Technical Report GL-98-17
August 1998

US Army Corps of Engineers
Waterways Experiment Station

Mapping Emplaced Articulated Concrete Mattress Using Geoelectrical and Electromagnetic Techniques

by Keith J. Sjostrom, Dwain K. Butler, Robert F. Ballard

Approved For Public Release; Distribution Is Unlimited

DTIC QUALITY INSPECTED 1

19980909 019

Prepared for U.S. Army Engineer Division, Lower Mississippi Valley

The contents of this report are not to be used for advertising, publication, or promotional purposes. Citation of trade names does not constitute an official endorsement or approval of the use of such commercial products.

The findings of this report are not to be construed as an official Department of the Army position, unless so designated by other authorized documents.

PRINTED ON RECYCLED PAPER

Technical Report GL-98-17
August 1998

Mapping Emplaced Articulated Concrete Mattress Using Geoelectrical and Electromagnetic Techniques

by Keith J. Sjostrom, Dwain K. Butler, Robert F. Ballard

U.S. Army Corps of Engineers
Waterways Experiment Station
3909 Halls Ferry Road
Vicksburg, MS 39180-6199

Final report

Approved for public release; distribution is unlimited

Prepared for U.S. Army Engineer Division, Lower Mississippi Valley
Vicksburg, MS 39180

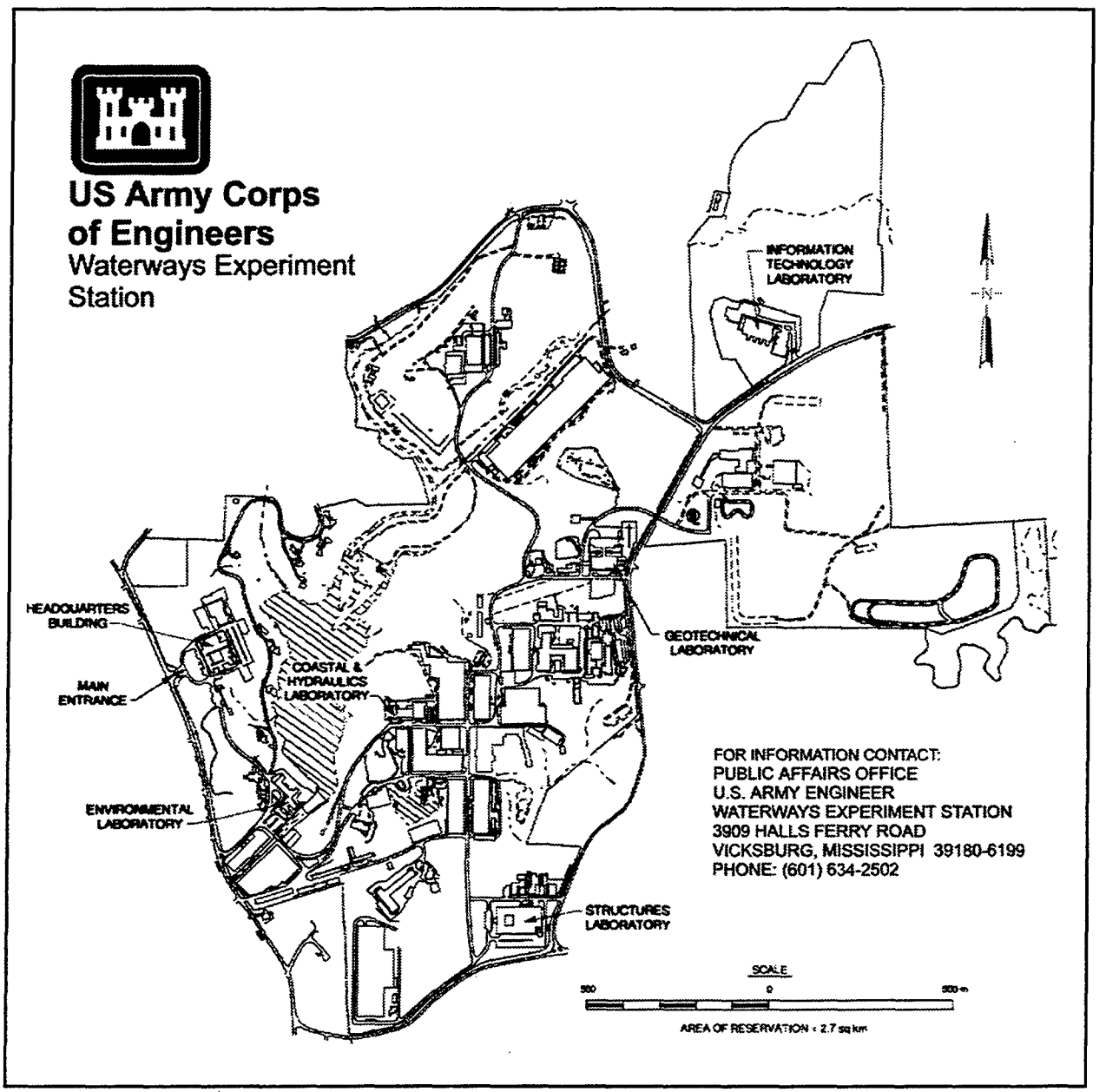

Waterways Experiment Station Cataloging-in-Publication Data

Sjostrom, Keith J.

Mapping emplaced articulated concrete mattress using geoelectrical and electromagnetic techniques / by Keith J. Sjostrom, Dwain K. Butler, Robert F. Ballard ; prepared for U.S. Army Engineer Division, Lower Mississippi Valley.

356 p. : ill. ; 28 cm. — (Technical report ; GL-98-17)

Includes bibliographic references.

1. Detectors — Geophysical methods. 2. Slopes (Soil mechanics) 3. Remote sensing. I. Butler, Dwain K. II. Ballard, Robert F. III. United States. Army. Corps of Engineers. Lower Mississippi Valley Division. IV. U.S. Army Engineer Waterways Experiment Station. V. Geotechnical Laboratory (U.S. Army Engineer Waterways Experiment Station) VI. Title. VII. Series: Technical report (U.S. Army Engineer Waterways Experiment Station) ; GL-98-17.

TA7 W34 no.GL-98-17

Contents

Preface v

Executive Summary vi

Conversion Factors, Non-SI to SI Units of Measurement ix

1—Introduction 1

Background 1
Geophysical Approach 1
Purpose and Scope 3

2—Articulated Concrete Mattress Revetments 4

Articulated Concrete Mattress 4
Test Sites 5

3—Self-Potential Method 7

Self-Potential Theory 7
Calculation of Self-Potential Response Profiles 8
Field Testing 9
Data Analysis and Results 10
Newly emplaced ACM 10
Older ACM under thin sediment cover 11
Older ACM under thick sediment cover 11
Multiple layers of ACM 12
No ACM present 13
Summary and Recommendations 13

4—Towed Electrical Resistivity Method 15

Electrical Resistivity Principles 15
Numerical Modeling of Resistivity Profiles 16
Field Testing 16
Stationary measurements 17
Underway measurements 18
Data Analysis and Results 18
Stationary measurements 19
Underway measurements 20
Summary and Recommendations 21

5—Correlation of Electrical Methods 23

6—Electromagnetic Methods 25
Concepts of Electromagnetic Surveying 25
Frequency domain EM method 25
Transient EM method 26
Feasibility Investigations and Numerical Modeling 27
Frequency domain EM method 27
Transient EM method 30
Field Testing 31
Waterborne FDEM method 31
Airborne FDEM method 32
Waterborne TDEM method 32
Data Analysis and Results 33
Waterborne FDEM method 33
Airborne FDEM method 36
Waterborne TDEM method 37
Summary and Recommendations 39
7—Conclusions 42
References 45
Figures 1-53
Appendix A: Phase II Report - Investigation of Articulated Concrete Mattress Using Self-Potential and Resistivity Methods A1
Appendix B: Phase III-A Report - Development of Self-Potential and Electrical Resistivity Methods for Investigation of Articulated Concrete Mattresses B1
Appendix C: Phase III-B Report - Development of Underway Electrical Resistivity Methods for Investigation of Articulated Concrete Mattresses C1
Appendix D: Self-Potential Type Curves Generated by Articulated Concrete Mattresses D1
Appendix E: Phase I Report - Airborne Electromagnetic Techniques to Delineate Reinforced Concrete Slabs Buried within River Bed Sediments E1
SF 298

Preface

A geophysical research program to detect, delineate, and assess emplaced articulated concrete mattresses along the Lower Mississippi River has been conducted by personnel of the Geotechnical Laboratory (GL), U.S. Army Engineer Waterways Experiment Station (WES). The research was performed under sponsorship of the U.S. Army Engineer Division, Lower Mississippi Valley (CELMV), and the associated U.S. Army Engineer Districts: New Orleans (CELMN), Vicksburg (CELMK), and Memphis (CELMM). The CELMV Project Coordinator was Mr. Steve Ellis.

The overall test program was conducted under the general supervision of Drs. W. F. Marcuson III, Director, GL, and A. G. Franklin, Chief, Earthquake Engineering and Geosciences Division (EEGD). Mr. Robert F. Ballard, Jr., was Program Manager and Dr. Dwain K. Butler and Mr. Keith J. Sjostrom were principal investigators. This report was prepared by Mr. Sjostrom, under the supervision of Mr. J. R. Curro, Jr., Chief, Engineering Geophysics Branch, GL, and Dr. Butler, under the supervision of Dr. A. G. Franklin, EEGD, GL. Data acquisition and analysis support for the self-potential and towed DC resistivity surveys was provided by Dr. Robert F. Corwin of SP Surveys, El Cerrito, CA. Electromagnetic data acquisition and analysis were provided by Dr. Edward Mozeley, Naval Research Laboratory, Stennis Space Center, Mississippi. Mr. Thomas S. Harmon, Jr., EEGD, acquired the side-scan sonar data presented in Figure 6. Mr. Rodney L. Leist and Ms. Lori M. Davis, EEGD, and Mr. Grady H. Holley, Applied Research Associates, Vicksburg, MS, assisted in the preparation of this report. Dr. L. D. Wakeley was Acting Chief, EEGD, and Dr. M. E. Hynes was Chief, Earthquake Engineering and Geophysics Branch at the time of publication of this report.

Acknowledgment is made to Messrs. Stuart Green, Tim McCarley, and other employees of DIMCO, Inc., Vicksburg, MS, for providing and piloting the research vessel, acquiring positioning and bathymetric information, and assisting in the collection of the geophysical data.

At the time of publication of this report, the Director of WES was Dr. Robert W. Whalin. Commander was COL Robin R. Cababa, EN.

The contents of this report are not to be used for advertising, publication, or promotional purposes. Citation of trade names does not constitute an official endorsement or approval of the use of such commercial products.

Executive Summary

Prior to this research initiative in 1991, limited techniques were available within the Corps of Engineers to determine the location and condition of emplaced ACM. Techniques available at the time were typically visual or direct contact procedures which, even under good conditions, proved marginal at best in the dynamic Mississippi River environment. Thereby, except for cases where the damage to an ACM extends far enough up the bank to be visible on-shore, there were no reliable procedures to verify the integrity or condition of an ACM after sinking.

Past attempts to locate and assess the condition of ACM by remote means have been only marginally successful. A conventional acoustic subbottom profiler test showed that under favorable conditions, reflected seismic signals could be used to locate ACM. Ground probing radar was feasibly demonstrated to Memphis District in 1985 and results indicated that bottom profiling could be conducted to depths of 25 ft and local disturbances along the ACM could be detected. In view of recent needs to perform detailed ACM site assessments, CELMV requested WES to submit a plan to thoroughly evaluate the use of geophysical methods to detect emplaced ACM and, from the candidate techniques selected, develop cost-effective and timely procedures for detecting, mapping, and determining the condition of ACM.

The plan was structured to address solutions to the problems of both ACM location and its behavior under a wide variety of river conditions. The investigation is organized in a series of sequential steps simply listed as Phases I, II, III, and IV.

Phase I: Feasibility Study of Candidate Techniques. This initial phase focused on the selection and evaluation of geophysical techniques applicable to determining the location and condition of in-service ACM. Prior to initiation of the study, CELMV engineers established the following criteria with which to evaluate any proposed geophysical method: (1) ability to detect ACM in water depths greater than 50 ft, (2) capable of detecting ACM buried under tens of feet of sediment, (3) delineating and resolving the limits of and depth to emplaced ACM, (4) capability of assessing ACM condition and integrity, and (5) cost-effectiveness and ease of use. WES scientists evaluated and tested a suite of candidate geophysical methods: self-potential (SP) method, towed DC electrical (TDC) resistivity, airborne and waterborne frequency-domain electromagnetics (FDEM), transient electromagnetics (TDEM), magnetics, ground

penetrating radar, direct current excitation, seismic reflection, and side scan sonar.

Phase II: Technique Optimization. Phase II concentrated on optimization of the Phase I techniques proven applicable to locating and determining the condition of ACM as per the criteria specified by CELMV. Only those techniques having the highest potential were considered. It was realized that no single geophysical technique works effectively over the total range of real-world conditions. Therefore, it was expected that more than one technique would be optimized to detect, delineate, map, and assess emplaced ACM in a variety of river conditions. To optimize a technique, additional field tests incorporating better data acquisition parameters or more robust data analysis algorithms are performed to fine-tune the interpretation of results. The testing was conducted at sites where conditions were adequately understood for proper technical evaluation.

Phase III: Procedural Development. Phase III was structured to concentrate on procedural development as related to the application of the geophysical methods in order to provide specific information about a revetment and developing the survey procedures for each technique. For the techniques optimized in Phase II, a logical test plan was developed for the selection and application of the geophysical techniques best suited to determine the parameters of specific ACM problems. A probable scenario would involve an analysis of typical problems, a determination of the manner in which ACM parameters should be obtained, selection of the most applicable techniques, development of test plans, conducting field tests, and finally, choosing the appropriate data presentation techniques to best resolve the problem.

The most promising techniques of those tested are SP, TDC resistivity, TDEM, and waterborne and airborne FDEM methods. Geophysical field investigations to develop, test, and refine each technique were conducted primarily at the Missouri Bend and Manchac Revetment sites along the Mississippi River, located downstream of Baton Rouge, LA, during the period December 1991 through September 1994. For each of the geophysical techniques developed and tested, the ACM is an excellent electrical target to detect and map. For rapid reconnaissance surveying to map the extent of a revetment field, the SP method proved to be simpliest and most cost-effective means developed. Airborne or waterborne FDEM methods also worked very well but were more costly. The TDC resistivity and TDEM systems, used as either a high-resolution or reconnaissance tool, proved equally capable of accurately determining the depth to the ACM even if the mattress is buried under tens of feet of sediment. Depth calculations to emplaced ACM along the Missouri Bend Revetment were within 10 percent of the depth values determined from 1992 hydrographic surveys. Interpreted depths along survey lines provided depth profiles of the in-service ACM. The SP method also provided depths of the riverward mat edge in all water depths. For condition assessment surveys to determine ACM integrity, the FDEM methods were demonstrated most effective in the ability to identify each 150 ft segment of a revetment, delimit mat edges, and identify areas of no mat or multiple mat layers. However, for any ACM mapping investigation, it is best to use at least two of the techniques developed in order to obtain the most useful results.

Phase IV: Procedural Implementation. Following the completion of Phase III, the strategy and procedures for routine application of the selected geophysical methods for ACM detection, mapping, and condition assessment surveys will be developed. For each individual geophysical technique, manuals are developed outlining survey procedures for identifying specific ACM criteria, scientific equipment required, guides for analyzing and interpreting the acquired data, and methods of data presentation. Included is the evaluation and recommendation of the feasibility and cost benefit of having the surveys conducted by WES, CELMV, or contractor personnel. Upon recognizing an ACM problem area, the prescribed methodologies developed in Phases III and IV must be followed to obtain the ACM parameters and information necessary to initiate remediation procedures.

Near the completion of Phase III, funding for this research program was discontinued. Phase IV of the program was never attained.

Conversion Factors, Non-SI to SI Units of Measurement

Non-SI units of measurement used in this report can be converted to SI units as follows:

Multiply	By	To Obtain
feet	0.3048	meters
inches	2.54	centimeters
inches	254.0	meters
knots	1.852	kilometers per hour
miles (U.S. statute)	1.6093	kilometers
miles per hour	1.6093	kilometers per hour
milliSiemens per foot	3.2808	milliSiemens per meter
ohm-feet	0.3048	ohm-meters
square feet	0.0929	square meters

1 Introduction

Background

Two of the U.S. Army Corps of Engineers (USACE) primary mission areas are the maintenance of the nation's navigable waterways and development of flood control measures. These tasks are most evident along the lower Mississippi River where revetments are used to maintain the river channel and prevent riverbank failure. Revetments are structures placed parallel to the river current for the purpose of stabilizing the concave banks in river bends, form a smooth bank line, and reduce the effects of erosion. Along the lower Mississippi River, articulated concrete mattresses (ACM's) are used exclusively for river bank protection (Figure 1).

Over time, ACM's are subjected to numerous cycles of high and low water levels, changing river velocities and currents, and structural fatigue. These factors may cause the ACM to become damaged, displaced by the undermining of streambed material, or buried by sediment material. The condition of ACM's must be routinely monitored to determine whether or not remedial or replacement measures need to be undertaken. Failure of an articulated concrete mattress during flood conditions could severely damage the integrity of the navigable channel and endanger the protective levees.

The U.S. Army Engineer Waterways Experiment Station (WES) was requested by the U.S. Army Engineer Division, Lower Mississippi Valley (CELMV) to develop a geophysical approach to rapidly detect, map, and determine the condition of in-service ACM's along the Mississippi River.

Geophysical Approach

Prior to this research initiative undertaken in 1991, limited techniques were available within the Corps of Engineers to determine the location and condition of emplaced ACM's. Techniques included side scan sonar surveys, underwater cameras and divers, and visual inspection of the on-shore portion of the mat. In each case, if the ACM was covered with sediment then these methods were useless in providing any information about the revetment. Also, except for cases where the damage to an ACM extends far enough up the bank to be

visible on-shore, there are no reliable procedures to verify the integrity or condition of an ACM after sinking. Verification by direct contact using a drill rig or probe is logistically difficult and can only provide a 'spot-check' of the ACM's depth.

Geophysical surveying techniques are remote sensing methods that can be applied to ACM inspection in a rapid, reconnaissance mode (detection and mapping) and in a high resolution mode (condition assessment). Rather than relying on direct contact or visual recognition, geophysical techniques exploit various physical processes to detect the contrast between the physical and chemical properties of the ACM and those of the river water and bottom sediments. Some of the physical processes include density, seismic/acoustic velocity and impedance, electrical resistivity and conductivity, dielectric permittivity, and magnetic susceptibility.

ACM detection refers to the capability of a geophysical method to determine the presence or absence of ACM beneath a point or location on the surface of the river. Detection by a particular geophysical technique can occur in two ways: (1) detection of a signal or anomaly that is above the background 'noise' level and occurs at a position, time, or depth consistent with that expected for the ACM and (2) detection or recognition of a signal pattern in an area that is consistent with the pattern expected from emplaced ACM. Mapping or delineation refers to ACM detection at multiple points in an area and therefore enabling the development of a map or plan view of the river surface showing locations where the mat is present or absent. If the ACM detection interpretation includes depth information, then contour maps of the interpreted mat depth may also be constructed. Resolution in the context of ACM detection and mapping refers to the accuracy with which features of the ACM can be mapped, e.g. location of riverward termination (toe), location of a revetment's upstream or downstream edge, location of missing ACM sections, and depth to an emplaced ACM. High resolution surveying also enables condition assessment of the emplaced ACM which refers to inference of multiple layers of ACM, deteriorated ACM conditions, missing sections of ACM, and holes in the ACM.

The WES in cooperation with several contractors developed a suite of geophysical techniques to rapidly assess the condition and location of in-service ACM's. During the research program, the following techniques were tested for feasibility and applicability in detecting and assessing ACM: self-potential, towed electrical resistivity, airborne and waterborne electromagnetics, magnetics, ground penetrating radar, direct current excitation, seismic reflection, and side scan sonar. Of all of the techniques tested, the first three listed (self-potential, towed electrical resistivity, and electromagnetics) met the CELMV requirements of rapidly detecting and mapping in-service ACM.

Purpose and Scope

The objectives of this research program are to develop rapid, safe, and cost-effective procedures for detecting, delineating, and assessing the condition of emplaced ACM along the Lower Mississippi River. Three of the ten geophysical methods evaluated during this program, self-potential, towed electrical resistivity, and electromagnetics, were selected for further development and are discussed in detail in Chapters 3, 4, and 6, respectively. Each chapter includes a discussion of the geophysical concepts, field testing procedures, data analysis methods, results of investigation, and a summary of the effectiveness in meeting the objectives of the ACM research program.

2 Articulated Concrete Mattress Revetments

Articulated Concrete Mattress

Bank protection procedures along the Lower Mississippi River entail the placement of revetments along the riverbank and dikes or weirs in the waterway for channel stabilization and control. A revetment, principally articulated concrete mattress (ACM) as shown in Figure 1, is a structure designed to continuously protect the banks of the Mississippi River from erosion and bank caving. The ACM protects the upper part of the riverbanks from wave action, protects the subacqueous bank from scouring or undercutting due to water currents, and is reasonably permanent (U.S. Army Corps of Engineers).

An ACM consists of an assemblage of concrete blocks reinforced and held together by a metal fabric to form a flexible but strong, protective blanket over the river bottom (Petersen 1986). The ACM must be flexible in order to mold itself to the irregularities of the riverbank during placement and cover the entire area to be protected. Flexibility also maintains the integrity of the ACM when uneven settlement or scouring occurs. The basic units of an ACM are the concrete blocks which have dimensions of 46 in. long by 14 in. wide by 3 in. thick. Each block is reinforced with corrosion-resistent stainless steel wire. The reinforcing cables of adjacent blocks are connected together leaving a 1-in. space between each block (Figure 2). This provides the flexibility in the revetment and the means for fabricating the blocks into a continuous mattress. A section of ACM comprised of the interconnected blocks is typically 150 ft wide and extends from the river bank to the center of the navigable channel. This length may vary from 500 to over 1,000 ft. Adjacent ACM sections are installed in an upstream direction by overlapping the downstream mattress section by five feet. The ACM sections are secured to the river bank with launching cables anchored into the bank material. This type of revetment is considered the 'standard' bank protection mechanism along the Lower Mississippi River (U.S. Army Corps of Engineers).

The ACM protect the riverbank during numerous cycles of high and low water levels, changing river velocities and currents, and toe scour and erosion. After decades of placement, these factors may eventually cause the ACM to deteriorate and disintegrate due to structural fatigue, degrade due to corrosion,

or become displaced by the undermining of streambed material. Flood events may also mangle (Figure 3), tear, or remove an ACM section from the riverbank. Physical damage, such as that caused by the mooring of barges, also lessens the integrity of a revetment. Damaged or displaced ACM sections are routinely monitored to determine whether or not remedial or replacement measures need to be undertaken.

Test Sites

Typical field sites were crucially important for evaluation of candidate geophysical methods and survey procedures for ACM detection and mapping. Two revetments were selected for study downstream of Baton Rouge, LA and represent the range of in-service ACM conditions. The revetments, constructed of overlapping ACM sections, are located between Mississippi River Mile (RM) 216 to 225 as illustrated in Figure 4 and identified as the Missouri Bend and Manchac Revetments. Positions along a revetment are given by range lines, e.g. U-100 or D-75. The range lines are situated perpendicular to the riverbank and referenced to a location on the crest of the levee. The prefixes 'U' and 'D' refer to range lines upstream or downstream, respectively of the reference range line located near the midpoint of the revetment or at the apex of the riverbend. The distance between adjacent range lines is 100 ft. The revetment test areas (indicated by river ranges) and general in-place conditions are described below.

Missouri Bend Revetment. The investigations performed at the Missouri Bend Revetment were concentrated between ranges U-70 to U-145 (Figure 5). The majority of the ACM in this reach, ranges U-70 to U-115, were placed in 1965 in water depths greater than 50 ft and extending 300 to 400 ft out into the river. Between ranges U-70 and U-87, the mat lies in water depths up to 100 ft and, according to USACE hydrographic surveys, is relatively clean or possibly buried by a few feet of sediment. Between ranges U-88 and U-114, hydrographic surveys indicate the ACM is buried by increasing amounts of sediment in the upstream direction. For example, sediment thickness above the mat along U-85 is approximately five feet whereby the average thickness along U-114 is 35 ft. Sediment thicknesses of over 50 ft may also be found along the revetment. Maximum water depths along this section range from 25 to 65 ft. In October 1992, 3,000 ft of new ACM were placed upstream of the existing revetment between ranges U-115 and U-145. No significant amounts of sediment had yet covered the ACM and maximum water depths ranged from 20 to 30 ft. The mat extends a distance of 500 ft into the river in this area. A side scan sonar image of the new mat, produced two weeks after placement, is illustrated in Figure 6.

Manchac Revetment. The Manchac Revetment test area between ranges U-80 and U-184 (Figure 7) has more complex and variable ACM conditions than the Missouri Bend Revetment. The majority of the revetment, ranges U-134 to U-184, was placed in 1983 and remains fairly clear of sediment between ranges U-134 and U-166 with less than five feet of siltation detected during the 1992 maintenance survey. Beginning near range U-166 and

extending upstream, the emplaced ACM are buried by increasingly greater amounts of sediment with thicknesses exceeding 40 ft at range U-184. The ACM between ranges U-96 and U-137 was placed in 1974 and also has little sediment cover. Visual inspection of the concrete mat along the riverbank in this section indicates torn sections and jumbled piles of blocks indicative of a highly worn ACM. Figure 3 is a photograph of the damaged ACM in this area. Additional sections of mat were placed over existing mattress for rehabilitation purposes between ranges U-123 and U-136 in October 1988, thereby providing an area with a double layer of ACM. Downstream of range line U-103, multiple layers of mat exist in areas of deep water. The ACM has little to no sediment cover except along the toe. However, indications of damage caused by the river current are evident along the bank line.

Arlington Revetment. Geophysical tests were also performed along the Arlington Revetment which is positioned along the eastern river bank between RM 223 and RM 228. The ACM was placed along this bankline during the period 1967 to the present. However, a barge repair facility and the constant presence of moored barges made any detailed mapping of ACM difficult. Therefore, this revetment was used primarily for 'proof-of-principle' investigations.

Plaquemine Bend Revetment. A series of airborne electromagnetic surveys (see Chapter 6) were conducted over the Plaquemine Bend Revetment in July 1994. The Plaquemine Bend Revetment is emplaced along the western riverbank downstream from the Manchac Revetment between RM 206 and RM 211. The age of the ACM ranges from 1947 to 1988.

3 Self-Potential Method

Self-Potential Theory

The SP method is based on the measurement of naturally occurring potential differences generated by electrochemical, electrokinetic, or thermoelectric mechanisms in the subsurface. SP anomalies are generated in water-covered areas when a metallic conductor, such as the metal reinforcing fabric of an ACM, extends from an electrochemically oxidizing region (near-surface river water) down to a electrochemically reducing environment such as the river bottom sediments. Electrochemical reactions, due to variations in oxygen content, take place within the system of the metal fabric of the ACM and surrounding medium. As a result, excess negative and positive ions are formed around the upper and lower parts of the ACM, respectively. Thus, an electric dipole, in which the metal fabric behaves essentially as a buried battery, is formed and an electric field produced (Skianis and Papadopoulos 1993). An electric current passes through the metal fabric from the negative pole to positive pole and the corresponding return current travels through the river water (see the upper sketch in Figure 8) and creates the observed SP signal at the surface of the water. A portion of the return current also flows through the streambed sediments. According to the SP mechanism described by Sato and Mooney (1960), SP signals are largest when the buried metal source does not corrode readily. Thus the stainless steel fabric of an ACM should be capable of generating a relatively large SP signal. The magnitude of the SP current increases as the electrochemical conditions near the bottom of the source body become more chemically reducing (Sato and Mooney 1960). As conditions are generally more reducing within streambed sediments than in overlying water, burial of the bottom portion of an ACM may actually increase the electrical current and magnitude of the SP signal when compared with unburied conditions. Further discussion on the generation of self-potentials by ACM can be found in Appendix A.

The contours of a SP field generated by an undamaged ACM parallel the river bank and show little lateral variation except at the upstream and downstream ends. Therefore, survey lines are performed perpendicular to shore to measure the diagnostic or characteristic SP signatures. The upper data profile illustrated in Figure 8 shows the total field SP signal for a generalized ACM geometry. Measuring the total field SP signal, however, requires towing two electrodes separated by a large distance such that as one electrode measures the SP field the other remains over an area of the river bottom with no ACM.

This survey configuration is logistically difficult to perform in the Mississippi River due to the strong water currents and frequent river traffic. Therefore, the SP measurements for this investigation were made using the 'gradient' technique in which the SP signals are measured by towing a pair of electrodes over the ACM and recording changes in potential. Because the electrode separation is small compared to the wavelength of the SP field, this configuration measures the rate of change or gradient of the total SP field. The lower data profile in Figure 8 illustrates the gradient signal for the geometry shown.

The locations of the inner (nearshore) and outer (offshore) limits of the mattress section are indicated by the points of the zero crossings of the gradient signal. The depths to the outer and inner ends of the section are related to the shape of the gradient profile and the characteristic wavelengths of the measured SP field. The amplitude of a gradient profile is a function of the magnitude of current flow in the metal fabric, mattress depth, and local geochemical conditions. Although amplitude information are not used directly in the interpretation routine, large amplitude signals are desirable because they are more readily detectable and higher signal-to-noise ratios allow improved resolution of zero crossings and profile shapes.

Calculation of Self-Potential Response Profiles

Modeling the SP response profiles is a process by which potential differences are calculated along the water surface for a variety of subsurface electrical conditions, ACM geometries, and survey configurations. Using a mathematical model, the generated profiles demonstrate the effects of varying parameters of interest for the purpose of SP survey design and guidance for interpretation of SP data collected over ACM. The SP source models are typical of those obtained from field measurements acquired during the course of the project. The models incorporate finite line sources, ACM geometries, and mat depths representative of ACM installations near Baton Rouge, LA.

Nine forward modeling simulations were investigated to analyze the various responses of the gradient electrode array to variations of the ACM source parameters, electrode configuration, and survey procedure. The situations investigated involved variation of the following parameters:

a. Electrode separation.

b. Depth of the outer edge of the ACM.

c. Position of the outer mat edge.

d. Dip angle of the ACM.

e. Offset of the survey line.

f. Line length of the source model.

g. Comparison of point and line source profiles.

Each of these forward modeling simulations are illustrated and discussed in detail in Appendix D. The results for each situation are further related to the collection and analysis of actual field data.

Field Testing

The SP signals were measured by towing a pair of electrodes perpendicularly to the river bank along the water surface and recording the potential difference between electrodes. The electrode spacing was 50 ft with the forward electrode positioned 100 ft behind the survey vessel. This electrode configuration, called an electrode dipole, was easy to deploy and gave detectable signals and good signal-to-noise ratios at all test sites. Larger electrode spacings were tested during the course of study which resulted in an increase in signal amplitudes. However, the amplitude gains of larger electrode spacings also increase noise levels and are more difficult to deploy and tow. Several towing configurations were tested in efforts to reduce data noise and enhance signal detection. It is important to remember that optimal SP data quality is achieved when the electrode dipole as well as the survey lines are performed perpendicular to the shore. Therefore, the best data will be usually obtained when the river currents are at their lowest velocity during low river stages.

The data acquisition system used consisted of a digital multimeter to measure the potential difference between the electrodes and transmit the voltage values to a computer. The digital voltage values, along with an acquisition time stamp, are transmitted to the computer via a RS-232 output port. The digitized SP values are plotted on the computer screen for real-time quality control and stored in a data file for later analysis. The data are also correlated with the corresponding survey vessel positioning information and measured water depths.

Field studies during the development and testing stages of the research project were conducted along the Mississippi River at the Missouri Bend (Figure 5) and Manchac Revetment (Figure 7) sites located downstream of Baton Rouge, LA. The SP surveys are designed to investigate five distinct site criteria for evaluation of the SP technique: recently placed ACM, older ACM buried with varying thicknesses of sediment, ACM emplaced in varying depths of water, multiple layers of ACM, and areas of possible ACM damage. Surveys were performed at these sites during December 1991, October 1992, August 1993, January 1994, and September 1994. While it is best to perform SP surveys during periods of low river levels, data collected during December 1991 and August 1993 were acquired when river levels were anomalously high. The results of the October 1992 and August 1993 field studies are provided in the reports presented in Appendices A and B, respectively. Data collected during the December 1991 and the two 1994 field studies were acquired during testing of other geophysical methods and not formally reported.

Data Analysis and Results

The SP data are interpreted using a modified version of the computer program SP1.BAS, described in Corwin and Butler (1989). The metal fabric of the mattress is modeled by a pair of linear sources of constant electrical current positioned longitudinally along the inner and outer edges of the ACM. The line sources are assumed to by in a homogeneous half-space. Referencing Figure 8, the offshore end of the ACM acts as a positive line source and generates the broad positive voltage variation detected at the right side of the gradient profile. A negative line source creates the large negative variation in the center and the positive signal at the left end of the profile. The (+) and (-) signs, see upper portion of Figure 8, denote the line current sources and are situated perpendicular to the plane of the paper. These sources may be thought of as the battery terminals in the analogy used earlier. This relatively simple model is common practice to interpret SP data conducted for mineral exploration and has been found to yield good estimates of the source parameters (depth and location) for SP signals generated by thin, dipping metallic structures. It should be noted that this model is not designed for multi-layered environments, such as a thick sediment layer overlying the ACM, and therefore the error factor for these cases will increase.

Measured values of the river water resistivity, current per unit length of each source, source length, location, and depth are used as input to the program. The analysis consisted of computing values of the total and gradient SP model and comparing the results with the measured gradient profiles. The lengths, depths, and position of the source lines are adjusted until the zero crossings, amplitudes, and peak-to-peak wavelengths of the model match that of the measured field profile. The zero crossings of the gradient (measured) curve denote the approximate location of the mat edges. Any significant deviation between the shapes of the calculated and measured profiles may indicate that the survey was not run exactly transverse to the ACM section, a portion of the ACM is damaged or missing, or variations in the geochemical environment.

A complete discussion of all the SP data collected during the October 1992 and August 1993 field investigations is given in the reports provided in Appendices A and B, respectively. Survey results from five representative conditions of in-service ACM along the Missouri Bend (Sjostrom and Corwin 1993) and Manchac Revetments are discussed below.

Newly emplaced ACM

Prior to the October 1992 SP survey, 3,000 ft of new ACM were placed along the river bank between ranges U-115 and U-145 of Missouri Bend (Figure 5). Surveys were performed on three range lines with data collected along range U-122 shown in the upper portion of Figure 9. Note that the shape of the gradient data curve corresponds to the theoretical curve described in Figure 8. The lower portion of Figure 9 illustrates the river bottom elevation measured during the SP survey and depths to the as-installed ACM (denoted by the '+' symbol) measured immediately after placement. Analysis of the SP data is

performed by comparing the measured SP gradient profile with a calculated profile using estimated source line depths and locations. The locations, depths, and intensities of the source lines are varied until a reasonable fit is obtained. Multiple source lines were computed which are typical of a relatively shallow and/or clean mat segment. The interpreted mat locations are indicated by the solid line as illustrated in the lower plot of Figure 9. The computed source depths for these ranges were essentially equal to the water depth as would be expected for newly-installed mat.

Older ACM under thin sediment cover

The area between ranges U-75 and U-87 of the Missouri Bend Revetment and ranges U-134 and U-170 of the Manchac Revetment are areas of older mat located in water depths greater than 50 ft and buried by sediment ranging in thickness from 0 to 10 ft. SP data measured along range U-75 at Missouri Bend in October 1992 and along range U-140 at the Manchac Revetment in August 1993 are presented in the upper portion of Figures 10 and 11, respectively. The measured depths to the river bottom and the as-installed elevation of the revetments, denoted by the '+' symbol, are illustrated in the lower portion of each figure. The gradient profile along each range line are similar to the data collected over new mat which indicates the mat is present and generating an SP signal. The amplitudes of the signal are smaller and may be attributed to the age of the emplaced ACM, greater water depths, or variations in the geochemical environment. Analysis of the data collected along range U-75 (Figure 10) indicates the outer limit of the mat is detected approximately 300 ft from shore (note the location of the zero crossing) at a depth of 120 ft with respect to the Low Water Reference Plane (LWRP). The interpreted electrochemical inner limit is located along the river bottom in 36 ft of water. It should also be noted that the mat could be seen along the shore in this area. The interpreted ACM results from data collected along range U-140 of the Manchac Revetment (Figure 11) indicates the outer limit of the mat is detected approximately 375 ft from shore at a depth of 110 ft LWRP. The inner limit was located just below the river bottom at the time of the survey. Each of these results correlate well with the as-installed information of the mat and the 1992 river bathymetry.

Older ACM under thick sediment cover

Between river ranges U-88 and U-114 of the Missouri Bend Revetment, the 1965 placed ACM are buried by tens of feet of sediment and is not visible along the river bank. Similarly, considerable siltation has also buried the ACM upstream of range U-166 of the Manchac Revetment. The recorded SP values collected along range U-95 at the Missouri Bend Revetment in October 1992 and measured elevations of both the river bottom and as-installed ACM are presented in the upper and lower portions of Figure 12, respectively. Likewise, the measured SP voltages recorded along range U-171 at the Manchac Revetment in August 1993, the 1992 river bottom elevations, and as-installed ACM depths are illustrated in Figure 13. The gradient signatures are similar to the other profiles previously presented but the amplitude of the signals are

much less. The lower amplitudes may be due to a combination of water depth, thickness of sediment overlying the mat, variations in the geochemical environment, or indications of a disintegrated or damaged area of ACM. The inner limit of the Missouri Bend ACM is interpreted just below the river bottom (see lower portion of Figure 12) and correlates well with the as-installed ACM elevation. The electrochemical outer limit of the ACM is computed at a depth of 280 ft below the water surface at a distance of approximately 200 ft from shore. At the Manchac Revetment test area, only one source line, representing the outer mat limit, was needed to interpret the data. The interpreted source point is located approximately 130 ft offshore at an elevation of -62 ft LWRP as illustrated in Figure 13. The results for the position of the outer source point contrast significantly from their respective as-installed ACM position. The results of both surveys underestimate the distance of the source point from the LWRP by over 100 ft. Although the depth of the outer source point along range U-171 correlates well with the as-installed depth at Manchac, this is not the case at the Missouri Bend site where the depth exceeds the as-installed depth by over 100 ft. Discrepencies in the depth parameter may be due to the fact that the emplaced ACM at Missouri Bend was located in deeper water at the time of the survey and buried by a greater thickness of sediment than the ACM at Manchac. As discussed in the description of the SP model, it is evident from the interpreted values that the SP model is unable to provide accurate estimates of the ACM parameters for situations where a thick layer of sediment overlies the ACM. Development of an SP model to handle multi-layer environments, namely water over sediment over ACM, is a mathematically rigorous and time-consuming project and was not within the scope of this research effort. However, for accurate estimates of the ACM parameters in all riverine environments, a multi-layer SP model should be studied in more detail if any additional study of the SP method is undertaken.

Multiple layers of ACM

Two areas along the Manchac Revetment study area have multiple layers of ACM. One such area is located between range lines U-123 and U-136 where the original ACM was placed along the riverbank in 1974 and an overlying layer was installed in 1988. Four survey lines were performed over this area in October 1992 with data collected along range U-130 shown in the upper portion of Figure 14. The plot of the gradient SP data curve has the expected characteristic signature with amplitudes greater than those recorded over new mat (Figure 9) and much greater than those from a single layer of older ACM. The lower portion of Figure 14 illustrates the recorded river bottom elevation and depths to the as-installed upper layer of ACM (denoted by the '+' symbol) measured immediately after placement. Analysis of the SP data revealed an interpreted depth to the outer edge of the mat of 100 ft LWRP as shown in the lower portion of Figure 14. The outer edge of the mat is detected approximately 380 ft from the riverbank. Another source is located closer to shore at a depth of 56 ft LWRP. These interpreted results correspond well to the as-installed depth information for the ACM. The SP method, however, is unable to resolve the depths to the individual mat layers.

No ACM present

Two surveys were performed upstream of the Missouri Bend Revetment along range U-154 in October 1992 to check the SP signal in areas with no ACM. The SP profile and river bathymetry are shown in Figure 15. It is readily apparent from the data that no ACM is detected along this range due to the lack of the characteristic SP gradient signature. No numerical data analysis was performed on this data.

Summary and Recommendations

Five field studies were conducted at the Missouri Bend and Manchac Revetment sites along the Mississippi River, located downstream of Baton Rouge, LA, during the period December 1991 through September 1994. The tests were used to develop a practical SP technique for use in differing site conditions (river stage, mat condition, water depth, sediment cover, etc.) for investigation of emplaced ACM. The SP data collected during all tests indicate that the metal reinforcing fabric does generate a large, readily detectable SP signal which is consistent with the expected electrical signatures. The best quality data are collected when the river flow velocities are at a minimum such that the survey track line and electrode dipole are perpendicular to the riverbank.

Analysis of the SP data provides locations and depths of the outer edge of the mat and inner source points where changes in the physical or geochemical condition occurs. Depths to source points along a river range provide an approximate depth profile of the in-service ACM. For good-quality SP data sets, the computed mattress location and depths correlate well with the as-installed ACM depths; even when ACM's are located in water depths up to 100 ft. At this level of development, the SP method is unable to resolve individual mat layers in areas of multi-layered ACM. For ACM buried under significant amounts of sediment or disintegrated and corroded ACM, lower amplitude SP signals are measured and result in discrepancies between the computed and as-installed ACM parameters.

Although the present state of the data acquisition and analysis process is reasonably efficient, modifications to survey setup, positioning data acquisition, computer software, and graphical output could significantly reduce the time needed to acquire and analyze the data. The reports presented in Appendices A and B include sections outlining suggested recommendations to enhance the current system. The SP data on which these conclusions are based were obtained from only two revetment sites. Although there was a wide variety of mat conditions at these two sites, it is recommended that additional sites be surveyed which may have differing site conditions that may affect the SP data in ways not detected at the two test sites. Development of a more robust, multi-layer SP model should also improve the accuracy of the computed ACM parameters.

The SP system developed under this research program is suitable for production use for investigation of in-service ACM. The SP data can be

interpreted to provide position and depth estimates of the outer edge of the mat and usually one or more mat points along the range line as well. This technique is most useful as a reconnaissance tool because of the ease in which the presence of ACM is detected and the mat limits determined. Other methods developed through this research program, namely the towed electrical resistivity and electromagnetics, may provided more detailed information about the physical condition of the mat.

4 Towed Electrical Resistivity Method

Electrical Resistivity Principles

Vertical electrical sounding methods examine the variation of resistivity with depth. This technique is primarily used on land to detect layers of earth material having significant resistivity contrasts with surrounding zones. This technique has also been applied and successfully used for a number of offshore engineering applications (Corwin 1983; Lavoie 1988).

Field studies using the towed DC electrical resistivity method (TDC) for ACM detection and mapping are performed using an inverted Schlumberger electrode array incorporated in a streamer cable towed in the water behind the survey vessel. A schematic of electrode array and deployment scheme are shown in Figure 16. The streamer cable consists of two closely spaced current electrodes located midway between logarithmically spaced pairs of potential electrodes. The electrode arrangement is symmetric about the midpoint of the array. Procedures using this array configuration entail leaving the current electrodes fixed and logarithmically increasing the distance between the potential electrodes and center point. An apparent electrical resistivity value is computed using the geometry of the electrode array, transmitted current, and measured voltage values. The resistivity measurements are correlated to the array midpoint.

As the potential electrode distance about the midpoint increases, the potential differences recorded reflect changes in the electric field, generated by the transmitted current, due to resistivity variations or layers deeper within the earth structure. The computed apparent resistivity values are plotted versus the potential electrode separation on logarithmic plots as shown in Figure 17 (the data and results presented in Figure 17 will be discussed later). The resulting apparent resistivity data curves are interpreted using computer algorithms to determine a model of the thickness and resistivity of the horizontal layers below the electrode array midpoint that best fits the data. A typical model of a buried mat would be comprised of a layer of water over sediment over the ACM. The stainless steel mesh of the ACM is modeled as a very thin layer having very low resistivity values.

The resultant information from a sounding location provides depths to the ACM below the center point of the array, resistivity values of the river water and overlying sediment (if present), and thicknesses of the water layer (water depth) and overlying sediment. Variations in the resistivity values of the ACM may also provide information on the condition of the emplaced revetment. A more in depth discussion of electrical resistivity techniques can be found in Telford, et al. (1976) and Department of Army (1979). Further discussions of this technique as related to the investigation of ACM are found in Appendices A, B, and C.

Numerical Modeling of Resistivity Profiles

Numerical modeling of the electrical resistivity response to an ACM is a process by which resistivity values are calculated along the water surface for a given set of subsurface geo-electrical models and ACM geometries including buried ACM. Numerous computer algorithms are readily available to perform these calculations. Using analytical models representative of ACM installations near Baton Rouge, LA, the numerical results demonstrate the effects of varying parameters of interest for the purpose of TDC survey design and interpretation of resistivity data collected over ACM. Results indicate that the calculated apparent resistivity value is sensitive to the metal fabric of the ACM even when the mat is buried under sediment. The study also indicated that the results can be interpreted to readily determine the presence or absence of and depth to ACM. Inferences about the condition of the ACM may also be derived. The results of the forward modeling exercise were not formally reported.

Field Testing

The production TDC resistivity system developed during this research effort includes a high-voltage power supply, transmitter-receiver unit, data acquisition hardware, and a towed electrode array. The transmitter-receiver unit is configured to allow manual or automated control of the current transmitter and data acquisition process. However, the system is also designed to be run manually if necessary. A complete description of all of the components comprising the TDC system is presented in Appendix C. A brief summary is outlined in the following paragraphs.

The towed electrode cable incorporates an inverted Schlumberger resistivity array (Figure 16) with a transmitter or current electrode spacing of two meters (6.56 ft) centered about the midpoint of the array. Eight pairs of receiver or potential electrodes are logarithmically spaced about the array midpoint at distances of 7.5, 10.0, 13.3, 17.8, 23.7, 31.6, 42.2, and 56.2 m (24.6, 32.8, 43.6, 58.4, 77.7, 103.6, 138.4, and 184.4 ft). During data acquisition, the center of the electrode array is positioned approximately 265 ft behind the research vessel thereby allowing adequate distance between the vessel and the potential electrode located at 56.2 m (184.3 ft). The end-to-end electrode

separation of 112.4 m (368.8 ft) allows detection of the mat at depths up to 100 ft below the river surface.

The transmitter-receiver components consist of a high-voltage power supply and transmitter-receiver switching unit. The prototype system, used during the September 1994 survey, was computer controlled using a personal computer. Earlier preliminary studies used equipment that was manually controlled. The voltage DC power supply, regulated to provide a current or voltage to a maximum of 3.5 amps or 300 volts, respectively, is commutated to a square wave signal by the switching unit with the waveform characteristics software controlled by the computer. The square-wave current is fed through the cable to the transmitter electrodes and the resulting potential differences in the water are measured between the eight pairs of receiving electrodes. The measured voltages are transmitted to the data acquisition system where they are digitized and filtered before being sent to the computer. The output current and measured voltage data are displayed in real time on the computer screen in graphical form and stored in a file. The computer program also computes apparent resistivity values using each of the eight voltage values, the output current value, and the geometric factor of the electrode array. These calculations are stored in a data file and may be graphically displayed on the computer screen during the survey if desired. Both the measured voltages and computed apparent resistivities are time stamped for correlation with the positioning information.

Field studies during the development and testing stages of the towed DC resistivity (TDC) system were conducted at both the Missouri Bend (Figure 5) and Manchac Revetment (Figure 7) sites. The TDC surveys are designed to investigate the same site criteria as the waterborne SP technique: recently placed ACM, ACM emplaced in varying depths of water, older ACM buried under varying thicknesses of sediment, multiple layers of ACM, and areas of possible ACM damage. Initial test studies were performed at these sites during October 1992 and August 1993. The initial studies were primarily designed to determine the resistivity structure of the water, sediments, and ACM and to analyze the characteristics of the equipment and data acquisition hardware. Data collection during these tests included stationary measurements over specific locations and some underway measurements. Surveys using the prototype production TDC system for underway data acquisition were conducted during late September 1994.

Stationary measurements

Stationary measurements using the TDC resistivity system were performed to initially test early versions of the data acquisition system and electrode array, evaluate the ACM as an electrical target, and determine the electrical characteristics of the Mississippi River water and sediments. Nine stationary measurements were performed along the Missouri Bend Revetment in October 1992. The center of the electrode array was positioned along range lines U-95, U-112, U-128, and U-158 to investigate the following conditions: older ACM buried by some sediment, older ACM underlying a thick sediment cover, new

ACM, and no ACM, respectively. No stationary soundings were performed at Manchac Revetment because of equipment malfunction.

Underway measurements

Initial testing of the TDC resistivity system in the underway mode was along the Missouri Bend Revetment in October 1992 (Appendix A). Resistivity measurements were collected along a survey line beginning at range line U-70 and extending to range U-160 to investigate the electrical characteristics of old mat, new mat, and no mat and monitor the transition between each area. Water depths below the electrode cable were maintained at 20 to 25 ft. Testing in August 1993 was performed at the Manchac Revetment to investigate the electrical properties of the mat, sediments, and water, characteristics of the electrical signal, and signal-to-noise ratios between the electrical signal and background values (Appendix B). Only a few tests were performed with the resistivity system before the electrode cable sank during a sharp turn and became snagged on the bottom. The array could not be retrieved.

Testing of the prototype computer-controlled TDC resistivity system was completed in September 1994 at the Missouri Bend and Manchac Revetments. Twenty-five profiles were performed with profiles run in both the upstream and downstream directions, at varying survey speeds, over differing conditions and ages of mat, and different equipment and data acquisition parameters. After evaluation of all the differing parameters, an optimal equipment and surveying configuration was determined and one profile line was made using this setup. The results of this test session are outlined in Appendix C. An additional survey program, scheduled for early 1995, incorporating the final TDC system upgrades and implementation of the optimal survey configurations was indefinitely postponed due to lack of funding.

Data Analysis and Results

The acquired apparent resistivity data are interpreted using a general-purpose modeling and interpretation computer program for the analysis of one-dimensional resistivity sounding data. The multiple layer analysis program, called INVES, in which the layers are assumed horizontal and infinite planes was written by Dr. Robert F. Corwin of SP Surveys, Inc. Initially, estimates of the layered model in terms of the number of layers, thickness, and resistivity are entered manually into the inversion program. For the investigations on the Mississippi River, the measured value of the river water resistivity is approximately 20 $\pm$5 ohm-m (ohm-meters). The resistivity of the river bottom sediments typically ranges from 10 to 50 ohm-m with an average value of 35 ohm-m. The metal fabric of the mattress is modeled as an individual layer. Laboratory analysis of the stainless steel reinforcing mesh determined the electrical resistivity of the wire to be 1.0×10^{-7} ohm-m and metal thickness to be 5.5×10^{-5} m (Mozley and Kooney 1991). Because the computer algorithm has difficulty handling very small resistivity and thickness values, an equivalent

mat layer thickness and resistivity value of 0.8 m and 0.01 ohm-m, respectively, were used. These values yield results very close to those obtained with the much smaller values.

Apparent resistivity values are calculated at each electrode separation using the estimated layered earth model. These values are compared to the measured field data through least squares analysis until a minimum error is obtained between the two data sets. The resultant earth model, continually adjusted during the iterative inversion process, indicates the interpreted depth to the emplaced ACM, thickness of sediment over the mat, and the resistivity of the sediment material. It should be noted that the resistivity values of the water and mat and the thickness of the ACM are fixed values. For stationary resistivity soundings, the resultant information provides a depth profile at a specific location along the revetment. Results from an underway resistivity survey include a depth profile to the sediment and ACM along a survey line. All information is correlated to the positioning information acquired during data acquisition.

Modeling studies performed on resistivity sounding data to determine the accuracy of the interpreted mat depths are discussed in Appendix B. By varying the model parameters, layer thickness (depth) and resistivity, it was found that the true elevation should be within ± 10 percent of the optimum value; i.e., the depth which provides the minimum least squares error between the actual and calculated resistivity values. However, the absolute accuracy of the interpreted ACM elevations can only be determined by comparison with actual 'ground truth' information. A deteriorated condition of the emplaced ACM may create large discrepancies between the actual and computed mat depths.

Analysis of the resistivity data incorporates the interpretation routine discussed earlier in this section. A complete discussion of the stationary and underway resistivity measurements collected during the October 1992 and September 1994 field investigations are given in the reports provided in Appendices A and C, respectively. A brief summary of the stationary and underway survey results are discussed below.

Stationary measurements

Stationary measurements using the TDC resistivity system were performed along the Missouri Bend Revetment in October 1992. The center of the electrode array was positioned along range lines U-95, U-112, U-128, and U-158 to investigate the following conditions: older ACM buried by little to no sediment, older ACM underlying a thick sediment cover, new ACM, and no ACM, respectively. The data collected from three resistivity tests are presented in Figure 17 along with a table of the interpreted models. It is clearly illustrated in this figure that the electrical response of the electrode array over emplaced ACM is characterized by a steeply dipping apparent resistivity curve. The position of the steep portion of the curve along the electrode separation axis is dependent on the thickness and resistivity values of the water and overlying sediment. The measured resistivities from the test over an area with no mat (range U-158) remained fairly uniform. Sediment resistivities ranged from

17.1 to 39.7 ohm-m which is consistent for unconsolidated and saturated sand/silt/clay sediments (Telford, et al. 1976). Interpretation of the sounding data collected along range U-128 over new ACM indicated the depth to mat is 27.9 ft (8.5 m). The measured water depth and depth to ACM at this location is 30 ft (9.2 m). The third sounding was performed over buried mat along range U-112. The interpreted results indicate the ACM is detected at a depth of 56.4 ft (17.2 m) and overlain by 37.4 ft (11.4 m) of sediment. The computed elevation of the ACM is 54.7 ft LWRP. At this location, the interpreted depth to the ACM is within two feet of the as-installed depth and the computed sediment thickness is approximately four feet less than the estimated thickness from the 1992 hydrographic survey. The sediment layer has an interpreted resistivity of 41.2 ohm-m. A full discussion of all the resistivity soundings can be found in Appendix A.

Underway measurements

Twenty-five resistivity surveys using the prototype computer-controlled TDC resistivity system were conducted in September 1994 at the Missouri Bend and Manchac Revetments. The results of these tests are discussed in Appendix C. The results of the initial testing in October 1992 are found in Appendix A. Following the September 1994 field investigation, it was determined that only one profile line, survey MB1 (Appendix C) along the Missouri Bend Revetment, was made using the optimal equipment and surveying configuration. This survey was performed in the upstream direction along the 30 ft water depth contour over the area of older mat (ranges U-70 to U-115) and along the 20 ft depth contour over the new mat and no mat areas.

An illustration of the measured apparent resistivity for each electrode separation versus the elapsed survey time is shown in Figure 18. It should be noted that a logarithmic display of the measured apparent resistivity values versus electrode separation for each measurement position is similar to any one of the three curves presented in Figure 17. A total of 149 soundings were acquired during the survey and each data set is correlated with survey positioning information to provide locations of each sounding on the river surface. The plot in Figure 18 is displayed in real-time during data acquisition and provides a great deal of preliminary information regarding the presence and relative elevation of the emplaced ACM. Different profile 'signatures' are associated with the differing areas of ACM and the transition areas from older mat to new mat and new mat to no mat are immediately evident as abrupt changes in the resistivity signatures. Also of interest is the higher resistivity bump detected at a distance of 3,000 ft along the survey line. This deviation may indicate a significant deepening of the mat or possible deterioration of the emplaced ACM. Analysis of each data set yielded interpreted depths to the mat and resistivity values of the river water and sediments. A plot of the interpreted depth to the ACM along with the measured water depth between ranges U-70 and U-130 is presented in Figure 19. The data sets for the depths to the river bottom and ACM have been smoothed to better illustrate the results of the survey. The as-installed depths below the water surface of the 1965 and 1992 placed ACM with respect to the September 1994 river level is also presented.

The area of new mat begins at range U-115 and interpreted depths to the ACM are at or near the river bottom as expected. Correlating the interpreted depths to the ACM with the as-installed depth information, deviations of less than two feet are typical. Between river ranges U-115 and U-120, greater differences exist between the as-installed and computed depths. These over estimated depth values are caused by the edge effects of the electrode array passing over the transition area between the older, deeper mat and the newer, shallower mat. As the 375 ft long electrode array passes over this area, portions of the measured voltages, especially at the outermost potential electrodes, are influenced by the laterally changing ACM conditions. Although the apparent resistivity values for each sounding represents the subbottom conditions, the horizontally layered-earth model has difficulty handling the complex geometry. Therefore, the computed depths are weighted averages of the actual ACM depths. The edge effects also affect the depth calculations of the older mat in the region between ranges U-110 and U-115.

Good correlation between the computed and as-installed ACM depths exists between ranges U-70 and U-90. Interpreted values are at depths of approximately 30 ft below the water surface and typically within four feet of the as-installed values. The area of higher resistivity values detected at 3,000 ft in Figure 18 is illustrated by the area of deeper ACM depths computed between ranges U-95 and U-105. The interpreted depths of the ACM in this section compares favorably with the as-installed placement depths as illustrated in Figure 19. Deviation between the depth values may be due to the undulating surface of the emplaced ACM, thickness of overlying sediment, and variations in the geochemical environment. The condition of the ACM in this area is unknown, however, as discussed in Appendix C, it is unlikely that a portion of the mat is missing because the changes in resistivity values are not as abrupt as those over the ACM transition areas indicated earlier.

Summary and Recommendations

Three field exercises were conducted at the Missouri Bend and Manchac Revetment sites during October 1992, August 1993, and September 1994. These tests were used to develop the TDC resistivity system and study the electrical characteristics of the river sediment and ACM, influence of electrical noise sources, and the effects of various acquisition parameters on the data collection process. The intent was to evaluate and implement a technique for determining the depth, extent, and possible condition of emplaced ACM at locations having different site parameters. The resistivity data collected during all tests indicated that the metal reinforcing fabric of the ACM is a readily detectable electrical target. The prototype system with the computer controlled current switching and data acquisition operated reliably under actual field conditions. The best quality data are collected when the survey track line and electrode array are aligned parallel to the riverbank. The data reduction and interpretation programs, using a layered earth model and fixed parameters to represent the ACM, provide good results when applied to actual field data.

Analysis of the TDC resistivity data provides estimated depths to the emplaced ACM, locations of mat boundaries, resistivity and thickness values of any overlying sediment cover, and possible delineation of anomalous areas. Interpreted depths along a survey line provide an approximate depth profile of the in-service ACM. Multiple passes, offset by a small distance, over an area of interest enables the possibility of producing a three-dimensional surface map of the ACM. For good-quality data sets, the ACM is detected and resolved to depths of 100 ft with the interpreted mattress depths typically within ± 10 percent of the actual depth value. During data acquisition, the TDC system displays the measured apparent resistivity values for each electrode separation in real-time to provide quality control and preliminary information regarding the presence and relative elevation of the emplaced ACM. Variations of the resistivity signatures can be associated with the differing ages and conditions of emplaced ACM and areas of transition. The transition areas investigated at Missouri Bend, such as from older mat to new mat, appear as abrupt changes in the resistivity signatures. Following interpretation of the data, test results at Missouri Bend correlate well with the as-installed ACM depths; even when ACM's are buried by tens of feet of sediment.

The TDC resistivity system developed to date under this research program is suitable for production surveying to investigate in-service ACM. The TDC system may be used either as a reconnaissance or high resolution investigation tool. In the reconnaissance mode, this system readily detects the presence of ACM, locations of the mat limits and transition areas, and relative depth information. This information can be obtained in real-time during data acquisition or following data analysis. As a high resolution tool, the TDC system provides depth profiles of the emplaced ACM parallel to the riverbank and delineation of any anomalous conditions which may be related to areas of deeper mat or deteriorated ACM.

Although the present TDC system hardware and software could be used for production operations, some modifications are necessary to help simplify field operations, prolong the operating life of the system components such as the electrode array and current switching box, and streamline the data interpretation process. An outline of system recommendations are discussed in Section VII of the report in Appendix C. Additional field studies and enhancement of the present interpretation algorithm are recommended to better resolve mat depths and determine the limits of accuracy of the interpreted ACM elevations under a variety of site conditions. The TDC resistivity data on which these conclusions and recommendations are based were obtained from primarily the Missouri Bend Revetment site. Additional survey tests were scheduled during 1995 to incorporate the final TDC system upgrades and implement the optimal survey procedures and configurations. However, this study was indefinitely postponed due to lack of funding.

5 Correlation of Electrical Methods

In geophysical investigations, it is desirable to use a suite of complimentary techniques to balance the limitations inherent to a particular technique and improve the accuracy of the final interpretation. The SP and TDC resistivity systems are complimentary techniques for conducting ACM investigations. SP profiles run along river range lines allow determination of the location and depth of the outer edge of the mat along with the location and depth of one or more additional points on the mat. TDC resistivity survey lines, performed parallel to the riverbank, permit calculation of ACM depth profiles with a lateral resolution of approximately 30 ft and depth resolution of ± 10 percent of the actual value. Good quality SP and TDC resistivity data for correlation of the two techniques were only acquired along the Missouri Bend Revetment between river ranges U-75 and U-125. This portion of the revetment encompasses, in upstream order, areas of older ACM under thin sediment cover, older mat buried under tens of feet of sediment, and newly placed ACM.

Within the area of investigation, older ACM originally placed in 1965 situated in water depths greater than 50 ft and covered by little to no sediment is located between river ranges U-75 and U-88. The characteristic signatures of the gradient SP profiles (Figure 10) and data collected with the underway TDC resistivity system (Figure 18) indicate the mat is present and readily detectable with either geophysical method. However, the amplitudes of the SP signals and resistivity values are less than those collected over newly placed ACM which may be attributed to the age and condition of the older ACM, greater water depths, or changes in the geochemical environment. Analysis of the SP data indicates the outer limits of the mat are easily detected and locations correlate well with the as-installed placement information. Interpreted depths of the toe of the ACM are, however, approximately 5 to 20 ft greater than the as-installed depths. Depth information provided by the inner SP source points correlates well with the as-installed ACM depth. Interpreted depths to the ACM as determined from the TDC data (Figure 19) are located along the river bottom surface and within ± 4 ft of the as-installed ACM depths.

Between river ranges U-88 and U-115, the ACM are buried by tens of feet of sediment. The measured SP values collected along range lines in this area maintain the characteristic gradient signatures but the amplitude of the signals are much less. The lower amplitudes may be due to a combination of the

thickness of sediment overlying the mat, the ACM located deeper below the water surface, variations in the geochemical environment, or indications of a disintegrated or damaged area of ACM. The interpreted locations and depths of the riverward edge of the ACM do not always agree to the as-installed ACM parameters. Two factors that may contribute to the differences in the resolved limits include the simple SP model is unable to accurately model ACM environments with thick sediment cover or the ACM has undergone disintegration and is not fully intact. However, another consideration is that the SP results are correct and the ACM has shifted since placement. Depth information computed from the inner SP source points remains consistent with the as-installed ACM depth measurements. The TDC resistivity data also indicates an anomalous area between river ranges U-90 and U-105 as described earlier in the report (see also Figures 18 and 19). The higher resistivity values measured with this technique indicate a significant deepening of the mat or possible deterioration of the emplaced ACM. ACM depth information calculated from each data set in this area found the maximum depth of the ACM along this survey line was 71 ft with an overlying sediment cover of approximately 45 ft. This depth and sediment thicknesss information correlates favorably with the as-installed placement depths. A stationary resistivity measurement performed along range U-112 yielded an interpreted depth to the ACM of 54.7 ft LWRP and overlain by over 40 ft of sediment. These results compare well with the as-installed ACM depths from 1965. Therefore, in areas of significant sediment cover over the existing ACM, the TDC resistivity system is able to provide better estimates of the depth to the emplaced ACM than the SP method.

Over the area of new mat, located upstream of range U-115, the results of SP investigations demonstrated that the riverward edges of the emplaced mat were easily located and mapped at depths which correspond to the as-installed depths measured immediately after placement. The SP surveys also provided 1 to 3 additional source points along the ACM with which depth information could be computed. The interpreted depths from the SP data are typically within two feet of the as-installed depths. Stationary and underway TDC resistivity measurements conducted over the same area also demonstrated good correlation between the interpreted and as-installed depths. Interpretation of the stationary sounding data collected in 30 ft of water along range U-128 indicated the depth to mat is 28.9 ft. Results computed over the new ACM from the underway TDC resistivity measurements when the electrode array is completely over the new mat (Figure 19) matches the as-installed depth information. Differences between the computed and as-installed depths between ranges U-115 and U-120 reflect the electrical effects of the electrode array being only partially over the new mat.

The combination of SP and TDC resistivity results provides useful and complimentary information regarding the location and depth of the in-service ACM. The SP method is more adept at delineating the outer or riverward edges of the mat as well as noting the presence of the ACM. The TDC resistivity system provides more accurate depth estimates than the SP method; especially in areas of significant burial. Further studies to include other geophysical data and drilling would be useful to verify results.

6 Electromagnetic Methods

Concepts of Electromagnetic Surveying

The SP method, discussed in Chapter 3, is a passive technique in that the survey method measures a field or effect that exists independently of the survey. The electromagnetic (EM) methods as well as the TDC method discussed in Chapter 4 are active techniques that use a source to produce the field or effect being measured. Further classification of the active techniques used for the ACM detection and mapping investigations are based on the physical way "depth sounding" is achieved. The TDC method achieves electrical resistivity versus depth information by increasing the electrode spacing and thereby changing the electrode geometry of the array. This procedure is called *geometric depth sounding*. In contrast, the two EM induction methods, frequency domain and time domain or transient, maintain a fixed geometry and achieve depth sounding by changing a source output parameter. This procedure is called *parametric depth sounding*. An advantage of the EM methods relative to the TDC method is that comparable depths of investigation can be achieved with much smaller surface arrays. The smaller array size also means a smaller subsurface zone of influence (or footprint) for the measurements which results in higher horizontal resolution.

Electromagnetic methods, both frequency domain and time domain methods, are attractive candidates for ACM detection and mapping because of their sensitivity to the conductive stainless steel reinforcing mesh of the ACM. The conductivity values of the reinforcing mesh are over 1,000 times more conductive than the Mississippi River water and sediments (Mozeley and Kooney 1991). The average measured conductivity of the river water and sediments is 45 and 28 mS/m (milliSiemens/meter), respectively. The EM induction methods can also be applied on the surface of the water (waterborne survey) or from the air (airborne survey). The possibility of an airborne survey method is extremely attractive from the standpoint of significantly increasing the areas covered per day and avoiding limitations due to river stage.

Frequency domain EM method

A frequency domain EM (FDEM) system developed by the Naval Research Laboratory (NRL) (Figure 20) was selected for ACM detection and mapping feasibility investigations. The system was originally developed for airborne

deployment as shown in Figure 21 to measure the bathymetry of shallow marine environments and map the water conductivity distribution in bays and estuaries. Within the towbody shown in Figure 20, the FDEM system consists of a transmitter and receiver coil situated a set distance apart. A schematic of the EM induction process is illustrated in Figure 22. The transmitter coil is energized with an alternating current to produce a time-varying magnetic field. The primary EM field from the transmitter induces currents in subsurface materials that oscillate at the same frequency as the primary field. Penetration into the subbottom of the primary field (related to depth of investigation) and distribution of the induced currents depends on the transmit frequency and conductivity structure of the subsurface material. The following guidelines are observed during surveying: (1) depth of investigation increases as transmit frequencies decrease and (2) depth of investigation increases as the electrical conductivity of the subsurface material decreases.

The induced currents in the subsurface produce secondary magnetic fields that are detected and measured by the receiver coil. The measured apparent conductivity is dependent upon the coil spacing, transmitter frequency, and the ratio between the primary and secondary magnetic fields. The secondary field is separated into a component in-phase with the primary field (also called the real component) and a quadrature component (also called the imaginary component) that is 90 deg out of phase with the primary field. The measured responses versus frequency form a parametric sounding data set that can be interpreted to provide electrical conductivity versus depth profiles. Further information concerning FDEM theory, survey methods, and data interpretation may be found in Butler (1986) and Nabighian (1987). An illustration of the FDEM towbody configured for waterborne survey deployment is shown in Figure 23. The survey platform is a non-conducting fiberglass pontoon boat.

Transient EM method

The transient or time domain EM (TDEM) system developed and field tested for the ACM detection and mapping investigations consists of a large transmitter loop and a small central receiver loop. The transmitter is energized with a current step that is held constant for a short period of time and then rapidly turned off. The rapid decay of the current in the transmitter loop induces eddy currents in subsurface materials below the transmitter. These induced currents, diffusing down and out away from the transmitter, produce secondary magnetic fields that are detected by the receiver coil. The measurements at the receiver coil are made during the off-time of the transmitter. A schematic of the concepts behind the TDEM method is illustrated in Figure 24.

The secondary magnetic field is measured at a number of discrete time intervals (typically 20 to 30) and the depth and conductivity of the material at the depth of the induced currents can be determined. After a sufficient time delay, the process is repeated with the transmitter loop energized with a current step of opposite polarity (Figure 24). The opposite polarity step is rapidly turned off and the decaying secondary field is then recorded. This constitutes one cycle in the testing procedure. The absolute values of the second response are measured and added to the first response. The resultant decay curve is the

average of the two responses. During a test, a specified number (e.g., 16, 32, or 64) of cycles are typically averaged to increase the signal to noise ratio of the recorded transient. The measured signal is converted to an apparent resistivity value and a plot of the apparent resistivity versus time is a depth sounding curve analogous to the apparent resistivity versus electrode spacing depth sounding for the electrical resistivity method (Figure 17). Analysis of the sounding curve provides the depth and apparent resistivity structure of the subsurface material. More information describing the TDEM method, survey methods, and data interpretation may be found in Butler and Fitterman (1986) and Nabighian (1987).

Feasibility Investigations and Numerical Modeling

FDEM and TDEM feasibility studies and forward modeling tests of the EM response to an ACM is a process by which conductivity values are calculated at the water surface for a variety of subsurface conditions and ACM geometries. Extensive numerical modeling studies were completed in August 1991 to test the effects of varying parameters of interest for the purpose of EM survey design and assistance in interpreting the conductivity data collected over ACM. Using numerical models representative of ACM installations near Baton Rouge, LA, the generated models demonstrate that the calculated apparent condictivity values are sensitive to the metal fabric of the ACM even when the mat is buried under sediment. The resultant information also indicated that the data can be interpreted to readily determine the presence or absence of and depth to the ACM. Inferences about the condition of the ACM may also be derived. The results of the forward modeling exercises are reported in Appendix E and summarized as follows.

Frequency domain EM method

Forward modeling is a technique for calculating the response of a geoelectrical model of the subsurface to an EM sounding technique. An extensive numerical forward modeling investigation was conducted for the FDEM technique using the parameters for the NRl EM system. Detailed results of this study are contained in Appendix E with only selected results discussed here. The numerical models are layered earth representations consisting of either: (1) water over sediment, (2) water over ACM over sediment, or (3) water over sediment over ACM over sediment. Model (1), also called the basic model, represents the normal background condition with no ACM present whereas model (3) represents ACM that has been buried by sediment. The layered geoelectrical model is shown in Figure 25.

To investigate the sensitivity of the numerical forward modeling methods to the electrical representation of the ACM, both thick and thin layer ACM models were considered with the overall conductance parameter (product of thickness and conductivity) set to a constant value. The conductivity values of the water and sediment layers are based on measured values of the river water and saturated clayey sediments. The thickness of the thin layer ACM model is

equivalent to the steel wire mesh of the ACM being flattened into a solid sheet. Model conductivity values are the same as typical values for steel (see Appendix E for a discussion of model parameters).

Two numerical EM forward modeling procedures were used for the feasibility investigations. The first is a one-dimensional (1-D) algorithm called BSAUT, developed by NRL, which simulates the response of a multi-layered model over a frequency range of 90 to 5,000 Hertz (Hz) using the dimensions and parameters of the EM system. The second procedure uses a three-dimensional (3-D) integral equation formulation of a model response to a 3-D body in multi-layered model. The 3-D program was checked against the 1-D predictions for the basic model in Figure 25 and gives virtually identical results. The 3-D model was then adopted to investigate lateral resolution capability for the FDEM system.

The total FDEM responses calculated using the BSAUT program for the thick and thin ACM models and for the basic model are shown in Figure 26. The water layer thickness (depth) is 15 m (49.2 ft) and it is assumed that the ACM has infinite length in each direction. Both the real (in-phase) and quadrature components of the responses are shown for each model. The responses are expressed in units of parts per million (ppm) and normalized to the primary field strength of the transmitter. The NRL FDEM system has an average noise level of 1.0 ppm. Referring to Figure 26, four key observations are noted from the modeling results:

a. Thick and thin layer ACM models give virtually identical responses.

b. The shapes of the basic model response curves are distinctly different from the ACM model response curves.

c. Responses for each model are large compared to the average system noise level.

d. The basic model responses are well separated from the ACM model responses over most of the frequency range.

The first observation indicates that the model parameters representing the ACM are unimportant as long as the conductivity value is large compared to the surrounding layers in the model and the conductance value is held constant at an appropriate value for steel. Observations 2, 3, and 4 each indicate that detection of the ACM with the NRL EM system are very good. Subtracting the basic model responses from the ACM model responses yields the anomalous ACM model responses shown in Figure 27. The illustration reemphasizes the large anomalous responses generated when ACM is present in the layered model.

The effect of variations in the water depth on signal level and curve shape for the basic model and anomalous ACM real responses are shown in Figures 28 and 29, respectively. Even for water depths of 30 m (100 ft), the real component of the ACM anomalous response (Figure 29) ranges from 500 to

1,000 ppm over the entire frequency range. Therefore, the ACM should be detectable to depths in excess of 30 m (100 ft).

Additional feasibility investigations with the 3-D forward modeling program address issues of ACM resolution such as: (1) detectability of small isolated ACM sections, (2) detectability of "holes" or missing sections in a large ACM field, and (3) accuracy in locating an edge of an ACM section. For case (1), a 6.0 m × 7.5 m (19.7 ft × 24.6 ft) ACM section is modeled at the water-sediment interface and buried by a 5 m (16.4 ft) thick layer of sediment. The water depth in each case is 15 m (49.2 ft) and the center of the transmitter/receiver couple is centered over the ACM section. The anomalous responses, both real and quadrature, are presented in Figure 30. The computed responses over the small ACM section are considerably reduced in magnitude compared to the results from the 1-D models (Figures 27 and 29). However, the responses generated by the small ACM section are still large compared to the average system noise level and, therefore, the small ACM section should be detectable for these conditions. Under real world conditions in which water depths, overlying sediment thicknesses, and water and sediment conductivity values vary, then the responses for a small ACM section buried at a depth of 5 m (16.4 ft) below the river bottom may be approaching the limit of what can be detected in practice.

Modeling exercises were also completed to investigate the ability of EM techniques to detect holes or missing sections of mat within a large ACM field. A numerical model was developed in which a 7.0 m × 6.0 m (23.0 ft × 19.7 ft) hole is considered in an ACM at a water depth of 15 m (49.2 ft). The anomalous real responses for a profile line along the X-direction are presented in Figure 31. The system frequency varies along the Y-axis to form the illustrated pseudo-section. The modeled hole is situated along the X-axis with the center positioned at X = 0 and the edges located at X = ±3.0 m (±10 ft). Referring to Figure 31, the boundary of the hole is approximately defined by the 25 ppm contour interval over most of the frequency range. An anomalous response of zero is found within the limits of the small hole. Therefore, in theory, holes as small as 6.0 m (19.7 ft) are easily detectable in water depths of 15 m (49.2 ft). The investigation of hole detectability as well as other numerical model investigations detailed in Appendix E lead to the conclusion that edges of ACM sections can be located with an accuracy of approximately ±1.0 m (3.3 ft) in water depths of 15 m (49.2 ft).

Theoretically, the EM response, R, from a transmitter/receiver couple coincident and positioned directly over an infinite extent, conductive, thin plate is proportional to the transmit frequency, f, divided by the square of the vertical distance, z^2, between the transmitter/receiver couple and target. The relationship between a waterborne FDEM survey response and airborne FDEM survey response over the same section of ACM is given by

$$\left(\frac{R_W}{\frac{f_W}{z_w^2}} \right) = \left(\frac{R_A}{\frac{f_A}{z_A^2}} \right)$$

where the subscript 'W' and 'A' indicate the parameters for the waterborne and airborne survey, respectively. Expressing the airborne EM response in terms of the waterborne EM response is determined through the relationship

$$R_A = R_W * \left(\frac{z_W^2}{f_W} \right) * \left(\frac{f_A}{z_A^2} \right)$$

Typically, the airborne EM response is less than the waterborne EM response because the distance between the ACM and transmitter/receiver couple is greater.

Transient EM method

Time domain or transient EM forward modeling was accomplished using the commercially available program TEMIX, developed by Interpex, Ltd., Golden, CO, and using the parameters of the transient system deployed for ACM applications. The program computes late stage apparent resistivity (Butler and Fitterman 1986) versus time for a specified layered model. Like the program BSAUT used for the frequency domain modeling, TEMIX is a 1-D model. The basic model and ACM model (thick layer) parameters used for the transient EM modeling are shown in Figure 25.

Apparent resistivity versus time response curves, also called sounding curves, for ACM situated at the water-sediment interface in water depths of 5 to 30 m (16.4 to 100 ft) are displayed in Figure 32. The curves are shown for times corresponding to the measurement range for the deployed transient system. The curves are clearly diagnostic of the depth to the ACM. Sounding curves using the basic model (no ACM) in the same water depth range are illustrated in Figure 33. Referring to Figures 32 and 33, it is easy to distinguish at any of the given water depths when ACM is present on the bottom surface.

A sounding curve for 40 ohm-m sediment, corresponding to a saturated sandy sediment, in a water depth of 5 m (16.4 ft) is also presented in Figure 33. While the basic model sounding curves for 5 ohm-m and 40 ohm-m sediment are easily distinguished, the sounding curves when ACM is present over 5 ohm-m sediment is indistinguishable from the sounding curve over 40 ohm-m sediment. Further TDEM modeling exercises determined that sounding curves for ACM buried under 5 m (16.4 ft) of sediment in water depths of 15 m (49.2 ft) are similar to sounding curves where ACM is situated at the water-sediment interface in 20 m (65.6 ft) of water. In each case, the ACM model proves to be an excellent transient EM target.

Field Testing

Field testing of the waterborne and airborne FDEM techniques and TDEM method were accomplished at the Arlington, Missouri Bend (Figure 5), Manchac (Figure 7), and Plaquemine Bend Revetments. Field studies during the development and testing stages of the EM techniques were designed to investigate the same site criteria as the waterborne SP and TDC techniques: recently placed ACM, ACM emplaced in varying depths of water, older ACM buried under varying thicknesses of sediment, multiple layers of ACM, and areas of possible ACM damage. In addition to ACM detection and mapping, the studies were also performed to provide ACM condition assessment information at each test site. Initial test studies of the waterborne FDEM technique were performed at Arlington and Manchac Revetments during December 1991. The initial studies were primarily designed to determine the conductivity profile of the water, sediments, and ACM and to analyze the characteristics of the sensors and data acquisition hardware. Field studies using the production waterborne FDEM system and prototype waterborne TDEM system were conducted during August and September 1993 along the Missouri Bend and Manchac Revetments. These tests were performed in the same areas as the SP and TDC resistivity studies in order to directly compare and evaluate all results for each method. Airborne FDEM exercises were conducted over the Missouri Bend, Manchac, and Plaquemine Bend Revetments during July 1994. It is noted that, other than the December 1991 feasibility study, EM field testing at the Arlington revetment was minimal due to the presence of numerous moored barges along the riverbank.

Waterborne FDEM method

The waterborne adaptation of the NRL airborne FDEM towbody is shown in Figures 23 and 34. The NRL EM system is the first of a new generation of digital, wideband EM systems that allow simultaneous generation of multiple frequencies. Typically, three to five frequencies are generated over the 50 to 5,000 Hz frequency range. In principal, however, any number of frequencies can be generated with this system.

The complete EM system consists of a kevlar towbody housing the transmitter/receiver couple, a tether containing the electronics cabling with which to tow the towbody, and the signal processing hardware. The towbody, shown in Figure 20, is 6.4 m (21 ft) in length and has a diameter of 0.56 m (1.8 ft). The towbody contains the transmitter coil, receiver coil, a bucking coil, and the electronics for the transmitter and receiver. The bucking coil (Figure 22) is used to effectively cancel the primary field from the transmitter at the location of the receiver coil. Appendix E contains a more detailed description of the NRL EM system and a discussion of its use for bathymetry mapping.

Because of the high cost of airborne surveying and the initially unknown detectability of ACM from the safe standoff height of the airborne towbody, WES and NRL considered it important to first verify the capability of the NRL

system from the river surface. To test the system on the river, a special non-conducting float was designed and constructed to hold the EM system towbody as shown in Figures 23 and 34. Waterborne deployment of the NRL system also allows for direct comparison with the survey times, logistical requirements, and results of the SP and TDC surveys. During waterborne deployment, the float supporting the AEM towbody is pulled behind a survey boat. A second boat, attached by a cable, trails the float and provides additional maneuvering capability and positioning control. Figure 35 presents the survey configuration during a waterborne FDEM test. Data measured at the receiver coil are transmitted via the tow cable to the signal processing hardware on the survey vessel. The processed data are recorded to magnetic tapes 30 times per second during a course of a survey line.

Production type surveys using the waterborne FDEM system with updated acquisition hardware were performed during late August and early September 1993 at the Missouri Bend and Manchac Revetments. Survey lines, referred to as P-lines, were performed parallel to the crest of the levee which are generally parallel to the riverbank. For example, the survey line P700 denotes a line 700 ft (approximately 213 m) riverward from the centerline of the levee crest. P-lines are perpendicular to the range lines (U-lines or D-lines) which define positions along a revetment (see Chapter 2). EM surveys were also performed along lines perpendicular to the riverbank. Positioning information was obtained using a Differential Global Positioning System (DGPS) with the GPS antenna located on the EM towbody float for more accurate data mapping.

Airborne FDEM method

Demonstrating the detectability of ACM by the waterborne FDEM surveys, an airborne field trial of the EM system was conducted over the Missouri Bend, Manchac Bend, and Plaquemine Bend Revetments in July 1994. The equipment for the airborne EM surveys are the same used for the waterborne surveys except the transmitter/receiver towbody is configured for airborne use (Figure 20). The airborne surveys were dispatched from the New Orleans Naval Air Station using a Sikorsky MH-53E helicopter staffed by personnel of the Naval Air Support Group, Panama City, Florida. Figure 21 shows the towbody in its airborne survey configuration suspended beneath the helicopter during liftoff. All airborne EM surveys were performed parallel to the riverbank. Positioning information is acquired using DGPS. During EM surveying, the helicopter flew at a nominal altitude of 60 m (196.8 ft), while the suspended towbody was maintained at an altitude range of 20 to 25 m (65.6 to 82.0 ft) above the river surface. Altitude was determined from the DGPS and a laser altimeter system. The EM surveys were conducted at helicopter airspeeds ranging from 130 to 150 km/hr (80 to 93 mi/hr).

Waterborne TDEM method

The concept of using the transient or time domain EM (TDEM) method for ACM detection and mapping was developed shortly after the initial waterborne FDEM tests in December 1991. The TDEM method has the advantages of

better determining the vertical resolution for layered geometries, multi-layered interpretation algorithms are readily available, has a smaller EM footprint, and has more rugged data acquisition components than the tested FDEM system. The TDEM system developed by NRL was tested at the Missouri Bend and Manchac Revetments during late August and early September 1993. Survey lines were conducted both parallel and perpendicular to the riverbank at each site.

The TDEM system was developed around the nonconductive pontoon float used for the waterborne FDEM system. The TDEM transmitter is a horizontal rectangular loop constructed of six turns of wire. The loop is constructed around the perimeter of the pontoon float at a height of 0.67 m (2.2 ft) above the water surface and has dimensions of 7.27 m × 2.48 m (23.8 ft × 8.1 ft). The effective area of the transmitter loop is approximately 18.0 m^2 (194.0 ft^2). The transmitter coil was energized with a current of 20 Amps which generates a dipole moment of 2,166 Amp-m^2. The TDEM receiver consists of three orthogonal multi-turn coils (designated Hx, Hy, and Hz) each having an effective area of 10,410 m^2. The receiver coils are positioned in the center of the transmitter loop and situated 0.1 m (0.3 ft) above the plane of the transmitter loop. After the current in the transmitter loop is shut off, the TDEM system samples the EM decay curve for 22 discrete time intervals over the time range of 6.28 to 212.8 microseconds for each transient signal. During TDEM surveying, the pontoon float is towed in the same manner as during waterborne FDEM survey operations (Figure 35).

Data Analysis and Results

Waterborne FDEM method

Initial waterborne FDEM tests evaluated the deployment and performance of the EM equipment and study the characteristics of the EM signatures over the in-service ACM. Figure 36 portrays results acquired over the Manchac Revetment along an 8,000 ft (2,438 m) segment of survey line P700. The illustrated segment begins near range U-70 (right side of figure) and proceeds upstream to range U-150. The real components of the EM signatures at frequencies of 150 and 390 Hz are displayed. Total acquisition time for these data was approximately 15 min and water depths along line P700 ranged from 35 to 40 ft (10.7 to 12.2 m). The results in Figure 36 are highlighted by the diagnostic nature of the EM response with regard to the ACM placement history. Various segments of the emplaced ACM were laid at four different times (1974, 1979, 1983, and 1988) along this reach of the Manchac Bend with some areas covered by two or three layers of ACM. The magnitude of the EM response not only detects the ACM but also appears to be diagnostic of the age and number of overlapping segments.

Several distinctive features of the EM response are indicated by letters A through F in Figure 36. These features are discussed below.

Areas A -- The three areas labeled A_1 ,A_2 , and A_3 have signal amplitudes in the range of 2,000 to 4,000 ppm. The signals also have a periodicity with wavelengths of approximately 125 to 150 ft (approximately 38 - 46 m) which correspond to the basic width of the individual ACM sections. This type of response is observed over extensive lengths of more recently placed ACM (post-1980) along both the Manchac and Arlington Revetments.

Area B -- An FDEM response minimum in the well-defined periodic pattern of the observed signal over a single layer of newer ACM. The signal minimum may be caused by missing portions of mat, deteriorated sections of ACM, or the EM system traversed off the outer edge of the mat for a short distance.

Area C -- The measured FDEM response has a very large amplitude ranging from 6,000 to 10,000 ppm and the signals are erratic. This observed data occurs over multiple layers of ACM yet some evidence of the 150 ft periodicity can be seen.

Area D -- Measured signals have large and erratic responses over a section of Manchac Revetment where only one layer of ACM is present. However, evidence along the riverbank suggests that this layer of ACM may be broken and jumbled (Figure 3) by the strong currents present during high river stages.

Area E -- An area having an intermediate type response over sections of older ACM (placed in 1974). The EM response magnitudes range from 1,000 to 2,000 ppm. The FDEM system easily indicates the presence of ACM and evidence of the 150 ft periodicity is also illustrated.

Area F -- The FDEM system measures an area having zero signal amplitude indicating no ACM is detected directly beneath the survey line. Within this area, the transmitter/receiver couple traversed across the outer edge of ACM and off the revetment as evidenced by examination of the survey track line positioning data. However, this is the typical EM response expected and observed when no ACM is present.

The portion of the 150 Hz EM response curve between the vertical dashed lines and labeled 'A' in Figure 36 is selected for further examination. A plan map of the ACM segments between river ranges U-83 and U-90 corresponding to this data set are presented in Figure 37. The track of survey line P700 is also shown. The river bottom bathymetry at the time of the survey as well as the track of each survey line performed in this section are presented in Figure 38. The real and imaginary components of the EM response for frequencies of 150, 390, and 4,110 Hz over the selected section are displayed in Figure 39. The periodic nature of the EM response is clearly evident for each frequency and it is interesting to note the subtle changes in the sinusoidal patterns. The vertical lines shown in each plot depict where the EM survey line crosses an ACM segment boundary or edge as shown in Figure 37. Note that

the EM amplitude response peaks near the center of each ACM segment and reaches a local minimum near the segment edges. The local minima are systematically displaced downstream from the as-laid positions of the segment edges suggesting that the river current pulls or flexes the physical segments in the downstream direction during placement operations.

A contour map of the real component of the 150 Hz EM response is shown in Figure 40. Areal delineation of the ACM segments is very good in the vicinity of the P700, P800A, P800B, and P800C survey lines. Further riverward of the P800-lines, the segments are not areally delineated due to the lack of sufficient EM response data in these areas. Also, the three lines perpendicular to shore do not systematically cross the ACM segment edges and, therefore, do not detect the response minima at the edges. The primary effect on the perpendicular profile lines is the response variation caused by the varying depths to the top of the ACM. FDEM response results using frequencies of 150, 390, and 4,110 Hz along survey line U-90A, performed perpendicular to the riverbank, are presented in Figure 41. The bottom plot displays the river bottom bathymetry beneath the survey line. The vertical line in each graph marks the riverward (left side of the figure) edge of the ACM segment. Referring to Figure 41, the EM amplitude response is clearly tracking the ACM as the water depths decrease. Based on this example, the ACM is detectable to depths of 100 ft (30 m) below the water surface. When signal levels of 200 to 1,000 ppm (depending on frequency) are taken into consideration following removal of any background response, the ACM should be detectable to even greater depths.

Additional waterborne FDEM surveys were performed along the Missouri Bend Revetment during late August - early September 1993. The survey tracklines of the EM system over a schematic of the in-service revetment are illustrated in Figure 42. The survey lines traverse the 1966 placed ACM (lower portion of the figure) before crossing over onto the newer ACM placed in 1992. The ACM segment boundaries are denoted by 'M' for the newer ACM (such as M1 and M10 shown) and 'm' for the older ACM (such as m1 and m10 shown). Segment boundary numbering increases away from the location where the older and newer ACM sections overlap near river range U-115. The tracklines are oriented approximately parallel to the riverbank and revetment. Unfortunately, none of the survey tracklines cross the junction between newer and older sections of the revetment. All the survey lines, with the exception of line P1100, traverse the newer ACM and closely parallel the older ACM between locations M1 and M10 (Figure 42). The magnitudes of the FDEM signal responses (real components only) for survey lines P700 and P1100 are presented in Figures 43 and 44, respectively. The EM responses were acquired using transmit frequencies of 90, 270, and 4,050 Hz. The river bottom bathymetry along both survey lines at the time of the survey are illustrated in the lowermost graph in each figure. The vertical lines in each graph of Figure 43 depict the ACM segment boundaries.

The results presented in Figure 43, acquired along survey line P700, provide the following observations of the EM response data over the newer ACM sections:

a. The EM response signals for each frequency exhibit large magnitude signal levels indicating the presence of the ACM. The EM signatures also demonstrate the sinusoidal periodicity associated with the detection of the individual ACM segments.

b. The local EM signal minima associated with the overlapping ACM segment boundaries are displaced downstream relative to the map locations as was also noted for the Manchac Revetment results.

c. The FDEM response magnitude drops rapidly and definitively as the survey line crosses from the new ACM to the older or no ACM areas at location M1. The survey results define the downstream edge of the 1992 revetment.

d. At the survey lines closest proximity to the 1966 placed (older) ACM, the EM response magnitude increases indicating the presence of the emplaced ACM. The outer edge of the older ACM in this vicinity is also buried by approximately 20 to 30 ft of sediment which may also effect the magnitude of the EM response.

The FDEM response magnitudes displayed in Figure 44 for data collected along survey line P1100 indicates a near-zero or less than zero value along the entire survey line. This is the expected result since the survey line does not traverse any ACM. Only near the termination point of the survey, which is close to the 1992 ACM, does the signal magnitude increase; thereby sensing the emplaced mat. In fact, line P1100 gets so close to the ACM that the signal magnitude recorded with the 4,050 Hz frequency begins to detect the individual ACM segments.

Attempts by NRL to determine depths to the in-service ACM at both Missouri Bend and Manchac Revetments were tried using a 3-D numerical model. The model, computer algorithm, and system parameters were so complex and involved that no reliable depth information could be achieved.

Airborne FDEM method

Airborne FDEM surveys were conducted over in-service ACM following demonstration of detectability and assessment of ACM using the waterborne FDEM deployment platform. Testing of the airborne FDEM system was conducted over the Missouri Bend, Manchac, and Plaquemine Bend Revetments to allow comparison with the waterborne FDEM survey results. It was shown during the forward modeling portion of the study that the measured EM response from the airborne surveys are consistent with those from the waterborne tests and differ only in response magnitude. Figure 45 contrasts the waterborne and airborne deployment modes for the FDEM system and illustrates typical results for comparable survey line lengths and ACM ages. The waterborne results, upper graph in Figure 45, were collected over ACM, placed in 1992, along Missouri Bend using a frequency of 270 Hz. The lower graph depicts results from an airborne survey over ACM, placed in 1993, at Plaquemine Bend using a frequency of 870 Hz. Both waterborne and airborne

results clearly detect the emplaced ACM. The acquired data are interpreted to delineate the edges of the revetment and detect the individual ACM segments. The responses drop to near-zero magnitude when the FDEM systems are no longer over ACM. The key differences in the airborne response compared to the waterborne results is the smaller overall magnitude of the signal and smaller amplitude of the periodic response of the ACM segments. The smaller overall magnitude of the airborne response relative to the waterborne responses can be attributed to the greater vertical distance between the ACM and the airborne transmitter/receiver couple. As a test to compare the magnitude of the airborne and waterborne EM responses, the value of the waterborne EM response (R_A=5,500 ppm) and system operating parameters for each method (f_A=870 Hz, z_A=20 m, f_W=270 Hz, z_W=5 m) are used as input to Equation 2. The calculated EM response expected for the airborne survey, R_A, is 1107 ppm which is almost exactly the EM response measured at Plaquemine Bend as indicated in Figure 45.

The airborne EM response data shown in the lower graph of Figure 45 is for survey line P16 over the Plaquemine Bend Revetment. The survey track line for P16, the only survey line which crosses the ACM, as well as the other survey lines at this site are illustrated in Figure 46. The EM response graphs, using a frequency of 870 Hz, for the five track lines are displayed in Figure 47. The results from survey line P16 clearly indicate the edge of the ACM at position M16 by the sharp increase in response magnitude from near-zero to approximately 1,000 ppm. Likewise, when the trackline crosses off the 1993-placed section of ACM at position M1, the response magnitude drops to approximately 200 ppm. The close proximity to the 1989-placed revetment is apparently responsible for the response not dropping to near-zero. The remaining four tracklines are all riverward of the Plaquemine Bend Revetment and illustrate EM response magnitudes less than 40 ppm. In fact, the response is so small that the basic system noise at the 1 to 2 ppm level is apparent. Other than the system noise, the only other characteristics in the responses of lines P18 through P21 reflect the affects of varying river bottom depths and broad, low-magnitude peaks at points of closest approach to the revetment.

Waterborne TDEM method

Waterborne TDEM surveys were conducted over the Missouri Bend and Manchac Revetments with profile lines performed parallel to the riverbank and lines looping perpendicular to and away from the shore. TDEM soundings were conducted at fixed time intervals approximately three seconds apart which result in distances between soundings dependent on survey vessel speed. The position of ten of 36 TDEM soundings acquired along range line U-128 of the Missouri Bend Revetment are shown in Figure 48. From sounding locations 384 to 395 where the boat maintains a constant speed, the distances between each sounding averages 25 to 30 ft.

The measured vertical component Hz of the TDEM data for five of the sounding locations (locations 384, 391, 392, 405, and 415), presented as signal decay curves, are presented in Figure 49. For sounding location 384, located well off the emplaced ACM, the signal decreases very rapidly to zero

magnitude by 0.5 millisecond (msec). In contrast, the decay curves for soundings 405 and 415, located directly over the ACM, have nearly identical responses and the signals decay more slowly. In fact, each sounding still has measurable response magnitudes at 3.0 msec after transmitter shut-off. The Hz signal responses for soundings 391, located just off the ACM (Figure 48), and 392, located over the edge of the ACM, exhibit predictable transitional behavior between the two extremes described above. Therefore, the vertical component of the transient EM signal is shown to be a sensitive indicator of the presence of ACM and a detector of ACM edges. Overall, the transmitted transient signal induces large currents in the highly conductive ACM which decay slowly and give rise to the slow decay curve detected by the receiver loops. In contrast, in areas where no ACM are present, the induced currents are much smaller in the less conductive water and sediment and, therefore, decay rapidly. The perceptibly small but diagnostic differences in the decay curves over ACM, such as illustrated by soundings 405 and 415 in Figure 49, can be analyzed using 1-D computer algorithms to determine ACM depth.

A TDEM profile line, labelled 'mb1,' was performed parallel to the riverbank between range lines U-75 and U-150 along the Missouri Bend Revetment. A schematic of the survey trackline is illustrated in Figure 50. This profile line traverses upstream along the center of the revetment. The survey line begins at location 'm28' (river range U-75), crosses onto the new mat at location 'm1/M1' (range U-115), and crosses the junction between new ACM and no ACM at location 'M21' (range U-145). The vertical component of the TDEM signal response recorded from the tenth sampling interval for all soundings along the profile are plotted to produce the profile in the upper graph of Figure 51. This sampling window, labeled W10 along the X-axis in Figure 49, was selected because it is well away from the large magnitude and saturated responses at early times while still giving good separation between off-ACM response (near-zero magnitude), transitional signal response, and on-ACM response. The TDEM response magnitudes for tenth sampling window are plotted every 20 to 30 ft along the profile line. The lower graph in Figure 51 illustrates the measured river bottom bathymetry during the TDEM survey.

The TDEM profile 'mb1' resembles the FDEM profiles presented earlier along the Missouri Bend Revetment. Like the FDEM profiles, the TDEM response curve exhibits the periodic magnitude variation characteristic of the individual ACM segments. Proceeding southward along the profile line (right to left on the graph), the response magnitude exhibits a prominent increase from near-zero to greater than 0.005 V/A (use the location 'W10' in Figure 49 as a comparison) as the northernmost edge of the new ACM is crossed. Over the new mat between locations M1 and M21, the response is consistently high and periodic which is indicative of the revetment being present, buried by little to no sediment, and in good condition. The somewhat decreased response magnitudes near locations M17 and M18 may indicate the system is near the riverward edge of the revetment. As the TDEM unit crosses the boundary from the 1992 to 1965 ACM, the response magnitude drops considerably to an average value of 0.001 V/A. Over the older mat between locations m1 and m28, the signal response magnitude becomes more erratic as the water depths and sediment thicknesses fluctuate. The erratic responses may also indicate areas of deteriorated ACM along the profile line.

While 3-D inversions of the TDEM data are desirable for ACM depth determinations, simplified 1-D inversions are sufficient and expected to be much better than for the case of FDEM data because of the smaller TDEM footprint. Figures 52 and 53 illustrate comparisons between measured water depths and calculated depths to ACM from the TDEM response data. The results presented in Figure 52 are for soundings 395 through 415 positioned as shown in Figure 48 along range line U-128 of the Missouri Bend Revetment. Calculated depths to the ACM correlate well with the measured river bottom depths. It is noted that this section of revetment was placed in 1992 and little to no sediment has been deposited over the mat. Therefore, the depth information for river bottom is also the depth to the ACM. The average percent difference between the measured water depths and computed depths to ACM is 6.7 percent. The results presented in Figure 53 are for soundings conducted along range U-96 over the section of ACM placed in 1966. In contrast to the first example, the ACM along this range line are, according to data from a 1992 hydrographic survey, buried under approximately 25 ft of sediment at the outer edge and by little to no sediment closer to shore. The measured water depths in Figure 53, collected during the TDEM survey, are probably to the top of the ACM near shore but to the top of the river bottom sediments further offshore. The computed depths to the ACM (Figure 53) illustrate that the ACM is placed at deeper depths at greater distances from the riverbank and the outer portion of the ACM is likely buried under at least 15 ft of sediment (dependent on the exact location of the soundings). The 1-D TDEM interpretation algorithm used to compute the ACM depths did not include a provision for a sediment layer and, therefore, the ACM depth values may contain some errors. These two examples illustrate the effective use of simple 1-D computer algorithms to analyze TDEM response data and compute depths to emplaced ACM.

The TDEM response data and depth calculations discussed in this section are the only data reported to date. The remainder of the TDEM data from both the Missouri Bend and Manchac Revetments have not been fully analyzed or formally reported. The TDEM technique was shown to be an excellent method for detecting ACM, delineating the edges of mat sections, and providing some condition assessment information of a revetment. However, because of the limited amount of data that was analyzed to provide depths to ACM, it is difficult to compare this technique with that of the SP and TDC resistivity methods. Overall, the TDEM technique should be an excellent technique for mapping and assessing emplaced ACM.

Summary and Recommendations

Three field studies were conducted at the Missouri Bend, Manchac, and Plaquemine Bend Revetment sites along the Mississippi River during the periods December 1991, August/September 1993, and July 1994. The first two studies were used to develop, test, and make modifications to waterborne FDEM technique at differing in-service ACM site conditions. The second investigation was also used for the development and testing of the waterborne TDEM equipment. The third study in July 1994 was used solely to evaluate

the airborne FDEM technique and its application to ACM detection and mapping. The data collected with each technique indicate that the metal reinforcing fabric of the ACM is an excellent electrical target and the measured EM response signals are consistent with expected electrical signatures.

Testing of the waterborne and airborne FDEM techniques indicate that the most useful, best quality FDEM data is typically collected when the survey track lines are parallel to the riverbank and, for waterborne deployment, the river flow velocities are at a minimum. Test results demonstrate that the FDEM systems easily detect the presence or absence of ACM and provide information assessing the probable physical condition. The magnitude of the EM response signatures acquired from the airborne deployment are less than those collected from the waterborne platform because of the greater vertical distance between the transmitter/receiver couple and electrical target. The advantage of airborne deployment is the considerable increase in data acquisition and a lack of impact of river state, barge and ship traffic, and general logistical problems which arise when towing equipment in strong river currents. The advantages of airborne surveys must be balanced against the disadvantages of high mobilization costs, logistical complexity of arranging surveys, and lack of access to some sites due to powerline crossings, moored barges, and bridges.

For both the waterborne and airborne FDEM deployments, each 150 ft wide segment of newer ACM is clearly detected and superimposed on a large background EM signal. For older or buried ACM, the individual segments are still evident, but the amplitude and definition of the periodic component of the signal is much less than for newer ACM. Multiple layers of ACM are indicated by large amplitude but erratic EM responses. The absense of ACM, such as indicated by profiling across the end or edge of an ACM field or segment or across a missing segment, is indicated by a transition to a constant, near-zero amplitude. Depth determinations for the ACM from both the waterborne and airborne FDEM methods were performed using both 1-D and 3-D interpretation algorithms. The 1-D routine to determine the depth to the ACM, however, did not provide the resolution or accuracy that could be attained with either the SP, TDC resistivity, or waterborne TDEM methods. The 3-D inversion program to generate a contour map of the ACM depths was never completed because of the complexity of the problem.

The FDEM system developed under this research program is most suitable for reconnaissance mapping of ACM. The technique can easily detect the presence of ACM and delimit individual mat sections and edges. The FDEM data also provides the most information about the physical condition of the mat. However, ACM depth information can be better obtained using the SP or TDC resistivity techniques discussed in this report. The present FDEM system hardware and software could be used for production operations if modifications are made to help simplify field operations, prolong the operating life of the system and signal processing components, and streamline the data interpretation process.

The TDEM system, like the TDC resistivity method, may be used either as a reconnaissance or high resolution investigation tool. In the reconnaissance

mode, this system readily detects the presence of ACM, locations of the mat limits and transition areas, and relative ACM depth information. The presence of ACM and location of the riverward mat edge are easily determined from the TDEM data as evidenced by the increase the decay times of the EM field. As a high resolution tool, the TDC system provides depth profiles of the emplaced ACM parallel and perpendicular to the riverbank and condition assessment information. The smaller footprint of the TDEM system has the capability of producing more detailed results than can be obtained with the waterborne FDEM or TDC systems. The TDEM system is also more rugged than the FDEM system and, therefore, not as susceptable to electronic equipment downtime.

Interpretation of each TDEM sounding can be performed using simple 1-D models of the water/sediment/ACM system to produce values of the ACM depth. This procedure is similar to analyzing the TDC resistivity data. Depth calculations to emplaced ACM along the Missouri Bend Revetment were within 10 percent of the depth values determined from a 1992 hydrographic survey. Monitoring individual time windows along survey lines performed parallel to the riverbank allow the waterborne TDEM method to provide information relating to the relative condition of the in-service ACM. The TDEM response curves, just like the FDEM method, illustrate the signatures of individual mat segments, edges of mat, and anomalous areas along the revetment.

The TDEM system developed under this research program is suitable for production surveying to investigate in-service ACM. However, some minor modifications to help simplify field operations and streamline the data acquisition and interpretation process are required. Additional modeling studies are recommended to better resolve mat depths and determine the limits of accuracy of the interpreted ACM elevations under a variety of site conditions. The TDEM response data on which these conclusions and recommendations are based were obtained from primarily the Missouri Bend Revetment site. Although a wide variety of mat conditions exist at this site, additional testing at other revetments will provide further information regarding the determination, accuracy, and resolution of mat depths over differing ages and conditions of ACM and in-depth condition assessment of ACM.

7 Conclusions

A suite of geophysical techniques to rapidly detect, map, and determine the condition of in-service ACM along the Mississippi River have been developed through a multi-phase research program. Three of the most promising techniques are the self-potential method, towed DC electrical resistivity, and electromagnetic methods. Geophysical field investigations to develop, test, and refine each technique were conducted primarily at the Missouri Bend and Manchac Revetment sites along the Mississippi River, located downstream of Baton Rouge, LA, during the period December 1991 through September 1994.

The SP system developed under this research program is suitable for production use for investigation of in-service ACM. The SP data collected during all tests indicate that the metal reinforcing fabric of the ACM does generate a large, readily detectable SP signal which is consistent with the expected electrical signatures. The most useful, best quality data is collected when the survey track line and electrode dipole are perpendicular to the riverbank and the river flow velocities are at a minimum.

Analysis of SP data provides locations to the outer edge of the mat, estimated depths to the outer edge, and inner source points where changes in the physical or geochemical condition occurs. Depths to source points along a river range also provide an approximate depth profile of the in-service ACM. For good-quality SP data sets, the computed mattress location and depths correlate well with the as-installed ACM depths; even when ACM's are located in water depths up to 100 ft. The SP method, however, is unable to resolve individual mat layers in areas of multi-layered ACM. For ACM buried under significant amounts of sediment or disintegrated and corroded ACM, lower amplitude SP signals are measured and result in discrepancies between the computed and as-installed ACM parameters. This technique is most useful as a reconnaissance tool because of the ease in which the presence of ACM is detected and the mat limits determined.

The designed TDC resistivity system is also suitable for production surveying to investigate in-service ACM. Resistivity data collected during all tests indicated that the metal reinforcing fabric of the ACM is a readily detectable electrical target and the computer controlled current switching and data acquisition system operated reliably under actual field conditions. The best quality data is collected when the survey track line and electrode array are aligned parallel to the riverbank.

The TDC system may be used either as a reconnaissance or high resolution investigation tool. During data acquisition, the TDC system displays the measured apparent resistivity values for each electrode separation in real-time to provide quality control and preliminary information regarding the presence and relative elevation of the emplaced ACM. Variations of the resistivity signatures can be associated with the differing ages and conditions of emplaced ACM and areas of transition between these ACM. Analysis of the TDC resistivity data provides estimated depths to the emplaced ACM, locations of mat boundaries, resistivity and thickness values of any overlying sediment cover, and possible delineation of anomalous areas. Interpreted depths along a survey line provide an approximate depth profile of the in-service ACM. Multiple passes, offset by a small distance, over an area of interest enables the possibility of producing a three-dimensional surface map of the ACM. For good-quality data sets, the ACM is detected and resolved to depths of 100 ft with the interpreted mattress depths typically within ± 10 percent of the actual depth value. Test results at Missouri Bend correlate well with the as-installed ACM depths; even when ACM's are buried by tens of feet of sediment.

Electromagnetic methods developed for ACM detection and mapping include waterborne frequency domain EM (FDEM), airborne FDEM, and waterborne time domain EM (TDEM). The results obtained from numerical modeling procedures and field measurements demonstrate that the waterborne FDEM system not only detects the presence of emplaced ACM, but also provides condition assessment information. For newer ACM and ACM in good condition, each 150 ft wide segment is detected and the characteristic signature of each segment is superimposed on the large EM signal for the entire revetment. The EM response over individual segments of older ACM or more deteriorated ACM have smaller amplitudes and the definition of the periodic component of the signal is less. Multiple layers of ACM are indicated by a large amplitude EM responses that have an erratic nature; thereby, masking the definition of the individual ACM segments.

Airborne FDEM surveys demonstrate similar capabilities for detection and mapping of emplaced ACM as the waterborne deployment mode. The decreased signal response from the ACM observed in the airborne results is entirely due to the increased distance between the EM towbody and ACM.

The waterborne TDEM method is also quite versatile for ACM detection, mapping, and depth calculations. The presence of ACM and location of the riverward edge of an ACM segment is easily determined as evidenced by the increase the decay times of the EM field. Interpretation of each TDEM sounding is performed using simple 1-D models of the water/sediment/ACM system; similar to the process of analyzing TDC resistivity data. Depth calculations to emplaced ACM along the Missouri Bend revetment were within 10 percent of the depth values determined from a 1992 hydrographic survey.

All of the EM methods and deployment modes exhibit the capability of detecting ACM segment edges and/or missing ACM segments. The detection depth capability for the EM methods is demonstrated to be at least 100 ft. Both the FDEM techniques and waterborne TDEM method can be used in both the reconnaissance mode or high-resolution mode for mapping in-service ACM.

The smaller footprint of the TDEM system has the capability of producing more detailed results than can be obtained with the waterborne FDEM or TDC systems. The waterborne and airborne FDEM methods have a better capability of assessing the condition of an ACM with respect to age and/or physical integrity.

For each of the geophysical techniques developed and tested, the ACM is an excellent electrical target to detect and map. For rapid reconnaissance surveying to map the extent of a revetment field, the SP method proved to be simplest and most cost-effective means developed. For condition assessment surveys of the current condition of an ACM, the FDEM was demonstrated most effective in its ability to identify each 150 ft segment of a revetment and identify areas of no mat or multiple mat layers. The TDC resistivity and TDEM systems proved equally capable of accurately determining the depth to the ACM even if the mattress is buried under tens of feet of sediment. However, for any ACM mapping investigation, it is best to use at least two of the techniques developed in order to obtain the most useful results.

References

Butler, D. K. (1986). "Military hydrology, Report 10: Asessment and field examples of continuous wave electromagnetic surveying for ground water," Miscellaneous Paper EL-79-6, U.S. Army Engineer Waterways Experiment Station, Vicksburg, MS.

Butler, D. K., and Fitterman, D. V. (1986). "Transient electromagnetic methods for groundwater exploration," Miscellaneous Paper GL-86-27, U.S. Army Engineer Waterways Experiment Station, Vicksburg, MS.

Corwin, R. F., Jr. (1983). "Marine permafrost detection using galvanic electrical resistivity methods," Proceedings of the 5th Annual Offshore Technology Conference, Houston, TX. 2-5 May 1983.

Corwin, R. F., Jr. and Butler, D. K. (1989). "Development of self-potential interpretation techniques for seepage detection," Technical Report REMR-GT-6, U.S. Army Corps of Engineers Waterways Experiment Station, Vicksburg, MS.

Department of the Army. (1979). "Geophysical exploration," Engineer Manual 1110-1-1802, Office of the Chief of Engineers, Washington, DC.

Lavoie, D., Mozley, E., Corwin, R., Lambert, D., and Valent, P. (1988). "The use of a towed, direct current, electrical resistivity array for classification of marine sediments," Proceedings of the Oceans 1988 Conference, Baltimore, MD. pp. 397-404.

Mozley, E. C., and Kooney, T. (1991). "Airborne electromagnetic techniques to delineate reinforced concrete slabs buried within river bed sediments." Phase I Report to USAE Waterways Experiment Station. Naval Oceanographic and Atmospheric Research Laboratory, Stennis Space Center, MS.

Nabighian, M. N. (1987). *Electromagnetic methods in applied geophysics*. Vol. 1, Society of Exploration Geophysicists, Tulsa, OK.

Petersen, M. S. (1986). *River engineering*. Prentice-Hall, New Jersey.

Sato, M., and Mooney, H. M. (1960). "The electrochemical mechanism of sulfide self-potentials," Geophysics, Vol. 25, no. 1, pp. 226-249.

Sjostrom, K. J., and Corwin, R. F., Jr. (1993). "Assessment of Mississippi River revetments using the self-potential method," Proceedings of the Symposium on the Application of Geophysics to Engineering and Environmental Problems, San Diego, CA. pp. 435-448.

Skianis, G. AI., and Papadopoulos, T. D. (1993). "A contribution to the study of the production mechanism of sulphide mineralization self-potential," First Break, Vol. 11, No. 4, pp. 119-125.

Telford, W. M., Geldart, L. P., Sheriff, R. E., and Keys, D. A. (1976). *Applied geophysics*. Cambridge University Press, New York, NY.

U.S. Army Corps of Engineers. (1984). Flood Control and Navigation Maps of the Mississippi River. 52nd Edition. Mississippi River Commission, Vicksburg, MS.

U.S. Army Corps of Engineers. (1986). "Master specifications for revetments." U.S. Army Engineer Division, Lower Mississippi Valley, Vicksburg, MS.

Figure 1. Articulated concrete mattress protecting a bank of the Lower Mississippi River

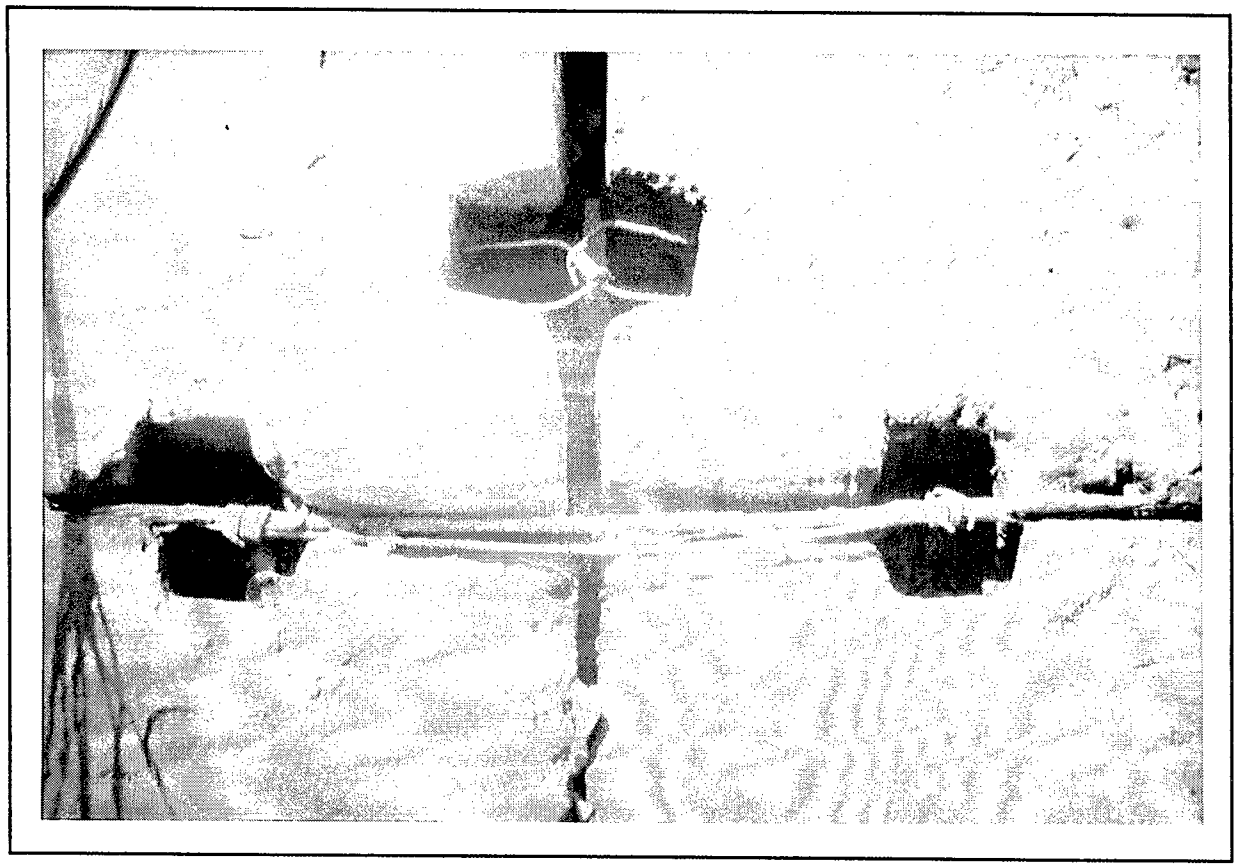

Figure 2. Stainless steel metal fabric of each concrete block attached to the ACM launching cable

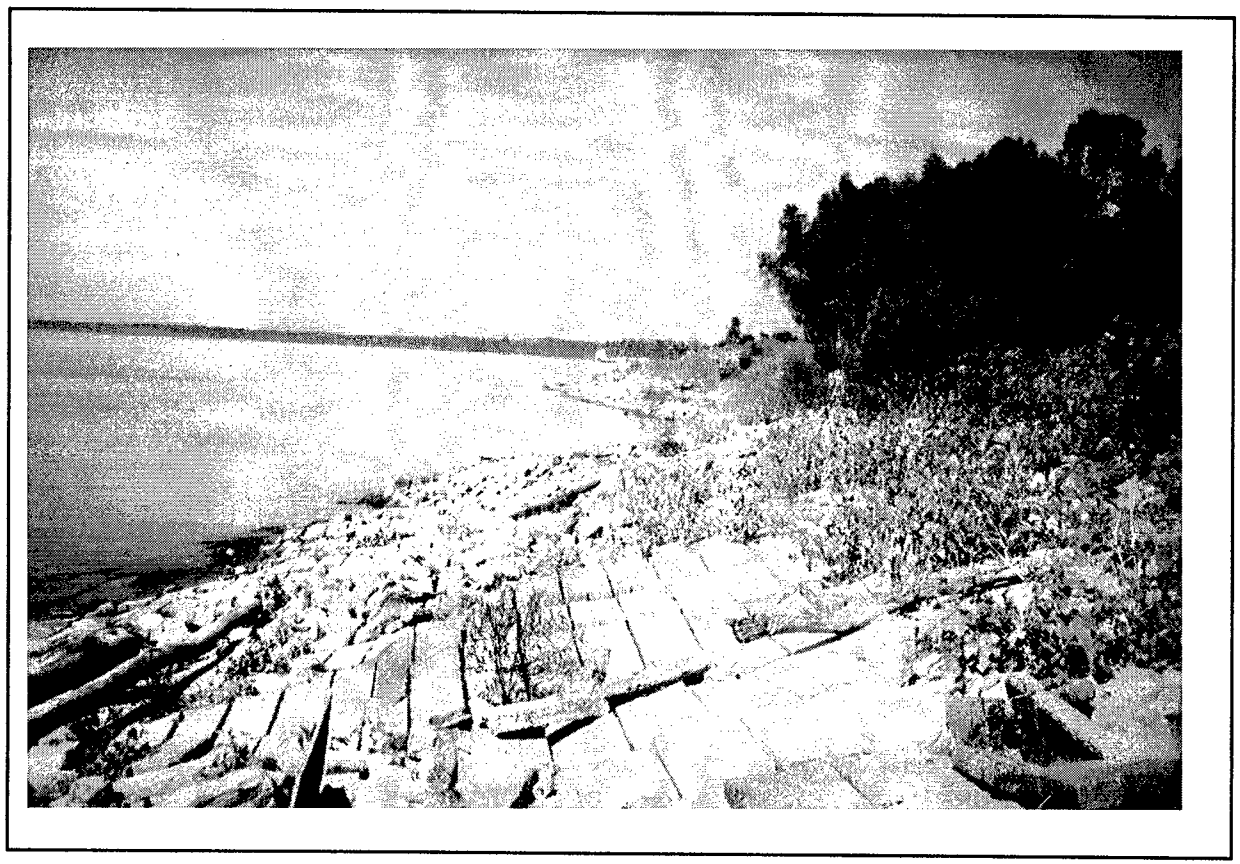

Figure 3. Damaged ACM along bankline of Mississippi River

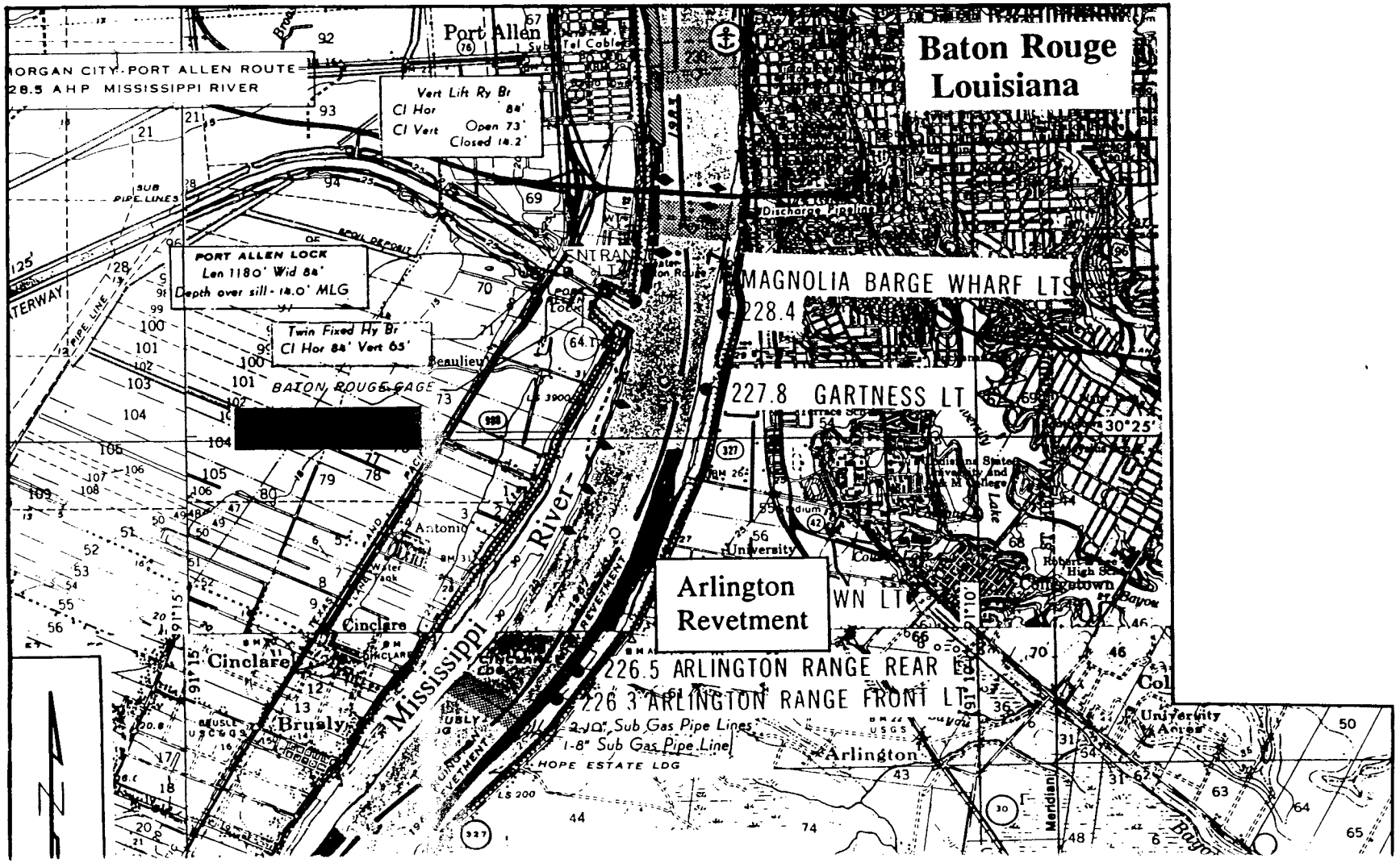

Baton Rouge
Louisiana
MORGAN CITY-PORT ALLEN ROUTE
28.5 AHP MISSISSIPPI RIVER
Vert Lift Ry Br
Cl Hor 84'
Cl Vert Open 73'
Closed 14.2'
PORT ALLEN LOCK
Len 1180' Wid 84'
Depth over sill - 14.0' MLG
Twin Fixed Hy Br
Cl Hor 84' Vert 65'
BATON ROUGE GAGE
MAGNOLIA BARGE WHARF LTS
228.4
227.8 GARTNESS LT
Arlington
Revetment
226.5 ARLINGTON RANGE REAR LT
226.3 ARLINGTON RANGE FRONT LT
2-10" Sub Gas Pipe Lines
1-8" Sub Gas Pipe Line
HOPE ESTATE LDG
Port Allen
Mississippi River
Cinclare
Brusly
Antonio
Arlington
University
Beaulieu
Discharge Pipeline

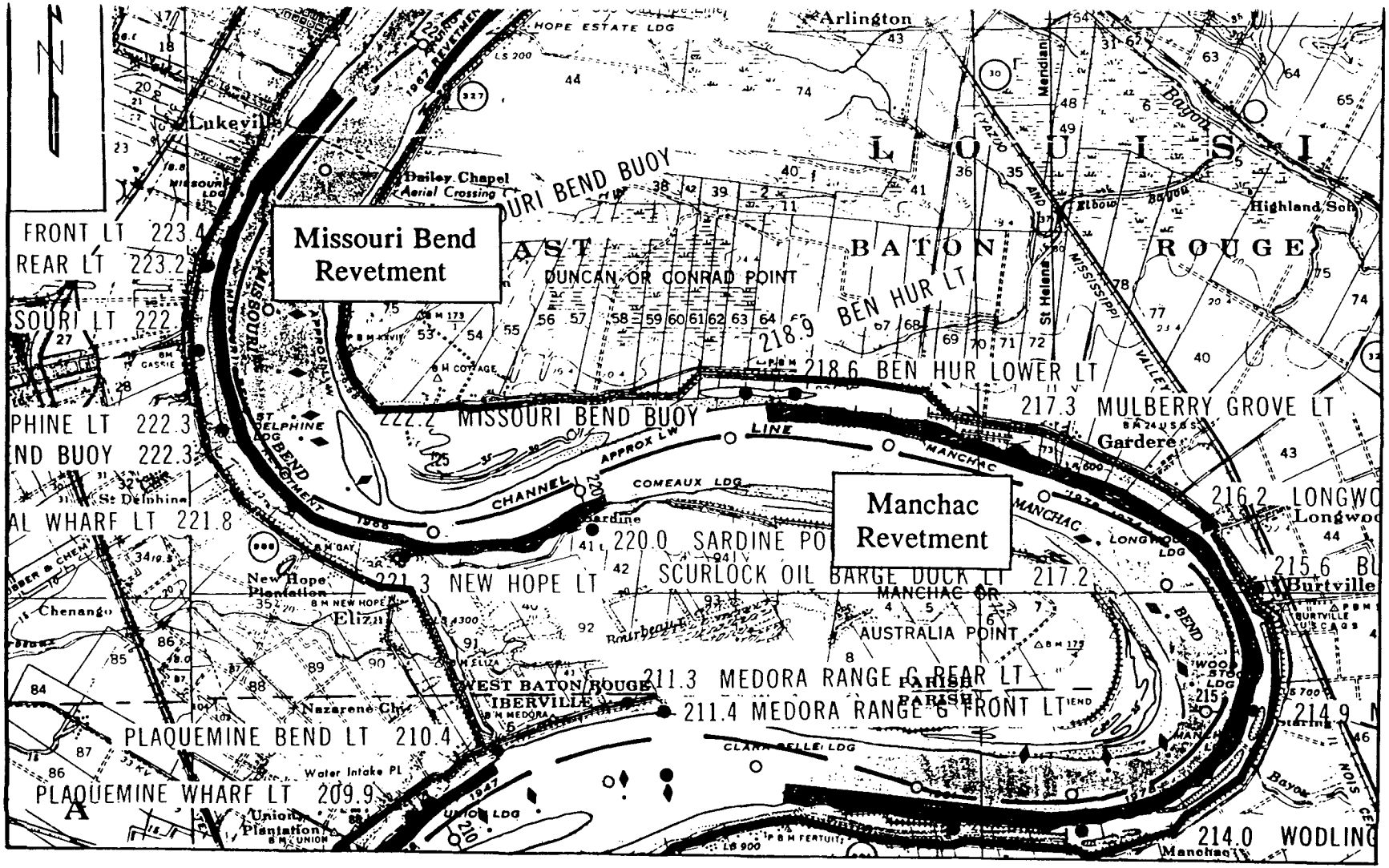

Figure 4. Site map showing the location of the Missouri Bend and Manchac Revetments along the Lower Mississippi River (U.S. Army Corps of Engineers 1984)

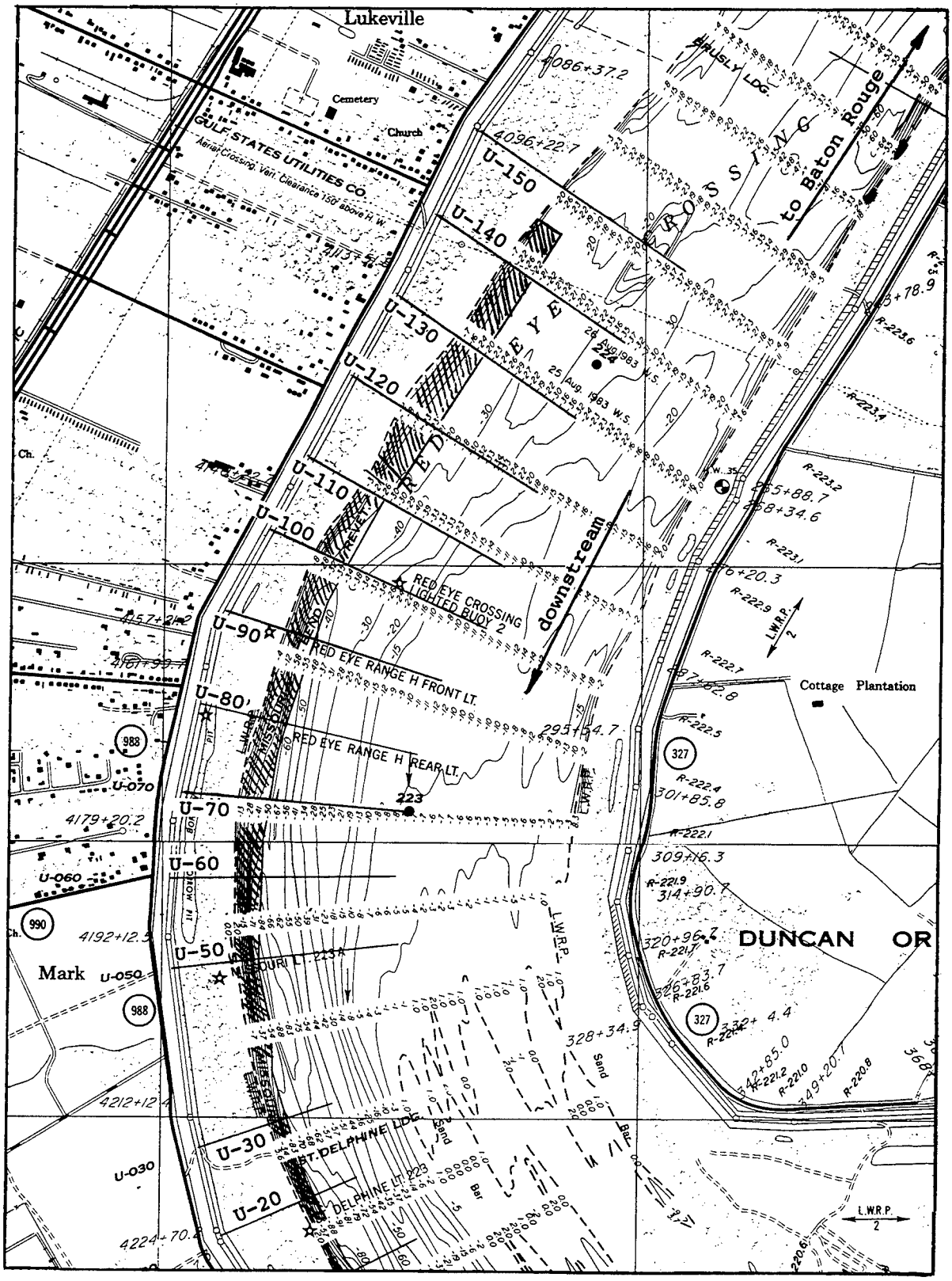

Figure 5. Site map of the Missouri Bend Revetment between ranges U-20 and U-150

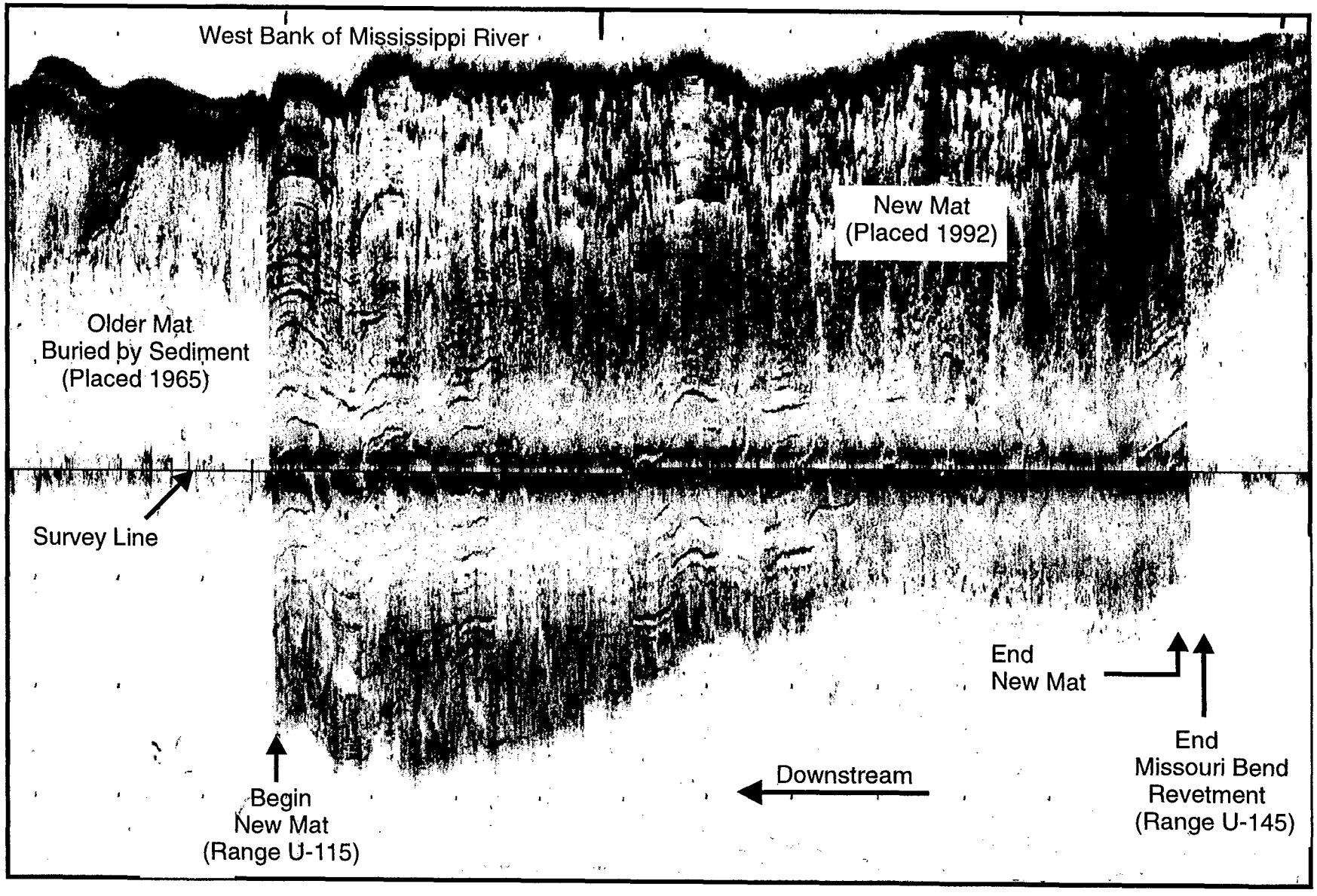

Figure 6. Side scan sonar image of new ACM, placed in 1992, between ranges U-115 and U-145, Missouri Bend Revetment

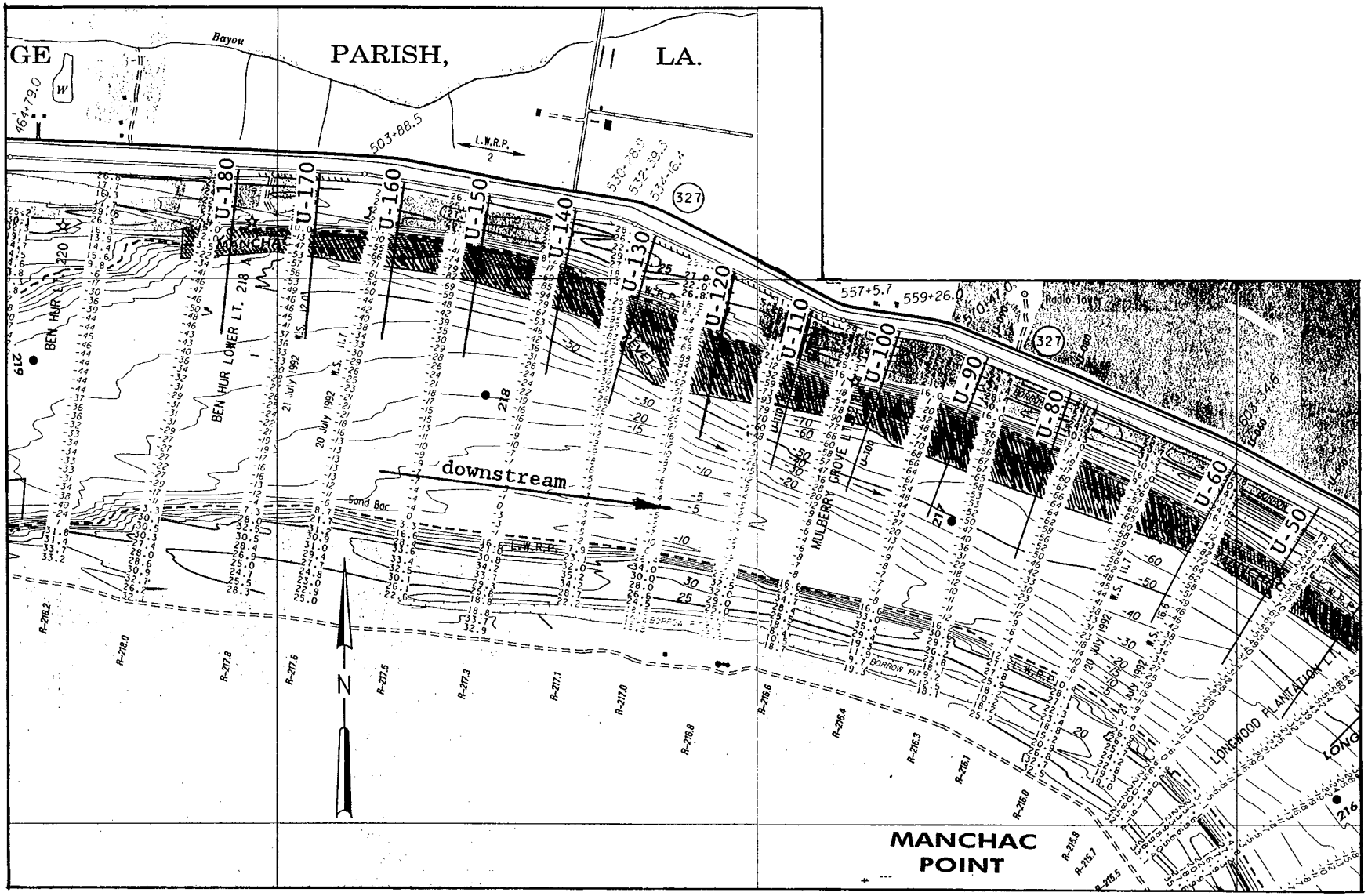

Figure 7. Site map of the Manchac Revetment between ranges U-50 and U-180

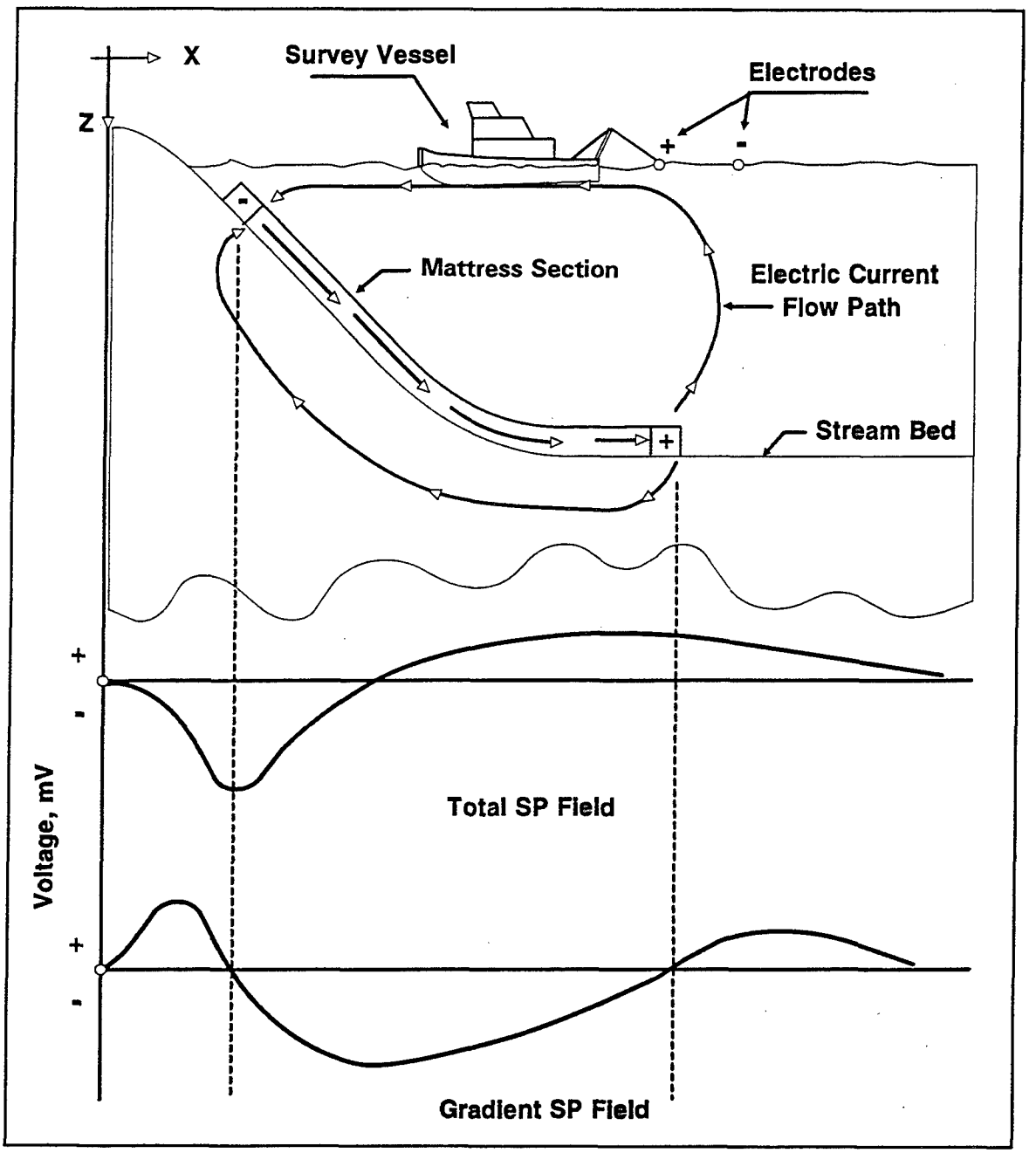

Figure 8. Schematic of the self-potential method

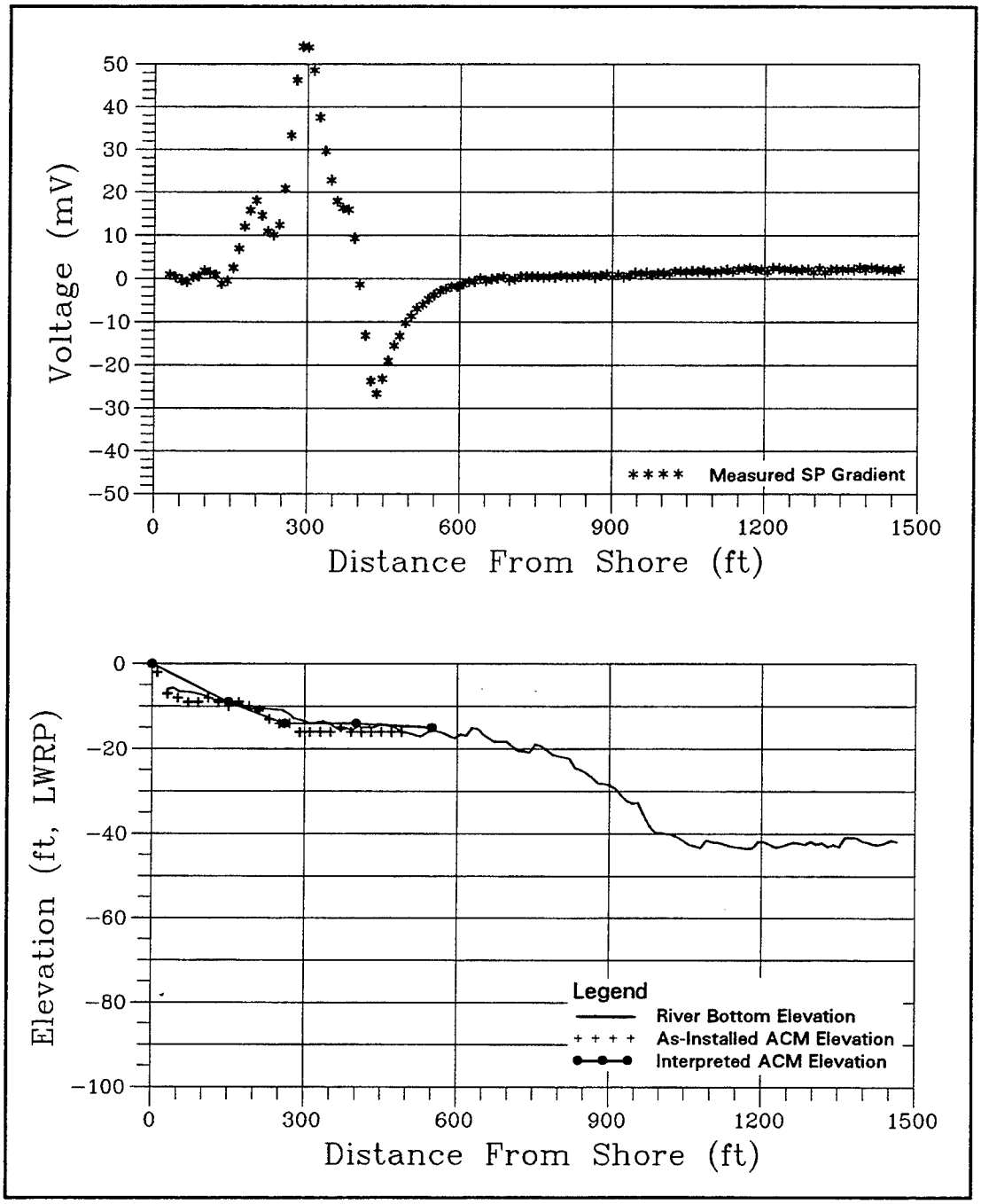

Figure 9. The measured SP gradient and bathymetry along range U-122, Missouri Bend Revetment. Interpreted depths to ACM are presented in the lower plot.

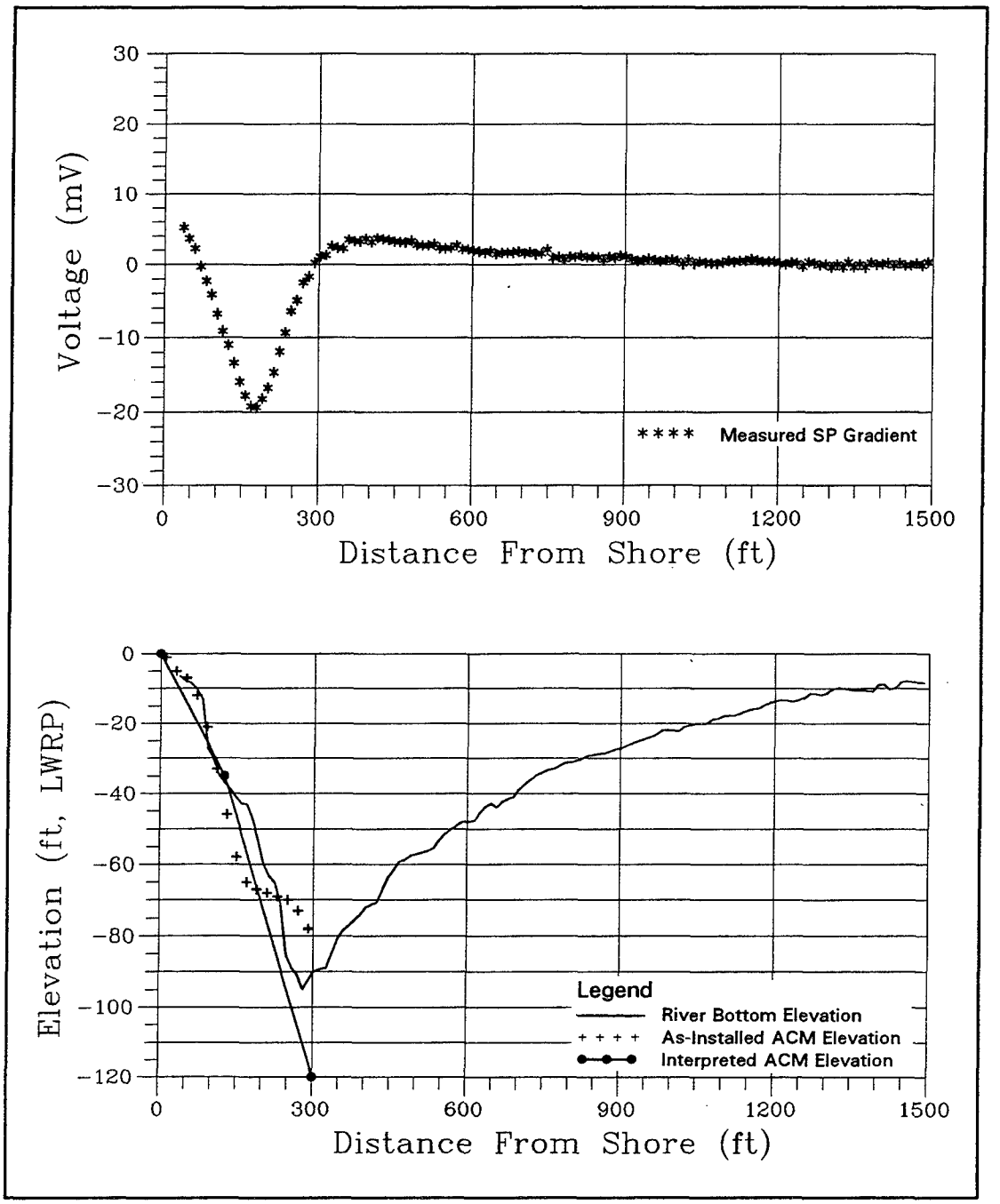

Figure 10. The measured SP gradient and bathymetry along range U-75, Missouri Bend Revetment. Interpreted depths to ACM are presented in the lower plot.

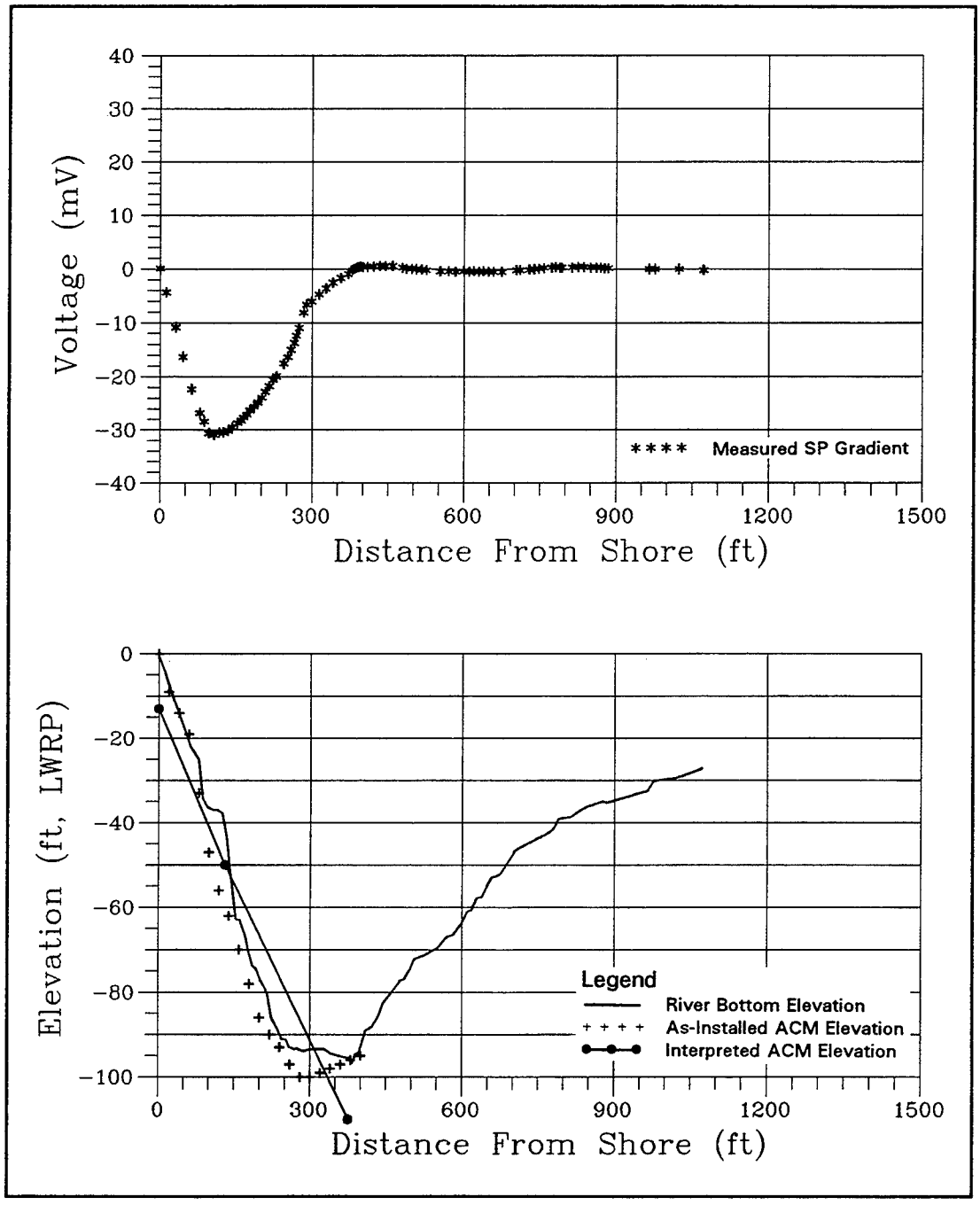

Figure 11. The measured SP gradient and bathymetry along range U-140, Manchac Revetment. Interpreted depths to ACM are presented in the lower plot.

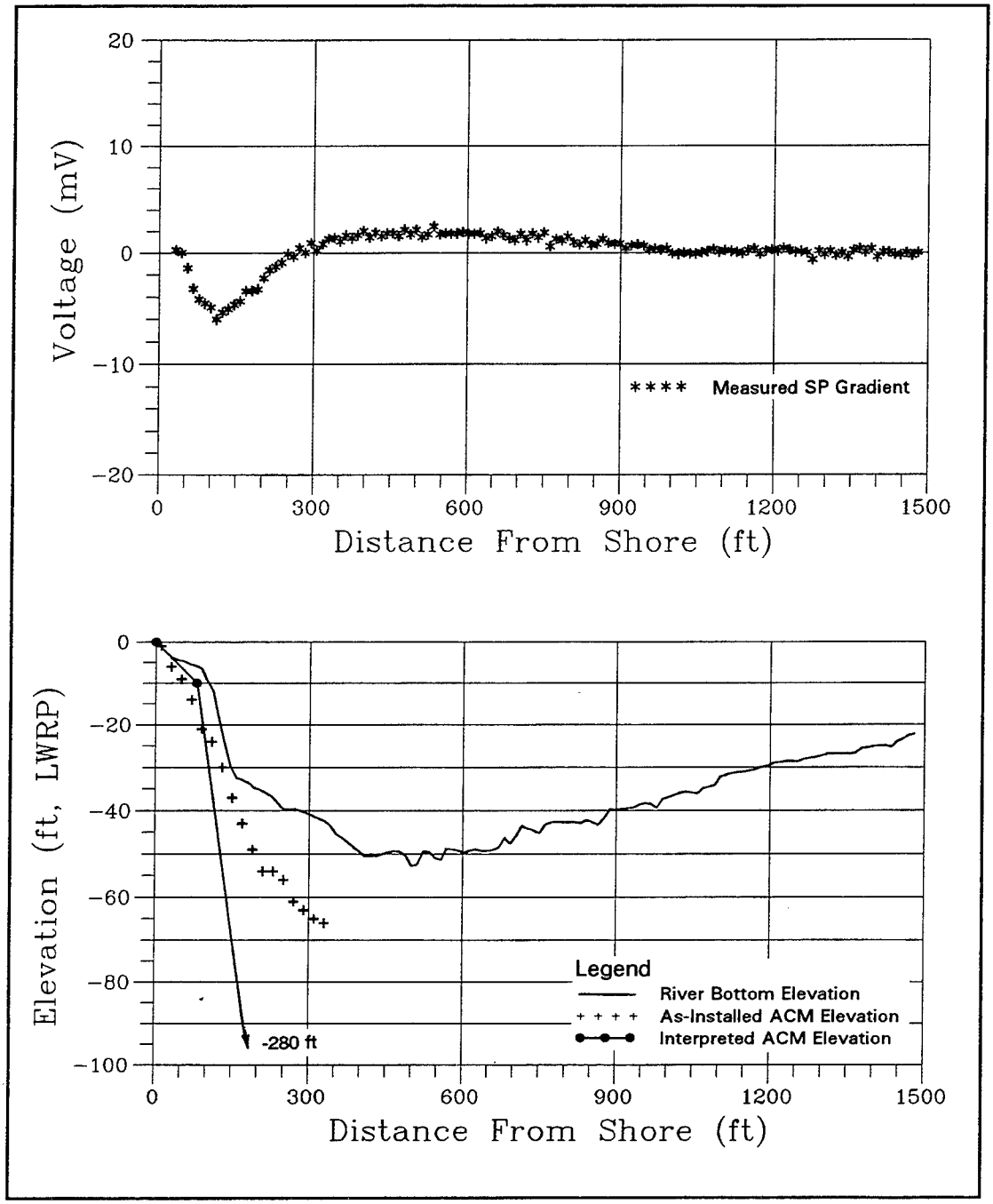

Figure 12. The measured SP gradient and bathymetry along range U-95, Missouri Bend Revetment. Interpreted depths to ACM are presented in the lower plot.

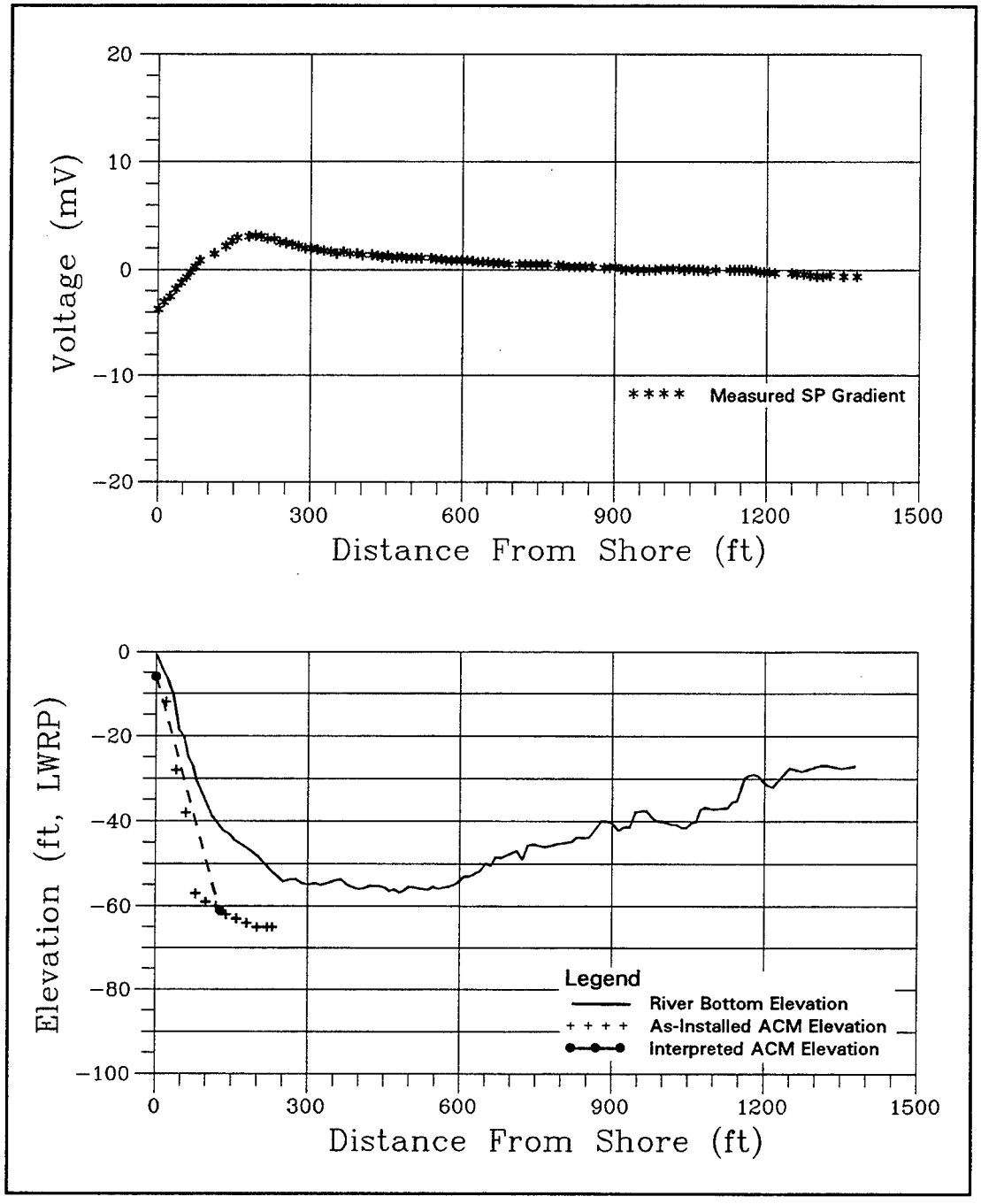

Figure 13. The measured SP gradient and bathymetry along range U-170, Manchac Revetment. Interpreted depths to ACM are presented in the lower plot.

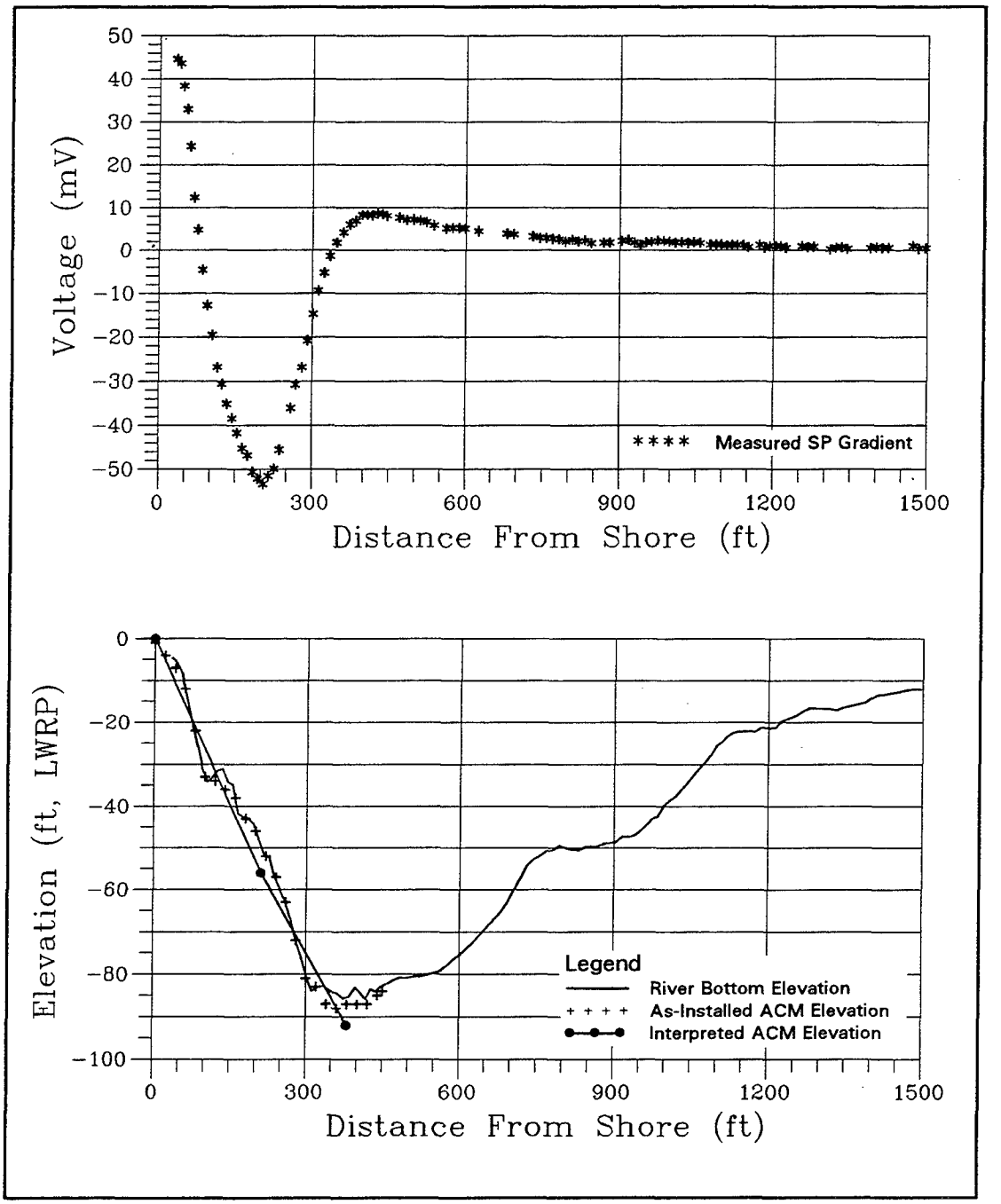

Figure 14. The measured SP gradient and bathymetry along range U-130, Manchac Revetment. Interpreted depths to ACM are presented in the lower plot.

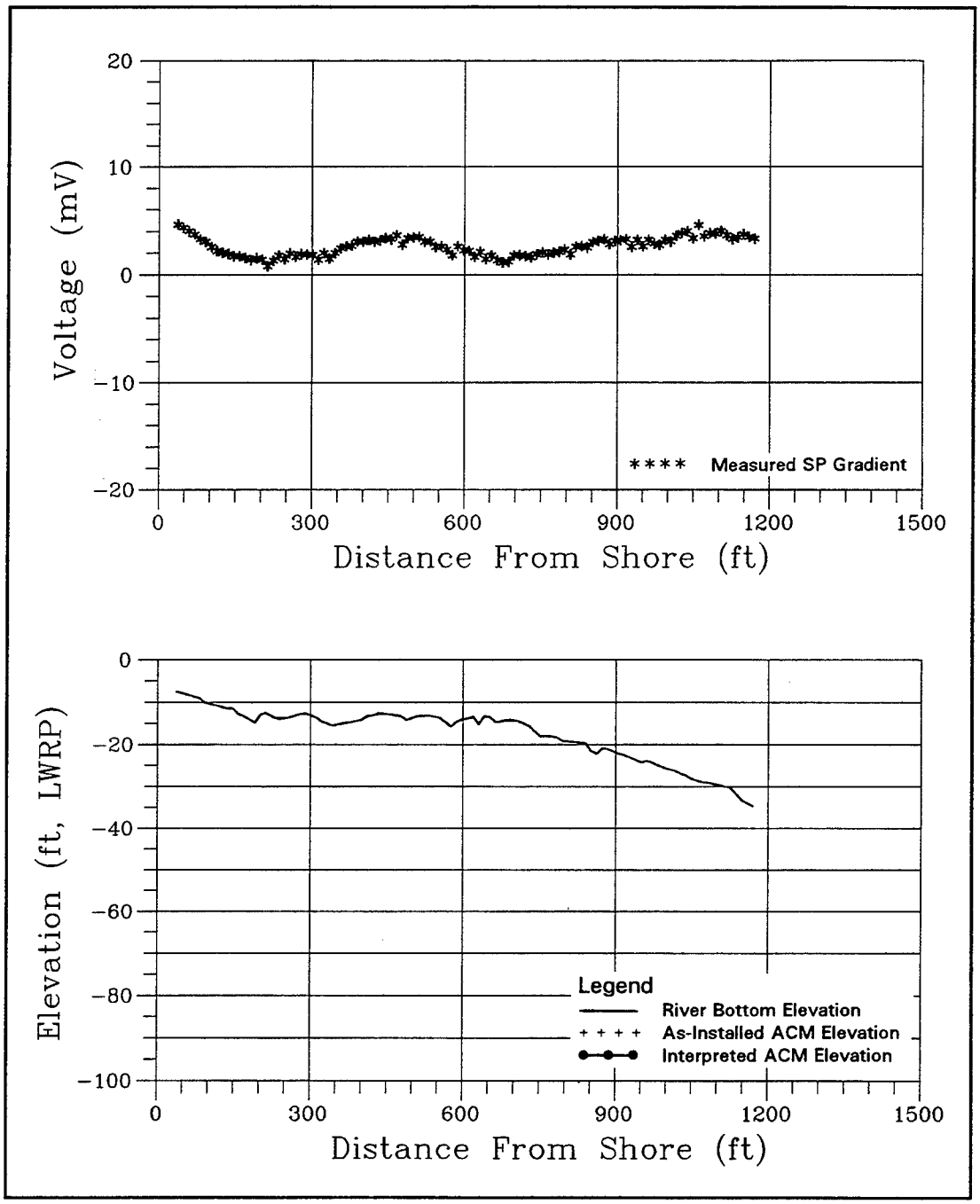

Figure 15. The measured SP gradient and bathymetry along range U-154, Missouri Bend Revetment.

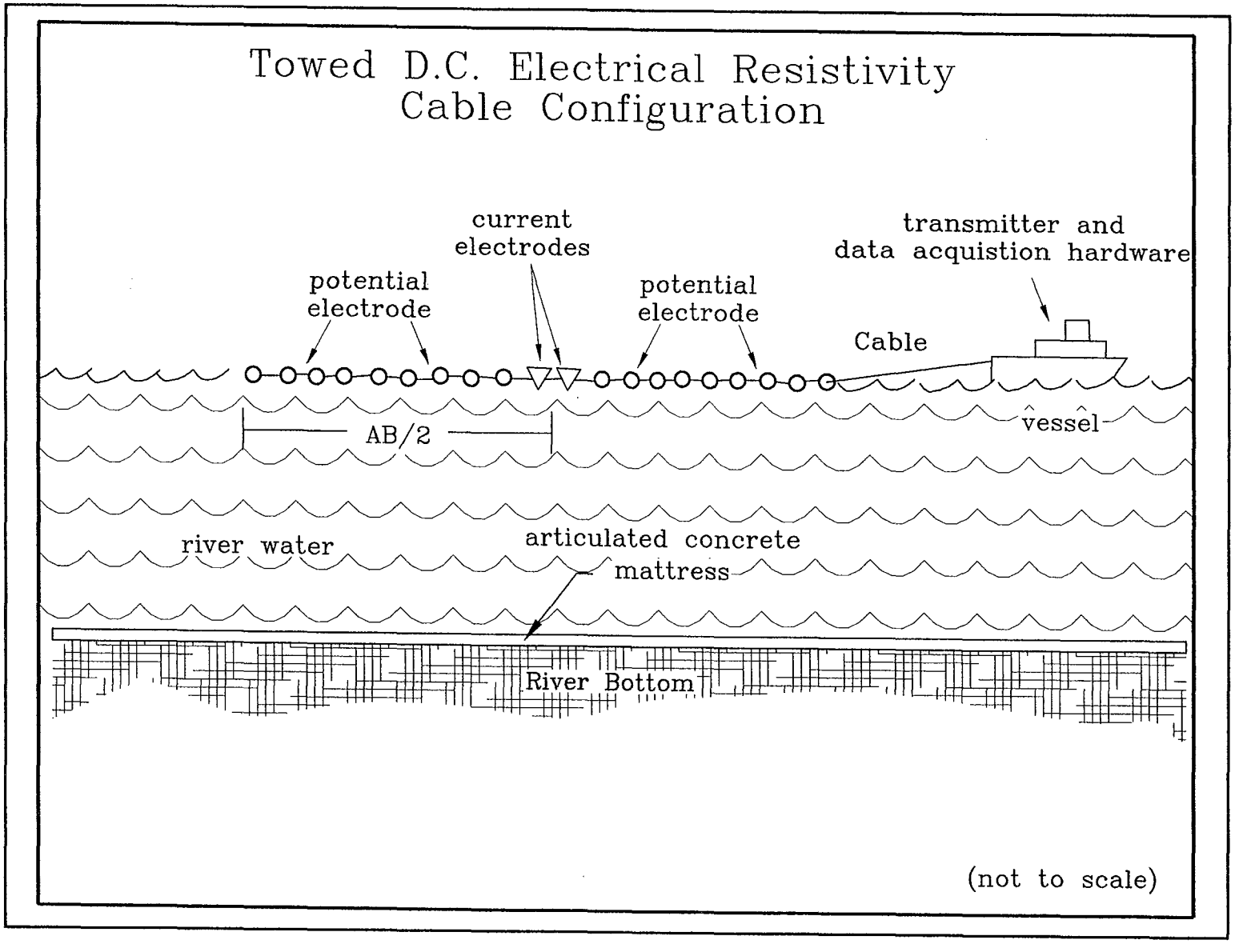

Figure 16. Schematic of the towed DC electrical resistivity system

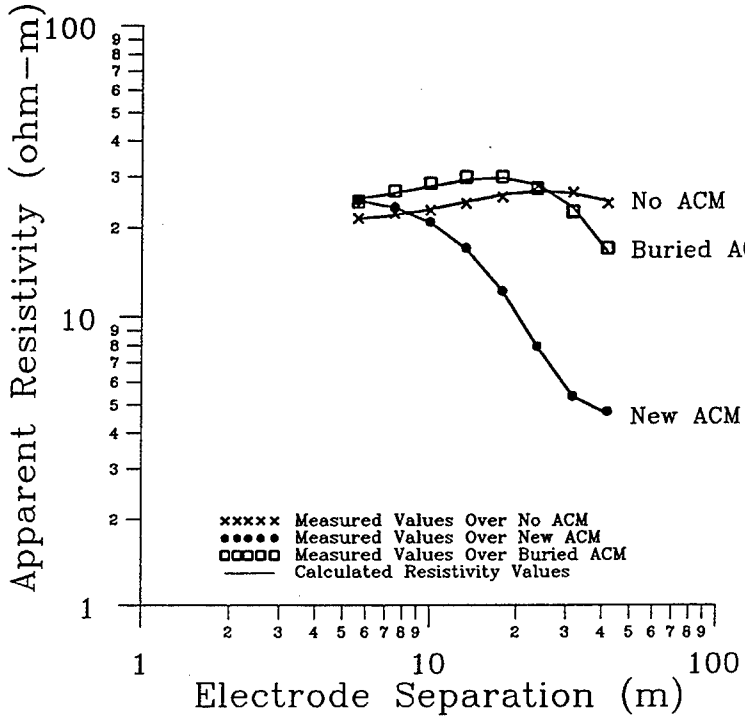

Interpretation of Resistivity Soundings

	Layer 1	Layer 2	Layer 3	RMS Error
Sounding Over New ACM				
Resistivity (ohm-m)	26.2	0.001	8.0	0.72 %
Thickness (m)	8.5	0.004	—	
Material	water	ACM	sediment	
Sounding Over Buried ACM				
Resistivity (ohm-m)	24.0	49.2	0.001	2.34 %
Thickness (m)	5.8	11.4	—	
Material	water	sediment	ACM	
Sounding Over No ACM				
Resistivity (ohm-m)	20.8	40.1	16.8	1.78 %
Thickness (m)	6.9	9.7	—	
Material	water	sediment	sediment	

Figure 17. TDC resistivity curves and corresponding interpretations

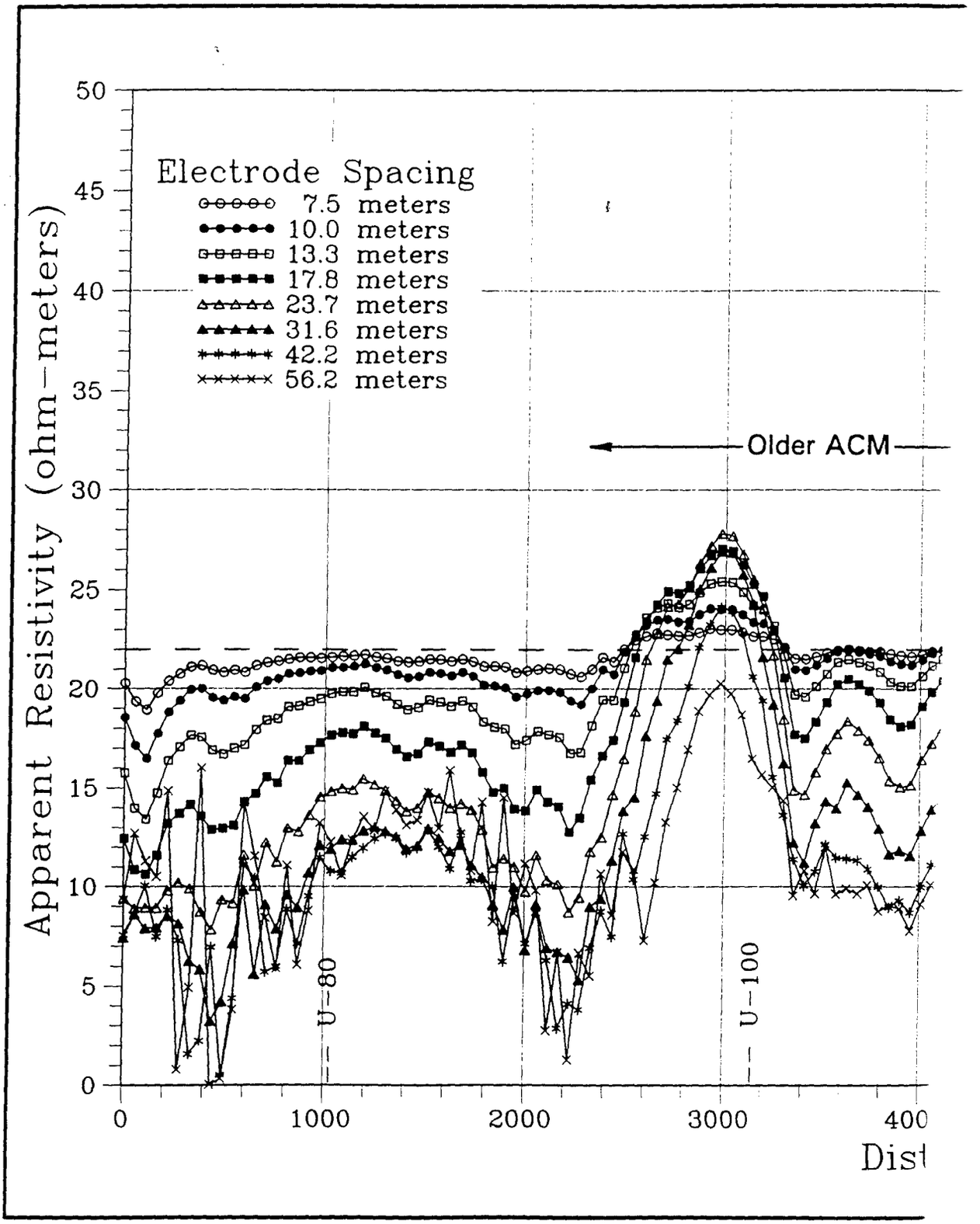

Figure 18. Apparent resistivity data versus distance measured with each electrode spacing, Missouri I

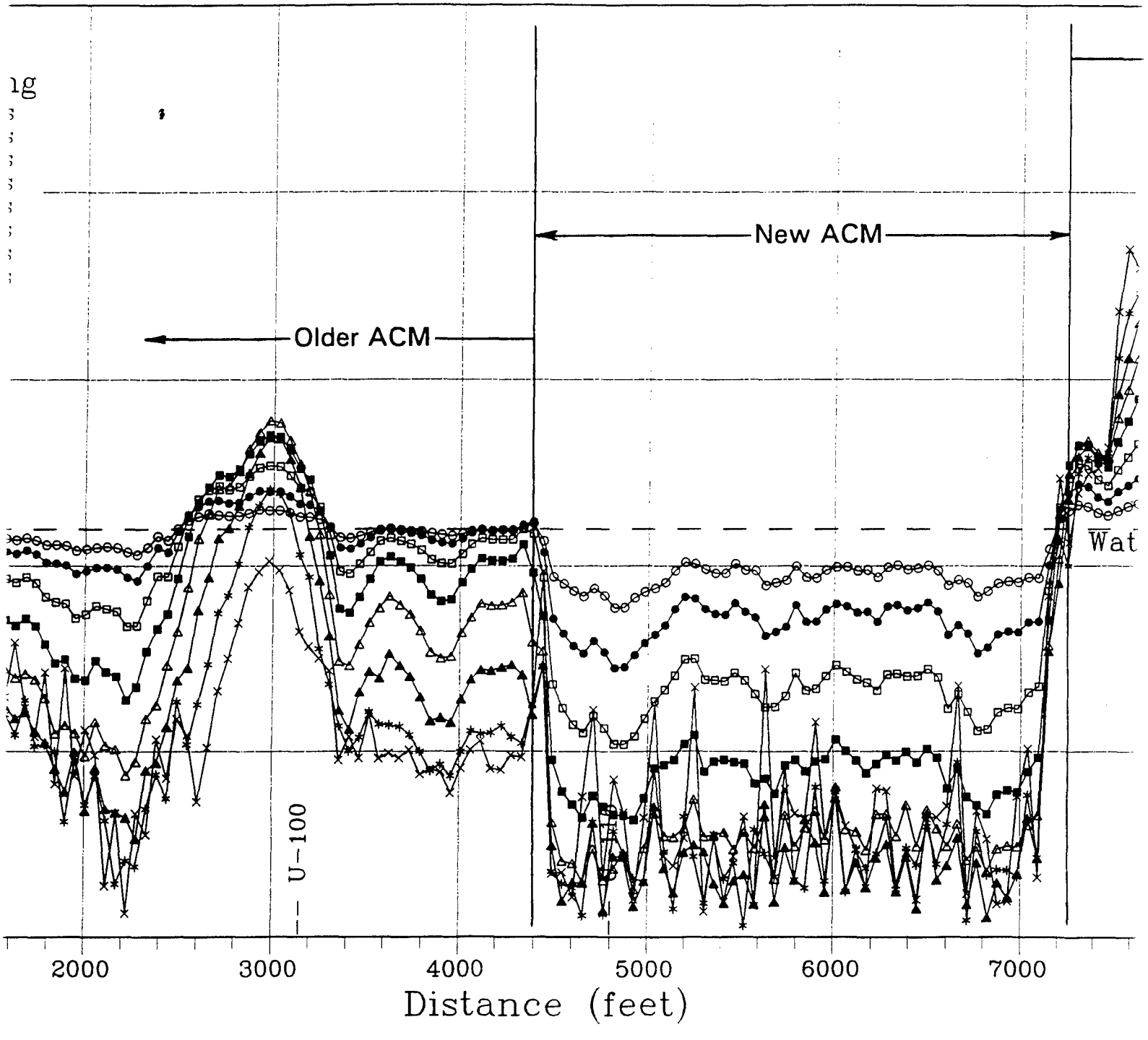

ance measured with each electrode spacing, Missouri Bend Revetment

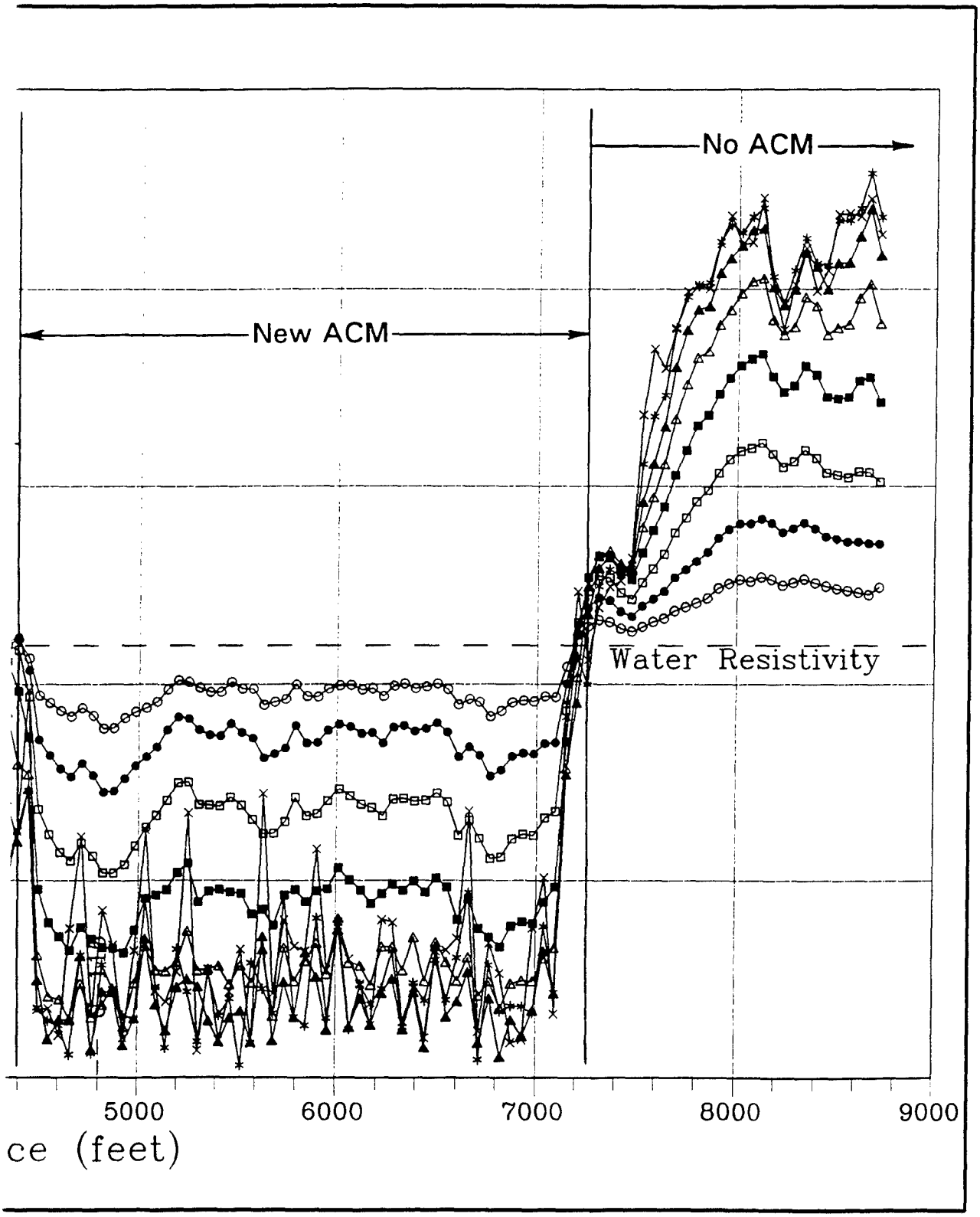
No ACM
New ACM
Water Resistivity
5000
6000
7000
8000
9000
ce (feet)

evetment

3

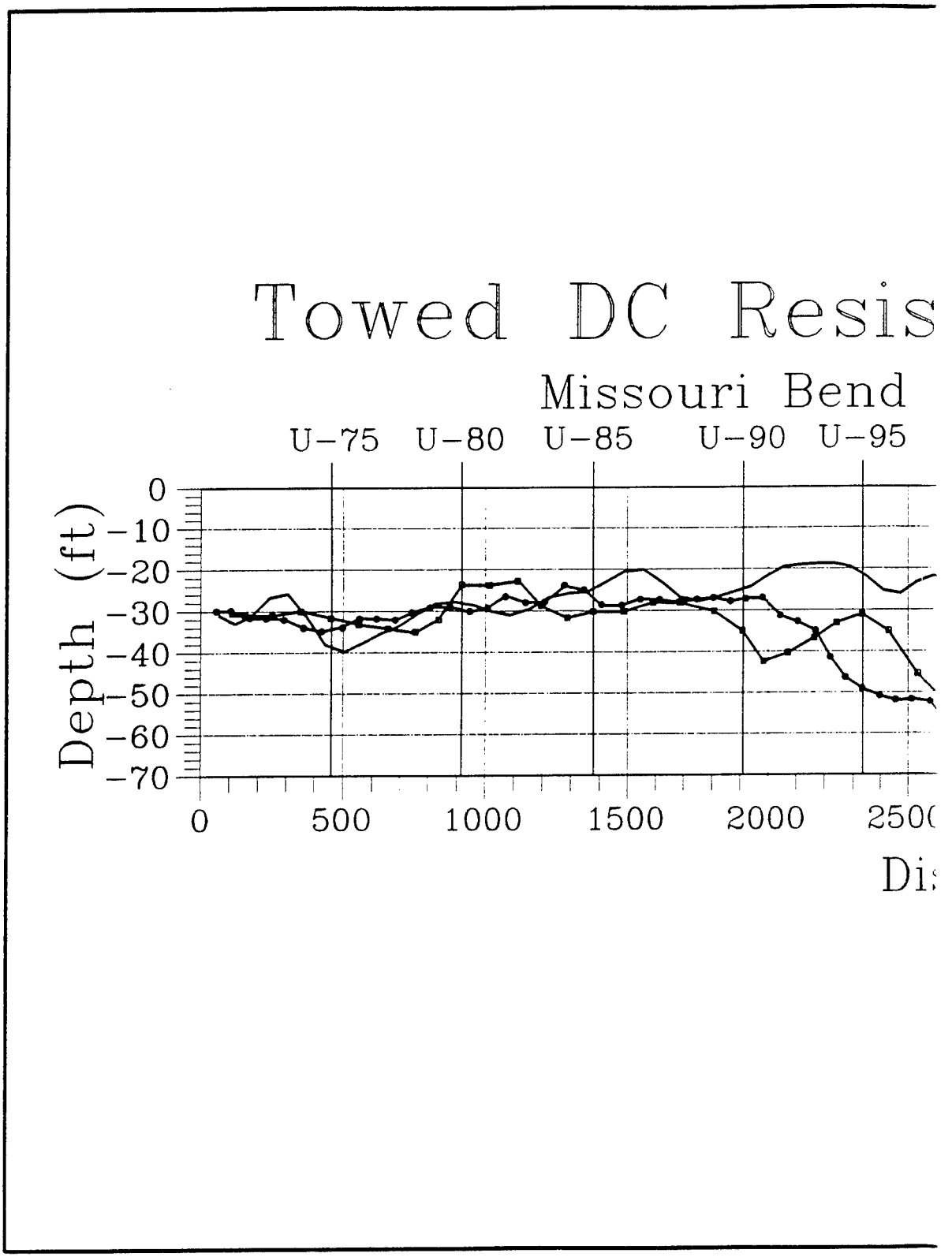

Figure 19. Computed ACM depths versus as-installed ACM depths, Missouri Bend Revetment

)wed DC Resistivity Profile

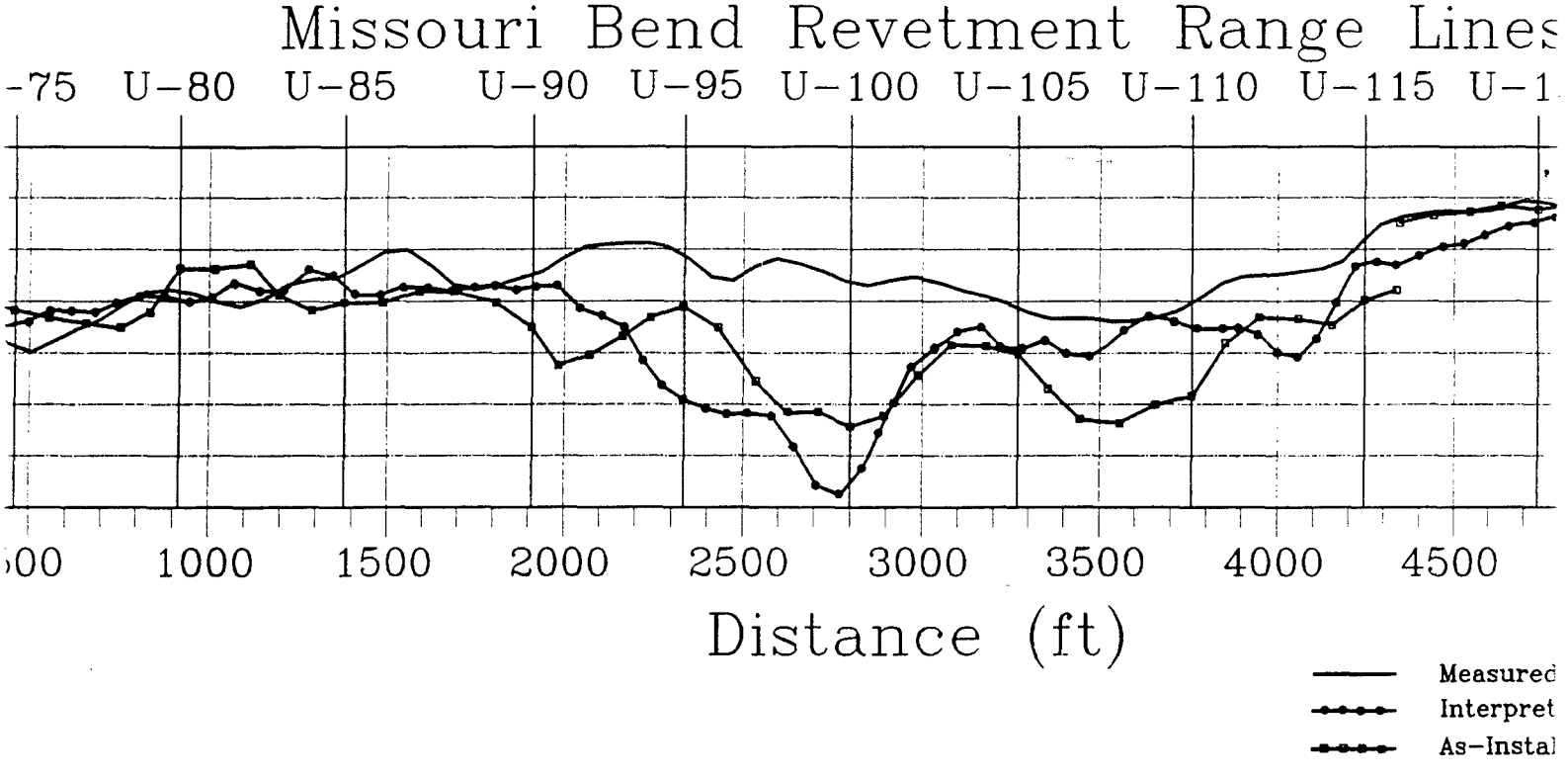

s versus as-installed ACM depths, Missouri Bend Revetment

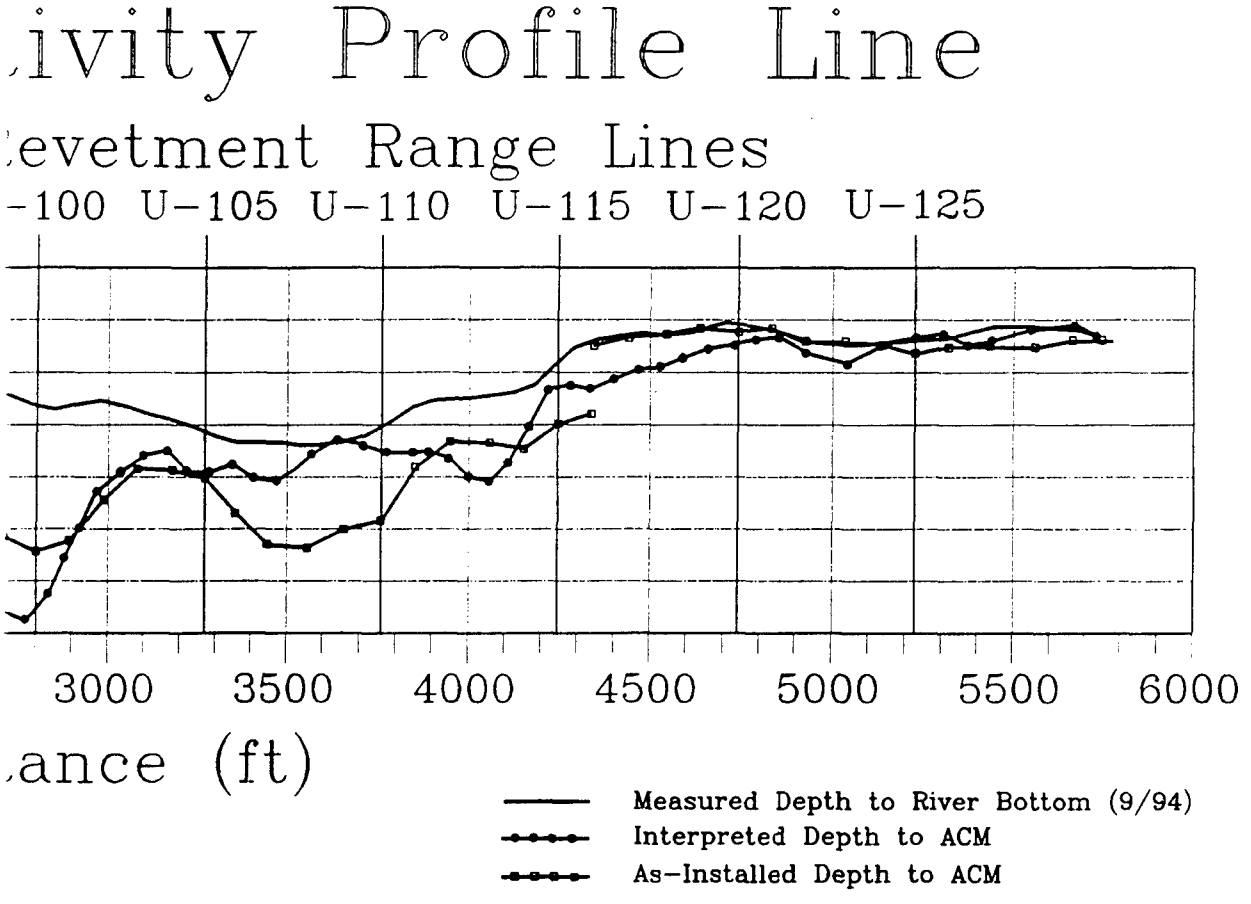
ivity Profile Line
evetment Range Lines
-100 U-105 U-110 U-115 U-120 U-125
3000
3500
4000
4500
5000
5500
6000
ance (ft)
Measured Depth to River Bottom (9/94)
Interpreted Depth to ACM
As-Installed Depth to ACM

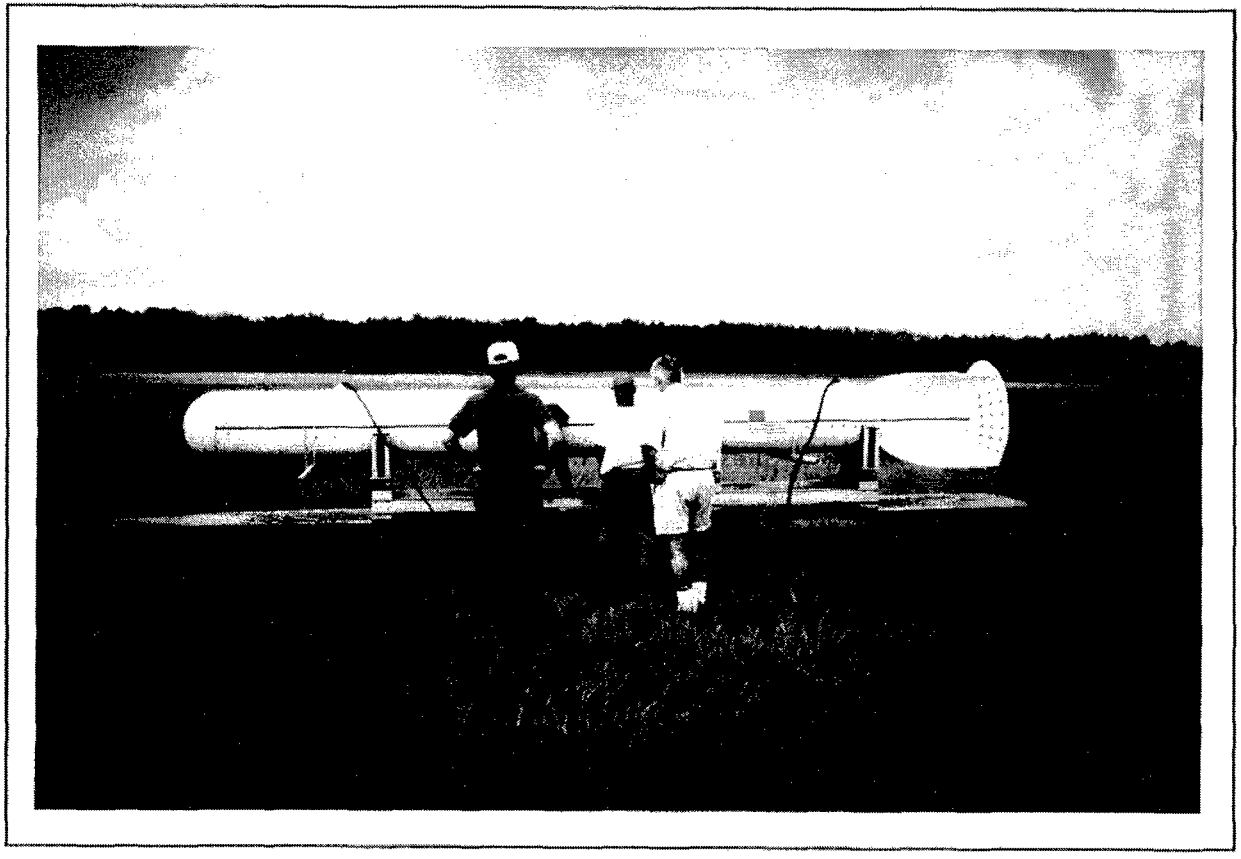

Figure 20. Frequency domain EM towbody configured for airborne deployment

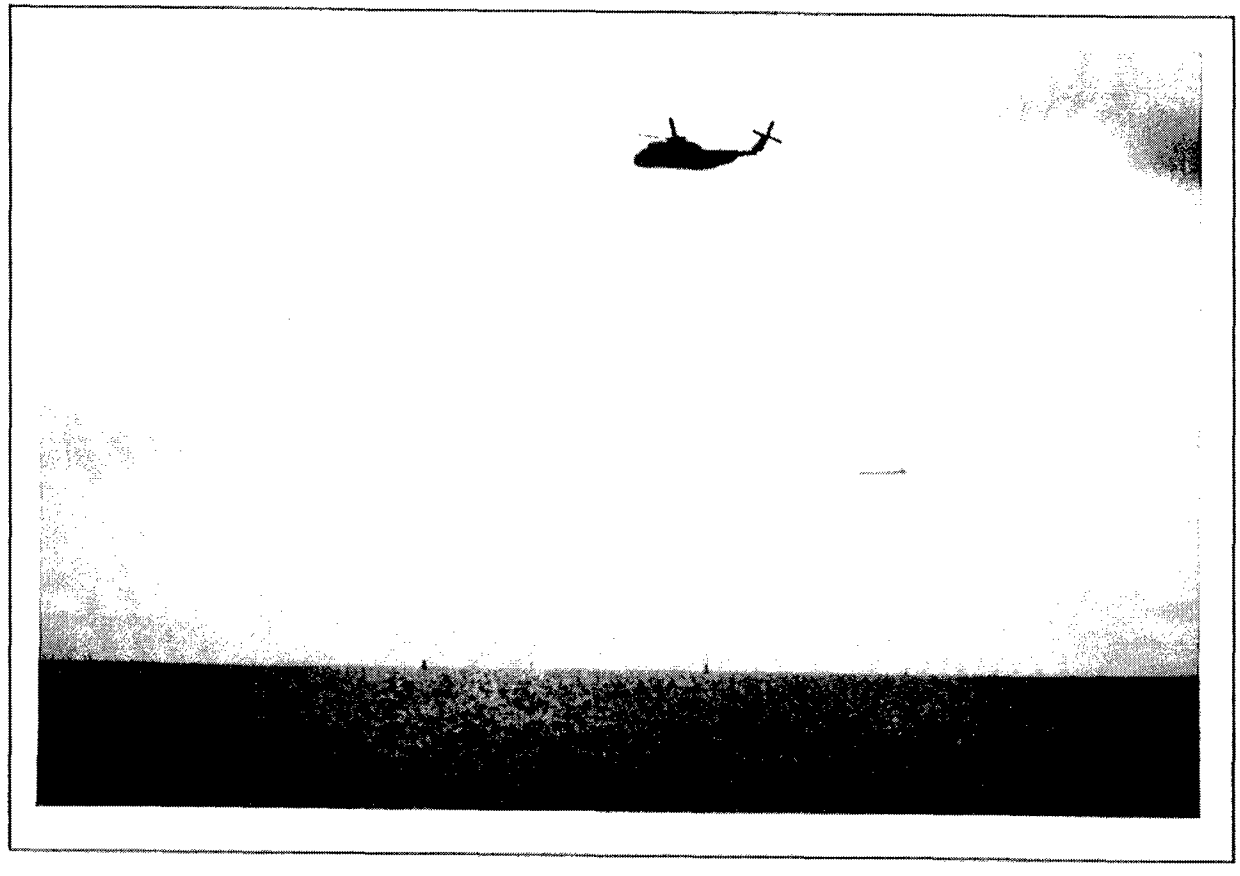

Figure 21. Airborne EM towbody suspended beneath helicopter during surveying

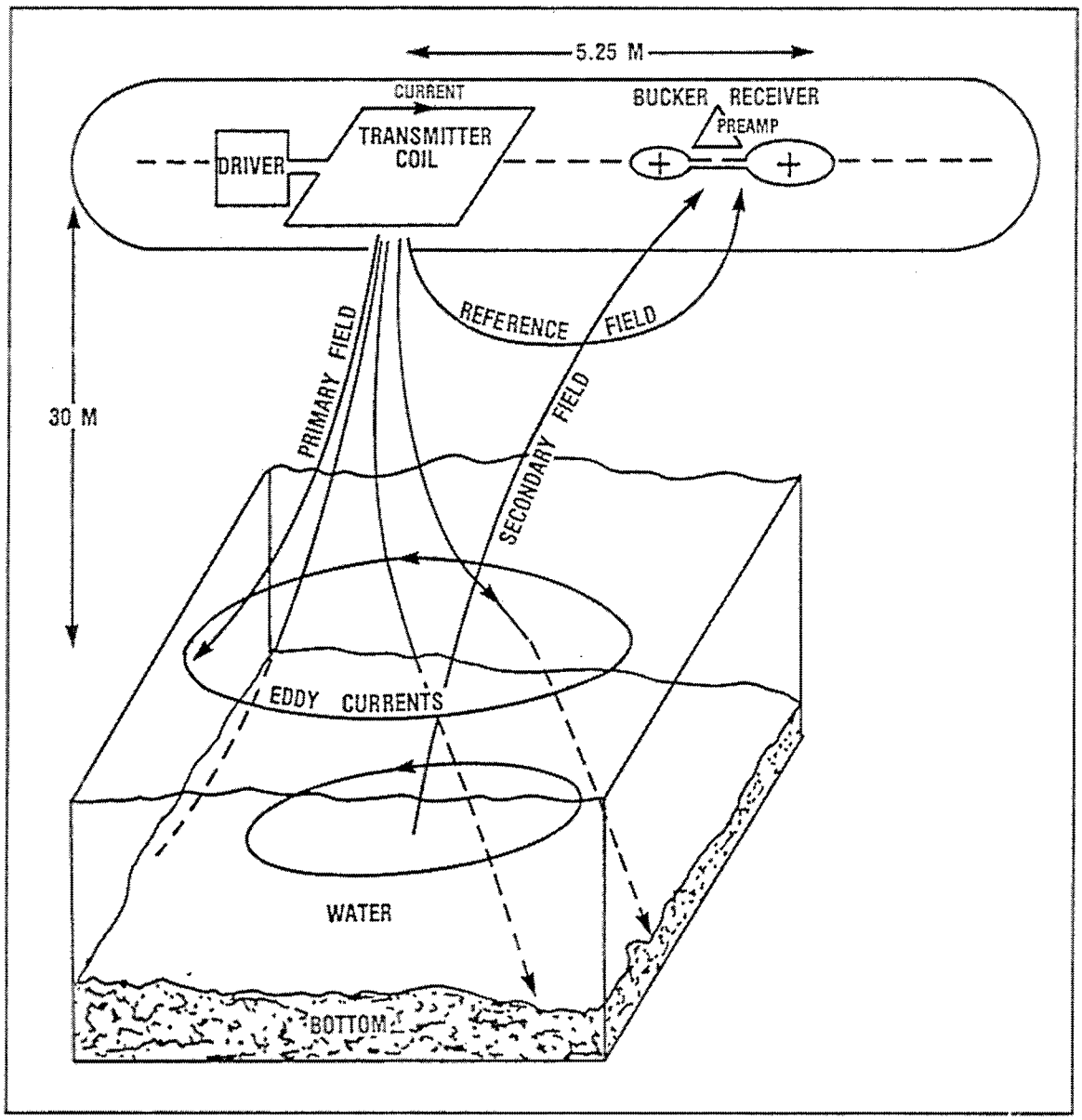

Figure 22. Schematic of primary components of AEM system and physical concepts of electromagnetic induction

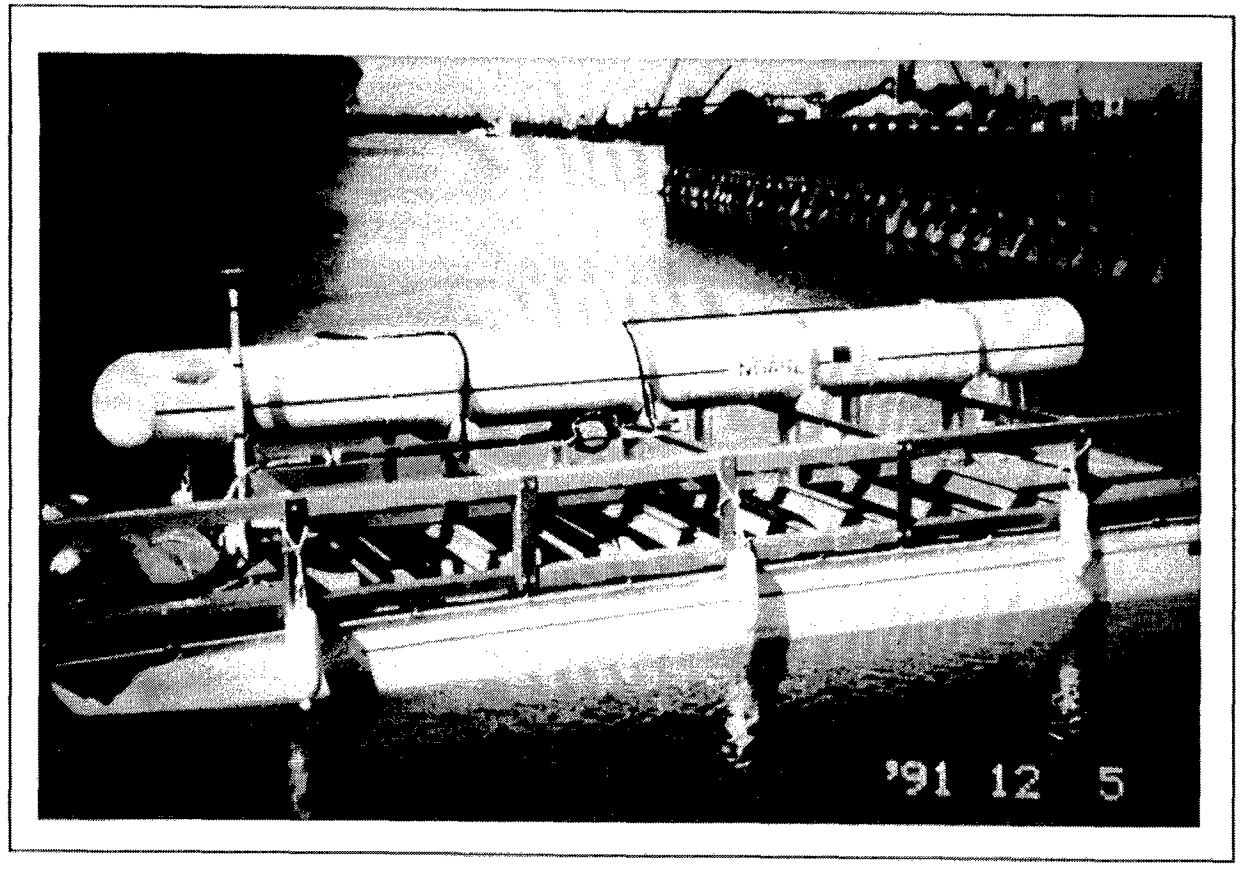

Figure 23. Airborne EM towbody configured for waterborne deployment on nonconducting pontoon float

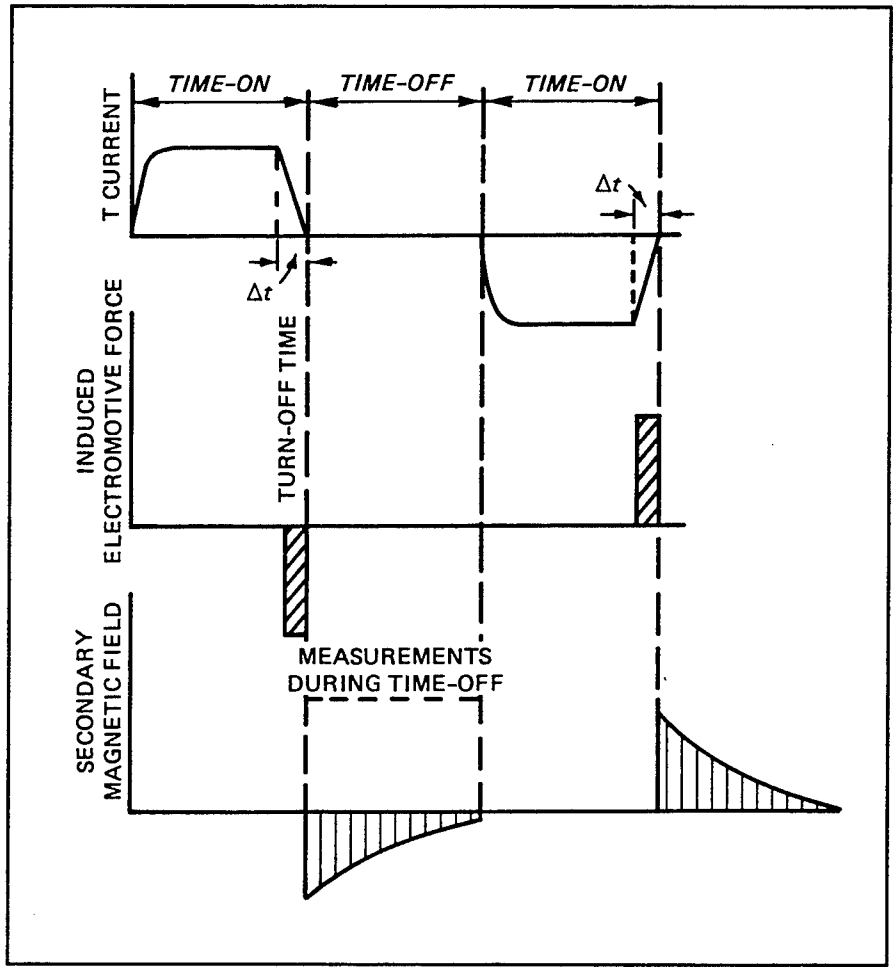

Figure 24. Concepts of transient or time domain EM method

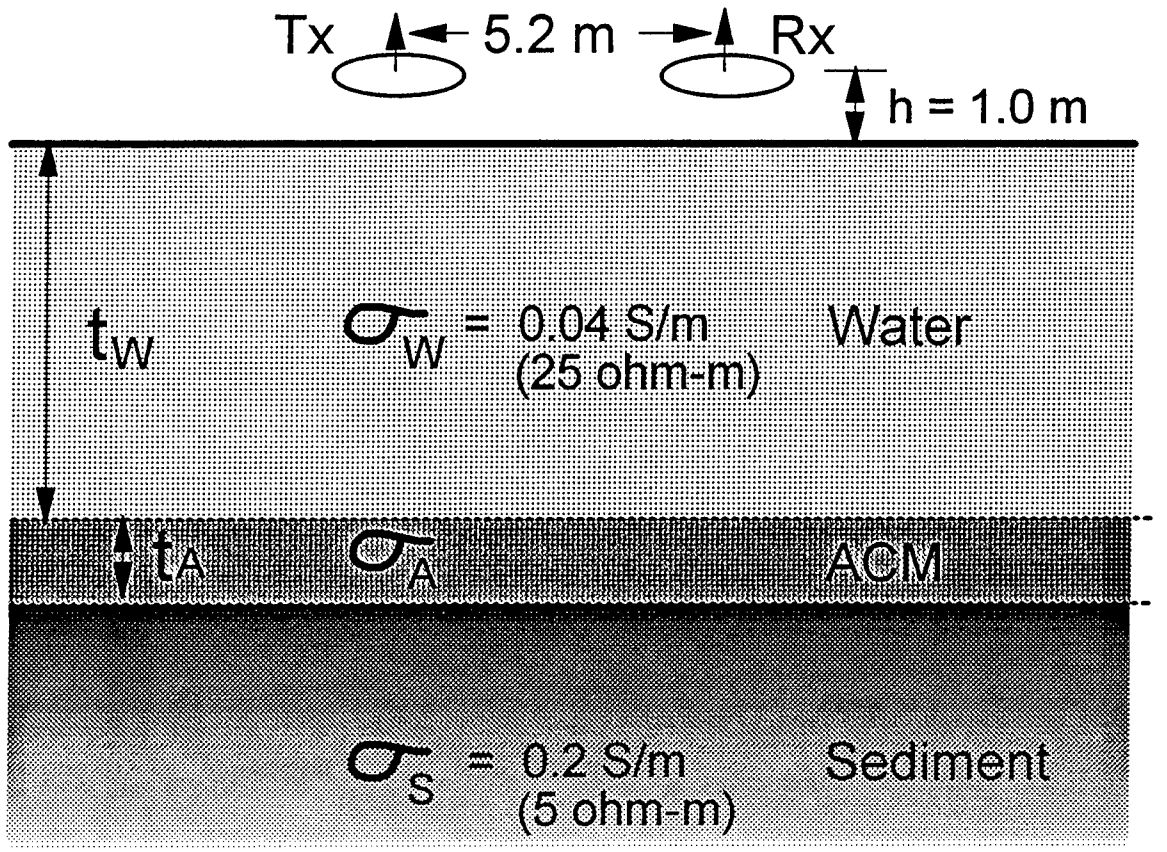

Basic Model: $t_A = 0$ (No ACM present)

Thick Layer ACM Model:

$t_A = 0.3$ m; $\sigma_A = 1816.7$ S/m

Thin Layer ACM Model:

$t_A = 5.45 \times 10^{-5}$ m; $\sigma_A = 1 \times 10^{7}$ S/m

For both Thick and Thin Layer ACM Models:

$\sigma_A t_A = 545$ S (Conductance)

Figure 25. Geoelectrical model for EM response calculations

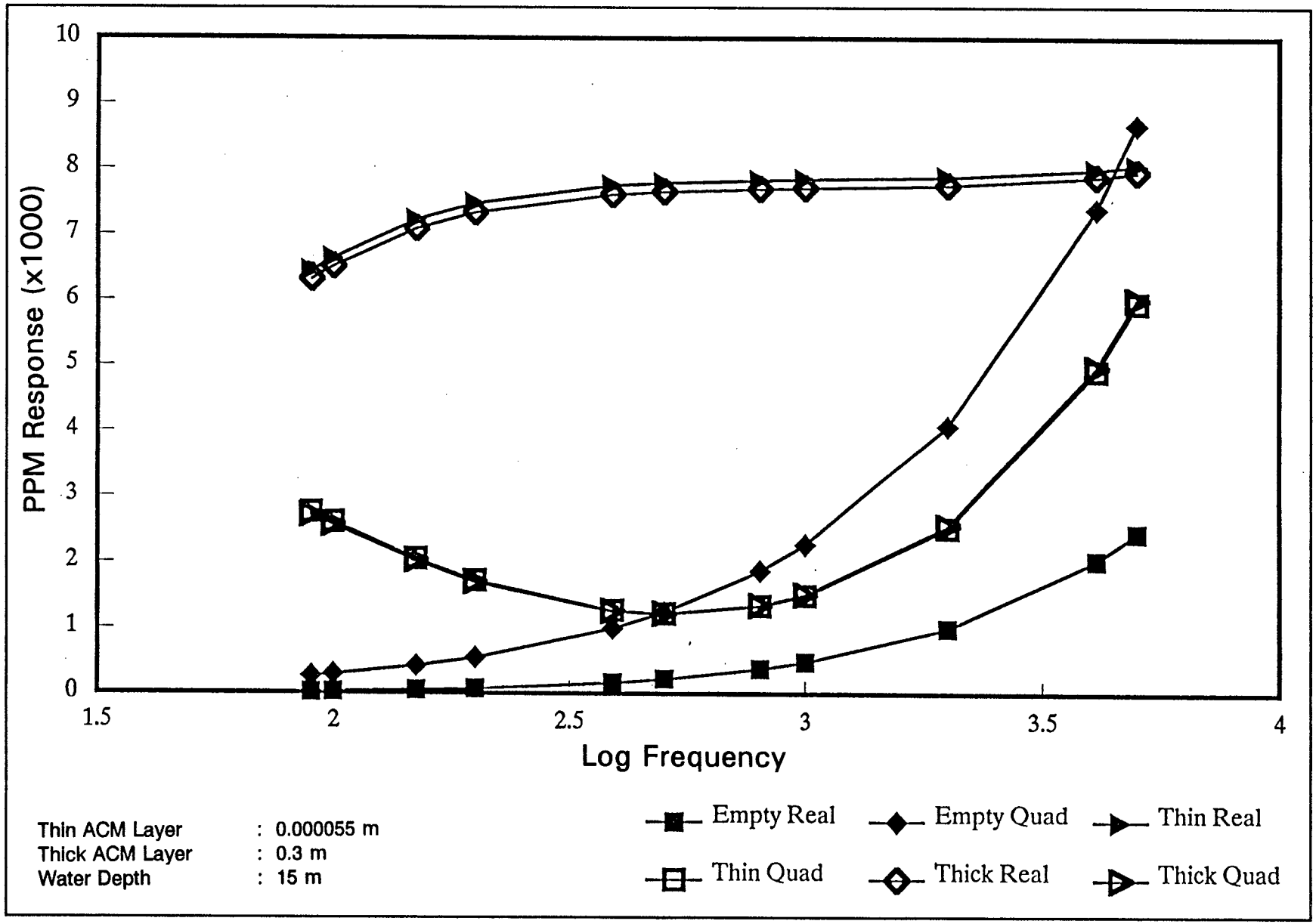

Figure 26. BSALIT 1-D total reponse calculations for basic background model (no ACM present) versus thick and thin ACM models

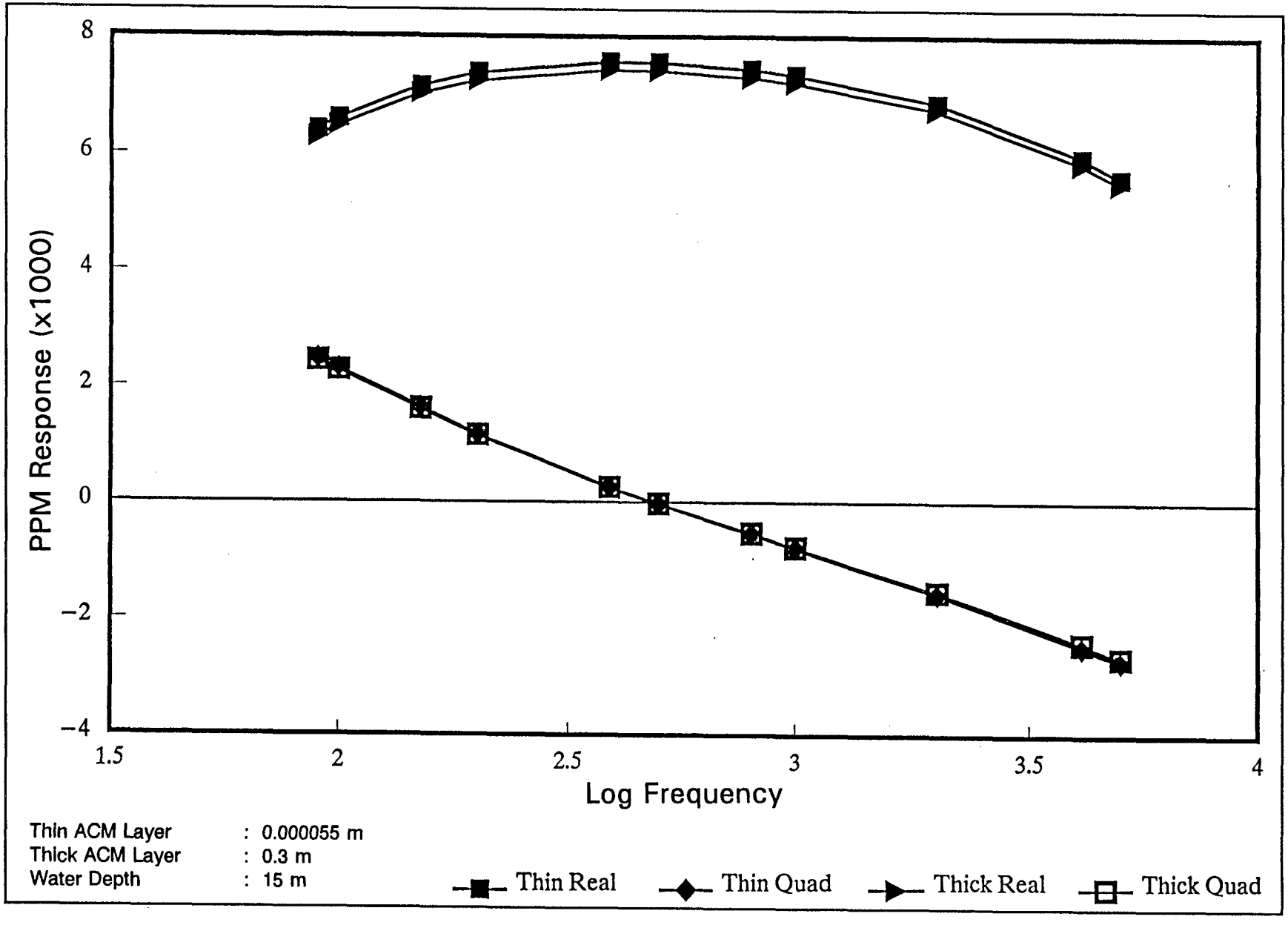

Figure 27. BSAUT 1-D anomalous response calculations for thick and thin ACM models

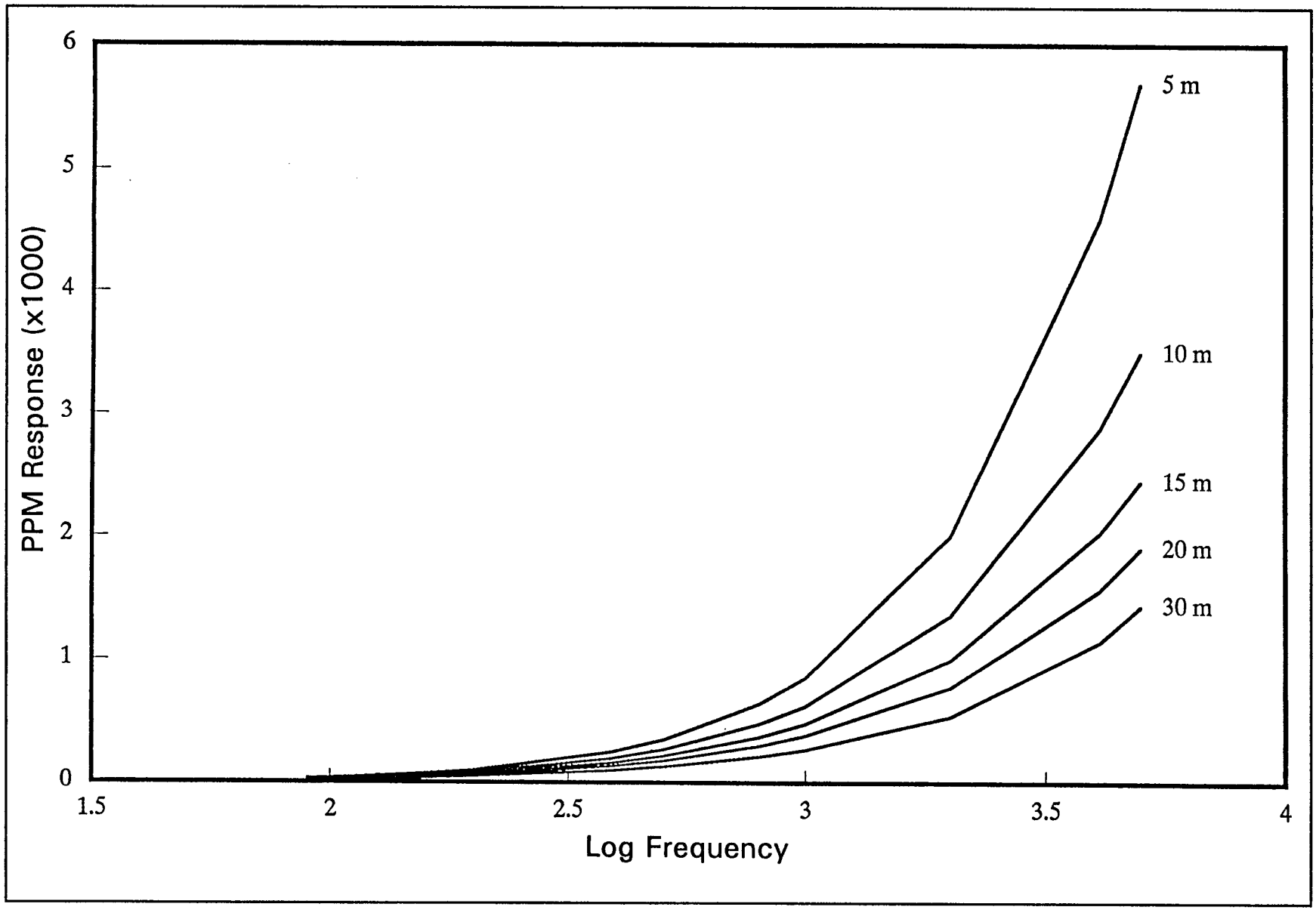

Figure 28. Response of the real component for the BSAUT 1-D basic model (no ACM) for varying water depths

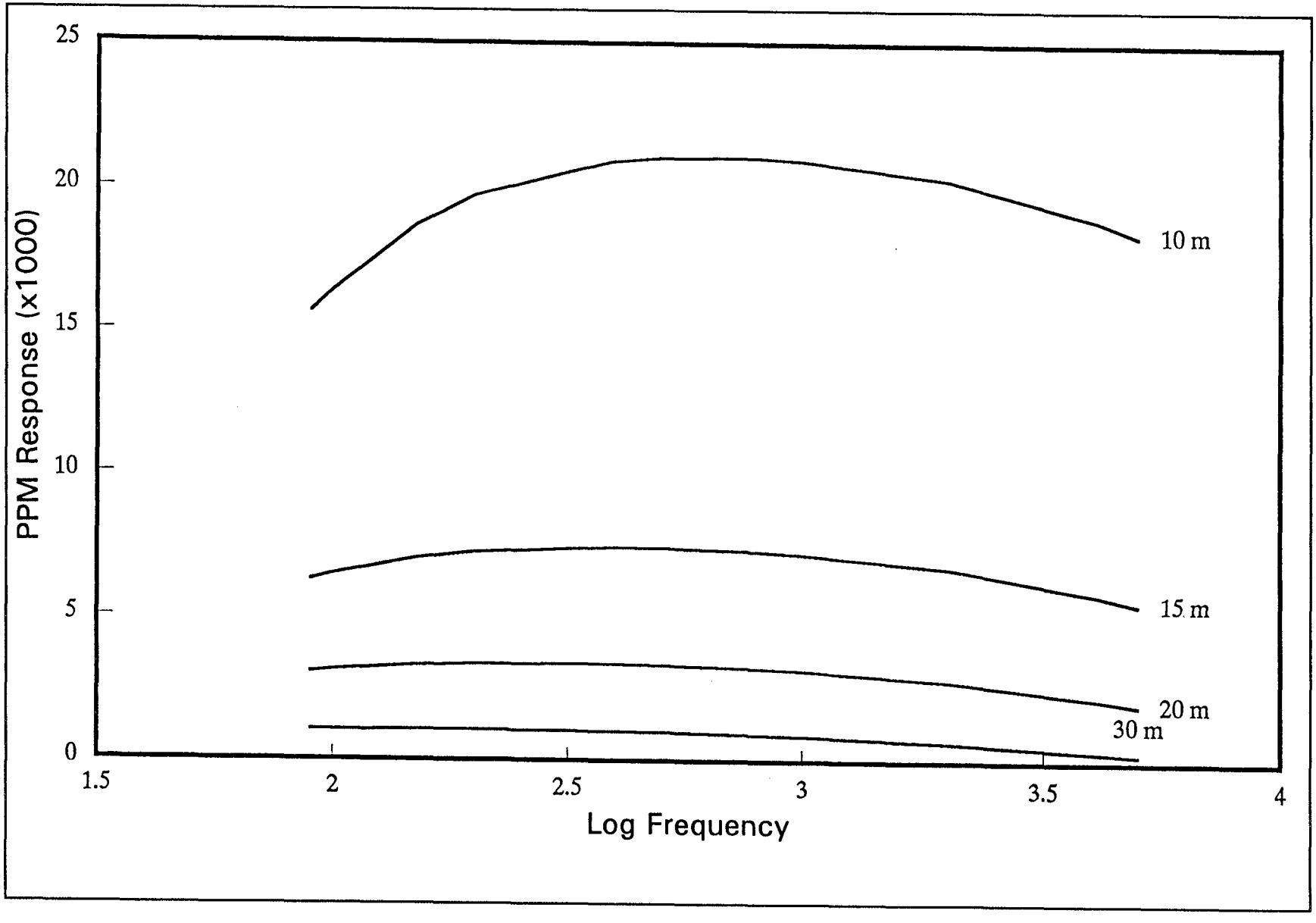

Figure 29. Variations of the BSAUT 1-D anomalous response for varying water depths when ACM is present

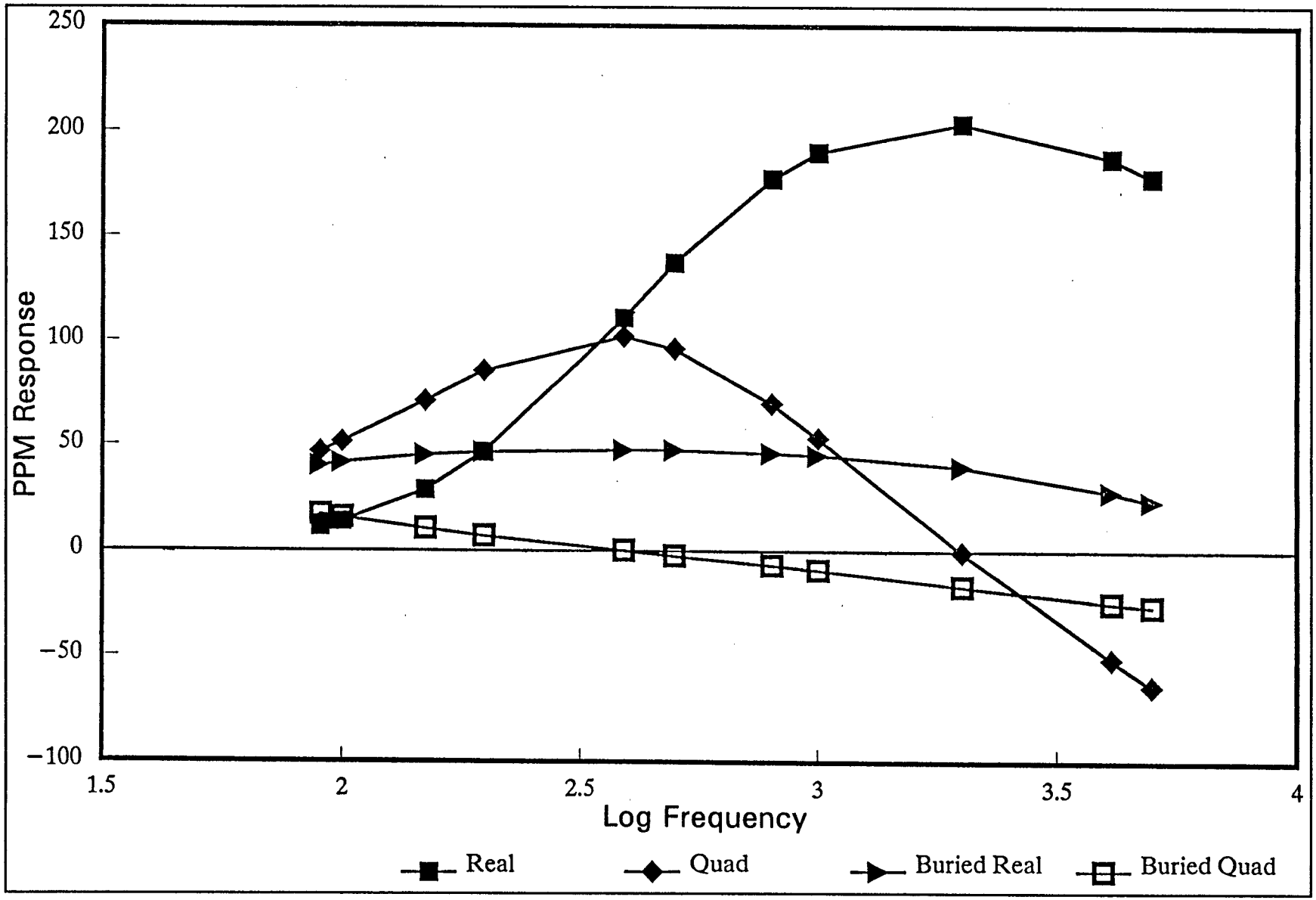

Figure 30. Anomalous response of identical 6.0 m x 7.5 m ACM sections; one at the water-sediment interface and the other buried under 5.0 m of 5.0 ohm-m sediment

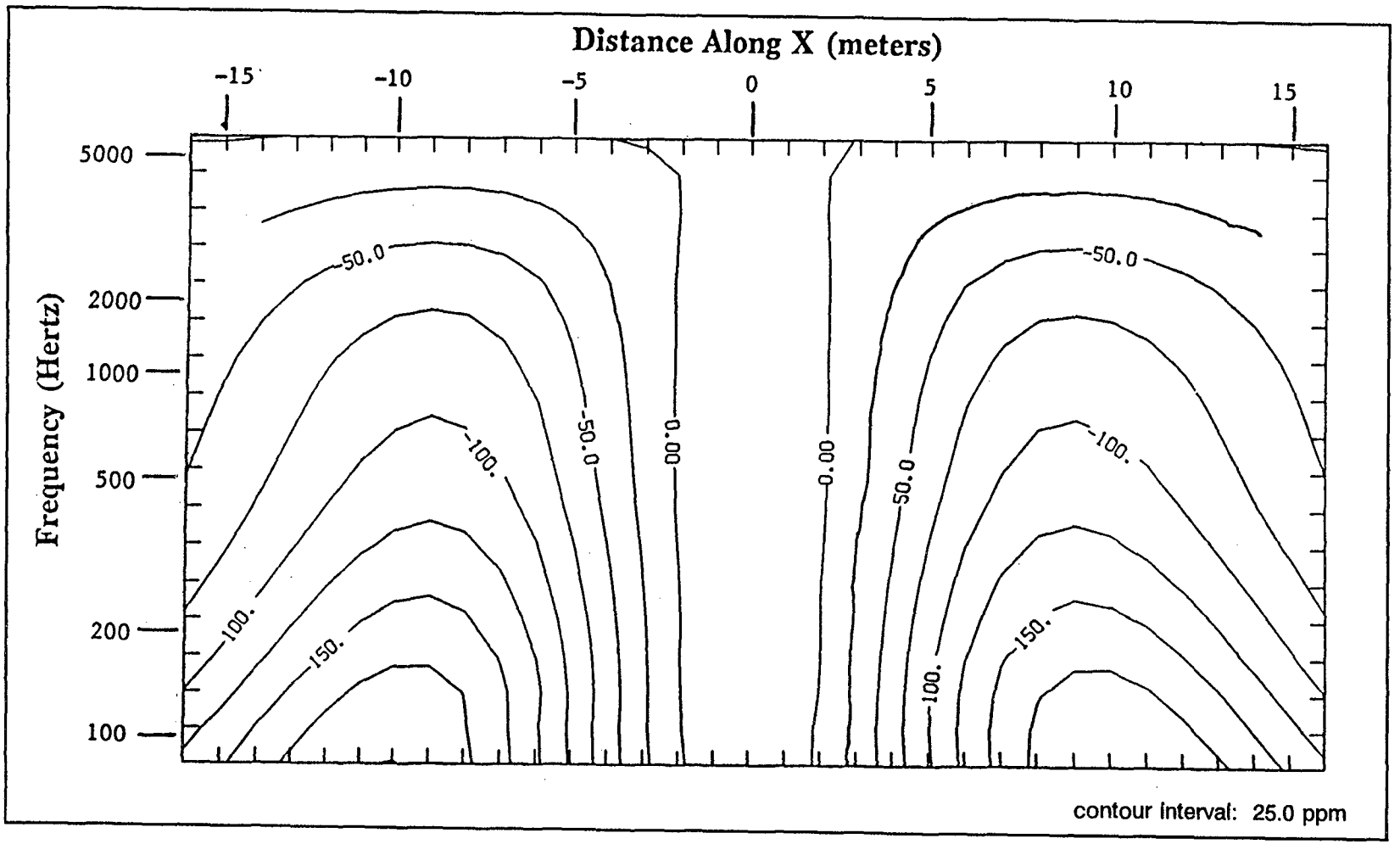

Figure 31. Anomalous real response pseudo-section for a 3-D model calculation of a 6.0 m x 7.5 m "hole" in an infinite ACM sheet

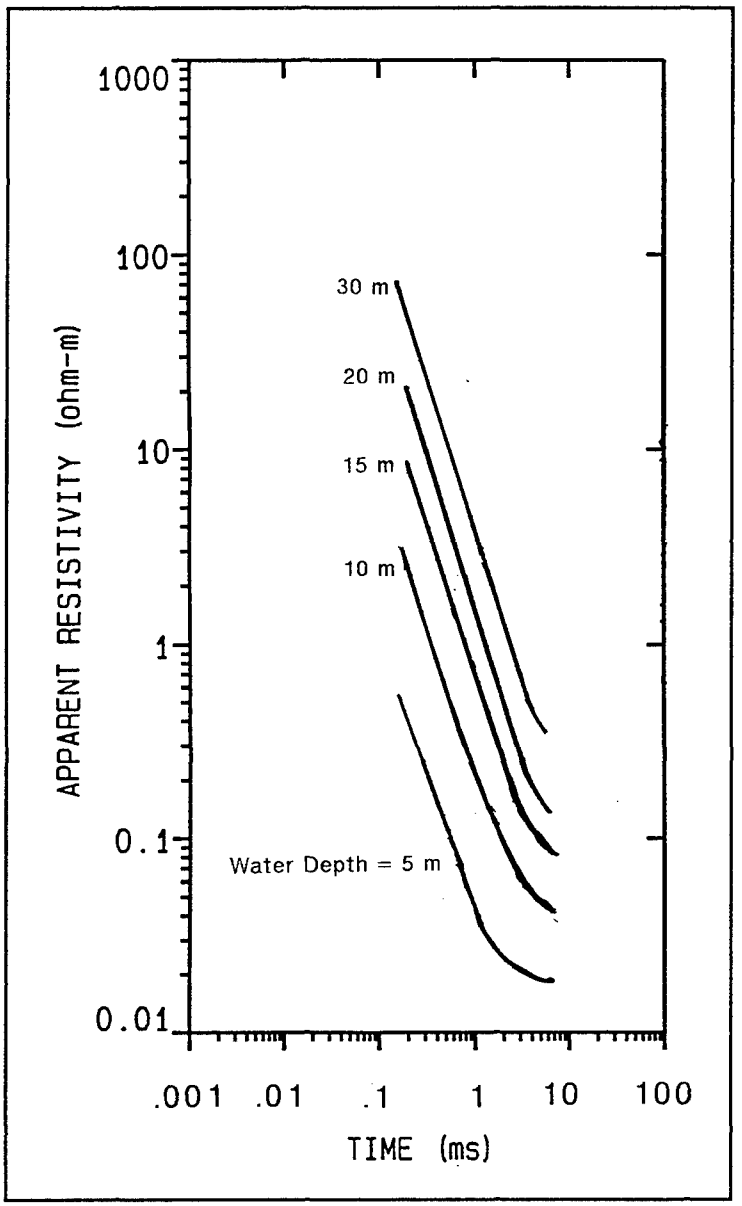

Figure 32. TDEM depth sounding curves for ACM overlying 5 ohm-m sediment in water depths ranging from 5 to 30 m

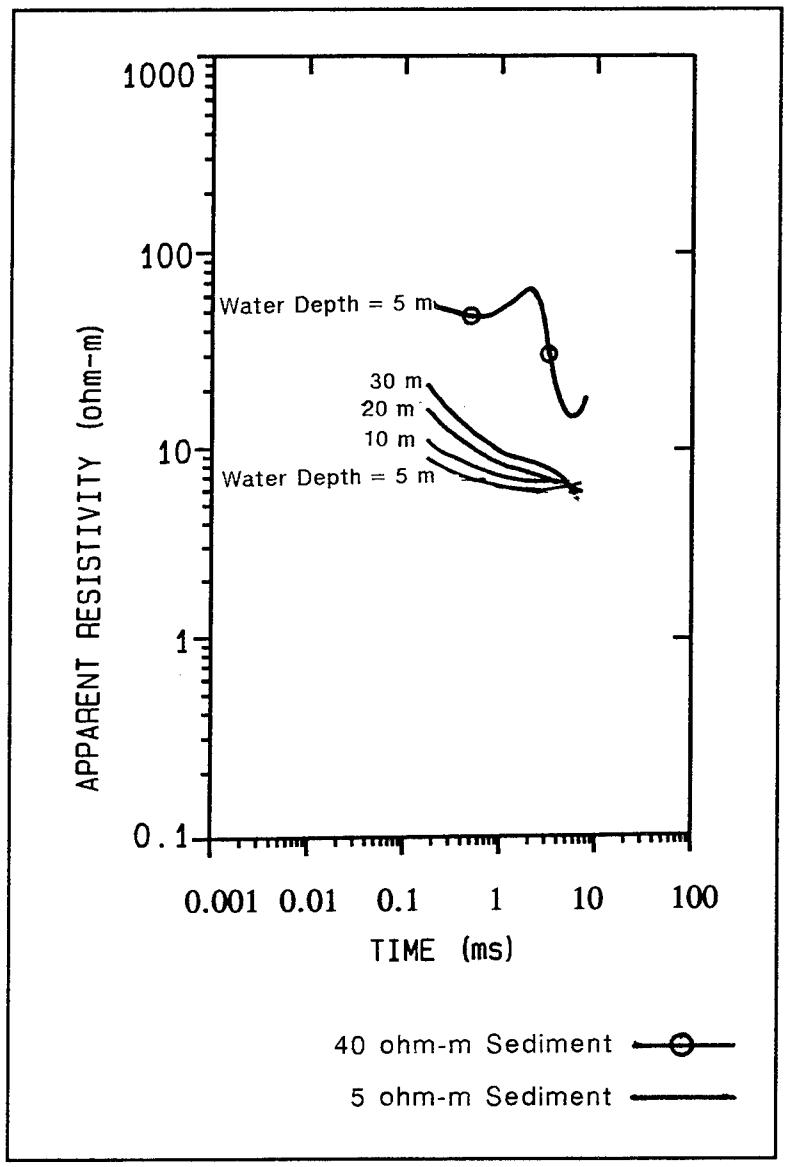

Figure 33. TDEM sounding curves using the basic model (no ACM) in varying water depths. Also, a sounding curve using 40 ohm-m sediment and 5 m water depth

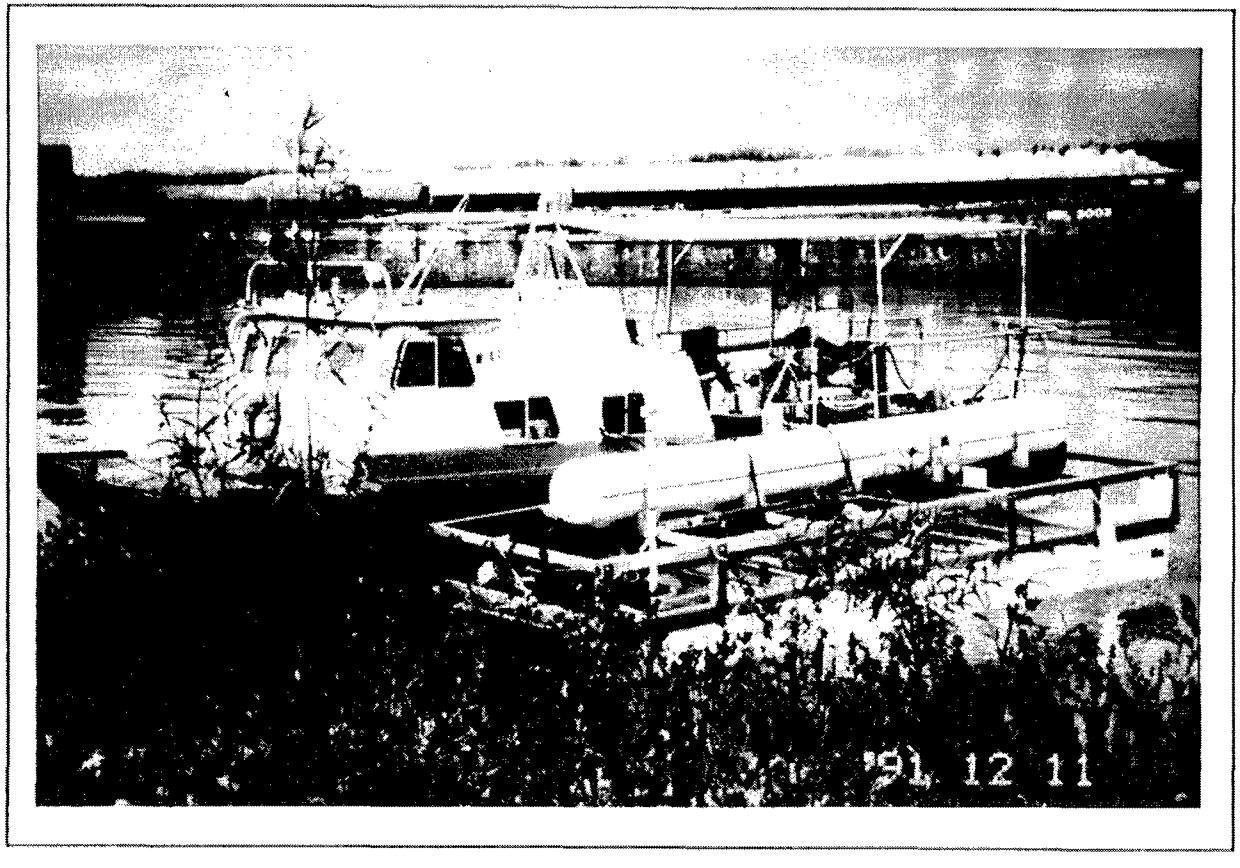

Figure 34. Waterborne deployment of FDEM system

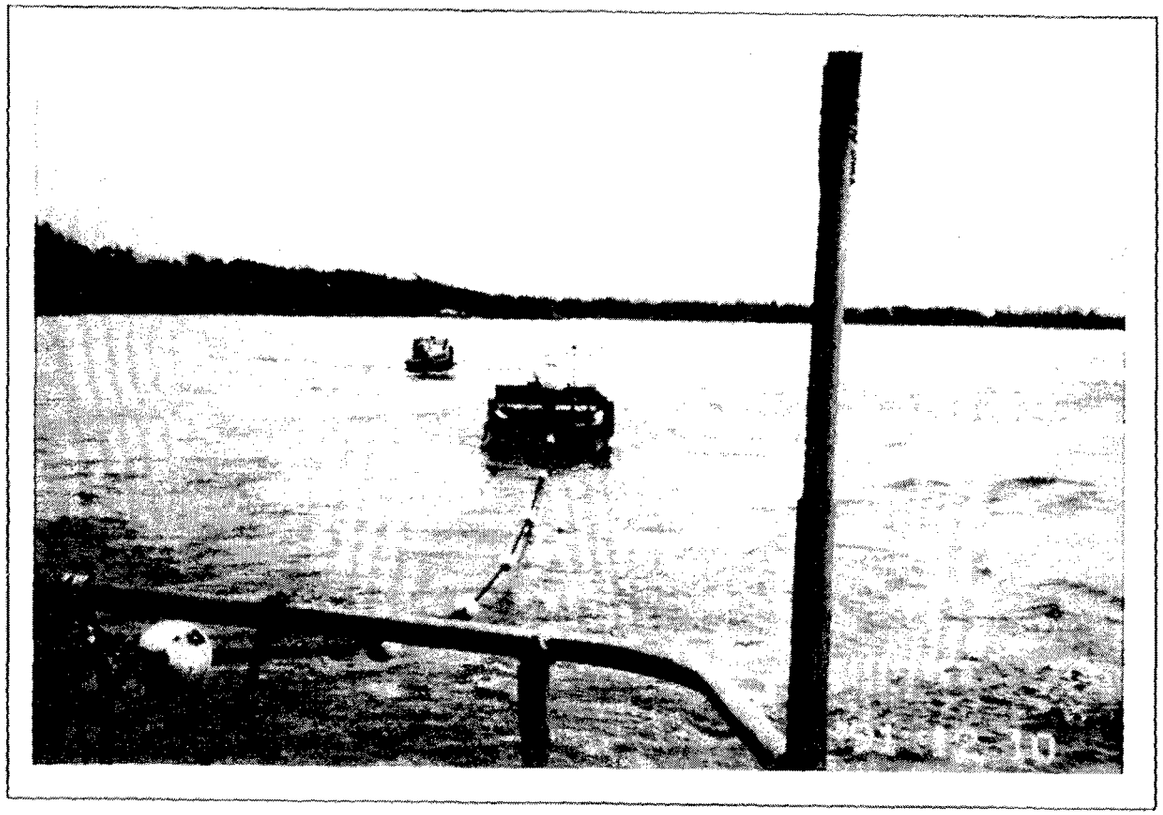

Figure 35. Waterborne FDEM system during surveying operation

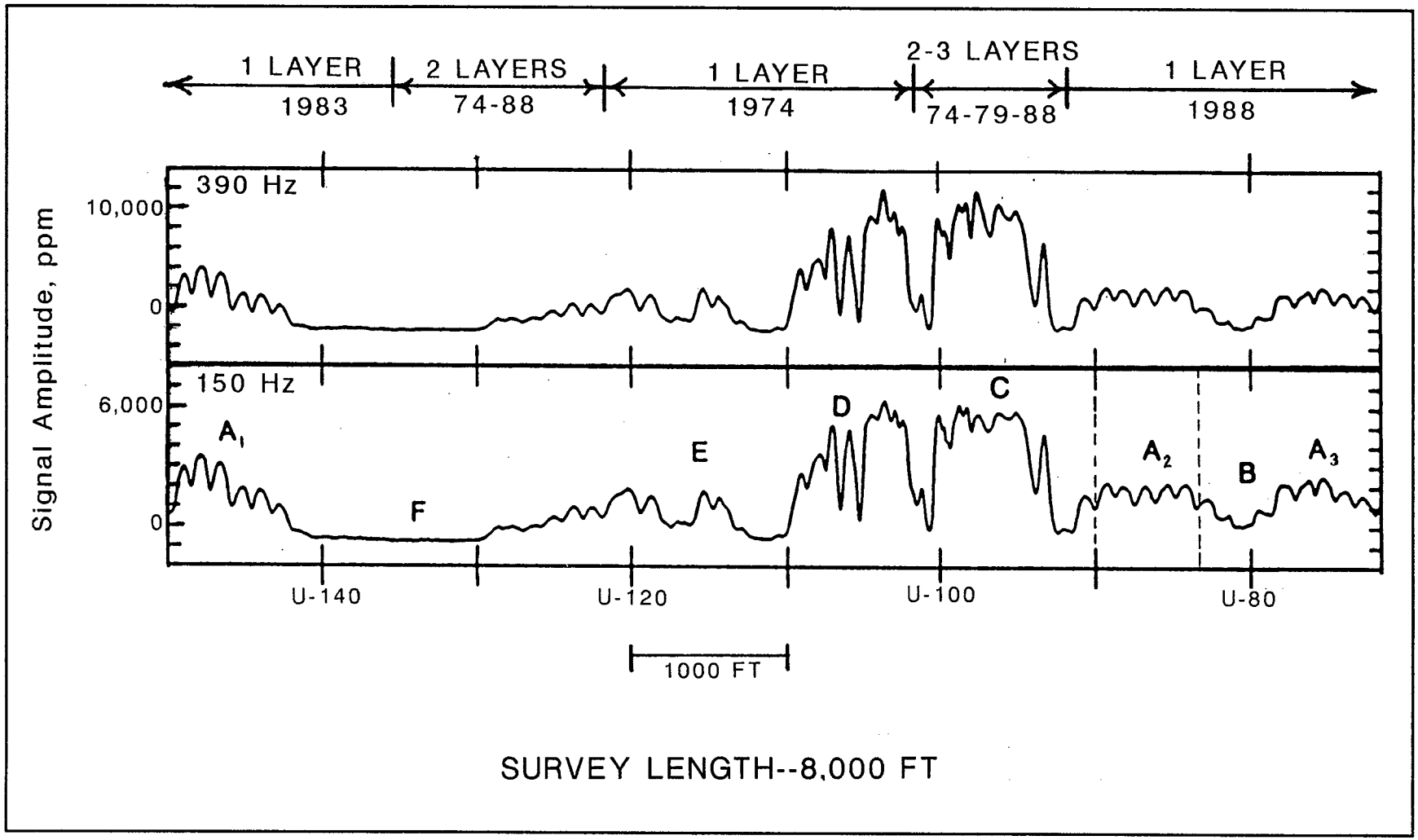

Figure 36. FDEM data collected along survey line P700, Manchac Revetment, to demonstrate potential for ACM condition assessment

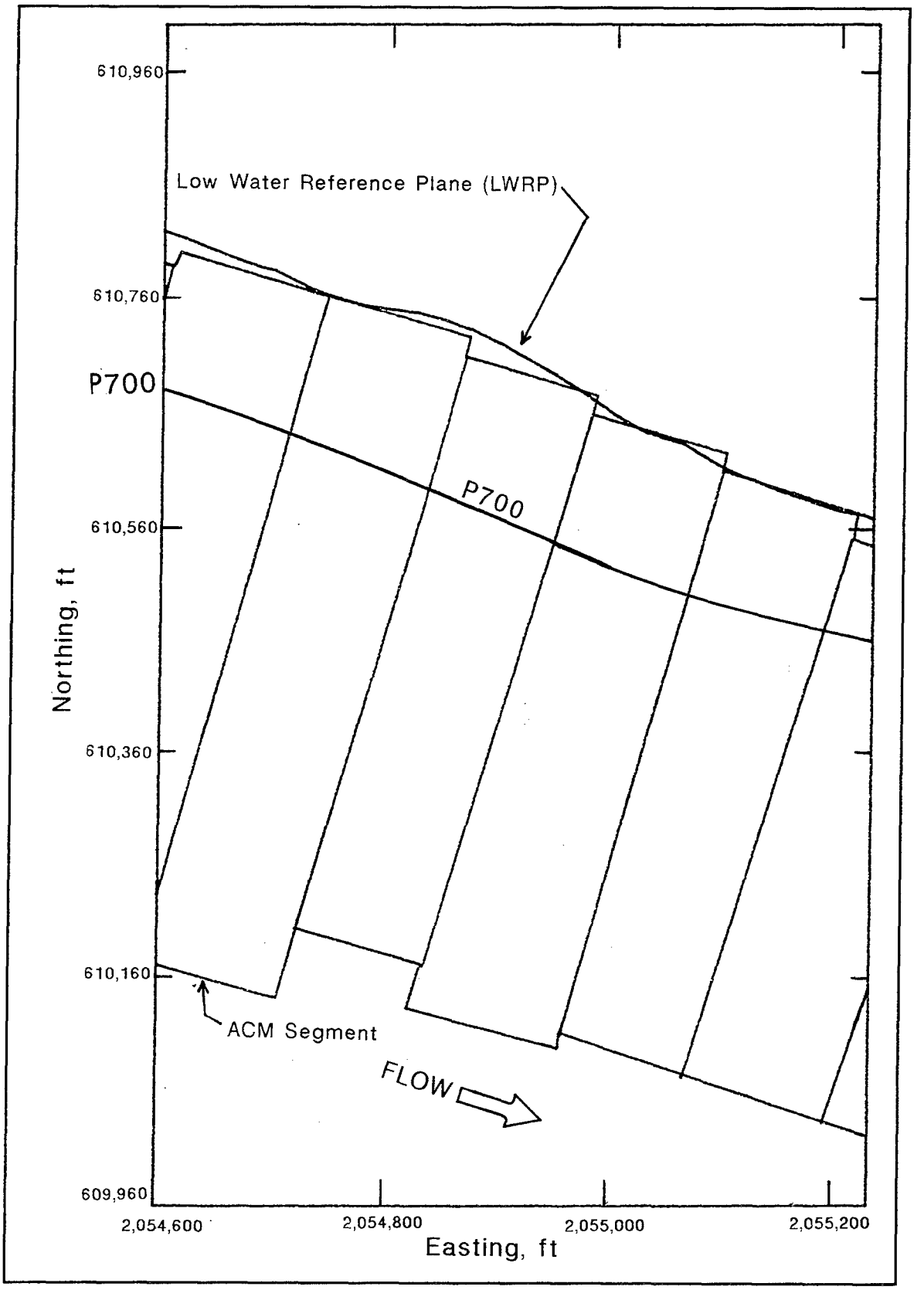

Figure 37. Plan map of ACM segments from range U-83 to U-90, Manchac Revetment (corresponds to region 'A_2' in Figure 36)

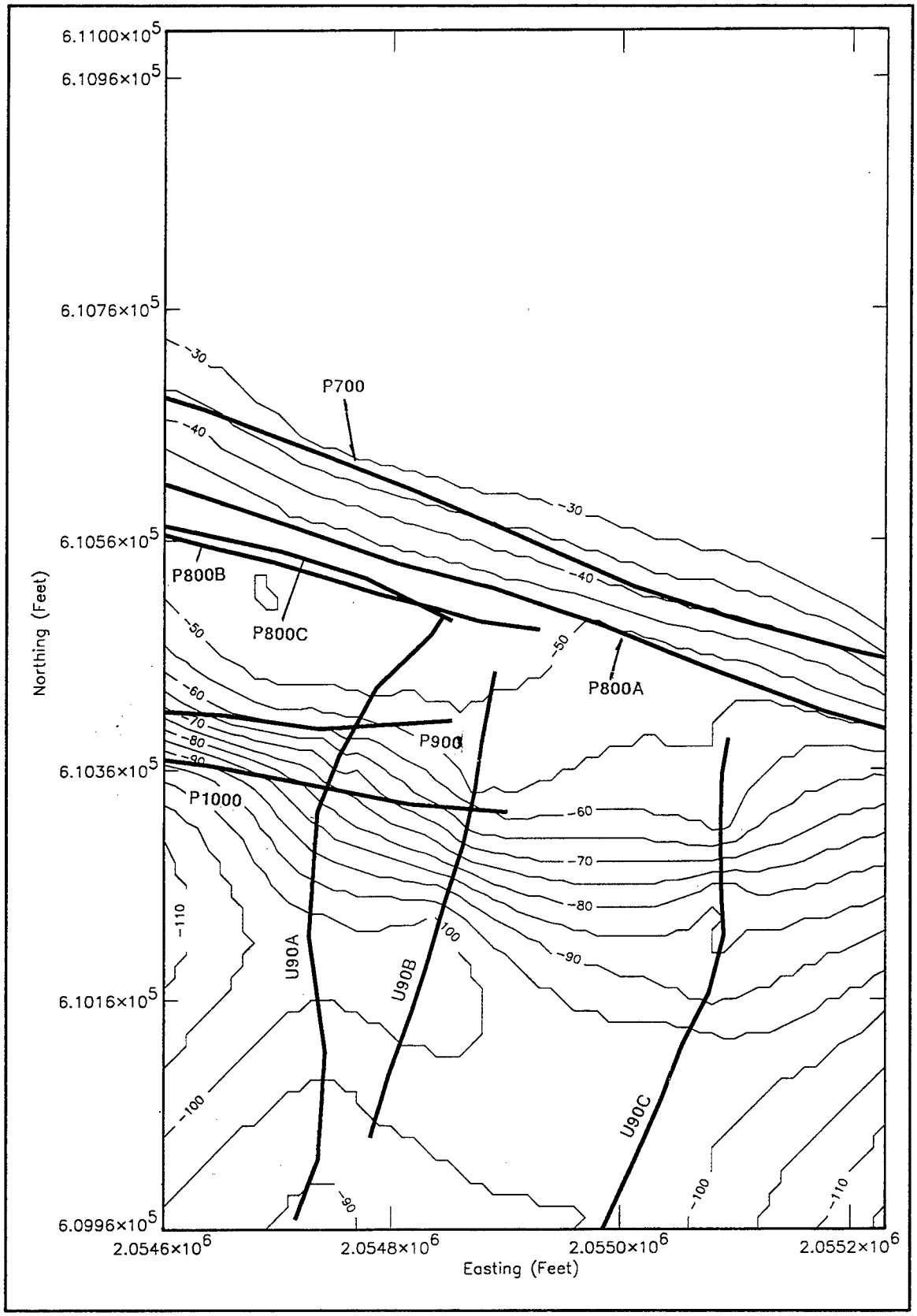

Figure 38. Location of FDEM survey lines and water depth contours for the area of Manchac Bend shown in Figure 37

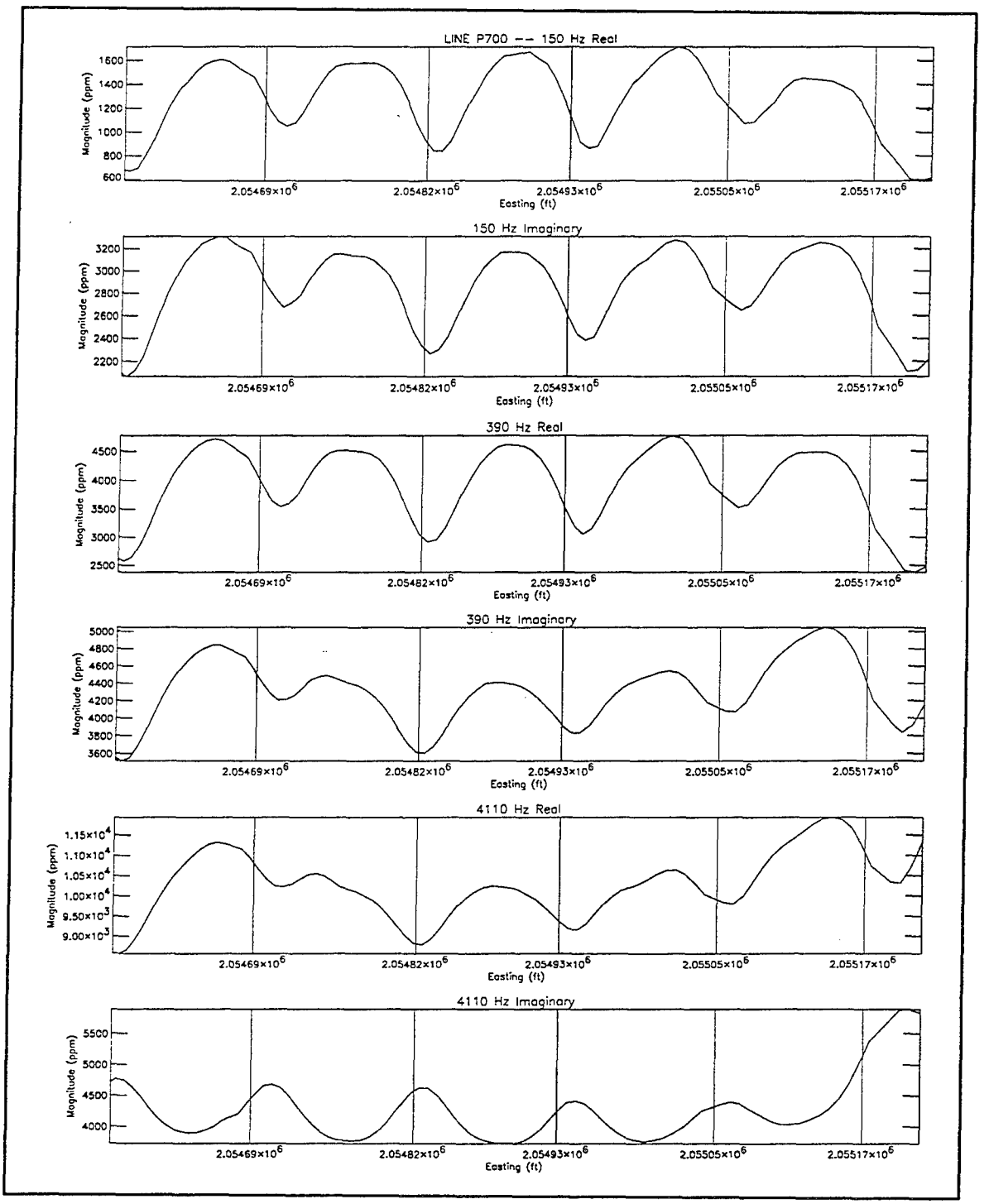

Figure 39. FDEM responses along survey line P700, Manchac Revetment (see Figure 37)

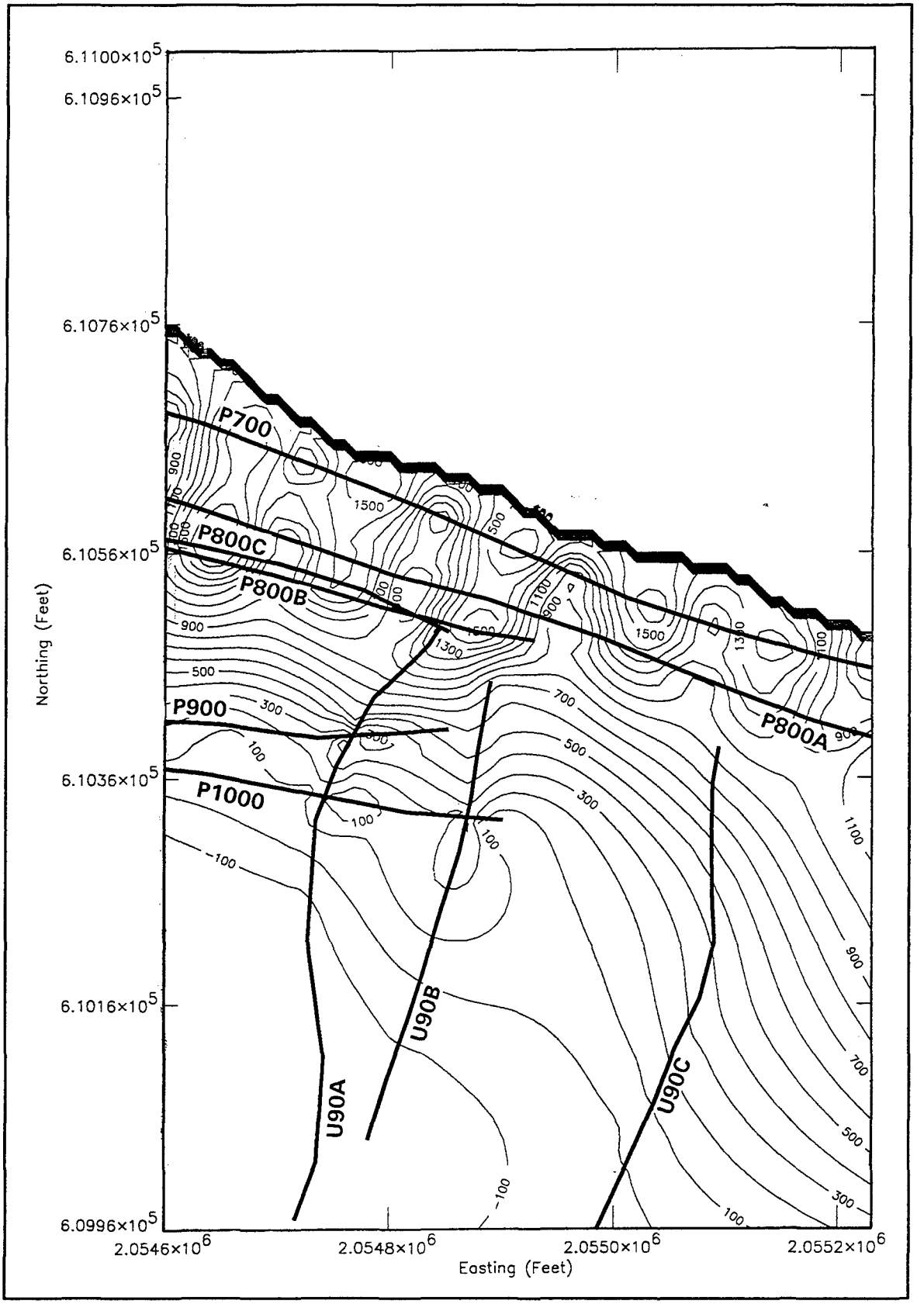

Figure 40. Contour map of real response at 150 Hz for selected area of Manchac Revetment

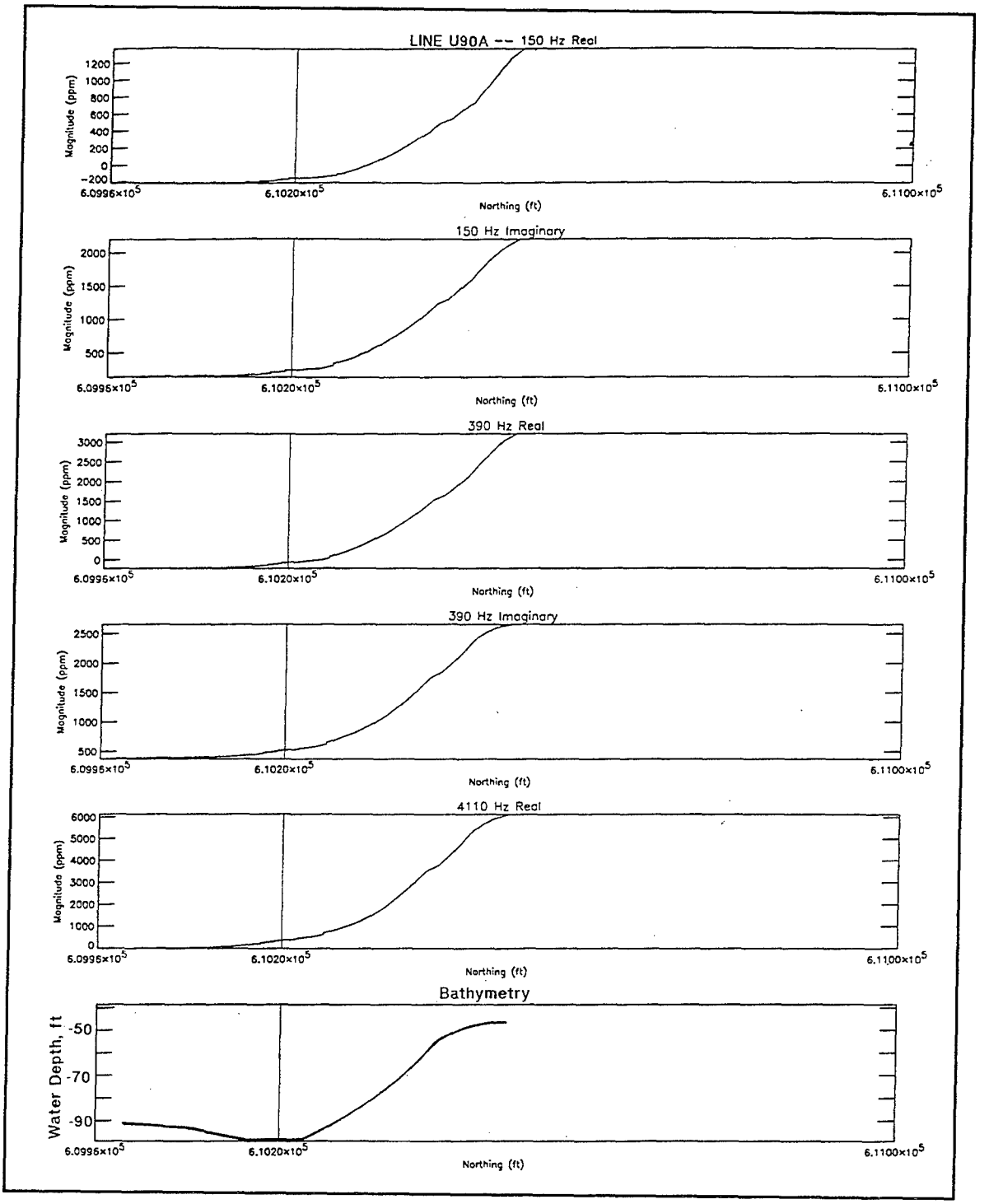

Figure 41. FDEM response for survey line U90A, Manchac Revetment

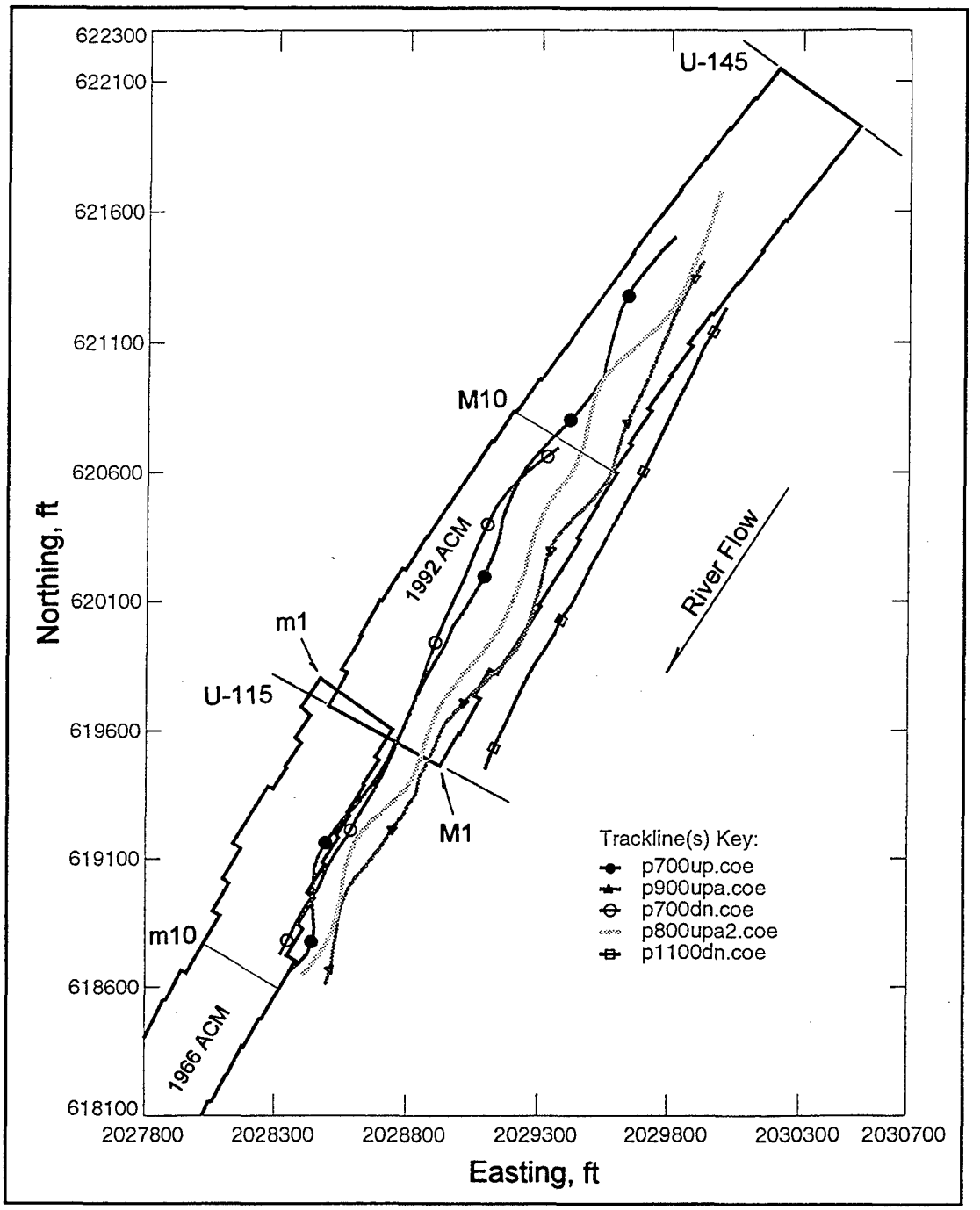

Figure 42. Location of FDEM survey lines, Missouri Bend Revetment

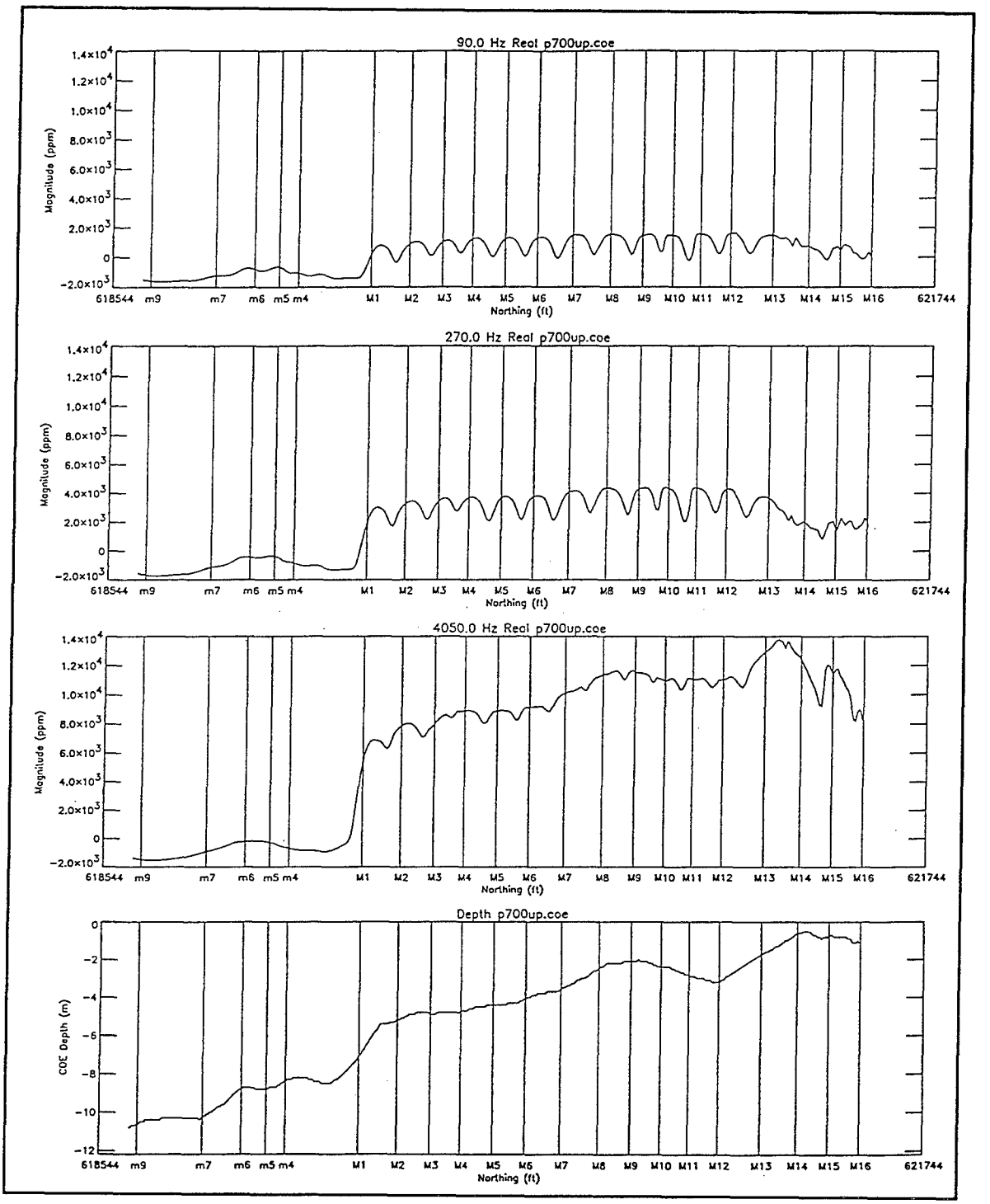

Figure 43. FDEM real responses for survey line P700, Missouri Bend Revetment

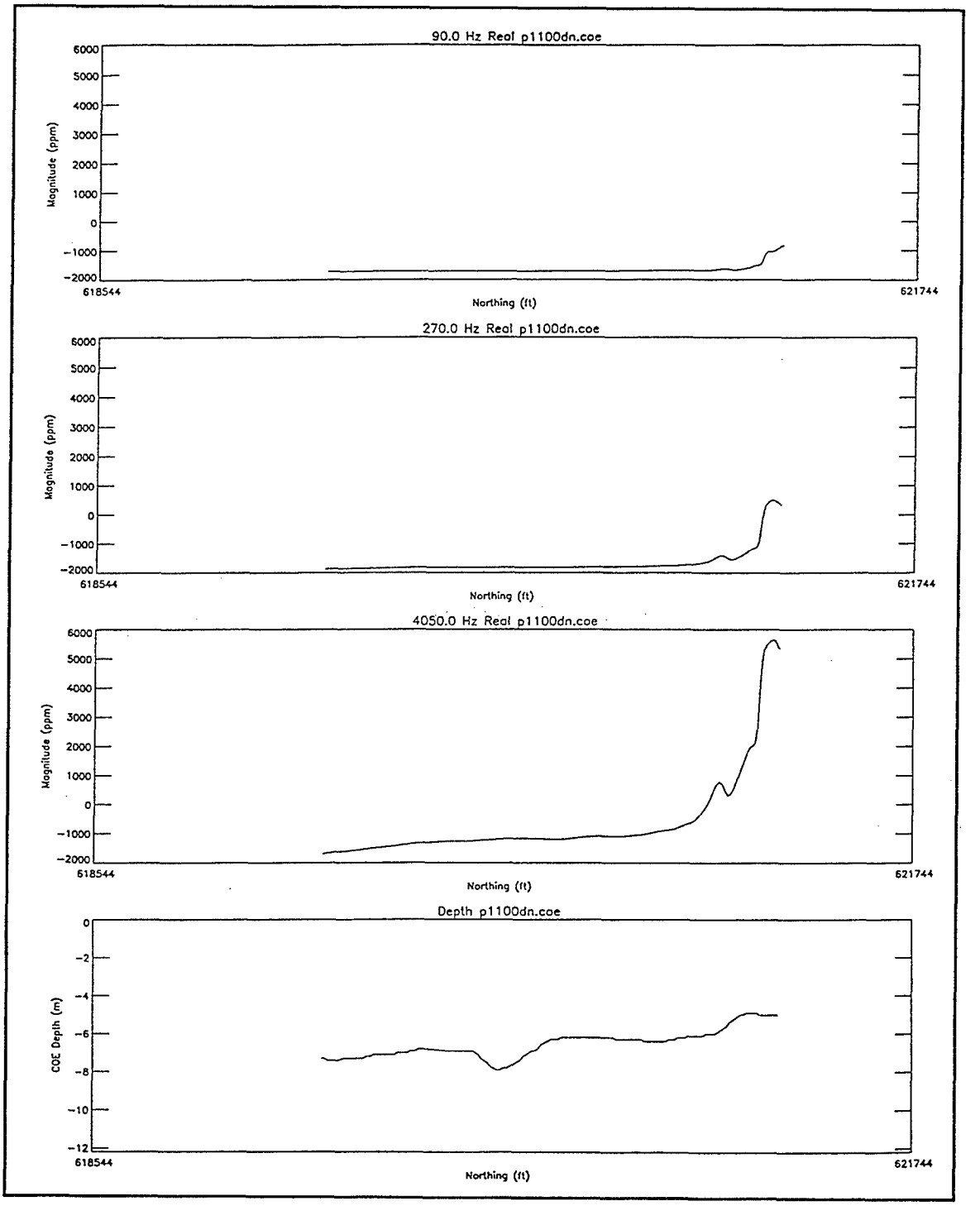

Figure 44. FDEM real responses for survey line P1100, Missouri Bend Revetment

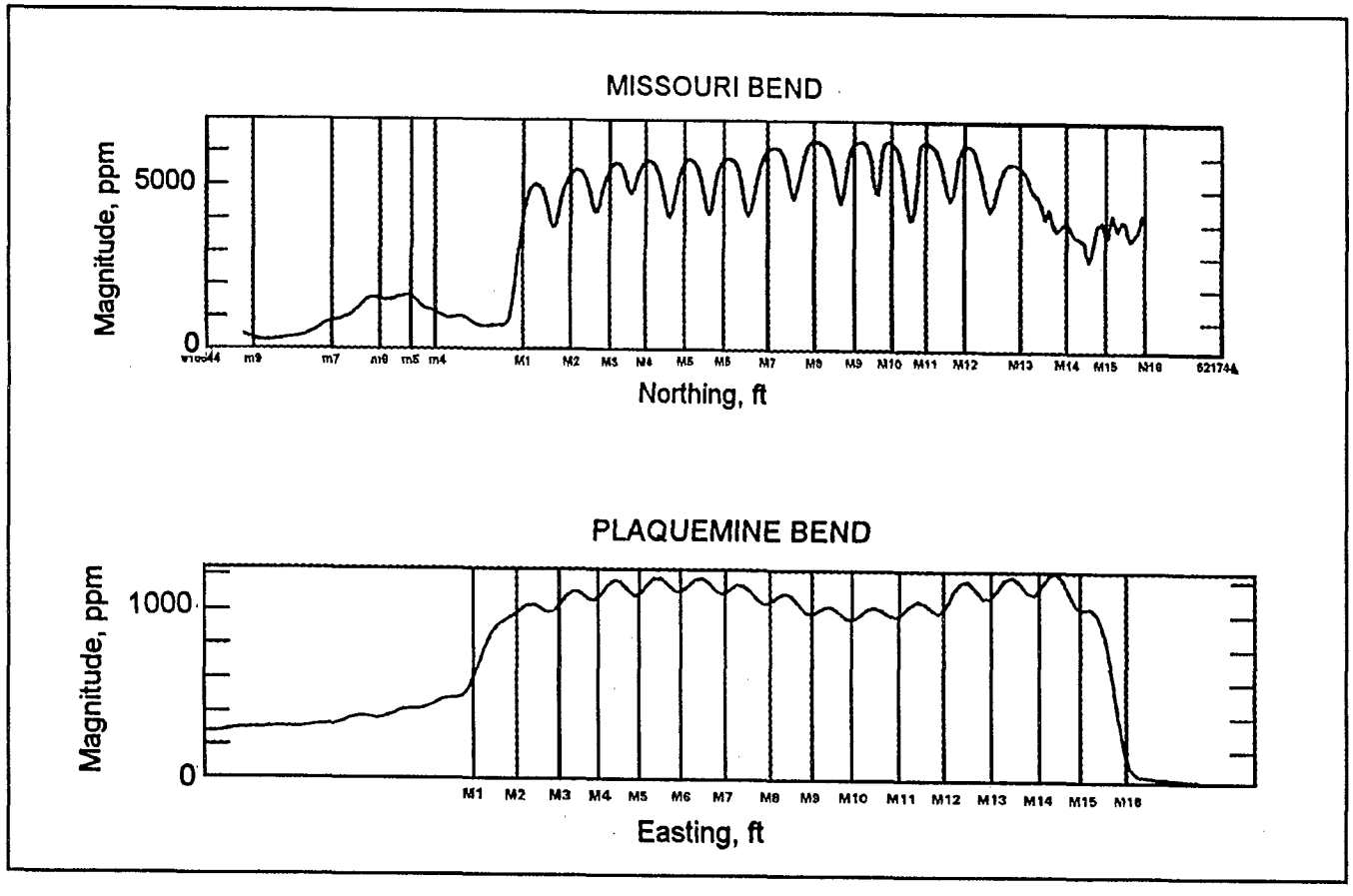

Figure 45. Comparison of waterborne (top) and airborne FDEM responses over characteristically similar ACM

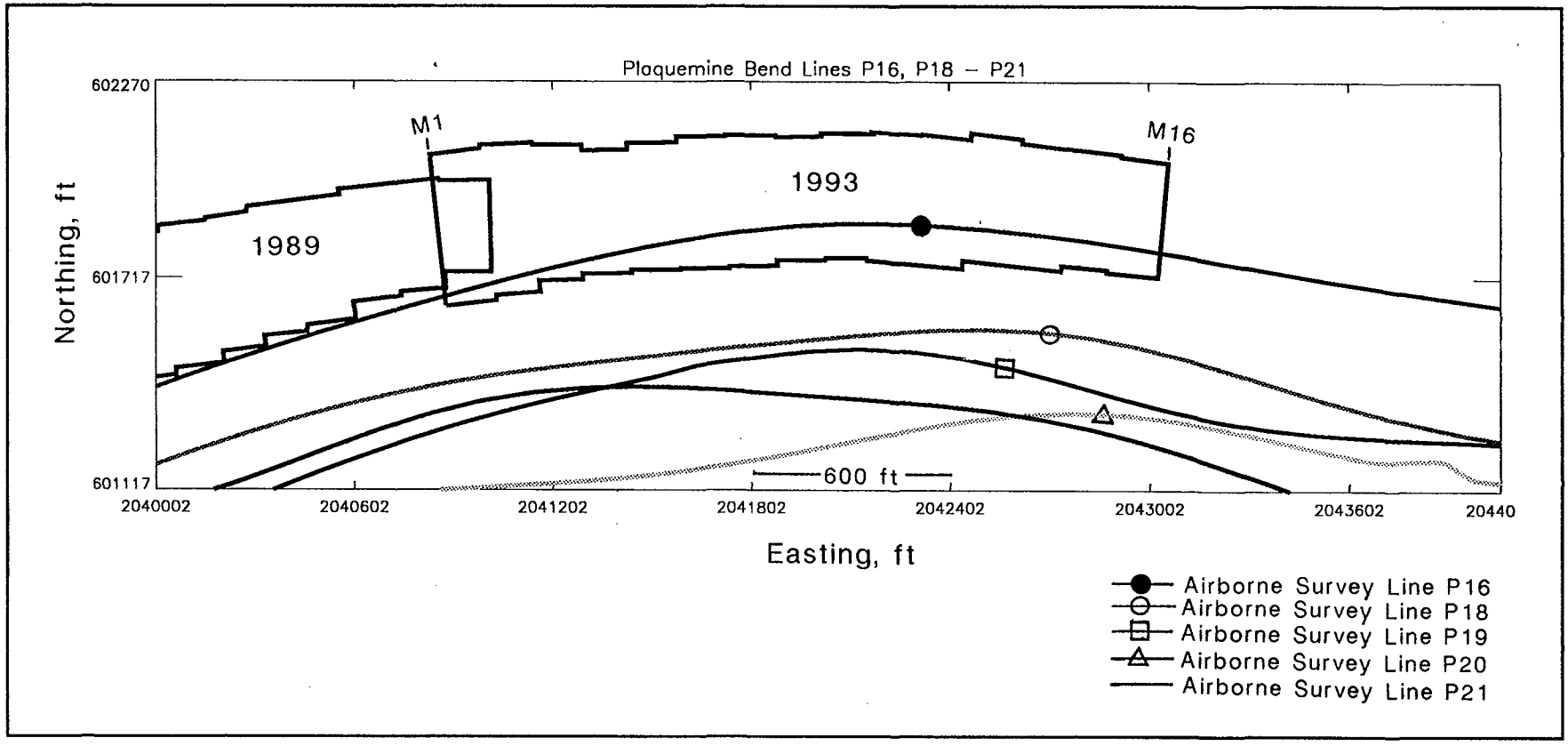

Figure 46. Location of airborne FDEM survey lines, Plaquemine Bend Revetment

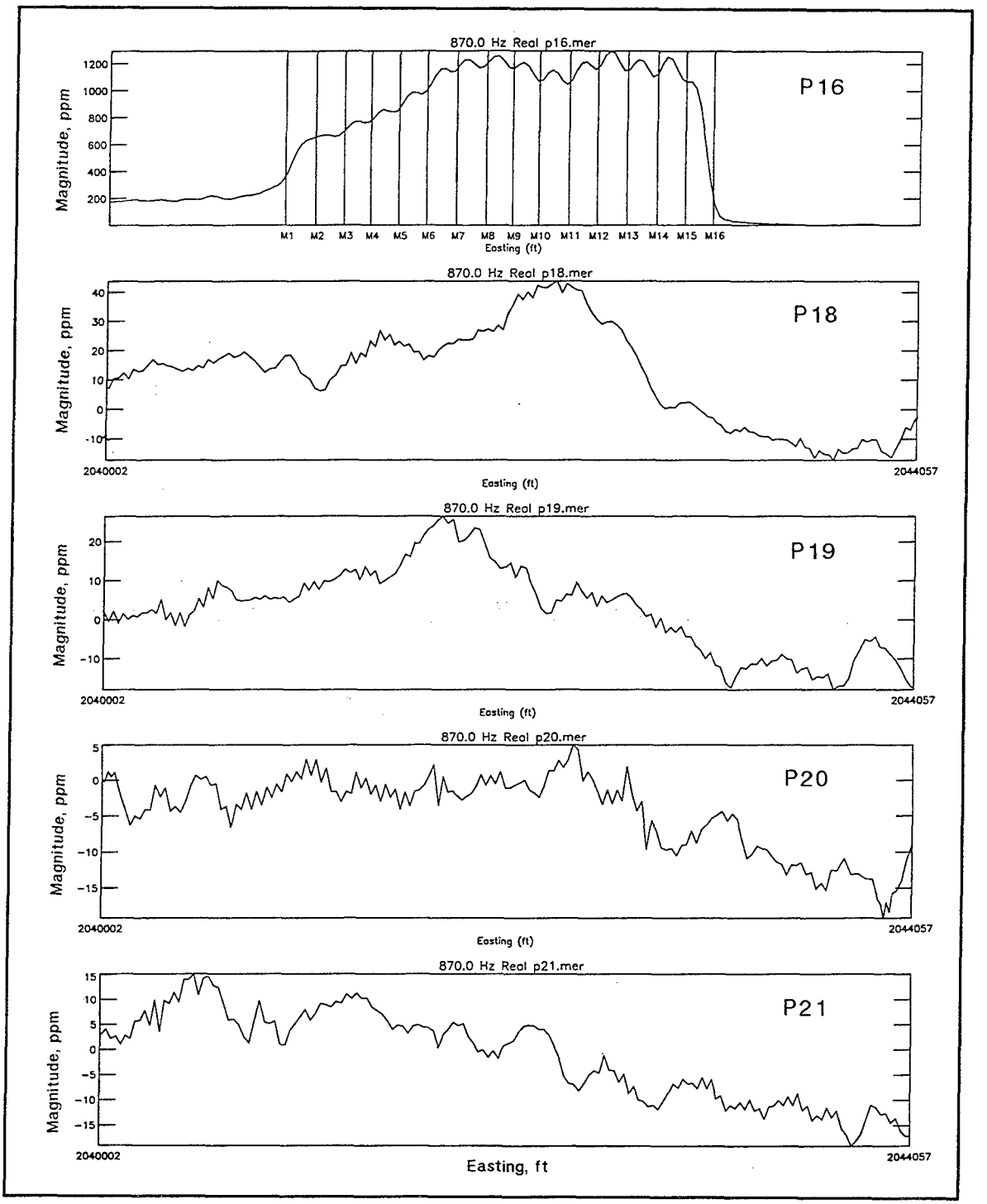

Figure 47. FDEM real responses at 870 Hz along survey lines P16 through P21, Plaquemine Bend Revetment

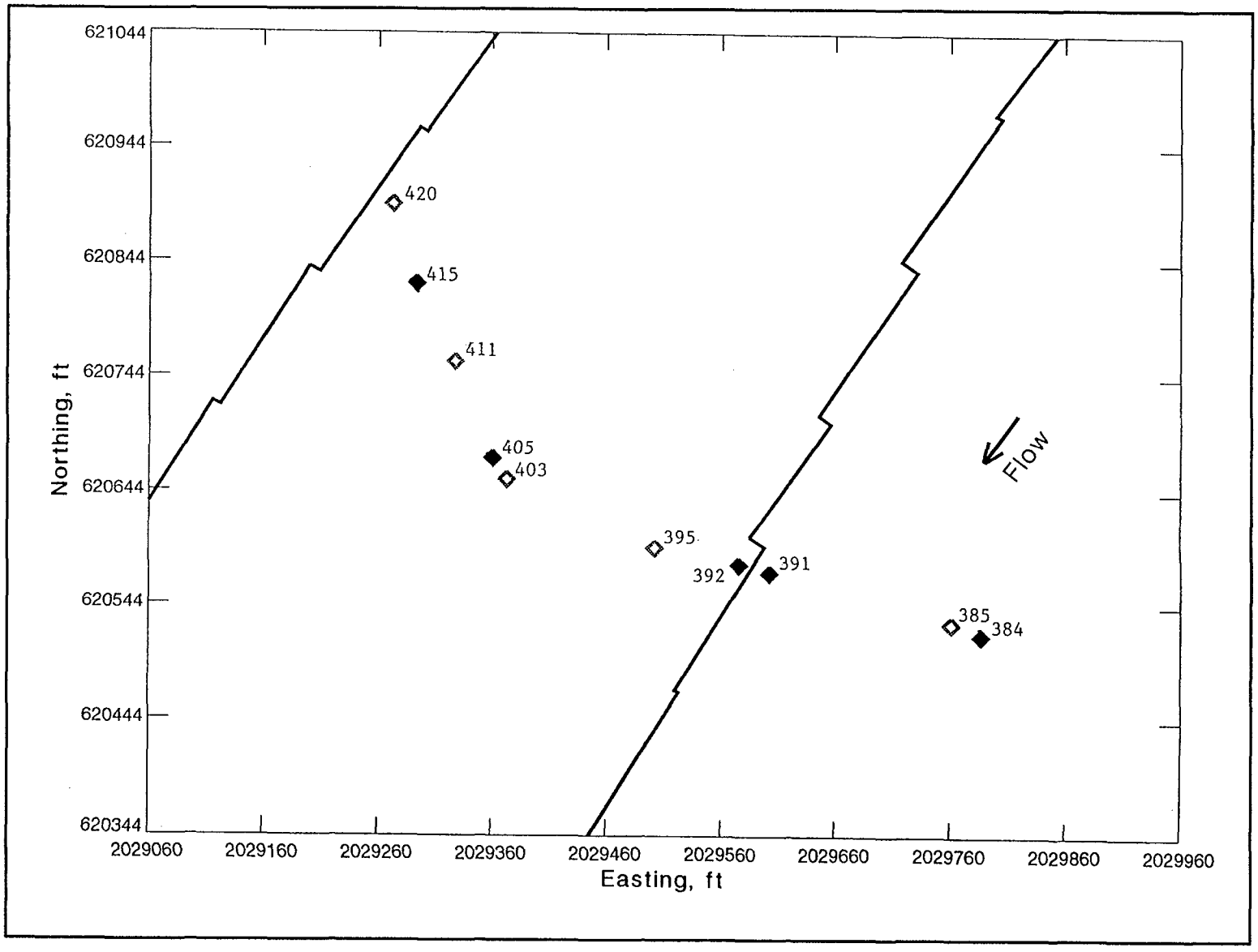

Figure 48. Selected TDEM sounding locations along range U-128, Missouri Bend Revetment

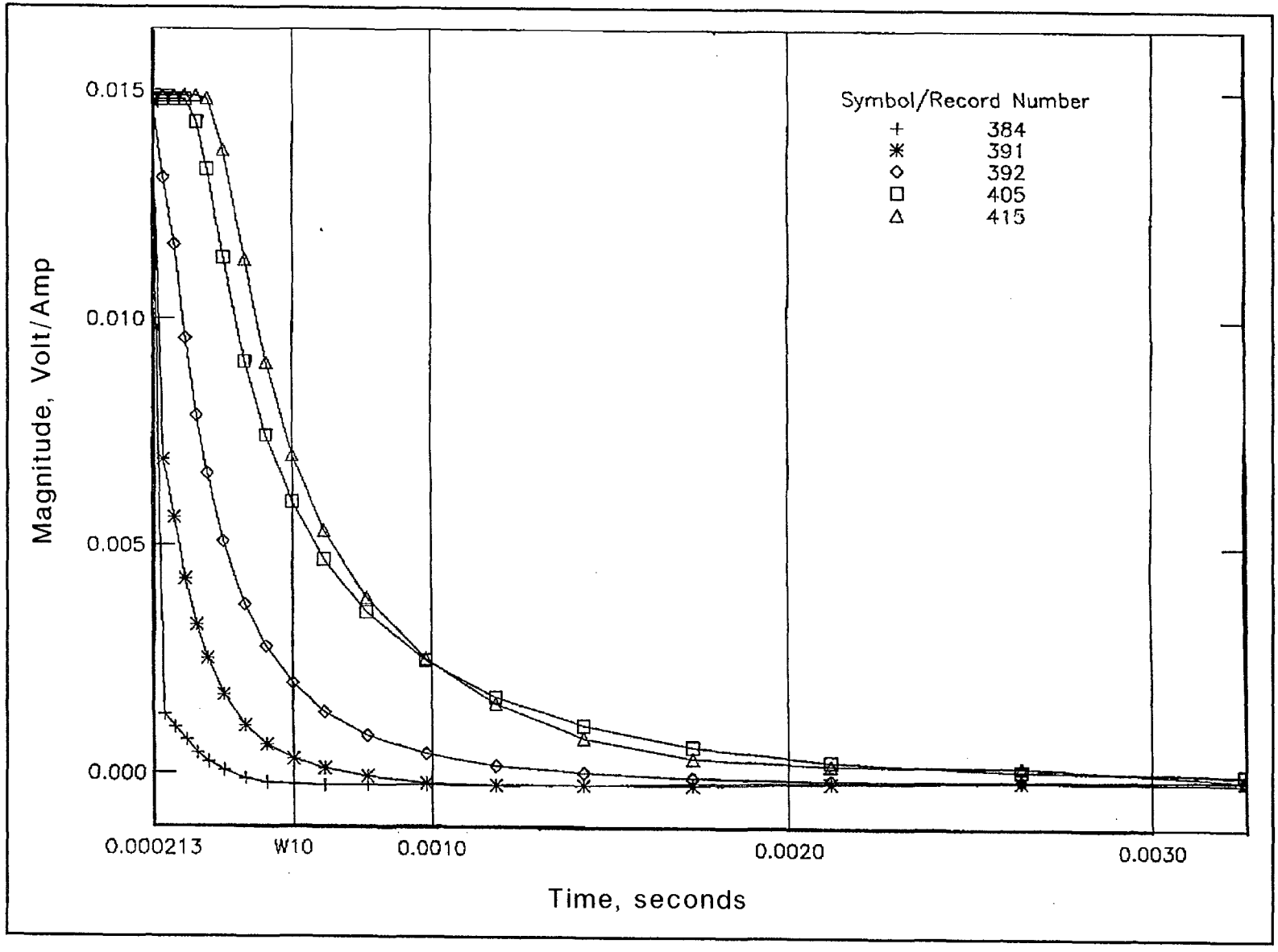

Figure 49. TDEM decay curves for five sounding locations (see Figure 48), range U-128, Missouri Bend Revetment

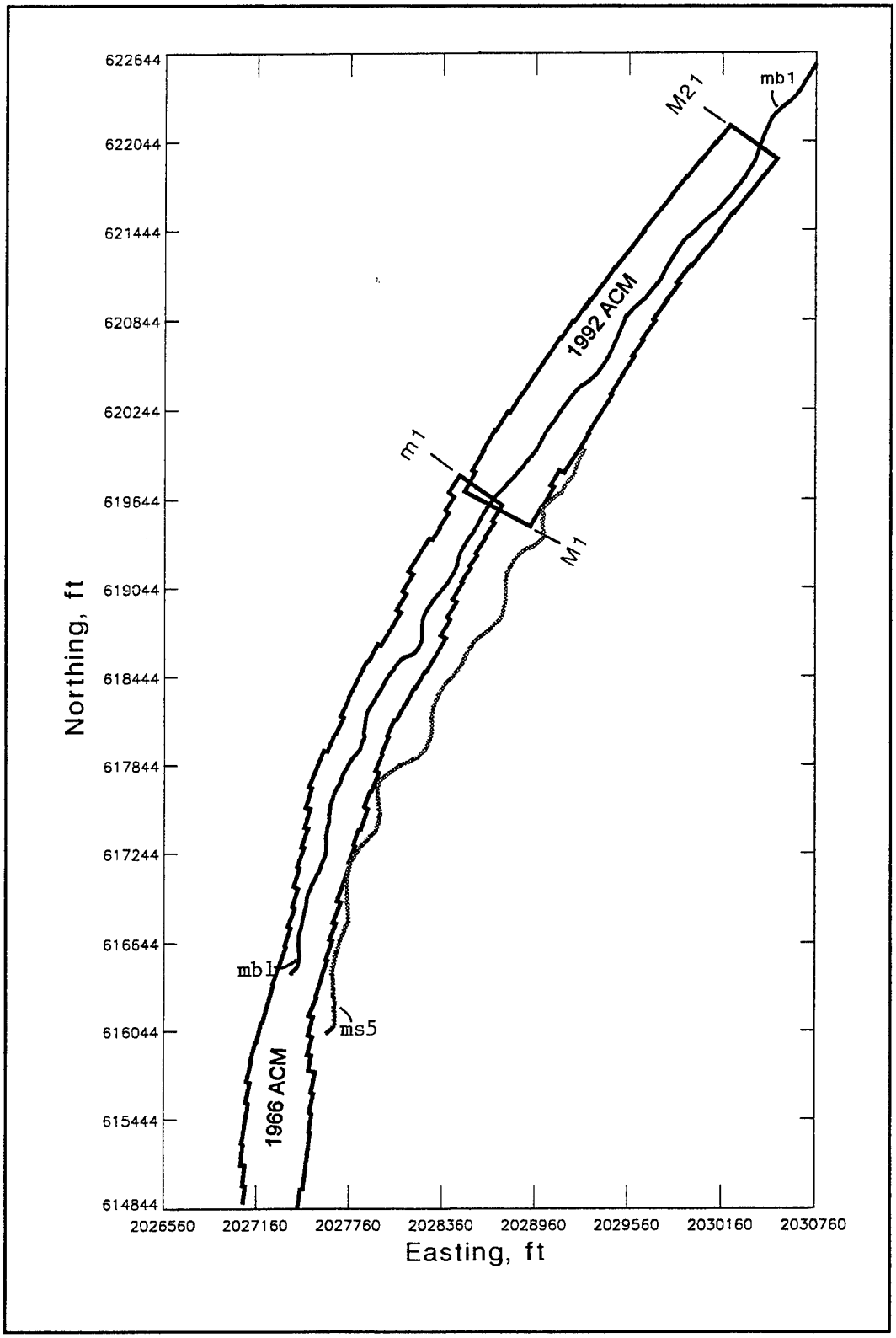

Figure 50. Location of TDEM survey lines MB1 and MS5, Missouri Bend Revetment

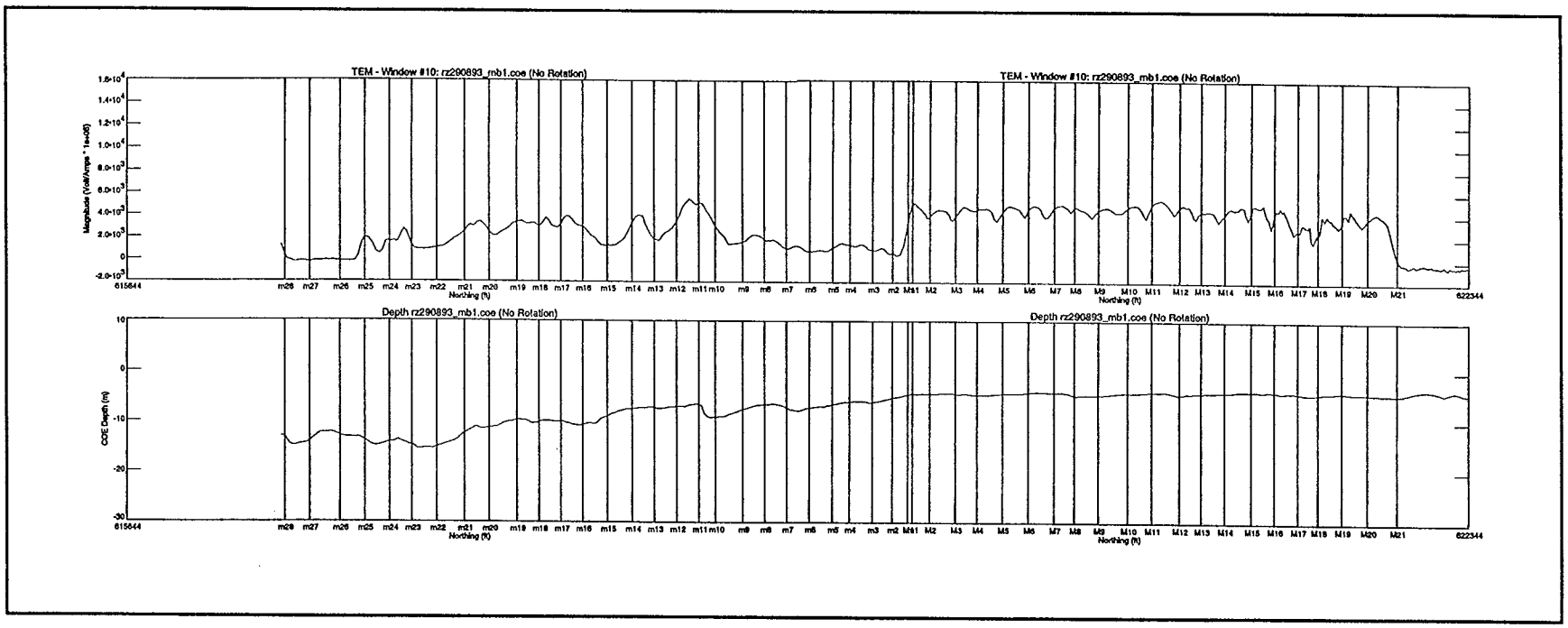

Figure 51. Measured TDEM response and water depth along survey line MB1, Missouri Bend Revetment

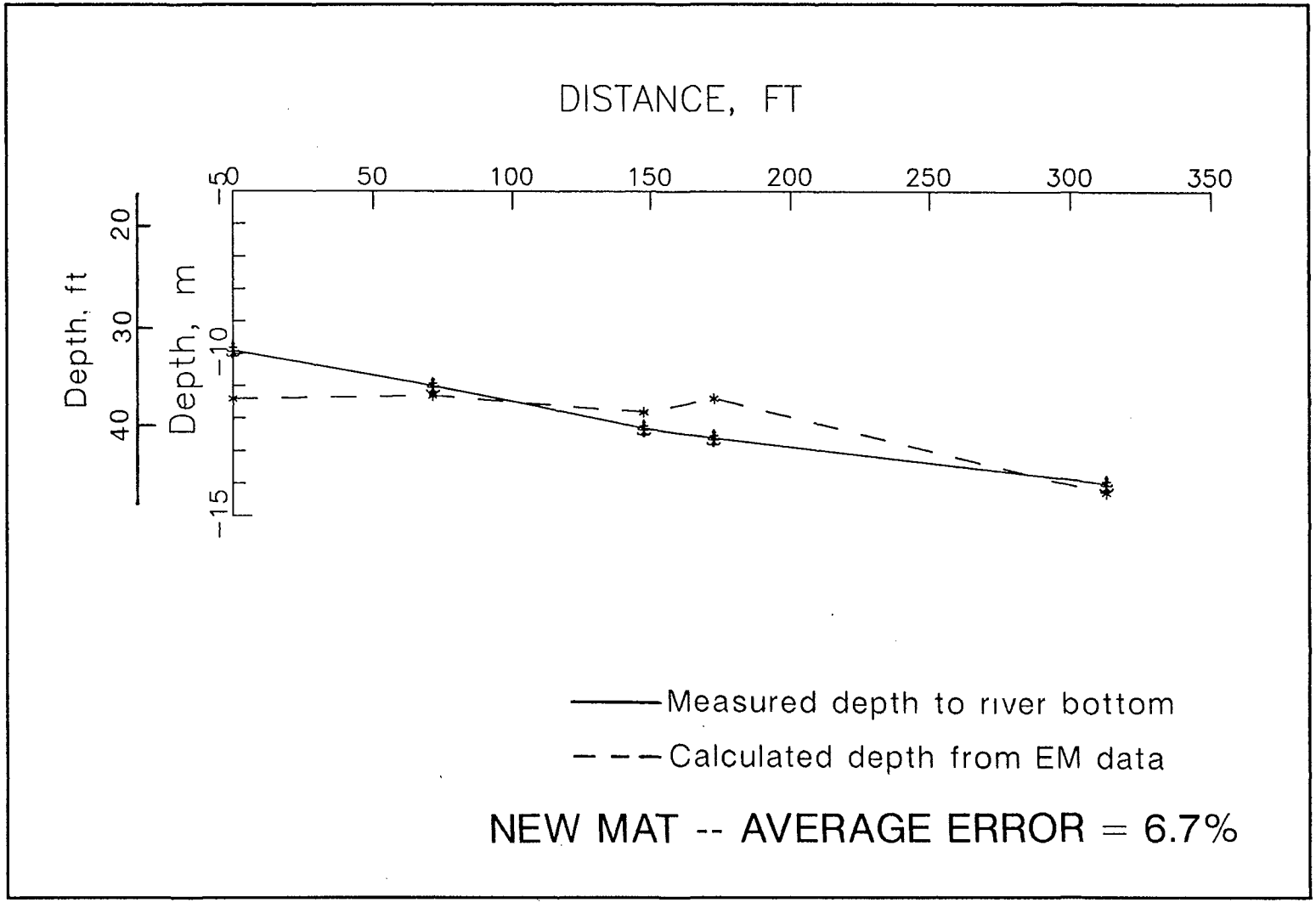

Figure 52. Computed ACM depths versus as-installed ACM depths, range U-128, Missouri Bend Revetment

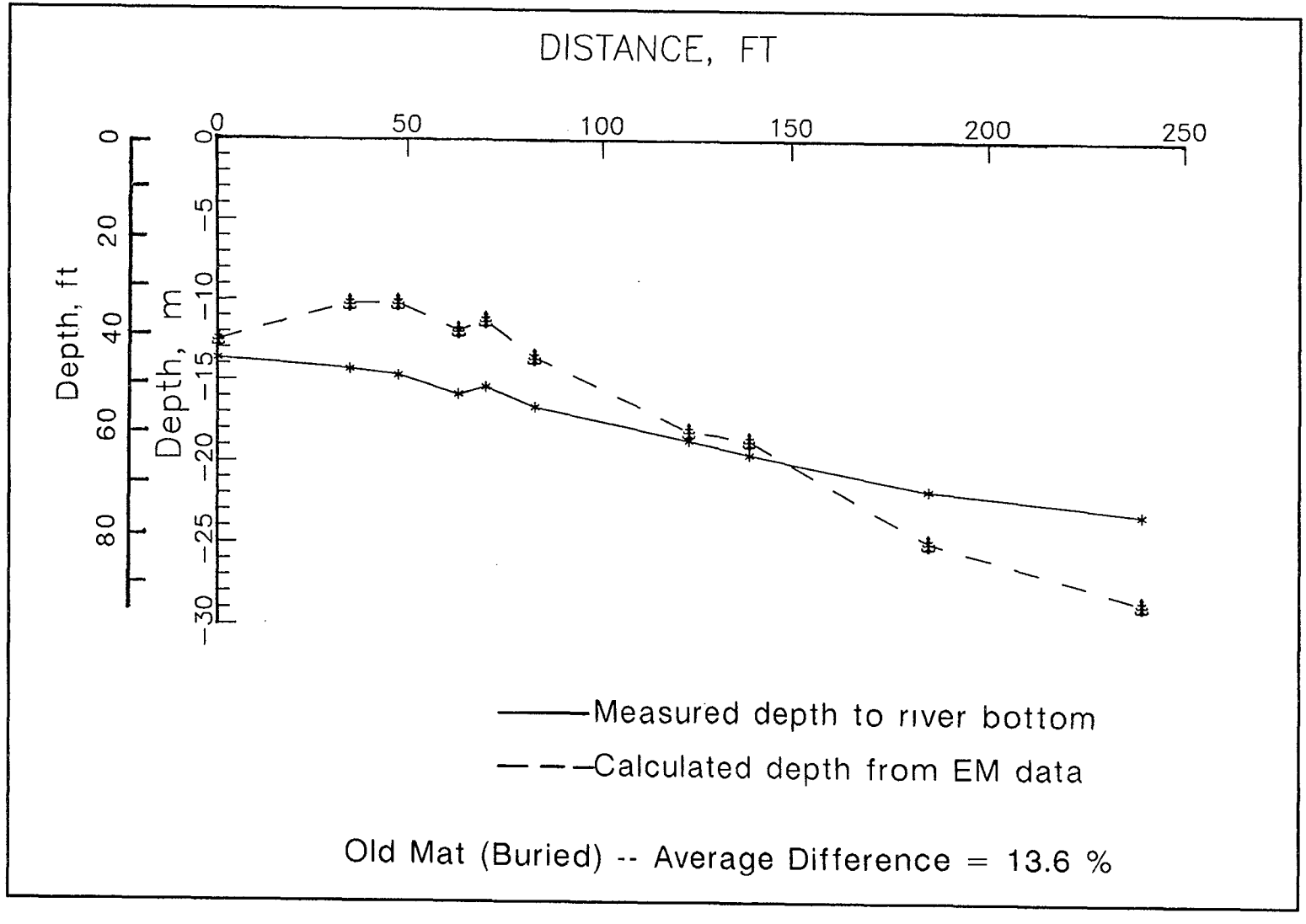

Figure 53. Computed ACM depths versus as-installed ACM depths, range U-96, Missouri Bend Revetment

Appendix A
Phase II Report - Investigation of Articulated Concrete Mattress Using Self-Potential and Resistivity Methods

PHASE II STUDY

INVESTIGATION OF ARTICULATED CONCRETE MATTRESSES USING SELF-POTENTIAL AND ELECTRICAL RESISTIVITY METHODS

Prepared for:

U.S. Army Engineer Waterways Experiment Station
ATTN: CEWES-CT-C
3909 Halls Ferry Road
Vicksburg, MS 39180-0631
Research Area GL-2 (Geophysics)

Contract No. DACW39-92-C-0112

Prepared by

Robert F. Corwin, Ph.D.
Consulting Geophysicist

SP SURVEYS
406 Sea View Drive
El Cerrito, CA 94530
(510) 527-2081

April 27, 1993

CONTENTS

page

I. INTRODUCTION 1

II. SUMMARY 1

III. DESCRIPTION OF TECHNIQUES 2

A. Self-Potential 2

B. Direct-Current Electrical Resistivity 4

1. Stationary Measurements 4

2. Towed Measurements 5

IV. RESULTS 5

A. Missouri Bend Revetment 5

1. Self-Potential 5

2. Electrical Resistivity 6

a. Stationary Measurements 6

b. Towed Measurements 7

B. Manchac Revetment 7

V. CONCLUSIONS AND RECOMMENDATIONS 9

REFERENCES 11

TABLES

FIGURES

TABLES

Table 1. SP Data Summary for Missouri Bend Revetment

Table 2. SP Data Summary for Manchac Revetment

FIGURES

1. ACM Self-Potential Mechanism and Data Profile
2. Self-Potential Measurement System
3. Measured and Calculated SP Data Profiles, Range U-89
4. Electrical Resistivity VES Field Measurement
5. Electrical Resistivity VES Data, Ranges U-158 and U-128
6. Towed Electrical Resistivity Cable Configuration

Missouri Bend Revetment

7. Mat Location from Self-Potential Data, Range U-75
7A. Measured and Calculated SP Data, Range U-75
8. Mat Location from Self-Potential Data, Range U-77
9. Mat Location from Self-Potential Data, Range U-79
10. Mat Location from Self-Potential Data, Range U-81
11. Mat Location from Self-Potential Data, Range U-83
12. Mat Location from Self-Potential Data, Range U-85
13. Mat Location from Self-Potential Data, Range U-87
14. Mat Location from Self-Potential Data, Range U-89
15. Mat Location from Self-Potential Data, Range U-90
16. Mat Location from Self-Potential Data, Range U-91
17. Mat Location from Self-Potential Data, Range U-93
18. Mat Location from Self-Potential Data, Range U-95
18A. Measured and Calculated SP Data, Range U-95
19. Mat Location from Self-Potential Data, Range U-100
20. Mat Location from Self-Potential Data, Range U-105
21. Mat Location from Self-Potential Data, Range U-110
22. Mat Location from Self-Potential Data, Range U-120
23. Mat Location from Self-Potential Data, Range U-122
23A. Measured and Calculated SP Data, Range U-122
24. Mat Location from Self-Potential Data, Range U-124
25. Mat Depths from Resistivity Soundings, Range U-128
26. Mat Depths from Resistivity Soundings, Range U-95
27. Mat Depths from Resistivity Soundings, Range U-112
28. Sample Towed Resistivity Data, Old Mat - New Mat Transition Area
29. Mat Depth Profile Interpreted from Towed Resistivity Data, Old Mat - New Mat Transition Area
30. Mat Depth Profile Interpreted from Towed Resistivity Data, Ranges U-93 - U-104.5
31A. Map of Mat Locations, Missouri Bend Ranges U-75 - U-89
31B. Map of Mat Locations, Missouri Bend Ranges U-90 - U-105
31C. Map of Mat Locations, Missouri Bend Ranges U-110 - U-124

32. Self-Potential Data and Mat Location, Range U-110
33. Self-Potential Data and Mat Location, Range U-111
34. Self-Potential Data and Mat Location, Range U-112
35. Self-Potential Data and Mat Location, Range U-114
36. Self-Potential Data and Mat Location, Range U-116
37. Self-Potential Data and Mat Location, Range U-118
38. Self-Potential Data and Mat Location, Range U-120
39. Self-Potential Data and Mat Location, Range U-124
40. Self-Potential Data and Mat Location, Range U-126
41. Self-Potential Data and Mat Location, Range U-128
42. Self-Potential Data and Mat Location, Range U-130
43A. Map of Mat Locations, Manchac Ranges U-110 - U-118
43B. Map of Mat Locations, Manchac Ranges U-120 - U-130
44. Self-Potential Data and Mat Location, Range U-166
45. Self-Potential Data and Mat Location, Range U-170
46. Self-Potential Data and Mat Location, Range U-176
47. Self-Potential Data Detail, Range U-176
48. Map of Mat Locations, Manchac Ranges U-166 - U-176

I. INTRODUCTION

This report presents the results of the Phase II study of the use of self-potential (SP) and towed direct-current electrical resistivity (TDC) methods for investigation of articulated concrete mattresses (ACM). Field measurements were conducted between 27 October and 3 November 1992 at the Missouri Bend and Manchac revetment sites near Baton Rouge, LA. The survey vessel "Mary Evans" and the differential GPS positioning information were provided by DIMCO, Inc. of Vicksburg, MS. River elevation during the survey period was about +8 ft.

II. SUMMARY

SP profiles were conducted in the region between ranges U-75 and U-124 at the Missouri Bend site. SP profiles at the Manchac site were conducted between ranges U-110 and U-130 and between ranges U-160 and U-180. TDC data were taken only at the Missouri Bend site. The SP profiles were run approximately along the range lines, perpendicular to the mat and the shoreline, using an electrode dipole towed behind or alongside the survey vessel. The SP data were of generally good quality, and could be interpreted with reasonable confidence using standard SP modeling techniques incorporated into a computer program developed for this application.

The region between ranges U-75 and U-124 at the Missouri Bend site encompassed a variety of mat conditions, with the mat lying on or just beneath the river bed in some areas and deeply buried in other areas. Three profiles (ranges U-120, U-122, and U-124) were run above a new mat section that had been installed just a few days before the measurements, and one profile (at about range U-154) was run in an area where no mat was present.

The SP profile run in the area where no mat was present shows only background variations. The three SP profiles run over the new mat give mat depths corresponding to the riverbed depth. SP profiles in the southern portion of the surveyed area (ranges U-75 through U-87) indicate that the mat is buried at relatively shallow depths in this area, with the outer end of the mat a few feet to about 60 ft beneath the river bed. A much different situation is observed between ranges U-89 and U-110. The mat in this area appears to plunge down steeply from the shoreline, at angles exceeding 70 degrees at some locations. The outer end of the mat in these areas is as much as 250 ft beneath the river bed, at water depths of only about 40 ft.

SP profiles at the Manchac site were run in an area of single to double mat transition (ranges U-110 - U-130) and in an area where the river bank had encroached on the mat (ranges U-160 - U-180). The SP data from ranges U-110 - U-130 indicated that the older mat between ranges U-110 and U-120 and the overlying newer mat between ranges U-124 and U-130 are close to as-installed locations and are not deeply buried. The transition area between

single and double mats (U-121 to U-123) produced erratic SP data that will require additional "ground truth" data for confident interpretation. The SP data from Manchac ranges U-160 to U-180 clearly indicated that the location of the outer end of the mat in this area is very close to the as-installed position, but that the depth of burial of the outer end of the mat increases from about 20 ft to about 60 ft with increasing degree of shoreline encroachment.

Two types of DC resistivity measurements were conducted at the Missouri Bend site. Vertical electric sounding (VES) readings were taken with the vessel stationary and the electrode cable (which incorporated 11 electrode pairs) extending downstream of the vessel. The VES data were interpreted to give the depths of the water column, riverbed sediments, and mat at a point beneath the center of the cable. Towed DC (TDC) resistivity readings were taken with the vessel underway, using only a single electrode pair. The TDC data were interpreted to give a rough estimate of the mat depth along the survey line.

Stationary VES measurements were taken at four locations. At range U-158, where no mat was installed, only the water and two riverbed sediment layers were seen in the interpreted VES data. Three measurements were conducted at range U-128, above the new mat. Results of these soundings clearly show a thin, highly conductive layer, corresponding to the metal fabric of the mat, at depths corresponding to that of the river bed. Two measurements were conducted at range U-112, in water depths of about 12 to 16 ft. Similar to the SP results at range U-110, the VES data indicate that the mat plunges steeply downward in this area, and is about 40 to 60 ft beneath the river bed at these relatively shallow water depths. Three VES measurements were taken at range U-95, in water depths of about 20 to 30 ft. The VES data indicate that the mat is located at or just beneath the river bed at these depths (the SP data at this site also indicate that the mat is shallow at this depth, but plunges steeply downward slightly further offshore).

Three sets of towed resistivity measurements were made along the 20-ft water depth contour. The estimated mat depths interpreted from these measurements were in reasonable agreement with those obtained from the SP and VES data, and indicated that towed DC resistivity measurements are feasible for this application.

III. DESCRIPTION OF TECHNIQUES

A. Self-Potential

Self-potential (SP) signals are generated when the metal fabric of an ACM interacts with changes in the oxygen content of the sediment or water in contact with the fabric (Sato and Mooney, 1960). These oxygen content variations cause an electric current to flow through the fabric, so that the fabric acts essentially as a buried battery. The corresponding return current through the

river water above the fabric (see the upper sketch on Figure 1) generates the observed SP signal at the surface of the water.

The (+) and (-) signs indicate line current sources perpendicular to the plane of the paper that are equivalent to "terminals" of the "battery" described above. The outer end of the ACM usually acts as the positive source line and generates the broad positive variation seen at the right side of the typical data profile shown on the lower portion of Figure 1. The negative source line generates the large negative variation in the center of the profile and the positive at the left end of the profile.

The negative source line may be located at the upper end of the ACM, at the shoreline, or at a point along the ACM where the oxygen content varies strongly (for example, where the ACM emerges from the river bed into the river water). Thus the depth and location of the upper source line will always correspond to those of the ACM at that point, but that point is not necessarily the location of the upper (inshore) end of the ACM. More complex signals, indicating multiple source lines, were observed in areas where the ACM was relatively shallow and the mat was buried at varying depths, or was alternately buried and exposed. Again, each of the interpreted source lines corresponds to a point on the ACM.

SP signals were measured by towing a pair (dipole) of electrodes along the water surface and recording the voltage between the electrode pair. In addition to the towed cable arrangement shown on Figure 2, a side-mounted electrode array also was used. In this arrangement, the electrodes were suspended from booms extending about 10 ft to the starboard side of the boat from the bow and stern (a separation of 25 ft).

The measurement system used for this work is shown on Figure 2. A Fluke model 45 digital multimeter with an RS-232 interface digitized the signal and transmitted the SP voltage to a computer for storage in a file that included the time of the measurement. The SP data file then was combined with a corresponding navigation file that included measurement time, vessel location, and water depth. Backup hard-copy SP records were obtained on a strip chart recorder.

Interpretation of ACM SP data is done by comparing the measured SP profile with a calculated profile using assumed source line depths and locations. The equation used for the line source calculation is given by Rao et al. (1970), and a computer algorithm based on this equation is described by Corwin and Butler (1989). For the ACM interpretation, the source lines were assumed to be parallel to the ACM, the line half-length was fixed at 1000 ft (essentially infinity), and the survey track lines were assumed to be centered over the source lines.

The depths, locations, and intensities of the source lines were varied until a reasonable fit was obtained between the measured and calculated profiles. Figure 3 shows measured and calculated SP data profiles for Missouri Bend range U-89, printed directly

from the computer program used for SP modeling and interpretation. Figures 14 and 31A show the corresponding mat location. Figures 7A, 18A, and 23A also show examples of measured and calculated data profiles for the Missouri Bend site, and Figures 32 - 47 show measured and calculated SP profiles for the Manchac site.

B. Direct-Current Electrical Resistivity

1. Stationary Measurements

The electrical resistivity (resistance to electric current flow) of metals is several orders of magnitude lower than that of water or soil. This infers that the metal fabric of an ACM should have a much lower electrical resistivity than the surrounding water or riverbed sediments, and that a technique that can determine the depth to such a low-resistivity target could be used for ACM investigations.

The direct-current (DC) vertical electric sounding (VES) resistivity technique is widely used for the determination of subsurface resistivity structure (Department of the Army, Corps of Engineers, 1979; Telford et al., 1976). An onshore VES is conducted by injecting electric current (I) into a pair of grounded metal stakes (current electrodes) and measuring the resultant voltage (V) at the surface using a second (potential) electrode pair (see Figure 4). An "apparent resistivity" value for the measurement (expressed in ohm-meters) is calculated by multiplying the ratio (V/I) by a geometric factor that depends on the electrode configuration and on the separation of the current electrodes (AB) and of the potential electrodes (MN).

By expanding the distance AB between the current electrodes, current is forced to flow more deeply into the earth, and resistivity information is obtained from increasing depths. The measured apparent resistivity values are plotted against the electrode separation on log-log axes (see Figure 5), and the resulting curve is interpreted in terms of the thickness and resistivity of horizontal layers underlying the center point of the electrode array. The stainless steel ACM fabric "target layer" would be expected to be very thin and to have a very low resistivity value.

To conduct VES measurements offshore, the current and potential electrodes were incorporated into a multiconductor cable that was towed behind the survey vessel (see Figure 6). The maximum current electrode separation AB/2 was 41.7 meters (137 ft), allowing an effective measurement depth of about 80 ft below the water surface. The stationary measurements were conducted with the vessel anchored and the cable extending downstream.

Sample results from two locations at the Missouri Bend site are shown on Figure 5. Range U-158 was in an area where no mat is installed. The interpreted model for this station shows a three-layer structure. The upper (20.8 ohm-m) layer represents the

river water, the second (39.7 ohm-m) layer represents sandy riverbed sediment, and the third (17.1 ohm-m) layer represents riverbed sediment having a relatively high clay content.

Range U-128 was above the new mat. The interpreted resistivity model for this station shows an upper (26.0 ohm-m) layer representing the river water, a second (0.001 ohm-m) layer representing the mat fabric, and a third (40.0 ohm-m) layer representing the underlying riverbed sediment. The depth of the mat is the same as the water depth, indicating that the mat is not buried at this point. The very low apparent resistivity values at large electrode separations are due to the presence of the low-resistivity mat fabric at a relatively shallow depth.

2. Towed Measurements

For production operations with the DC method, it would be desirable to obtain measurements with the vessel underway. To test the feasibility of underway data acquisition, a series of towed measurements was made along the 20-ft depth contour using a single current electrode pair (AB/2 = 23.7 m). As seen on Figure 5, the measured apparent resistivity at this electrode separation is much lower when the mat is present at shallow depths than when the mat is not present. As the depth to the mat increases, the measured apparent resistivity also increases. Thus the values of the measured apparent resistivity at a single electrode separation can be used to obtain rough estimates of the depth to the mat, as described in Section IV.

IV. RESULTS

A. Missouri Bend Revetment

1. Self-Potential

Figures 7 - 24 show water depth profiles and mat locations interpreted from SP data. Figures 7A, 18A, and 23A show examples of the measured and modeled SP data profiles for ranges U-75, U-95, and U-122, respectively. As discussed in Section III, the SP data provide a point corresponding to the location and depth of the outer limit of the mat, and one or more additional points corresponding to locations along the mat where there is a strong change in the surrounding oxygen content. The dashed lines on the figures indicate the inferred location of the mat fabric between the points determined by the SP data. Approximate locations of the as-installed outer mat limit along each range were obtained from Corps of Engineers Record Map drawing H-13-23991. Table 1 summarizes the SP data interpretations for each profile. Figures 31A, 31B, and 31C show maps of the interpreted mat locations.

Between ranges U-75 (Figure 7) and U-87 (Figure 13), the mat appears to be buried at relatively shallow depths below the river bed and outer mat limits are close to as-installed locations. On Figure 31A, the location of the offshore end of the mat

interpreted from the SP data for ranges U-75, U-77, and U-79 is somewhat offshore of the mapped as-installed location. Because there is no reason to expect the mat to have shifted in this direction, this apparent offset may have been due to an error in the plotting of the original mat location or to accumulation of slight positioning errors in the extreme southern portion of the survey area.

Between ranges U-89 (Figure 14) and U-110 (Figure 21), the mat appears to plunge very steeply downward in the offshore direction, extending to depths of about 170 to almost 300 ft below the water surface. Along some of these ranges (e.g., U-95; Figure 18) the inshore portion of the mat is close to the river bed at about 30 ft water depth and the mat appears to plunge downward at an angle of about 75 degrees past this point. The resistivity data at this station (discussed in the next section) appear to support this interpretation. In contrast, at range U-110 (Figure 21), the mat appears to be about 100 ft deep at a water depth of only 15 ft. The resistivity data at nearby range U-112 also show a considerable amount of sediment covering the mat at water depths of 10 to 15 ft.

Ranges U-120, U-122, and U-124 (Figures 22, 23, and 24) were above the new mat. As discussed in Section III, mats lying at or just below the riverbed tend to generate multiple line sources corresponding to local changes in the surrounding oxygen content. All of the interpreted source depths for these three ranges were essentially equal to the water depth, as would be expected for a newly-installed mat.

2. Electrical Resistivity

a. Stationary Measurements

Results of the stationary VES at about range U-158 are tabulated on Figure 5. As discussed in Section III, no evidence of a thin, low-resistivity layer corresponding to the mat fabric is seen at this site. Summarized results from the three soundings at range U-128 (new mat) are shown on Figure 25. These results indicate the presence of the mat fabric at depths corresponding to the water depth, as expected for a newly-installed mat.

Locations of the three soundings conducted at range U-95 are shown on Figure 31B and interpreted results of these soundings are shown on Figure 26. Similar to range U-128, the depth of the mat fabric is the same as the water depth, implying that the mat is not buried at these points. This is in agreement with the SP data along this range (Figure 18), which show the mat location at the river bed at a depth of about 35 ft. However, the SP data also show the mat plunging steeply downward just offshore of this depth. Soundings conducted just slightly further offshore probably would have detected this situation (as was the case at range U-112, discussed below).

The SP data at range U-110 (Figure 21) indicate that the mat is

deeply buried even at relatively shallow water depths. This is in agreement with the VES data at nearby range U-112 (Figure 27), which show the mat at a depth of about 50 ft at 11 ft water depth and at a depth of about 80 ft in 15 ft water depth.

b. Towed Measurements

As discussed in Section III, the main purpose of the towed DC resistivity measurements was to obtain signal-to-noise ratios and other information to help determine the feasibility of taking resistivity data with the vessel underway. This was accomplished by towing the cable along a constant depth contour (20 ft) while transmitting a constant current (1000 mA) through a single pair of current electrodes (AB/2 = 23.7 m) and recording the signal across the potential electrodes (potential electrode separation MN/2 was 1.10 m). To minimize the effects of electrode polarization and SP variations, the current was transmitted in the form of a square wave with a period of a few seconds.

Figure 28 shows a sample of the recorded data, for a run extending across the old mat - new mat transition at about range U-114. Peak-to-peak amplitudes of the signal appear to be resolvable within one mV or better, and the transition between the deeply-buried old mat and the shallow new mat is readily apparent. Determination of the actual depth to the mat along these profiles would require the use of a multichannel data acquisition system to obtain a complete data set such as those shown on Figure 5. However, a rough estimate of the mat depth can be obtained by comparing the signal amplitude for AB/2 = 23.7 m with those measured for the stationary soundings at this electrode spacing. This procedure was used to obtain the depth estimates discussed in the following paragraph.

Figure 29 shows water depth and estimated mat depth for the old mat - new mat profile described above. The old mat depth of about 80 ft is comparable to that determined by the SP and stationary VES data at a water depth of 20 ft in this area of deeply-buried old mat. As expected, the new mat lies at or just beneath the river bed. Figure 30 shows the results of a towed resistivity profile run between ranges U-93 and U-104.5. The depth to the mat varies from about 30 to 60 ft along the 20-ft water depth contour. This is in reasonable agreement with the SP and VES data in this area. Although the estimated depths shown on Figures 29 and 30 were calculated at 50-ft intervals along the survey line, smaller intervals (5 or 10 ft) could have been used if desired.

B. Manchac Revetment

SP surveys were conducted at two different areas of this revetment. The area between ranges U-110 and U-130 included an older (1974) mat which was overlaid by newer (1988) mat between ranges U-123 and U-130 (see Figure 43B). The region between ranges U-160 and U-180 was of interest because it included an area (ranges U-170 to U-180) where considerable sedimentation had

occurred, to the point where the mat was no longer visible on shore even at low river levels.

SP profiles and interpreted mat locations for the area between ranges U-110 and U-130 are shown on Figures 32 - 42. Figures 43A and 43B show maps of interpreted mat locations, and Table 2 summarizes the SP data interpretations for this area. At some locations, points on the mat are shown "suspended" in the water above the river bed (e.g., range U-112, Figure 34). At such points, the mat actually is on or just below the river bed, and the interpreted elevation above the river bed indicates the uncertainty in the depth interpretation.

For the region of older single mat between ranges U-110 and U-120, the SP interpretations indicate that the mat generally follows the riverbed profile, buried at depths of a few feet to several tens of feet. An exception to this is seen at range U-116, where there appears to have been considerable additional sediment deposition above the central portion of the mat. Because the riverbed profile has changed since the mat was installed, the outer end of the mat in this region averages about 50 ft closer to shore than it was at the time of installation.

The SP data for the region between ranges U-121 and U-124 could not be interpreted in terms of reasonable mat locations and depths. This probably is due to the junction between the old and overlying new mats, which generates erratic SP currents that cannot be modeled using simple line sources. A similar problem was noted at the junction of the old and new mat areas at the Missouri Bend revetment. More study of modeling techniques, based on "ground truth" data of actual multiple mat configurations, is needed in these junction areas. The newer (1988) mat between ranges U-124 and U-130 appears to closely follow the river bed. Because there has been little change in the river bed profile since the mat was installed in this region, the interpreted outer limit of the mat is close to the as-installed location (see Figure 43B).

Selected profiles for the region between ranges U-160 and U-180 are shown on Figures 44 - 47. The data for range U-166 (Figure 44) is representative of the area between U-160 and U-169, where the mat is visible on shore. The data for range U-176 (Figure 46) is representative of ranges U-171 to U-180, where the mat is not visible on shore; and range U-170 (Figure 45) represents the transition area. Figure 47 shows details of the very low-amplitude measured and calculated SP profiles at range U-176. Figure 48 shows a plan map of the interpreted mat locations. For all three profiles, the outer end of the mat appears to be very close to the as-installed location.

At range U-166 (Figure 44), the outer end of the mat appears to be buried about 22 ft below the river bed. At U-170 (Figure 45), the depth of burial of the outer end of the mat is greater (about 35 ft), and the outer end is so close to shore that this is the only point on the mat that is detected by the SP measurement. At

range U-176 (Figure 46), the outer end of the mat is covered by about 60 ft of sediment, and is very close to shore. As for range U-170, the outer end at range U-176 is so close to shore that this is the only point on the mat that is detected by the SP measurement. The increasing depth of burial and encroachment of the shoreline interpreted from the SP data between ranges U-160 and U-180 correlates with the observed shore conditions.

V. CONCLUSIONS AND RECOMMENDATIONS

The objectives of this Phase II study were (1) to further develop the SP method for practical application to ACM investigations, and (2) to determine the feasibility of the TDC technique for ACM investigations. The results described in this report indicate that both the SP and TDC resistivity methods appear to provide useful information regarding mat depth and location, even in areas where the mat is deeply buried within the riverbed sediments. The SP data obtained from this study provide the information necessary to develop SP equipment, survey techniques, and interpretation procedures for routine production use. The resistivity data obtained from this study indicate that the TDC method is feasible for ACM investigations, and provide information needed to further develop instrumentation, survey techniques, and interpretation procedures for this method.

SP and DC measurements conducted over a section of new mat give interpreted depths corresponding to that of the river bed, furnishing "ground truth" data for relatively shallow mat depths. The steep offshore plunge and great burial depth of the mat in some areas were seen on independent SP and DC data sets, providing more confidence than would the results of either technique alone. However, additional independent confirmation by drilling and/or by other geophysical techniques would help validate these results and provide accuracy limits for the interpreted mat depths and locations.

Drilling or some other direct exploration technique would provide the most convincing confirmation of the mat depths interpreted from the SP and DC data in areas of deep burial. An additional option would be to conduct a closely integrated suite of geophysical measurements in one or more areas of interpreted deep burial. This would include detailed SP and VES data as well as electromagnetic (EM) readings such as those being investigated by the Navy as part of the ACM program. As the stainless steel fabric of the mat appears to be magnetic, towed magnetometer readings also may be helpful.

Reasonable agreement regarding the mat depth and location interpreted from the results of these independent data sets would strongly increase confidence that the geophysical data are providing realistic estimates of mat conditions in deep-burial areas. This type of study could be conducted using presently-available SP, DC, EM, and magnetic equipment. Because of the availability of previous geophysical data and the variety of mat

conditions, Missouri Bend and/or Manchac would be preferred sites for this study.

Regarding additional development of the SP technique, a variety of electrode configurations and data acquisition methods were tested as part of the field study. The field configuration (shown on Figure 2) that was used to obtain the data analyzed for this report performed well, and provided the information needed to generate a final design for a production system.

For the 1992 field study, different computer programs were used to acquire the SP data, to graphically display the field data, to reduce the acquired data, to combine the SP and navigation data files, and to interpret the SP data. While each of these programs performed satisfactorily, data processing could be made much more efficient by reducing the number of programs used, with the ultimate goal of combining data acquisition, display, reduction, and interpretation in a single program. It also is recommended that a joint effort be conducted with the contractor that provides positioning information to develop a technique to combine the navigation and SP data files during the acquisition process (rather than as a post-acquisition step as presently done). This would save considerable processing time and would allow real-time evaluation of survey results.

The results of the TDC investigation indicate that further development of the TDC technique is warranted. The stationary VES technique can be used to obtain "spot" mat depth information, but the necessity of positioning and anchoring the survey vessel for each reading makes this a slow process. The towed single-channel tests indicated that signal levels and signal-to-noise ratios for underway TDC data are acceptable, and that a multichannel TDC system could provide closely-spaced mat depth information along the course of the survey vessel. Development of the TDC concept would include the design of a multichannel data acquisition system, assembly of a suitably powerful and sensitive transmitter-receiver system, construction of a towed cable with electrode separations large enough to delineate deeply-buried mats, and production of software for data reduction and interpretation.

In any geophysical investigation, it is desirable to use as many different techniques as possible to balance the limitations inherent in any one method and to improve the accuracy of the final interpretation. Advantages of the SP method for ACM investigations include the use of simple and reliable equipment and the ability to detect deeply-buried mats using a relatively short towed cable. The results of this study indicate that the SP measurements are particularly effective for determining the depth and location of the outer limit of the mat. However, SP measurements are best made on profiles along ranges perpendicular to shore, requiring relatively low river flow conditions. Also, the SP data indicate only individual points on the mat rather than providing a continuous profile.

In contrast, the TDC method requires more elaborate equipment and data reduction procedures, as well as a longer and heavier cable than used for SP measurements. However, TDC profiles can be run parallel to shore, and provide an almost continuous record of mat depth along the survey profile. Thus The SP and TDC methods are complementary, and the combined use of both techniques would provide a better picture of mat conditions in a given survey area than would the use of either technique alone. As the EM method also provides unique advantages (including better horizontal resolution of mat features than possible with SP or TDC measurements, and the possibility of airborne deployment), it would be desirable to combine SP, TDC, and EM surveys (and possibly magnetic surveys) whenever possible at a given site.

REFERENCES

Corwin, R.F., and Butler, D.K., 1989, Geotechnical applications of the self-potential method, Report 3, Development of self-potential interpretation techniques for seepage detection: Department of the Army, US Army Corps of Engineers, Technical Report REMR-GT-6.

Department of the Army, Corps of Engineers, 1979, Geophysical Explorations: Engineer Manual 1110-1-1802.

Rao, B.S.R., Marthy, I.V.R., and Reddy, S.J., 1970, Interpretation of self-potential anomalies of some geometric bodies: Pure and Applied Geophysics, vol 78, no. 1, p 66-77.

Sato, M., and Mooney, H.M., 1960, The electrochemical mechanism of sulfide self-potentials: Geophysics, vol 25, no 1, p. 226-249.

Telford, W.M., Geldart, L.P., Sheriff, R.E., and Keys, D.A., 1976, Applied Geophysics: Cambridge Univ. Press.

TABLE 1

DATA SUMMARY FOR MISSOURI BEND REVETMENT

Nominal Range Line	U-75	U-77	U-79	U-81	U-83	U-85	U-87	U-89	U-9
Data Profile	MB41	MB42	MB43	MB44	MB45	MB46	MB47	MB48	MB1
Field SP Data File (*.ED)	MB41	MB42	MB43	MB44	MB45	MB46	MB46	MB48	MB1
Positioning Data File (*.NAV)	MB3017ED	MB3019ED	MB3020ED	MB3022ED	MB3023ED	MB3023ED	MB3024ED	MB3025ED	MB2
Combined Data File (*.DAT)	MB41	MB42	MB43	MB44	MB45	MB46	MB47	MB48	MB1
SP Model File (*.MOD)	MB41	MB42	MB43	MB44	MB45	MB46	MB47	MB48	MB1
Output Data File (*.DAT)	MB41AOUT	MB42OUT	MB43OUT	MB44AOUT	MB45AOUT	MB46OUT	MB47OUT	MB48OUT	MB1
Output GRAPHER File (*.DAT)	MB41GRF	MB42GRF	MB43GRF	MB44GRF	MB45GRF	MB46GRF	MB47GRF	MB48GRF	MB1
GRAPHER Plot File (*.GRF)	U75	U77	U79	U81	U83	U85	U87	U89	U90
POL. CORR. (mV)	-2.5	-2.0	-2.0	-2.0	-2.0	-2.0	-1.5	-2.0	+1.0
Chi Squared	60.5	40.6	25.2	39.5	139.8	175	147	42.5	58.2
SOURCE LINES (line half-length = 1000 ft, parallel to mat)									
X1 (ft)	2450	2200	1760	2800	2491	2378	1745	1823	2015
I1 (mV/ft)	+.0055	+.0500	+.0055	+.00618	+.0105	+.00832	+.08484	+.0070	+.01
H1 (depth to source, ft)	115	130	165	136.5	105	92.4	96.6	160	220
E1 (EASTING)	2027571	2027590	2027624	2027623	2027625	2027688	2027728	2027785	2027
N1 (NORTHING)	616124	616250	616466	616626	616825	616975	617104	617339	6174
D1 (depth to river bed, ft)	92	92	93	91	87	81	76	65	51
X2	2600	2330	1939	2936	2590	2511	1890	1965	2060
I2	-.003267	-.00198	-.00515	-.0200	-.00700	-.0051	-.0051	-.0022	-.00
H2	48.5	48	61	48	55	37.5	32	45.3	60
E2	2027422	2027464	2027452	2027491	2027525	2027565	2027590	2027657	2027
N2	616140	616278	616519	616664	616840	617016	617149	617394	6174
D2	60	69	50	53	58	29	36	36	43

TABLE 1 (continued)

DATA SUMMARY FOR MISSOURI BEND REVETMENT

Nominal Range Line	U-91	U-93	U-95	U-100	U-105	U-110	U-120	U-122	U-1
Data Profile	MB49	MB50	MB51	MB60	MB61	MB62	MB52	MB53	MB5
Field SP Data File (*.ED)	MB49	MB50	MB51	MB60	MB61	MB62	MB52	MB53	MB5
Positioning Data File (*.NAV)	MB3026ED	MB3027ED	MB3028ED	MB31ED	MB32ED	MB3331ED	MB3029ED	MB3030ED	MB3
Combined Data File (*.DAT)	MB49	MB50	MB51	MB60	MB61	MB62	MB52	MB53	MB5
SP Model File (*.MOD)	MB49	MB50	MB51	MB60	MB61	MB62	MB52	MB53	MB5
Output Data File (*.DAT)	MB49OUT	MB50AOUT	MB51OUT	MB60OUT	MB61OUT	MB62OUT	MB52OUT	MB53OUT	MB5
Output GRAPHER File (*.DAT)	MB49GRF	MB50GRF	MB51GRF	MB60GRF	MB61GRF	MB62GRF	MB52GRF	MB53GRF	MB5
GRAPHER Plot File (*.GRF)	U91	U93	U95	U100	U105	U110	U120	U122	U12
POL. CORR. (mV)	-1.0	-1.5	-2.0	0	0	+1.5	-2.0	-2.0	-2.0
Chi Squared	39	35.1	37.2	39.5	81.1	23.3	2405	1015	1041
SOURCE LINES (line half-length = 1000 ft, parallel to mat)									
X1 (ft)	1710	1750	2012	2900	2900	1100	1900	720	1150
I1 (mV/ft)	+.0130	+.009	+.0065	+.0060	+.0050	+.0060	-.0060	-.0030	-.00
H1 (depth to source, ft)	273	250	290	241.5	226	200	25	20	25
E1 (EASTING)	2027733	2027786	2027865	2028088	2028287	2028556	2029202	2029417	2029
N1 (NORTHING)	617517	617705	617876	618294	618707	619210	619834	620173	6203
D1 (depth to river bed, ft)	48	43	44	33	26	22	25	22	23
X2	1779	1800	2088	3038	3041	1150	2050	790	1280
I2	-.00332	-.0030	-.0011	-.0011	-.00010	-.00010	+.0025	-.0040	+.00
H2	60	60	33.9	34	34	100	25	20	25
E2	2027665	2027737	2027808	2027960	2028170	2028516	2029079	2029350	2029
N2	617535	617712	617925	618350	618785	619241	619922	620196	6203
D2	37	33	29	28	9	18	25	23	22
X3							2200	875	1430
I3							+.0010	+.0025	+.00
H3							15	25	15
E3							2028971	2029268	2029
N3							630026	620218	6203
D3							18	22	15
X4								980	
I4								+.0015	
H4								18	
E4								2029168	
N4								620242	
D4								19	

TABLE 2

DATA SUMMARY FOR MANCHAC REVETMENT

Nominal Range Line	U-110	U-111	U-112	U-114	U-116	U-118
Data Profile	MA2	MA15	MA3	MA1	MA4	MA7
Field SP Data File (*.ED)	MA2	MA15	MA3	MA1	MA4	MA7
Positioning Data File (*.NAV)	MA312ED	MA3115ED	MA313ED	MA311ED	MA314ED	MA317ED
Combined Data File (*.DAT)	MA2	MA15	MA3	MA1	MA4	MA7
SP Model File (*.MOD)	MA2	MA15	MA3	MA1	MA4	MA7
Output Data File (*.DAT)	MA2BOUT	MA15OUT	MA3OUT	MA1OUT	MA4OUT	MA7OUT
Output GRAPHER File (*.DAT)	MA2GRF	MA15GRF	MA3GRF	MA1GRF	MA4GRF	MA7GRF
GRAPHER Plot File (*.GRF)	MAU110	MAU111	MAU112	MAU114	MAU116	MAU118
POL. CORR. (mV)	0	0	0	0	-0.5	-0.6
Chi Squared	1545	1223	1109	1371	4806	1458
SOURCE LINES (line half-length = 1000 ft, parallel to mat)						
X1 (ft)	1000	1000	880	1020	850	1210
I1 (mV/ft)	-.009	-.007	-.0030	-.0020	-.0020	-.0025
H1 (depth to source, ft)	92	80	82	100	100	100
E1 (EASTING)	2052997	2052897	2052808	2052575	2052336	2052270
N1 (NORTHING)	610800	610808	610820	610882	611046	611052
D1 (depth to river bed, ft)	79	80	80	63	105	94
X2	1115	1169	1050	1120	970	1410
I2	-.009	+.0083	+.0017	+.0020	+.0080	-.0090
H2	60	43.5	40	80	85	30
E2	2053006	2052919	2052843	2052613	2052380	2052309
N2	610915	610970	610986	610974	611158	611246
D2	43	39	47	63	57	28
X3	1290	1230	1090	1325	1130	1500
I3	+.018	-.005	-.0025	-.0010	-.0120	-.0080
H3	10	22.5	20	25	40	15
E3	2053050	2052926	2052852	2052673	2052437	2052319
N3	611170	611036	611025	611169	611307	611335
D3	-	17	17	26	21	20
X4				1390	1165	
I4				+.0010	+.0120	
H4				10	15	
E4				2052683	2052450	
N4				611234	611340	
D4				16	20	

TABLE 2 (continued)

DATA SUMMARY FOR MANCHAC REVETMENT

Nominal Range Line	U-120	U-122	U-124	U-126	U-128	U-130	U-166	U-170	U-176
Data Profile	MA6	MA8	MA9	MA10	MA11	MA12	MA19	MA21	MA24
Field SP Data File (*.ED)	MA6	MA8	MA9	MA10	MA11	MA12	MA19	MA21	MA24
Positioning Data File (*.NAV)	MA316ED	MA318ED	MA319ED	MA3110ED	MA3111ED	MA3112ED	MA3119ED	MA3121ED	MA312
Combined Data File (*.DAT)	MA6	MA8	MA9	MA10	MA11	MA12	MA19	MA21	MA24
SP Model File (*.MOD)	MA6	MA8	MA9	MA10A	MA11	MA12	MA19	MA21	MA24
Output Data File (*.DAT)	MA6OUT	MA8OUT	MA9OUT	MA10OUT	MA11OUT	MA12OUT	MA19OUT	MA21OUT	MA240
Output GRAPHER File (*.DAT)	MA6GRF	MA8GRF	MA9GRF	MA10GRF	MA11GRF	MA12GRF	MA19GRF	MA21GRF	MA24G
GRAPHER Plot File (*.GRF)	MAU120	MAU122	MAU124	MAU126	MAU128	MAU130	MAU166	MAU170	MAU17
POL. CORR. (mV)	0	0	-1.0	0	0	0	0	+0.3	+0.4
Chi Squared	4288	-	1343	686	531	1839	37.8	38.2	16.7
SOURCE LINES (line half-length = 1000 ft, parallel to mat)									
X1 (ft)	1256	950	1500	1660	1440	1700	1450	1740	1900
I1 (mV/ft)	-.0080	-.0020	+.0050	+.0090	+.011	+.014	+.0055	+.0028	+.002(
H1 (depth to source, ft)	75	30	120	100	100	100	100	90	90
E1 (EASTING)	2052042	-	2051775	2051626	2051435	2051290	2048195	2047794	204727
N1 (NORTHING)	611238	-	611220	611336	611424	611459	612317	612383	61244(
D1 (depth to river bed, ft)	61	-	97	106	101	93	77	57	34
X2	1400	1125	1610	1820	1605	1870	1550		
I2	-.0110	-.0110	-.0070	-.0130	-.0100	-.0132	-.0048		
H2	20	80	75	65	65	65	60		
E2	2052106	-	2051829	2051686	2051513	2051345	2048229		
N2	611366	-	611316	611484	611569	611619	612411		
D2	28	-	64	46	65	54			
X3	1700	1200	1725	1950					
I3	+.0035	+.0080	-.0060	+.0060					
H3	10	10	40	10					
E3	2052220	-	2051873	2051731					
N3	611650	-	611422	611606					
D3	-	-	43	15					
X4			1950						
I4			+.0100						
H4			10						
E4			2051960						
N4			611660						
D4			-						

FIGURES

FIGURE 1

ACM Self-Potential Mechanism and Data Profile

(not to scale)

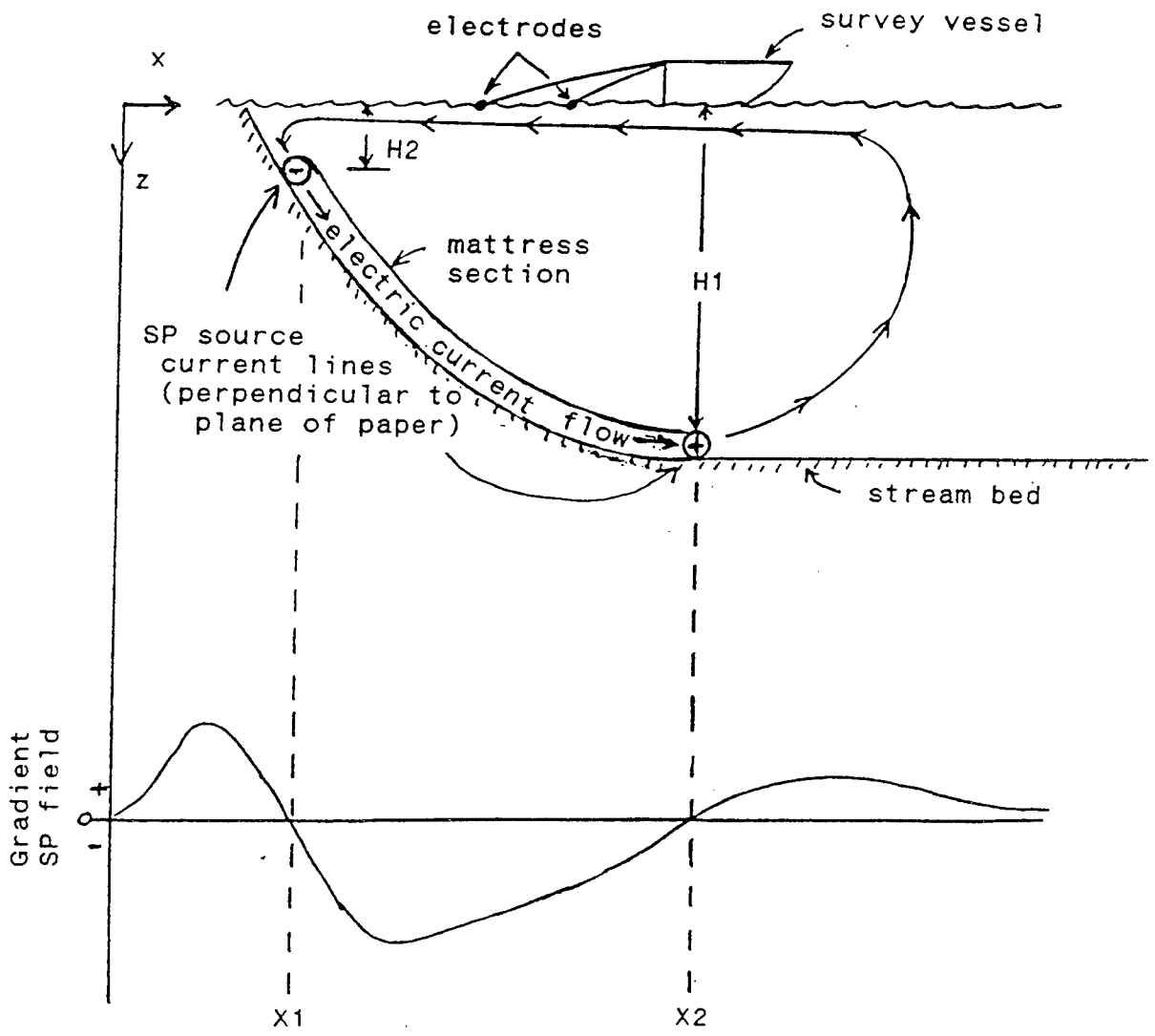

FIGURE 2

Self-Potential Measurement System

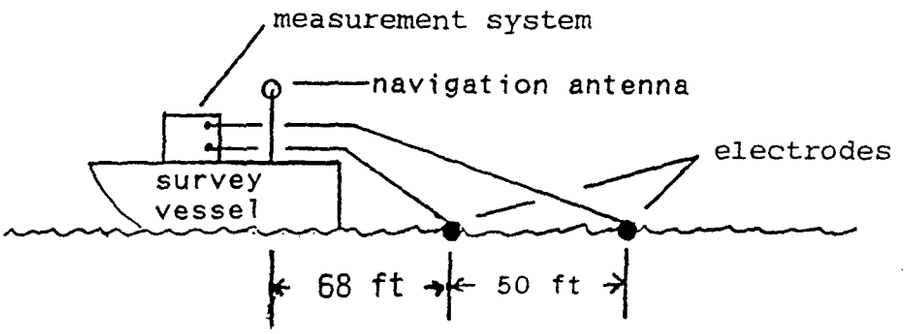

Measurement System Schematic

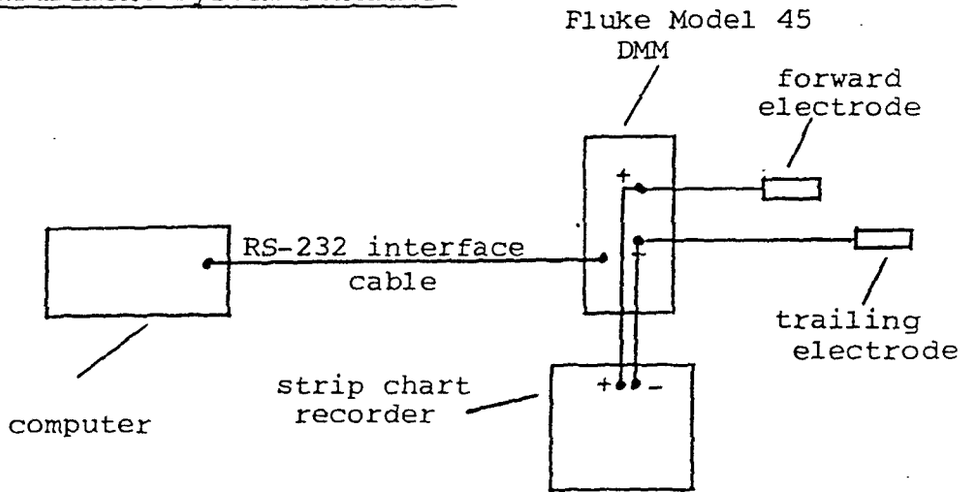

FIGURE 3

Measured and Calculated SP Data Profiles

Range U-89 Missouri Bend

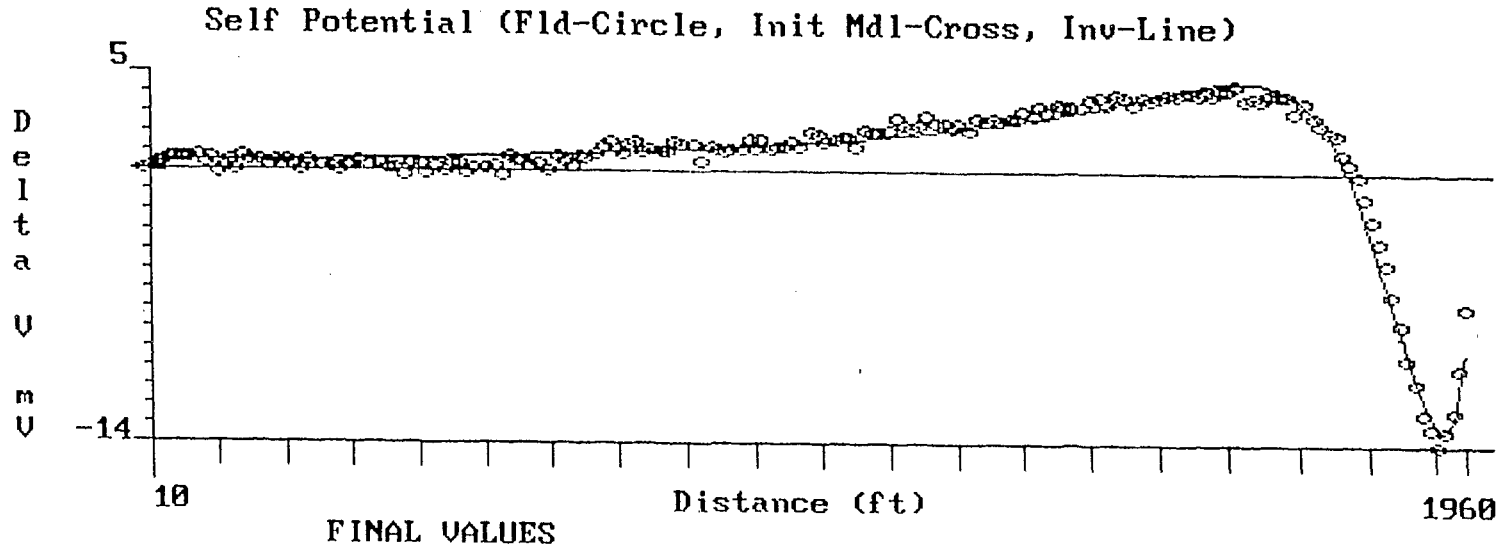

FINAL VALUES

Line 1
Current = .007
Length = 1000
X = 1823 Y = 0
H = 160

Line 2
Current = -.0022
Length = 1000
X = 1965 Y = 0
H = 45.3

FIGURE 4

Electrical Resistivity Vertical Electric Sounding (VES)

(from Corps of Engineers EM-1110-1-1802)

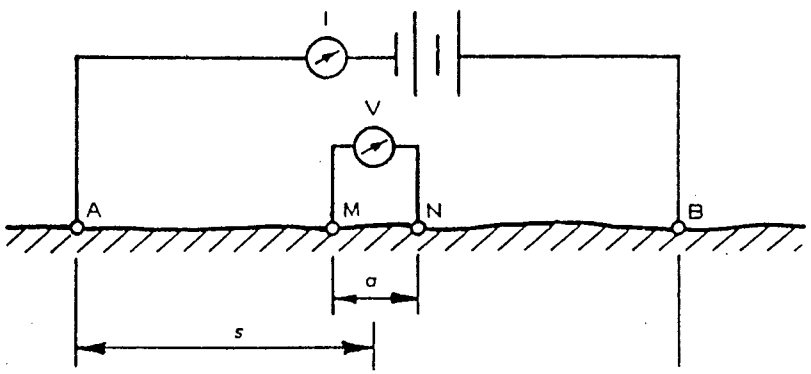

SCHLUMBERGER ARRAY

FIGURE 5

ELECTRICAL RESISTIVITY SOUNDINGS
RANGES U-158 (NO MAT) AND U-128 (NEW MAT)
MISSOURI BEND SITE

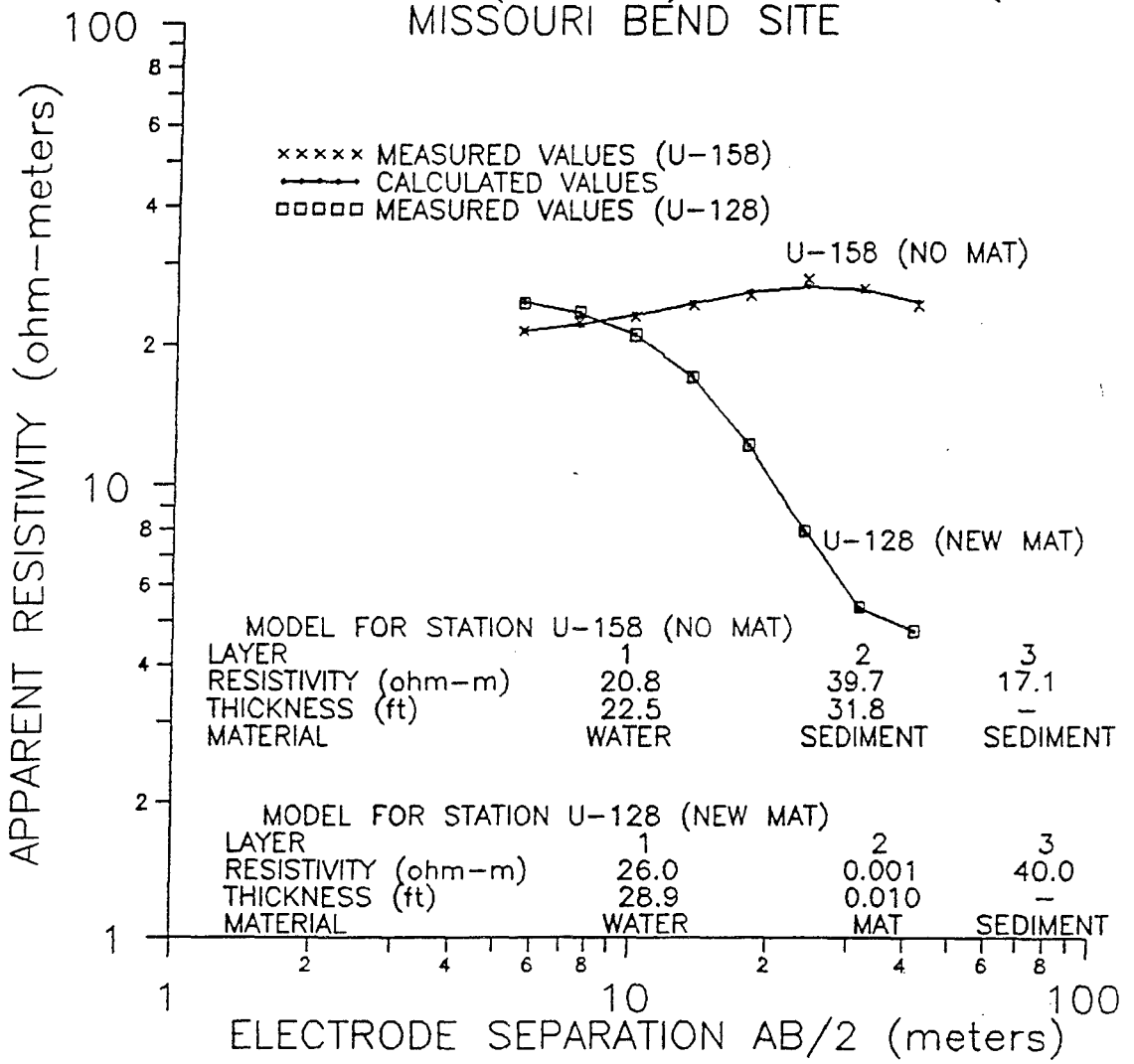

FIGURE 6

Towed Electrical Resistivity Cable Configuration

(not to scale)

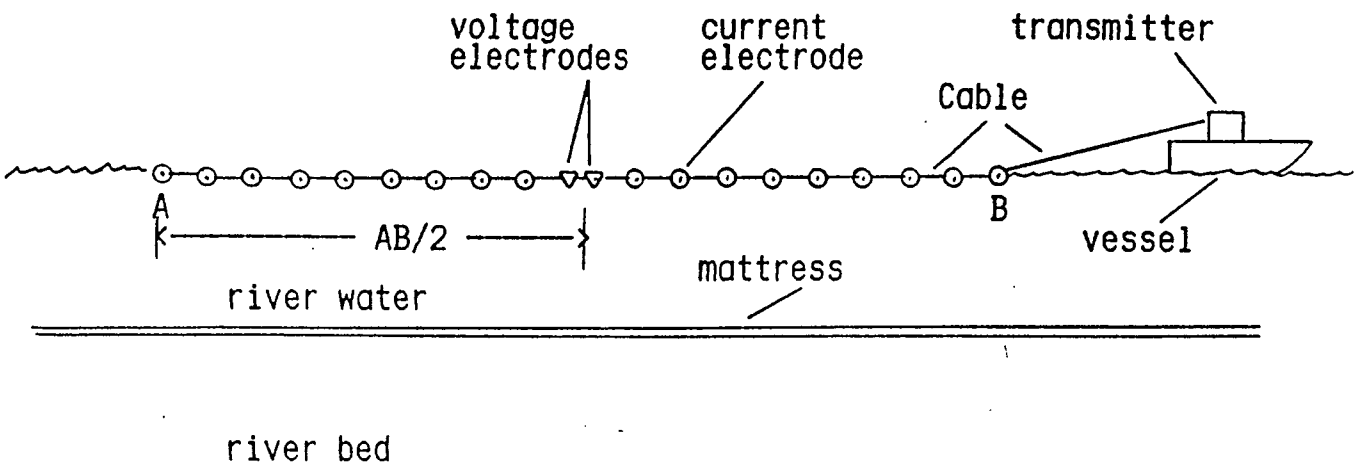

FIGURE 7

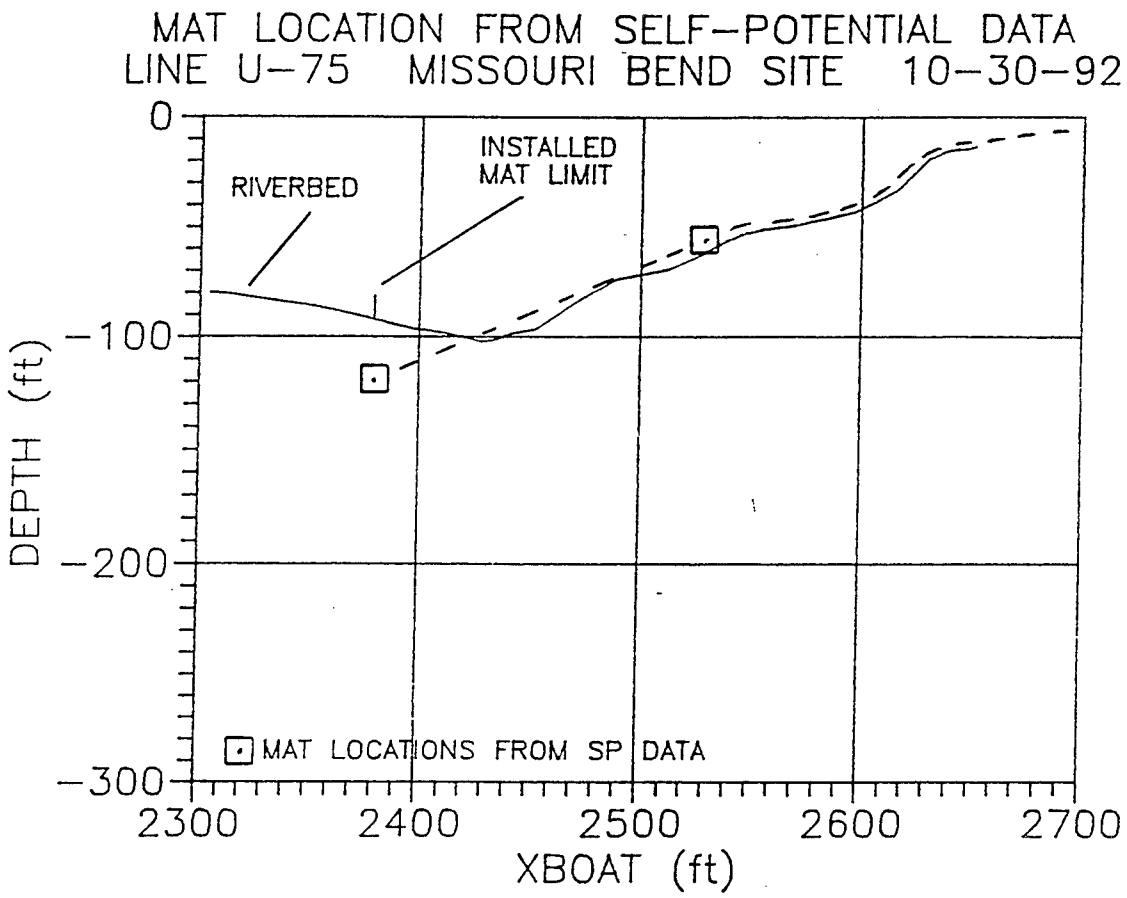
MAT LOCATION FROM SELF-POTENTIAL DATA
LINE U-75 MISSOURI BEND SITE 10-30-92
0
-100
-200
-300
DEPTH (ft)
RIVERBED
INSTALLED
MAT LIMIT
MAT LOCATIONS FROM SP DATA
2300
2400
2500
2600
2700
XBOAT (ft)

FIGURE 7A

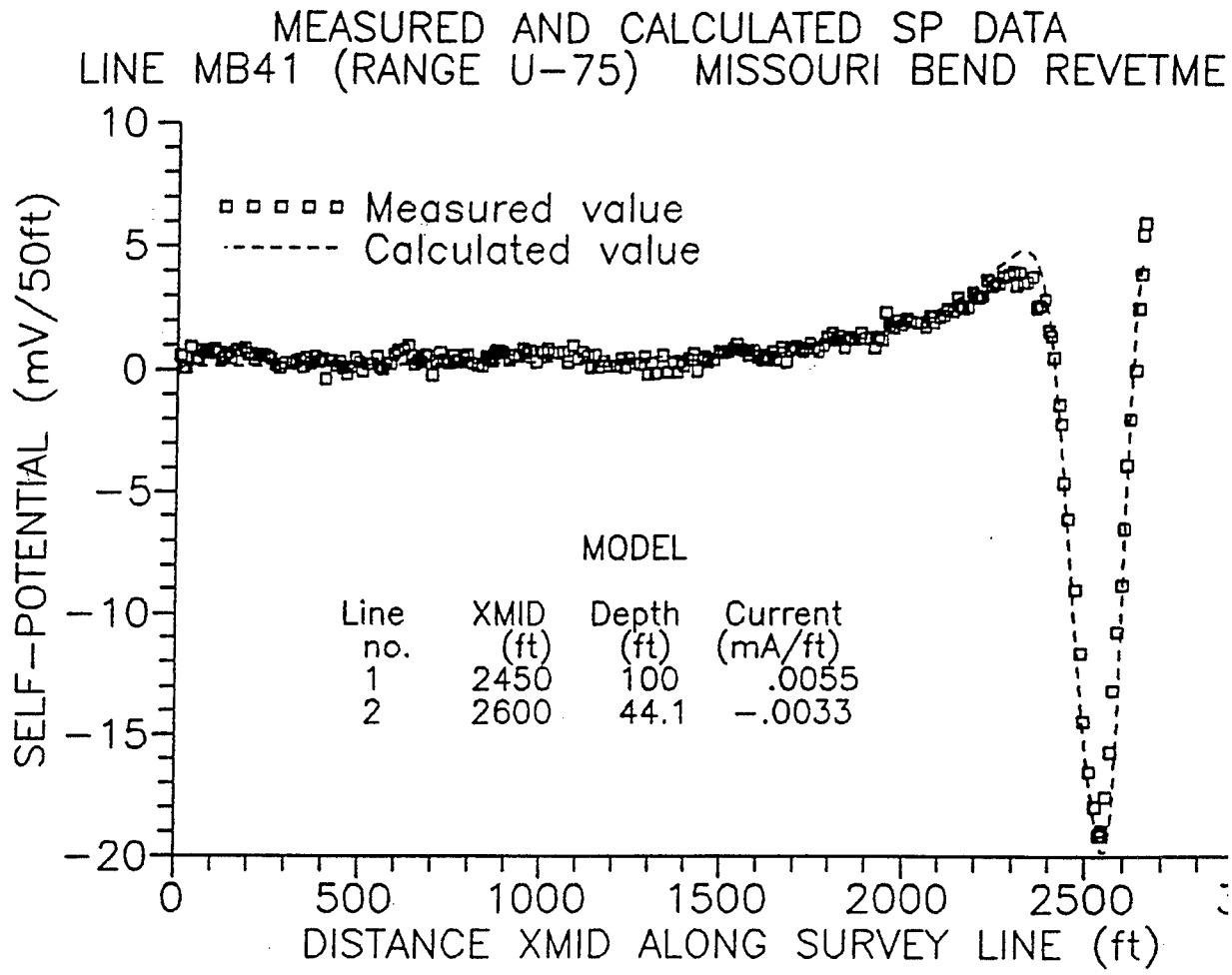
MEASURED AND CALCULATED SP DATA
LINE MB41 (RANGE U-75) MISSOURI BEND REVETME
Measured value
Calculated value
MODEL
Line no. | XMID (ft) | Depth (ft) | Current (mA/ft)
1 | 2450 | 100 | .0055
2 | 2600 | 44.1 | -.0033
SELF-POTENTIAL (mV/50ft)
10
5
0
-5
-10
-15
-20
0
500
1000
1500
2000
2500
DISTANCE XMID ALONG SURVEY LINE (ft)

FIGURE 8

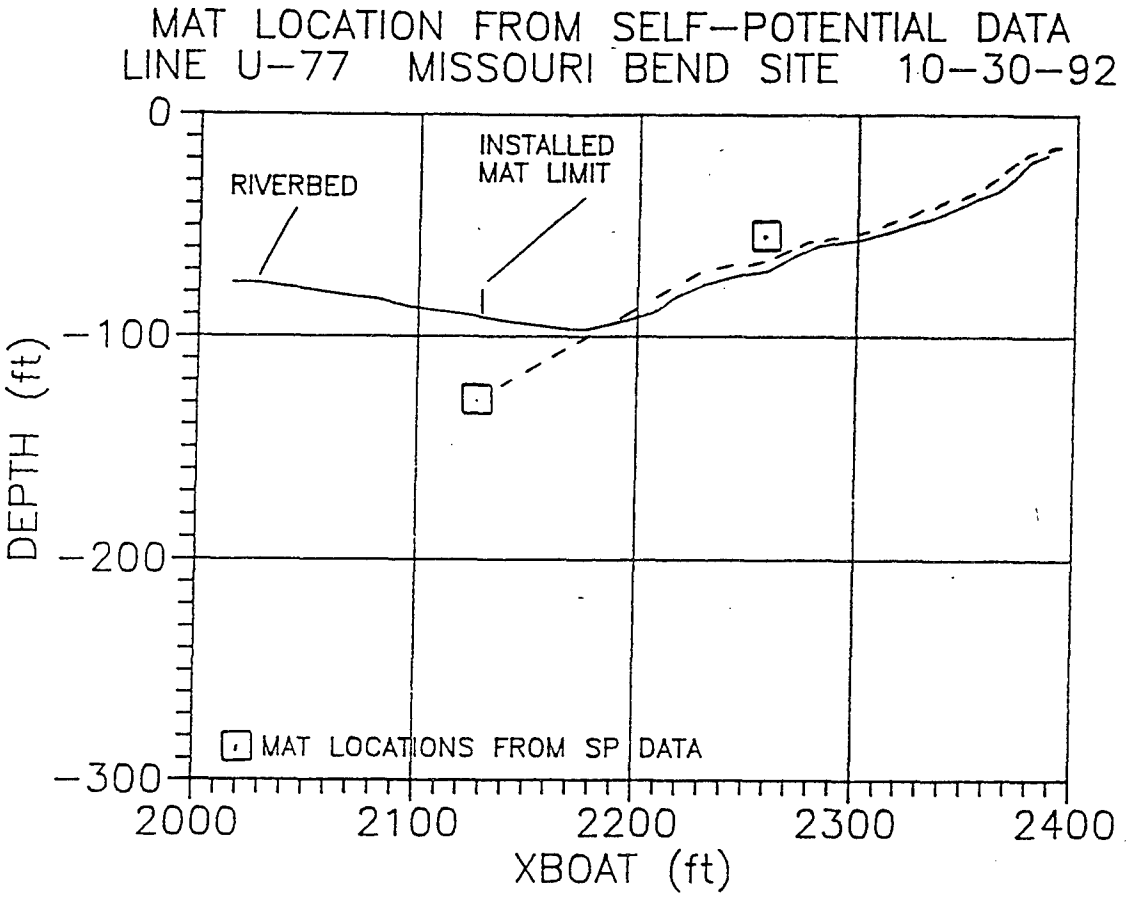
MAT LOCATION FROM SELF-POTENTIAL DATA
LINE U-77 MISSOURI BEND SITE 10-30-92
0
-100
-200
-300
DEPTH (ft)
RIVERBED
INSTALLED
MAT LIMIT
MAT LOCATIONS FROM SP DATA
2000
2100
2200
2300
2400
XBOAT (ft)

FIGURE 9

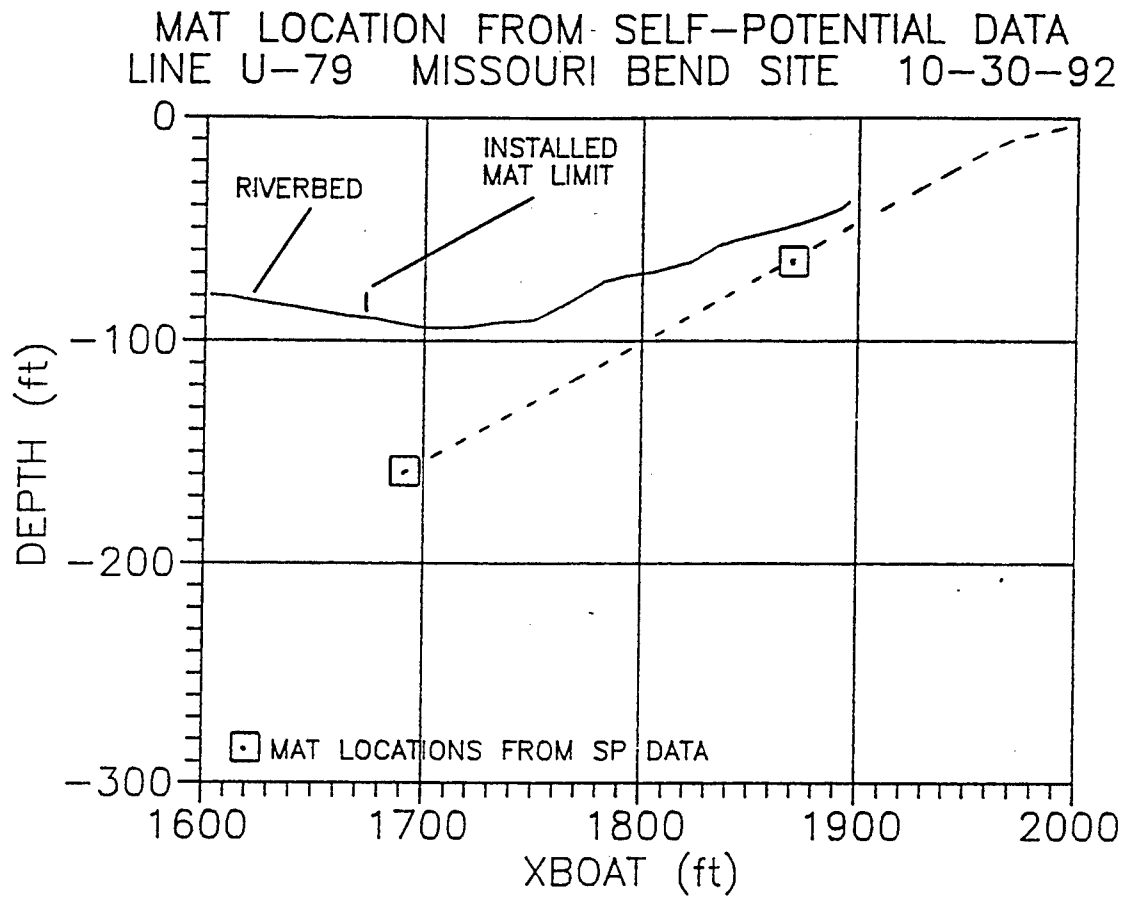
MAT LOCATION FROM SELF-POTENTIAL DATA
LINE U-79 MISSOURI BEND SITE 10-30-92
0
-100
-200
-300
DEPTH (ft)
RIVERBED
INSTALLED
MAT LIMIT
MAT LOCATIONS FROM SP DATA
1600
1700
1800
1900
2000
XBOAT (ft)

FIGURE 10

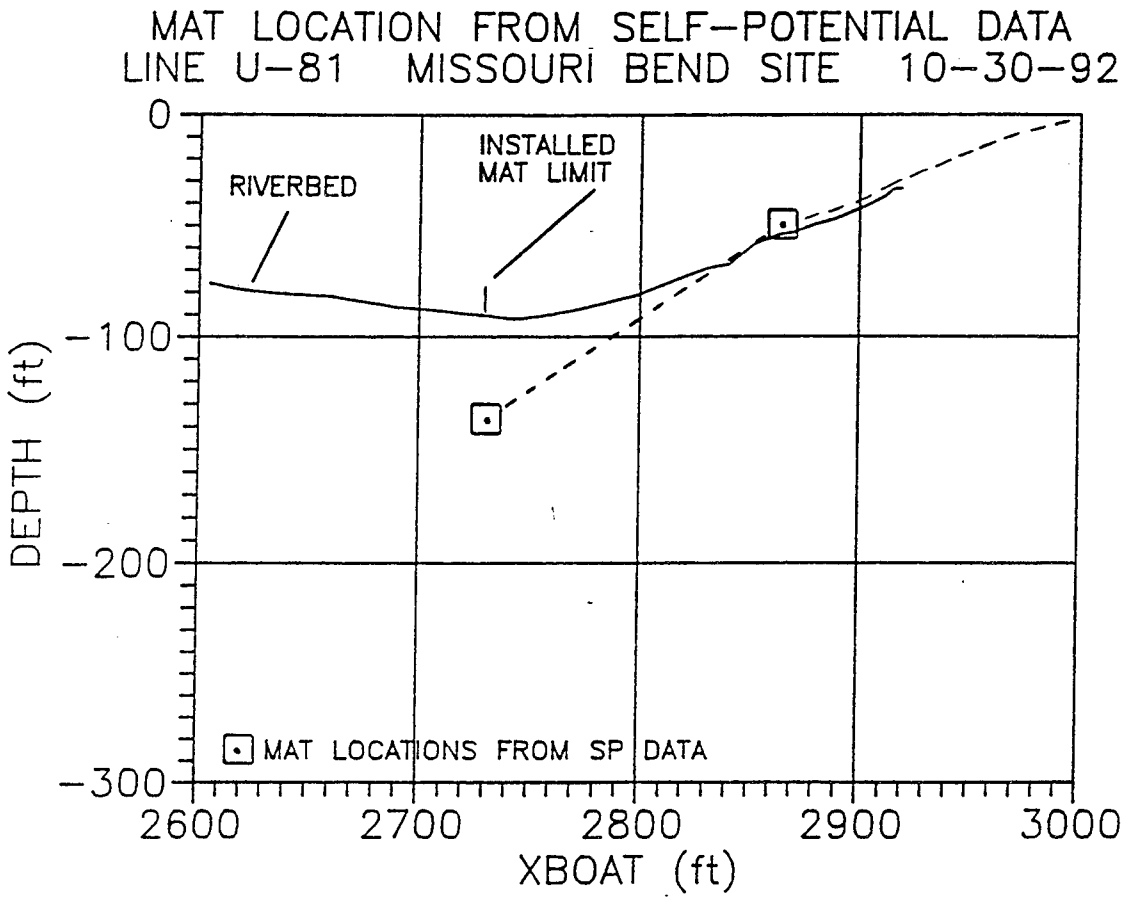
MAT LOCATION FROM SELF-POTENTIAL DATA
LINE U-81 MISSOURI BEND SITE 10-30-92
0
-100
-200
-300
DEPTH (ft)
RIVERBED
INSTALLED
MAT LIMIT
MAT LOCATIONS FROM SP DATA
2600
2700
2800
2900
3000
XBOAT (ft)

FIGURE 11

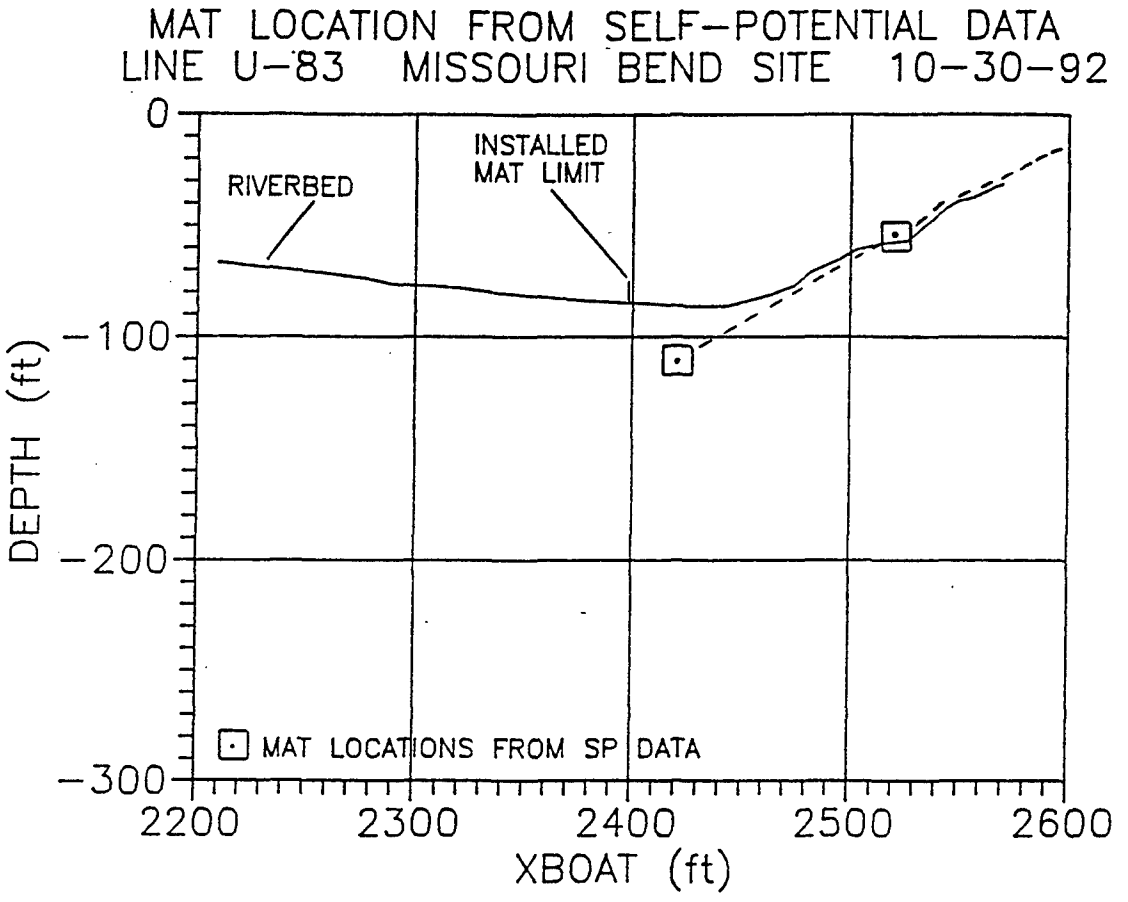
MAT LOCATION FROM SELF-POTENTIAL DATA
LINE U-83 MISSOURI BEND SITE 10-30-92
0
-100
-200
-300
DEPTH (ft)
RIVERBED
INSTALLED
MAT LIMIT
MAT LOCATIONS FROM SP DATA
2200
2300
2400
2500
2600
XBOAT (ft)

FIGURE 12

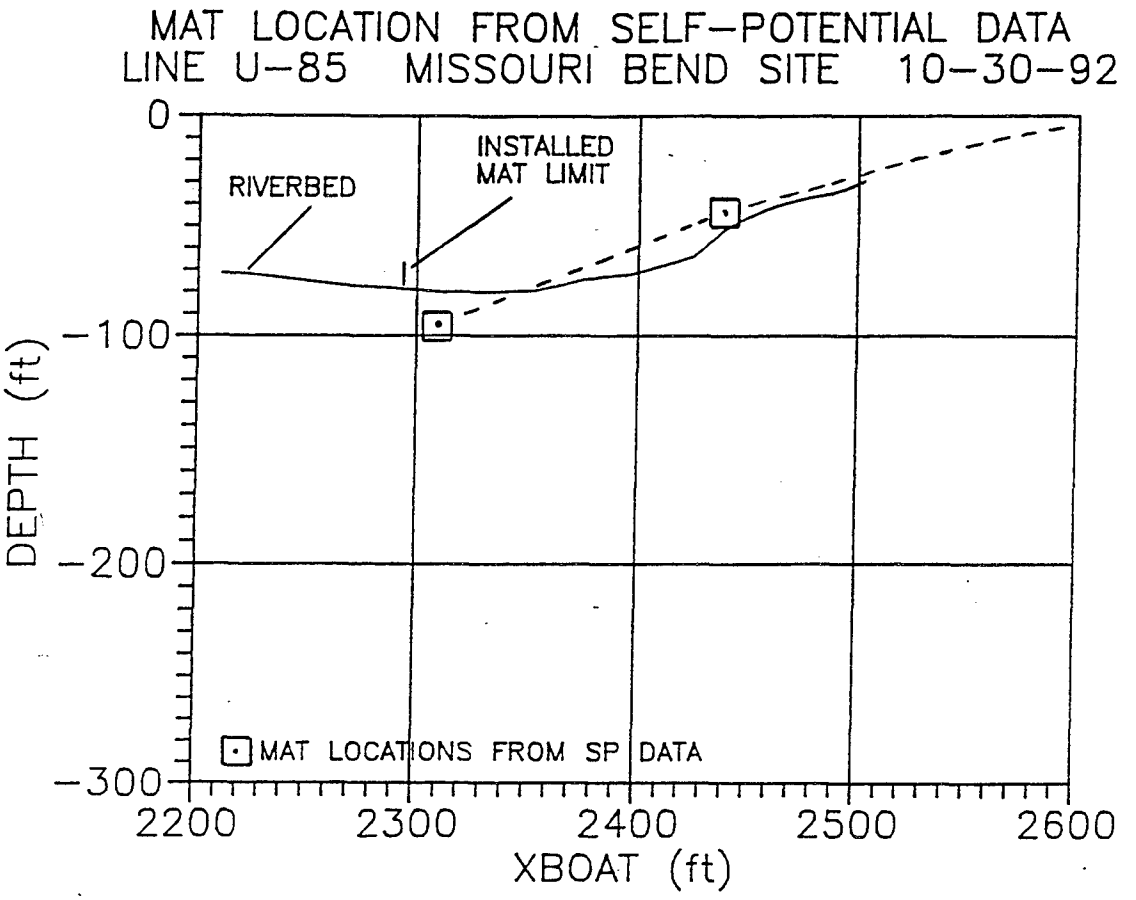
MAT LOCATION FROM SELF-POTENTIAL DATA
LINE U-85 MISSOURI BEND SITE 10-30-92
0
-100
-200
-300
DEPTH (ft)
RIVERBED
INSTALLED
MAT LIMIT
MAT LOCATIONS FROM SP DATA
2200
2300
2400
2500
2600
XBOAT (ft)

FIGURE 13

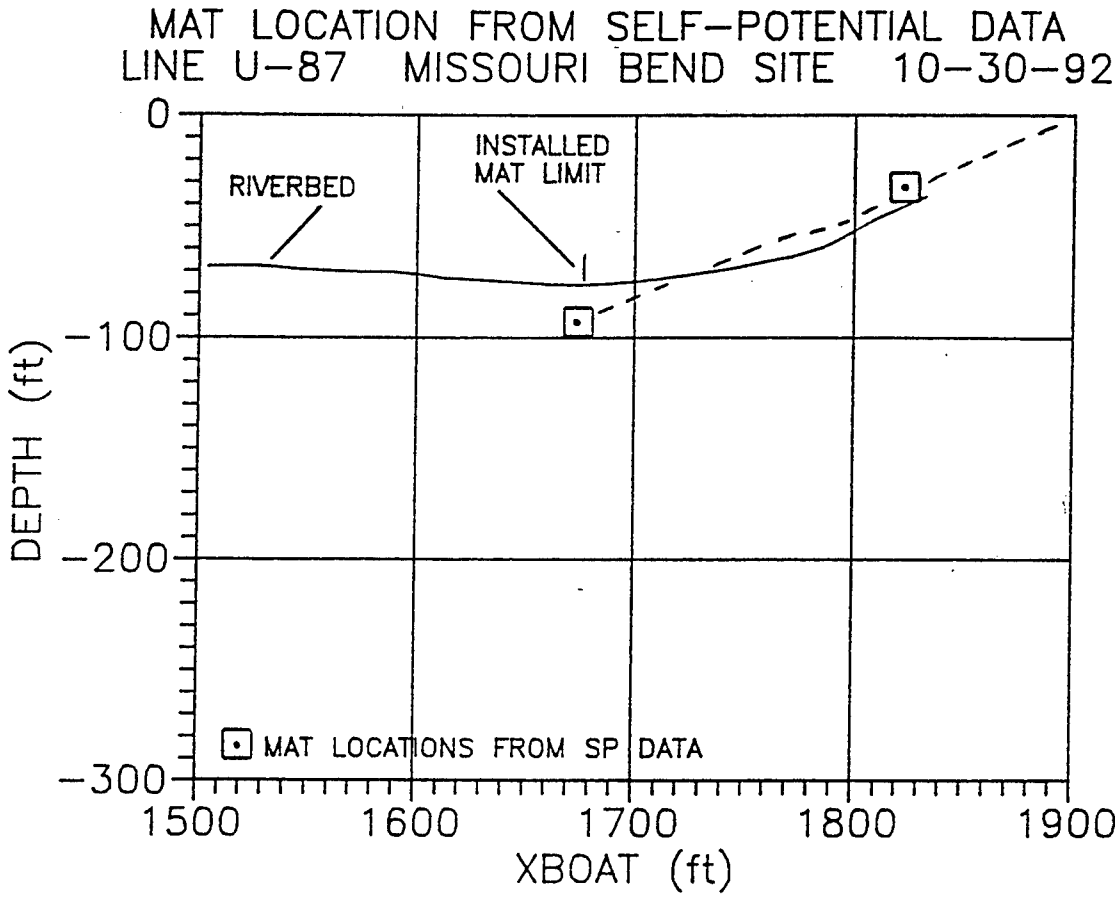
MAT LOCATION FROM SELF-POTENTIAL DATA
LINE U-87 MISSOURI BEND SITE 10-30-92
0
-100
-200
-300
DEPTH (ft)
RIVERBED
INSTALLED
MAT LIMIT
MAT LOCATIONS FROM SP DATA
1500
1600
1700
1800
1900
XBOAT (ft)

FIGURE 14

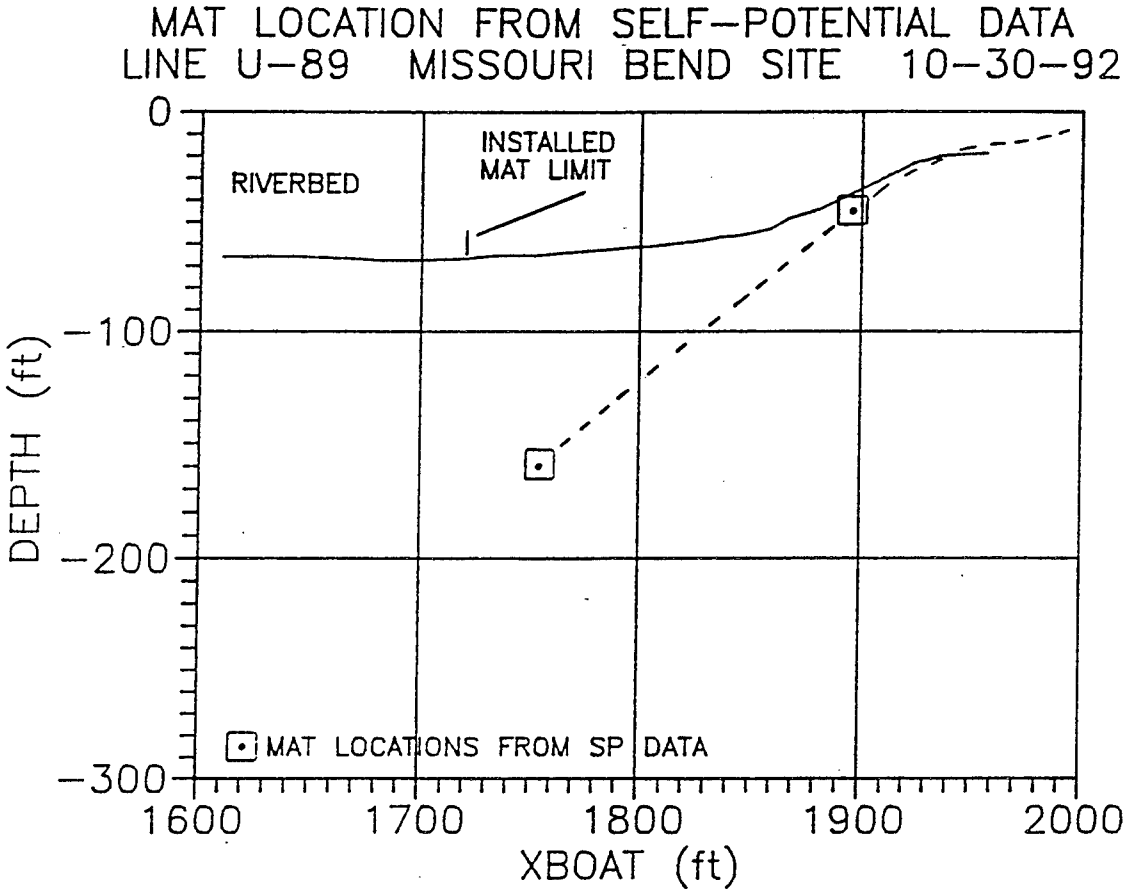
MAT LOCATION FROM SELF-POTENTIAL DATA
LINE U-89 MISSOURI BEND SITE 10-30-92
0
-100
-200
-300
DEPTH (ft)
RIVERBED
INSTALLED
MAT LIMIT
MAT LOCATIONS FROM SP DATA
1600
1700
1800
1900
2000
XBOAT (ft)

FIGURE 15

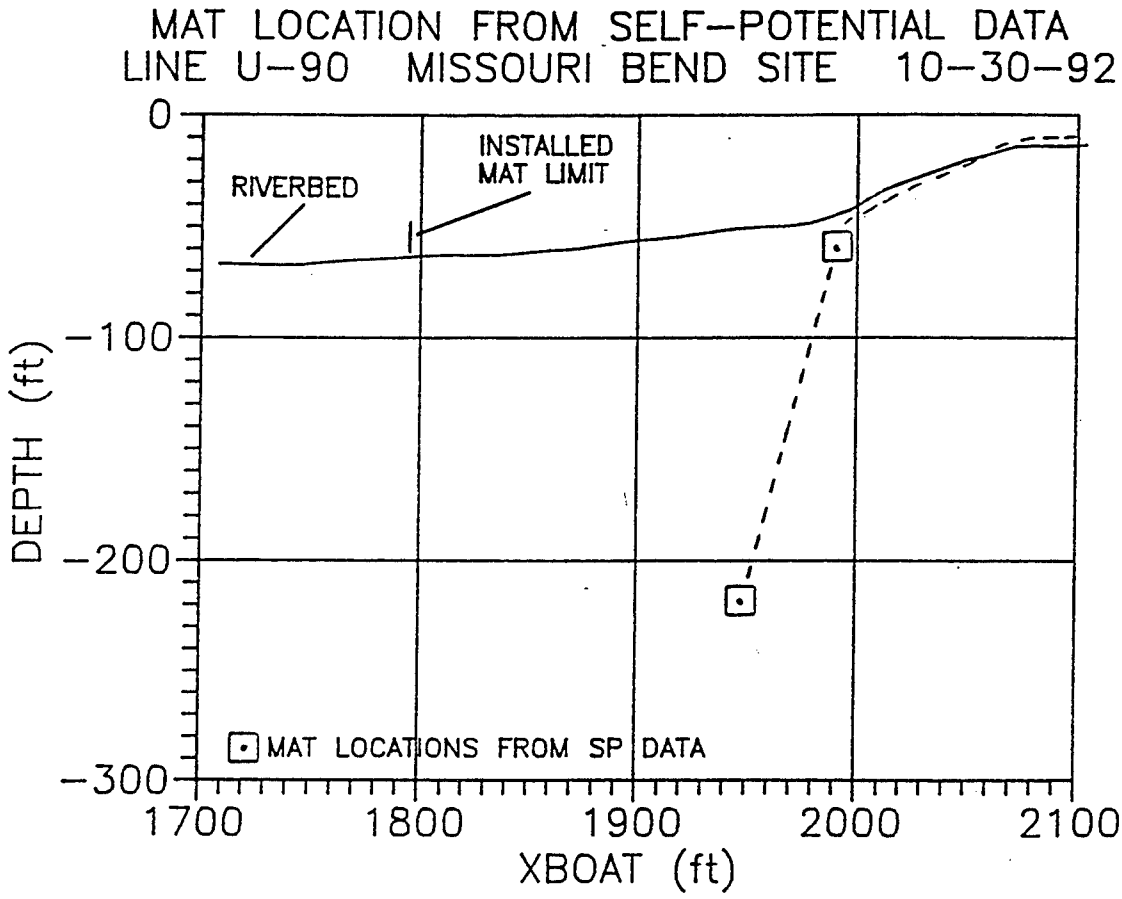
MAT LOCATION FROM SELF-POTENTIAL DATA
LINE U-90 MISSOURI BEND SITE 10-30-92
0
-100
-200
-300
DEPTH (ft)
RIVERBED
INSTALLED
MAT LIMIT
MAT LOCATIONS FROM SP DATA
1700
1800
1900
2000
2100
XBOAT (ft)

FIGURE 16

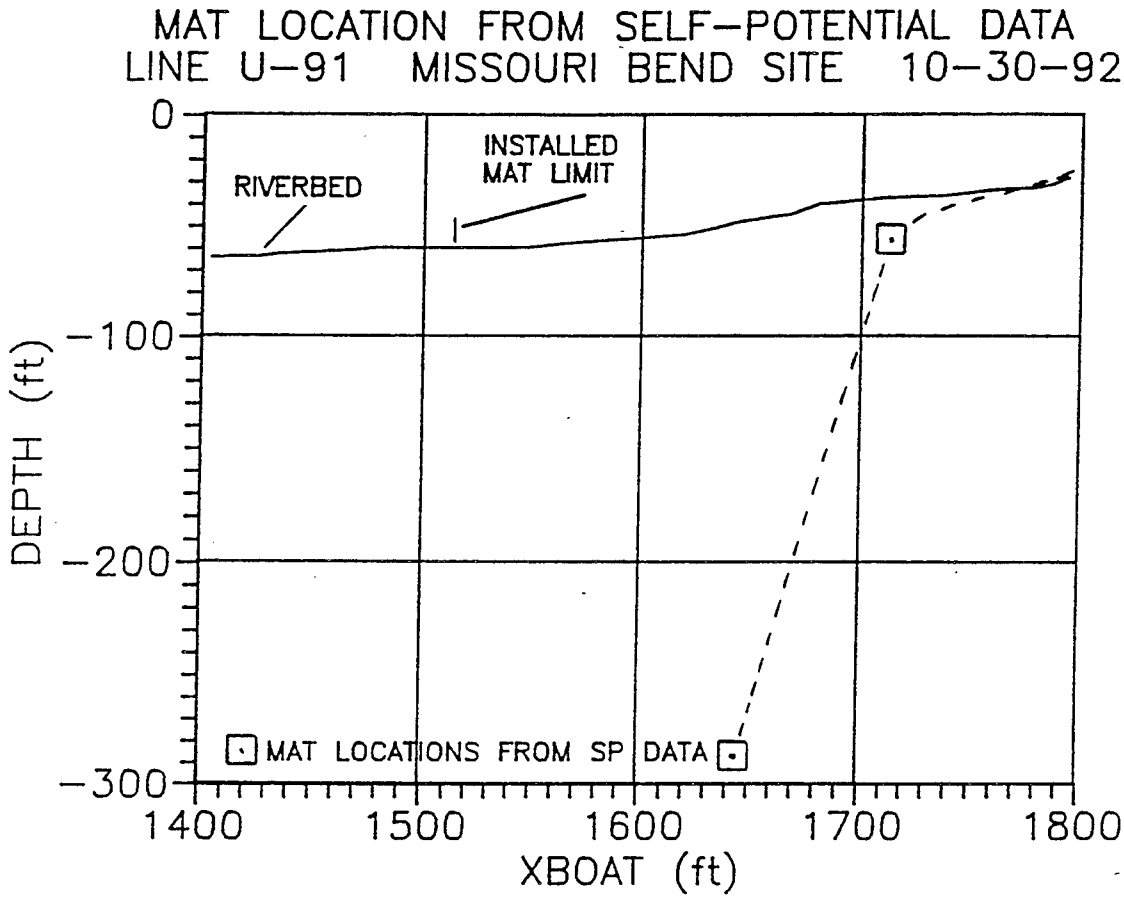
MAT LOCATION FROM SELF-POTENTIAL DATA
LINE U-91 MISSOURI BEND SITE 10-30-92
0
-100
-200
-300
DEPTH (ft)
RIVERBED
INSTALLED
MAT LIMIT
MAT LOCATIONS FROM SP DATA
1400
1500
1600
1700
1800
XBOAT (ft)

FIGURE 17

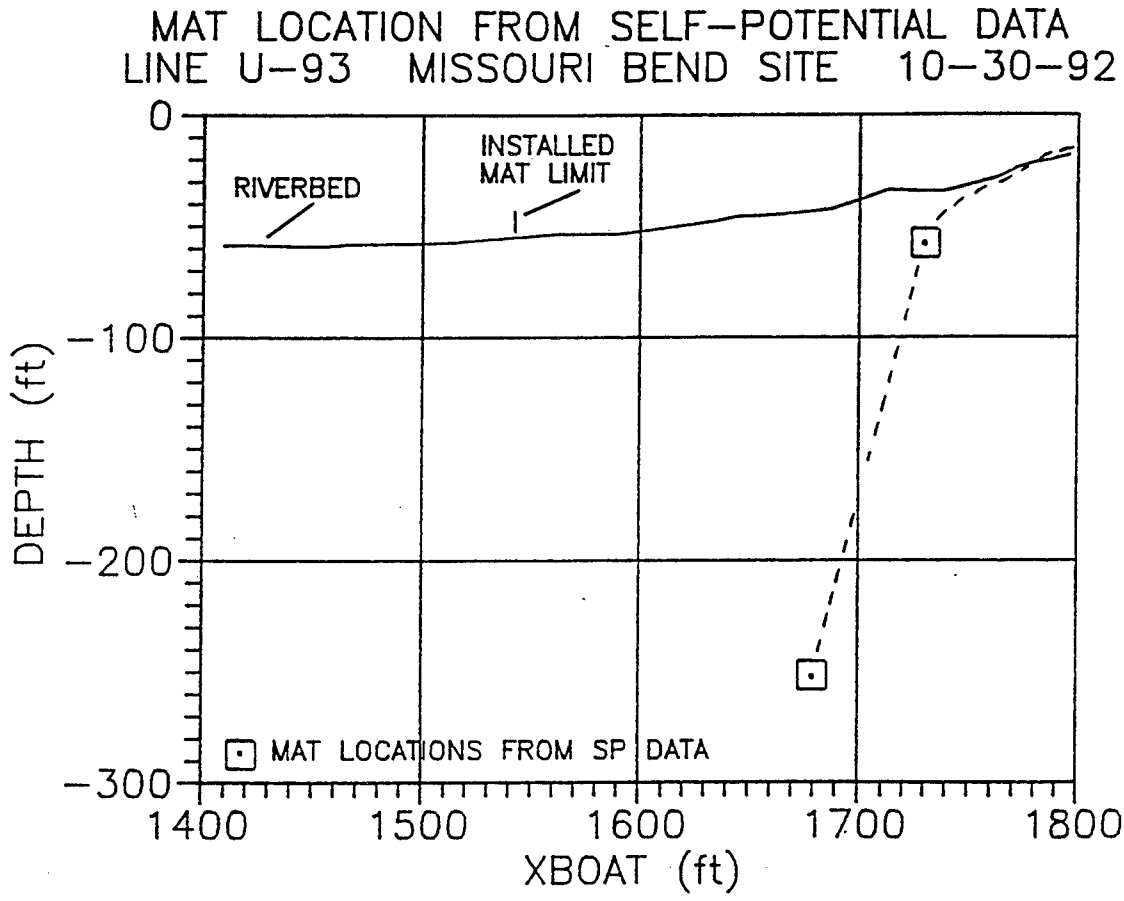
MAT LOCATION FROM SELF-POTENTIAL DATA
LINE U-93 MISSOURI BEND SITE 10-30-92
0
-100
-200
-300
DEPTH (ft)
RIVERBED
INSTALLED
MAT LIMIT
MAT LOCATIONS FROM SP DATA
1400
1500
1600
1700
1800
XBOAT (ft)

FIGURE 18

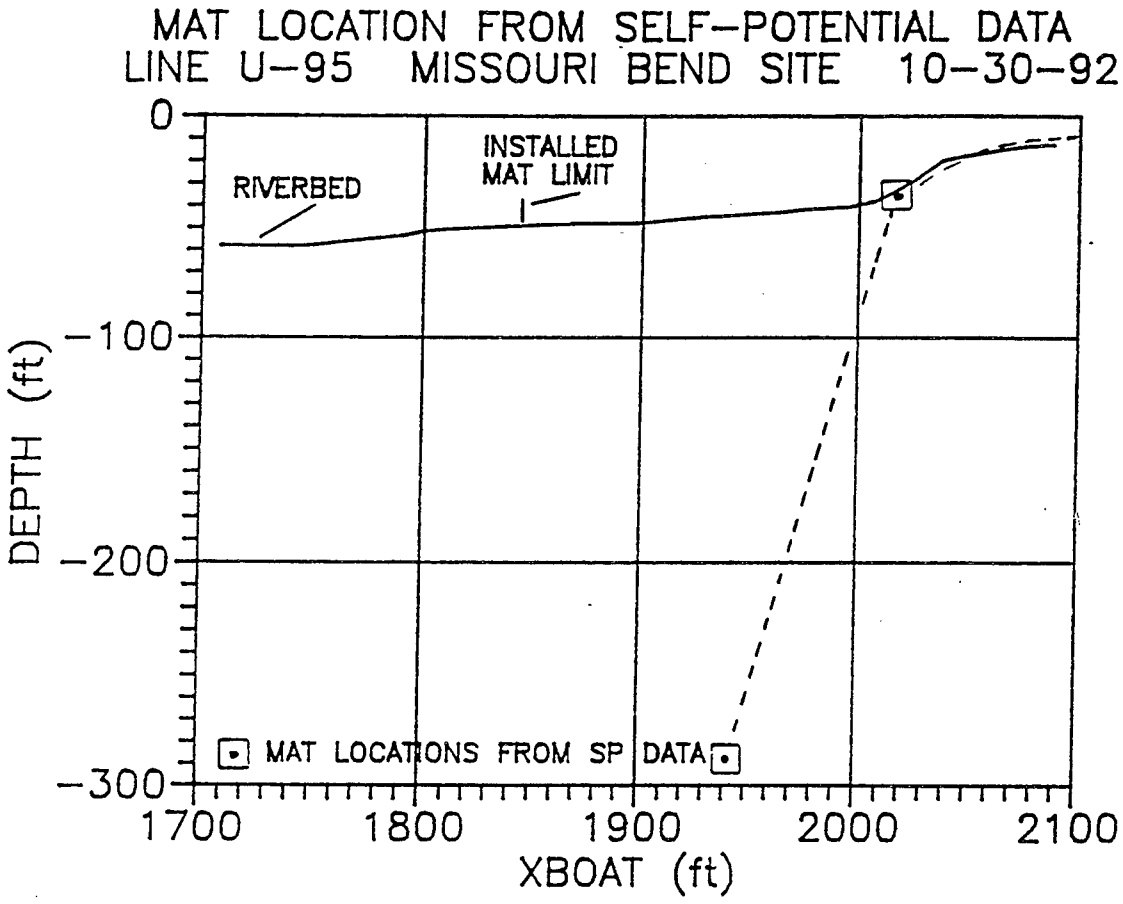
MAT LOCATION FROM SELF-POTENTIAL DATA
LINE U-95 MISSOURI BEND SITE 10-30-92
0
-100
-200
-300
DEPTH (ft)
RIVERBED
INSTALLED
MAT LIMIT
MAT LOCATIONS FROM SP DATA
1700
1800
1900
2000
2100
XBOAT (ft)

FIGURE 18A

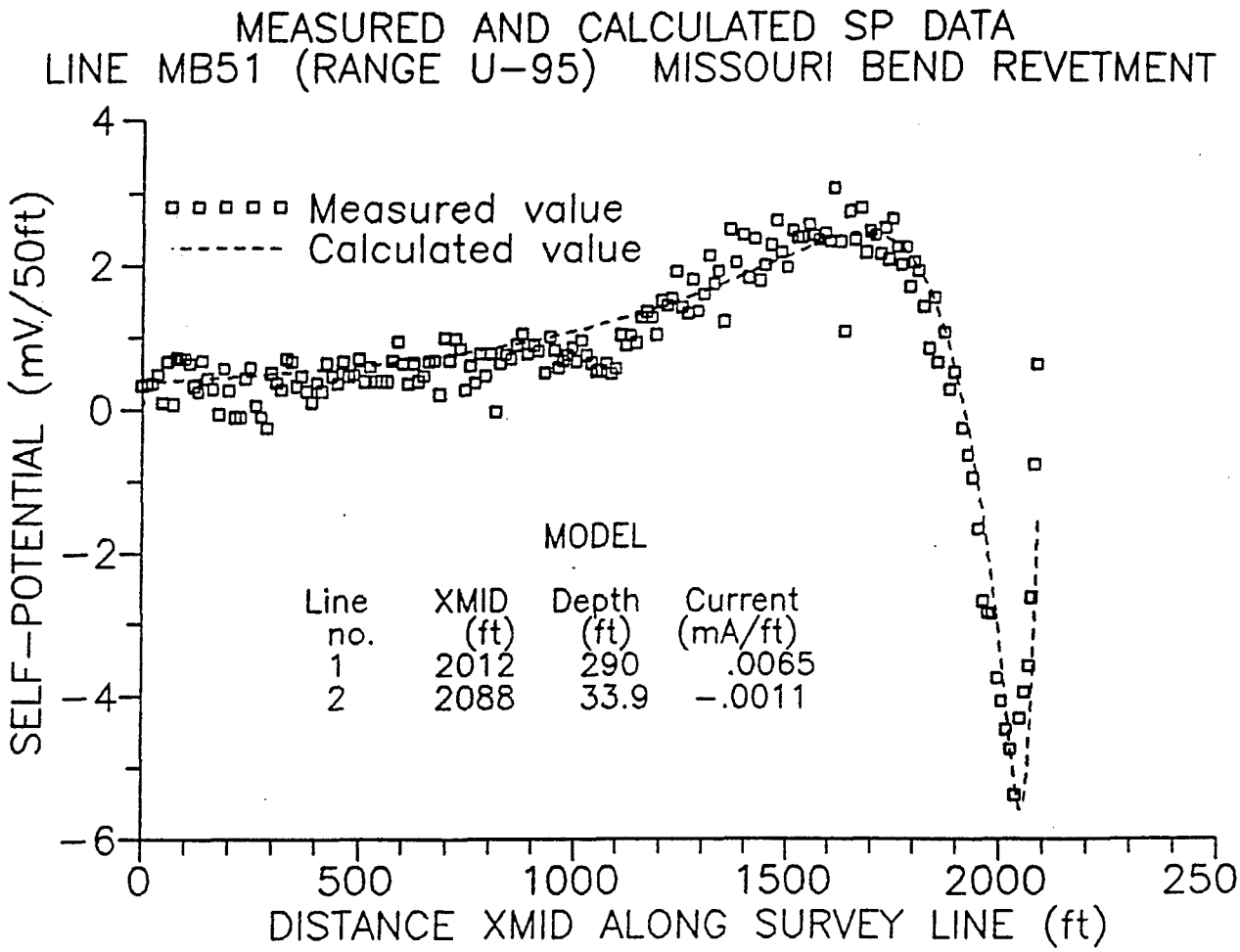
MEASURED AND CALCULATED SP DATA
LINE MB51 (RANGE U-95) MISSOURI BEND REVETMENT
Measured value
Calculated value
MODEL
Line no. | XMID (ft) | Depth (ft) | Current (mA/ft)
1 | 2012 | 290 | .0065
2 | 2088 | 33.9 | -.0011
SELF-POTENTIAL (mV/50ft)
4
2
0
-2
-4
-6
0
500
1000
1500
2000
250
DISTANCE XMID ALONG SURVEY LINE (ft)

FIGURE 19

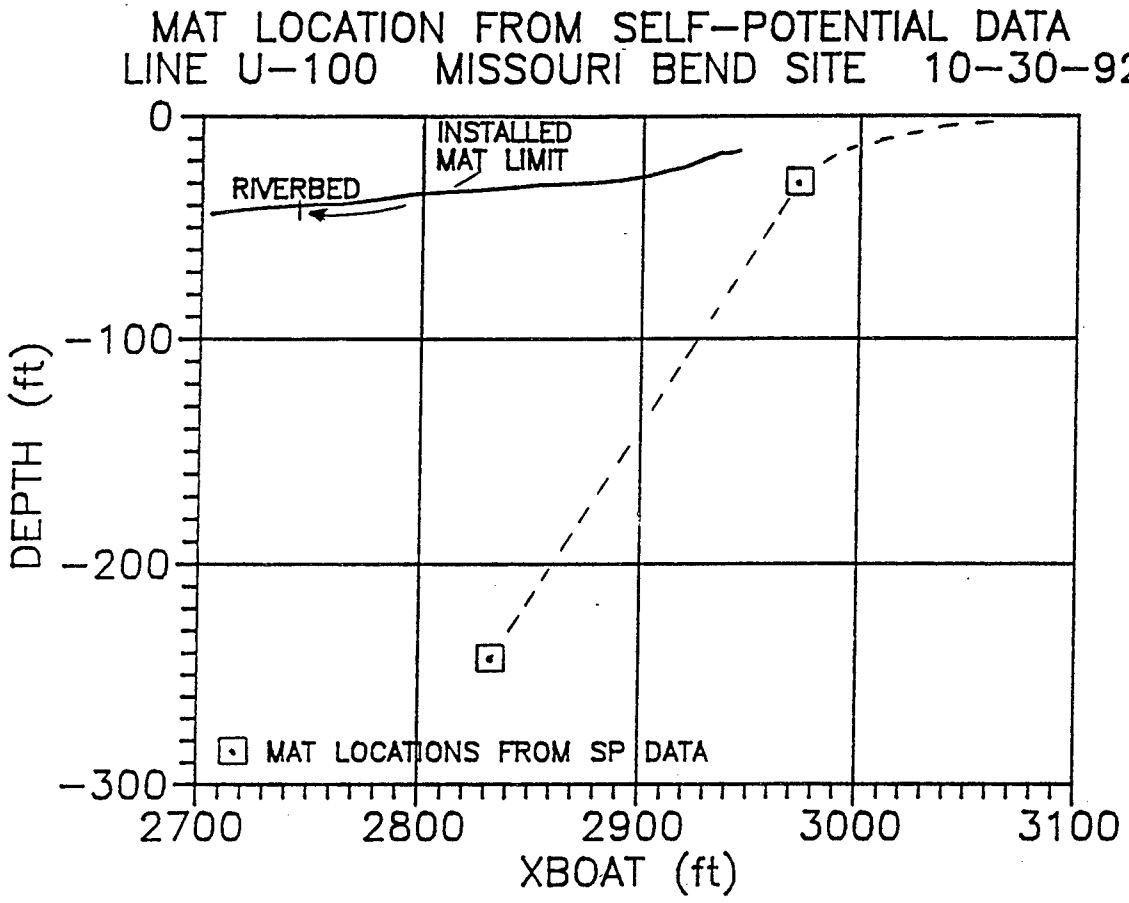
MAT LOCATION FROM SELF-POTENTIAL DATA
LINE U-100 MISSOURI BEND SITE 10-30-92
0
-100
-200
-300
DEPTH (ft)
INSTALLED
MAT LIMIT
RIVERBED
MAT LOCATIONS FROM SP DATA
2700
2800
2900
3000
3100
XBOAT (ft)

FIGURE 20

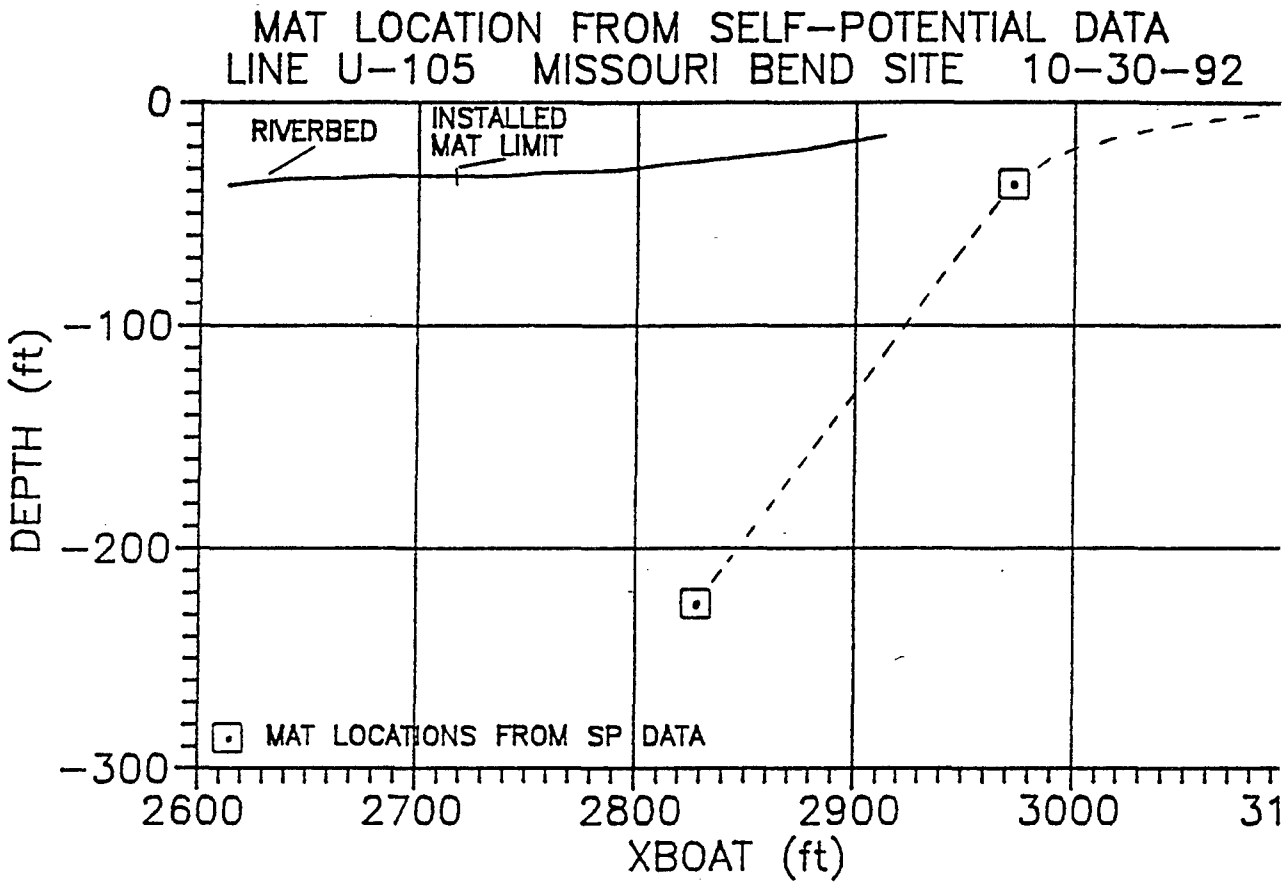
MAT LOCATION FROM SELF-POTENTIAL DATA
LINE U-105 MISSOURI BEND SITE 10-30-92
RIVERBED
INSTALLED MAT LIMIT
MAT LOCATIONS FROM SP DATA
DEPTH (ft)
0
-100
-200
-300
2600
2700
2800
2900
3000
31
XBOAT (ft)

FIGURE 21

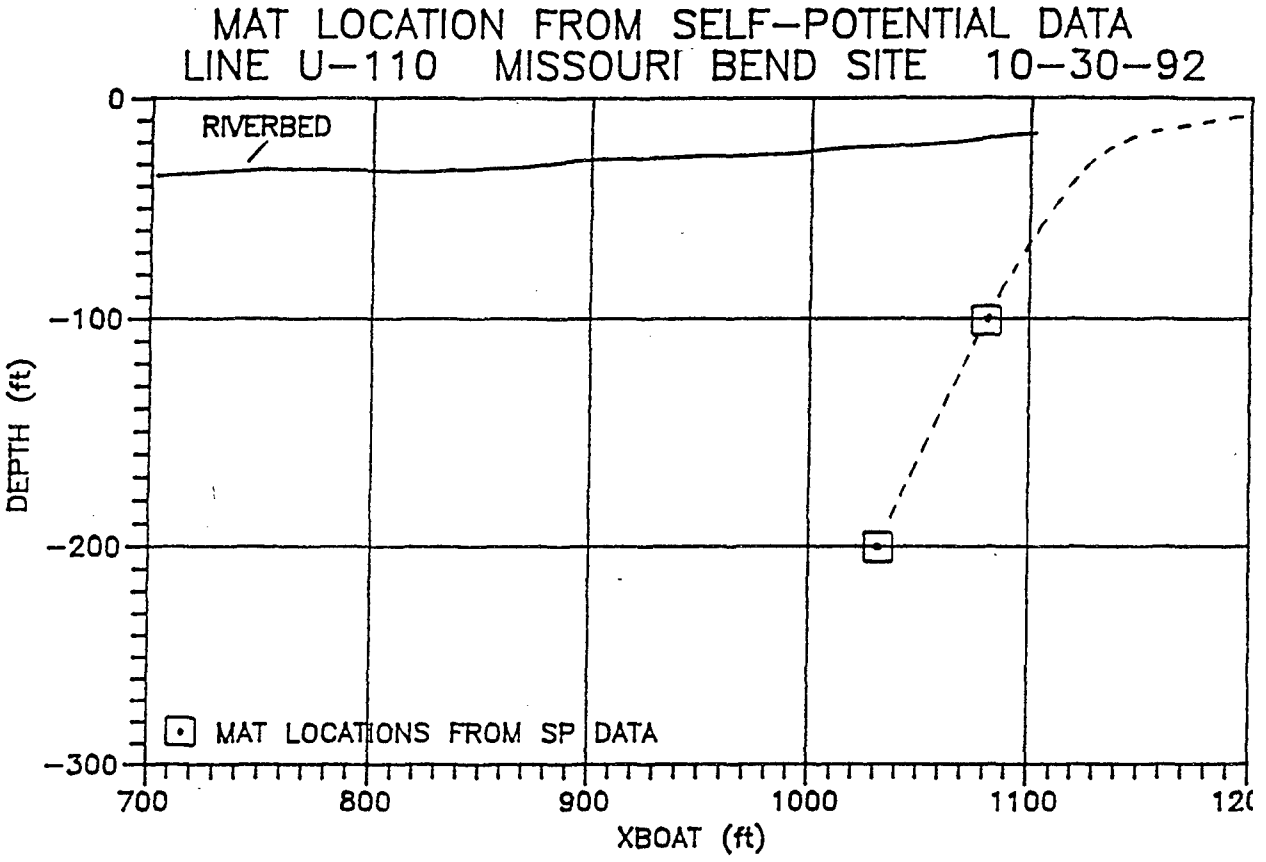
MAT LOCATION FROM SELF-POTENTIAL DATA
LINE U-110 MISSOURI BEND SITE 10-30-92
RIVERBED
MAT LOCATIONS FROM SP DATA
DEPTH (ft)
XBOAT (ft)
0
-100
-200
-300
700
800
900
1000
1100

FIGURE 22

MAT LOCATION FROM SELF-POTENTIAL DATA
LINE U-120 (NEW MAT) MISSOURI BEND SITE 10-30-9

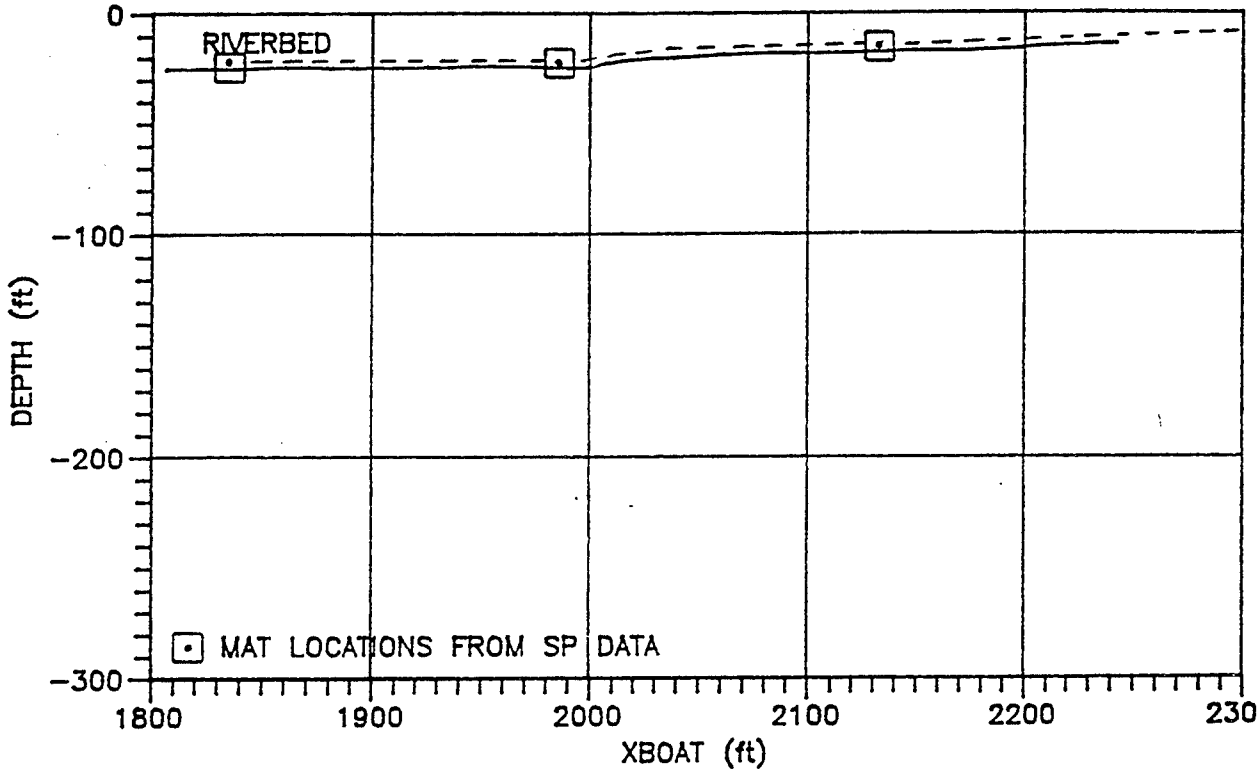

FIGURE 23

MAT LOCATION FROM SELF-POTENTIAL DATA
LINE U-122 (NEW MAT) MISSOURI BEND SITE 10-30-9

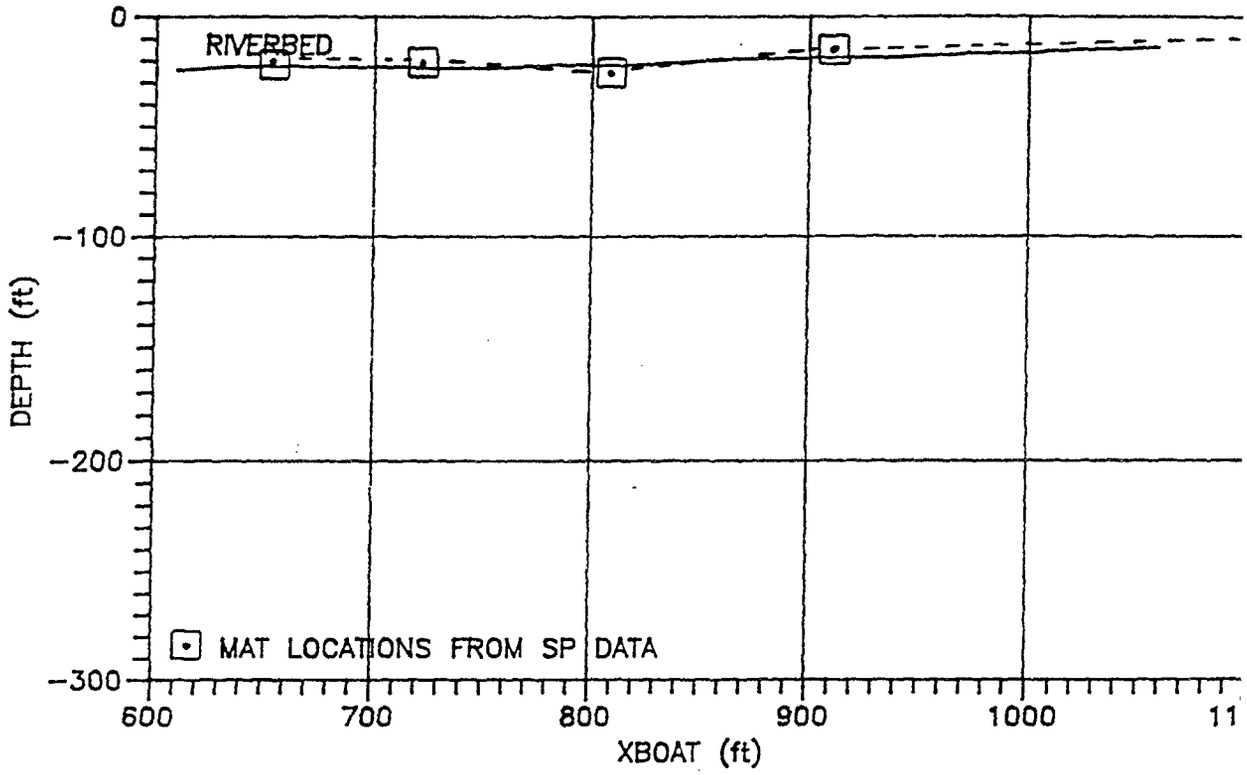

FIGURE 23A

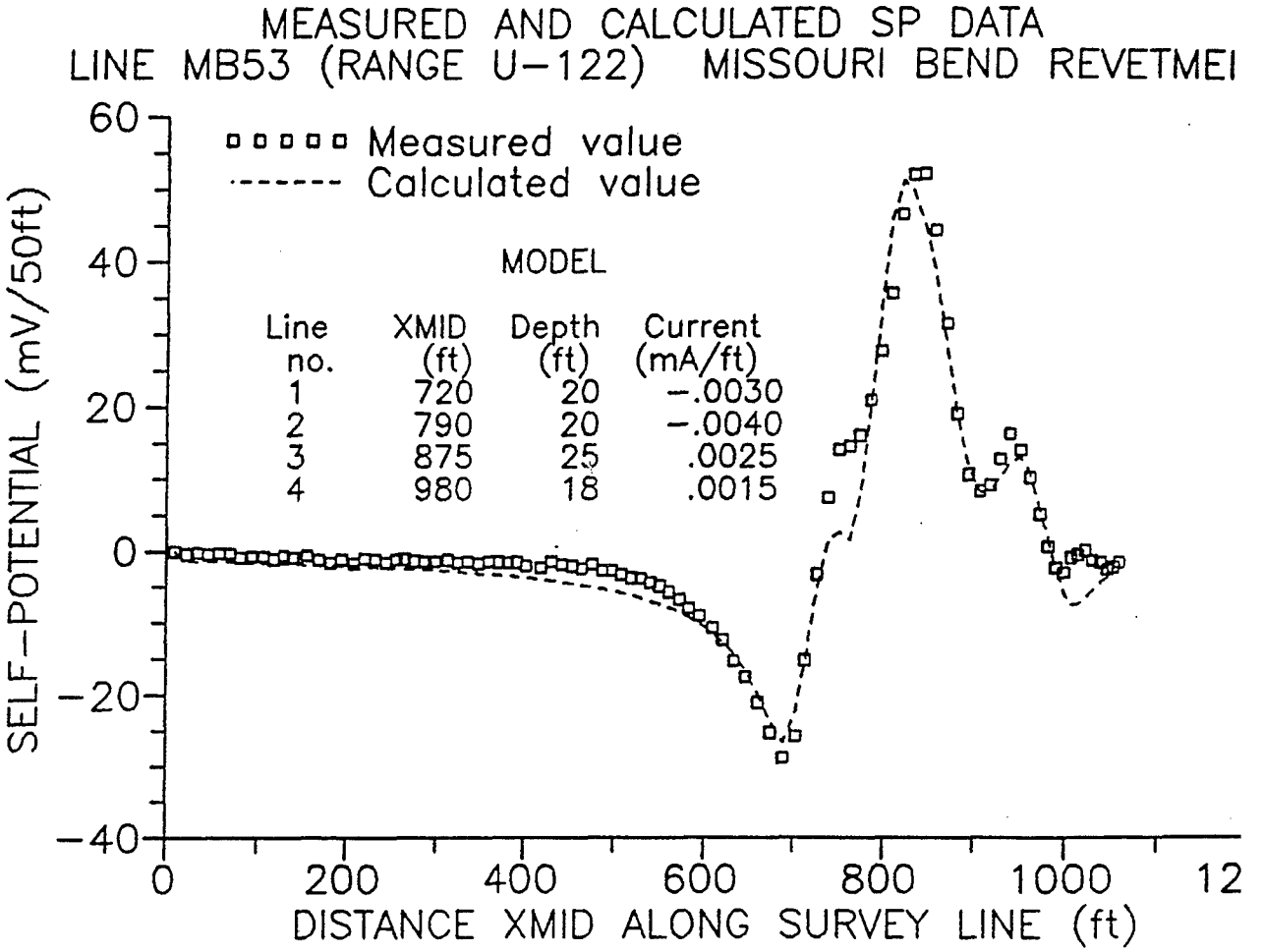
MEASURED AND CALCULATED SP DATA
LINE MB53 (RANGE U-122) MISSOURI BEND REVETMEI
Measured value
Calculated value
MODEL
Line no. | XMID (ft) | Depth (ft) | Current (mA/ft)
1 | 720 | 20 | -.0030
2 | 790 | 20 | -.0040
3 | 875 | 25 | .0025
4 | 980 | 18 | .0015
SELF-POTENTIAL (mV/50ft)
60
40
20
0
-20
-40
0
200
400
600
800
1000
12
DISTANCE XMID ALONG SURVEY LINE (ft)

FIGURE 24

MAT LOCATION FROM SELF-POTENTIAL DATA
LINE U-124 (NEW MAT) MISSOURI BEND SITE 10-30-9

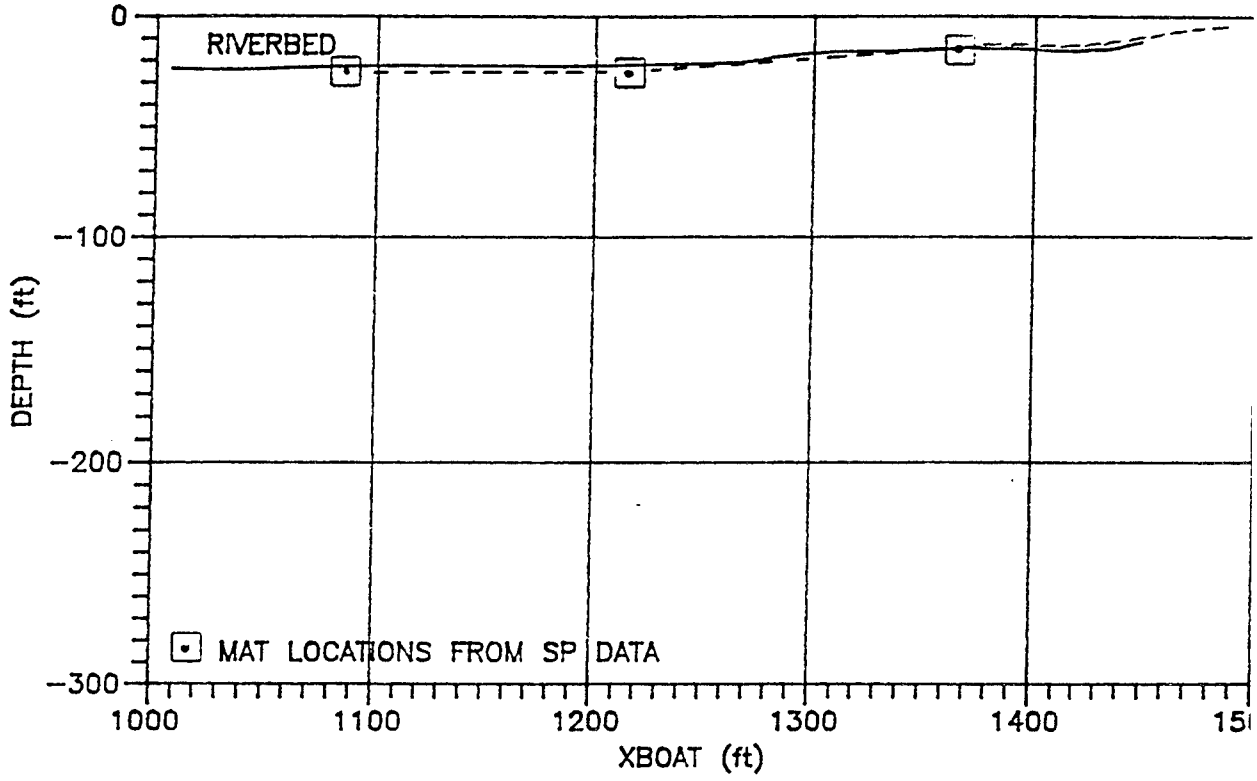

FIGURE 25

MAT DEPTHS FROM RESISTIVITY SOUNDINGS
RANGE U-128 MISSOURI BEND SITE -- NEW MAT
(Resistivity Values in Ohm-Meters)

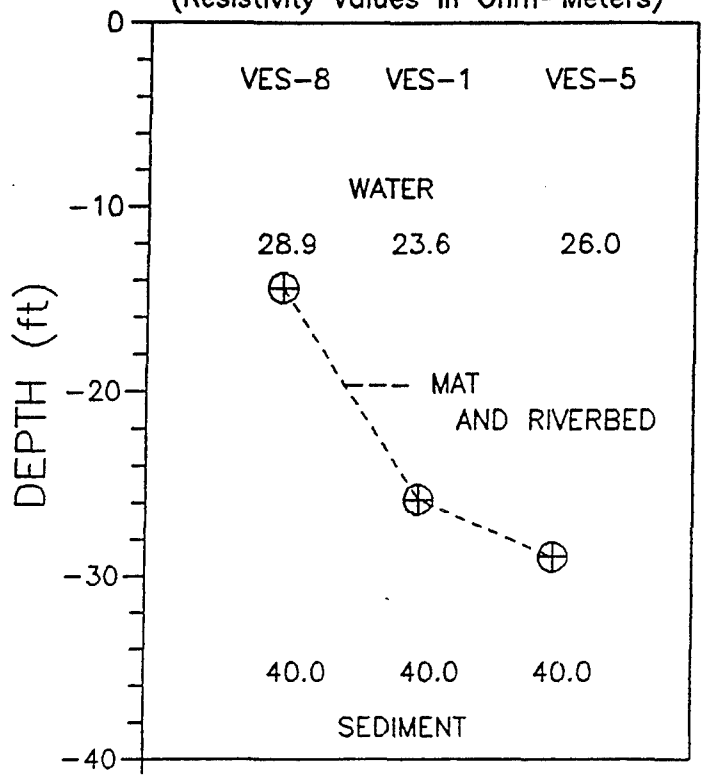

FIGURE 26

MAT DEPTHS FROM RESISTIVITY SOUNDINGS
RANGE U-95 MISSOURI BEND SITE
(Resistivity Values in Ohm-Meters)

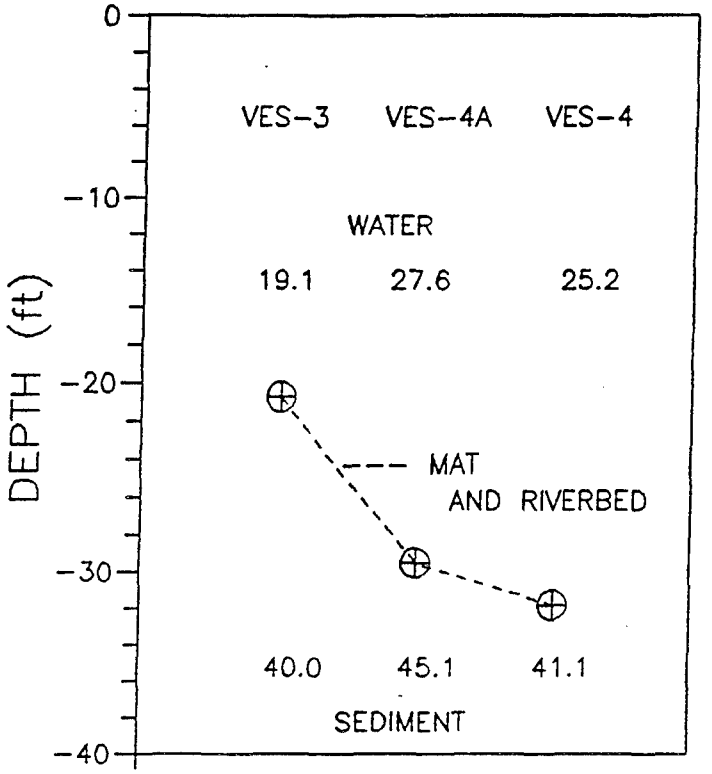

FIGURE 27

MAT DEPTHS FROM RESISTIVITY SOUNDINGS
RANGE U-112 MISSOURI BEND SITE
(Resistivity Values in Ohm-Meters)

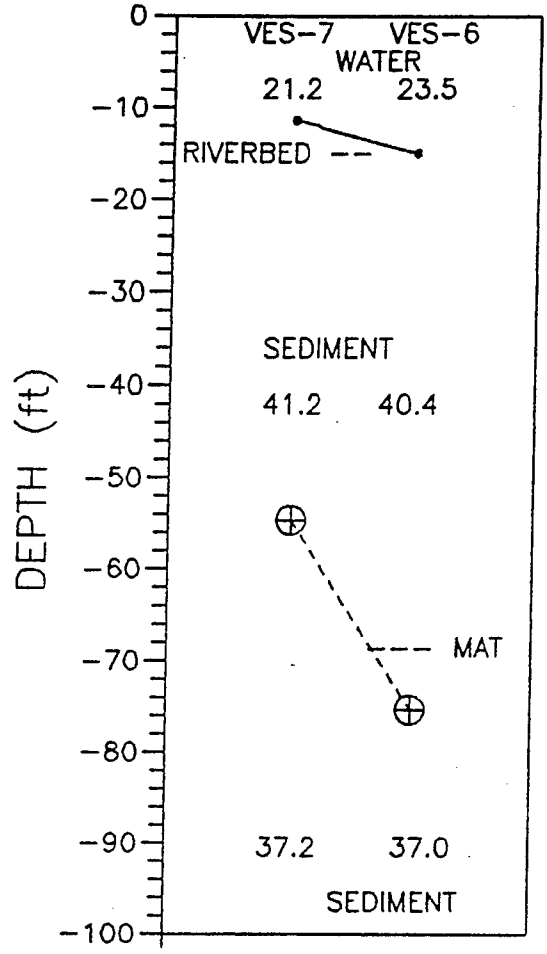

FIGURE 28

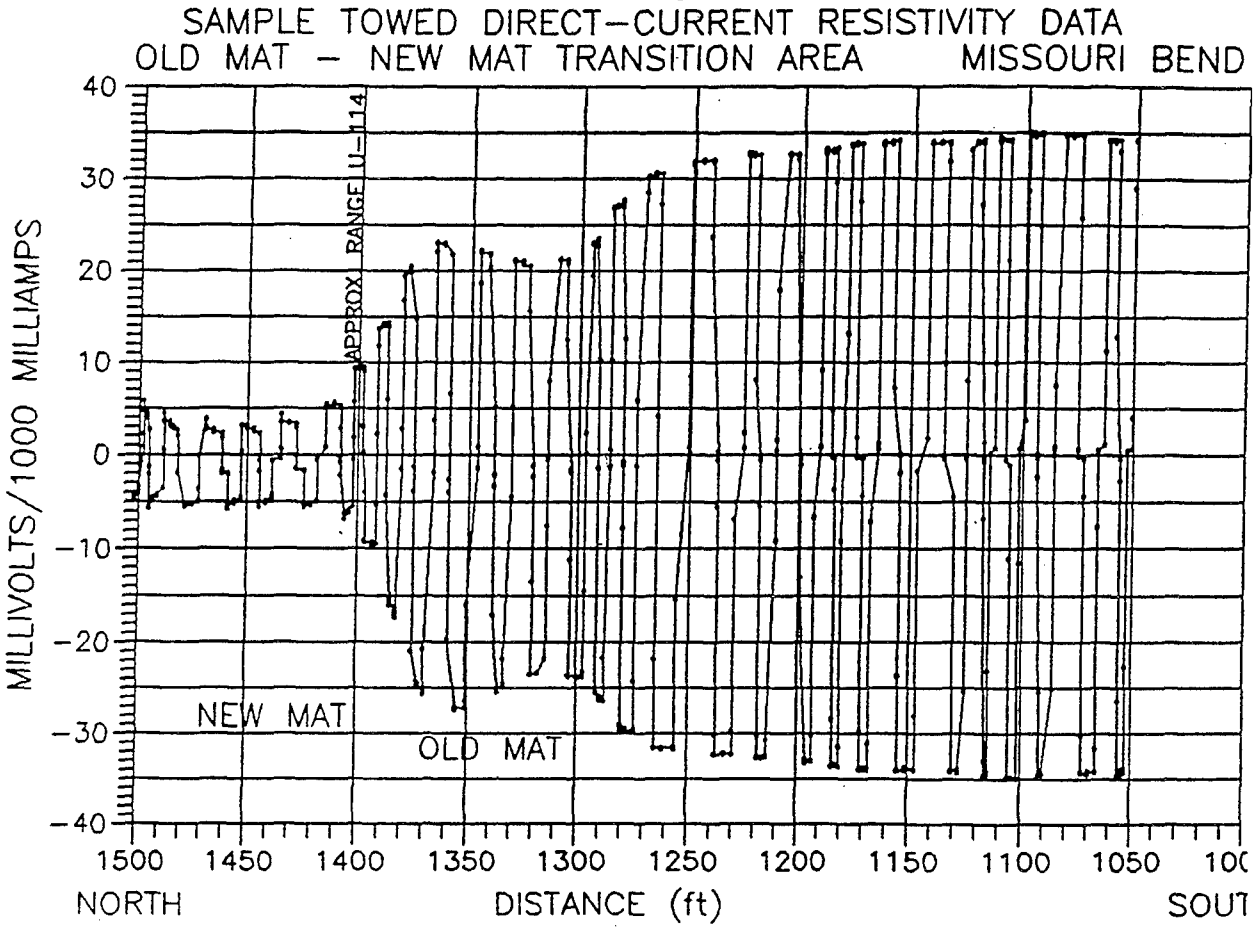
SAMPLE TOWED DIRECT-CURRENT RESISTIVITY DATA
OLD MAT - NEW MAT TRANSITION AREA MISSOURI BEND
MILLIVOLTS/1000 MILLIAMPS
40
30
20
10
0
-10
-20
-30
-40
APPROX. RANGE LI-114
NEW MAT
OLD MAT
1500
1450
1400
1350
1300
1250
1200
1150
1100
1050
NORTH
DISTANCE (ft)
SOUT

FIGURE 29

APPROXIMATE MAT DEPTH CALCULATED FROM SINGLE-CHANNEL TOWED RESISTIVITY DATA
ALONG 20 FT DEPTH CONTOUR OLD MAT - NEW MAT TRANSITION AREA
MISSOURI BEND SITE 2 NOVEMBER 1992

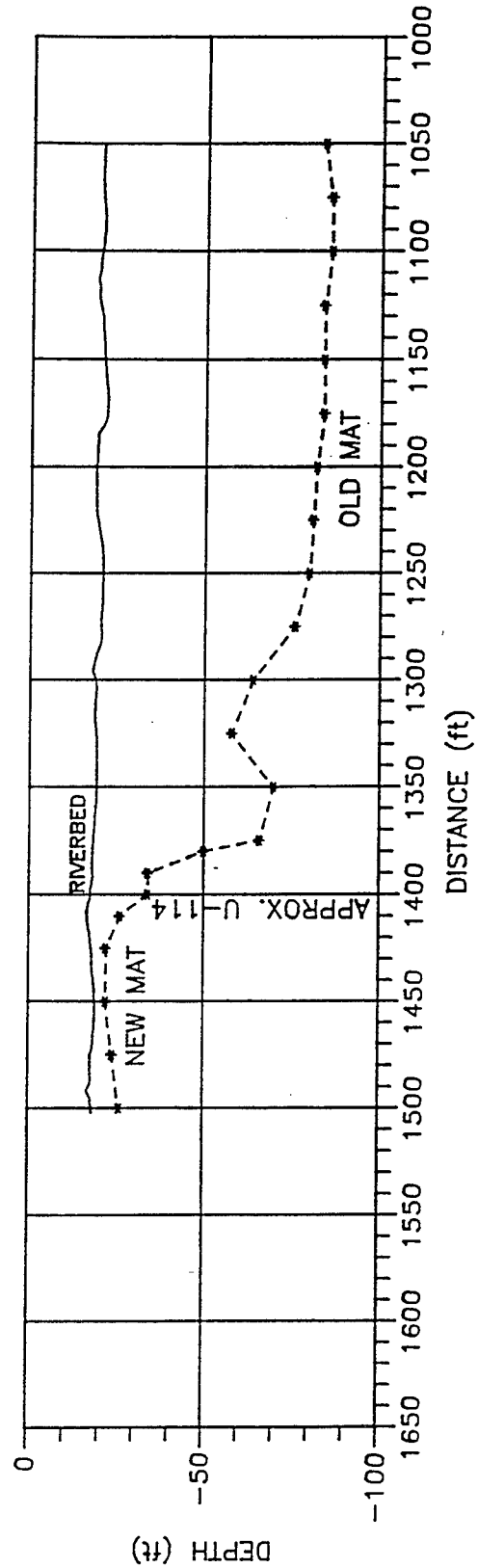

FIGURE 30

APPROXIMATE MAT DEPTH CALCULATED FROM SINGLE-CHANNEL TOWED RESISTIVITY DATA
FOLLOWING 20 FT DEPTH CONTOUR RANGES U-93 TO U-104.5
MISSOURI BEND SITE

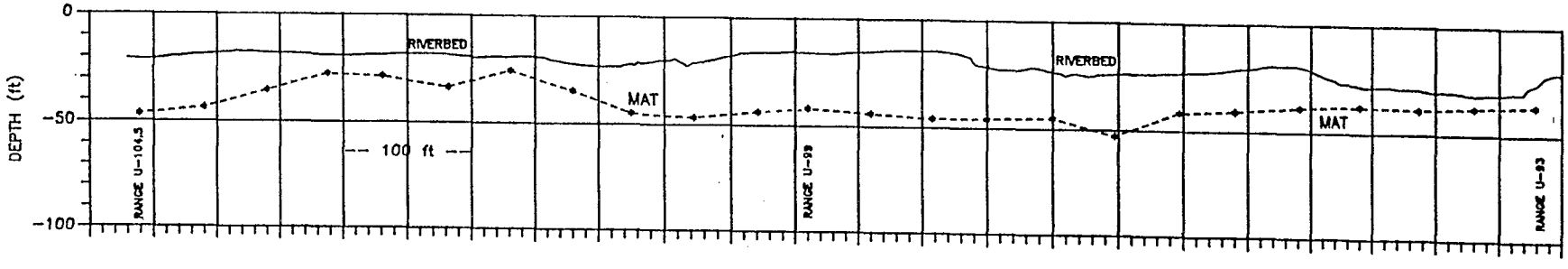

FIGURE 31A

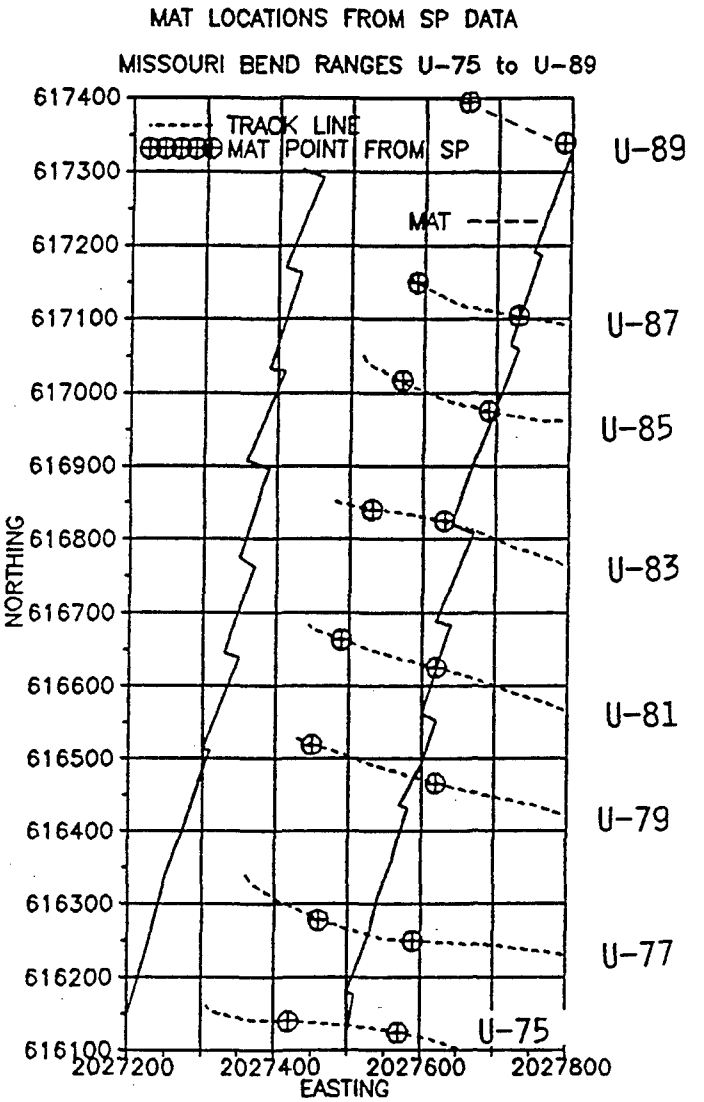
MAT LOCATIONS FROM SP DATA
MISSOURI BEND RANGES U-75 to U-89
TRACK LINE
MAT POINT FROM SP
MAT
U-89
U-87
U-85
U-83
U-81
U-79
U-77
U-75
NORTHING
617400
617300
617200
617100
617000
616900
616800
616700
616600
616500
616400
616300
616200
616100
2027200
2027400
2027600
2027800
EASTING

FIGURE 31B

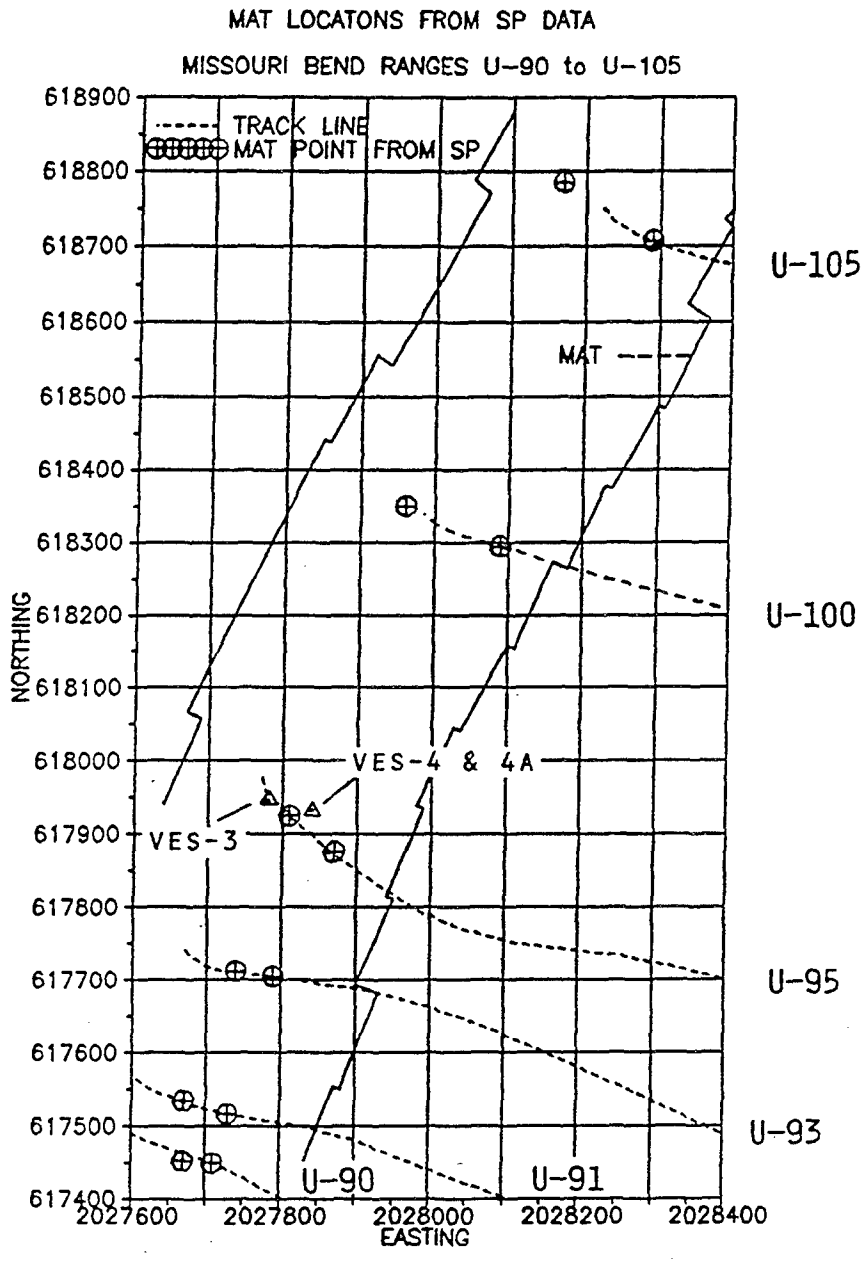
MAT LOCATONS FROM SP DATA
MISSOURI BEND RANGES U-90 to U-105
TRACK LINE
MAT POINT FROM SP
MAT
U-105
U-100
U-95
U-93
U-91
U-90
VES-4 & 4A
VES-3
NORTHING
EASTING
618900
618800
618700
618600
618500
618400
618300
618200
618100
618000
617900
617800
617700
617600
617500
617400
2027600
2027800
2028000
2028200
2028400

FIGURE 31C

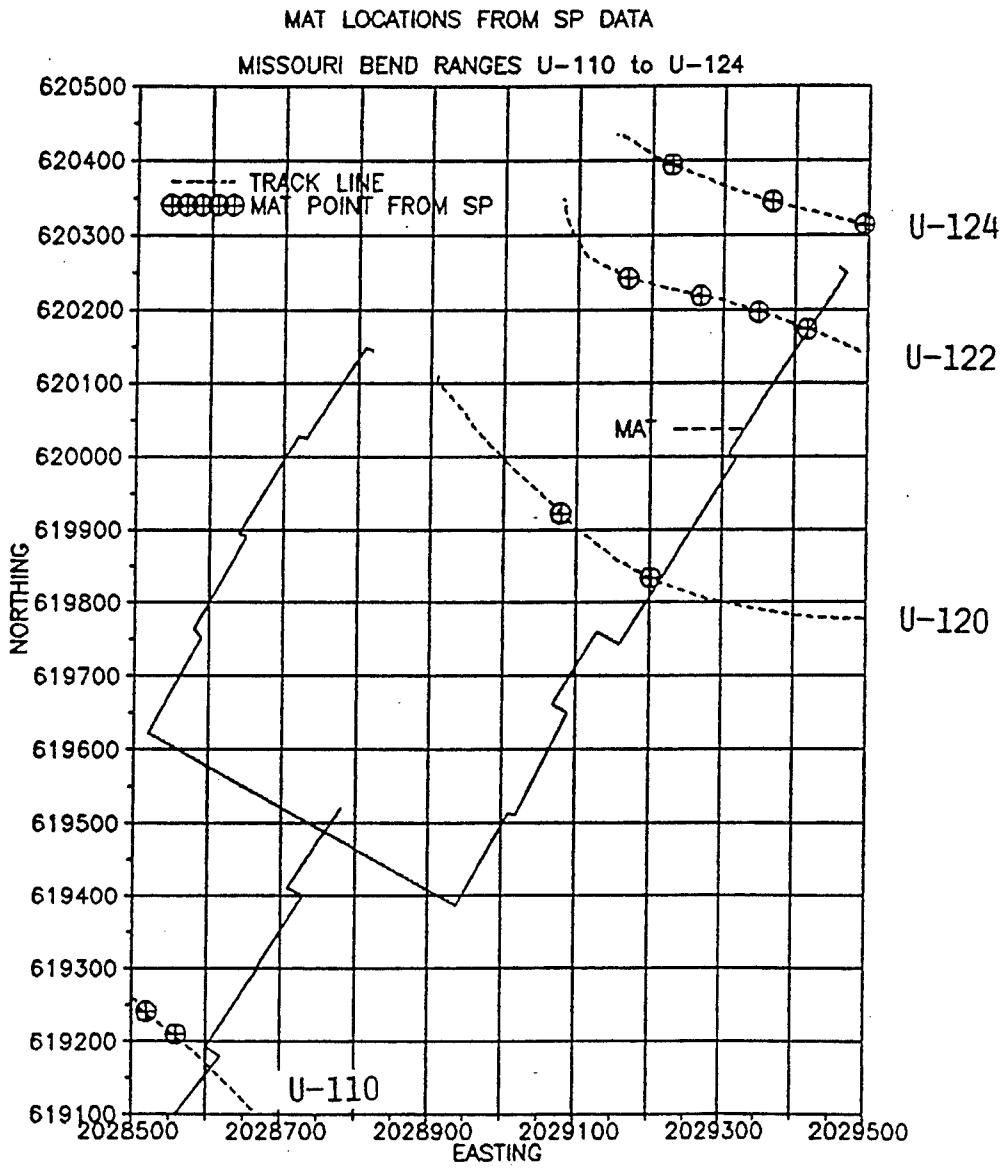
MAT LOCATIONS FROM SP DATA
MISSOURI BEND RANGES U-110 to U-124
TRACK LINE
MAT POINT FROM SP
MAT
U-124
U-122
U-120
U-110
NORTHING
620500
620400
620300
620200
620100
620000
619900
619800
619700
619600
619500
619400
619300
619200
619100
2028500
2028700
2028900
2029100
2029300
2029500
EASTING

FIGURE 32

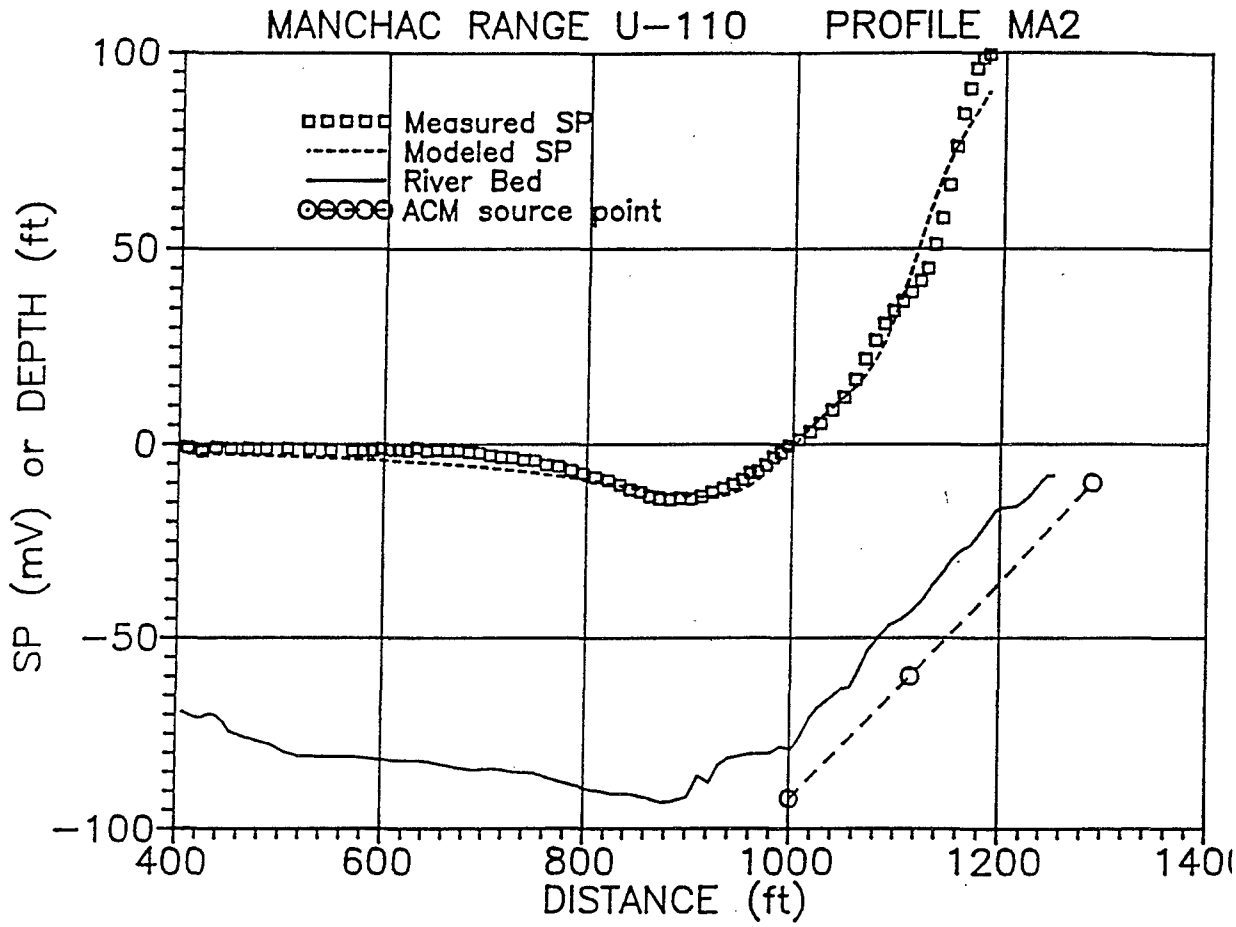
MANCHAC RANGE U-110 PROFILE MA2
Measured SP
Modeled SP
River Bed
ACM source point
SP (mV) or DEPTH (ft)
100
50
0
-50
-100
400
600
800
1000
1200
1400
DISTANCE (ft)

FIGURE 33

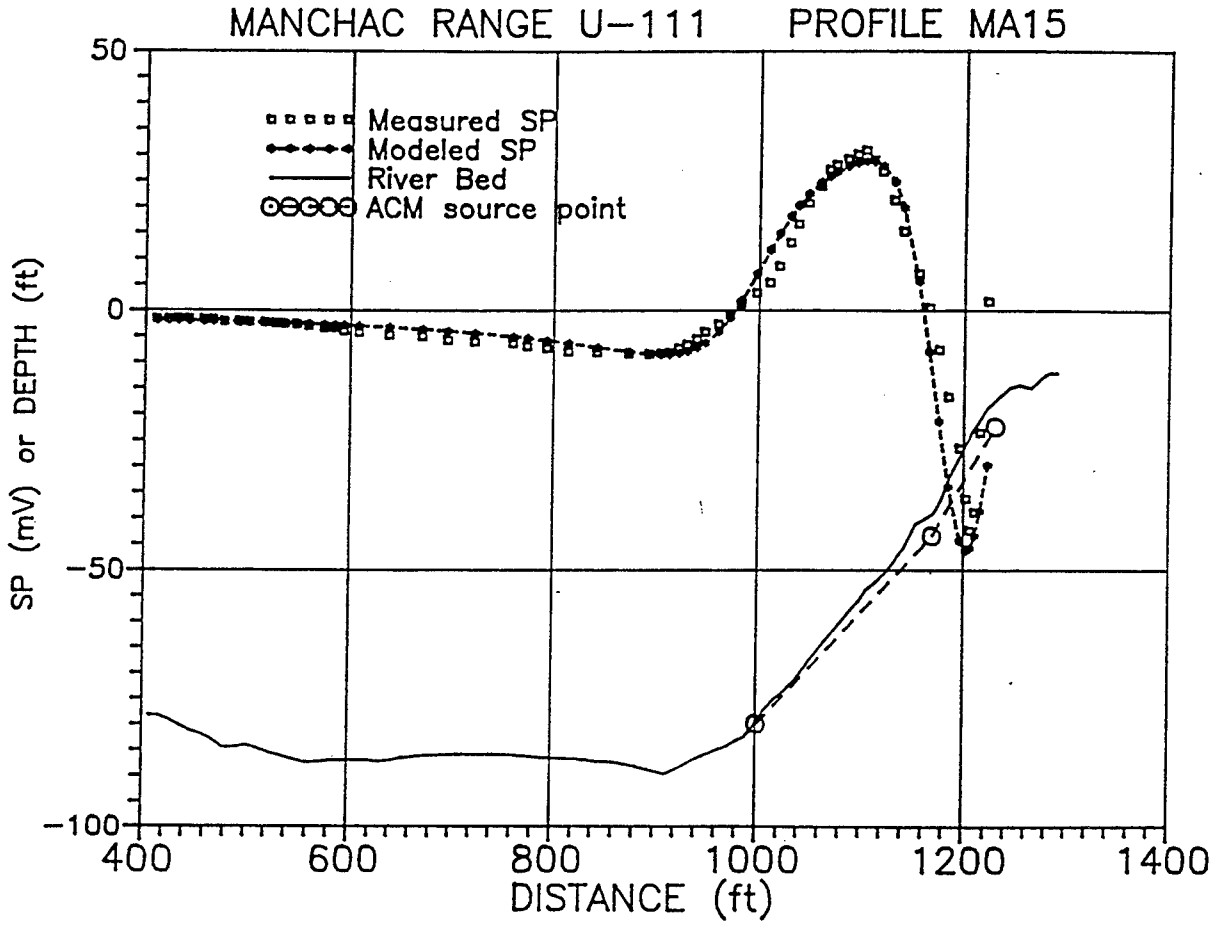
MANCHAC RANGE U-111 PROFILE MA15
Measured SP
Modeled SP
River Bed
ACM source point
SP (mV) or DEPTH (ft)
50
0
-50
-100
400
600
800
1000
1200
1400
DISTANCE (ft)

FIGURE 34

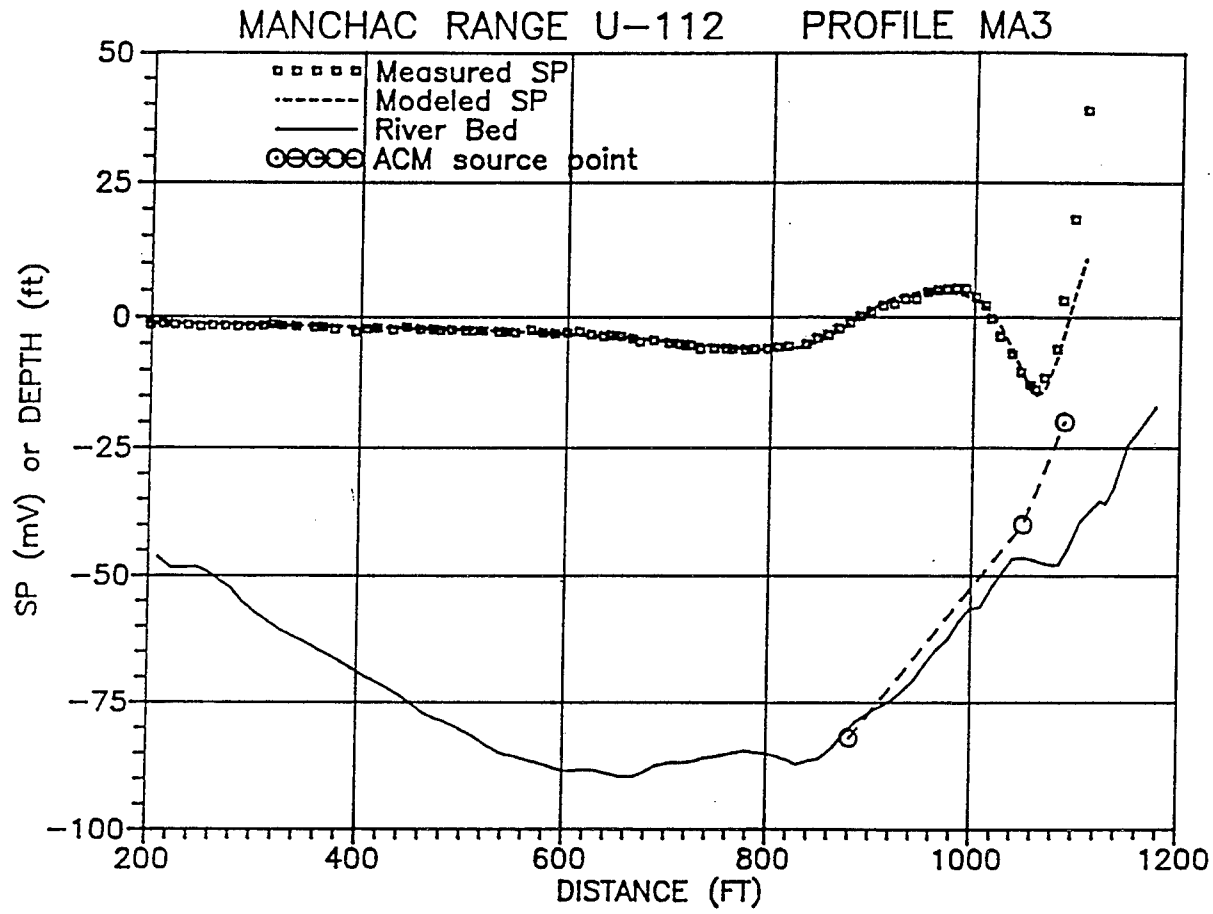
MANCHAC RANGE U-112 PROFILE MA3
Measured SP
Modeled SP
River Bed
ACM source point
SP (mV) or DEPTH (ft)
50
25
0
-25
-50
-75
-100
200
400
600
800
1000
1200
DISTANCE (FT)

FIGURE 35

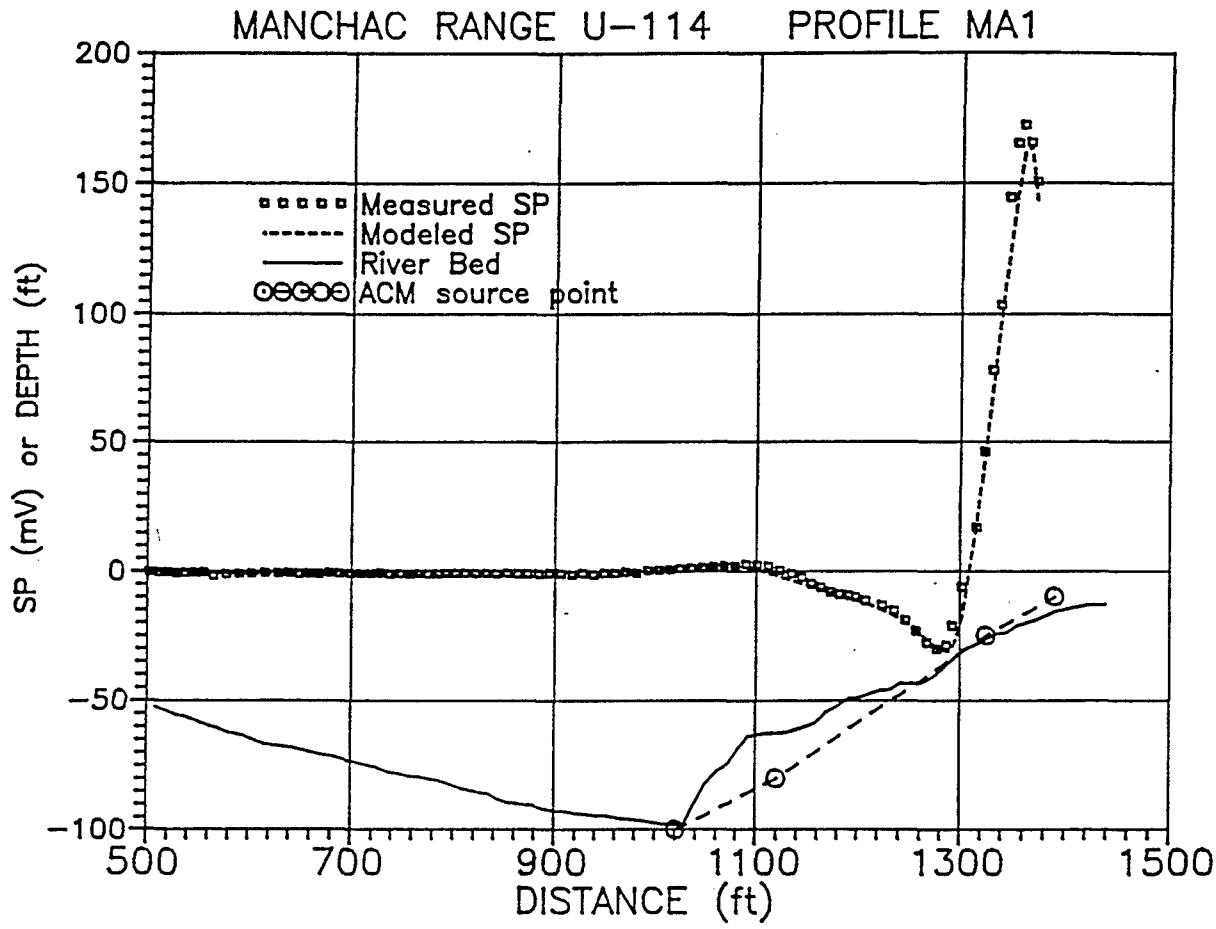
MANCHAC RANGE U-114 PROFILE MA1
Measured SP
Modeled SP
River Bed
ACM source point
SP (mV) or DEPTH (ft)
200
150
100
50
0
-50
-100
500
700
900
1100
1300
1500
DISTANCE (ft)

FIGURE 36

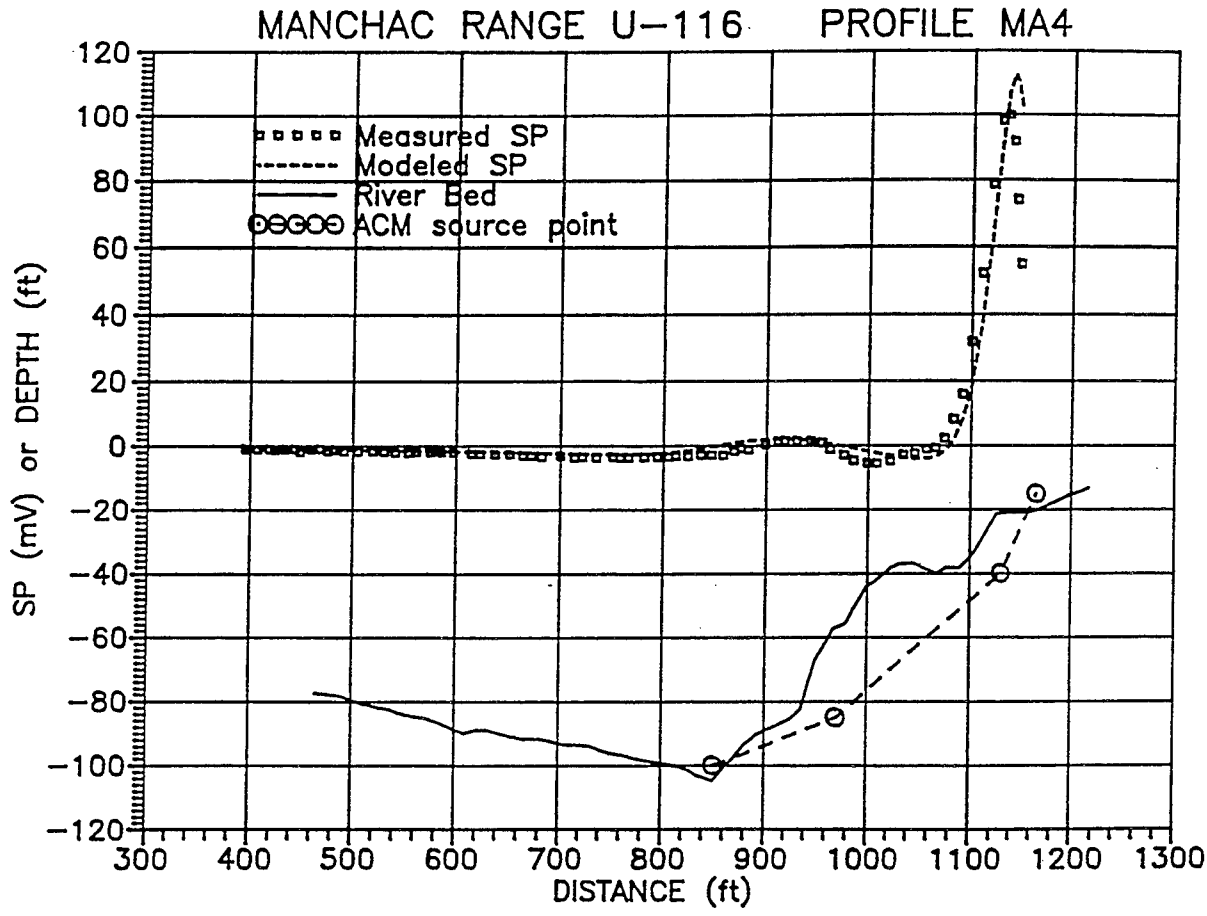
MANCHAC RANGE U-116 PROFILE MA4
Measured SP
Modeled SP
River Bed
ACM source point
SP (mV) or DEPTH (ft)
DISTANCE (ft)
120
100
80
60
40
20
0
-20
-40
-60
-80
-100
-120
300
400
500
600
700
800
900
1000
1100
1200
1300

FIGURE 37

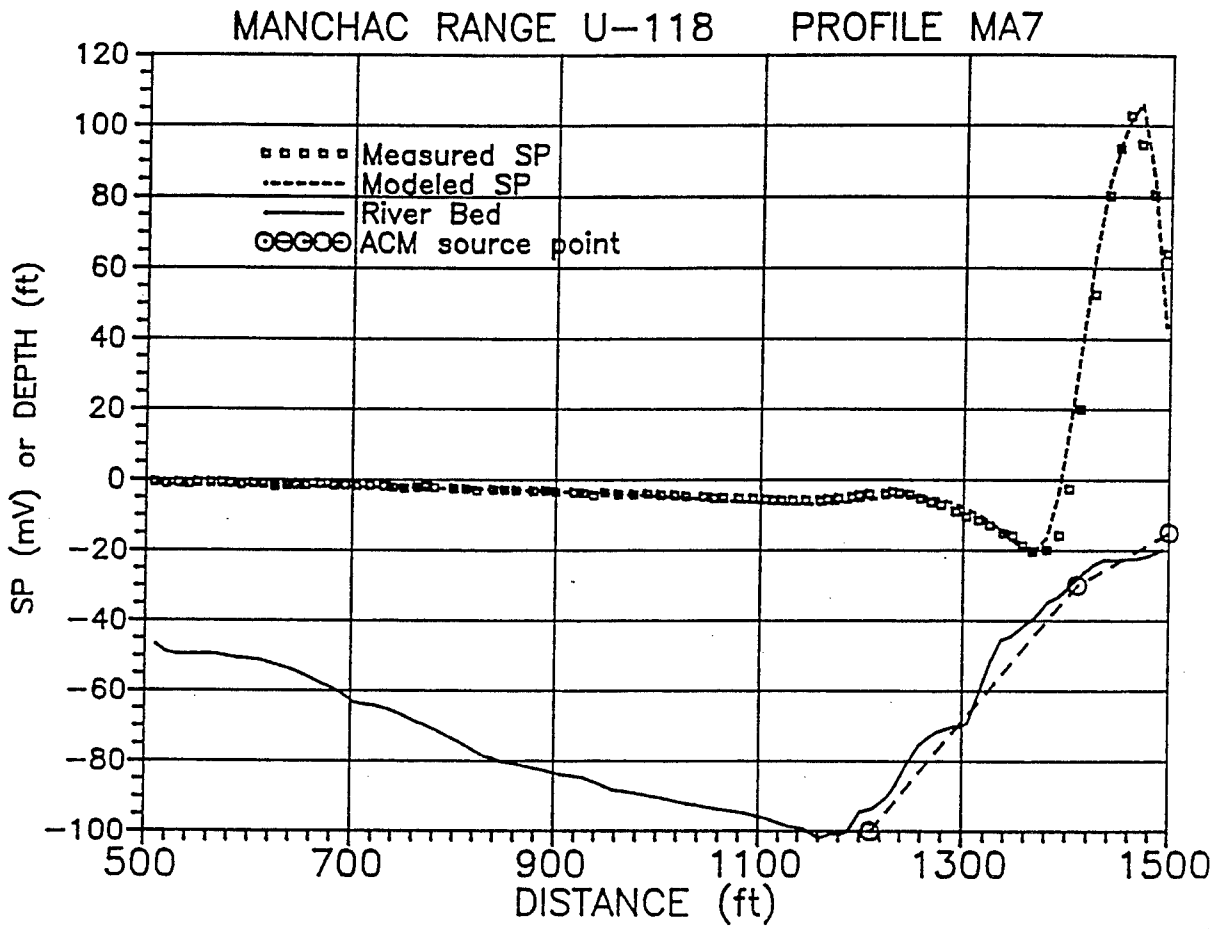
MANCHAC RANGE U-118 PROFILE MA7
Measured SP
Modeled SP
River Bed
ACM source point
SP (mV) or DEPTH (ft)
120
100
80
60
40
20
0
-20
-40
-60
-80
-100
500
700
900
1100
1300
1500
DISTANCE (ft)

FIGURE 38

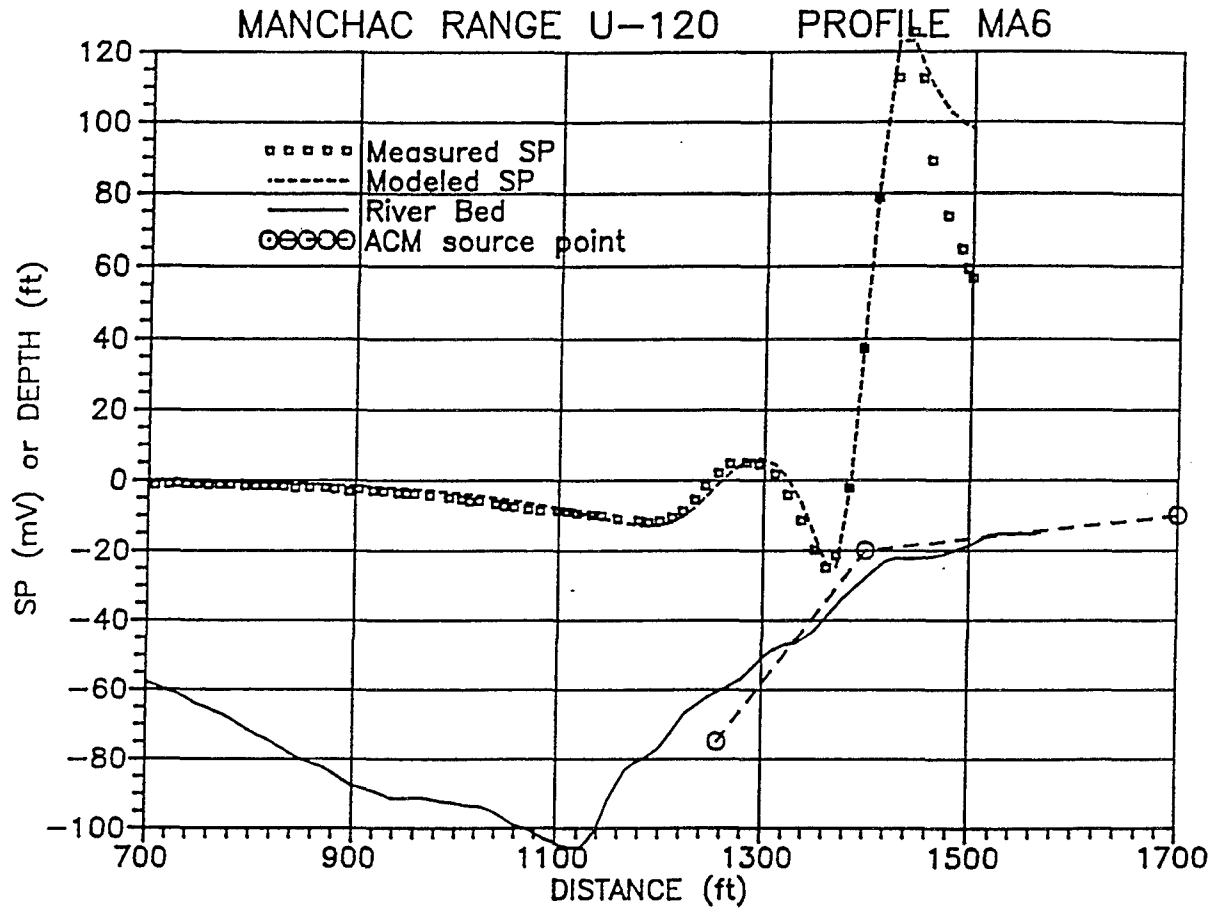
MANCHAC RANGE U-120 PROFILE MA6
Measured SP
Modeled SP
River Bed
ACM source point
SP (mV) or DEPTH (ft)
DISTANCE (ft)
120
100
80
60
40
20
0
-20
-40
-60
-80
-100
700
900
1100
1300
1500
1700

FIGURE 39

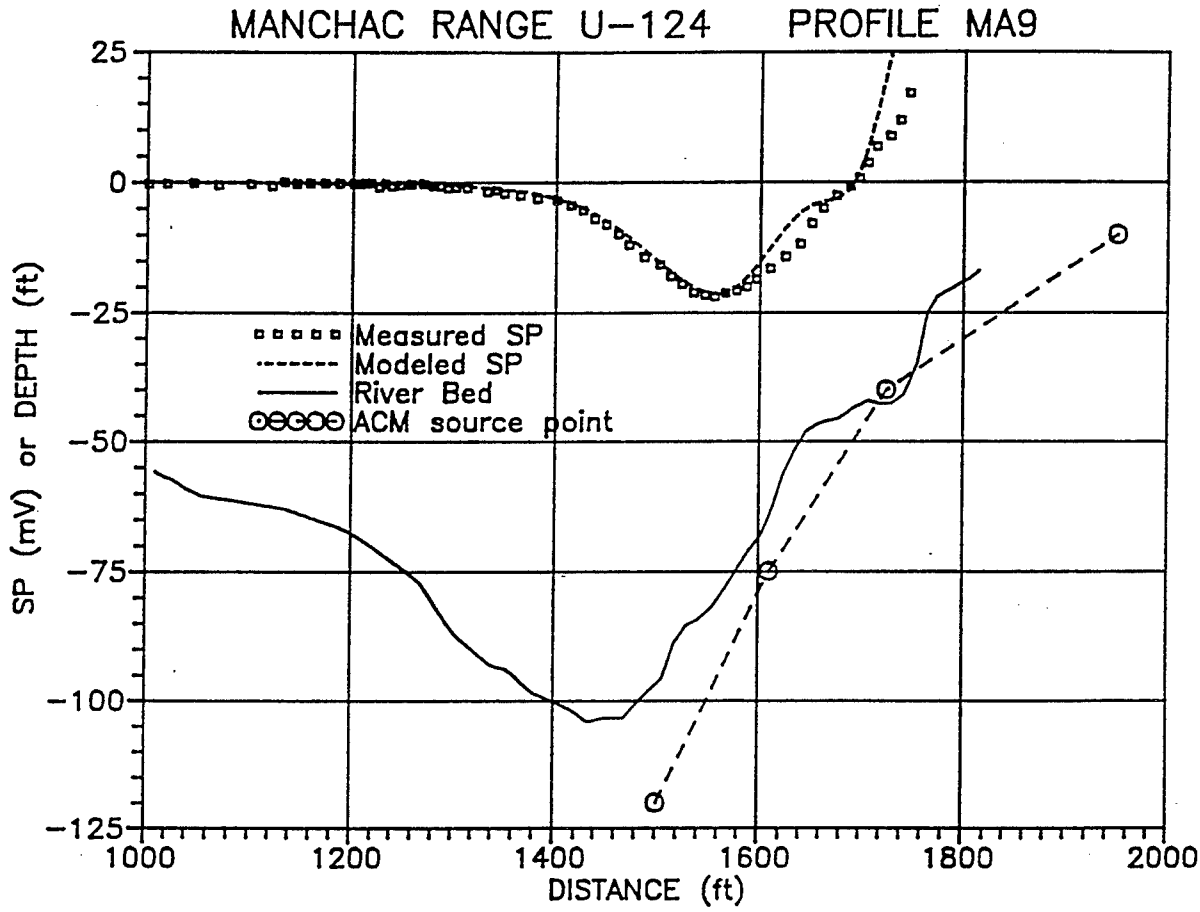
MANCHAC RANGE U-124 PROFILE MA9
25
0
-25
-50
-75
-100
-125
SP (mV) or DEPTH (ft)
Measured SP
Modeled SP
River Bed
ACM source point
1000
1200
1400
1600
1800
2000
DISTANCE (ft)

FIGURE 40

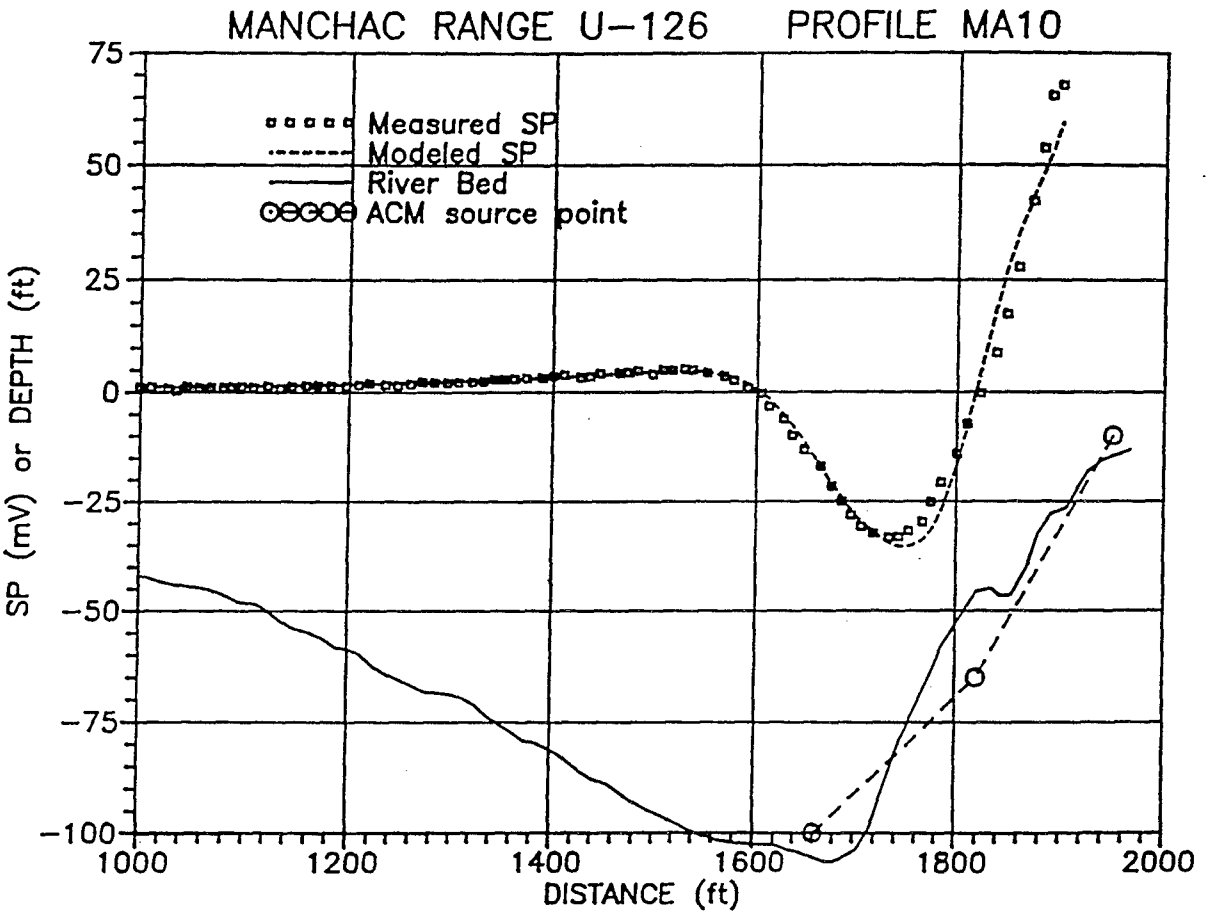
MANCHAC RANGE U-126 PROFILE MA10
Measured SP
Modeled SP
River Bed
ACM source point
SP (mV) or DEPTH (ft)
75
50
25
0
-25
-50
-75
-100
1000
1200
1400
1600
1800
2000
DISTANCE (ft)

FIGURE 41

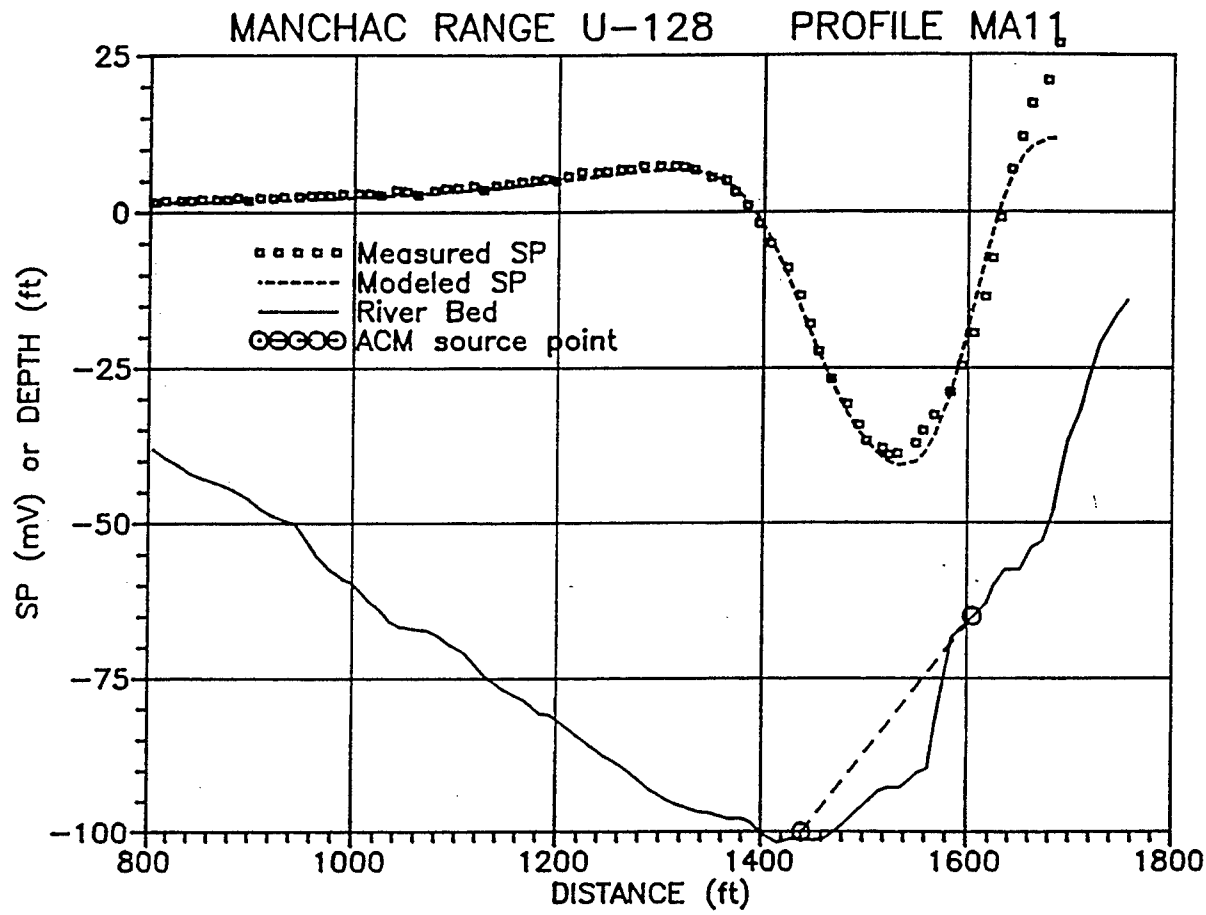
MANCHAC RANGE U-128 PROFILE MA11
25
0
-25
-50
-75
-100
800
1000
1200
1400
1600
1800
SP (mV) or DEPTH (ft)
DISTANCE (ft)
Measured SP
Modeled SP
River Bed
ACM source point

FIGURE 42

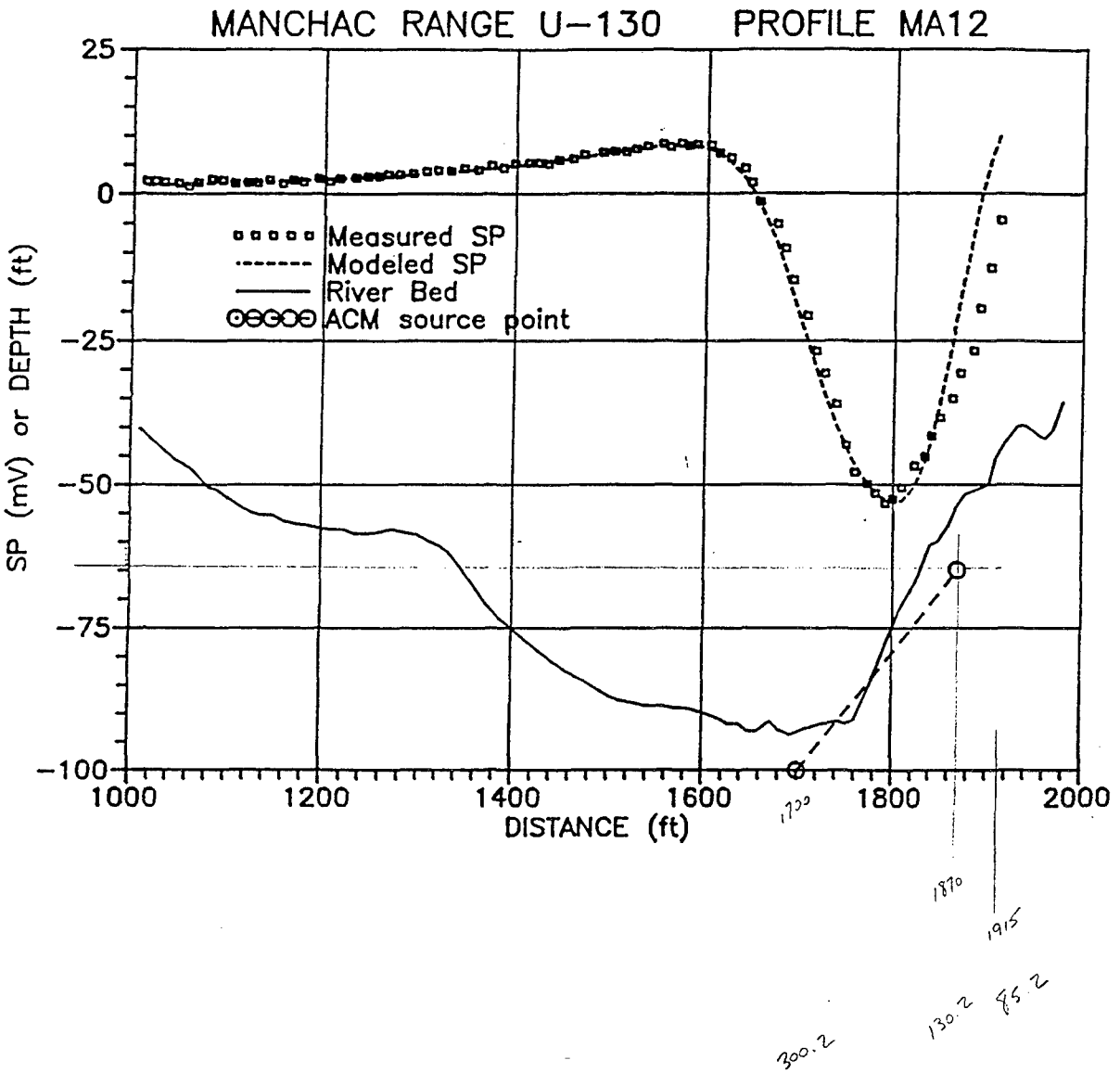
MANCHAC RANGE U-130 PROFILE MA12
SP (mV) or DEPTH (ft)
25
0
-25
-50
-75
-100
1000
1200
1400
1600
1800
2000
DISTANCE (ft)
Measured SP
Modeled SP
River Bed
ACM source point
1720
1870
1915
300.2
130.2
85.2

FIGURE 43A

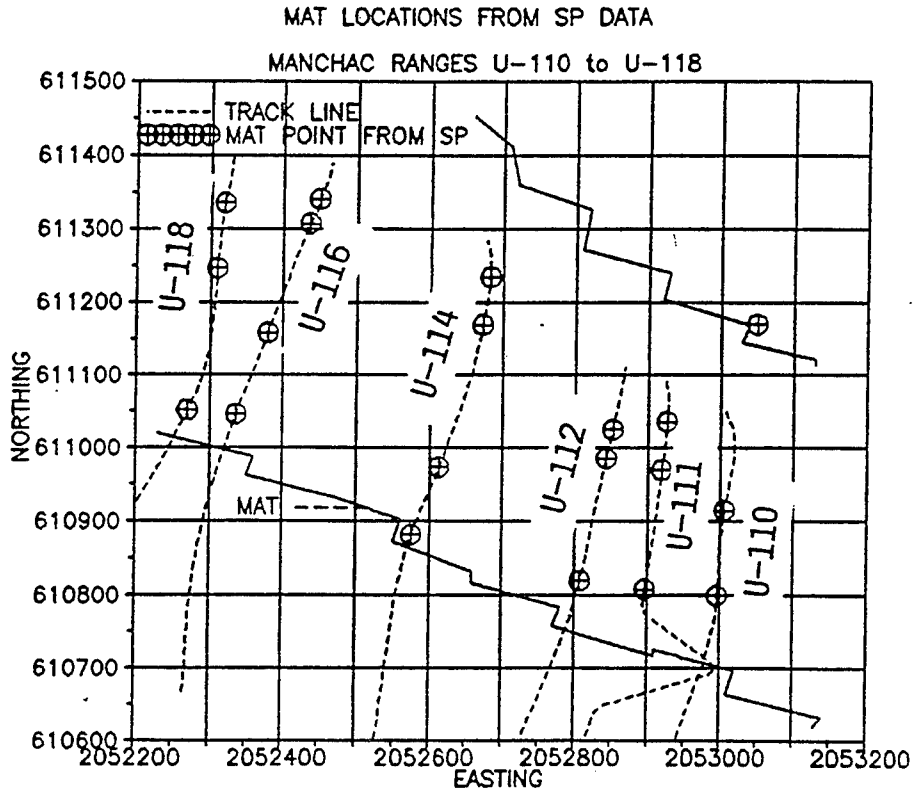
MAT LOCATIONS FROM SP DATA
MANCHAC RANGES U-110 to U-118
TRACK LINE
MAT POINT FROM SP
MAT
U-118
U-116
U-114
U-112
U-111
U-110
NORTHING
611500
611400
611300
611200
611100
611000
610900
610800
610700
610600
2052200
2052400
2052600
2052800
2053000
2053200
EASTING

FIGURE 43B

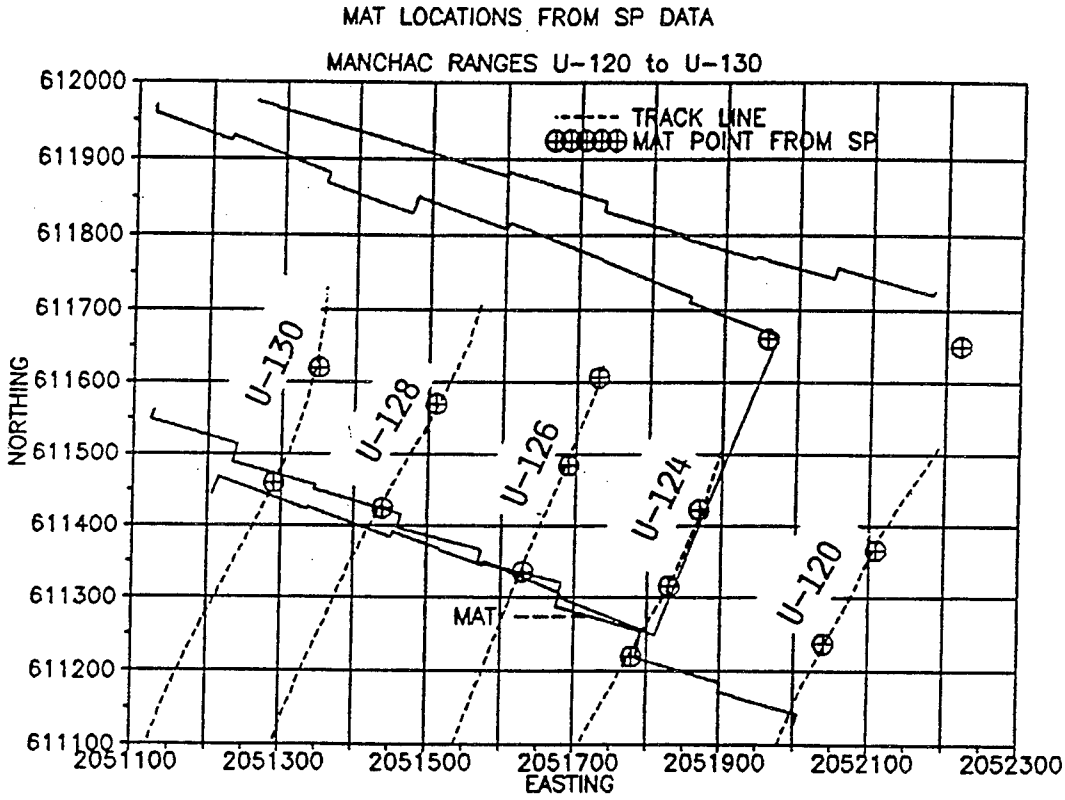
MAT LOCATIONS FROM SP DATA
MANCHAC RANGES U-120 to U-130
TRACK LINE
MAT POINT FROM SP
U-130
U-128
U-126
U-124
U-120
MAT
NORTHING
612000
611900
611800
611700
611600
611500
611400
611300
611200
611100
2051100
2051300
2051500
2051700
2051900
2052100
2052300
EASTING

FIGURE 44

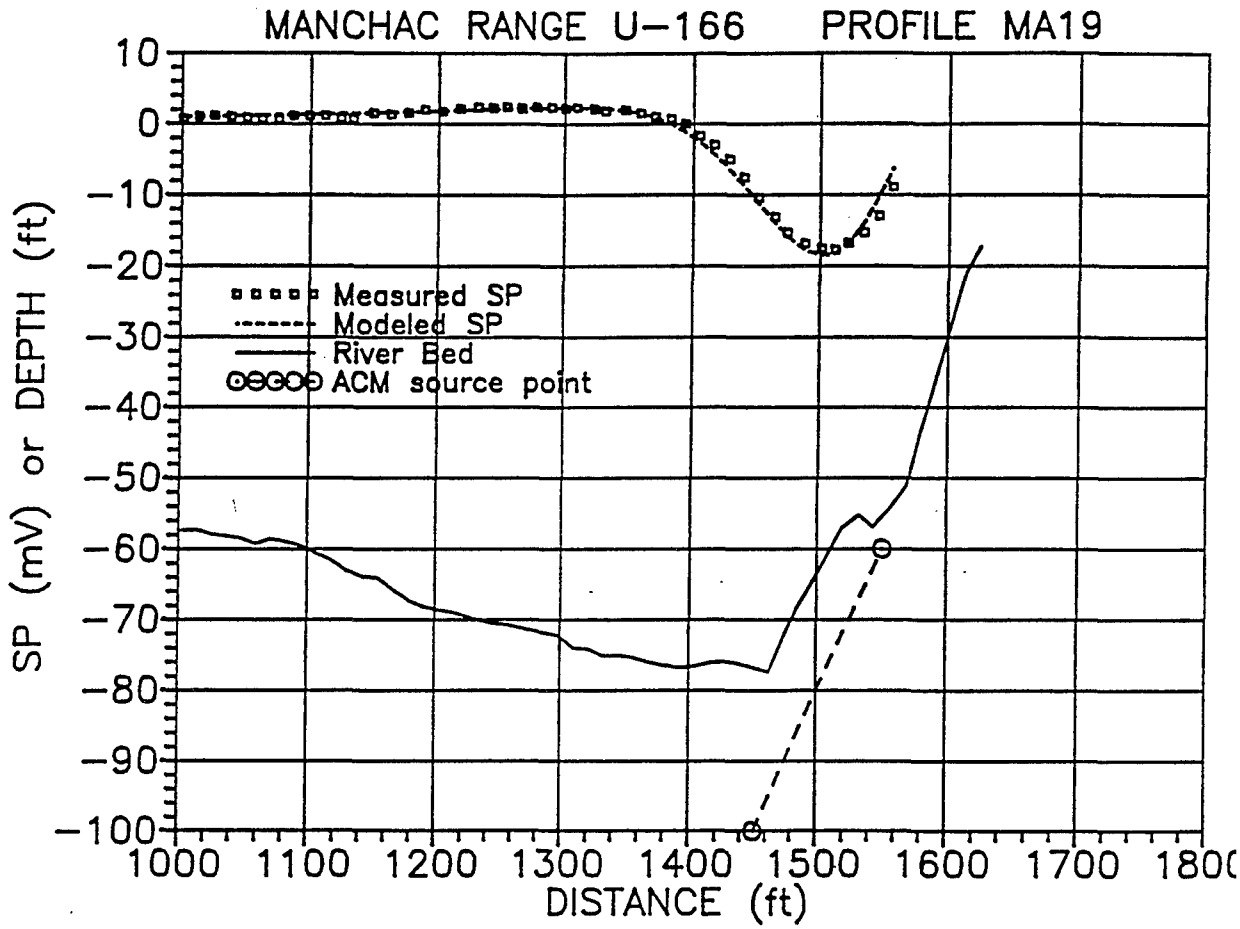
MANCHAC RANGE U-166 PROFILE MA19
SP (mV) or DEPTH (ft)
10
0
-10
-20
-30
-40
-50
-60
-70
-80
-90
-100
1000 1100 1200 1300 1400 1500 1600 1700 180
DISTANCE (ft)
Measured SP
Modeled SP
River Bed
ACM source point

FIGURE 45

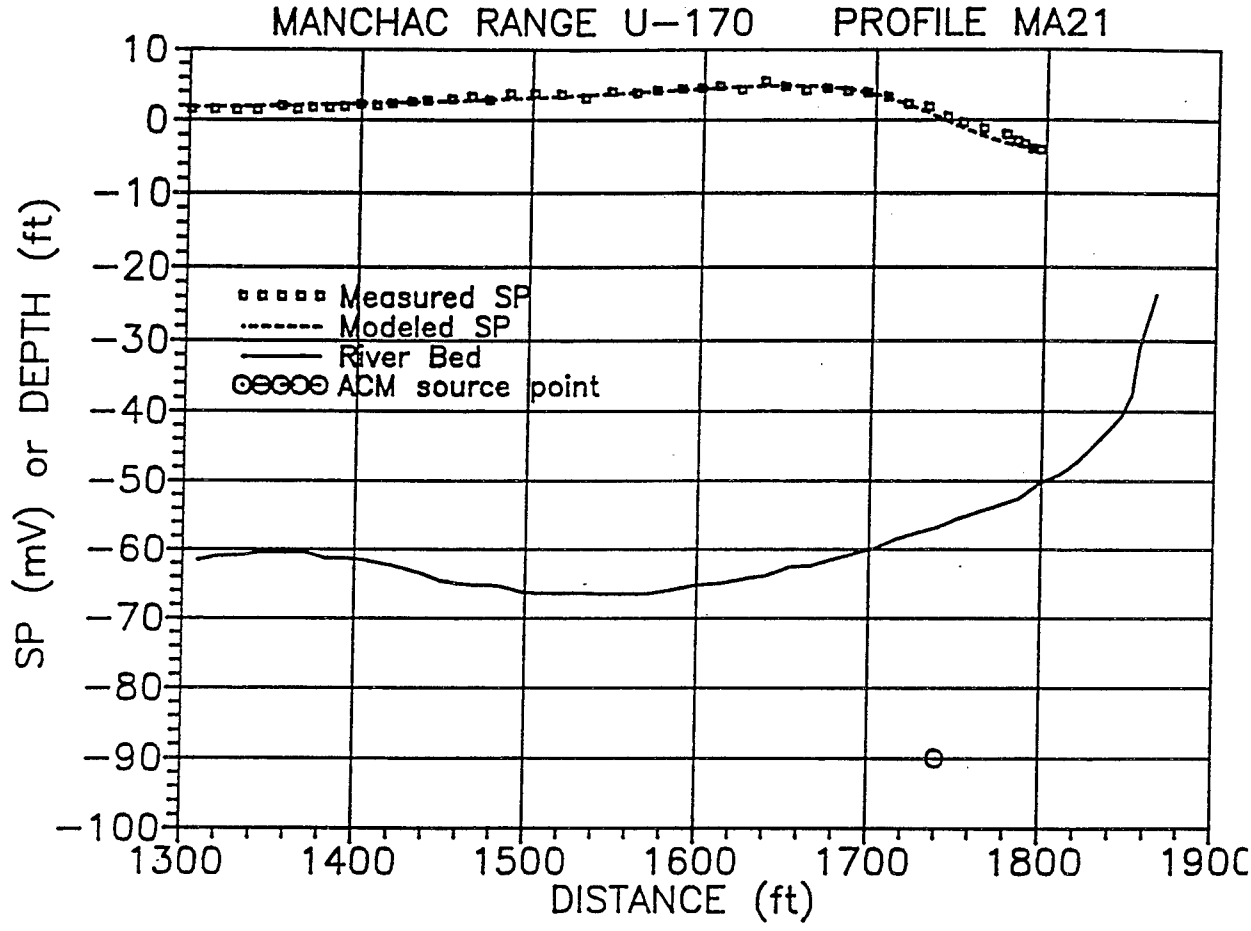
MANCHAC RANGE U-170 PROFILE MA21
10
0
-10
-20
-30
-40
-50
-60
-70
-80
-90
-100
SP (mV) or DEPTH (ft)
Measured SP
Modeled SP
River Bed
ACM source point
1300
1400
1500
1600
1700
1800
190C
DISTANCE (ft)

FIGURE 46

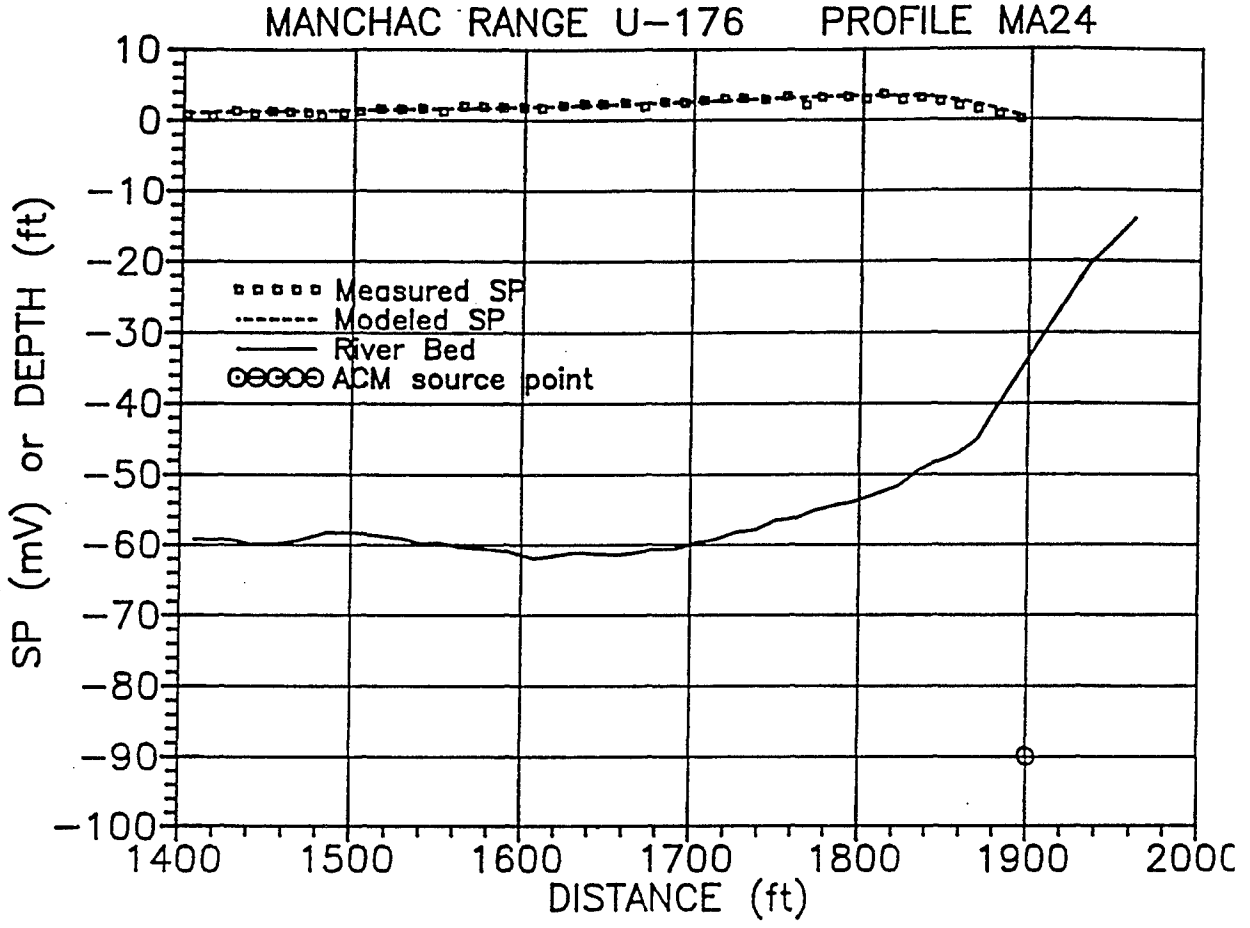
MANCHAC RANGE U-176 PROFILE MA24
SP (mV) or DEPTH (ft)
10
0
-10
-20
-30
-40
-50
-60
-70
-80
-90
-100
1400
1500
1600
1700
1800
1900
2000
DISTANCE (ft)
Measured SP
Modeled SP
River Bed
ACM source point

FIGURE 47

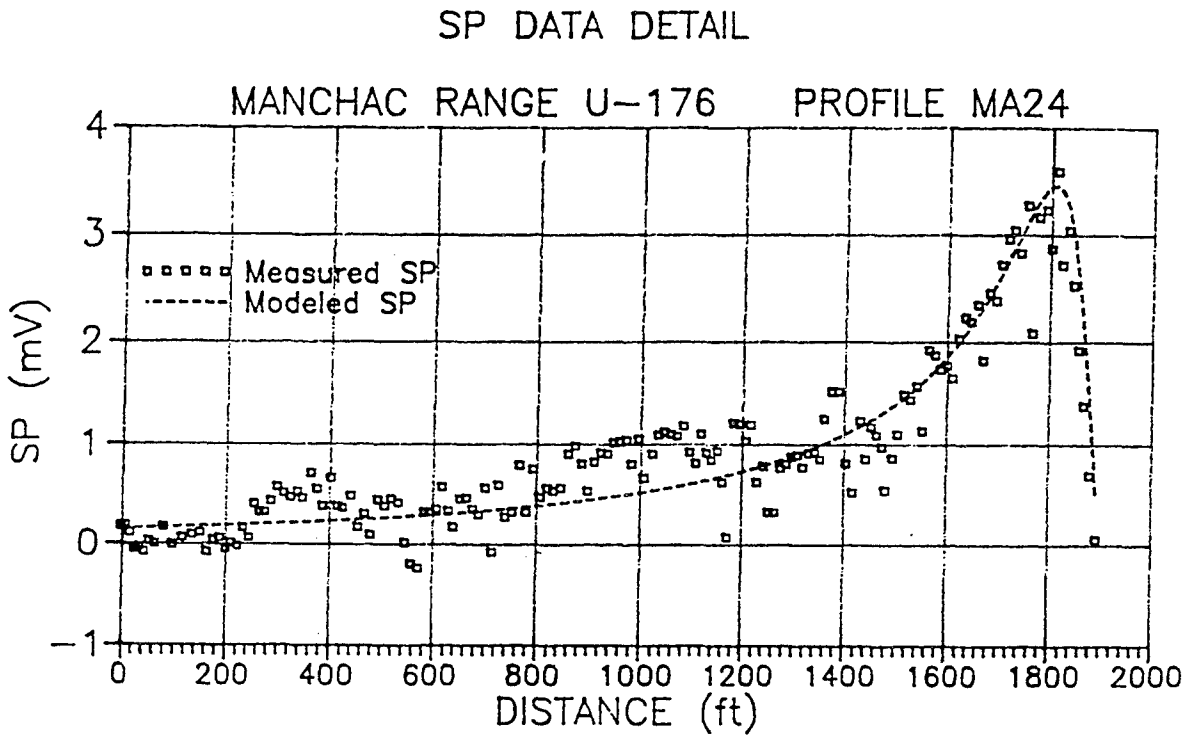
SP DATA DETAIL
MANCHAC RANGE U-176 PROFILE MA24
Measured SP
Modeled SP
SP (mV)
4
3
2
1
0
-1
0
200
400
600
800
1000
1200
1400
1600
1800
2000
DISTANCE (ft)

FIGURE 48

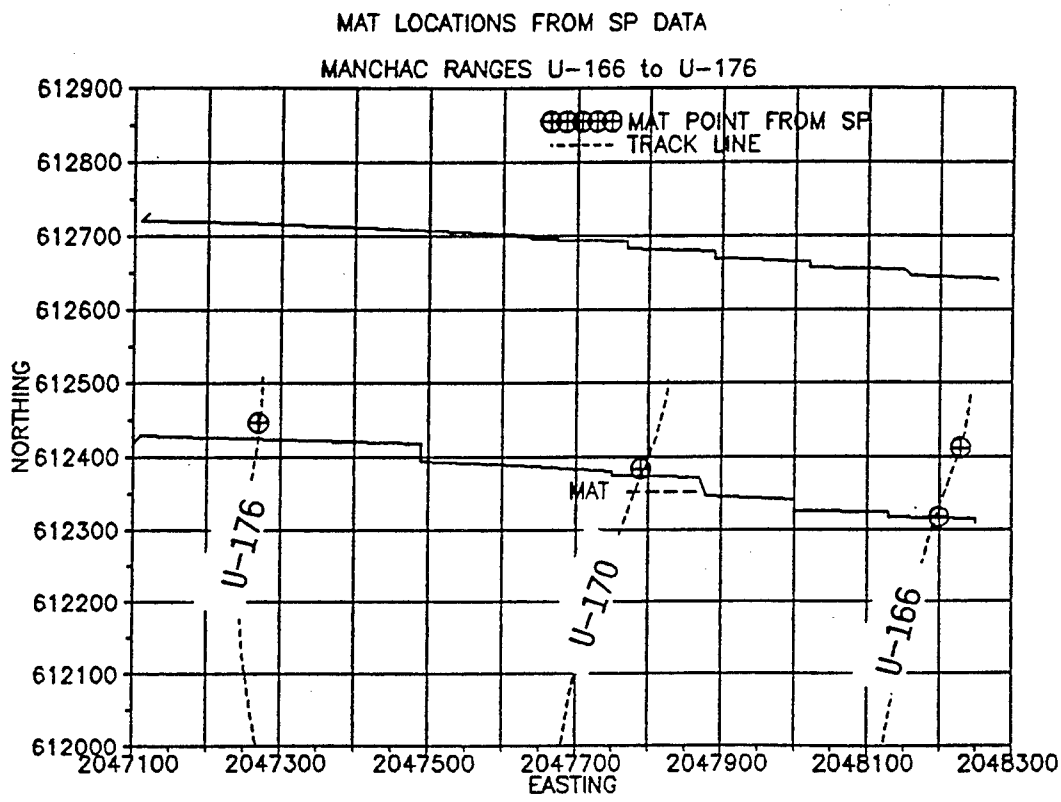
MAT LOCATIONS FROM SP DATA
MANCHAC RANGES U-166 to U-176
MAT POINT FROM SP
TRACK LINE
MAT
U-176
U-170
U-166
NORTHING
612900
612800
612700
612600
612500
612400
612300
612200
612100
612000
2047100
2047300
2047500
2047700
2047900
2048100
2048300
EASTING

Appendix B
Phase III-A Report - Development of Self-Potential and Electrical Resistivity Methods for Investigation of Articulated Concrete Mattresses

PHASE III-A STUDY

DEVELOPMENT OF SELF-POTENTIAL AND ELECTRICAL RESISTIVITY METHODS FOR INVESTIGATION OF ARTICULATED CONCRETE MATTRESSES

Prepared for:

U.S. Army Engineer Waterways Experiment Station
ATTN: CEWES-CT-C
3909 Halls Ferry Road
Vicksburg, MS 39180-0631
Research Area GL-2 (Geophysics)

Contract No. DACA39-93-C-0084

Prepared by:

Robert F. Corwin, Ph.D.
Consulting Geophysicist

SP SURVEYS
406 Sea View Drive
El Cerrito, CA 94530
(510) 527-2081

January 26, 1994

PHASE III-A STUDY

DEVELOPMENT OF SELF-POTENTIAL AND ELECTRICAL RESISTIVITY METHODS FOR INVESTIGATION OF ARTICULATED CONCRETE MATTRESSES

Prepared for:

U.S. Army Engineer Waterways Experiment Station
ATTN: CEWES-CT-C
3909 Halls Ferry Road
Vicksburg, MS 39180-0631
Research Area GL-2 (Geophysics)

Contract No. DACA39-93-C-0084

Prepared by:

Robert F. Corwin, Ph.D.
Consulting Geophysicist

SP SURVEYS
406 Sea View Drive
El Cerrito, CA 94530
(510) 527-2081

January 26, 1994

CONTENTS

page

I. INTRODUCTION 1

II. SUMMARY 2

III. SELF-POTENTIAL MEASUREMENTS 3

A. Self-Potential System 3

B. Missouri Bend Revetment SP Surveys 3

1. Ranges U-81 - U-89 3

2. Ranges U-90 - U-96 4

3. Ranges U-110 - U-124 4

C. Manchac Revetment SP Surveys 4

1. Ranges U-89 - U-91 5

2. Ranges U-109 - U-111 5

3. Ranges U-139 - U-141 5

4. Ranges U-169 - U-171 5

IV. ELECTRICAL RESISTIVITY INVESTIGATION 6

A. Signal Characteristics 6

1. Electrical Properties of Mat and Surroundings .. 7

2. Signal Levels 8

B. Noise Measurements 11

V. CONCLUSIONS AND RECOMMENDATIONS 13

REFERENCES 14

TABLES

Table 1. Missouri Bend Revetment Mat Location Parameters

Table 2. Manchac Revetment Mat Location Parameters

FIGURES

1. Offshore Self-Potential Measurement System
2. Self-Potential Data Acquisition System Schematic

Missouri Bend Revetment SP Measurements

3. Mat Locations from Self-Potential Data, Ranges U-75 - U-89
4. Mat Locations from Self-Potential Data, Ranges U-90 - U-105
5. Mat Locations from Self-Potential Data, Ranges U-110 - U-124
6. Profile Data and Mat Point Locations, Nominal Range U-81
7. " U-82
8. " U-83
9. " U-84
10. " U-85
11. " U-87
12. " U-88
13. " U-89
14. " U-90
15. " U-91
16. " U-94
17. " U-95
18. " U-96
19. " U-110
20. " U-111
21. " U-112
22. " U-113
23. " U-120
24. " U-122
25. " U-124

Manchac Revetment SP Measurements

26. Mat Locations from Self-Potential Data, Ranges U-89 - U-91
27. Mat Locations from Self-Potential Data, Ranges U-109 - U-118
28. Mat Locations from Self-Potential Data, Ranges U-139 - U-141
29. Mat Locations from Self-Potential Data, Ranges U-166 - U-176
30. Profile Data and Mat Point Locations, Nominal Range U-89
31. " U-90
32. " U-91
33. " U-109
34. " U-110
35. " U-111
36. " U-139
37. " U-140
38. " U-141
39. " U-169
40. " U-170
41. " U-171

FIGURES
(continued)

Resistivity Investigation Data

42. TDC Signal and Depth Profile, MN/2 = 41.7 m, Manchac Range U-90
43. TDC Signal and Depth Profile, MN/2 = 31.6 m, Manchac Range U-90
43A. TDC Signal and SP Model, MN/2 = 31.6 m, Manchac Range U-90
44. TDC Signal and Depth Profile, MN/2 = 23.7 m, Manchac Range U-90
45. TDC Signal and Depth Profile, MN/2 = 17.8 m, Manchac Range U-90
46. TDC Signal and Depth Profile, MN/2 = 13.3 m, Manchac Range U-90
47. Measured TDC Background Noise Using Data Acquisition Board

I. INTRODUCTION

This report presents the results of a Phase III-A study of the use of self-potential (SP) and towed direct-current electrical resistivity (TDC) methods for investigation of articulated concrete mattresses (ACM). The investigation had the following four major objectives:

(1) Testing of an operational SP system and comparison of the SP data with that obtained at the same sites in October 1992

(2) Acquisition of TDC field test data needed for further development of the TDC technique

(3) Confirmation of geophysical data with "ground truth" obtained by a concurrent drilling program

(4) Determination of the most efficient combination of geophysical techniques for ACM investigations.

The Phase III-A operational SP system was designed and constructed using information obtained from the Phase II study (Corwin, 1993) of the use of the SP and TDC methods for ACM investigations. This publication will be referenced as the Phase II report throughout this report. The Phase II report includes detailed descriptions of the theoretical background of the SP and TDC techniques, which will not be repeated in the present report.

The computer program SPGEN used to interpret the SP data, along with associated documentation, was furnished to USACE as part of the Phase II study. Details of the Phase III-A production SP system components, field procedures, and data acquisition and reduction techniques are given in a separate report (Corwin, 1994), referenced as the SP system report.

Phase III-A field measurements were conducted between 23 and 28 August 1993 at the Missouri Bend and Manchac revetment sites near Baton Rouge, LA. The survey vessel "Mary Evans" and the differential GPS positioning information were provided by DIMCO, Inc. of Vicksburg, MS. Because SP data quality is adversely affected by strong river currents, it was originally intended that these field measurements be conducted at low river level, as were the previous Phase II measurements. However, because of unusual rainfall and flooding in the summer of 1993, river levels were considerably higher than anticipated in August 1993. River elevation during the survey period was about +30 ft at the Missouri Bend site and about +29 ft at the Manchac site. For the previous October 1992 Phase II investigation to which the present data will be compared, river elevation was about +8 ft at both sites. The effects of this high river level and associated strong currents are discussed later in this report.

As mentioned above, two objectives of the Phase III-A program were to compare SP and TDC interpretations of mat parameters with those obtained from a "ground truth" drilling program and from

other geophysical techniques (specifically, magnetics and electromagnetics [EM]). Due to the high river level and strong currents, it was not possible to conduct the drilling program, and the magnetic and EM data were not available at the time of this writing. Therefore, data verification in the present report will be limited to comparisons between SP measurements taken in October 1992 and August 1993.

II. SUMMARY

The production SP system operated as intended, furnishing good-quality SP data even under difficult (high-water) survey conditions. The system was reliable, and needed no maintenance or repairs during the survey period. The useability of the SP data depended on the quality of the track lines. Where current conditions allowed the track lines to be oriented along the range lines and the course of the vessel to be reasonably straight, the interpreted SP data gave mat positions and depths that were close to as-installed values or to those determined from the Phase II survey, for which most of the track lines were of good quality. Although reasonable interpretations usually could be obtained even when track lines deviated significantly from the range lines, the accuracy of the interpreted mat locations and depths generally was not as good for such lines.

SP data quality also was affected in areas of transition from deeply buried old mat to adjacent shallow new mat. In such areas, the strong SP signal from the shallow new mat overwhelmed the weaker SP signal from the deep old mat for a distance of a few hundred feet along the old mat, making it impossible to determine the parameters of the old mat in this region. Once away from the influence of the new mat, the small old-mat SP signal could be interpreted with no difficulty.

The resistivity data obtained as part of this investigation provided information needed to select transmitter and cable parameters for a future production TDC system. The field data indicated that usable signal-to-noise levels can be obtained over representative mat configurations, but that high-frequency noise will have to be filtered from the signal to attain these levels. The field tests indicated that analog filtering can produce the desired noise reduction, and further testing as part of a proposed Phase III-B study will determine whether analog or digital filtering is optimal for this application. Also to be determined are techniques for mitigating the effects of long-period SP variations on TDC signals to allow effective TDC data acquisition in areas of strong SP signals.

III. SELF-POTENTIAL MEASUREMENTS

A. Self-Potential System

The measurement system used to acquire the SP data is shown in Figure 1. Dipole separation (DI) was 50 ft and the distance from the navigation antenna to the dipole center point (AN) was 125 ft. A schematic of the SP data acquisition system is shown in Figure 2. More details of the equipment and instrumentation are given in the SP system report.

The interpretation algorithm used in program SPGEN (Rao et al., 1970) requires that the track line be straight and orthogonal to the mat. It is evident from the figures discussed below that these conditions were not met for some of the track lines, both at the Missouri Bend and the Manchac sites. The cause of these deviations from ideal track line profiles was the strong and irregular current flow due to the high river level, which made it impossible to hold the survey vessel to a straight track or a consistent orientation. For comparison, the Phase II track lines conducted in October 1992 generally were considerably straighter and better oriented (see Figures 31A - 31C, 43A, and 48 of the Phase II report).

B. Missouri Bend Revetment SP Surveys

SP survey lines were run in three areas of the Missouri Bend revetment, covering ranges U-81 - U-96, U-110 - U-113, and U-120 - U-124. Mat location parameters for the Missouri Bend revetment are summarized in Table 1.

1. Ranges U-81 - U-89

Track lines and mat points for ranges U-81 - U-89 are shown on Figure 3 (corresponding to Figure 31A of the Phase II report). Mat point locations from the Phase II study also are shown on Figure 3, but Phase II track lines have been omitted for clarity. Plots of the Phase III-A measured and calculated SP data, river bed profiles, and mat point locations for these ranges are shown on Figures 6 - 13. Note that, due to the difficulty of maintaining the desired track lines, some of the indicated nominal range lines are not in the proper sequence (e.g., nominal range U-83 is north of nominal range U-84).

The ranges for which the track lines were reasonably straight and orthogonal (U-81, 82, 83, and 85) gave mat locations close to as-installed values and mat depths similar to those determined from Phase II measurements. Mat location and depth for range U-84 appear to be reasonable even though the track line was not well-oriented. The three northernmost lines (U-87, 88, and 89) were very poorly oriented, and gave mat locations that were not consistent with as-installed values or those determined from Phase II measurements. The displacement of the interpreted mat points from the river bed for ranges U-88 and U-89 (Figures 12 and 13) indicates that the interpretation is not valid for these

skewed track lines. Note that, even though the mat parameters are not well determined, the presence of the mat still is detected under these adverse conditions.

2. Ranges U-90 - U-96

Track lines and mat points for these ranges are shown on Figure 4 (corresponding to Figure 31B of the Phase II report). Mat point locations from the Phase II study also are shown on Figure 4, but Phase II track lines have been omitted for clarity. Plots of the Phase III-A measured and calculated SP data, river bed profiles, and mat point locations for these ranges are shown on Figures 14 - 18.

Similar to the lines discussed above, track lines that were reasonably well-oriented (e.g., U-96) gave interpreted mat positions that were very close to those determined from the Phase II data. While the other Phase III-A lines on Figure 4 were not as well-oriented as those for the Phase II survey, the interpreted Phase III-A mat locations are reasonably close to those previously determined for Phase II.

3. Ranges U-110 - U-124

Track lines and mat points for these ranges are shown on Figure 5 (corresponding to Figure 31C of the Phase II report). Mat point locations from the Phase II study also are shown on Figure 5, but Phase II track lines have been omitted for clarity. Plots of the Phase III-A measured and calculated SP data, river bed profiles, and mat point locations for these ranges are shown on Figures 19 - 25.

Although lines U-110 and U-111 are not well oriented, they give reasonable locations for the edge of the mat. However, all four of the southern lines (U-110, 111, 112, and 113) show a spurious mat point (denoted by the ? symbol) well to the east of the mat. These spurious points are caused by the southeastern corner of the new mat just to the north of these ranges. For lines U-112 and U-113, the influence of the strong SP signal from the new mat along with the poor orientation of the lines makes it impossible to properly interpret the data from these lines, and the locations and profiles for U-112 and U-113 shown on Figures 5, 21, and 22 are not usable.

In contrast, track lines for the three profiles conducted over the new mat (ranges U-120, 122, and 124) were very well oriented. Interpreted mat locations and depths for these profiles agreed well with as-installed locations and measured water depths, indicating that the mat had not significantly changed position since it was installed in 1992.

C. Manchac Revetment SP Surveys

SP survey lines were run in four areas of the Manchac revetment, covering ranges U-89 - U-91, U-109 - U-111, U-139 - U-141, and

U-169 - U-171. Mat location parameters for the Manchac revetment are summarized in Table 2.

1. Ranges U-89 - U-91

Track lines and mat points for ranges U-89 - U-91 are shown on Figure 26 (this area was not surveyed for the Phase II study). Plots of the Phase III-A measured and calculated SP data, river bed profiles, and mat point locations for these ranges are shown on Figures 30, 31, and 32. Although the track lines are only moderately well oriented, the SP interpretations give mat position and depth estimates that correlate well with as-installed positions and measured water depths.

2. Ranges U-109 - U-111

Track lines and mat points for these ranges are shown on Figure 27 (corresponding to Figure 43A of the Phase II report). Mat point locations from the Phase II study also are shown on Figure 27, but Phase II track lines have been omitted for clarity. Plots of the Phase III-A measured and calculated SP data, river bed profiles, and mat point locations for these ranges are shown on Figures 33, 34, and 35.

The three track lines are fairly well oriented, and interpreted mat locations and depths agree reasonably well with both as-installed values and previous Phase II interpretations. Spurious points, indicated by the ? symbol, are seen well to the south of the mat on lines U-109 and U-110. These points may have been due to metallic debris on the river bed that apparently was not present during the Phase II measurements.

3. Ranges U-139 - U-141

Track lines and mat points for these ranges are shown on Figure 28 (this area was not surveyed as part of the Phase II study). Plots of the measured and calculated SP data, river bed profiles, and mat point locations for these ranges are shown on Figures 36, 37, and 38. Although the track lines are of only fair to moderate quality, interpreted mat locations and depths appear to correlate quite well with as-installed values for all three ranges.

4. Ranges U-169 - U-171

Track lines and mat points for these ranges are shown on Figure 29 (corresponding to Figure 48 of the Phase II report). Mat point and track line locations from the Phase II study also are shown on Figure 29. Plots of the Phase III-A measured and calculated SP data, river bed profiles, and mat point locations for these ranges are shown on Figures 39, 40, and 41. Note that the mapped location of the Phase III-A track line for range U-170 appears to differ considerably from that for the Phase II survey. The reason for this discrepancy is not clear.

Although the track lines and SP data for these three profiles appear to be of reasonably good quality, the location of the outer edge of the mat interpreted from the Phase III-A data differs considerably from the as-installed locations and the Phase II interpretations, which were very close to the as-installed locations. As the lateral accuracy of the interpreted position of the outer edge of the mat is probably within about +/- 20 ft, this would appear to indicate that the outer edge of the mat was 50 - 100 ft closer to shore in 1993 than in 1992. However, because the interpreted depths for 1993 are no greater than those for 1992, this type of movement appears unlikely. Thus, in conjunction with the discrepancy in the track line locations, it appears that there may have been a problem with the Phase III-A positioning of the vessel in this area.

IV. ELECTRICAL RESISTIVITY INVESTIGATION

Electrical resistivity measurements conducted as part of the Phase II investigation indicated that the stainless steel fabric of the mat could be detected using direct-current (DC) resistivity measurements conducted from a cable towed along the surface of the river, and that these towed DC (TDC) measurements could be interpreted to give reasonable estimates of the depth of the mat. The operating theory and equipment configuration for a TDC system are discussed in detail in the Phase II report.

The purpose of the present Phase III-A investigation was to obtain additional, more detailed information regarding the electrical properties of the mat and surroundings, and also to determine realistic TDC signal and noise levels that could be used to design an operational multi-channel TDC system. Once signal and noise levels are known, estimates of the accuracy of mat parameters determined from TDC measurements can be made and optimal TDC survey configurations and procedures can be determined. These topics are discussed in the following sections.

A. Signal Characteristics

The amplitude of the measured TDC signal depends on the amplitude of the transmitted current, the electrode configuration and spacing, and the geometry and electrical characteristics of the mat and the surrounding water and riverbed sediments. For the inverse Schlumberger resistivity configuration used for this study, the ratio of measured voltage to transmitted current is given by

$$(1) \qquad V/I = (\rho_a * (2[AB/2])) / (\pi * ([MN/2]^2 - [AB/2]^2)),$$

where V = measured signal voltage (mV)
I = transmitted current (mA)
ρ_a = apparent resistivity (ohm-meters)
[AB/2] = current (inner) electrode separation (meters)
[MN/2] = voltage (outer) electrode separation (meters).

For TDC measurements to be useful, the desired signal V must be large enough to be reliably distinguished from the noise present across the voltage electrodes (discussed in section B below). From Equation (1), the parameters affecting V are the apparent resistivity rho_a, the transmitted current I, and the values of electrode separations [AB/2] and [MN/2].

1. Electrical Properties of Mat and Surroundings

The value of rho_a is a complex function of the resistivity and geometry of the mat, the river water, and the riverbed sediments. If resistivity values for the mat, water, and sediments are known, assuming that these three constituents are flat-lying, infinite layers allows calculation of rho_a values using available algorithms (Telford et al., 1976) and computer programs. Future studies of the TDC method will include examination of more complex (and realistic) two-dimensional geometries.

The measured value of the river water resistivity has been about 20 +/- 5 ohm-m for the Phase I, II, and III-A studies. The Phase II vertical electric soundings (VES) indicated that the river bed resistivity ranged from about 20 to 40 ohm-m, with 40 ohm-m being a more representative value. For the present modeling studies, it is assumed that water resistivity is 20 ohm-m and riverbed resistivity is 40 ohm-m.

Because the metal fabric of the mat is not actually a sheet but instead is a rectangular wire mesh, its thickness and resistivity for modeling purposes are obtained by calculating the volume of metal per unit area of the mat, assuming that this volume of metal is in the form of a continuous sheet of constant thickness, and using the known resistivity of the stainless steel wire material.

Following the above procedure, Mozley and Kooney (1991) determined that the mat contained 44.4 m of wire of diameter 3.8 E-03 m (0.15 inches) in a mat section of 1.2 m x 7.6 m (4 ft x 25 ft), giving a wire volume of about 5 E-4 cubic m in a volume of 9.1 square m, and an equivalent metal thickness of about 5.5 E-05 meters (about 0.0022 inches). Mozley and Kooney list the electrical resistivity of stainless steel as about 1.0 E-07 ohm-m, but reference to standard industrial materials handbooks indicates that this value is low, and that most stainless steels average about 7 E-07 ohm-m.

For a layer of very low resistivity compared to those above and below it, the ratio of layer thickness divided by layer resistivity is defined as the equivalent conductance of the layer. Calculations of rho_a for layered structures of this type indicate that rho_a is controlled primarily by the equivalent conductance of the low-resistivity layer rather than actual values of the layer thickness and resistivity. Thus the estimated equivalent conductance of the mat fabric is about 5.5 E-05 m / 7 E-07 ohm-m, or about 80 Siemens (S).

Because the computer programs used for resistivity modeling have difficulty handling very small resistivity and thickness values, this concept is useful for calculating rho_a values for the mat. For example, using an equivalent mat layer thickness of 0.80 m and resistivity of 0.01 m, which can be more easily handled by most computer programs, gives results very close to those obtained for the smaller thickness and resistivity values.

Tests of the accuracy of the assumed equivalent conductance value of 80 S were performed using Phase II VES data from the Missouri Bend revetment site. If a reasonable fit to the field curve and reasonable values for the mat depth and sediment and water resistivity could be obtained while holding the conductance of the mat fixed at 80 S, the 80 S value probably is close to the true value for that particular location. However, if the mat conductance had to be changed from the 80 S value to obtain reasonable depth and resistivity estimates, this indicated that the in-situ conductance value was not actually 80 S.

Results of these tests indicated that the 80 S value worked well at some sites, but was up to about an order of magnitude too high at others. Causes of this variation probably include the condition of the wire (loss of material by corrosion, surface deposits, etc), the condition of the mat concrete, and the non-horizontal orientation of the mat. A lower mat conductance value would tend to decrease the detectability of the mat using DC or EM methods, so the use of a lower conductance value (e.g., 10 S) would tend to provide more conservative estimates of mat detection capability using TDC methods. A 10 S conductance value was used for the example studies described below.

2. Signal Levels

As shown in Equation (1), TDC signal strength depends on the electrode configuration, on the transmitter current I, and on rho_a, which in turn depends on the depths and resistivities of the river water, mat, and riverbed sediments. The brief example shown below is representative of many such parametric studies of mat detectability that would be performed as part of the design of a production TDC system. For this example, it was assumed that the resistivity of the river water is 20 ohm-m, resistivity of the riverbed sediments is 40 ohm-m, that the mat conductance is 10 S, that the transmitter electrode separation AB/2 is 1.1 m, and that the receiver (voltage) electrode separation MN/2 is 41.7 m (these were actual cable values for the Phase II and Phase III-A field measurements). Also assumed is the 1500 mA maximum transmitter current value attainable using a 300 V transmitter output with the Phase II resistivity cable.

Using these values, a study was made of the differences between the signal levels observed when the mat is or is not present for different combinations of water depth and mat depth. The calculated signal levels are listed in Table A on the following page.

TABLE A: Calculated Signal Levels With and Without Mat

Case no.	1	2	3	4	5	6
Water depth (ft)	33	56	108	108	108	108
Mat depth (ft)	33	56	108	164	220	328
Signal w/mat (mV)	2.4	4.7	8.9	11.1	11.7	12.0
Signal w/o mat (mV)	17.5	14.8	12.2	12.2	12.2	12.2
mV difference	15.1	10.1	3.3	1.1	0.5	0.2

From the results of the Phase II and III-A field studies and of the noise studies discussed in the following section, differences of about 1 mV or greater should be distinguishable from TDC field data under good conditions. Therefore the presence of the mat should be easily detected and its depth well resolved for cases 1, 2, and 3; the mat would be detected but its depth resolution not as good for case 4; and both detectability and resolution would be marginal for cases 5 and 6. Note that these conclusions apply only for the single electrode spacing set (AB/2 = 1.1 m; MN/2 = 41.7 m) and transmitter current of 1500 mA. Thus determining the actual detectability of the mat for these different cases would involve performing these calculations for all the different electrode spacings in the array and comparing the complete sounding curves for each different case.

The Phase II field investigation included a number of TDC profiles run parallel to the shore line, using a standard (not inverted) Schlumberger array with current electrode spacing AB/2 of 23.7 m and potential electrode spacing MN/2 of 1.10 m. Signal amplitudes in 20 ft of water, using 1000 mA of transmitted current, were about 35 mV above deeply buried old mat and about 5 mV above newly-emplaced mat, in reasonable agreement with the magnitudes tabulated above. For the Phase III-A field investigation, it was desired to obtain TDC data along, rather than perpendicular to, the range lines. Also, because the noise level might be greater for the inverted array (due to the larger potential electrode separations), it was desired to acquire TDC data using an inverted Schlumberger array that would more closely resemble a multi-channel production configuration.

In order to determine whether the calculated signal levels shown above are realistic for actual operating conditions for survey profiles run along range lines, it was intended to obtain sample multi-channel TDC data as part of the Phase III-A field investigation. However, the resistivity cable and the multi-channel data acquisition system were damaged by the unexpected strong river currents before the multi-channel data could be obtained; and the resistivity cable was torn from the vessel and lost when the end of the cable snagged on the bottom and the vessel was caught in a powerful eddy.

Therefore, the multi-channel system was simulated by towing the cable repeatedly over a single survey line and recording the data for different electrode spacings using the single-channel SP data

acquisition system. These measurements were made at Manchac ranges U-90 and U-140, both of which also had been surveyed with the SP system. The results from range U-90 are discussed below. The SP and riverbed profiles and the interpreted mat location for this range are shown on Figures 26 and 31.

The TDC measurements at Manchac range U-90 were made using an inverted Schlumberger configuration with the electrode pair at AB/2 = 3.16 m serving as the current transmitter and the wire-wrap electrode pairs at MN/2 = 13.3, 17.8, 23.7, 31.6, and 41.7 m used as voltage receivers. The SP program SPGEN was used to merge the TDC data with the navigation data and to create GRAPHER plot files for the profiles shown on Figures 42 - 46.

The profile of Figure 42 (MN/2 = 41.7 m) illustrates several features of TDC profiles run along range lines (the very large DC signal offset of about -200 mV is due to the cable damage noted above). The zero-to-peak signal amplitude in the "background" area well offshore of the mat is about 45 mV. Correcting the 3.16 m actual AB/2 spacing to 1.1 m spacing assumed for Table A and correcting the actual current of 1415 mA to the assumed current of 1500 mA, the background signal amplitude for this profile would be about 15 mV, which compares well with the 14.8 to 12.2 mV values shown in Table A for MN/2 = 41.7 m in 56 to 108 ft water depth, with no mat present.

A second TDC profile feature is the presence of a very large SP variation over the mat. The polarity of the variation is reversed from that seen on the SP profile (Figure 31) because the polarity of the TDC system was opposite that of the SP system, but the absolute shapes of the SP profile and the mean of the TDC profile are very similar. The amplitudes of the SP variations on the SP and TDC profiles are proportional to the respective dipole separations (50 ft for SP, 274 ft for TDC with AB/2 = 41.7 m).

Figure 43 shows the TDC profile for MN/2 = 31.6 m, which is generally similar to that for 41.7 m. Figure 43A shows the same profile with the calculated SP model curve for range U-90 (model MN1B, Table 2) superimposed on the TDC data profile. The only change in the source model from that used for the SP data was reversal of the source current polarities to account for the different electrode polarity. For input to program SPGEN, antenna distance AN for the TDC array was 250 ft and dipole length DI was 207 ft (twice the MN/2 value of 31.7 m). Also, the base level BA of the field data was shifted +200 mV to correct for the electrode polarization. Considering that the track lines were not identical for the SP and TDC runs, the fit between the SP model curve and the mean (zero-current level) of the TDC profile is reasonable.

From Figure 43A, it is apparent that the peak-to-peak amplitude of the TDC signal (and associated apparent resistivity) decrease strongly as the center point of the array passes over the outer edge of the mat at X = 1060 ft, and continue to decrease with increasing distance. However, the steep gradient of the SP curve

makes it extremely difficult to determine the actual TDC signal amplitude for distances greater than about 1200 ft. This presents a difficulty for the use of TDC methods along range lines for which large SP anomalies are present. Methods will have to be developed to compensate for this problem to allow determination of signal amplitudes for large electrode spacings if the TDC method is to be used under these conditions. For example, reducing the vessel speed in such areas would decrease the spatial steepness of the SP gradient, allowing better resolution of the TDC signal amplitude.

Figures 44, 45, and 46 show the TDC profiles for progressively smaller MN/2 values (23.7, 17.8, and 13.3 m). Because of the smaller electrode spacing and the associated shallower depth of investigation, peak-to-peak TDC signal amplitudes remain large even above the mat. Also, the smaller electrode spacing reduces the SP effect, making it easier to resolve TDC signal amplitudes. However, because of the shallower depth of investigation of these smaller spacings, they may not be providing data helpful for determining the depth of the mat. Further modeling and field tests will be used to help resolve this question.

B. Noise Measurements

Because it is the signal-to-noise ratio rather than the absolute signal level alone that determines the resolution of TDC data, it is important to determine the noise levels associated with TDC readings. Some TDC noise sources are briefly noted below.

1. Environmental sources

    a) SP signals from ACM and other metal sources (as discussed in previous section).
    b) Water salinity: higher salinity gives lower noise (and signal) levels; signal/noise ratio usually remains about constant.
    c) Water currents: motion of water in Earth's magnetic field generates voltages, so changes in current velocity or direction produce baseline shift.
    d) Waves: wave particle motion produces electric signals that are a major source of short-period noise; amplitude increases with increasing wave height.

2. Operational sources

    a) Electromagnetic interference (EMI) from sources on vessel (radios, engine ignition, electric motors, etc).
    b) Cable motion in Earth's magnetic field; due to boat motion and to cable vibration (strumming). Cable motion noise usually increases with increased boat speed and larger electrode separation.

Noise may be short-period (less than the typical transmitted current pulse of a few seconds) or long-period (greater than a few seconds). SP signals and water current effects generally are

relatively long-period; wave noise, cable strumming, and EMI generally are relatively short-period; and boat motion effects (roll, pitch, yaw, turns to correct course) usually are of similar period to the transmitted signal.

The SP systems used for ACM studies used two different types of digital multimeters (DMM's) for single-channel data acquisition (Fluke model 45; Micronta model 22-182). Extensive experience with these SP systems indicates that, using these DMM's, the typical maximum peak-to-peak "envelope" of short-period noise in background areas is of the order of about +/- 0.1 to +/- 0.5 mV, with occasional larger excursions (see for example Figures 19 - 22 and 39 - 41 of this report and Figures 18A and 47 of the Phase II report). These noise levels have proven to be low enough to allow effective SP measurements in all the surveyed revetment areas.

To examine the nature of short-period noise for a multi-channel TDC data acquisition system using a high-speed data acquisition board instead of the relatively slow DMM's, measurements were made using a Keithley model DAS-1401 8-channel data acquisition board installed in an expansion chassis connected to a notebook computer. The SP electrode array (50-ft separation) was towed at about 5 kt in a deep-water area free of SP effects and the data recorded on channel 1 at a gain of 100 and a sampling frequency of about 3 Hz.

The upper plot on Figure 47 shows the noise recorded with the electrodes connected directly to the input of the data acquisition board. The peak-to-peak amplitude of the measured noise is about +/- 10 mV, more than an order of magnitude greater than that typically seen when using the DMM's. Thus the DC measurement circuitry of the DMM's apparently incorporates a very effective low-pass filter that greatly attenuates the actual short-period noise across the electrodes. From the discussion and examples in the previous section, it is clear that a +/- 10 mV noise level is unacceptable for TDC measurements, and that some form of filtering of the raw TDC signal will be needed.

To test the effect of filtering the signal entering the data acquisition board, a run was made using the same setup as described above, but with an active low-pass filter (designed primarily for 60 Hz reduction) connected across the input to the board. The lower plot on Figure 47 shows the data for this run. It is apparent that the use of the filter has reduced the amplitude of the short-period noise by a factor of about 10 to 20, to a level close to that for the DMM's. Therefore the use of front-end analog filtering in conjunction with a high-speed, multi-channel data acquisition board should allow acquisition of TDC data with acceptable short-period noise levels. Another approach to noise reduction may be the use of digital post-processing (stacking) rather than (or in conjunction with) analog filtering.

V. CONCLUSIONS AND RECOMMENDATIONS

The SP system provided generally acceptable results under very difficult high-water conditions, and good results for low-water conditions. Limitations of the SP technique include the necessity of running along range lines, subjecting the vessel to the effects of water currents and passing ship traffic; and difficulty in obtaining usable data in areas where the strong signal from a shallow mat interferes with the weaker signal from an adjacent deeper mat.

The SP system as presently configured is ready for use for production surveys. Such use probably will indicate the desirability of further system development and modifications. One recommended area for future development is streamlining of the data acquisition - reduction - interpretation procedure to improve the efficiency of the process. This would include real-time combination of the positioning and SP data with provision for real-time display of the vessel track line, SP data, target range line, and mat outline. Also desirable would be modification of program SPGEN to allow in-program display of plan views of interpreted mat locations, as-installed mat outlines, and range lines instead of having to shell out to GRAPHER for these functions as presently required.

A second area of interest would be studies of the physical basis of the SP signal generated by the ACM, and development of analytical modeling and interpretation techniques based on these studies. Sato and Mooney (1960) and Sill (1983) have developed the mechanisms and techniques for such modeling. Although the present geometric modeling scheme based on simple line sources (Rao et al., 1970) appears to give very reasonable results, confidence in the SP technique would be improved if the effects on the SP data of environmental variables such as wire conductivity, electrochemical properties of the water and sediments, and depth of burial of the mat were better understood.

The results of the resistivity studies indicate that high-frequency noise levels for representative operating conditions and electrode separations can be kept to levels below about +/- 0.5 mV, and that, using practical values for electrode separation and transmitter current, signal level differences needed to resolve mat parameters at depths of less than 150 ft for representative mat configurations are a few mV or greater. Thus it should be possible to design a practical TDC system that will detect a mat and resolve its depth with reasonable accuracy for most depths of interest.

Of concern for the use of TDC methods with profiles run along range lines is the interference of very large SP signals generated by relatively shallow mats. While such signals are ideal for SP studies, they may make it very difficult to determine TDC signal levels in the critical area above the mat. Additional studies are needed to determine what data analysis or operational procedures can be used in such cases.

REFERENCES

Corwin, R.F., 1993, Phase II Study, Investigation of articulated concrete mattresses using self-potential and electrical resistivity methods: Report prepared for U.S. Army Engineer Waterways Experiment Station, Contract No. DACW39-92-C-0112, April 27, 1993.

Corwin, R.F., 1994, System documentation: Self-Potential technique for investigation of articulated concrete mattresses: Report prepared for U.S. Army Engineer Waterways Experiment Station, Contract No. DACA39-93-C-0084.

Mozley, E.C., and Kooney, T., 1991, Airborne electromagnetic techniques to delineate reinforced concrete slabs buried within river bed sediments: Naval Oceanographic and Atmospheric Research Laboratory, Phase I Report to USACE, WES, Vicksburg, MS.

Rao, B.S.R., Murthy, I.V.R., and Reddy, S.J., 1970, Interpretation of self-potential anomalies of some geometric bodies: Pure and Applied Geophysics, v. 78, no. 1, p. 66-77.

Sato, M., and Mooney, H.M., 1960, The electrochemical mechanism of sulfide self-potentials: Geophysics, v. 25, no. 1, p. 226-249.

Sill, W.R., 1983, Self-potential modeling from primary flows: Geophysics, v. 48, no. 1, p 76-86.

Telford, W.M., Geldart, L.P., Sheriff, R.E., and Keys, D.A., 1976, Applied Geophysics: Cambridge Univ. Press.

TABLES

TABLE 1

MISSOURI BEND MAT LOCATION PARAMETERS FROM SP DATA

Range (nominal)	Run	Model	line no	Curr.	Xmid	Depth	Water depth	EAST	NORTH
U-81	MO1	MO1A	1	+11.96	1601	159	89	2027630	616732
			2	-11.61	1798	118	53	7450	821
U-82	MO4	MO4A	1	+11.96	1601	159	92	2027614	616730
			2	-11.61	1798	118	64	7453	843
U-83	MO5	MO5A	1	+17.0	1601	164	90	2027634	616882
			2	-14.6	1750	60	65	7485	889
U-84	MO6	MO6A	1	+16.95	1593	143	89	2027610	616843
			2	-12.51	1705	76	83	7499	828
U-85	MO7	MO7B	1	+17.7	1460	135	85	2027662	616912
			2	-14.7	1593	97	85	7545	976
U-87	MO9	MO9A	1	+15.6	1109	143	87	2027662	617110
			2	-14.8	1275	65	69	7511	043
U-88	MO10	MO10A	1	+8.67	829	99	82	2027698	617361
			2	-10.6	941	42	64	7592	617323
U-89	MO13	MO13A	1	+7.49	635	105	78	2027710	617395
			2	-9.39	760	41	65	7586	384
U-90	MO15	MO15A	1	+12.5	1470	163	74	2027781	617510
			2	-11.0	1630	80	62	7621	517
U-91	MO17	MO17B	1	+19.0	1068	140	81	2027743	617435
			2	-16.0	1120	66	70	7697	460
U-94	MO19A	MO19A	1	+10.5	1700	140	71	2027811	617815
			2	-9.0	1770	66	66	7741	807
U-95	MO18	MO18A	1	+10.5	2700	140	70	2027846	617780
			2	-9.0	2770	66	55	7745	815
U-96	MO20	MO20B	1	+11.3	1906	143	67	2027882	617905
			2	-9.6	1988	70	67	7815	952

TABLE 1
(continued)

MISSOURI BEND MAT LOCATION PARAMETERS FROM SP DATA

Range (nominal)	Run	Model	line	Curr.	Xmid	Depth	Water depth	EAST	NORTH
U-110	MO25	MO25A	1	+0.50	1350	120	48	2028804	618973
			2	-1.10	1680	100	56	8556	9152
			3	+0.90	1885	100	53	8357	9165
U-111	MO22	MO22C	1	+0.30	1400	138	44	2028887	619102
			2	-1.00	1770	90	57	8560	196
			3	+0.35	1900	50	54	8430	197
U-112	MO21A	MO21A	1	+0.80	1770	200	50	2028775	619288
			2	-1.60	2020	120	57	8533	330
U-113	MO23	MO23A	1	+0.75	1770	75	47	2028861	619368
			2	-1.50	2040	120	53	8598	411
U-120	MO27	MO27C	1	-3.30	1566	50	48	2029168	619881
			2	+2.80	1606	50	44	9129	891
			3	-3.80	1750	40	43	9024	982
			4	+1.20	1480	50	48	9251	862
U-122	MO26A	MO26A	1	+1.30	2270	55	46	2029358	620022
			2	-3.50	2340	60	43	9299	061
			3	+3.90	2430	60	41	9219	099
			4	-3.20	2600	40	40	9066	172
			5	+1.95	2750	50	36	8926	224
U-124	MO28	MO28A	1	+2.20	1850	45	44	2029407	620198
			2	-3.50	2115	45	42	9194	344

TABLE 2

MANCHAC MAT LOCATION PARAMETERS FROM SP DATA

Range (nominal)	Run	Model	line no	Curr.	Xmid	Depth	Water depth	EAST	NORTH
U-89	MN2A	MN2C	1	+15.5	887	105	108	2054814	610163
			2	-21.2	1008	90	89	4891	255
			3	-9.95	1110	62	53	4910	352
			4	+11.33	1273	36	50	4884	505
U-90	MN1	MN1B	1	+13.85	1061	128	103	2054717	610159
			2	-17.99	1241	95	74	4793	317
			3	-14.33	1370	66	52	4796	445
			4	+12.82	1500	37	48	4815	572
U-91	MN3	MN3B	1	+10.00	650	120	103	2054567	610177
			2	-17.00	910	90	80	4721	386
			3	-15.00	990	62	57	4759	455
			4	+11.00	1112	50	48	4766	577
U-109	MN5	MN5A	1	+3.2	569	100	108	2052961	610528
			2	-8.0	790	105	96	3064	722
			3	+4.57	1073	45	30	3105	999
U-110	MN4	MN4B	1	+1.33	600	100	104	2052891	610510
			2	-2.61	872	105	106	2933	774
			3	-5.36	1073	80	66	3023	952
			4	+5.90	1135	45	44	3046	611009
U-111	MN6A	MN6A	1	-10	520	100	102	2052885	610834
			2	+7.5	630	60	71	2923	936
			3	-1.5	740	45	50	2900	611043
U-139	MN8B	MN8B	1	+8	1560	150	127	2050470	611876
			2	-18	1790	85	83	0596	612064
			3	+1.5	1890	40	49	0613	160
U-140	MN7	MN7A	1	+8	810	140	124	2050414	611886
			2	-16	1050	85	72	0399	612119
			3	+5	1220	30	23	0432	285
U-141	MN9	MN9A	1	+8	1630	150	123	2050286	611936
			2	-21	1870	75	73	0390	612151
			3	+6	2000	30	28	0446	266
U-169	MN11	MN11A	1	+3.01	1725	100	77	2047719	612442
U-170	MN10	MN10A	1	+2.2	1330	91	72	2047636	612482
U-171	MN12	MN12A	1	+1.66	1272	91	70	2047580	612489

FIGURES

FIGURE 1

OFFSHORE SELF–POTENTIAL MEASUREMENT SYSTEM
(not to scale)

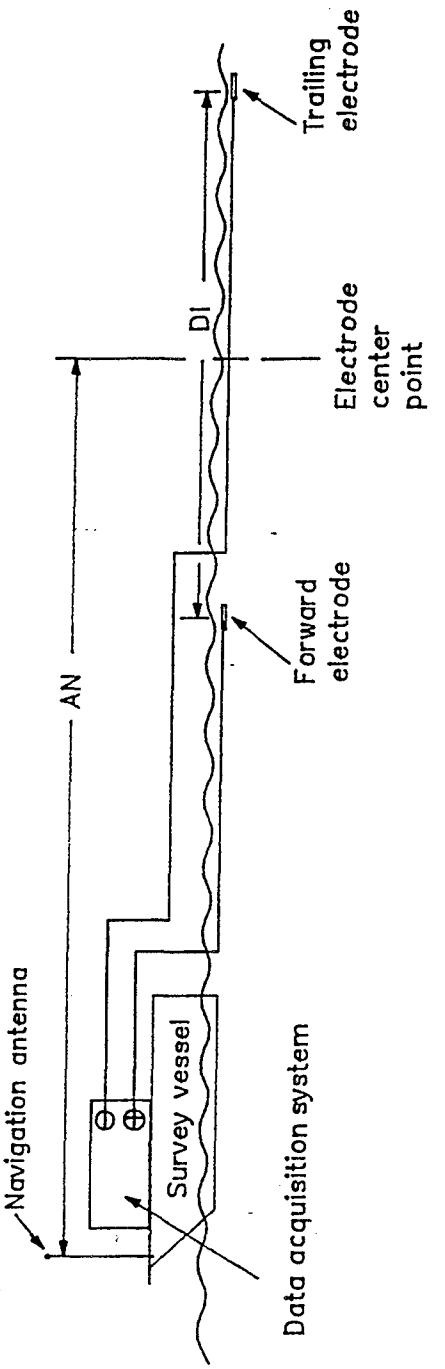

FIGURE 2

OFFSHORE SELF-POTENTIAL DATA ACQUISITION SYSTEM SCHEMATIC

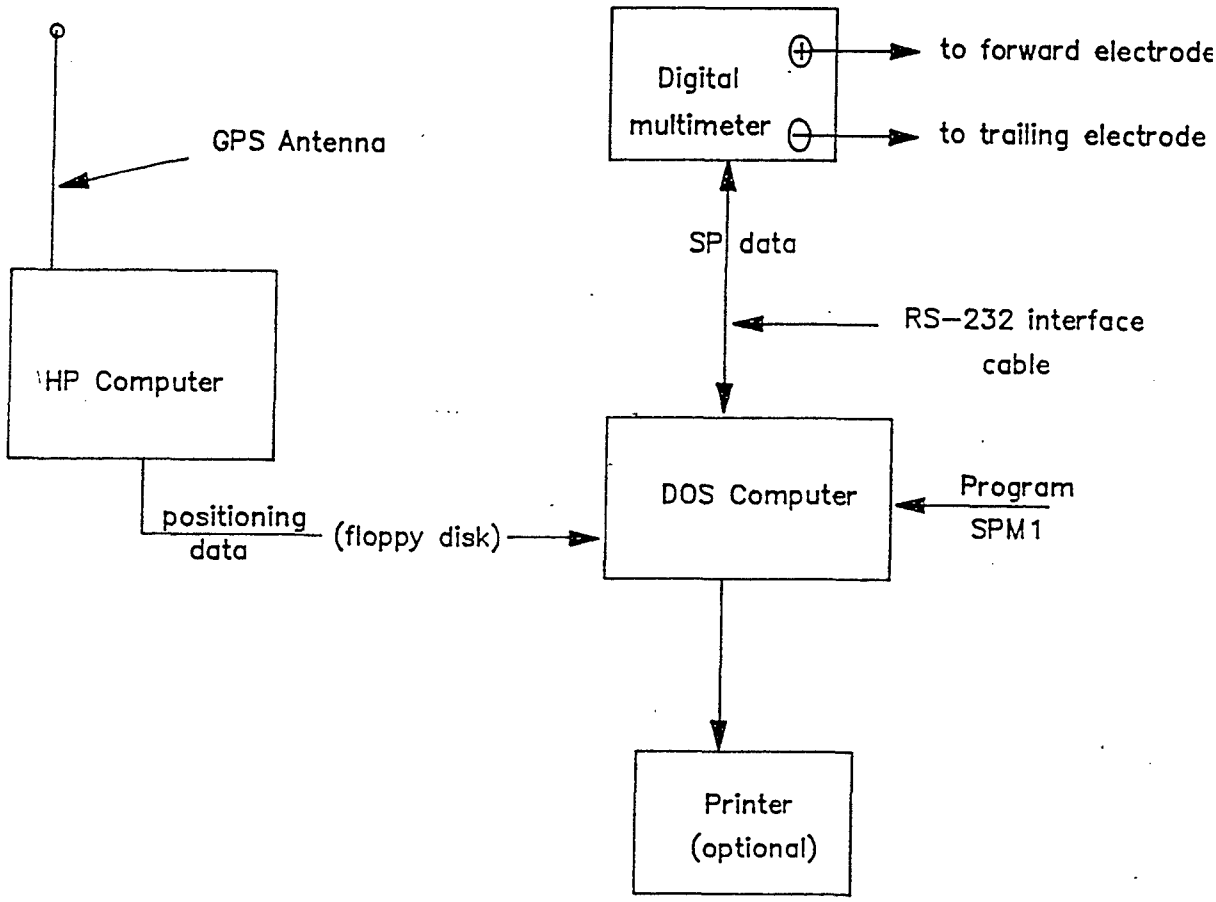

FIGURE 3

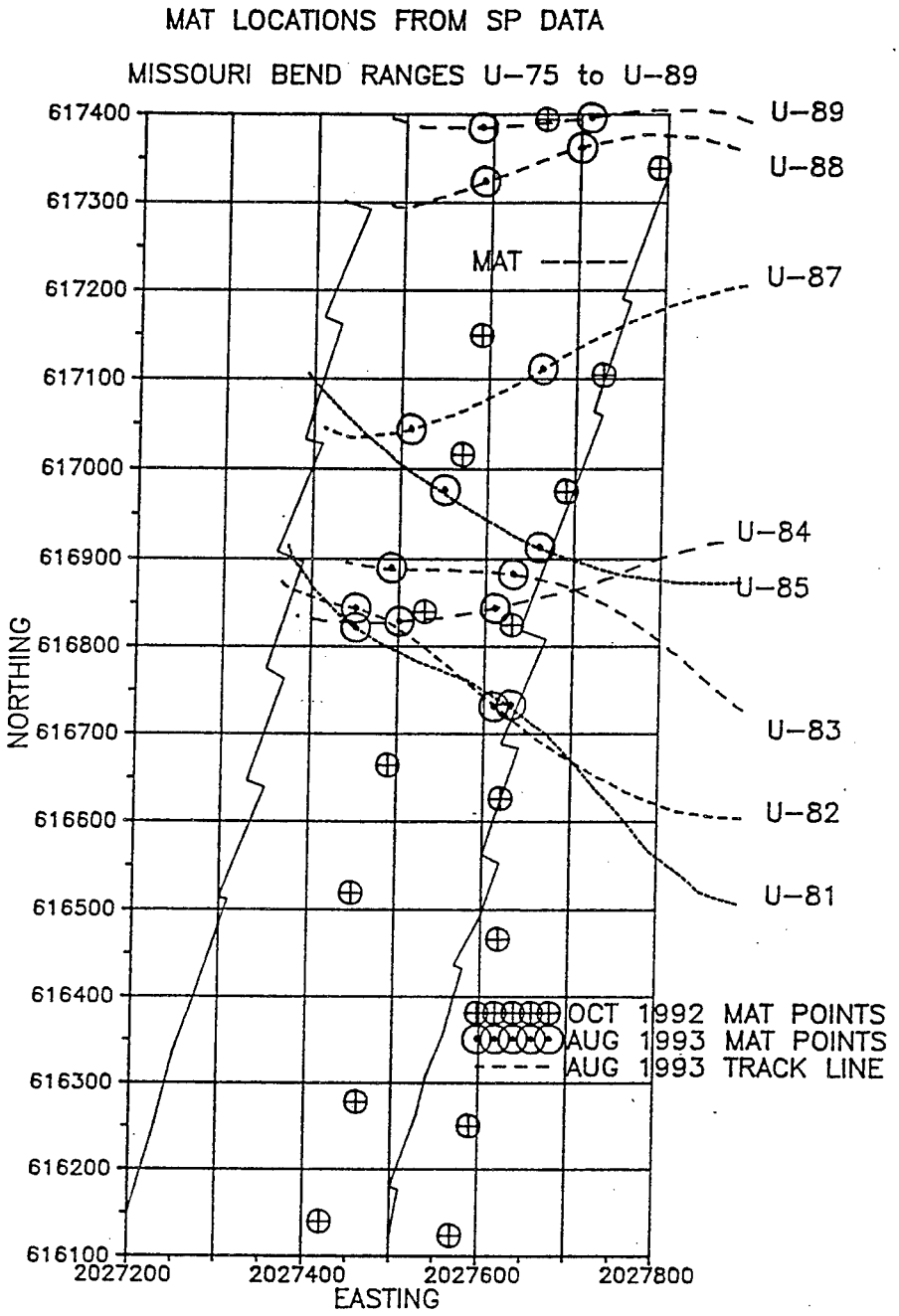
MAT LOCATIONS FROM SP DATA
MISSOURI BEND RANGES U-75 to U-89
617400
617300
617200
617100
617000
616900
616800
616700
616600
616500
616400
616300
616200
616100
NORTHING
2027200
2027400
2027600
2027800
EASTING
U-89
U-88
MAT
U-87
U-84
U-85
U-83
U-82
U-81
OCT 1992 MAT POINTS
AUG 1993 MAT POINTS
AUG 1993 TRACK LINE

FIGURE 4

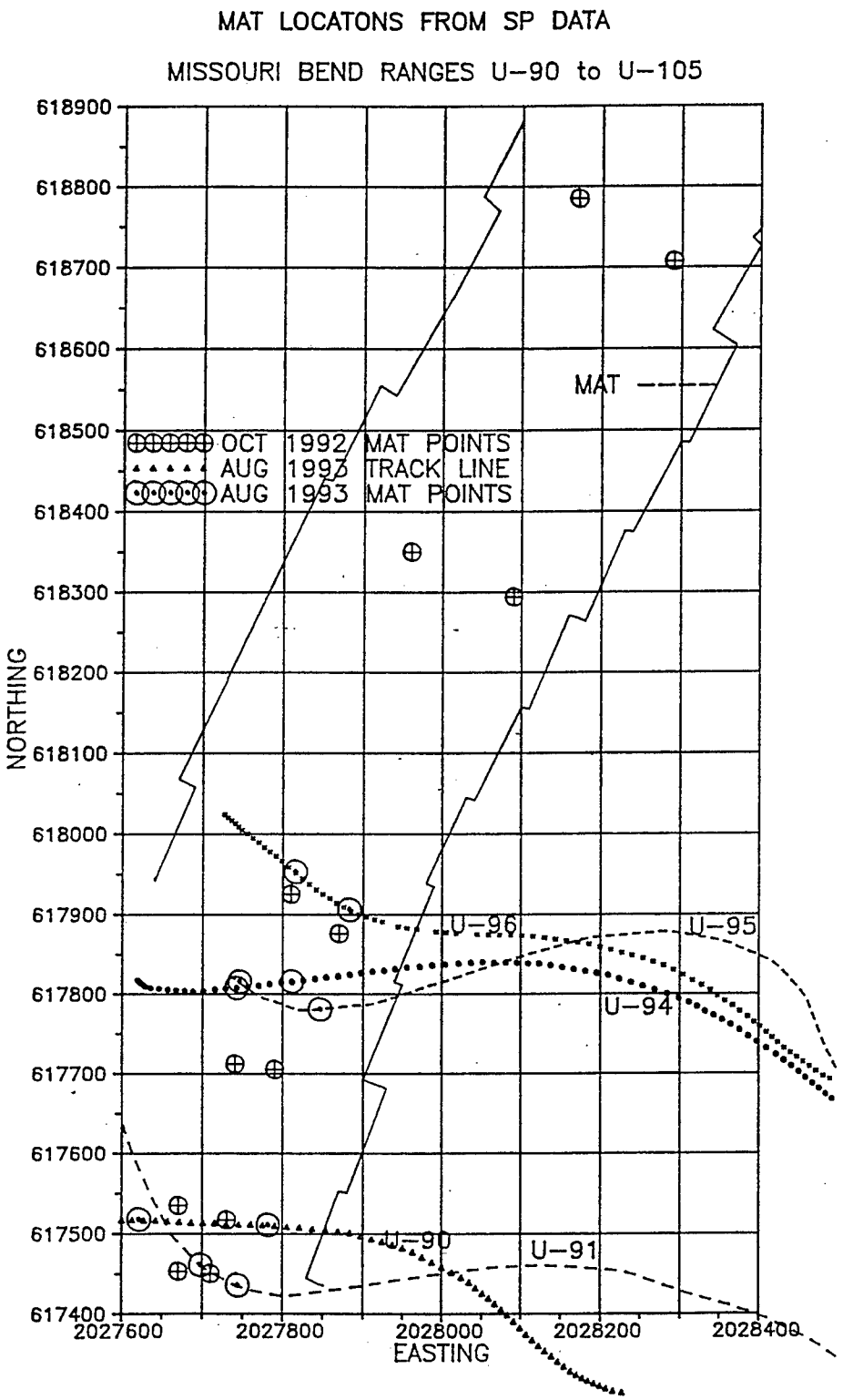
MAT LOCATONS FROM SP DATA
MISSOURI BEND RANGES U-90 to U-105
618900
618800
618700
618600
618500
618400
618300
618200
618100
618000
617900
617800
617700
617600
617500
617400
NORTHING
2027600
2027800
2028000
2028200
2028400
EASTING
OCT 1992 MAT POINTS
AUG 1993 TRACK LINE
AUG 1993 MAT POINTS
MAT
U-96
U-95
U-94
U-90
U-91

FIGURE 5

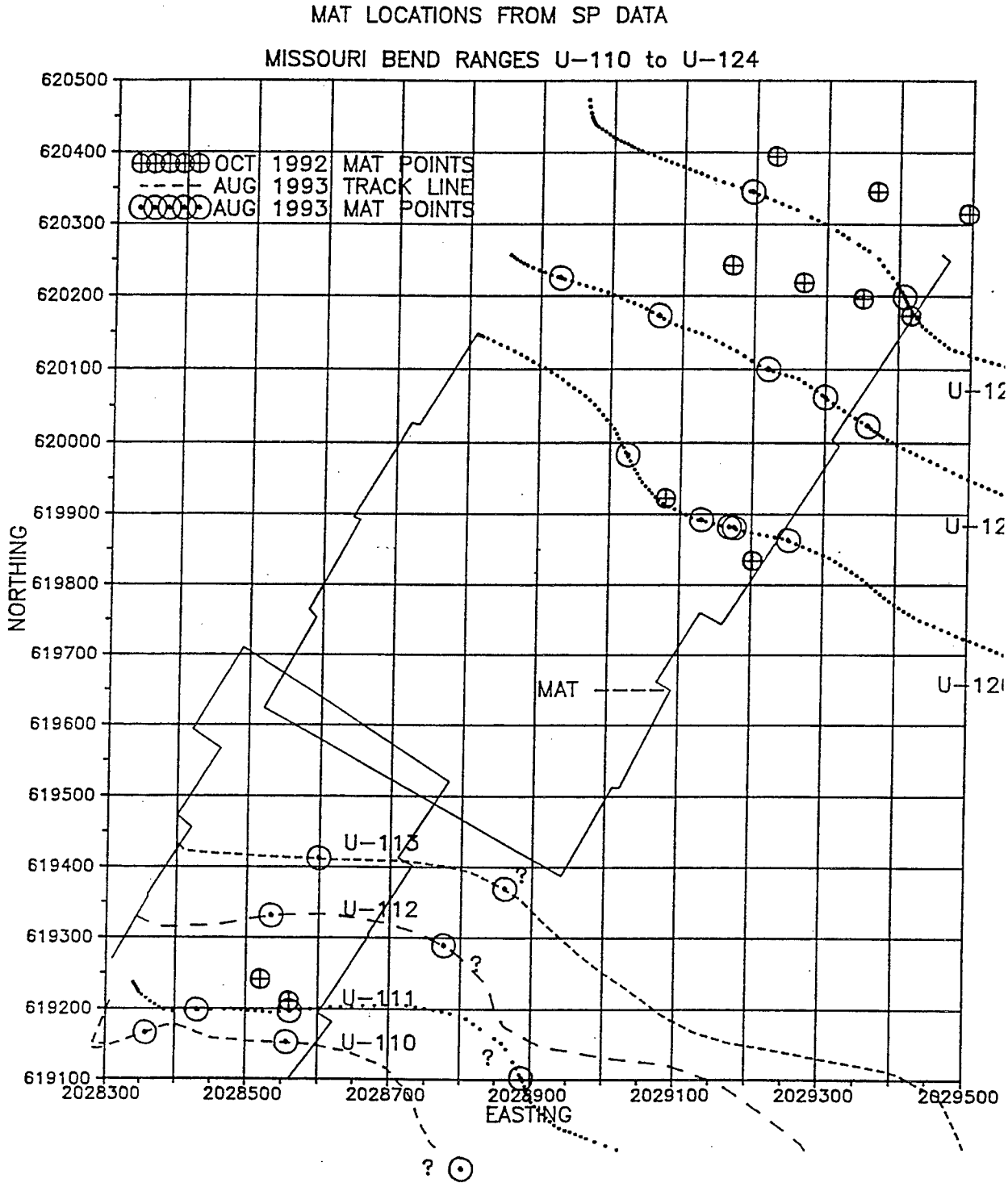
MAT LOCATIONS FROM SP DATA
MISSOURI BEND RANGES U-110 to U-124
OCT 1992 MAT POINTS
AUG 1993 TRACK LINE
AUG 1993 MAT POINTS
NORTHING
EASTING
620500
620400
620300
620200
620100
620000
619900
619800
619700
619600
619500
619400
619300
619200
619100
2028300
2028500
2028700
2028900
2029100
2029300
2029500
U-12
U-12
U-12
MAT
U-113
U-112
U-111
U-110

FIGURE 6

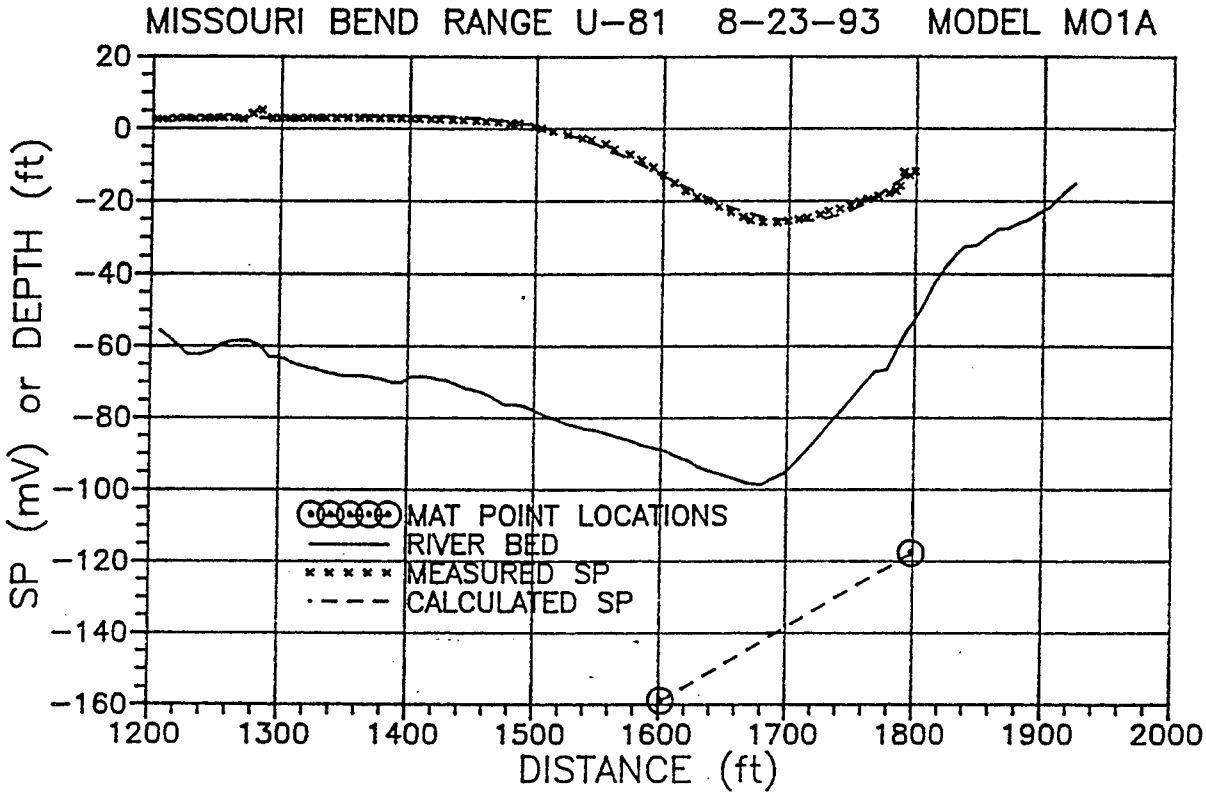
MISSOURI BEND RANGE U-81 8-23-93 MODEL MO1A
SP (mV) or DEPTH (ft)
20
0
-20
-40
-60
-80
-100
-120
-140
-160
1200
1300
1400
1500
1600
1700
1800
1900
2000
DISTANCE (ft)
MAT POINT LOCATIONS
RIVER BED
MEASURED SP
CALCULATED SP

FIGURE 7

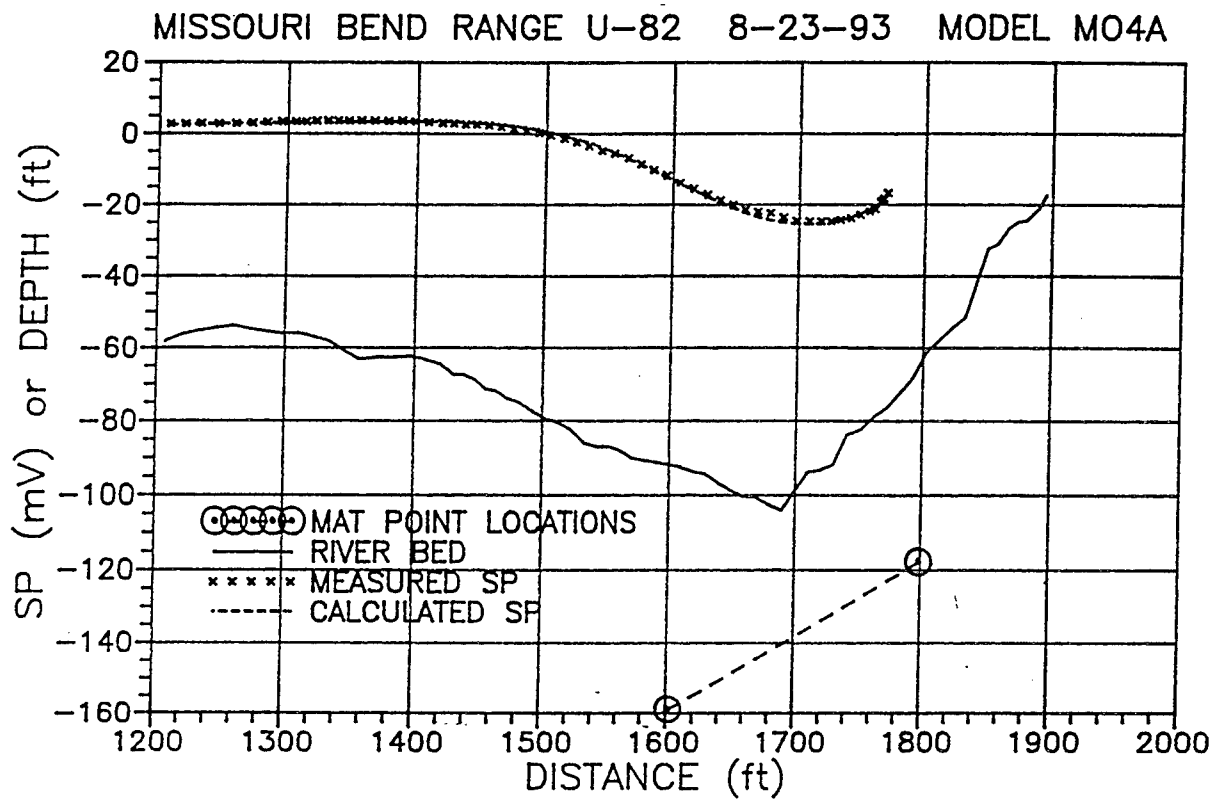
MISSOURI BEND RANGE U-82 8-23-93 MODEL MO4A
SP (mV) or DEPTH (ft)
20
0
-20
-40
-60
-80
-100
-120
-140
-160
1200
1300
1400
1500
1600
1700
1800
1900
2000
DISTANCE (ft)
MAT POINT LOCATIONS
RIVER BED
MEASURED SP
CALCULATED SP

FIGURE 8

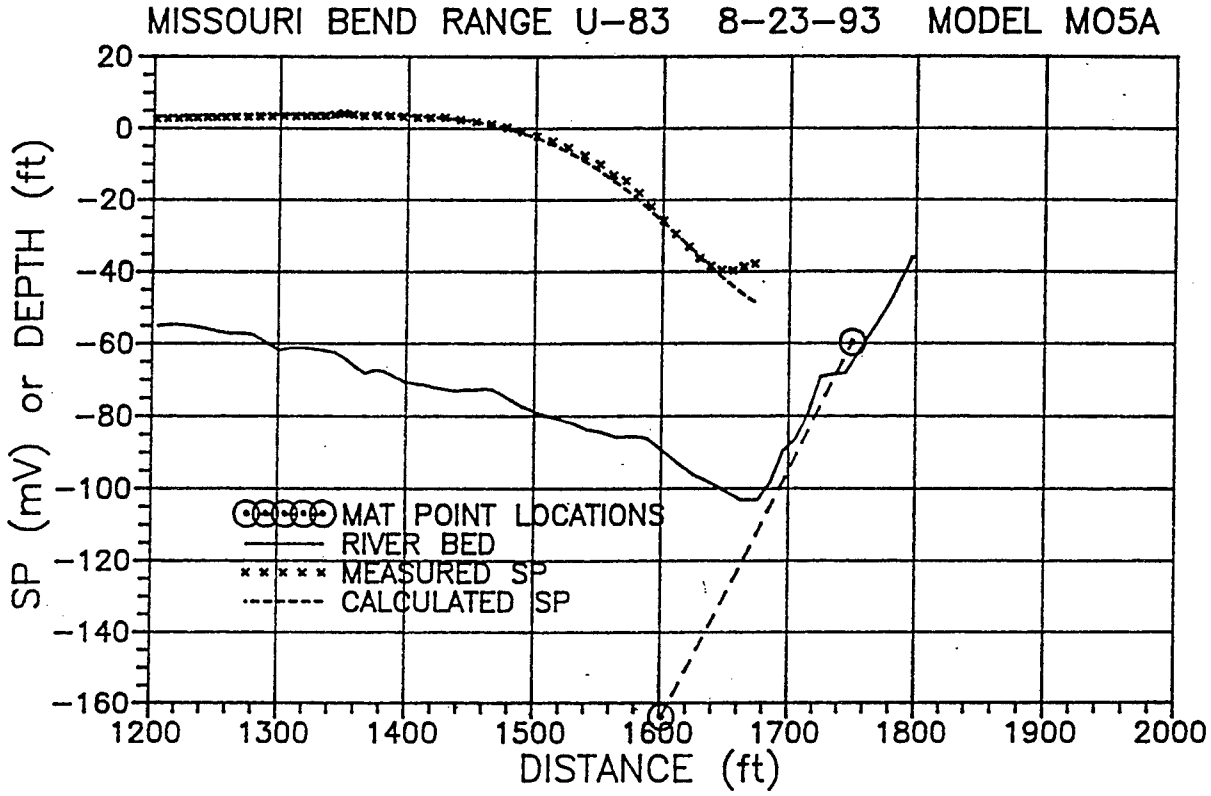
MISSOURI BEND RANGE U-83 8-23-93 MODEL MO5A
SP (mV) or DEPTH (ft)
20
0
-20
-40
-60
-80
-100
-120
-140
-160
1200
1300
1400
1500
1600
1700
1800
1900
2000
DISTANCE (ft)
MAT POINT LOCATIONS
RIVER BED
MEASURED SP
CALCULATED SP

FIGURE 9

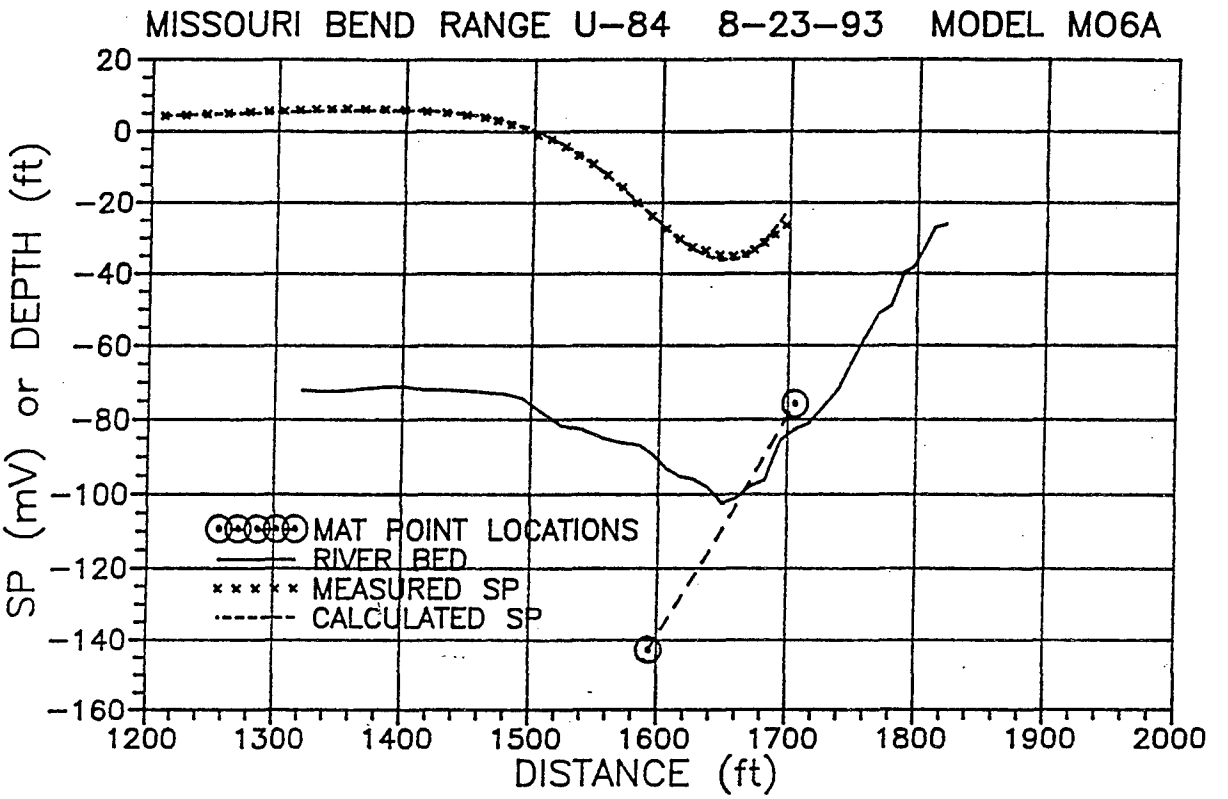
MISSOURI BEND RANGE U-84 8-23-93 MODEL MO6A
SP (mV) or DEPTH (ft)
20
0
-20
-40
-60
-80
-100
-120
-140
-160
1200
1300
1400
1500
1600
1700
1800
1900
2000
DISTANCE (ft)
MAT POINT LOCATIONS
RIVER BED
MEASURED SP
CALCULATED SP

FIGURE 10

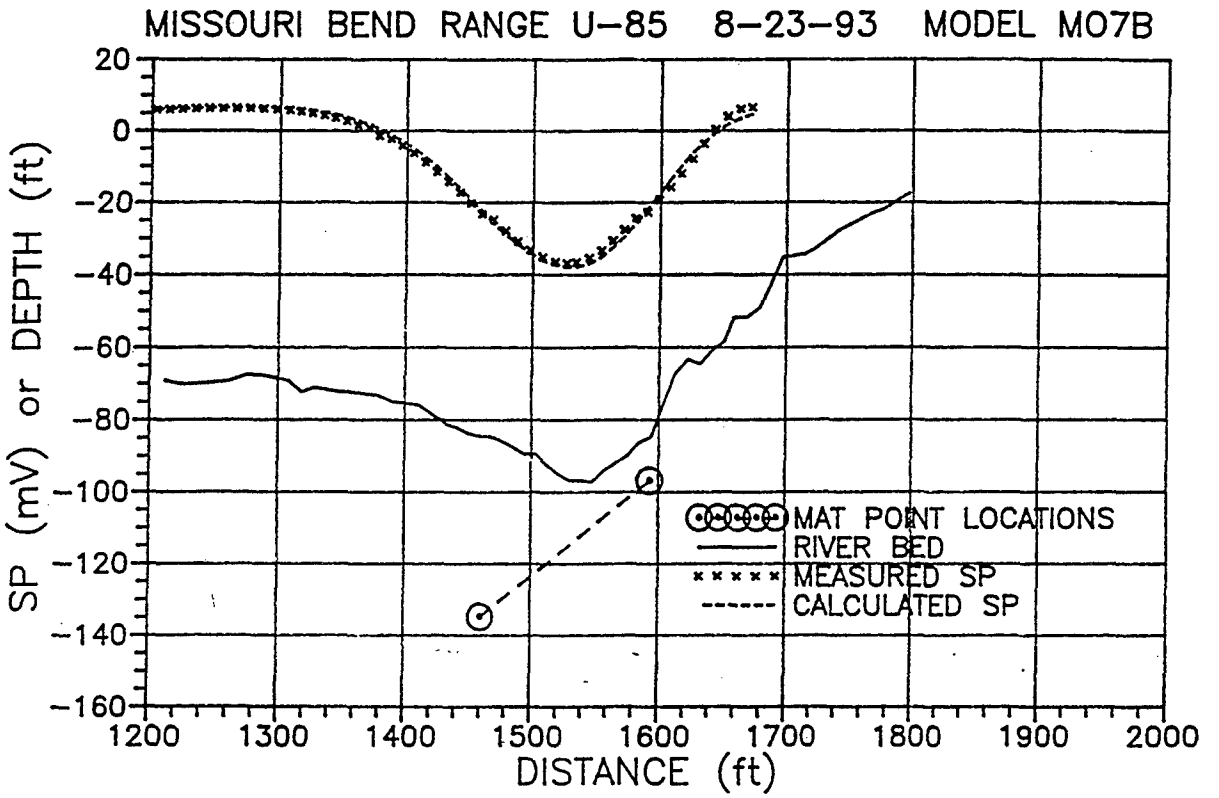
MISSOURI BEND RANGE U-85 8-23-93 MODEL MO7B
SP (mV) or DEPTH (ft)
20
0
-20
-40
-60
-80
-100
-120
-140
-160
1200
1300
1400
1500
1600
1700
1800
1900
2000
DISTANCE (ft)
MAT POINT LOCATIONS
RIVER BED
MEASURED SP
CALCULATED SP

FIGURE 11

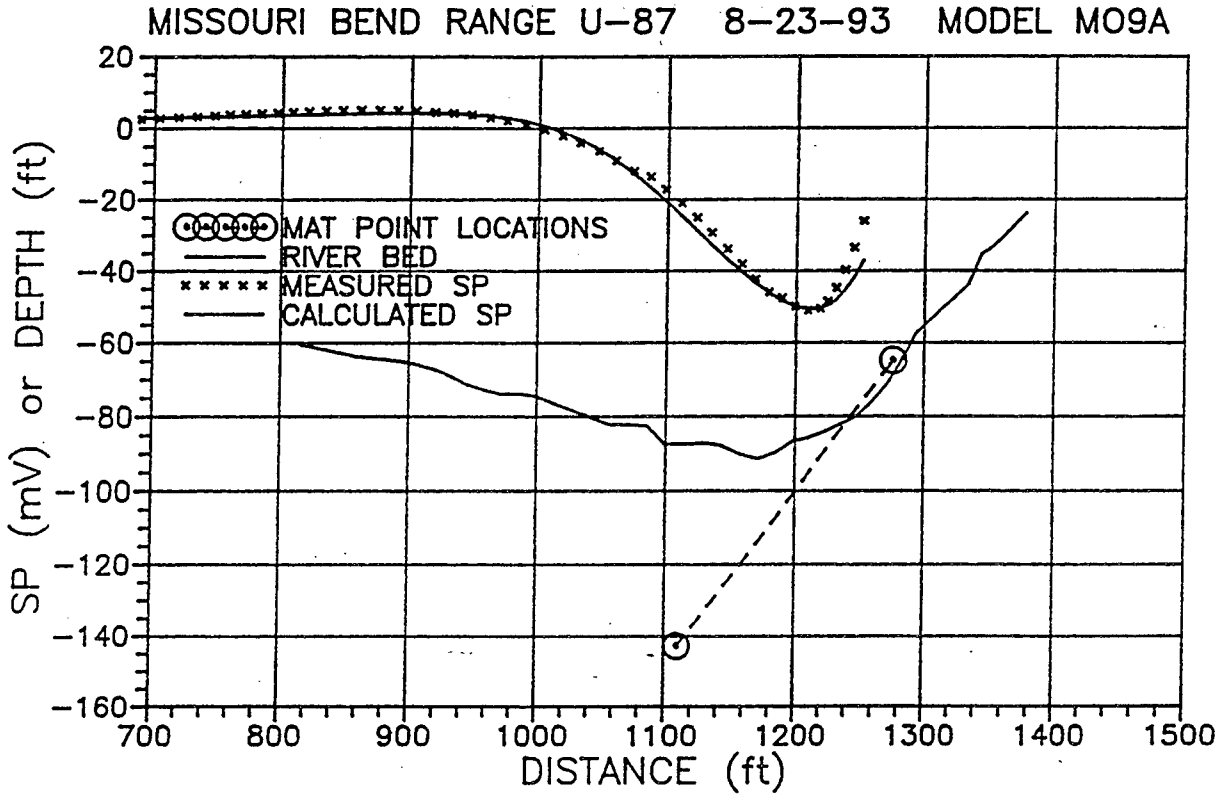
MISSOURI BEND RANGE U-87 8-23-93 MODEL MO9A
SP (mV) or DEPTH (ft)
DISTANCE (ft)
MAT POINT LOCATIONS
RIVER BED
MEASURED SP
CALCULATED SP
20
0
-20
-40
-60
-80
-100
-120
-140
-160
700
800
900
1000
1100
1200
1300
1400
1500

FIGURE 12

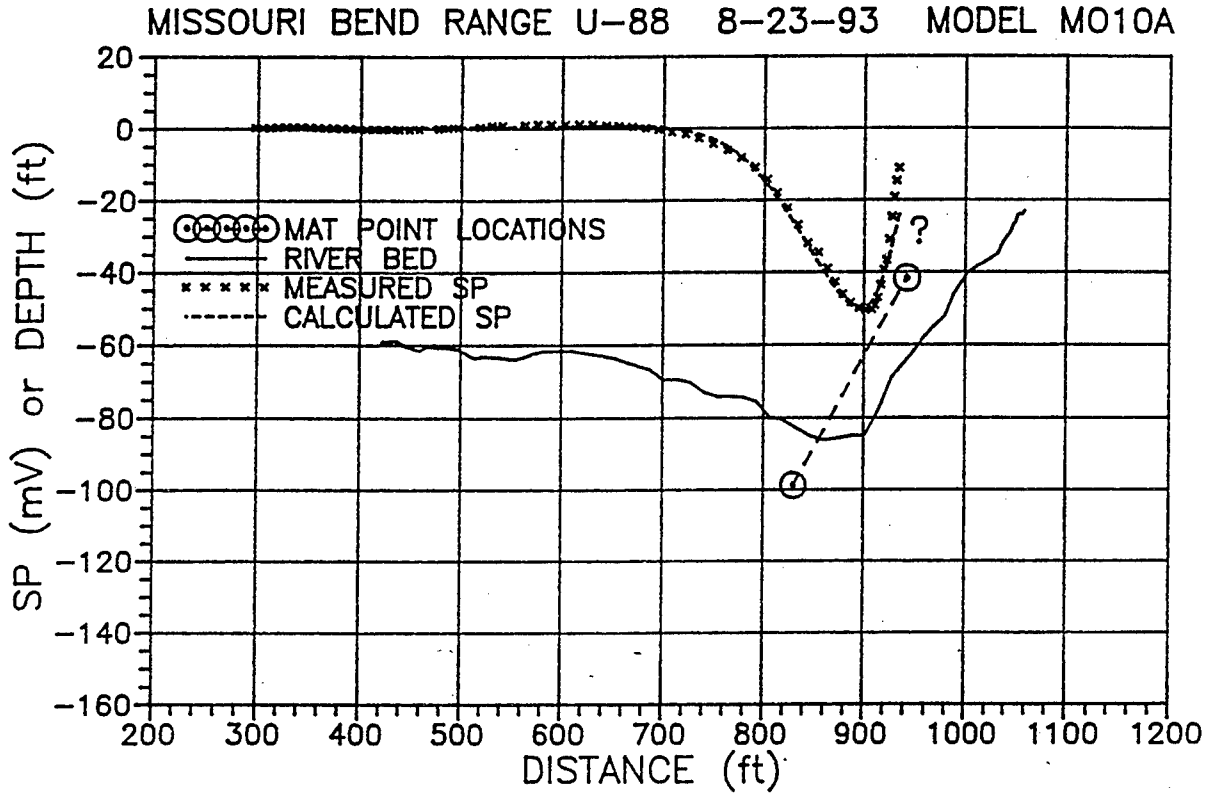
MISSOURI BEND RANGE U-88 8-23-93 MODEL M010A
SP (mV) or DEPTH (ft)
20
0
-20
-40
-60
-80
-100
-120
-140
-160
MAT POINT LOCATIONS
RIVER BED
MEASURED SP
CALCULATED SP
?
200
300
400
500
600
700
800
900
1000
1100
1200
DISTANCE (ft)

FIGURE 13

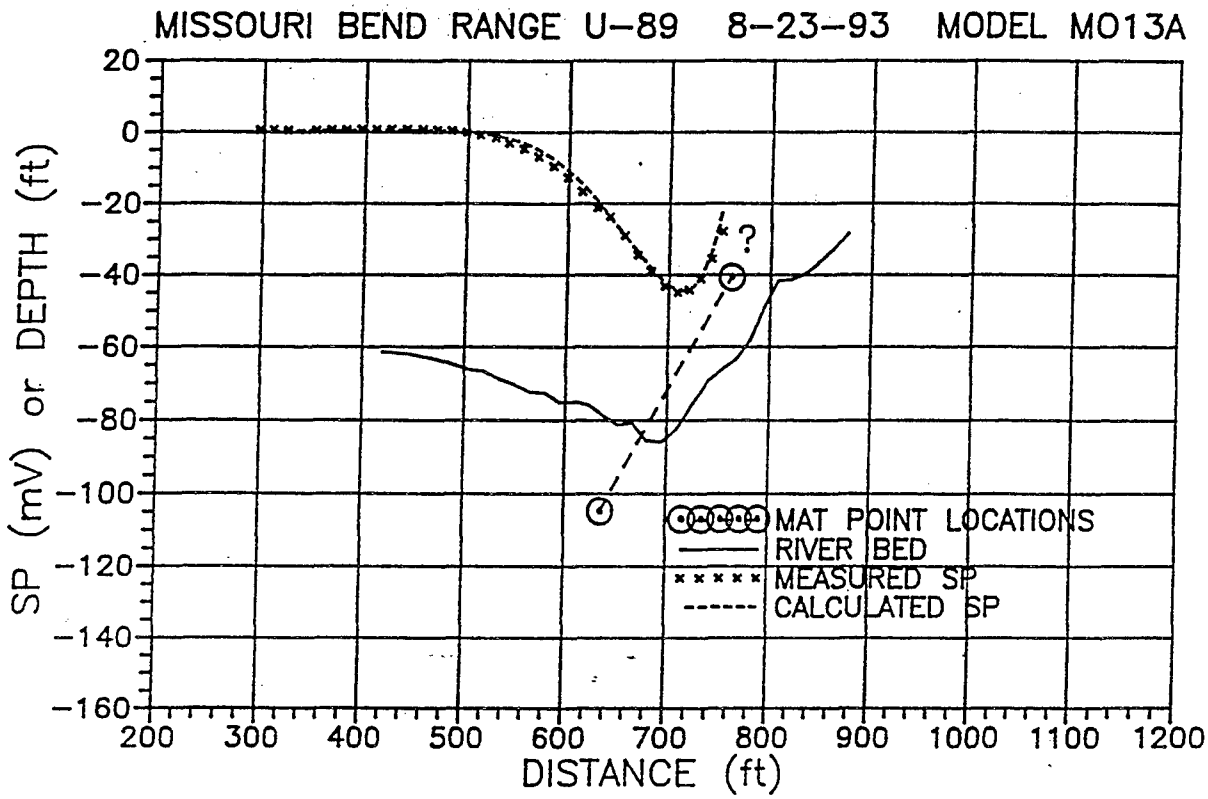
MISSOURI BEND RANGE U-89 8-23-93 MODEL MO13A
SP (mV) or DEPTH (ft)
20
0
-20
-40
-60
-80
-100
-120
-140
-160
200
300
400
500
600
700
800
900
1000
1100
1200
DISTANCE (ft)
?
MAT POINT LOCATIONS
RIVER BED
MEASURED SP
CALCULATED SP

FIGURE 14

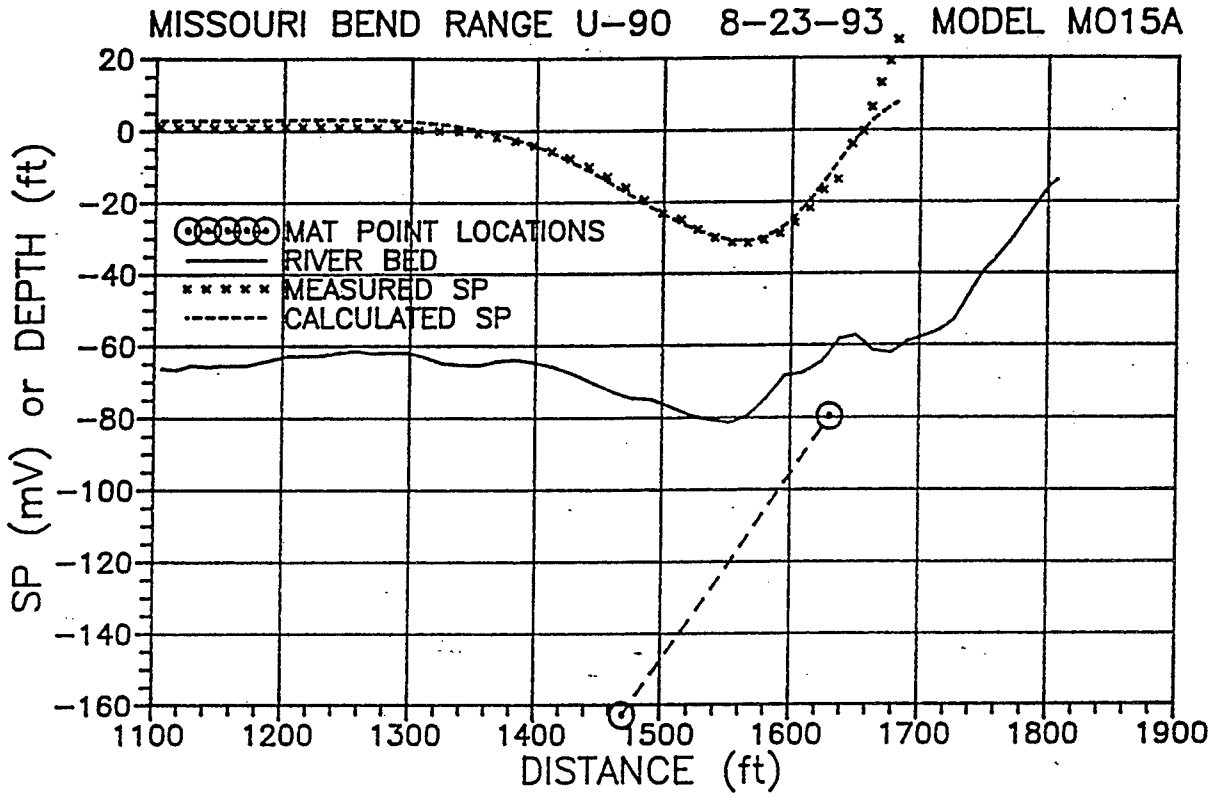
MISSOURI BEND RANGE U-90 8-23-93 MODEL MO15A
SP (mV) or DEPTH (ft)
20
0
-20
-40
-60
-80
-100
-120
-140
-160
MAT POINT LOCATIONS
RIVER BED
MEASURED SP
CALCULATED SP
1100
1200
1300
1400
1500
1600
1700
1800
1900
DISTANCE (ft)

FIGURE 15

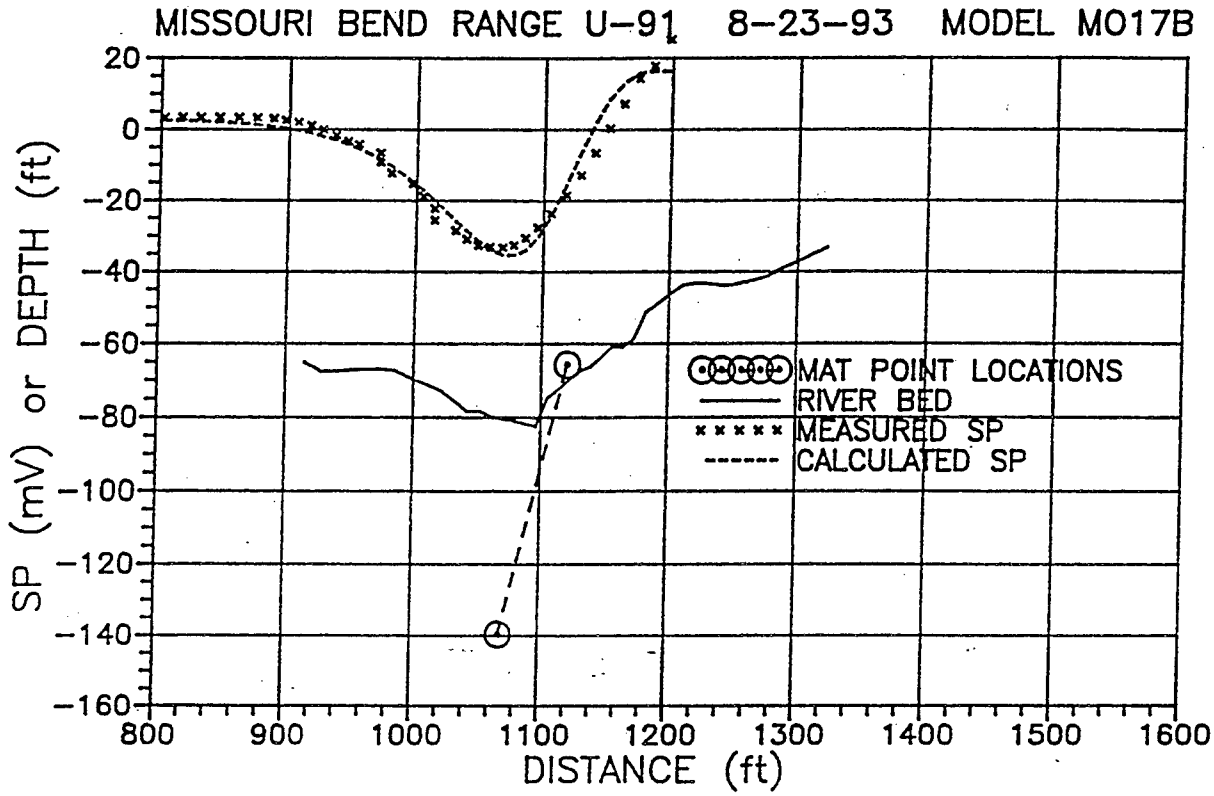
MISSOURI BEND RANGE U-91 8-23-93 MODEL M017B
SP (mV) or DEPTH (ft)
20
0
-20
-40
-60
-80
-100
-120
-140
-160
800
900
1000
1100
1200
1300
1400
1500
1600
DISTANCE (ft)
MAT POINT LOCATIONS
RIVER BED
MEASURED SP
CALCULATED SP

FIGURE 16

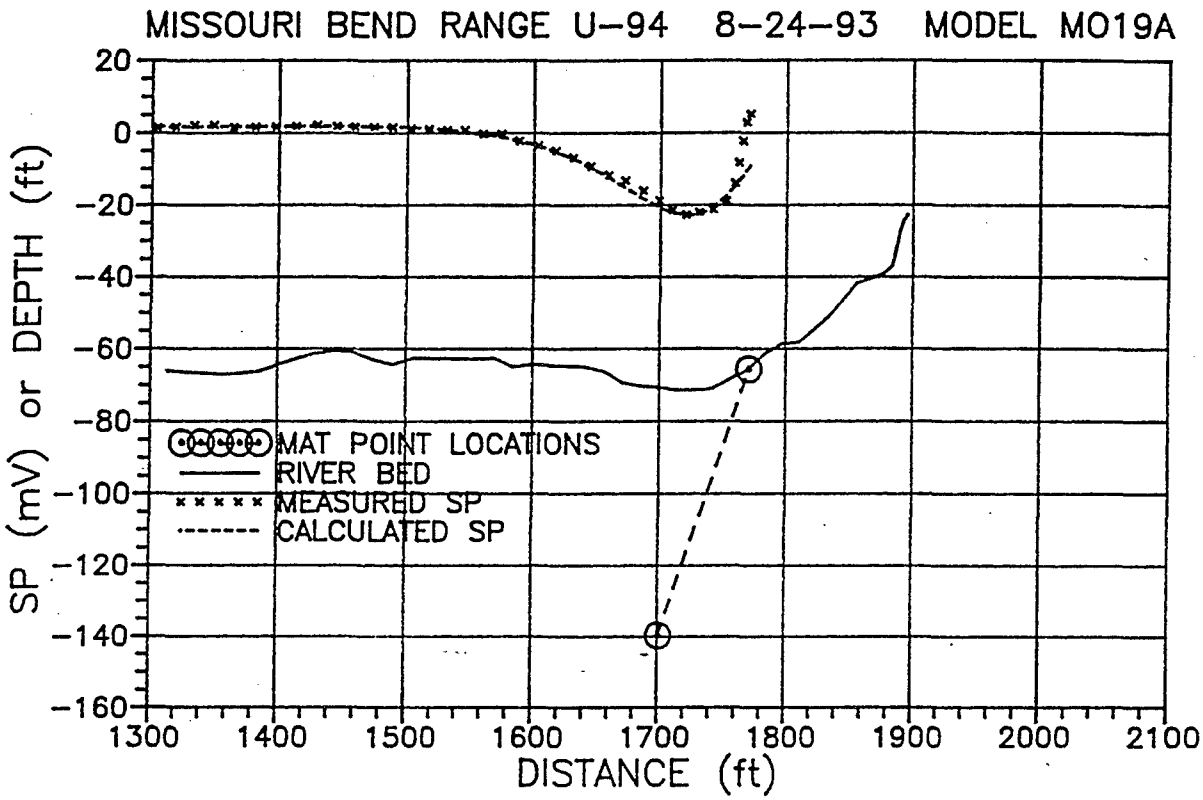
MISSOURI BEND RANGE U-94 8-24-93 MODEL MO19A
SP (mV) or DEPTH (ft)
20
0
-20
-40
-60
-80
-100
-120
-140
-160
1300
1400
1500
1600
1700
1800
1900
2000
2100
DISTANCE (ft)
MAT POINT LOCATIONS
RIVER BED
MEASURED SP
CALCULATED SP

FIGURE 17

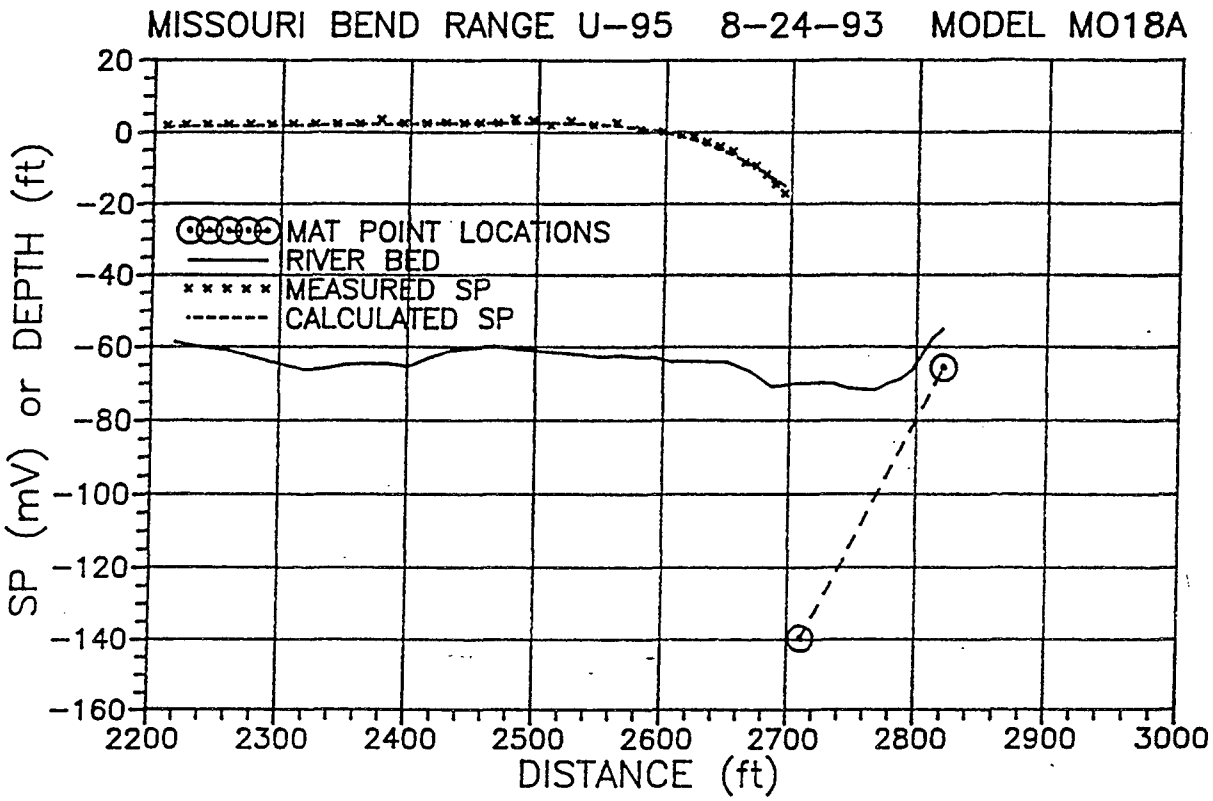
MISSOURI BEND RANGE U-95 8-24-93 MODEL MO18A
SP (mV) or DEPTH (ft)
DISTANCE (ft)
MAT POINT LOCATIONS
RIVER BED
MEASURED SP
CALCULATED SP
20
0
-20
-40
-60
-80
-100
-120
-140
-160
2200
2300
2400
2500
2600
2700
2800
2900
3000

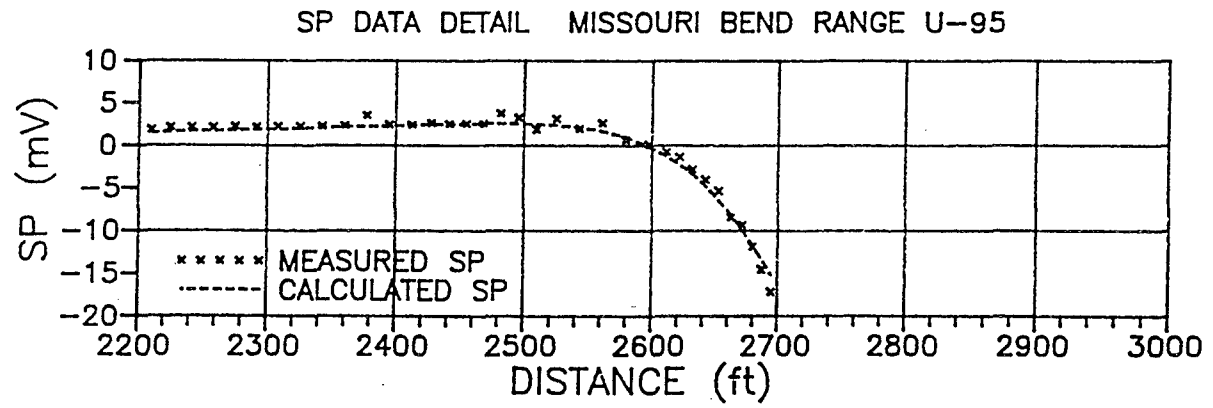
SP DATA DETAIL MISSOURI BEND RANGE U-95
SP (mV)
DISTANCE (ft)
MEASURED SP
CALCULATED SP
10
5
0
-5
-10
-15
-20
2200
2300
2400
2500
2600
2700
2800
2900
3000

FIGURE 18

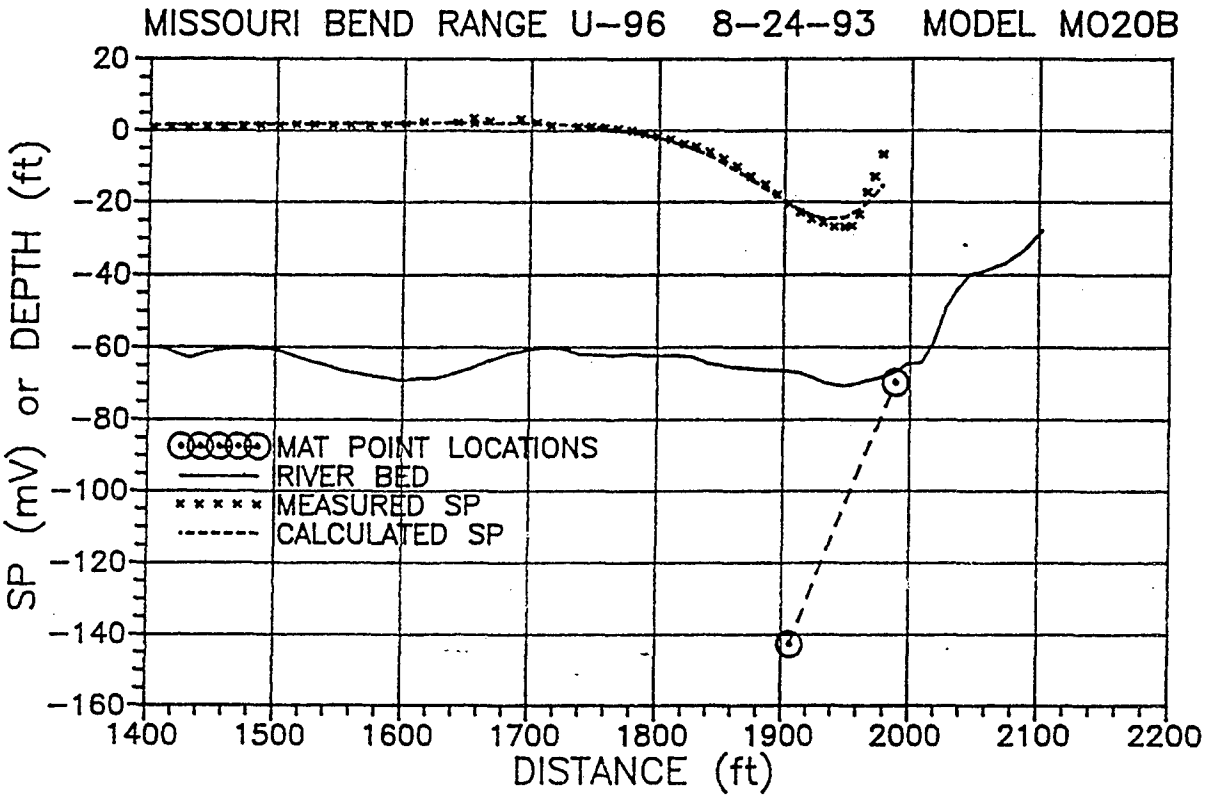
MISSOURI BEND RANGE U-96 8-24-93 MODEL MO20B
SP (mV) or DEPTH (ft)
20
0
-20
-40
-60
-80
-100
-120
-140
-160
1400
1500
1600
1700
1800
1900
2000
2100
2200
DISTANCE (ft)
MAT POINT LOCATIONS
RIVER BED
MEASURED SP
CALCULATED SP

FIGURE 19

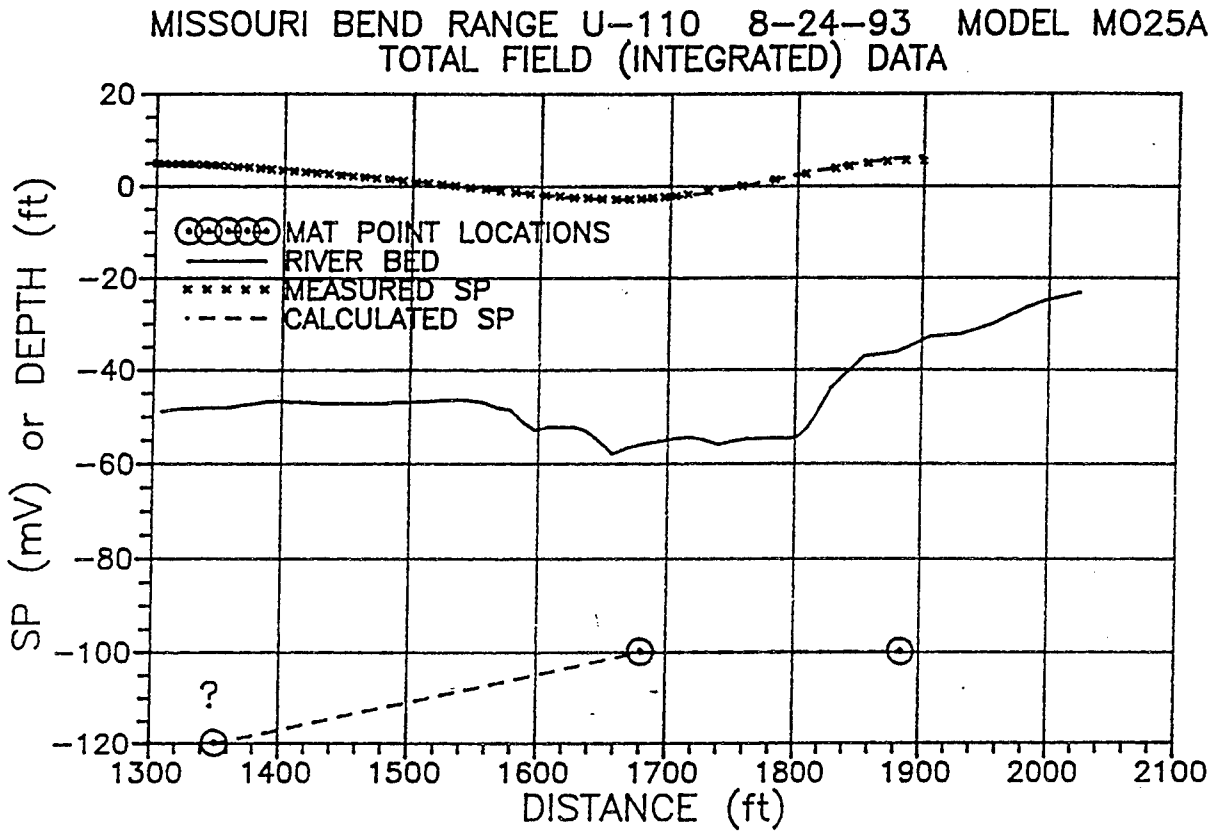
MISSOURI BEND RANGE U-110 8-24-93 MODEL MO25A
TOTAL FIELD (INTEGRATED) DATA
MAT POINT LOCATIONS
RIVER BED
MEASURED SP
CALCULATED SP
?
SP (mV) or DEPTH (ft)
DISTANCE (ft)
20
0
-20
-40
-60
-80
-100
-120
1300
1400
1500
1600
1700
1800
1900
2000
2100

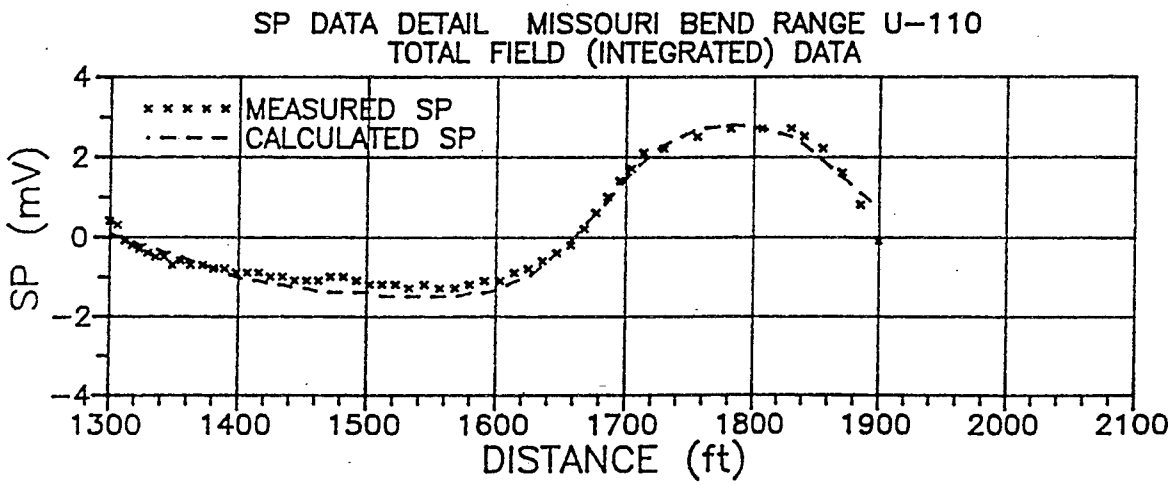
SP DATA DETAIL MISSOURI BEND RANGE U-110
TOTAL FIELD (INTEGRATED) DATA
MEASURED SP
CALCULATED SP
SP (mV)
DISTANCE (ft)
4
2
0
-2
-4
1300
1400
1500
1600
1700
1800
1900
2000
2100

FIGURE 20

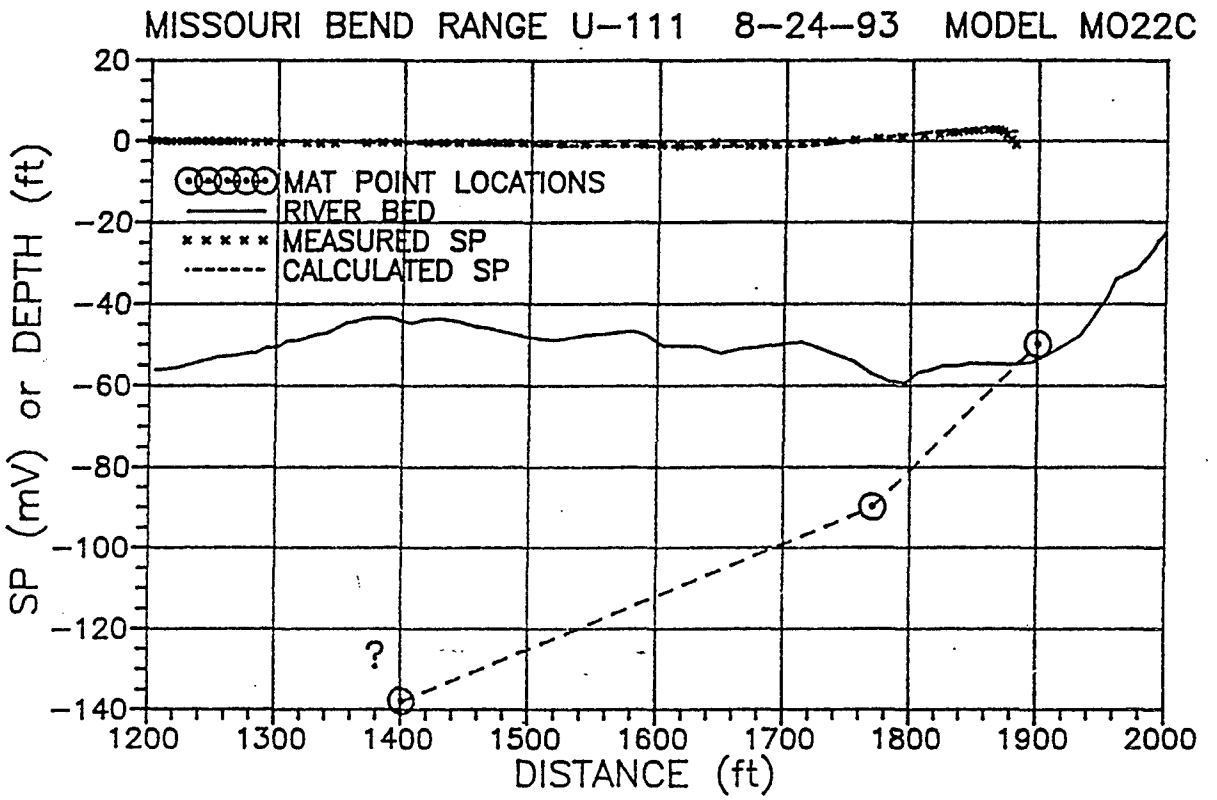
MISSOURI BEND RANGE U-111 8-24-93 MODEL MO22C
MAT POINT LOCATIONS
RIVER BED
MEASURED SP
CALCULATED SP
SP (mV) or DEPTH (ft)
DISTANCE (ft)
?

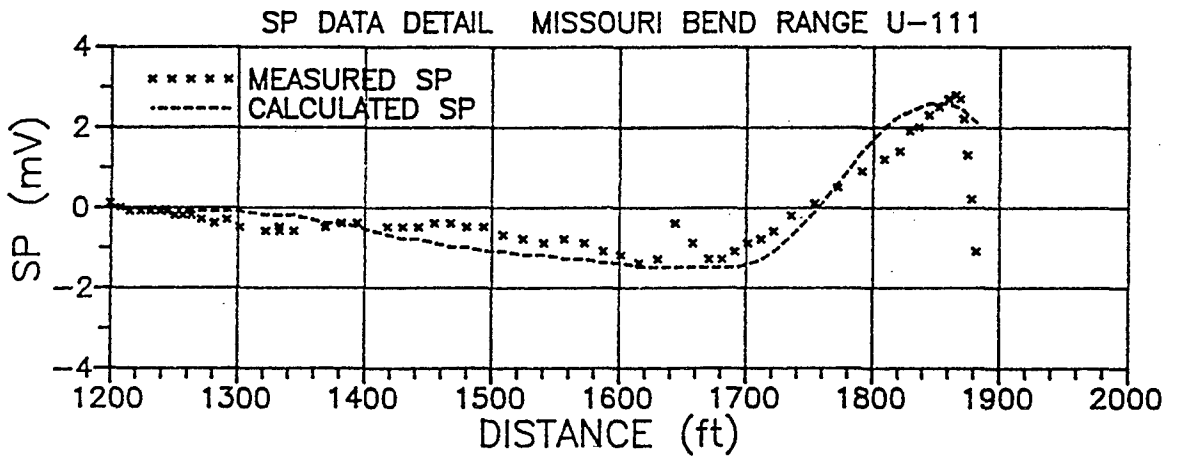
SP DATA DETAIL MISSOURI BEND RANGE U-111
MEASURED SP
CALCULATED SP
SP (mV)
DISTANCE (ft)

FIGURE 21

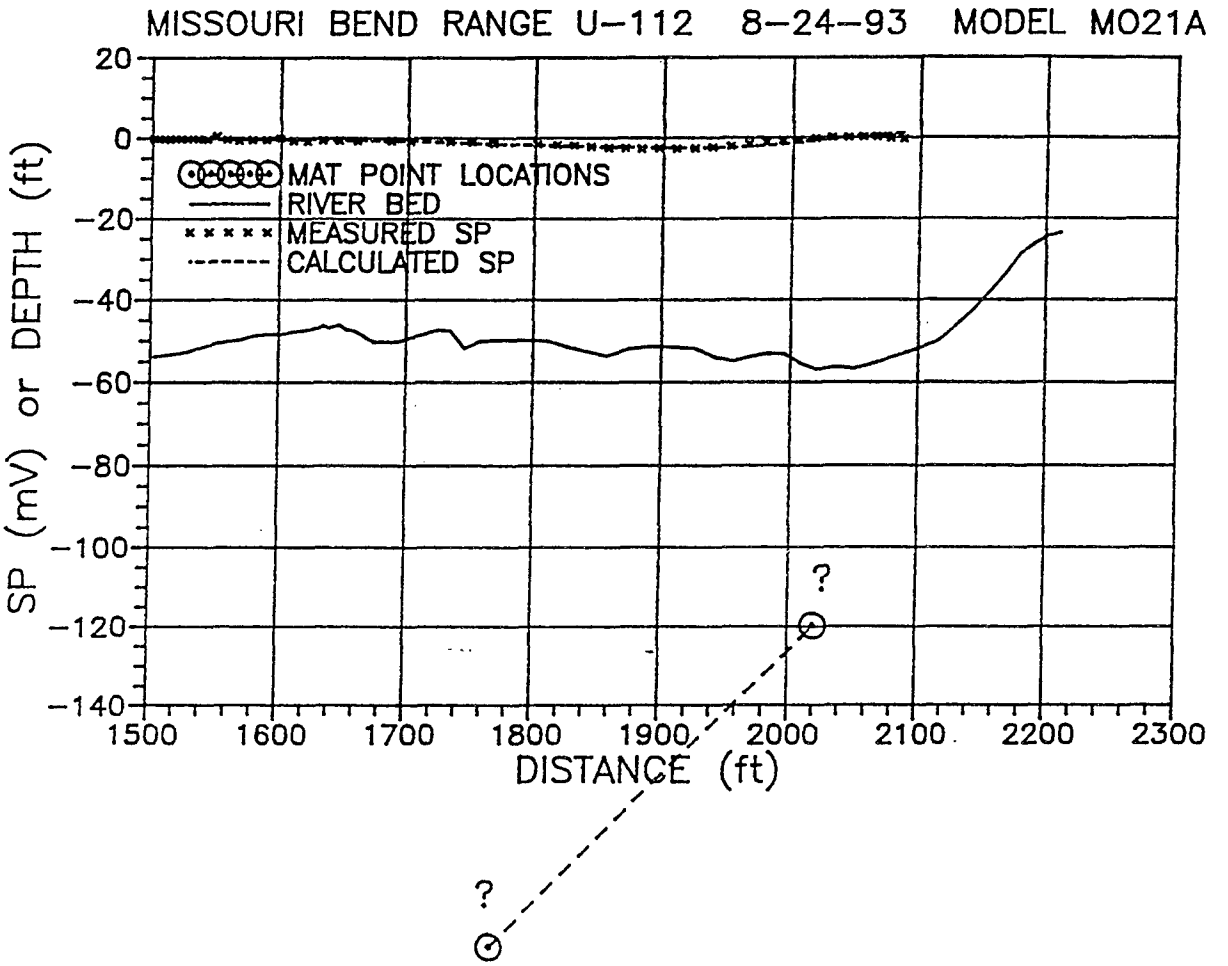
MISSOURI BEND RANGE U-112 8-24-93 MODEL MO21A
MAT POINT LOCATIONS
RIVER BED
MEASURED SP
CALCULATED SP
SP (mV) or DEPTH (ft)
DISTANCE (ft)
?
?

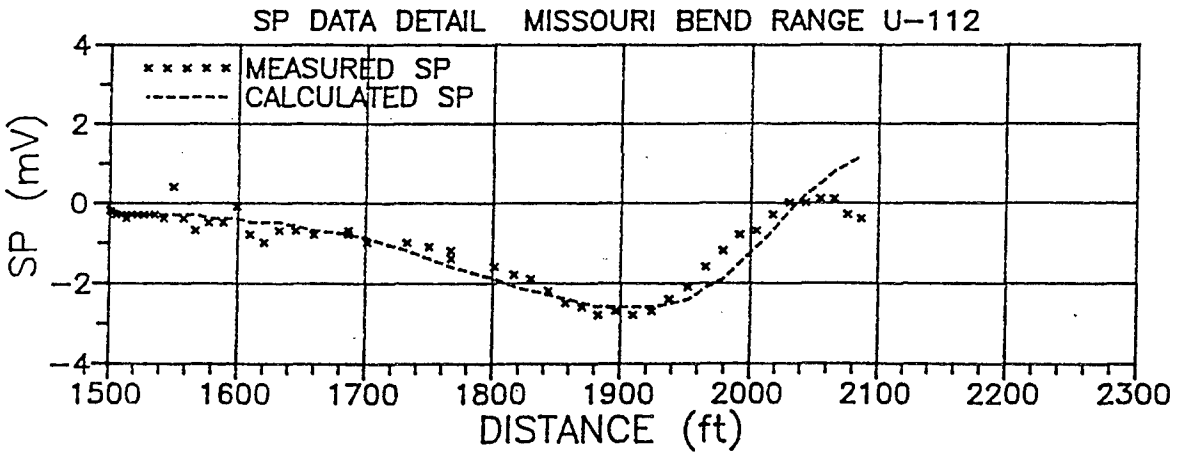
SP DATA DETAIL MISSOURI BEND RANGE U-112
MEASURED SP
CALCULATED SP
SP (mV)
DISTANCE (ft)

FIGURE 22

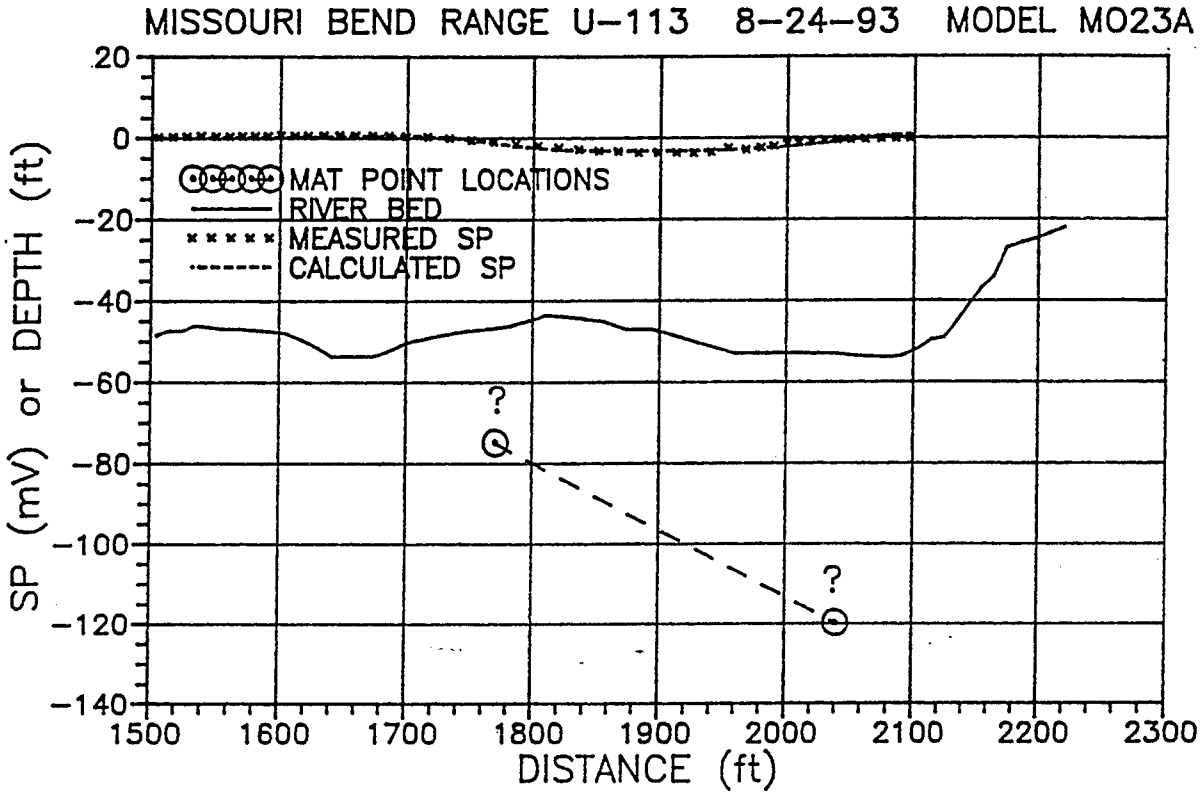
MISSOURI BEND RANGE U-113 8-24-93 MODEL MO23A
MAT POINT LOCATIONS
RIVER BED
MEASURED SP
CALCULATED SP
SP (mV) or DEPTH (ft)
DISTANCE (ft)
20
0
-20
-40
-60
-80
-100
-120
-140
1500
1600
1700
1800
1900
2000
2100
2200
2300
?
?

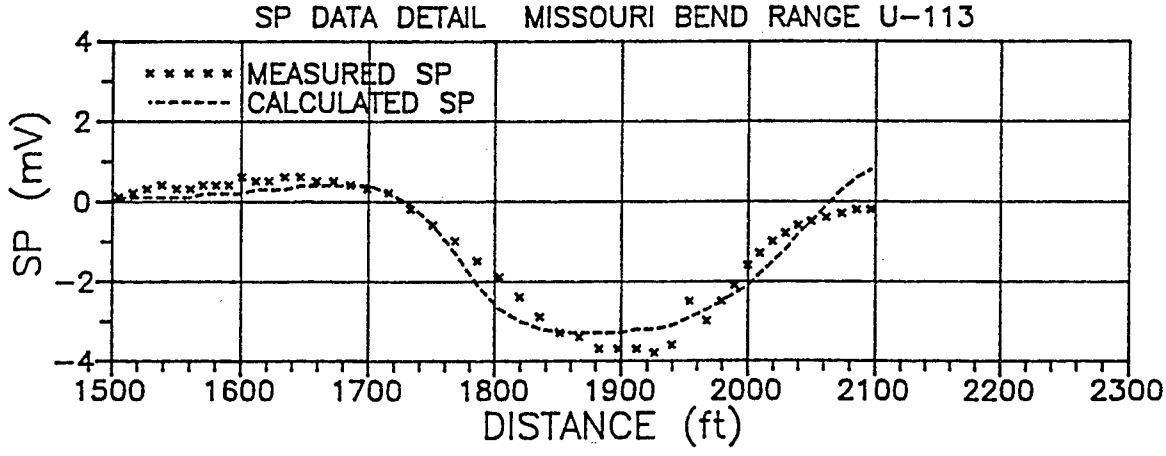
SP DATA DETAIL MISSOURI BEND RANGE U-113
MEASURED SP
CALCULATED SP
SP (mV)
DISTANCE (ft)
4
2
0
-2
-4
1500
1600
1700
1800
1900
2000
2100
2200
2300

FIGURE 23

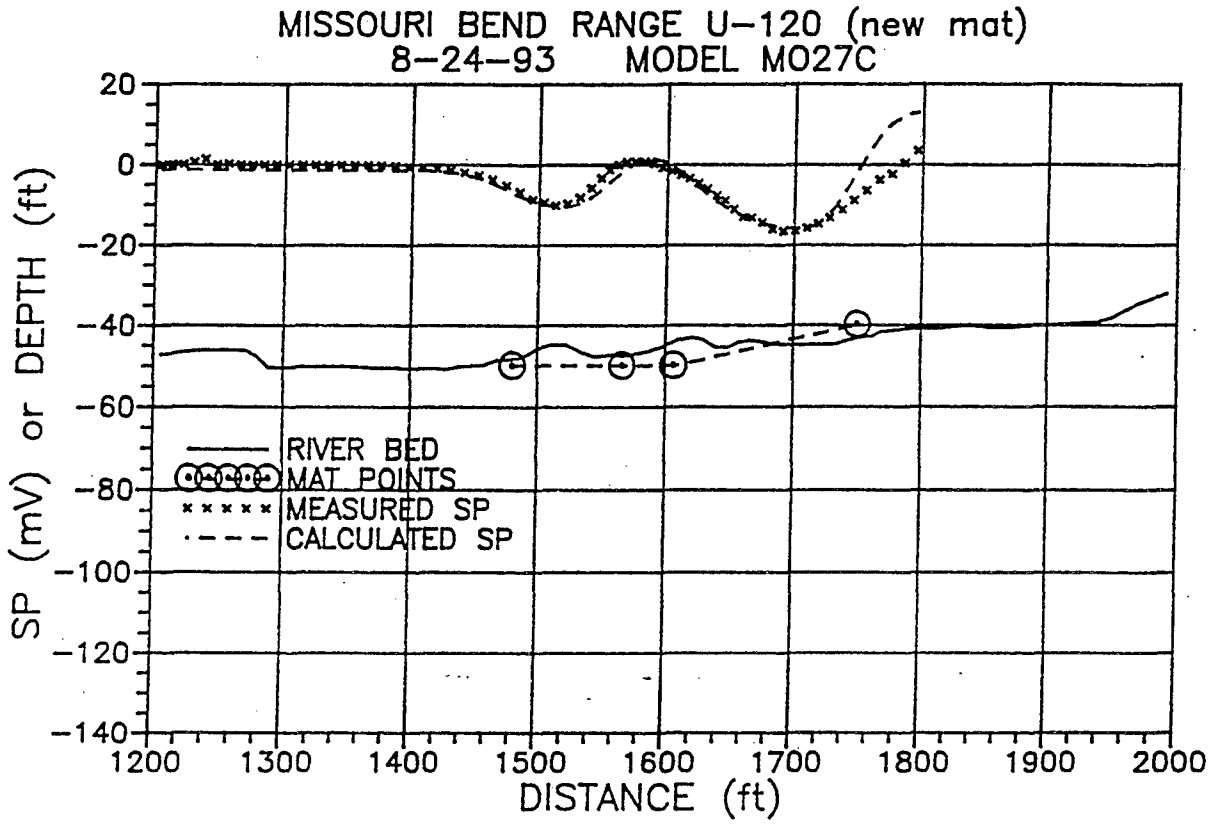
MISSOURI BEND RANGE U-120 (new mat)
8-24-93 MODEL M027C
SP (mV) or DEPTH (ft)
20
0
-20
-40
-60
-80
-100
-120
-140
RIVER BED
MAT POINTS
MEASURED SP
CALCULATED SP
1200
1300
1400
1500
1600
1700
1800
1900
2000
DISTANCE (ft)

FIGURE 24

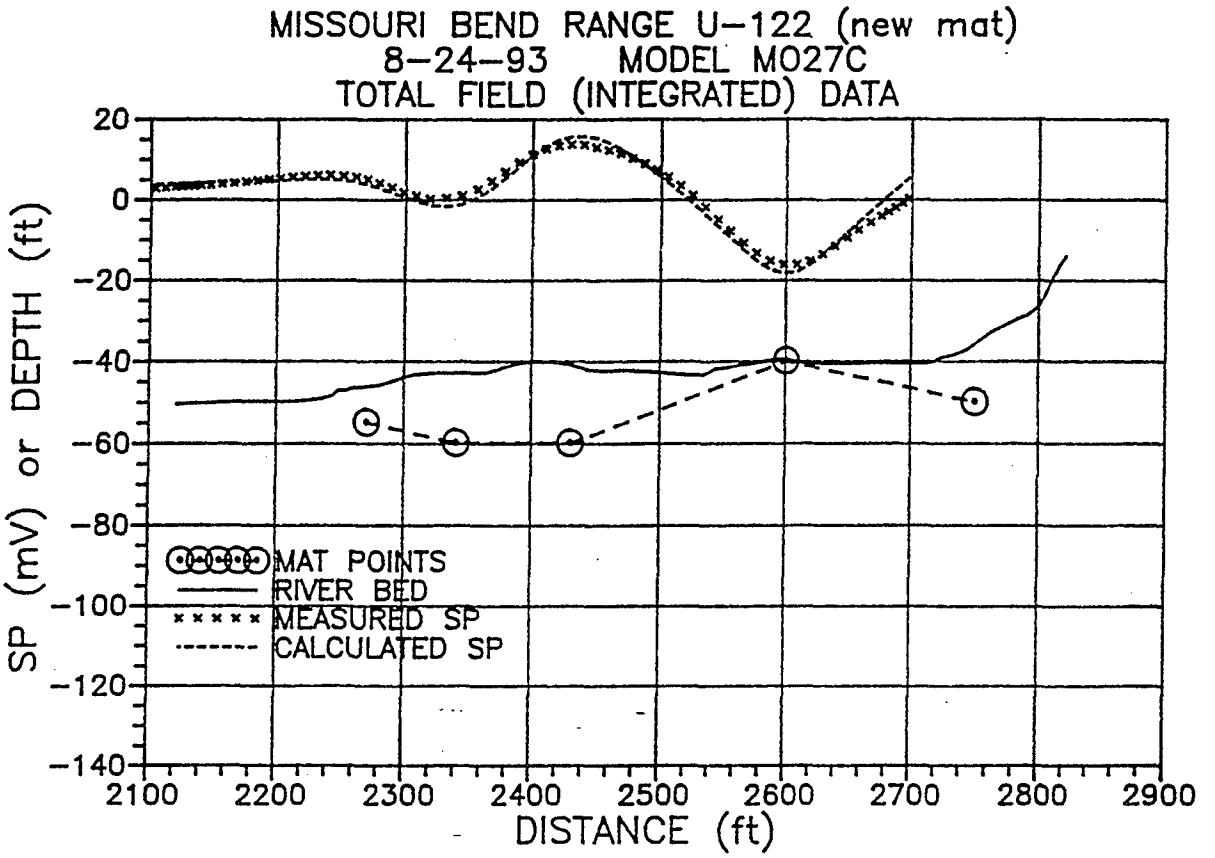
MISSOURI BEND RANGE U-122 (new mat)
8-24-93 MODEL M027C
TOTAL FIELD (INTEGRATED) DATA
SP (mV) or DEPTH (ft)
20
0
-20
-40
-60
-80
-100
-120
-140
2100
2200
2300
2400
2500
2600
2700
2800
2900
DISTANCE (ft)
MAT POINTS
RIVER BED
MEASURED SP
CALCULATED SP

FIGURE 25

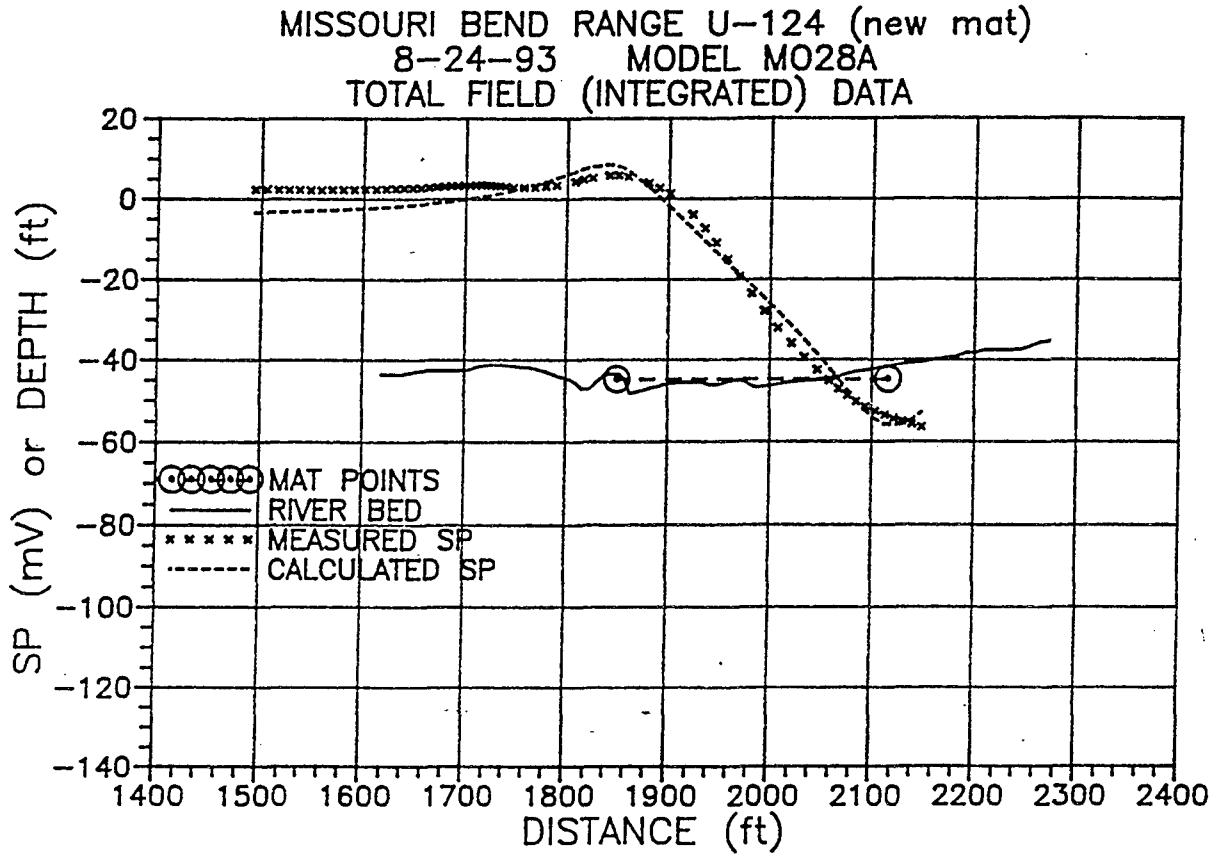
MISSOURI BEND RANGE U-124 (new mat)
8-24-93 MODEL MO28A
TOTAL FIELD (INTEGRATED) DATA
SP (mV) or DEPTH (ft)
20
0
-20
-40
-60
-80
-100
-120
-140
MAT POINTS
RIVER BED
MEASURED SP
CALCULATED SP
1400
1500
1600
1700
1800
1900
2000
2100
2200
2300
2400
DISTANCE (ft)

FIGURE 26

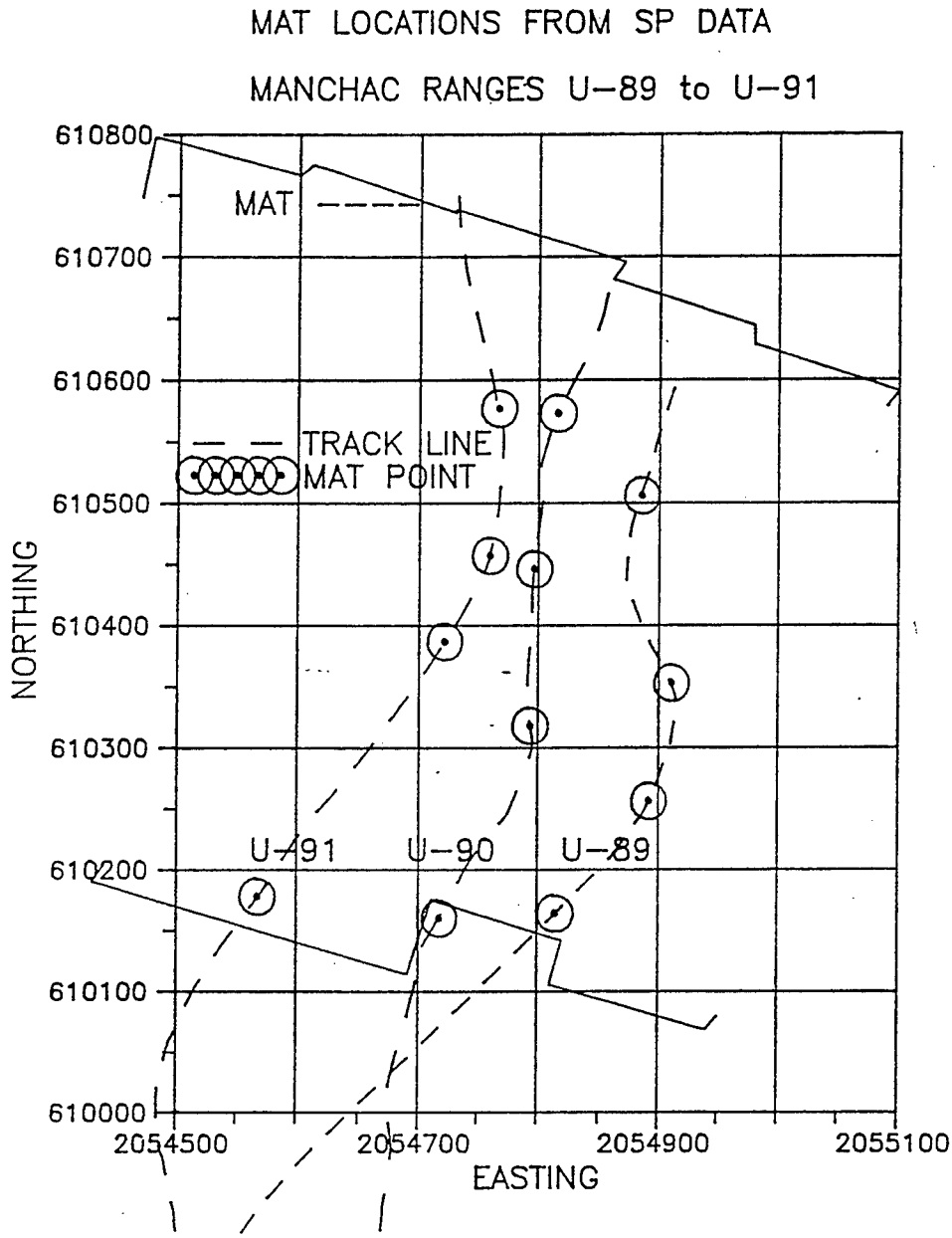
MAT LOCATIONS FROM SP DATA
MANCHAC RANGES U–89 to U–91
MAT
TRACK LINE
MAT POINT
U–91
U–90
U–89
NORTHING
610800
610700
610600
610500
610400
610300
610200
610100
610000
2054500
2054700
2054900
2055100
EASTING

FIGURE 27

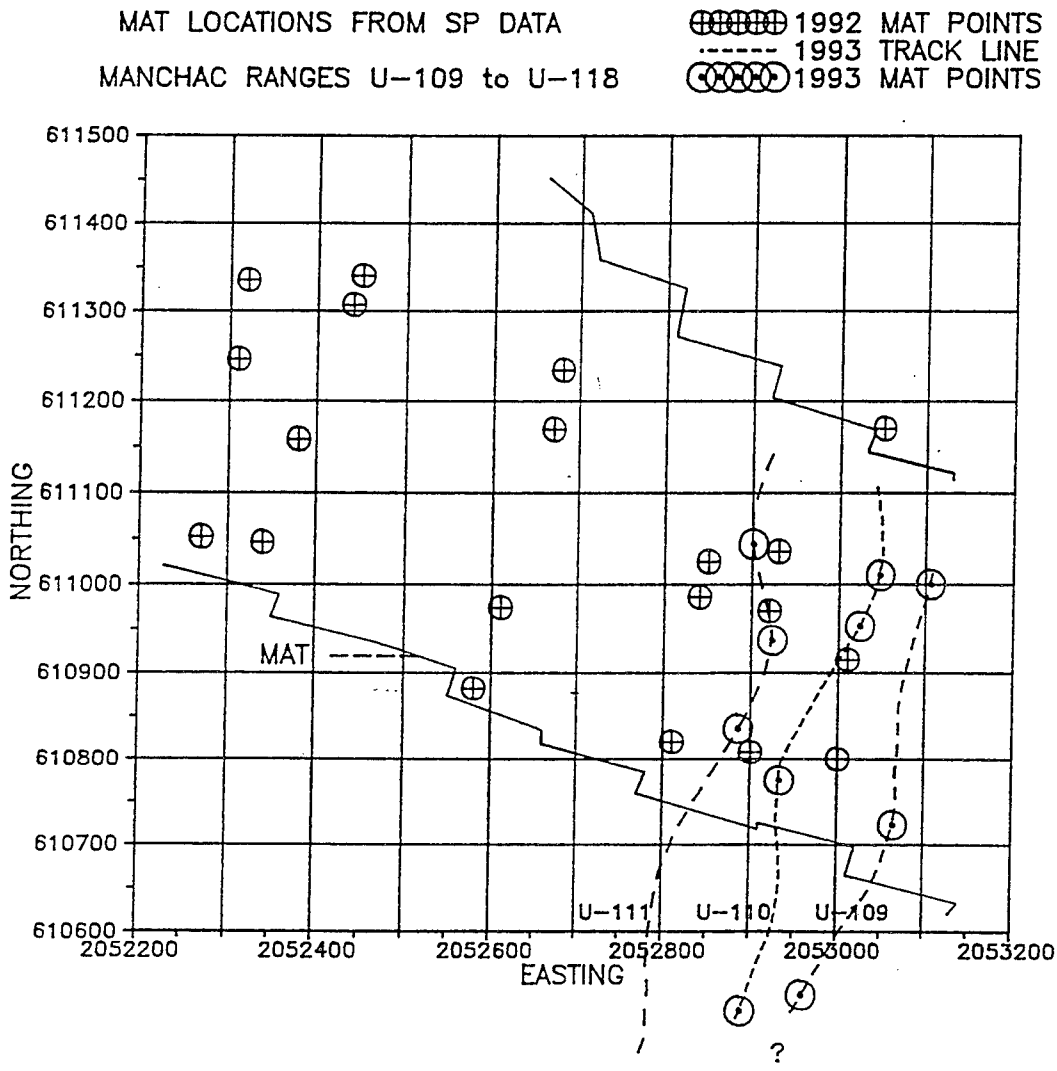
MAT LOCATIONS FROM SP DATA
MANCHAC RANGES U-109 to U-118
1992 MAT POINTS
1993 TRACK LINE
1993 MAT POINTS
NORTHING
611500
611400
611300
611200
611100
611000
610900
610800
610700
610600
MAT
U-111
U-110
U-109
?
2052200
2052400
2052600
2052800
2053000
2053200
EASTING

FIGURE 28

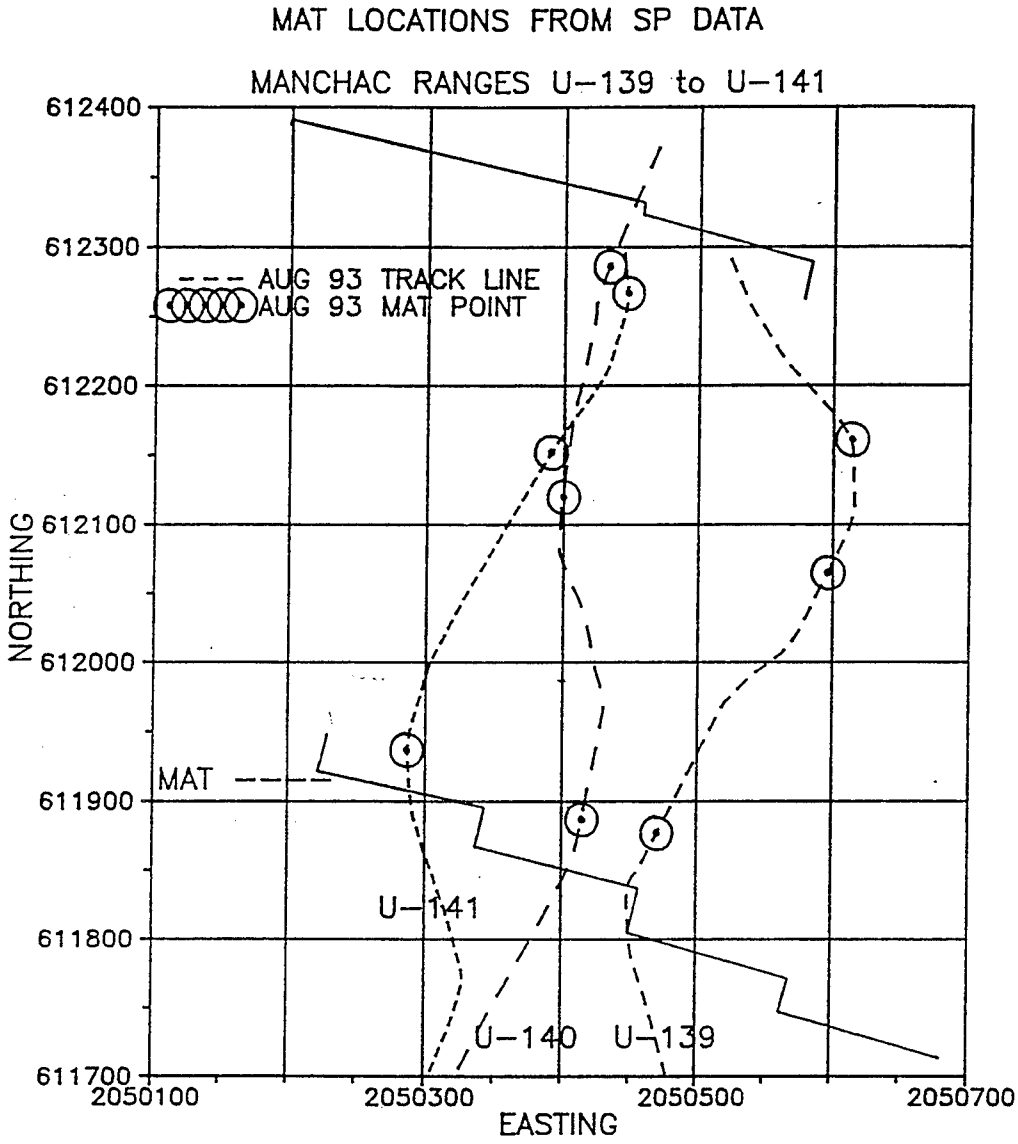
MAT LOCATIONS FROM SP DATA
MANCHAC RANGES U-139 to U-141
AUG 93 TRACK LINE
AUG 93 MAT POINT
MAT
U-141
U-140
U-139
NORTHING
612400
612300
612200
612100
612000
611900
611800
611700
2050100
2050300
2050500
2050700
EASTING

FIGURE 29

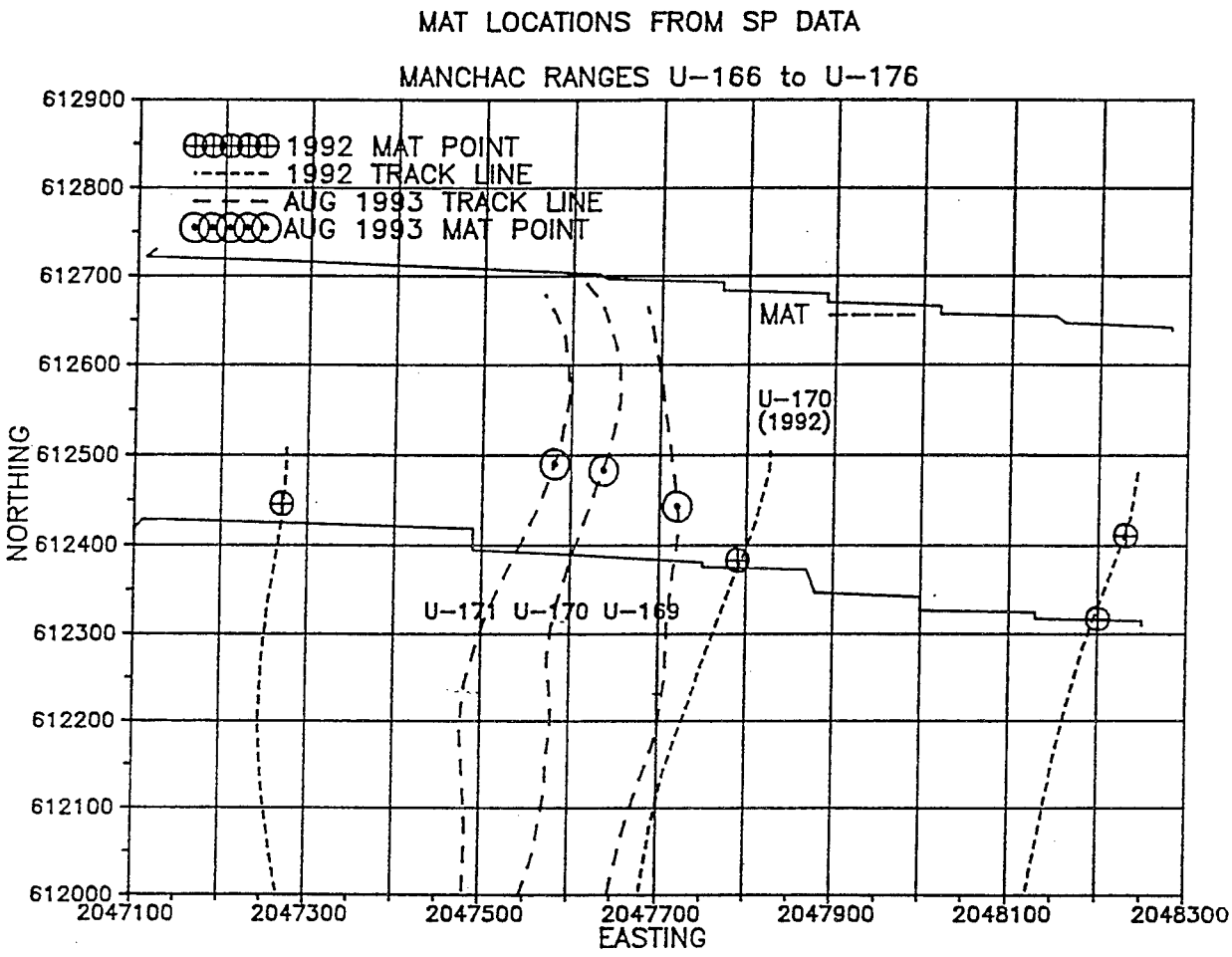
MAT LOCATIONS FROM SP DATA
MANCHAC RANGES U-166 to U-176
1992 MAT POINT
1992 TRACK LINE
AUG 1993 TRACK LINE
AUG 1993 MAT POINT
MAT
U-170
(1992)
U-171 U-170 U-169
NORTHING
612900
612800
612700
612600
612500
612400
612300
612200
612100
612000
2047100
2047300
2047500
2047700
2047900
2048100
2048300
EASTING

FIGURE 30

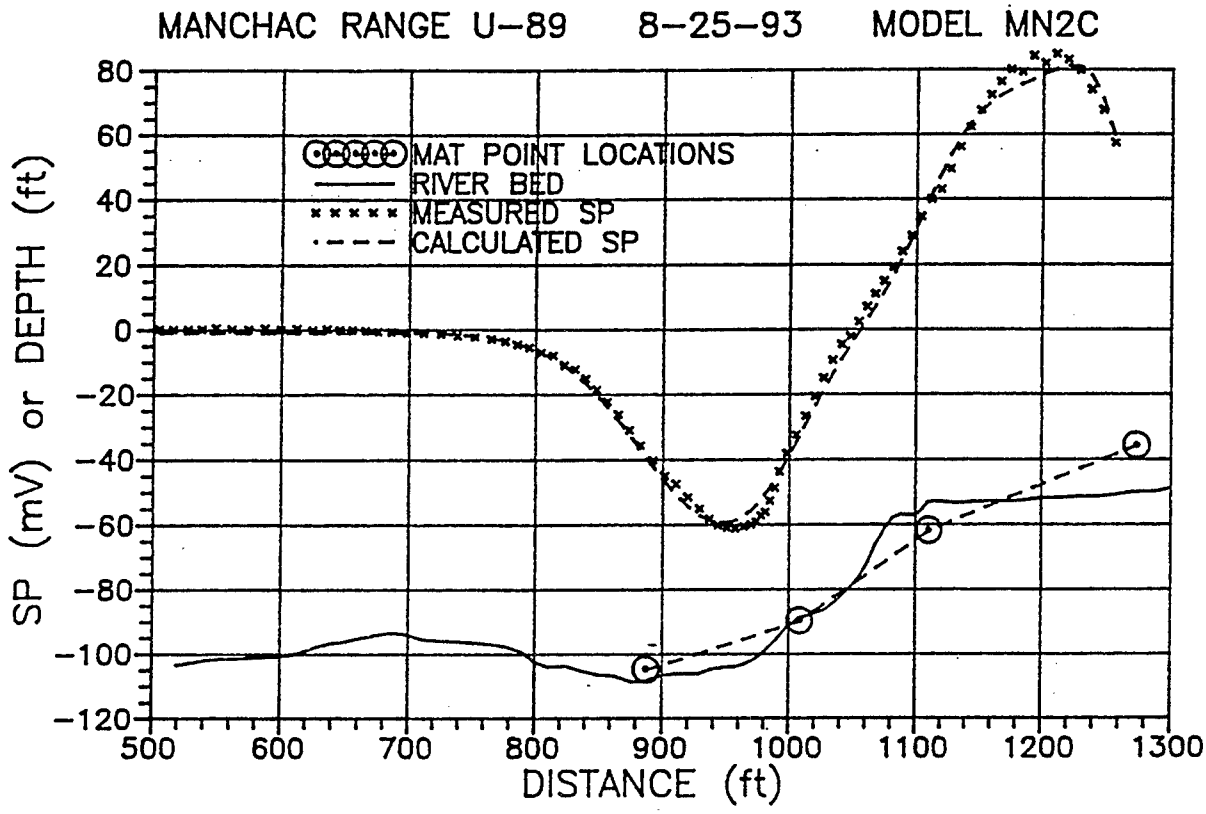
MANCHAC RANGE U-89 8-25-93 MODEL MN2C
MAT POINT LOCATIONS
RIVER BED
MEASURED SP
CALCULATED SP
SP (mV) or DEPTH (ft)
DISTANCE (ft)
80
60
40
20
0
-20
-40
-60
-80
-100
-120
500
600
700
800
900
1000
1100
1200
1300

FIGURE 31

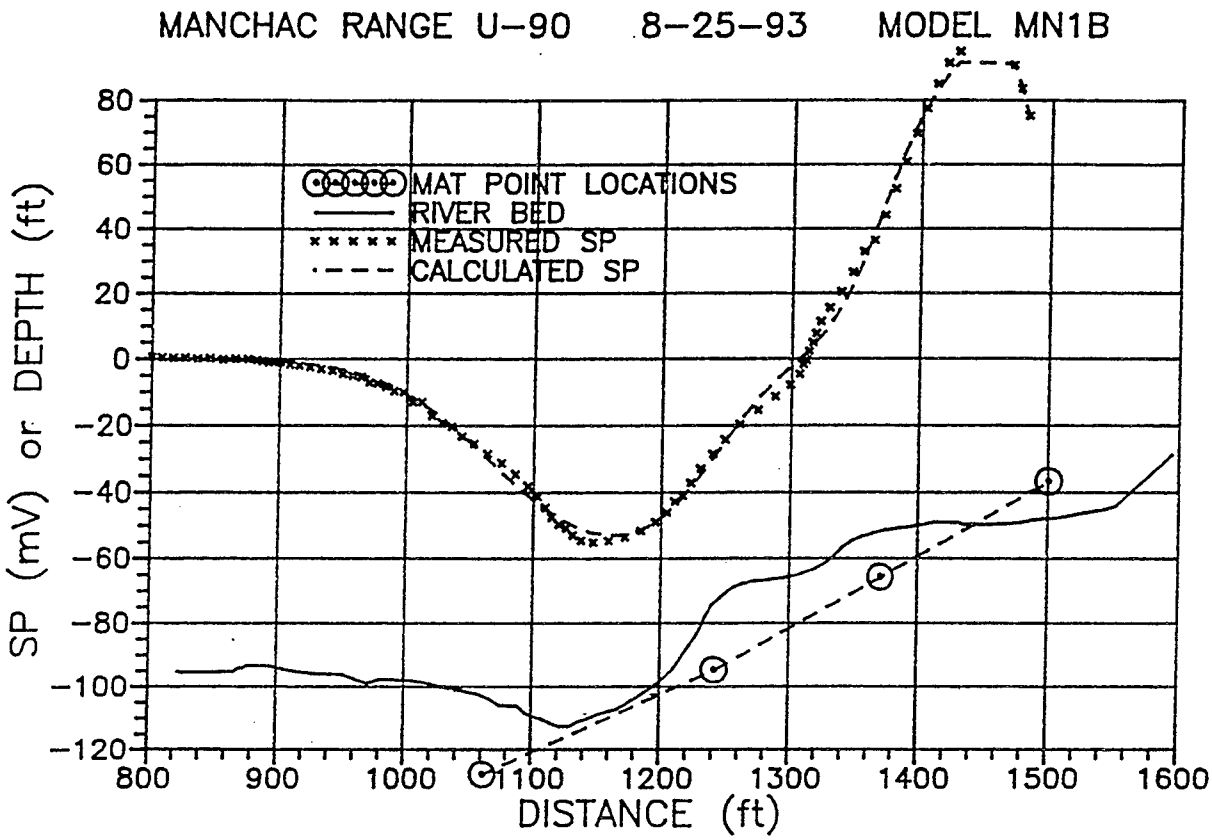
MANCHAC RANGE U-90 8-25-93 MODEL MN1B
MAT POINT LOCATIONS
RIVER BED
MEASURED SP
CALCULATED SP
SP (mV) or DEPTH (ft)
DISTANCE (ft)
80
60
40
20
0
-20
-40
-60
-80
-100
-120
800
900
1000
1100
1200
1300
1400
1500
1600

FIGURE 32

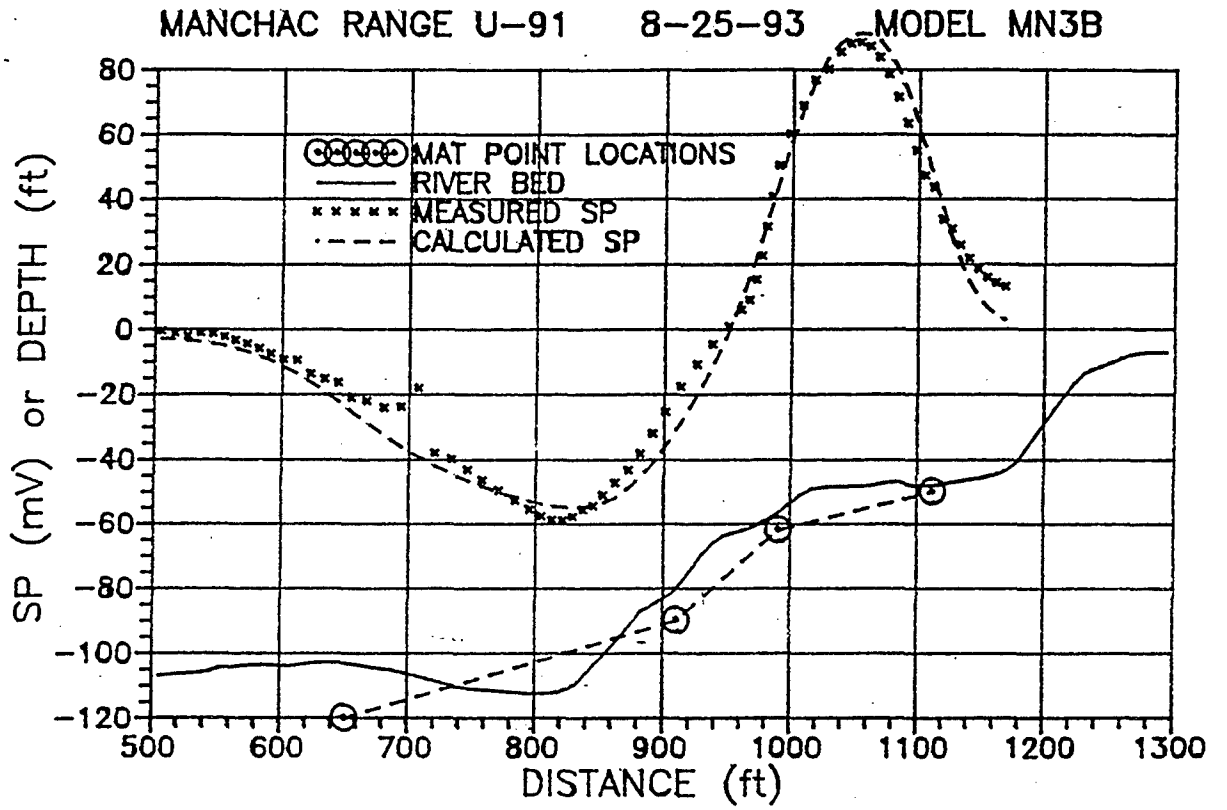
MANCHAC RANGE U-91 8-25-93 MODEL MN3B
MAT POINT LOCATIONS
RIVER BED
MEASURED SP
CALCULATED SP
SP (mV) or DEPTH (ft)
DISTANCE (ft)
80
60
40
20
0
-20
-40
-60
-80
-100
-120
500
600
700
800
900
1000
1100
1200
1300

FIGURE 33

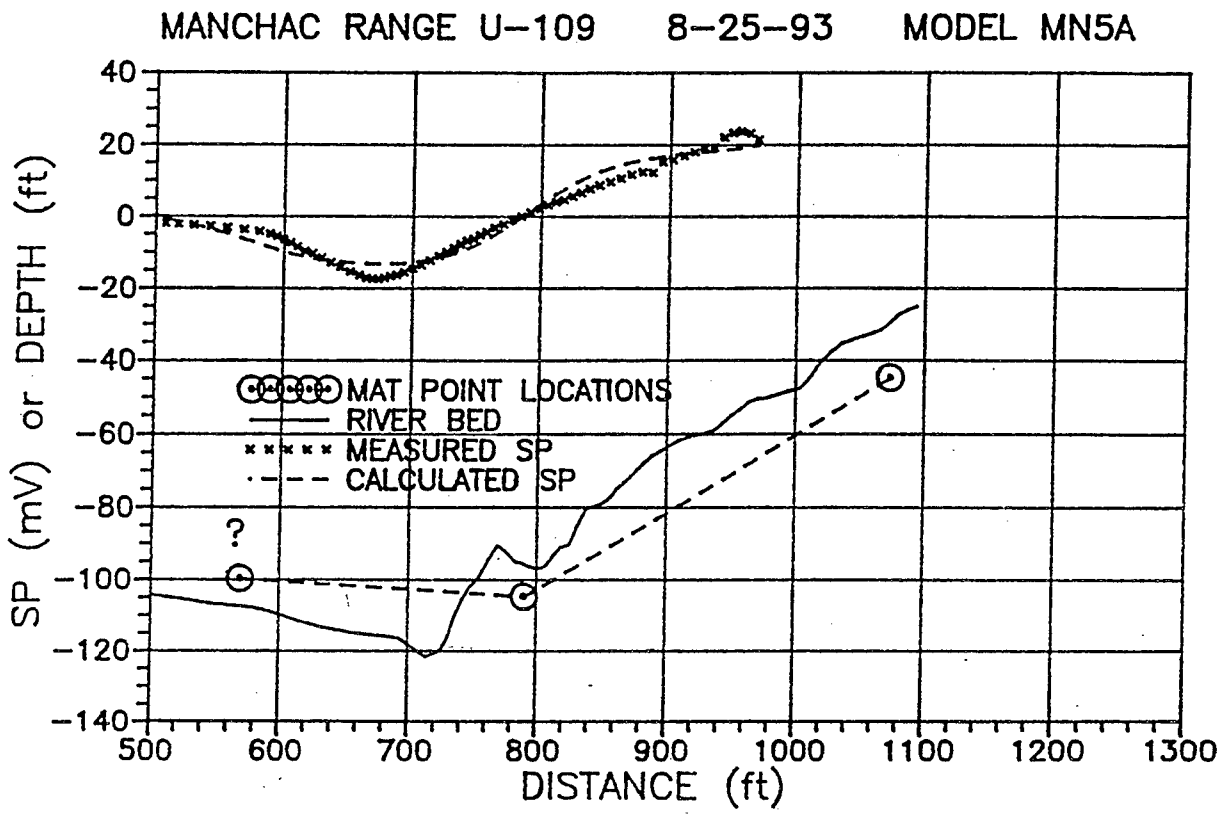
MANCHAC RANGE U-109 8-25-93 MODEL MN5A
SP (mV) or DEPTH (ft)
DISTANCE (ft)
MAT POINT LOCATIONS
RIVER BED
MEASURED SP
CALCULATED SP
?
40
20
0
-20
-40
-60
-80
-100
-120
-140
500
600
700
800
900
1000
1100
1200
1300

FIGURE 34

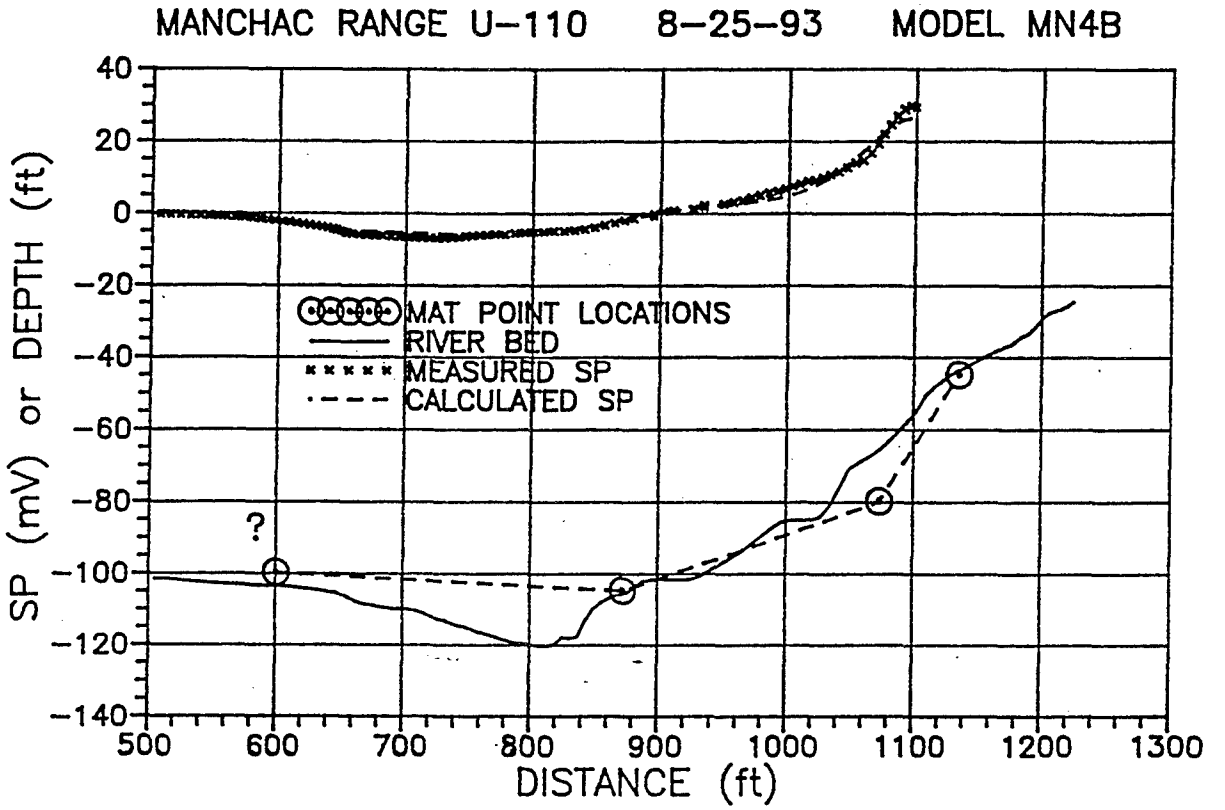
MANCHAC RANGE U-110 8-25-93 MODEL MN4B
SP (mV) or DEPTH (ft)
DISTANCE (ft)
MAT POINT LOCATIONS
RIVER BED
MEASURED SP
CALCULATED SP
?
40
20
0
-20
-40
-60
-80
-100
-120
-140
500
600
700
800
900
1000
1100
1200
1300

FIGURE 35

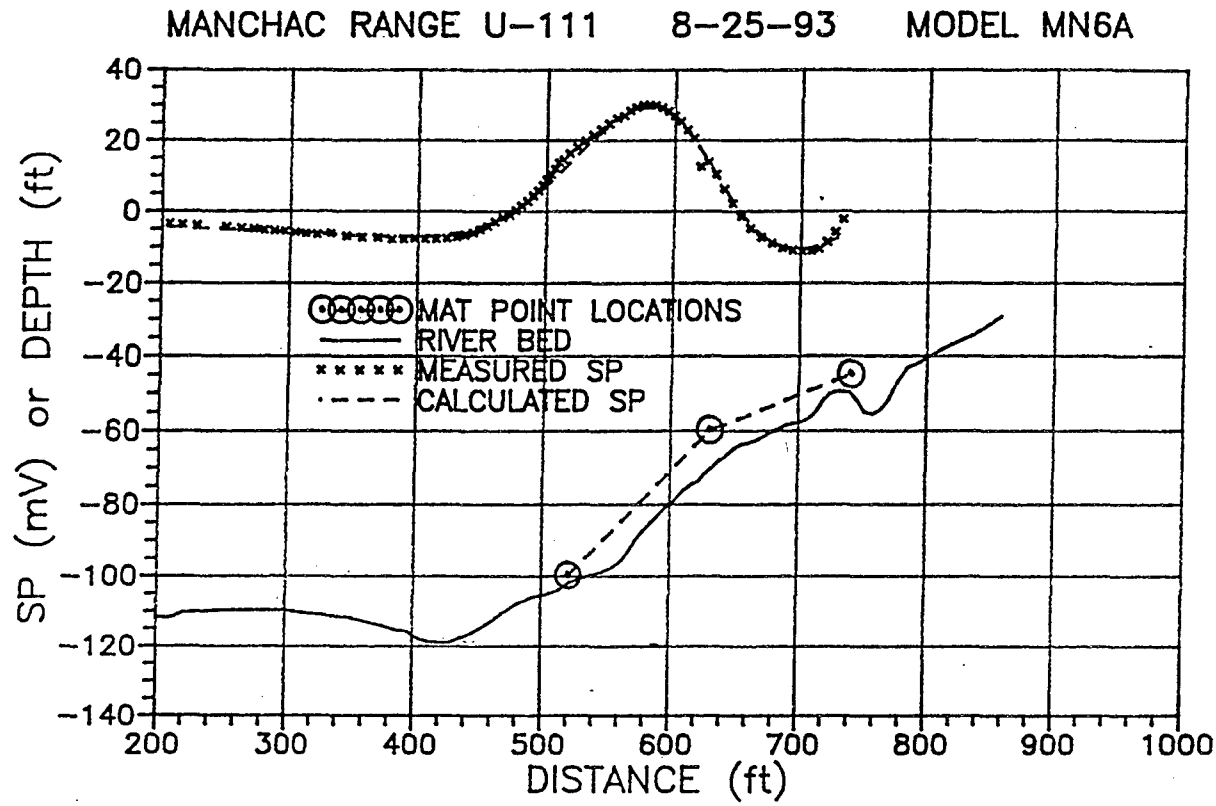
MANCHAC RANGE U-111 8-25-93 MODEL MN6A
SP (mV) or DEPTH (ft)
DISTANCE (ft)
MAT POINT LOCATIONS
RIVER BED
MEASURED SP
CALCULATED SP
40
20
0
-20
-40
-60
-80
-100
-120
-140
200
300
400
500
600
700
800
900
1000

FIGURE 36

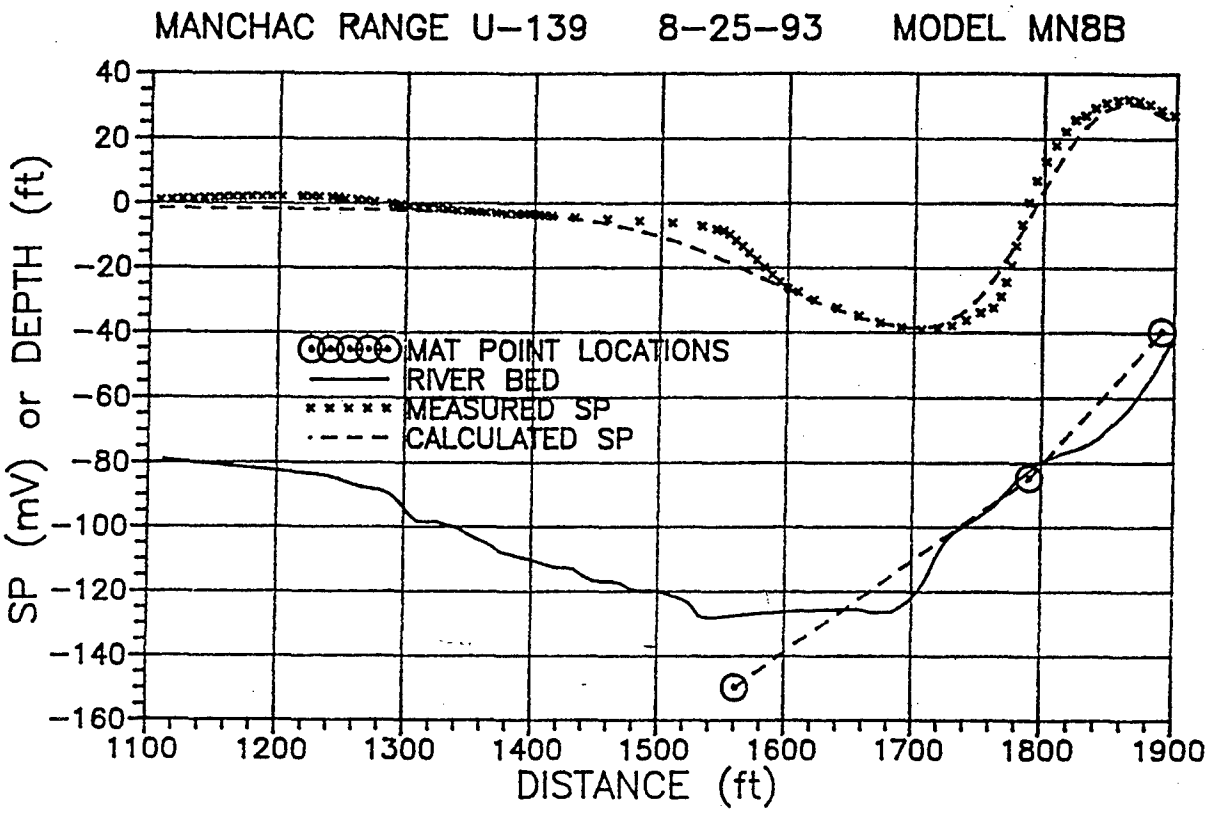
MANCHAC RANGE U-139 8-25-93 MODEL MN8B
SP (mV) or DEPTH (ft)
40
20
0
-20
-40
-60
-80
-100
-120
-140
-160
1100
1200
1300
1400
1500
1600
1700
1800
1900
DISTANCE (ft)
MAT POINT LOCATIONS
RIVER BED
MEASURED SP
CALCULATED SP

FIGURE 37

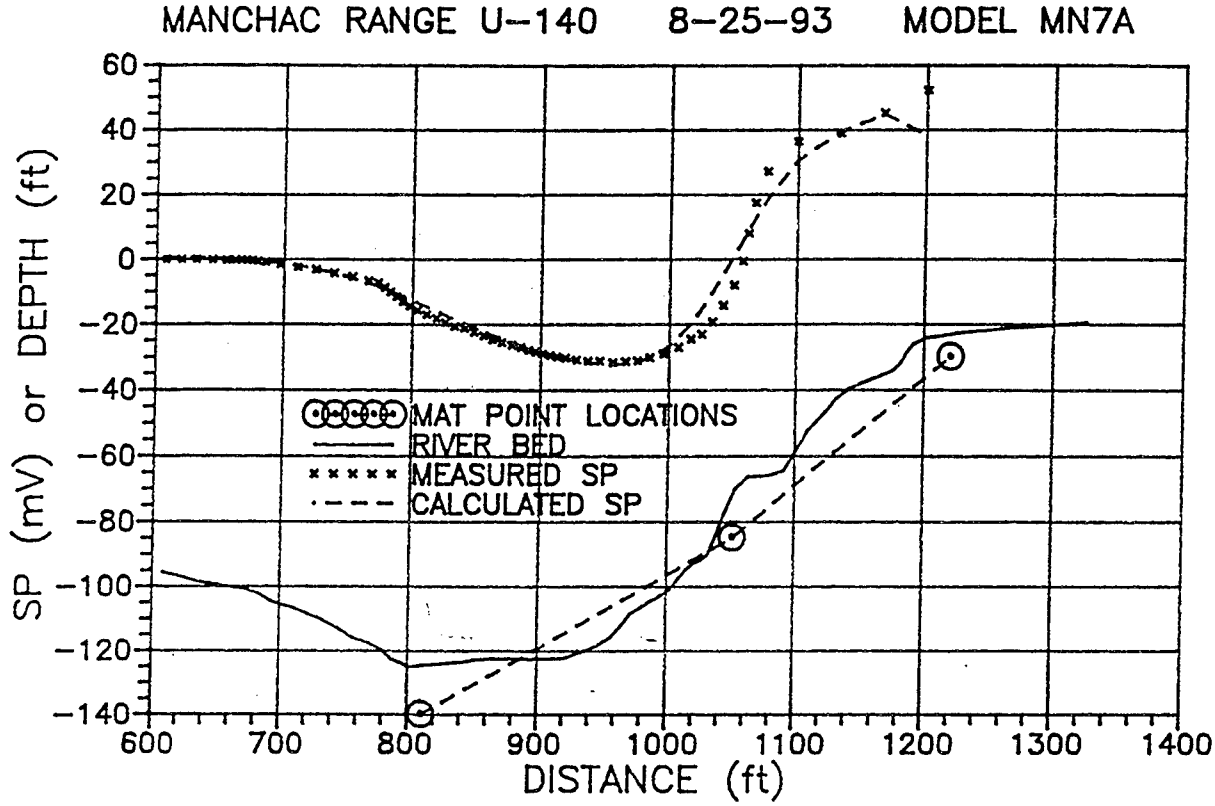
MANCHAC RANGE U–140 8–25–93 MODEL MN7A
SP (mV) or DEPTH (ft)
60
40
20
0
–20
–40
–60
–80
–100
–120
–140
600
700
800
900
1000
1100
1200
1300
1400
DISTANCE (ft)
MAT POINT LOCATIONS
RIVER BED
MEASURED SP
CALCULATED SP

FIGURE 38

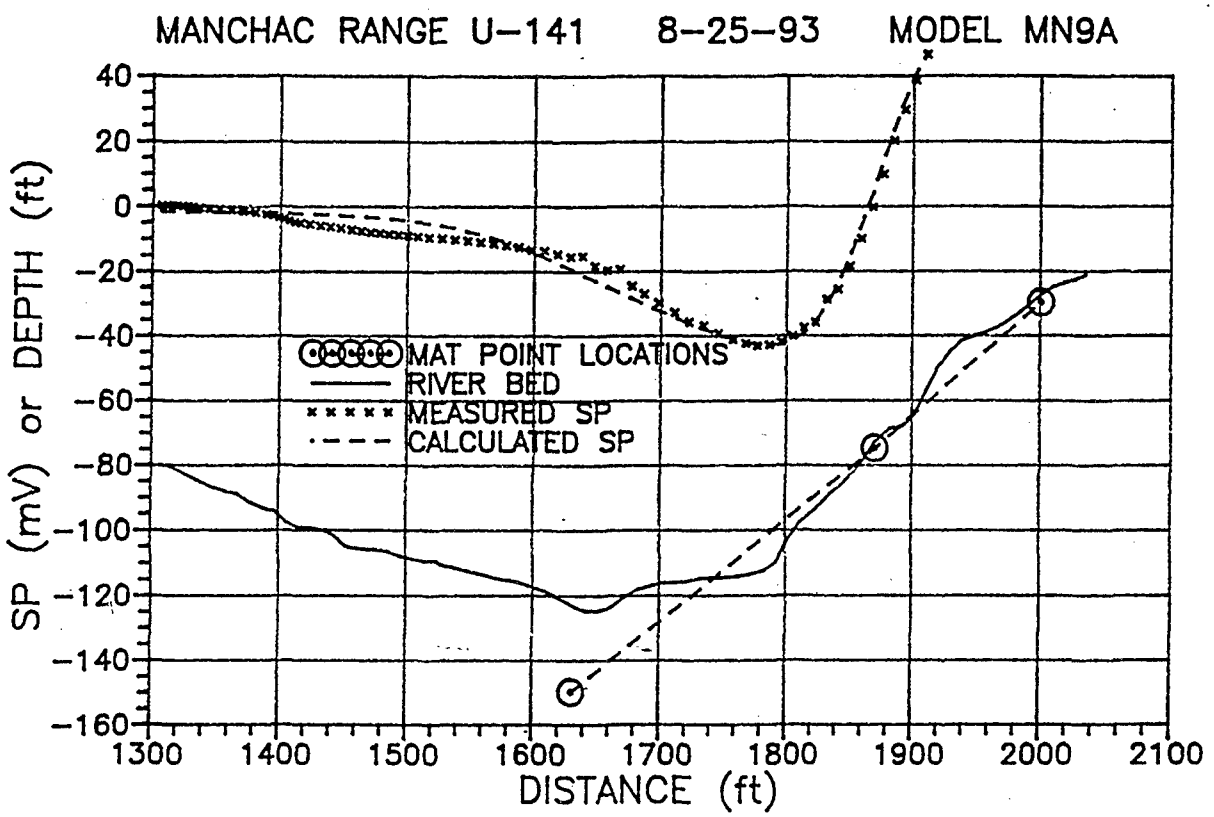
MANCHAC RANGE U-141 8-25-93 MODEL MN9A
SP (mV) or DEPTH (ft)
DISTANCE (ft)
MAT POINT LOCATIONS
RIVER BED
MEASURED SP
CALCULATED SP
40
20
0
-20
-40
-60
-80
-100
-120
-140
-160
1300
1400
1500
1600
1700
1800
1900
2000
2100

FIGURE 39

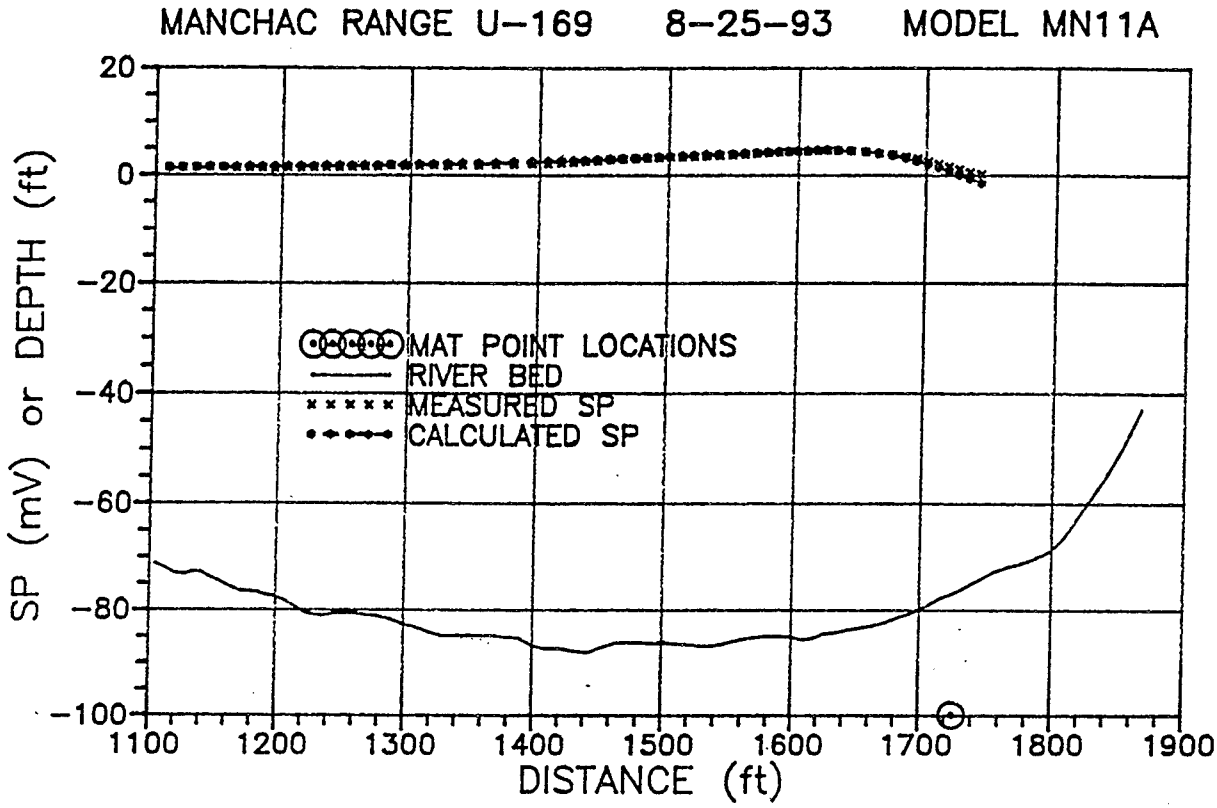
MANCHAC RANGE U–169 8–25–93 MODEL MN11A
SP (mV) or DEPTH (ft)
20
0
–20
–40
–60
–80
–100
MAT POINT LOCATIONS
RIVER BED
MEASURED SP
CALCULATED SP
1100
1200
1300
1400
1500
1600
1700
1800
1900
DISTANCE (ft)

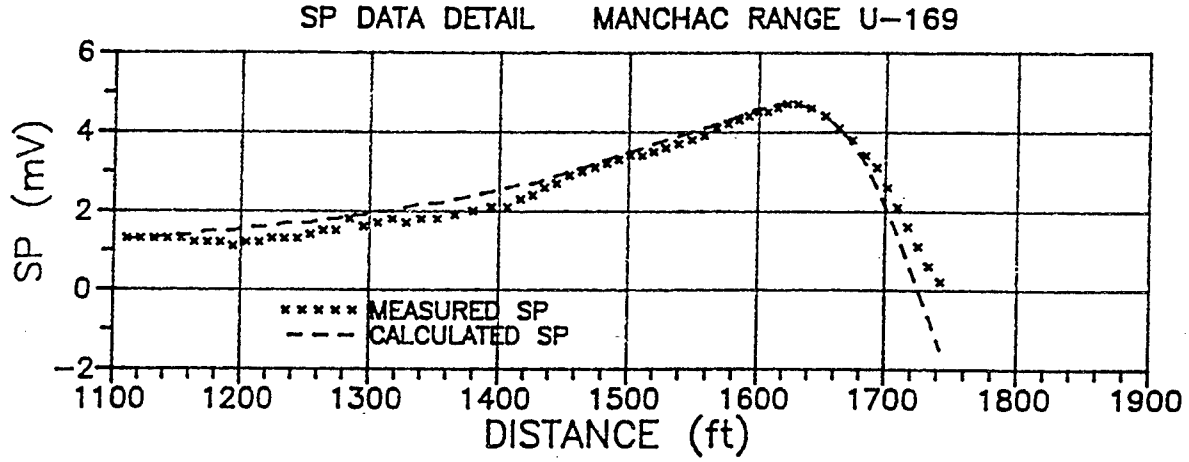
SP DATA DETAIL MANCHAC RANGE U–169
SP (mV)
6
4
2
0
–2
MEASURED SP
CALCULATED SP
1100
1200
1300
1400
1500
1600
1700
1800
1900
DISTANCE (ft)

FIGURE 40

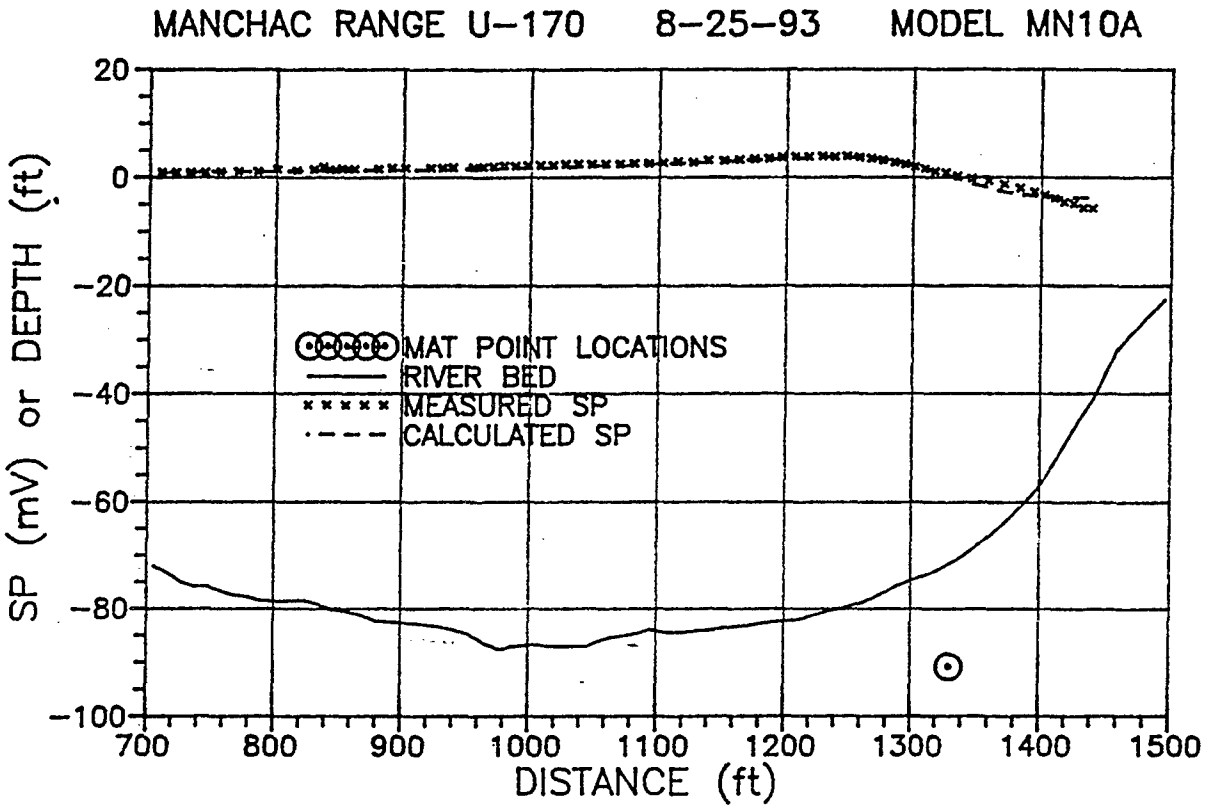
MANCHAC RANGE U-170 8-25-93 MODEL MN10A
SP (mV) or DEPTH (ft)
DISTANCE (ft)
MAT POINT LOCATIONS
RIVER BED
MEASURED SP
CALCULATED SP
20
0
-20
-40
-60
-80
-100
700
800
900
1000
1100
1200
1300
1400
1500

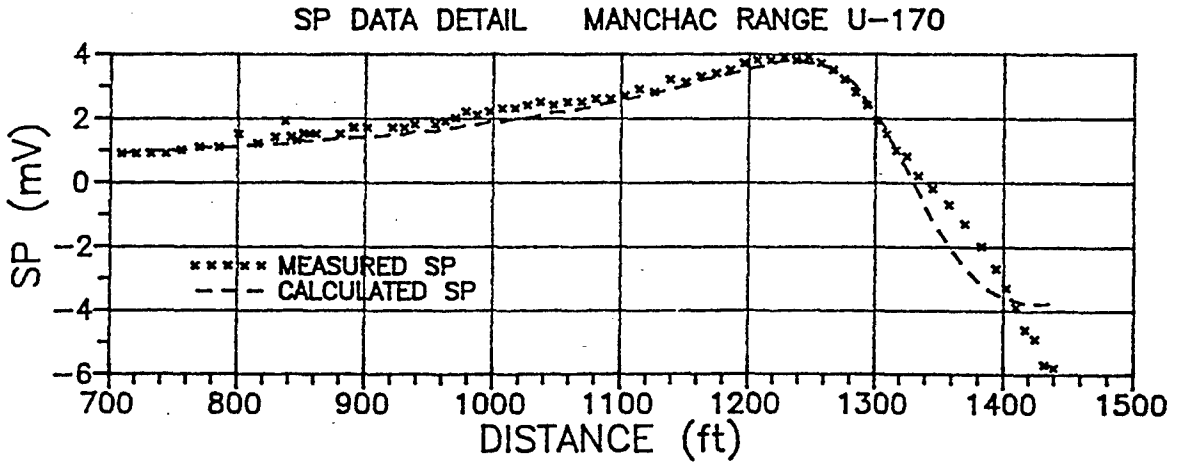
SP DATA DETAIL MANCHAC RANGE U-170
SP (mV)
DISTANCE (ft)
MEASURED SP
CALCULATED SP
4
2
0
-2
-4
-6
700
800
900
1000
1100
1200
1300
1400
1500

FIGURE 41

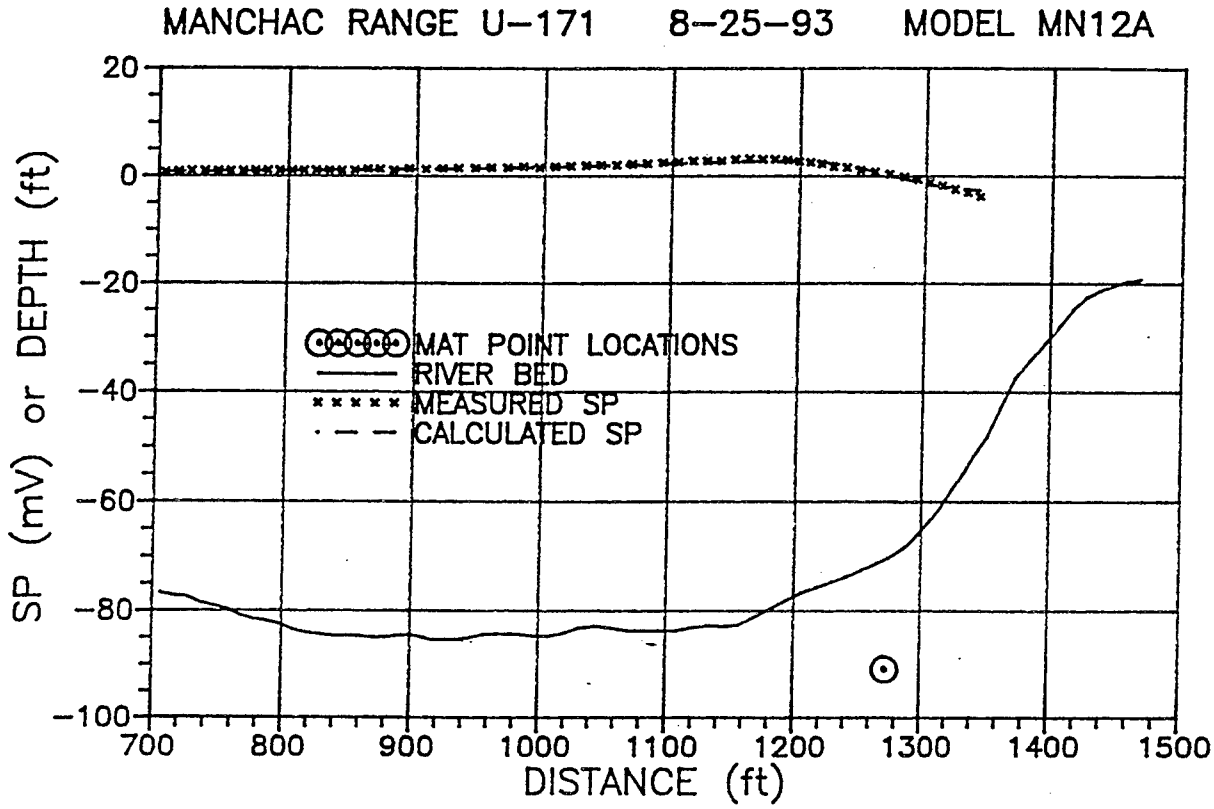
MANCHAC RANGE U–171 8–25–93 MODEL MN12A
SP (mV) or DEPTH (ft)
20
0
-20
-40
-60
-80
-100
MAT POINT LOCATIONS
RIVER BED
MEASURED SP
CALCULATED SP
700
800
900
1000
1100
1200
1300
1400
1500
DISTANCE (ft)

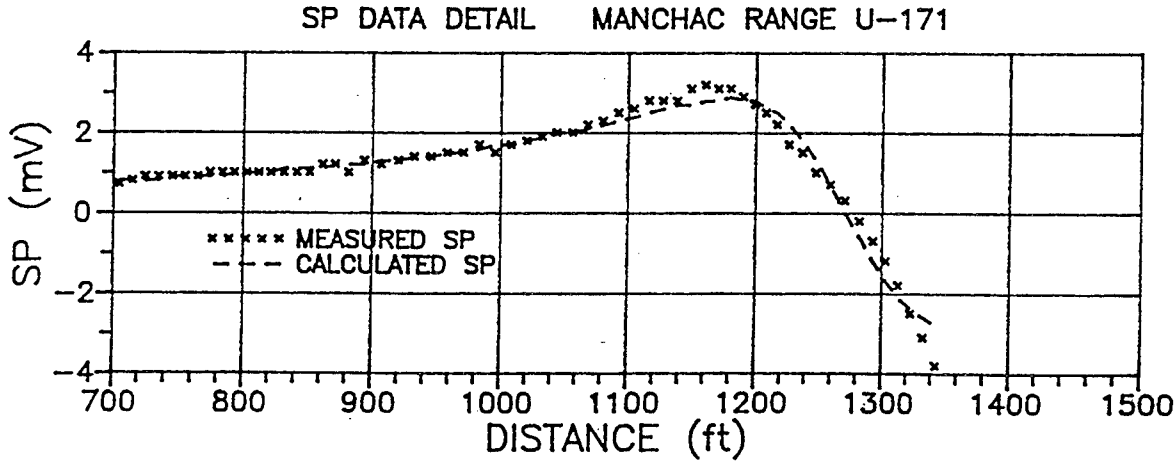
SP DATA DETAIL MANCHAC RANGE U–171
SP (mV)
4
2
0
-2
-4
MEASURED SP
CALCULATED SP
700
800
900
1000
1100
1200
1300
1400
1500
DISTANCE (ft)

FIGURE 42

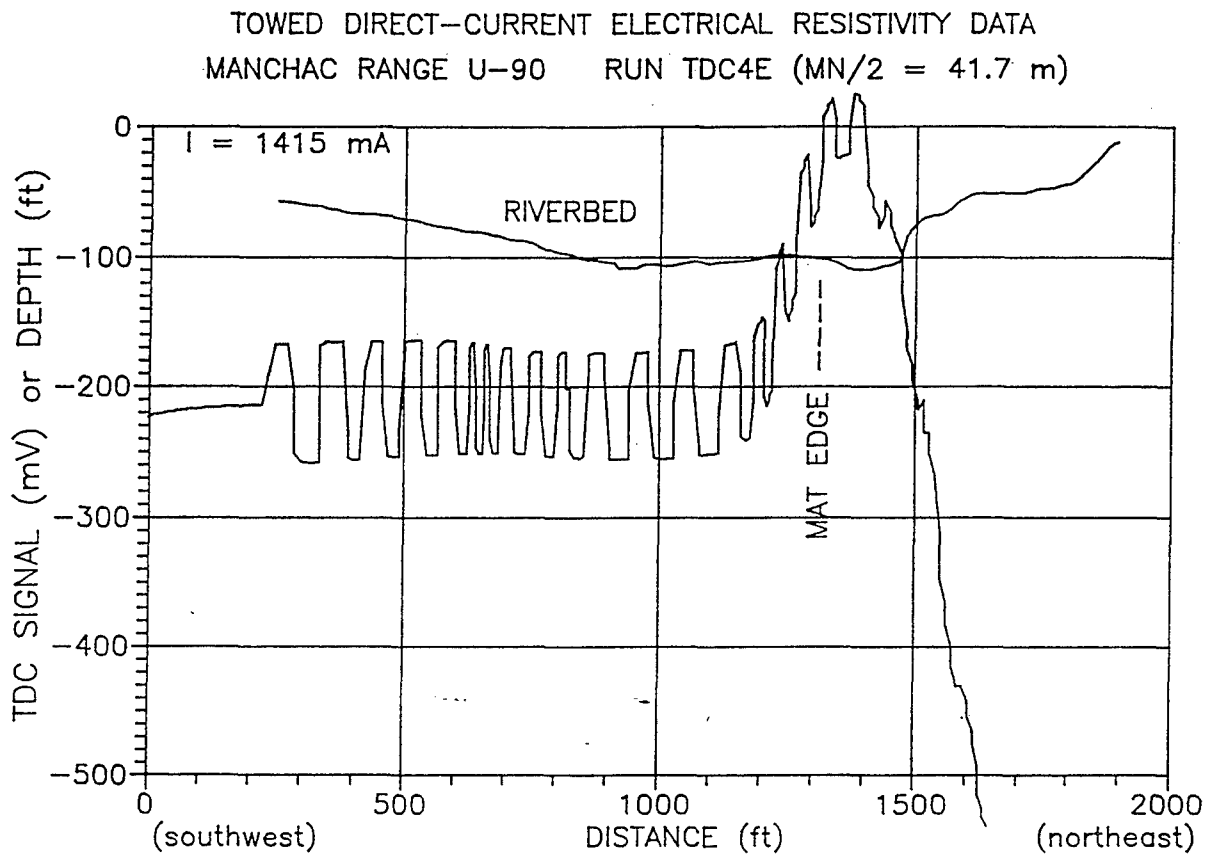
TOWED DIRECT–CURRENT ELECTRICAL RESISTIVITY DATA
MANCHAC RANGE U–90 RUN TDC4E (MN/2 = 41.7 m)
I = 1415 mA
RIVERBED
MAT EDGE
TDC SIGNAL (mV) or DEPTH (ft)
0
−100
−200
−300
−400
−500
0
500
1000
1500
2000
(southwest)
DISTANCE (ft)
(northeast)

FIGURE 43

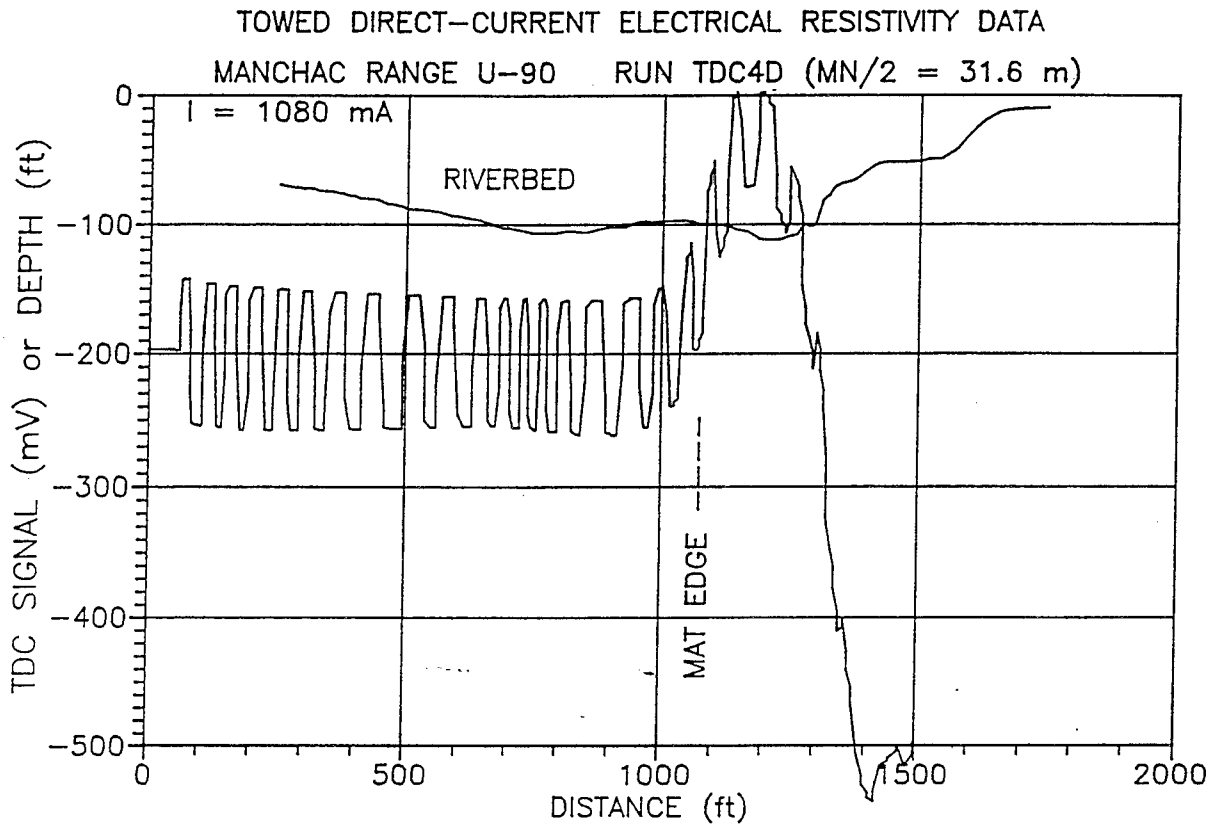
TOWED DIRECT–CURRENT ELECTRICAL RESISTIVITY DATA
MANCHAC RANGE U–90 RUN TDC4D (MN/2 = 31.6 m)
I = 1080 mA
RIVERBED
MAT EDGE
TDC SIGNAL (mV) or DEPTH (ft)
0
−100
−200
−300
−400
−500
0
500
1000
1500
2000
DISTANCE (ft)

FIGURE 43A

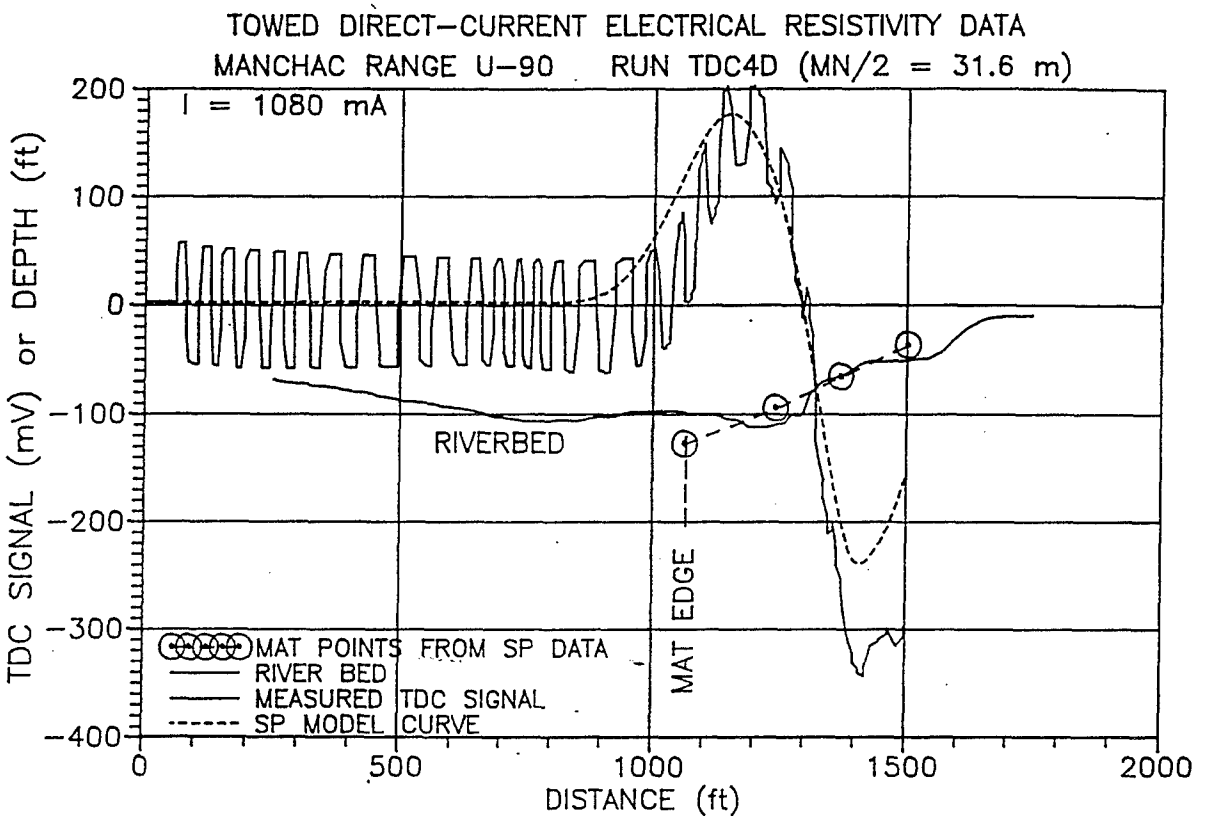
TOWED DIRECT–CURRENT ELECTRICAL RESISTIVITY DATA
MANCHAC RANGE U–90 RUN TDC4D (MN/2 = 31.6 m)
I = 1080 mA
TDC SIGNAL (mV) or DEPTH (ft)
200
100
0
−100
−200
−300
−400
RIVERBED
MAT EDGE
MAT POINTS FROM SP DATA
RIVER BED
MEASURED TDC SIGNAL
SP MODEL CURVE
0
500
1000
1500
2000
DISTANCE (ft)

FIGURE 44

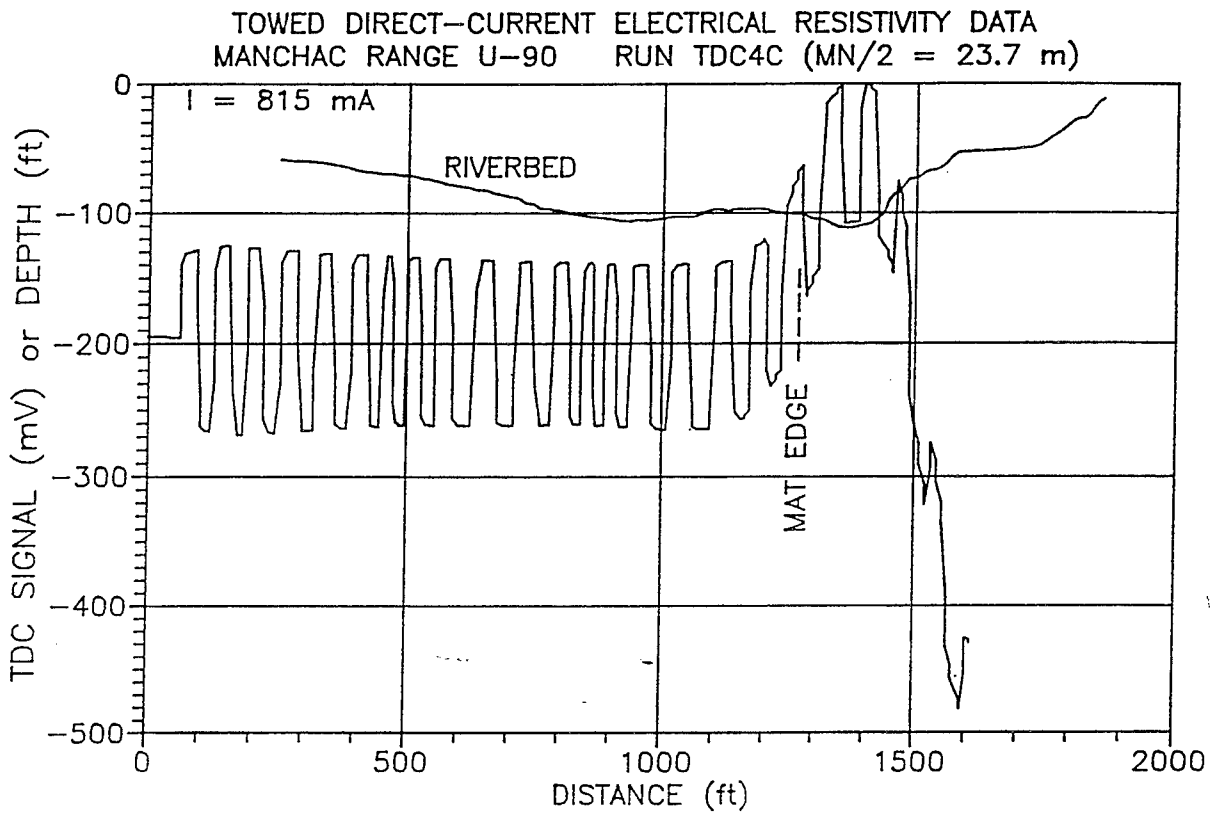
TOWED DIRECT–CURRENT ELECTRICAL RESISTIVITY DATA
MANCHAC RANGE U–90 RUN TDC4C (MN/2 = 23.7 m)
I = 815 mA
RIVERBED
MAT EDGE
TDC SIGNAL (mV) or DEPTH (ft)
0
–100
–200
–300
–400
–500
0
500
1000
1500
2000
DISTANCE (ft)

FIGURE 45

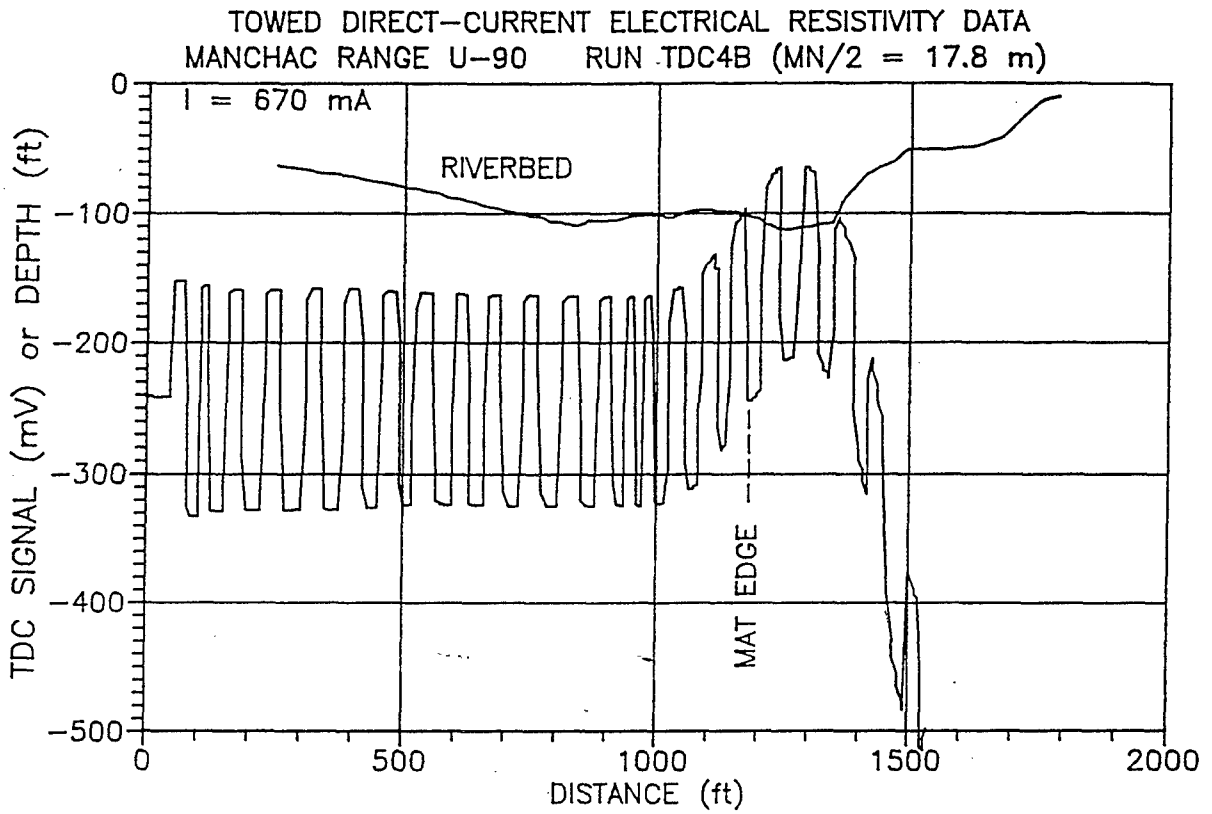
TOWED DIRECT–CURRENT ELECTRICAL RESISTIVITY DATA
MANCHAC RANGE U–90 RUN TDC4B (MN/2 = 17.8 m)
I = 670 mA
RIVERBED
MAT EDGE
TDC SIGNAL (mV) or DEPTH (ft)
0
−100
−200
−300
−400
−500
0
500
1000
1500
2000
DISTANCE (ft)

FIGURE 46

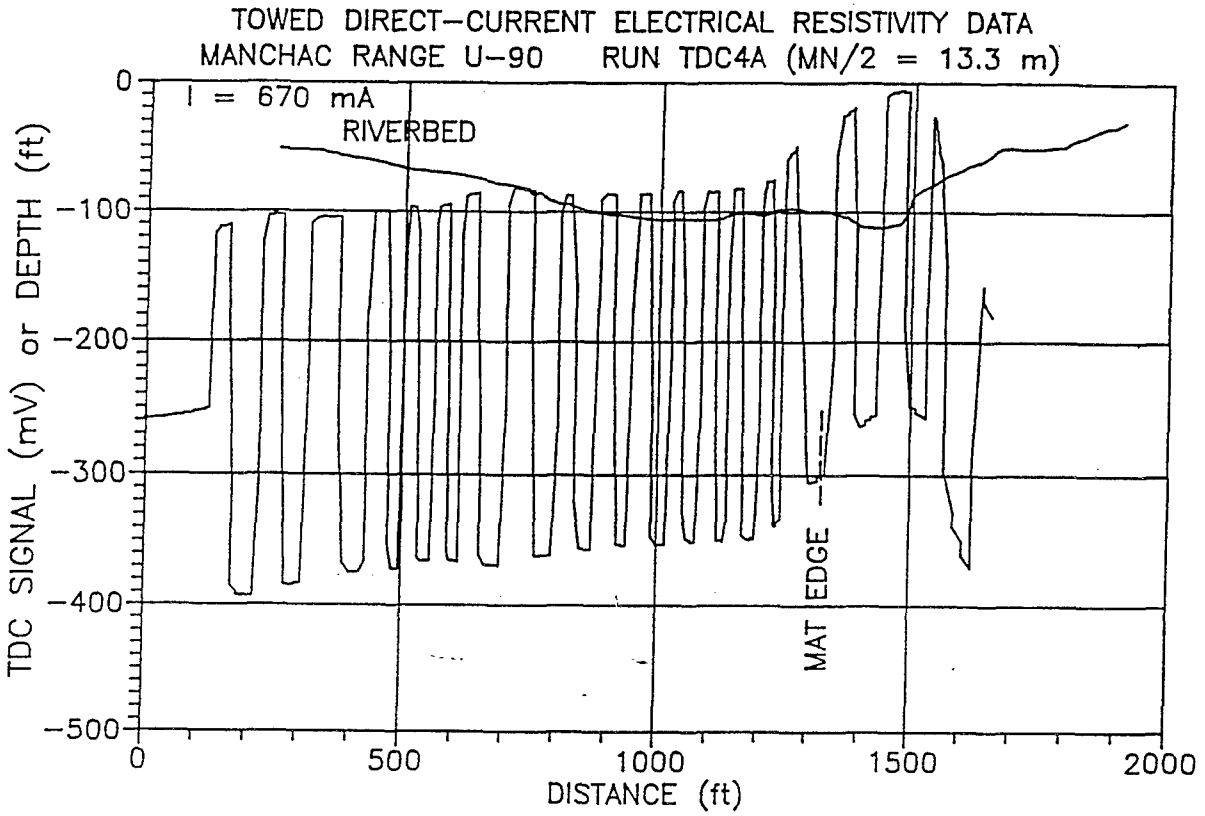
TOWED DIRECT–CURRENT ELECTRICAL RESISTIVITY DATA
MANCHAC RANGE U–90 RUN TDC4A (MN/2 = 13.3 m)
I = 670 mA
RIVERBED
MAT EDGE
TDC SIGNAL (mV) or DEPTH (ft)
0
–100
–200
–300
–400
–500
0
500
1000
1500
2000
DISTANCE (ft)

FIGURE 47

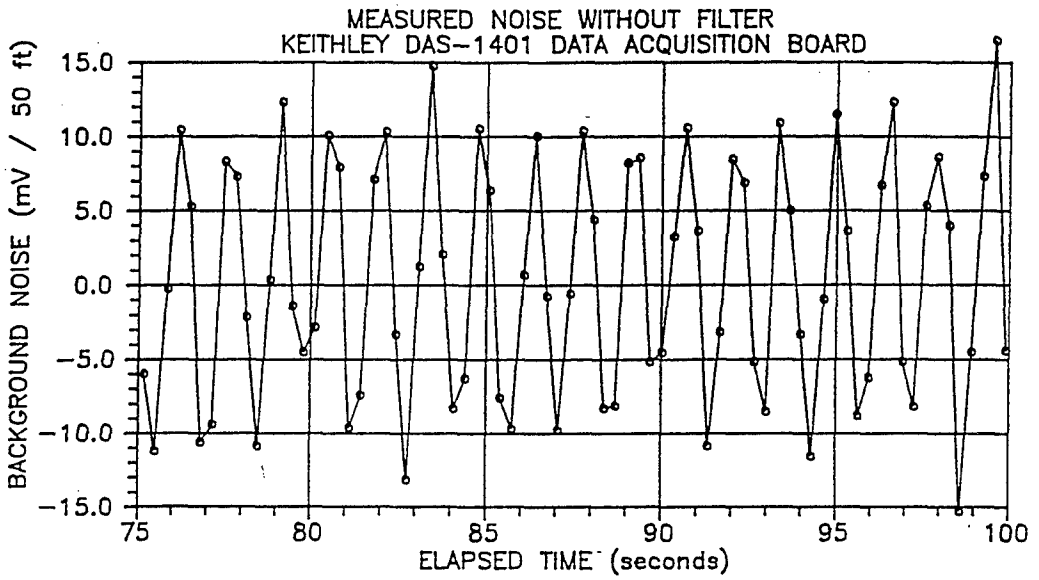
MEASURED NOISE WITHOUT FILTER
KEITHLEY DAS-1401 DATA ACQUISITION BOARD
BACKGROUND NOISE (mV / 50 ft)
15.0
10.0
5.0
0.0
-5.0
-10.0
-15.0
75
80
85
90
95
100
ELAPSED TIME (seconds)

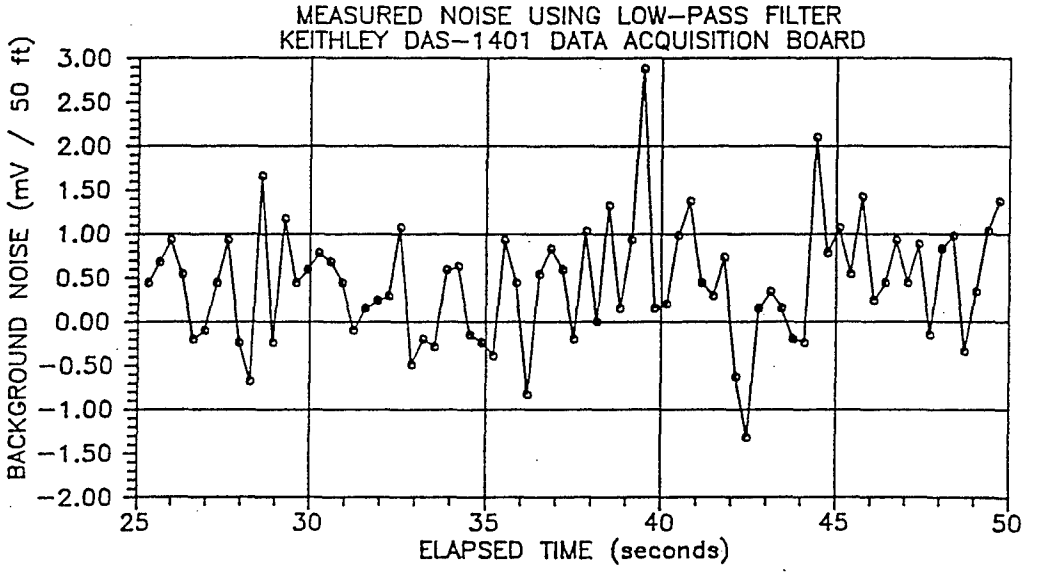
MEASURED NOISE USING LOW-PASS FILTER
KEITHLEY DAS-1401 DATA ACQUISITION BOARD
BACKGROUND NOISE (mV / 50 ft)
3.00
2.50
2.00
1.50
1.00
0.50
0.00
-0.50
-1.00
-1.50
-2.00
25
30
35
40
45
50
ELAPSED TIME (seconds)

Appendix C
Phase III-B Report - Development of Underway Electrical Resistivity Methods for Investigation of Articulated Concrete Mattresses

PHASE III-B STUDY

DEVELOPMENT OF UNDERWAY ELECTRICAL RESISTIVITY METHODS FOR INVESTIGATION OF ARTICULATED CONCRETE MATTRESSES

Prepared for:

U.S. Army Engineer Waterways Experiment Station
ATTN: CEWES-CT-C
3909 Halls Ferry Road
Vicksburg, MS 39180-0631
Research Area GL-2 (Geophysics)

Contract No. DACW39-94-C-0035

Prepared by:

Robert F. Corwin, Ph.D.
Consulting Geophysicist

SP SURVEYS
406 Sea View Drive
El Cerrito, CA 94530
(510) 527-2081

March 2, 1995

CONTENTS

page

I. INTRODUCTION 1

II. SUMMARY 1

III. TDC SYSTEM DESIGN 2

A. Transmitter-Receiver System 3

B. TDC Cable 4

C. Data Acquisition System 5
1. External data logger 5
2. Internal data acquisition board 6

IV. INTERPRETATION OF TDC DATA 7

V. FIELD INVESTIGATION 8

A. Field Program 8

B. Profiles MB1 and MB2 (Missouri Bend Revetment) .. 10
1. Profile MB1 10
2. Profile MB2 12

C. Accuracy of Interpreted Mat Depths 13

VI. CONCLUSIONS 14

VII. RECOMMENDATIONS 14

A. System Components 15
1. Power supply 15
2. Transmitter-receiver unit 15
3. Cable 15
4. Data acquisition system 15

B. Data Interpretation 16
1. Further analysis of September 1994 field data . 16
2. Program INVES 16
3. Modeling studies 17

C. Field Investigation 17

REFERENCES 18

TABLES

Table 1. Sample Voltage Data File

Table 2. Sample Resistivity Data File

Table 3. Sample Positioning Data File

Table 4. Sample Merged Data File

Table 5. Sample INVES Output File

Table 6. Sample Mat and River Bed Elevation Data

FIGURES

1. Towed Direct-Current Electrical Resistivity System

2. Mat Depth Resolution Study, Station MB1-108

3. Mat Depth Resolution Study, Station MB1-252

4. Mat and River Bed Elevation Plots, Profile MB1, Missouri Bend

5. Survey Line Locations, Profiles MB1 and MB2, Missouri Bend

6. Apparent Resistivity Plots, Profile MB1, Missouri Bend

7. Plan Map, Area of Buried Mat, Profiles MB1 and MB2, Missouri Ben

8. Apparent Resistivity Plots, Profile MB2, Missouri Bend

APPENDIXES

A. Listing for Program TDCMRG

B. Listing for Program FCON

C. Listing for Program TDCTAB

I. INTRODUCTION

Because an articulated concrete mattress (ACM) may become buried, displaced, or damaged by water movement or other causes, a need exists within the Corps of Engineers (USACE) for techniques to detect buried, missing or damaged areas of an ACM. A series of investigations of the use of self-potential (SP) and direct-current (DC) electrical resistivity methods for this purpose have been conducted for the USACE Waterways Experiment Station (WES).

The results of the first research program ("Monitoring of Articulated Concrete Mattresses using Direct-Current Excitation and Self-Potential Techniques, Phase I, Feasibility Study"; WES Contract No. DACW-39-91-M-3669) indicated that the SP and towed direct-current electrical resistivity (TDC) methods appeared to be feasible for this purpose. The results of the second (Phase II) program ("Investigation of Articulated Concrete Mattresses Using Self-Potential and Electrical Resistivity Methods"; WES Contract No. DACW-39-92-C-0112) showed that SP measurements conducted on cross-river profiles provide a practical reconnaissance technique for mapping ACM locations and depths, and that the TDC method can provide detailed delineation of ACM depths along profiles run parallel to the river bank.

The results of the third (Phase III-A) program ("Development of Self-Potential and Electrical Resistivity Methods for Investigation of Articulated Concrete Mattresses", Contract No. DACW39-93-C-0084) furnished USACE with specifications for a production SP system and provided the design parameters needed for an operational TDC system. These design parameters were used as input to the Phase III-B program.

The present report describes the results of the Phase III-B program that was conducted to develop and test an operational TDC system and associated interpretation routines suitable for production field surveys for ACM investigations. The report includes descriptions of the TDC system and interpretation procedures, along with a discussion of field test results.

II. SUMMARY

The production TDC system includes a high-voltage power supply, a transmitter-receiver unit, a data acquisition system, and a towed cable. The transmitter-receiver unit is configured to allow complete computer control of the current transmitter and the data acquisition process. The system also can be controlled manually if desired. The test profile described in Section V was run under full computer control, which provided real-time display of the voltage waveforms and measured apparent resistivities, and required the operator only to provide initial setup and to monitor the displayed data.

The towed cable incorporated an inverted Schlumberger resistivity array with transmitter electrode spacing AB/2 of 2 m

and 8 receiver electrode pairs with MN/2 spacings ranging from 7.5 to 56.2 m. An output voltage of about 240 VDC maintained a regulated output current of 3000 mA into the transmitter electrodes, sufficient to generate detectable signal levels for all receiver electrode pairs.

Two types of data acquisition systems were tested: an external data logger and an internal data acquisition board. After appropriate setup parameters were established, both systems performed well. A current half-cycle length of 6 seconds provided enough time for filtering high-frequency noise from the signal. At a towing speed of about 3.5 mph over-the-ground, this 6-second period gave a spacing of about 30 ft between measurement stations.

TDC test profile MB1 was run on September 24, 1994 at the Missouri Bend revetment site. The profile was run in the upstream direction between about ranges U-75 and U-170. River surface elevation was about +6.5 ft NGVD. This profile covered areas of both shallow and buried old mat, new mat, and no mat, and followed the 30-ft depth contour above the old mat and the 20-ft depth contour above the new mat.

The field data were reduced and interpreted using the programs developed for this investigation, and were displayed as a plot of interpreted mat elevation vs. distance along the survey profile. The results indicated that the mat was at or within a few feet of the river bed over the new mat and a portion of the old mat. However, an area of more deeply buried old mat was seen between about ranges U-95 and U-108. The mat reached a minimum elevation of -71 ft NGVD at about range U-101, where the water depth was about 25 ft. Thus the mat was covered by about 45 ft of sediment at this point. A brief resolution study of the TDC data indicated that the interpreted -71 ft mat elevation should be within about +/- 10% of the true elevation value.

III. TDC SYSTEM DESIGN

The operational TDC system includes a towed multi-electrode cable, a transmitter-receiver system, and instrumentation for data acquisition, display, reduction, and storage. Figure 1 shows diagrams of the TDC system. The output of the high-voltage DC power supply is commutated to a square-wave signal by the switching system. The output waveform characteristics are software-controlled by the computer. The square-wave current is fed through the cable into the transmitter electrodes A and B. The resulting voltage differences in the water are measured by the receiving electrodes M1 - M8 and N1 - N8 and transmitted through the receiver cables to the data acquisition unit. The data acquisition unit digitizes and filters the voltage signals and transmits them to the computer.

The output current and received voltages are displayed in real time on the computer screen in graphical form, and are stored in a voltage file on the hard drive of the computer. The operating

software also converts the raw voltage data to apparent resistivity values, displays them on the screen, and stores them as a separate resistivity file. Both the voltage and the resistivity files include the time of each TDC measurement. This permits later merging of the TDC and positioning files so that the position of each TDC measurement can be determined.

Components of the TDC system are described in the following sections. Details of the data reduction and interpretation software and procedures are given in Section IV.

A. Transmitter-Receiver System

The transmitter-receiver system (Figure 1) includes a 120 VAC motor-generator, a high-voltage power supply, and the transmitter-receiver unit (TRU). The 2.5 kW motor-generator provided power for the high-voltage power supply, the system computer, the data acquisition unit, and the 12-volt supply incorporated in the transmitter-receiver unit. During a period when the 2.5 kW generator was inoperative, the entire TDC system was powered by the same motor-generator used for the positioning system and the vessel's air conditioner. No ground loops or other operating problems were observed with this setup.

The computer used to control the system operation was a standard PC-compatible notebook model. This particular model incorporated an expansion port connector to allow use of an external unit for installation of a data acquisition board. If it is desired to use an internal data acquisition board for future operations, the computer must either allow internal installation of additional boards or must incorporate an expansion port as described above.

Two high-voltage power supplies were tested for this project. The first, used for most of the tests, was a Model EMS 300-3.5 unit manufactured by Electronic Measurements Inc. This is a 1000 watt switching power supply that provides regulated current or voltage to a maximum of 300 VDC or 3.5 amps DC. The second power supply was a 2500 watt linear unit manufactured by SP SURVEYS. This unit can provide up to 700 VDC or 6.5 amps DC, but, unlike the EMS unit, the output is not regulated.

The TRU provides the switching circuitry to commutate the DC current, and functions as the interface between the power supply, computer, data acquisition unit, and towed cable. The TRU incorporates a manual drum switch that allows optional manual operation of the current switching process as well as a means of completely disconnecting the high-voltage output from the towed cable. Automated switching of the high-voltage input is performed by a pair of Kilovac Model AP10AA57 vacuum relays. These relays have an expected life cycle of at least 100,000 operations when switching the maximum 300 VDC, 3.5 amp output of the EMS power supply. Coil voltage for these relays is 12 VDC.

The signal to activate the Kilovac relays is sent through the parallel port of the computer to a B&B Model PPIO control unit.

This unit activates a small reed relay in the TRU, which in turn drives an intermediate relay that controls the output to the activating coil of the Kilovac relay. A shunt resistor in the current output line of the TRU provides a voltage proportional to the transmitted current for input to the data acquisition unit. 12 VDC power for the PPIO unit and the relay coils is provided by a 12 volt, 4 amp DC power supply built into the TRU and powered by 120 VAC from the motor-generator.

B. TDC Cable

The TDC cable incorporates transmitting and receiving electrodes with associated wiring, a stress member, sufficient flotation to ensure positive buoyancy, a container for cable storage and deployment, and connectors to interface the cable to the transmitter-receiver unit and the data acquisition system. In order to allow for inspection and possible repair of the cable, a modular construction was used. The central member of the cable is a 508-ft length of 5/16 in diameter polypropylene rope, with a breaking strength of 2100 lb. Cables for the transmitting and receiving electrodes are secured to the rope using plastic cable ties. Flotation is provided by five floats attached to the rope at approximately uniform intervals.

The electrode array uses an inverted Schlumberger configuration, with a transmitter electrode separation AB/2 of 2.00 meters. Receiver electrode separations MN/2 are tabulated below.

Pair No.	1	2	3	4	5	6	7	8
MN/2 (m)	7.50	10.0	13.3	17.8	23.7	31.6	42.2	56.2

This arrangement sets the distance from the stern of the towing vessel to the center point of the electrode array to about 265 ft, removing the cable from the wake of the vessel and allowing adequate distance between the metal hull of the vessel and the +56.2 m receiving electrode. Figure 1 shows the deployment of the cable for the September 1994 field investigation.

The wires to the transmitting electrodes are stranded 18-gage hookup wire, UL style 1015, with 600-V rated PVC insulation (Belden # 8918 or equivalent). The cables to the receiving electrodes are 8-conductor, stranded 22-gage with a 0.032 in PVC outer jacket (Belden # 9421). The transmitting electrodes are 2-ft lengths of tinned copper braid, clamped to the ends of the transmitter wires. The receiving electrodes are Sensorex #97048 Ag-AgCl reference electrodes. These electrodes use a gelled KCl filling solution, with electrical contact to the water made through a porous junction. The bodies of the electrodes are clear epoxy plastic. The electrodes are spliced to the 8-conductor cables and clamped to the rope.

The maximum outer electrode separation of 56.2 m allows detection of the mat at depths of at least 100 ft below the river surface. A more detailed discussion of detection depth and accuracy is included in Section V.

C. Data Acquisition System

The data acquisition system includes a data acquisition unit, an IBM-compatible personal computer (PC), and associated software. Two different data acquisition units, an external data logger and an internal data acquisition board, were tested for this project. These units are described in the following sections. A discussion of the comparative advantages and disadvantages of the two units is included in Section VII.

1. External data logger

The Fluke Hydra model 2625A Data Logger used for this study is a self-contained unit powered by 120 VAC from the motor-generator (a 12 VDC battery pack also can be used). The Hydra can scan up to 21 differential input channels. The measured signals are digitized, filtered, and transmitted to the PC through an RS-232 (COMM) port. For the TDC system, channel 0 measures the current shunt voltage (300 VDC maximum common mode) and channels 1-8 measure the receiving electrode voltage differences.

The scan rate can be set to either "fast" or "slow". For DC voltage measurements, the 10-channel scan rate is 13.4 channels/second at the fast rate and 3.8 channels/second at the slow rate. Because the slower scan rate allows more time for filtering high-frequency noise from the incoming signal, the accuracy and resolution of the data are considerably better at the slow scan rate. The tradeoff for this improved signal quality when using the slow rate is slower data acquisition, i.e., for a given vessel speed, the spacing between individual soundings is about four times greater at the slow rate as compared with the fast rate. Comparisons of data obtained at the different scan rates are discussed in Section V.

The operating software for the TDC system with the Hydra data logger is program HYDAQ, written in Microsoft QuickBASIC. This program performs the following functions:

(1) Controls the switching of the transmitter current
(2) Controls the scanning and data acquisition procedure for the Hydra
(3) Reads the digitized output of the Hydra and calculates the associated voltage values
(4) Calculates the measured apparent resistivity for each electrode separation
(5) Provides a real-time scrolling on-screen display of the apparent resistivity values along with a graphic strip-chart display of the transmitted current and receiver electrode voltages
(6) Writes two files to disk:
    a) A voltage file that includes the measurement time and the recorded current and voltage values (see Table 1 for example voltage file). This file can be used to create a graphic display of the current and voltage waveforms.

b) A resistivity file that includes the measurement time and the calculated apparent resistivities for each station (see Table 2 for example resistivity file). As discussed later, the data from this file are used as input to the program used to interpret layer depths and thicknesses.

As mentioned previously, the program controls the transmitted current waveform by signals sent through the parallel port of the PC to a B&B PPIO parallel port input/output converter incorporated in the transmitter-receiver unit (TRU). The desired switching intervals are input to the program as part of the setup routine conducted before beginning data acquisition. Under control of the program, the PPIO unit activates the appropriate relays in the TRU to open the high-voltage Kilovac relays, reverse the output polarity, and close the high-voltage relays. As discussed later, the half-wavelength of the transmitted current square wave ranged from 2 to 6 seconds, with an open-circuit interval of a few hundred milliseconds between half-cycles to allow activation of the polarity-reversing relays.

The data acquisition process is keyed to the time when the current polarity is reversed. A "grab delay" time interval (typically about 1/2 of the half-cycle time) is specified as part of the initial setup procedure. After the polarity is switched, the computer waits for the specified grab delay interval for transient effects to die out and then initiates the scanning procedure to measure the input voltages, calculate the apparent resistivities, and write the data to the output files.

2. Internal data acquisition board

The second tested data acquisition unit was a Keithley DAS 1601 data acquisition board. This 8-channel, 12-bit board is designed to be installed in an open slot of a PC. For the notebook PC used for this project, the board was installed in an external chassis connected to the expansion port of the computer.

The nominal scan speed of this board is much greater than that of the Hydra; about 100,000 samples per second or 8000 8-channel scans per second. However, because the board does not provide built-in high-frequency noise filtering, provision for such filtering must be made. This can be done by using external low-pass circuitry on the input or by software routines in the data acquisition program. The software developed for the TDC program incorporated noise reduction routines which operated essentially in the same fashion as those included in the built-in Hydra operating system. These routines slowed the board scan rates to values similar to those of the Hydra for an equivalent degree of high-frequency noise reduction.

Unlike the Hydra, the high common-mode voltage present at the current shunt resistor does not allow the output of the shunt to be directly input to the board. This means that some other provision must be made to monitor the transmitter current. For

the regulated-current power supply used for most of the TDC measurements, the constant current can be entered as part of the initial setup of the data acquisition program. For an unregulated supply, instruments are available to isolate the high common-mode voltage from the board input. Although not used for the present project, such an instrument could be incorporated into future TDC systems.

The operating software for the TDC system with the Keithley data acquisition board is program KDAQ, written in Microsoft QuickBASIC. With the exception of some of the setup parameters, the operation of this program is essentially identical to that of program HYDAQ described above. Both programs provide the same control over the transmitted waveform and the data acquisition process, and write similar output files.

IV. INTERPRETATION OF TDC DATA

The general procedure for interpreting the TDC data is as follows:

1. The TDC resistivity output file is merged with the positioning data file to determine the position of each TDC station.
2. The resistivity-electrode separation data set for each desired station is extracted from the resistivity output file and input to the interpretation program INVES.
3. The data set is interpreted in terms of the thickness, depth, elevation, and resistivity of the layers at the station. If the mat is present at the station, it will be one of the interpreted layers.

The procedure described above involves the use of four different programs. The procedure and programs are described in more detail below. The example data files are those from profile MB1 at the Missouri Bend site, discussed in Section V.

The HYDAQ output files MBV1.DAT (voltage) and MBR1.DAT (resistivity) for this profile are shown in Tables 1 and 2, respectively. Note that the first column for each of these files is a "sequence number" that serves as a label to identify the data set for each individual station. The corresponding DIMCO positioning file MBR1.NAV is shown in Table 3. Files MBR1.DAT and MBR1.NAV are input to the merging program TDCMRG (Appendix A), which generates the merged output file MBR1.OUT (Table 4). The first column of this merged file is the sequence number, followed by information about the position of the vessel's navigation antenna and of the center point of the TDC array. All subsequent interpretation is keyed to the position of the array center point for the desired sequence number.

The resistivity file MBR1.DAT then is input to file conversion program FCON (Appendix B). This program prompts the user to enter the desired sequence numbers to be interpreted, extracts the information from the desired lines of the input file, and creates output files of the appropriate format for direct input to

interpretation program INVES. The input data for sequence number 108 is listed at the bottom of Table 5 (discussed below).

Program INVES is a general-purpose modeling and interpretation program for the analysis of one-dimensional (layered) resistivity sounding data. A copy of the description and operating manual for INVES, along with the program disk, have been delivered to WES. The output of INVES is a file containing the input data, interpreted layering, and quality-of-fit information for the interpreted sounding. Table 5 shows a sample INVES output file for sequence number 108 on profile MB1, and Figures 2 and 3 (discussed in more detail in Section V-C) show plots of the measured and calculated data for this station and for station 252 on the same profile.

As INVES is presently written, output model values are shown in the same units as the electrode spacings; which in this case are meters. Program TDCTAB (Appendix C) is used to convert the layer thicknesses to feet, calculate depths and elevations, and determine which layer is the mat. The program prompts the user to enter the sequence number and thickness and resistivity data from each INVES output file, all of which are entered manually. TDCTAB then performs the preceding calculations and presents the results in tabular form.

Using a line editor, these results then are appended manually to the merged output file, and unwanted columns showing the time and vessel position are removed to create a final output table such as that shown in Table 6. A graph showing the measured riverbed elevation and interpreted mat elevation vs distance XMID along the profile is shown on Figure 4. The data for this plot were taken from Table 6.

The procedure described above is involved and time-consuming. For future application, the auxiliary programs such as TDCMRG, FCON, and TDCTAB will be incorporated into INVES and the unit conversions and output tabulations will be done internally. This will allow much faster and more efficient data interpretation.

V. FIELD INVESTIGATION

A. Field Program

The Phase III-B field investigation was conducted between 20 and 24 September 1994 at the Missouri Bend and Manchac revetment sites near Baton Rouge, Louisiana. River gage during this period was about +6.5 ft NGVD. Measured river water resistivity was about 22 ohm-m. The survey vessel "Mary Evans" and differential GPS positioning data were provided by DIMCO, Inc. of Vicksburg, MS

As part of the investigation, the GPS antenna was installed on a small raft, fabricated by DIMCO, that was towed behind the vessel at the center point of the TDC array. The purpose of this was to provide a more accurate position for the array center point. This

arrangement worked well until electronic problems were encountered, at which time the GPS antenna on the vessel was used to acquire positioning data. The data for profile MB1 discussed below were run with the antenna on the survey vessel; profile MB2 was run with the antenna on the raft at the array center point.

The field study included 25 TDC runs designed to determine the optimum equipment configuration and survey procedures, as well as a series of SP profiles to provide supplementary data for the TDC interpretations. The variables for the TDC runs included:

(a) Profiles run in both the upstream and downstream directions, at different towing speeds

(b) Profiles over areas of old mat, new mat, shallow mat, deep mat, and no mat

(c) Use of the EMI and the SP SURVEYS power supplies, with both regulated and unregulated current and varying output voltage

(d) Use of both the external data logger and the internal data acquisition board, with different switching, filtering, and wavelength setups, and with automatic and manual switching.

Conclusions obtained from these tests included the following:

(1) Towing the array in the upstream direction at a speed of about 3.5 mph over the ground gave the best combination of data quality and vessel course control.

(2) The cable design and deployment described in Section III-B appeared to provide usable data for mat depths of at least 100 ft below the river surface. In areas where the mat was shallow, the very low apparent resistivity values reduced the signal strength of the largest few electrode pairs to the point where the data from those pairs was not usable. However, at these shallow mat depths the data from the outer electrodes was not needed to determine the depth to the mat. In areas where the mat was deep or missing, the higher apparent resistivities produced larger signals and good signal-to-noise ratios for all electrode pairs.

(3) While the unregulated SP SURVEYS power supply provided usable data, the regulated EMI unit gave much steadier readings when the transmitter electrode depth varied as a result of wave activity. A transmitter supply voltage of 240 VDC maintained a regulated output current of 3000 mA.

(4) When using the EMI power supply with the internal Keithley board, it appeared that the board was picking up some high-frequency noise from the power supply. For future operations with an internal board, additional shielding and locating the power supply at a position other than directly beneath the board should reduce this problem. Because of the built-in shielding of the external data logger, this problem was

not observed when using the EMI power supply with the external logger.

(5) If sufficient filtering time was allowed (about a 6-second half-period), very good data quality was obtained from both the Hydra data logger and the internal Keithley board. For the Hydra unit, the required filtering time was achieved by using the slow data acquisition rate. For the Keithley board, the filtering was optimized by using the 6-second half-period and by choosing appropriate sampling and filtering constants as part of the setup procedure.

(6) At the 3.5 mph (5.2 ft/sec) survey speed, the 6-second half-cycle timing gives a lateral resolution of about 30 ft between soundings. If more closely-spaced readings are desired, it may be possible to reduce the 6-second half-cycle time somewhat. Also, depending on the river current velocity, the survey speed could be reduced slightly.

(7) The fully-automated mode of TDC data acquisition, with all switching and data acquisition functions controlled by the computer, worked very well. In this mode, after initiating the data acquisition process the operator needed only to monitor the computer screen as the measurements were being made.

Disks containing the field data for all the tests described above have been delivered to WES. The results of one of these tests, Missouri Bend profile MB1, are described in detail in section B below. Profile MB1 was the final run in the field program, and was the only run made using the optimum equipment configuration, including the slow data acquisition rate for the Hydra data logger. Profile MB2 was made using the fast data acquisition rate of the Hydra data logger, so the readings were noisier than those for profile MB1. Therefore, the results from profile MB2 were not interpreted in terms of mat elevations for this report. As discussed in Section VII, because profile MB2 was run in shallow water, the data quality may be sufficient to determine the depth to the mat with acceptable accuracy.

B. Profiles MB1 and MB2

1. Profile MB1

Profile MB1 was run in the upstream direction, at an over-the-ground speed of about 3.5 mph (5.2 ft/sec). The profile was run as closely as possible over the 30-ft water depth contour above the old mat. To maintain a reasonably straight survey line, the 20-ft depth contour was followed in the area above the new mat.

The voltage and resistivity field data files for profile MB1 are shown in Tables 1 and 2. Note that the interval between resistivity readings is 12 seconds rather than 6 seconds described in (5) and (6) above. This was due to a bug in the data acquisition program, which has been corrected. A portion of the

corresponding DIMCO positioning file is shown in Table 3, and Table 4 shows the merged TDC and positioning data. A plan map of the survey line, taken from the data of Table 4, is shown on Figure 5. Note that all coordinates are referenced to the position of the center point of the TDC array (XMID) rather than the position of the survey vessel.

A plot of the measured apparent resistivity for each electrode separation vs. elapsed time is shown on Figure 6. This plot is of interest because it can be generated either real-time during the survey or directly following the completion of the field profile, and provides a great deal of preliminary information regarding the presence and relative elevation of the mat. Different profile "signatures" are associated with different areas of the mat, and the transitions from old mat to new mat, and from new mat to no mat, are immediately evident. Of particular interest is the high-resistivity "bump" centered at an elapsed time of about 1300 seconds. This high-resistivity deviation indicates an area of significant deepening of the mat. The quantitative elevation changes associated with this deepening are discussed below.

The total length of the profile was 9194 ft, and 149 readings were obtained, giving an average spacing of about 62 ft. Of these 149 readings, 107 were interpreted using program INVES. These included all 71 readings taken above the old mat and 36 of the 52 readings taken above the new mat. Several of the 26 readings made in the no-mat area past the end of the new mat also were interpreted, and gave interesting information regarding the geology of the river bed in this area. However, only the readings made in the old-mat and new-mat areas are discussed below.

The interpreted data were processed as described in Section IV and are summarized in Table 6. A plot of the mat elevation interpreted from the TDC data and the riverbed elevation obtained from the positioning data is shown on Figure 4. The x-axis parameter XMID represents distance travelled along the survey profile shown on Figure 5.

It is important to note that the mat elevations plotted on Figure 4 represent "first-pass" interpretations of the field data, with only minimal efforts made to delete obviously noisy data values or to use known parameters such as water depth and resistivity to constrain the interpretations. This accounts for the roughness of the elevation profile and the placement of the mat above the river bed at some points. Also, some of the deviations of the elevation profile probably are caused by the electrode cable not following exactly the course of the vessel, which would result in the TDC measurement being made at a different water depth than that recorded on the vessel.

A second pass through the data interpretation process would have resulted in a smoother mat elevation profile. However, it is evident from Figure 4 that the interpreted mat elevation is essentially the same as the riverbed elevation from XMID = 300 to

2400 ft over the old mat and from XMID = 5500 to 7700 ft over the old mat, indicating that the mat in these areas is continuous and lies at or just below the river bed. Visually smoothing the elevation profile between about XMID = 3800 and 5500 ft indicates that both the old and the new mat in this area are covered by about 5 to 10 ft of sediment.

Between about XMID = 2400 and 3800 ft the mat appears to dip beneath the river bed, reaching a maximum burial depth of about 40 to 50 ft. This area corresponds to the high-resistivity deviation seen on Figure 6. It is possible that this apparent deepening actually represents an area of missing or discontinuous mat. However, as seen on Figure 6, the transition from existing mat to no mat at an elapsed time of 2250 seconds is much more abrupt than seen in the high-resistivity area between about 1180 and 1400 seconds. Therefore it appears more likely that the area between XMID = 2400 and 3800 ft represents a true deepening of a continuous mat section. Note that the apparent sharp dropoff of the mat is greatly exaggerated by the factor of 100 between the scales of the x- and y-axes of Figure 4.

Figure 7 covers the area of interpreted buried mat on profile MB1. The plot shows the survey line for profile MB1, the as-installed outline of the mat, and locations of SP profiles conducted in this area. Profile MB1 passes over the inshore ends of the interpreted mat points for the SP lines on ranges U-100 and U-105, and is inshore of all SP mat points for the profile along range U-95. Note that the SP mat points do not necessarily correspond to the limits of the mat; rather they represent points where there are changes in geochemical conditions along the mat.

The SP data gave elevations of the inshore mat points in this area that were between about -24 and -40 ft. Thus, although the SP data do not contradict the area of buried mat interpreted from the TDC data, they cannot provide any direct indication of such an area. As discussed in Section VII, it would be desirable to obtain additional, detailed TDC and SP coverage in this area to determine how well mat elevations calculated from the two techniques agree, and to see whether the SP data can provide additional support for the burial of the mat in this area.

2. Profile MB2

Figures 5 and 7 show the survey line location for profile MB2, and Figure 8 shows the apparent resistivity plots for this profile. This profile was run in the upstream direction at a nominal water depth of 20 ft over the old mat and 15 ft over the new mat and no-mat areas. The data were recorded with the Fluke Hydra data logger using the fast data acquisition rate.

Comparison between Figures 6 and 8 shows the considerably higher noise level of the data resulting from use of the fast data acquisition rate. Because of the extreme noise variations of the data from the 42.2 and 56.2 m receiver dipoles, the data from these dipoles are not shown on the plot. However, it is evident

that the general form of the profile MB2 plots is comparable to that of the MB1 plots, with similar indications of areas of shallow old mat, buried old mat, new mat, and no mat. Because of the shallower water depth, the information from the larger electrode separations is not necessary to determine the depth to the mat. Therefore, it is possible that some useful indication of the mat elevation could be obtained from the MB2 data.

C. Accuracy of Interpreted Mat Depths

The absolute accuracy of interpreted mat elevations can only be determined by comparison with actual "ground truth" data. At this time, there is no ground truth data available in areas where the mat appears to be buried beneath the river bed. However, in areas where it is reasonably certain that the mat lies on or just below the river bed (e.g., the shallow old mat and recently-installed new mat at Missouri Bend), the average mat elevations interpreted from the TDC data are within a few feet of the riverbed elevation. The total depth from the water surface to the mat ranges from about 15 to 40 ft in these areas.

Modeling studies can be used to help estimate the resolution of mat elevation attainable from the TDC measurements. Figure 2 shows the TDC data from station 108 on profile MB1, an area of interpreted shallow old mat. The total interpreted depth from the water surface to the mat was about 40 ft, giving an interpreted mat elevation of -33 ft. The -33 ft value gave a very good fit to the field data. Elevations that are 10% greater or less than the -33 ft value give fits that are significantly worse. Therefore the true elevation should be within +/- 10% of the optimum value.

Figure 3 shows similar plots for station 252 on profile MB1, an area of interpreted deeply-buried old mat. Water depth at this station was about 25 ft, and the interpreted mat elevation was -67 ft NGVD, placing the mat about 74 ft below the river surface. Varying the mat elevation by +/- 10% of the nominal -67 ft value gave data fits that were significantly worse than those provided by the -67 ft elevation. Although the deviations from the optimum fit were not as large as those seen for shallower mat elevations, it appears that the mat elevation still should be resolvable within +/- 10% at a total depth of 74 ft.

The 74 ft depth at station 252 represents about the greatest mat depth surveyed for the September 1994 field investigation. From the results described above, it appears that the present TDC system should be able to maintain resolutions of +/- 10% to +/- 20% for total mat depths of up to at least 100 ft beneath the river surface. Future TDC investigations should include profiles run at greater water depths, over areas of deeper mat. Resolution studies like those described above then can be used to determine the practical limits of mat detectability and depth resolution for the present array configuration, and to furnish information about possible modifications needed for TDC measurements conducted over very deeply buried mats.

VI. CONCLUSIONS

The results of the field tests indicated that the production TDC system and associated software performed as intended. The computer-controlled current switching and data acquisition process operated reliably under actual field conditions. The towed cable did not develop any problems during the course of testing. The data reduction and interpretation programs functioned properly and gave reasonable results when applied to actual field data.

The Phase III-A report included an extensive discussion of the need for high-frequency filtering to produce acceptable signal-to-noise ratios. The filtering procedures for both the external data logger and the internal data acquisition board accomplished the necessary high-frequency noise reduction and provided data quality sufficient to allow detection and resolution of mat depths of 100 ft. The high-voltage power supply provided sufficient current for the desired signal-to-noise ratios.

Reduction and interpretation of the field test profile data provided a mat elevation profile that showed the mat to be within a few feet of the river bed in most areas. The old mat appeared to be more deeply buried along one 1300-ft portion of the survey profile, reaching a maximum depth of burial of about 45 ft beneath the river bed. The total interpreted depth of the mat beneath the water surface in this area was about 74 ft. Resolution studies of the TDC sounding curves indicated that the actual mat elevation should be within +/- 10% of the interpreted value for this burial depth. For the present system configuration, mat depth resolution probably is no worse than about +/- 20% for total burial depths of up to 100 ft.

The SP system developed for the Phase III-A investigation and the TDC system described in this report provide complementary techniques for conducting ACM investigations. SP profiles run along the range lines provide location and depth of the outer edge of the mat, along with the location and depth of one or more additional points on the mat. TDC survey lines run in the upstream direction give mat elevation profiles with a lateral resolution of about 30 ft along the profile. Thus the combination of the SP and TDC data can provide useful information regarding the location and depth of the mat.

VII. RECOMMENDATIONS

Although the present TDC hardware and software could be used immediately for production operations, some modifications and upgrades would help to simplify field operations, prolong the operating life of the components, streamline the interpretation process, and provide better indications of the reliability of the interpreted mat depths. Some recommendations for future TDC system development are presented below.

A. System Components

1. Power supply

The EMI power supply worked well and could be incorporated into a future system with no modifications other than provision of a protective housing. It should be noted that the 300-volt, 3-amp unit used for this investigation was selected for operation in relatively fresh (20 ohm-meter) river water. TDC operations conducted in salt water would require a lower-voltage, higher-current unit. Some modifications would have to be made to the transmitter-receiver unit to handle such higher currents.

2. Transmitter-receiver unit

The prototype unit functioned well, and could be essentially replicated for future systems. One useful modification might be to have the computer directly control the high-voltage power supply rather than using the Kilovac relays for this function.

3. Cable

The prototype modular cable worked well for testing purposes. However, for long-term operation it probably would be desirable to construct an integrated cable, with all the individual conductors within a single jacket. Incorporation of a second pair of transmitter electrodes with a larger spacing (e.g., AB/2 of 10 meters) might help to provide better signal-to-noise levels for the outer voltage electrodes in areas of deeply buried mat. Installing the GPS positioning antenna on a small raft at the center point of the TDC array improved the positioning accuracy of the measurement, and should be incorporated into future configurations.

4. Data acquisition system

Both the Hydra logger and the Keithley board provided acceptable data. The Hydra provided the following advantages: (1) operation through the serial port (making it easier to use a portable computer without card slots); (2) better filtering of external electromagnetic interference (it could be used when installed next to the EMI power supply; the Keithley board could not); (3) the current shunt output could be directly input to one of the data acquisition channels of the Hydra; buffering must be provided for the board; (4) The Hydra offers up to 21 channels of data acquisition; the board is limited to 8 channels total (including a current channel, if used).

The advantages of the internal board are: (1) it is considerably less expensive than the Hydra unit; (2) because its inherent data acquisition speed is much greater than that of the Hydra and its high-frequency filtering routines can be modified under program control, it offers the possibility of optimizing the filtering process to permit greater data acquisition rates than achievable by the Hydra (which only offers the "slow" and "fast" data

acquisition rates). This in turn would permit better lateral resolution of mat properties at a given vessel speed.

For operations conducted with no further development it probably would be preferable to use the Hydra unit for data acquisition. However, it is recommended that a provision to buffer the shunt current for input to the board be developed, and that some additional field trials be conducted to determine whether the board can provide significantly greater acquisition rates than the Hydra in actual field use.

The data acquisition programs HYDAQ and KDAQ generally worked very well, and would require only some cleaning up of setup routines to remove procedures that were not found to be needed during the field testing. It also would be helpful to provide a real-time on-screen graphic display of the apparent resistivity profiles, similar to those shown in Figures 6 and 8.

To expedite field operations, it would be helpful to develop a technique for real-time input of the positioning data into the geophysical (TDC) files. This would eliminate the necessity of merging the TDC and positioning files before analyzing the TDC data, and would allow immediate inspection of the TDC data with respect to the location of the survey profile, to determine whether the indicated mat conditions and elevations are consistent with the survey profile location.

B. Data interpretation

1. Further analysis of September 1994 field data

Of all the test TDC profiles conducted as part of the September 1994 field investigation, only profile MB1 at the Missouri Bend site was run using the equipment configuration that gave the highest data quality. However, additional information regarding mat elevations possibly could be obtained from the data from some of the other TDC profiles. For example, because profile MB2 was run in relatively shallow water, the data from this profile may be able to provide usable mat depths even though it is considerably noisier than that for profile MB1.

2. Program INVES

As discussed in Section IV, the modeling and inversion routines of program INVES appear to be working well, but some input-output modifications would help to streamline the interpretation process. Several of these modifications are presently being made, and when completed will be incorporated into INVES. For future production applications, it might be helpful to develop a capability for batch inversion of a series of soundings, rather than doing each inversion individually as the program is presently set up.

Once the modifications are completed, the upgraded program could be tested by interpreting some additional data from the September

1994 field investigation. This testing should indicate what additional changes, if any, would be desirable.

3. Modeling studies

Resolution studies like those discussed in Section V-C are helpful in determining the limits of accuracy of the interpreted mat elevations. Additional studies of this type using data from the September 1994 investigation (and from a possible future field investigation, as discussed below) would help to better establish the resolution of the mat depth estimates for a variety of site conditions.

There are a number of "second-order" resistivity effects that could affect the accuracy of TDC data interpretation. The algorithm for program INVES is written for a mat that is a flat-lying layer of infinite lateral extent, and thus does not determine the effects of the mat dip or edges. These effects could be significant, especially in areas where measurements are made near the inner or outer limits of the mat, where there is a gap in the mat, or where the mat dips steeply offshore. Studies made using 2-dimensional resistivity computer modeling routines would help to determine whether and how these effects are to be considered when interpreting TDC field data.

Another possibility for studying two-dimensional effects is the use of analog (tank) models. Analog modeling is particularly helpful in cases where the resistivity target is a thin, low-resistivity layer such as an ACM. Model tank facilities such as those available at WES and some universities could be used to construct a scale model of the mat field and river bed, with measurements made using a scaled-down resistivity array. These models also could be used for SP studies.

C. Field Investigation

A field investigation in the Missouri Bend revetment area, possibly conducted in the late summer or fall of 1995, could provide additional information regarding the accuracy and resolution of mat depth interpretations provided by geophysical methods and about the utility of improvements in equipment and survey techniques.

As discussed in Section V, TDC survey profile MB1 was run in relatively shallow water, close to the onshore limit of the mat. Unfortunately, this happened to be an area where SP survey coverage was limited. It would be very helpful to run additional TDC profiles in this area at greater water depths, to determine how well the system performs in areas where the mat is deeper. A series of closely-spaced SP lines run along and between the range lines could be used to determine how well the TDC and SP interpretations correlate along the profile. This detailed coverage would allow profiling and contouring of the mat elevations interpreted from the TDC and SP data, for comparison with initial mat emplacement data. Detailed coverage at the

upstream end of the new mat would provide information regarding the sensitivity of the TDC measurements to sections of missing or discontinuous mat.

A particular target of this detailed survey would be the area of interpreted deep burial centered in the vicinity of range U-101. Along with the TDC and SP coverage in this area, it would be helpful to examine any available EM data and possibly to consider a drilling program to confirm the geophysical interpretations.

The field investigation also could be used to test any of the equipment and software improvements suggested above that had been made in the interim, and to try some new field procedures that could improve the data acquisition process. These could include the deployment of the GPS antenna at the center point of the TDC array, as well as conducting the TDC profiles along straight lines rather than following depth contours.

REFERENCES

Monitoring of articulated concrete mattresses using direct-contact excitation and self-potential techniques, Phase I, Feasibility study: Report prepared for U.S. Army Engineer Waterways Experiment Station, Contract No. DACW39-91-M-3669, May 19, 1992.

Phase II Study, Investigation of articulated concrete mattresses using self-potential and electrical resistivity methods: Report prepared for U.S. Army Engineer Waterways Experiment Station, Contract No. DACW39-92-C-0112, April 27, 1993.

Phase III-A Study, Development of self-potential and electrical resistivity methods for investigation of articulated concrete mattresses: Report prepared for U.S. Army Engineer Waterways Experiment Station, Contract No. DACW39-93-C-0084, January 26, 1994.

TABLES

TABLE 1

SAMPLE VOLTAGE DATA FILE (MBV1.DAT, partial)

MO BEND 9-24 94 30 FT DEPTH
HSLOW.EXE EMI TX
MBV1.DAT 09-24-1994 Delay1= 200 Delay2= 200 Source rate= 6
A(1 to 7): 7.5 10 13.3 17.8 23.7 31.6 42.2 56.2 B= 2

N	TIME(N)	Elasped	ma	V1	V2	V3	V4	V5	V6	V7	V8
27	13:48:40.47	676.85	-3018.30	-1449.50	-704.70	-329.80	-154.00	-83.22	-64.83	-52.80	-58.97
28	13:48:43.33	680.04	-3021.00	-1452.40	-706.80	-333.70	-160.90	-90.94	-72.33	-61.57	-66.10
29	13:48:46.46	682.84	3017.30	1376.80	646.40	281.10	113.20	45.28	3.32	-19.28	-34.68
30	13:48:49.43	686.13	3019.10	1386.70	657.60	291.20	117.20	44.14	1.45	-23.75	-34.70
31	13:48:52.56	688.93	-3016.90	-1398.90	-662.40	-306.30	-145.00	-82.16	-63.74	-67.38	-61.70
32	13:48:55.36	692.12	-3017.70	-1425.90	-690.30	-324.80	-151.50	-79.28	-62.48	-66.27	-59.38
33	13:48:58.54	694.92	3019.00	1394.90	666.60	300.10	119.00	36.68	-8.65	-28.34	-33.62
34	13:49:01.46	698.22	3014.60	1425.50	698.10	318.10	127.40	42.08	-7.29	-21.68	-28.70
35	13:49:04.64	701.02	-3019.60	-1472.70	-723.90	-340.70	-161.30	-83.73	-62.82	-52.68	-48.98
36	13:49:07.44	704.20	-3016.70	-1512.10	-758.20	-365.60	-173.70	-93.02	-63.84	-52.26	-45.01
37	13:49:10.63	707.00	3017.80	1482.80	727.30	328.50	127.60	41.97	5.80	-12.31	-13.13
38	13:49:13.54	710.24	3020.80	1504.40	744.90	344.30	134.60	45.99	6.43	-8.59	-7.28
39	13:49:16.72	713.05	-3020.70	-1518.30	-770.40	-384.60	-185.90	-88.81	-60.53	-45.27	-23.49
40	13:49:19.47	716.23	-3020.40	-1555.40	-802.90	-406.10	-197.50	-94.60	-62.23	-44.90	-8.91
41	13:49:22.66	719.03	3017.10	1482.80	746.30	357.70	149.70	50.72	4.63	-1.90	38.55
42	13:49:25.57	722.27	3019.50	1515.90	770.80	368.90	152.50	47.52	2.96	4.37	55.49
43	13:49:28.81	725.18	-3016.40	-1552.50	-793.10	-394.40	-188.30	-90.02	-45.66	-2.69	56.77
44	13:49:31.61	728.32	-3019.00	-1564.50	-801.30	-397.90	-186.40	-85.42	-37.55	16.31	66.73
45	13:49:34.80	731.12	3016.30	1518.80	773.50	368.60	147.00	50.40	29.71	59.54	78.90
46	13:49:37.71	734.47	3019.70	1531.50	788.20	383.60	164.70	68.83	50.55	77.19	78.49
47	13:49:40.89	737.27	-3019.80	-1564.50	-800.10	-389.40	-164.10	-40.25	26.92	71.89	62.33
48	13:49:43.75	740.45	-3017.10	-1559.20	-798.40	-387.00	-157.60	-25.64	43.21	70.57	55.59
49	13:49:46.88	743.26	3018.20	1564.40	822.50	423.80	220.00	142.04	120.50	97.86	69.83
50	13:49:49.73	746.50	3016.50	1572.30	841.10	449.80	248.00	164.09	129.94	100.33	53.62
51	13:49:52.92	749.24	-3017.30	-1531.50	-755.90	-329.00	-87.20	38.94	77.56	75.66	7.36
52	13:49:55.72	752.43	-3016.30	-1514.60	-740.30	-313.30	-73.10	47.32	79.77	71.78	4.70
53	13:49:58.91	755.28	3019.00	1606.40	870.80	480.30	272.90	176.33	124.69	72.79	22.95
54	13:50:01.76	758.52	3019.10	1601.00	870.00	477.30	267.40	170.34	118.67	53.39	34.07
55	13:50:04.95	761.33	-3020.00	-1505.30	-725.10	-303.80	-75.50	35.38	59.98	28.95	34.89
56	13:50:07.75	764.51	-3019.20	-1503.70	-736.10	-320.00	-92.10	18.87	35.29	31.63	39.15
57	13:50:10.99	767.37	3020.00	1552.10	812.40	417.40	210.10	110.23	45.08	45.18	47.03
58	13:50:13.85	770.22	3022.60	1530.50	790.80	392.50	179.50	73.15	12.72	38.45	44.40
59	13:50:16.65	772.97	-3017.00	-1543.90	-785.70	-384.10	-177.10	-78.63	-16.57	29.32	45.54
60	13:50:19.39	776.16	-3018.50	-1553.10	-799.90	-408.20	-209.60	-102.14	-28.65	21.39	44.36
61	13:50:22.64	778.96	3020.30	1488.60	724.60	298.80	72.40	-10.09	-13.10	17.84	42.44
62	13:50:25.60	782.36	3017.30	1471.70	706.00	288.50	70.80	-14.80	-29.19	3.52	36.58
63	13:50:28.79	785.16	-3020.70	-1592.40	-839.70	-442.90	-233.70	-131.89	-85.26	-32.61	17.80
64	13:50:31.59	788.35	-3021.00	-1592.50	-842.40	-444.80	-237.60	-138.79	-99.58	-56.14	4.76
65	13:50:34.77	791.15	3017.80	1491.70	736.00	326.70	104.30	-0.88	-47.06	-45.12	11.80
66	13:50:37.74	794.06	3021.20	1522.00	770.50	357.10	125.70	11.54	-67.20	-72.37	-30.70
67	13:50:40.54	796.86	-3019.50	-1548.60	-794.60	-404.00	-213.10	-134.04	-112.33	-98.35	-54.44
68	13:50:43.29	800.05	-3020.40	-1557.70	-797.60	-395.90	-196.50	-120.15	-106.12	-95.59	-69.99
69	13:50:46.47	802.85	3019.90	1543.50	798.40	392.40	172.10	53.08	-25.48	-55.36	-51.06
70	13:50:49.38	806.09	3020.20	1547.20	803.70	400.50	181.90	71.05	-3.70	-50.15	-52.09
71	13:50:52.57	808.89	-3019.60	-1568.70	-807.10	-403.10	-185.20	-72.64	-39.44	-66.33	-71.38
72	13:50:55.32	812.08	-3017.40	-1579.40	-819.00	-414.00	-194.10	-76.90	-33.14	-46.92	-68.28
73	13:50:58.50	814.88	3018.20	1553.80	804.60	398.20	180.40	78.30	33.09	13.08	-35.40
74	13:51:01.41	818.12	3021.30	1562.10	816.10	411.90	192.50	85.25	39.26	31.02	-19.29
75	13:51:04.54	820.86	-3017.50	-1579.60	-820.70	-412.50	-194.60	-83.69	-31.98	-3.51	-23.11
76	13:51:07.34	824.11	-3020.70	-1584.50	-827.20	-421.40	-200.70	-82.10	-29.24	-3.29	-2.45

TABLE 2

SAMPLE RESISTIVITY DATA FILE (MBR1.DAT)

MO BEND 9-24-94 HSLOW.EXE
U/S EMI TX 3000MA LCP = 284 ft
MBR1.DAT 09-24-1994 Delay1= 200 Delay2= 200 Source rate= 6
A(1 to 8): 7.5 10 13.3 17.8 23.7 31.6 42.2 56.2 B= 2

N	TIME(N)	Elasped	R1	R2	R3	R4	R5	R6	R7	R8	
24	13:48:34.54	670.92	20.28	18.56	15.75	12.45	9.42	7.43	7.57	9.31	1.5 cycle
28	13:48:46.46	682.95	19.37	17.14	13.98	10.86	8.89	8.61	8.60	12.71	1.5 cycle
32	13:48:58.54	695.03	18.93	16.48	13.43	10.63	8.94	7.90	10.07	11.31	1.5 cycle
36	13:49:10.63	707.06	19.79	17.74	14.73	11.58	8.93	7.94	7.48	10.51	1.5 cycle
40	13:49:22.66	719.09	20.40	18.82	16.37	13.21	9.81	8.51	8.82	14.86	1.5 cycle
44	13:49:34.80	731.23	20.77	19.41	17.05	13.71	10.21	8.13	7.29	0.80	1.5 cycle
48	13:49:46.88	743.31	21.12	19.96	17.67	14.15	9.90	6.24	1.57	4.94	1.5 cycle
52	13:49:58.91	755.34	21.19	20.02	17.57	13.58	8.73	5.83	2.23	16.02	1.5 cycle
56	13:50:10.99	767.42	20.96	19.56	16.92	12.90	7.83	3.22	6.94	0.04	1.5 cycle
60	13:50:22.64	779.12	20.83	19.41	16.69	12.95	9.34	4.21	0.51	0.33	1.5 cycle
64	13:50:34.77	791.26	20.95	19.60	16.99	13.10	9.17	7.14	4.38	3.82	1.5 cycle
68	13:50:46.47	802.90	20.84	19.50	17.17	14.29	11.62	9.84	11.12	14.28	1.5 cycle
72	13:50:58.50	814.93	21.19	20.09	17.95	14.71	10.03	5.59	10.44	11.55	1.5 cycle
76	13:51:10.53	826.96	21.34	20.39	18.41	15.54	12.23	9.10	5.71	8.44	1.5 cycle
80	13:51:22.72	839.16	21.41	20.50	18.48	15.25	11.26	7.88	5.98	5.89	1.5 cycle
84	13:51:34.48	850.85	21.50	20.77	19.09	16.38	12.98	9.60	8.87	11.08	1.5 cycle
88	13:51:46.45	862.88	21.58	20.79	19.13	16.37	12.78	8.97	7.13	6.08	1.5 cycle
92	13:51:58.43	874.86	21.59	20.88	19.35	16.92	13.62	10.69	9.53	8.80	1.5 cycle
96	13:52:10.45	886.89	21.57	20.92	19.50	17.28	14.55	12.09	11.48	13.24	1.5 cycle
100	13:52:22.59	898.97	21.61	21.08	19.77	17.65	14.81	11.88	10.78	12.27	1.5 cycle
104	13:52:34.68	911.05	21.65	21.08	19.85	17.78	14.98	12.39	10.71	10.58	1.5 cycle
108	13:52:46.32	922.75	21.68	21.13	19.84	17.73	14.90	12.37	11.50	12.37	1.5 cycle
112	13:52:58.46	934.84	21.74	21.27	20.07	18.12	15.46	12.84	11.94	13.55	1.5 cycle
116	13:53:10.60	947.03	21.62	21.08	19.80	17.76	15.17	13.02	12.43	12.85	1.5 cycle
120	13:53:22.30	958.78	21.56	20.97	19.62	17.52	14.87	12.81	12.68	14.83	1.5 cycle
124	13:53:34.49	970.92	21.41	20.73	19.21	16.96	14.34	12.55	12.48	13.88	1.5 cycle
128	13:53:46.13	982.57	21.36	20.55	18.94	16.57	13.81	11.91	11.70	13.13	1.5 cycle
132	13:53:58.22	994.65	21.38	20.61	19.04	16.72	13.98	12.06	11.93	13.37	1.5 cycle
136	13:54:10.36	1006.79	21.50	20.84	19.44	17.32	14.78	12.95	12.89	14.76	1.5 cycle
140	13:54:22.06	1018.49	21.49	20.78	19.32	17.10	14.49	12.47	12.02	12.96	1.5 cycle
144	13:54:34.25	1030.63	21.40	20.66	19.11	16.79	13.98	11.79	10.91	15.88	1.5 cycle
148	13:54:46.33	1042.76	21.51	20.85	19.40	17.16	14.21	12.12	12.77	12.34	1.5 cycle
152	13:54:57.92	1054.46	21.39	20.65	19.10	16.79	13.90	11.08	10.31	10.81	1.5 cycle
156	13:55:10.12	1066.55	21.15	20.20	18.35	15.80	12.91	10.49	10.38	14.29	1.5 cycle
160	13:55:22.31	1078.69	21.16	20.16	18.07	14.78	10.97	9.08	10.00	8.26	1.5 cycle
164	13:55:33.90	1090.33	21.12	20.05	17.98	14.99	11.44	7.84	6.24	14.52	1.5 cycle
168	13:55:45.98	1102.41	20.83	19.58	17.19	13.95	11.00	9.99	9.56	8.68	1.5 cycle
172	13:55:58.12	1114.55	20.92	19.74	17.41	13.85	9.76	6.80	7.13	11.18	1.5 cycle
176	13:56:09.82	1126.25	21.00	19.92	17.86	14.89	11.61	9.11	8.70	9.83	1.5 cycle
180	13:56:21.85	1138.33	21.05	19.93	17.69	14.31	10.33	6.91	6.28	2.76	1.5 cycle
184	13:56:33.99	1150.42	20.99	19.83	17.55	14.06	10.13	6.72	2.87	6.66	1.5 cycle
188	13:56:46.02	1162.45	20.76	19.39	16.75	12.79	8.72	6.43	4.11	1.28	1.5 cycle
192	13:56:57.71	1174.15	20.61	19.20	16.78	13.49	9.45	5.28	3.80	6.64	1.5 cycle
196	13:57:09.85	1186.28	21.00	20.01	18.13	15.40	11.78	8.99	6.89	5.51	1.5 cycle
200	13:57:21.88	1198.31	21.61	20.99	19.45	16.61	12.52	9.38	8.76	10.67	1.5 cycle
204	13:57:33.97	1210.40	21.38	20.74	19.43	17.40	14.65	11.34	7.47	8.56	1.5 cycle
208	13:57:45.66	1222.10	22.02	21.88	21.06	19.32	16.46	13.84	12.70	11.77	1.5 cycle

212 13:57:57.75	1234.23	22.48	22.77	22.63	21.62	18.87	14.52	10.38	10.89	1.5 cycle
216 13:58:09.83	1246.26	22.67	23.22	23.61	23.40	21.49	17.62	12.53	7.29	1.5 cycle
220 13:58:21.86	1258.29	22.83	23.49	24.09	24.24	22.78	19.40	14.70	10.21	1.5 cycle
224 13:58:33.50	1269.94	22.75	23.53	24.30	24.91	24.17	21.50	17.43	13.26	1.5 cycle
228 13:58:45.64	1282.07	22.70	23.38	24.12	24.80	24.29	22.04	18.41	15.00	1.5 cycle
232 13:58:57.78	1294.21	22.70	23.41	24.27	25.21	25.12	23.27	20.13	16.92	1.5 cycle
236 13:59:09.43	1305.80	22.85	23.74	24.83	26.04	26.30	25.00	22.09	18.86	1.5 cycle
240 13:59:21.45	1317.89	23.05	24.04	25.29	26.69	27.18	26.09	23.25	19.68	1.5 cycle
244 13:59:33.54	1330.02	22.99	24.02	25.39	27.03	27.82	26.92	24.11	20.26	1.5 cycle
248 13:59:45.57	1342.00	23.00	24.00	25.35	26.93	27.69	26.84	23.92	19.76	1.5 cycle
252 13:59:57.60	1354.03	22.88	23.74	24.87	26.23	26.75	25.73	22.83	18.69	1.5 cycle
256 14:00:09.62	1366.06	22.65	23.35	24.20	25.24	25.51	24.26	20.61	16.47	1.5 cycle
260 14:00:21.21	1377.64	22.64	23.29	23.99	24.64	24.07	21.61	19.39	15.66	1.5 cycle
264 14:00:33.35	1389.73	22.52	22.98	23.17	22.98	21.69	19.21	15.53	15.02	1.5 cycle
268 14:00:45.38	1401.76	22.10	22.11	21.66	20.57	18.46	16.23	13.62	14.35	1.5 cycle
272 14:00:57.30	1413.79	21.54	20.99	19.72	17.69	14.87	12.24	11.39	9.56	1.5 cycle
276 14:01:09.33	1425.76	21.52	20.94	19.60	17.50	14.64	11.21	10.05	10.82	1.5 cycle
280 14:01:21.41	1437.84	21.63	21.22	20.12	18.33	15.79	13.21	10.77	9.67	1.5 cycle
284 14:01:33.11	1449.54	21.82	21.55	20.75	19.31	16.97	14.33	12.15	12.02	1.5 cycle
288 14:01:45.14	1461.57	21.95	21.88	21.36	20.23	17.73	13.96	11.48	9.63	1.5 cycle
292 14:01:57.22	1473.65	22.02	21.96	21.51	20.51	18.37	15.27	11.43	9.91	1.5 cycle
296 14:02:09.36	1485.79	21.95	21.87	21.36	20.24	17.91	14.64	11.34	9.67	1.5 cycle
300 14:02:20.95	1497.49	21.89	21.78	21.19	19.90	17.41	14.06	10.91	10.08	1.5 cycle
304 14:02:33.20	1509.69	21.88	21.66	20.86	19.30	16.52	12.97	10.01	8.77	1.5 cycle
308 14:02:45.23	1521.66	21.77	21.39	20.35	18.46	15.37	11.66	8.97	9.04	1.5 cycle
312 14:02:56.93	1533.36	21.69	21.25	20.13	18.09	15.03	11.84	9.30	8.90	1.5 cycle
316 14:03:09.01	1545.44	21.64	21.22	20.14	18.20	15.14	11.58	8.70	7.78	1.5 cycle
320 14:03:21.20	1557.64	21.75	21.49	20.66	19.11	16.39	12.84	9.98	9.10	1.5 cycle
324 14:03:32.90	1569.33	21.88	21.80	21.18	19.83	17.23	13.90	11.12	10.08	1.5 cycle
328 14:03:45.04	1581.42	21.97	21.96	21.51	20.41	17.98	14.42	10.94	10.57	1.5 cycle
332 14:03:57.02	1593.50	21.88	21.89	21.42	20.29	17.85	14.35	11.00	9.07	1.5 cycle
336 14:04:09.10	1605.53	21.95	21.94	21.43	20.28	17.89	14.54	11.39	9.01	1.5 cycle
340 14:04:20.85	1617.28	21.93	21.91	21.45	20.39	18.05	14.68	10.80	9.81	1.5 cycle
344 14:04:32.94	1629.31	22.07	22.21	22.00	21.16	18.57	14.14	10.44	9.69	1.5 cycle
348 14:04:44.97	1641.40	22.29	22.40	21.75	19.66	15.91	12.01	12.57	12.54	1.5 cycle
352 14:04:56.99	1653.43	21.35	20.73	19.36	17.29	15.41	14.67	14.60	19.72	1.5 cycle
356 14:05:08.69	1665.12	19.44	17.17	13.65	9.56	6.18	4.93	3.56	3.43	1.5 cycle
360 14:05:20.72	1677.21	19.05	16.37	12.35	7.85	4.09	1.93	2.87	3.49	1.5 cycle
364 14:05:32.86	1689.35	18.66	15.70	11.47	7.14	3.96	2.94	2.65	2.14	1.5 cycle
368 14:05:44.50	1700.94	18.36	15.28	11.01	6.45	2.96	2.90	1.15	7.56	1.5 cycle
372 14:05:56.53	1712.96	18.78	15.96	11.92	7.61	4.75	6.13	6.20	12.25	1.5 cycle
376 14:06:08.73	1725.16	18.40	15.37	11.27	7.03	3.06	1.42	1.21	3.15	1.5 cycle
380 14:06:20.81	1737.24	17.74	14.50	10.41	6.62	3.68	4.35	5.73	8.51	1.5 cycle
384 14:06:32.45	1748.83	17.77	14.56	10.40	6.57	4.53	4.33	4.50	6.73	1.5 cycle
388 14:06:44.54	1760.97	18.28	15.20	10.83	6.33	2.58	1.66	3.19	2.03	1.5 cycle
392 14:06:56.51	1773.05	18.60	15.84	11.79	7.49	4.80	3.02	2.98	6.44	1.5 cycle
396 14:07:08.65	1785.08	18.79	16.29	12.73	9.08	6.67	7.04	9.06	12.58	1.5 cycle
400 14:07:20.68	1797.11	19.11	16.79	13.32	9.26	5.45	3.72	4.59	4.38	1.5 cycle
404 14:07:32.27	1808.70	19.74	17.66	14.10	9.54	5.38	2.38	1.52	3.83	1.5 cycle
408 14:07:44.30	1820.73	20.21	18.33	14.97	10.40	5.84	4.57	6.50	5.35	1.5 cycle
412 14:07:56.44	1832.81	20.12	18.24	15.02	10.89	7.43	4.97	4.34	13.46	1.5 cycle
416 14:08:08.52	1844.90	19.84	17.69	13.91	8.92	5.42	4.60	1.83	1.39	1.5 cycle
420 14:08:20.44	1856.87	19.62	17.42	13.85	9.46	5.51	2.90	5.30	5.47	1.5 cycle
424 14:08:32.47	1868.95	19.61	17.36	13.78	9.57	5.66	1.83	3.14	1.92	1.5 cycle
428 14:08:44.22	1880.65	20.13	17.99	14.25	9.43	4.74	3.04	4.02	4.36	1.5 cycle
432 14:08:56.36	1892.74	19.78	17.53	13.84	9.35	5.67	3.38	0.61	6.51	1.5 cycle
436 14:09:08.39	1904.82	19.76	17.23	13.10	8.30	4.80	1.79	5.80	1.70	1.5 cycle
440 14:09:20.47	1916.90	18.96	16.24	12.40	8.56	6.51	7.17	4.52	14.45	1.5 cycle
444 14:09:32.23	1928.60	19.11	16.45	12.43	7.74	3.14	1.88	3.27	4.27	1.5 cycle
448 14:09:44.36	1940.80	19.24	16.73	13.01	9.26	6.60	4.83	9.19	7.99	1.5 cycle

452	14:09:56.12	1952.55	20.00	17.89	14.24	9.56	4.89	3.09	3.08	6.66	1.5 cycle
456	14:10:08.15	1964.63	19.39	16.99	13.29	8.94	5.88	6.34	2.65	6.41	1.5 cycle
460	14:10:20.23	1976.72	19.37	17.02	13.41	9.47	6.82	5.09	8.10	11.60	1.5 cycle
464	14:10:31.93	1988.36	19.79	17.65	14.08	9.59	5.25	2.43	3.04	5.47	1.5 cycle
468	14:10:44.07	2000.50	19.95	17.97	14.67	10.64	7.51	8.11	7.67	7.91	1.5 cycle
472	14:10:56.10	2012.53	19.97	17.83	14.32	10.04	5.82	2.55	2.46	6.01	1.5 cycle
476	14:11:08.24	2024.67	19.74	17.48	13.91	9.52	5.68	4.02	4.72	4.74	1.5 cycle
480	14:11:19.88	2036.37	19.80	17.53	13.73	8.84	4.68	2.68	3.72	2.65	1.5 cycle
484	14:11:31.96	2048.50	19.39	16.99	13.31	9.33	6.64	4.29	4.52	8.02	1.5 cycle
488	14:11:44.10	2060.53	19.93	17.81	14.15	9.81	6.64	5.02	6.40	7.89	1.5 cycle
492	14:11:55.75	2072.18	20.05	17.90	14.20	9.51	5.44	2.44	2.59	2.83	1.5 cycle
496	14:12:07.88	2084.32	19.79	17.59	14.04	9.96	7.12	4.33	4.78	4.56	1.5 cycle
500	14:12:19.91	2096.34	19.88	17.73	14.10	9.42	4.89	1.54	3.90	2.04	1.5 cycle
504	14:12:32.05	2108.48	20.05	18.03	14.47	10.14	6.87	6.66	5.97	6.41	1.5 cycle
508	14:12:43.75	2120.13	19.75	17.55	14.00	9.67	5.84	3.10	3.93	6.46	1.5 cycle
512	14:12:55.78	2132.27	18.96	16.28	12.32	8.01	4.88	3.85	6.07	7.05	1.5 cycle
516	14:13:07.86	2144.35	19.25	16.80	13.09	9.06	6.09	5.34	9.39	13.54	1.5 cycle
520	14:13:19.51	2155.94	19.10	16.36	12.16	7.55	4.13	1.77	0.92	2.35	1.5 cycle
524	14:13:31.70	2168.13	18.35	15.30	11.12	7.11	4.86	4.01	5.68	6.79	1.5 cycle
528	14:13:43.78	2180.16	18.64	15.62	11.22	6.62	3.49	1.05	3.34	5.27	1.5 cycle
532	14:13:55.76	2192.19	19.07	16.29	12.12	7.66	4.74	2.92	3.62	1.77	1.5 cycle
536	14:14:07.84	2204.22	19.17	16.46	12.37	7.90	4.89	2.12	3.58	1.91	1.5 cycle
540	14:14:19.43	2215.92	19.13	16.43	12.32	7.82	4.87	3.39	3.26	7.59	1.5 cycle
544	14:14:31.51	2228.00	19.38	16.96	13.18	8.90	6.02	6.40	7.64	10.15	1.5 cycle
548	14:14:43.54	2239.97	19.34	17.00	13.52	9.67	6.56	4.24	4.28	3.20	1.5 cycle
552	14:14:55.57	2252.00	20.92	20.04	18.63	17.05	15.70	15.40	19.09	18.37	1.5 cycle
556	14:15:07.60	2264.03	22.58	23.03	23.16	22.54	20.38	19.06	21.41	24.71	1.5 cycle
560	14:15:19.25	2275.68	22.96	23.87	24.72	25.39	24.96	23.57	19.99	21.25	1.5 cycle
564	14:15:31.33	2287.76	23.30	24.40	25.50	26.47	26.51	25.88	24.98	23.93	1.5 cycle
568	14:15:43.41	2299.84	23.19	24.26	25.40	26.45	26.73	26.42	25.81	24.97	1.5 cycle
572	14:15:55.44	2311.93	22.86	23.70	24.65	25.69	26.09	25.90	25.48	25.23	1.5 cycle
576	14:16:07.52	2324.07	22.71	23.46	24.32	25.31	25.78	25.86	26.06	26.37	1.5 cycle
580	14:16:19.33	2335.76	22.95	23.98	25.16	26.65	27.93	29.22	31.16	33.65	1.5 cycle
584	14:16:31.36	2347.79	23.20	24.33	25.85	27.76	29.45	31.16	33.57	36.98	1.5 cycle
588	14:16:43.45	2359.88	23.36	24.71	26.57	28.96	31.14	33.04	34.63	36.01	1.5 cycle
592	14:16:55.15	2371.58	23.75	25.41	27.67	30.58	33.45	36.08	38.03	38.03	1.5 cycle
596	14:17:07.45	2383.88	23.93	25.80	28.40	31.84	35.20	37.93	39.61	39.89	1.5 cycle
600	14:17:19.09	2395.52	24.13	26.21	29.22	33.09	36.53	38.97	40.16	40.20	1.5 cycle
604	14:17:31.12	2407.61	24.38	26.68	29.82	33.65	36.87	39.15	40.33	40.05	1.5 cycle
608	14:17:43.20	2419.64	24.88	27.39	30.69	34.71	38.21	40.83	42.39	42.32	1.5 cycle
612	14:17:54.96	2431.39	25.09	27.81	31.37	35.50	38.95	41.55	43.22	43.67	1.5 cycle
616	14:18:07.04	2443.47	25.31	28.12	31.82	36.15	39.80	42.20	42.83	42.26	1.5 cycle
620	14:18:19.13	2455.56	25.21	28.11	31.96	36.49	40.40	42.97	43.63	42.35	1.5 cycle
624	14:18:31.26	2467.70	25.42	28.35	32.22	36.73	40.55	43.05	44.07	44.58	1.5 cycle
628	14:18:43.02	2479.40	25.31	28.14	31.67	35.58	38.46	40.11	40.63	40.05	1.5 cycle
632	14:18:55.05	2491.59	25.02	27.66	31.00	34.79	37.69	39.20	39.28	37.96	1.5 cycle
636	14:19:06.80	2503.29	25.14	27.86	31.27	35.11	38.08	39.99	40.93	40.24	1.5 cycle
640	14:19:18.89	2515.32	25.33	28.16	31.84	36.12	39.61	41.86	42.57	42.07	1.5 cycle
644	14:19:30.97	2527.45	25.13	27.86	31.44	35.68	39.15	41.15	41.30	39.92	1.5 cycle
648	14:19:43.05	2539.48	24.97	27.45	30.70	34.55	37.68	39.99	41.20	40.94	1.5 cycle
652	14:19:54.81	2551.24	24.84	27.35	30.58	34.46	38.05	41.31	43.44	43.74	1.5 cycle
656	14:20:06.94	2563.38	24.75	27.19	30.46	34.53	38.22	41.35	43.46	43.80	1.5 cycle
660	14:20:19.03	2575.46	24.65	27.19	30.77	35.35	39.55	42.65	44.04	43.65	1.5 cycle
664	14:20:30.67	2587.16	24.53	27.11	30.72	35.54	40.24	44.01	45.80	44.52	1.5 cycle
668	14:20:42.81	2599.19	24.92	27.09	30.25	34.29	38.26	41.70	43.61	42.75	1.5 cycle
672	14:20:54.57	2611.00	17.11	17.76	18.92	20.17	20.85	20.38	18.70	18.31	1.5 cycle
676	14:21:06.54	2622.92	30.78	14.14	254.60	460.69	476.33	439.38	340.16	2183.27	1.5 cycle

TABLE 3

SAMPLE POSITIONING DATA FILE
(MBR1.NAV, partial)

NORTH EAST ELEV DEPTH TIME

```
2,615619,2.027178E+6,-25.4,31.9,"13:49:20.56 "
3,615624,2.027178E+6,-24.2,30.7,"13:49:21.57 "
4,615629,2.027177E+6,-24,30.5,"13:49:22.56 "
5,615634,2.027177E+6,-23.3,29.8,"13:49:23.56 "
6,615642,2.027177E+6,-20.6,27.1,"13:49:25.57 "
7,615647,2.027177E+6,-20.7,27.2,"13:49:26.56 "
8,615651,2.027177E+6,-18.9,25.4,"13:49:27.56 "
9,615655,2.027177E+6,-18.2,24.7,"13:49:28.56 "
10,615659,2.027177E+6,-18.8,25.3,"13:49:29.57 "
11,615664,2.027177E+6,-17.4,23.9,"13:49:30.56 "
12,615667,2.027177E+6,-17.2,23.7,"13:49:31.57 "
13,615672,2.027178E+6,-17.3,23.8,"13:49:32.57 "
14,615676,2.027179E+6,-16.7,23.2,"13:49:33.57 "
15,615681,2.027179E+6,-15.8,22.3,"13:49:34.57 "
16,615685,2.02718E+6,-15.7,22.2,"13:49:35.57 "
17,615690,2.027181E+6,-15.9,22.4,"13:49:36.57 "
18,615694,2.027182E+6,-16.3,22.8,"13:49:37.57 "
19,615698,2.027183E+6,-16.6,23.1,"13:49:38.56 "
20,615702,2.027185E+6,-16.3,22.8,"13:49:39.56 "
21,615707,2.027186E+6,-15.6,22.1,"13:49:40.57 "
22,615717,2.027188E+6,-19.3,25.8,"13:49:42.57 "
23,615722,2.027189E+6,-20.4,26.9,"13:49:43.57 "
24,615727,2.02719E+6,-19.5,26,"13:49:44.57 "
25,615732,2.027191E+6,-19.4,25.9,"13:49:45.57 "
26,615737,2.027193E+6,-18.6,25.1,"13:49:46.57 "
27,615742,2.027194E+6,-19.2,25.7,"13:49:47.56 "
28,615762,2.027199E+6,-21.7,28.2,"13:49:51.57 "
29,615767,2.0272E+6,-21.8,28.3,"13:49:52.57 "
30,615773,2.027201E+6,-21.2,27.7,"13:49:53.57 "
31,615778,2.027202E+6,-21.1,27.6,"13:49:54.56 "
32,615783,2.027203E+6,-20.6,27.1,"13:49:55.57 "
33,615788,2.027204E+6,-20.3,26.8,"13:49:56.57 "
34,615798,2.027206E+6,-20.3,26.8,"13:49:58.57 "
35,615803,2.027207E+6,-20.4,26.9,"13:49:59.57 "
36,615808,2.027208E+6,-21,27.5,"13:50:00.57 "
37,615813,2.027209E+6,-22.6,29.1,"13:50:01.57 "
38,615833,2.027214E+6,-24.8,31.3,"13:50:05.57 "
39,615838,2.027215E+6,-26.4,32.9,"13:50:06.57 "
40,615842,2.027217E+6,-26.5,33,"13:50:07.57 "
41,615852,2.027219E+6,-25,31.5,"13:50:09.57 "
42,615856,2.027221E+6,-23.9,30.4,"13:50:10.57 "
43,615861,2.027222E+6,-24.3,30.8,"13:50:11.56 "
44,615870,2.027224E+6,-25.3,31.8,"13:50:13.57 "
45,615875,2.027226E+6,-26.1,32.6,"13:50:14.56 "
46,615879,2.027228E+6,-27.5,34,"13:50:15.57 "
47,615883,2.027229E+6,-27.7,34.2,"13:50:16.57 "
48,615887,2.02723E+6,-28,34.5,"13:50:17.57 "
49,615901,2.027234E+6,-28.6,35.1,"13:50:20.57 "
50,615905,2.027235E+6,-29.9,36.4,"13:50:21.57 "
51,615933,2.027243E+6,-33.1,39.6,"13:50:27.56 "
52,615938,2.027244E+6,-35.8,42.3,"13:50:28.57 "
```

TABLE 4

SAMPLE MERGED DATA FILE (MBR1.OUT)

					AT BOAT				AT TDC CENTER			
NTDC	TIME	TSEC	XBOAT	XMID	NORTH	EAST	DEPTH	ELEV	NORTH	EAST	DEPTH	ELEV
44	"13:49:34	731	284	0	615682	2027179	-22	-16	0	0	0	0
48	"13:49:46	743	342	58	615739	2027193	-25	-19	0	0	0	0
52	"13:49:58	755	405	121	615800	2027206	-27	-20	0	0	0	0
56	"13:50:10	767	465	181	615858	2027221	-31	-24	0	0	0	0
60	"13:50:22	779	519	235	615910	2027236	-37	-30	0	0	0	0
64	"13:50:34	791	579	295	615968	2027249	-41	-35	615692	2027182	-23	-16
68	"13:50:46	803	636	352	616025	2027254	-40	-34	615748	2027195	-26	-19
72	"13:50:58	815	699	415	616088	2027261	-36	-29	615810	2027209	-27	-21
76	"13:51:10	827	767	483	616156	2027269	-28	-21	615876	2027227	-33	-26
80	"13:51:22	839	830	546	616216	2027287	-35	-28	615936	2027242	-39	-32
84	"13:51:34	851	886	602	616269	2027304	-43	-36	615991	2027251	-41	-34
88	"13:51:46	863	944	660	616324	2027320	-50	-43	616049	2027257	-39	-32
92	"13:51:58	875	1005	721	616385	2027331	-46	-39	616110	2027264	-33	-26
96	"13:52:10	887	1070	786	616448	2027343	-42	-36	616173	2027274	-30	-23
100	"13:52:22	899	1135	851	616513	2027349	-42	-35	616235	2027294	-38	-31
104	"13:52:34	911	1202	918	616580	2027360	-40	-33	616300	2027313	-47	-40
108	"13:52:46	923	1270	986	616647	2027369	-35	-28	616366	2027327	-47	-41
112	"13:52:58	935	1336	1052	616712	2027378	-32	-26	616431	2027340	-43	-37
116	"13:53:10	947	1399	1115	616772	2027398	-35	-29	616494	2027347	-42	-35
120	"13:53:22	959	1462	1178	616833	2027417	-34	-28	616556	2027356	-40	-34
124	"13:53:34	971	1524	1240	616892	2027435	-38	-31	616617	2027365	-37	-31
128	"13:53:46	983	1588	1304	616954	2027449	-39	-33	616681	2027374	-34	-27
132	"13:53:58	995	1657	1373	617022	2027455	-35	-29	616747	2027390	-34	-28
136	"13:54:10	1007	1722	1438	617087	2027466	-31	-25	616809	2027410	-35	-28
140	"13:54:22	1018	1786	1502	617149	2027479	-32	-25	616870	2027428	-36	-30
144	"13:54:34	1031	1852	1568	617214	2027493	-34	-28	616934	2027444	-39	-32
148	"13:54:46	1043	1920	1636	617281	2027506	-27	-21	617002	2027453	-36	-30
152	"13:54:57	1054	1988	1704	617347	2027518	-27	-21	617069	2027463	-33	-26
156	"13:55:10	1067	2058	1774	617416	2027535	-23	-17	617138	2027476	-32	-25
160	"13:55:22	1079	2128	1844	617481	2027561	-33	-26	617206	2027491	-34	-27
164	"13:55:33	1090	2190	1906	617539	2027581	-36	-29	617267	2027503	-29	-22
168	"13:55:45	1102	2255	1971	617602	2027599	-34	-28	617331	2027515	-27	-21
172	"13:55:58	1115	2323	2039	617668	2027613	-33	-26	617397	2027531	-24	-18
176	"13:56:09	1126	2388	2104	617732	2027627	-31	-24	617458	2027552	-29	-23
180	"13:56:21	1138	2453	2169	617794	2027647	-32	-25	617520	2027574	-35	-28
184	"13:56:33	1150	2521	2237	617857	2027670	-23	-17	617584	2027594	-35	-28
188	"13:56:46	1162	2585	2301	617916	2027696	-27	-21	617647	2027609	-33	-27
192	"13:56:57	1174	2643	2359	617968	2027721	-24	-17	617703	2027621	-32	-25
196	"13:57:09	1186	2704	2420	618020	2027753	-26	-19	617762	2027636	-31	-25
200	"13:57:21	1198	2762	2478	618067	2027787	-25	-19	617817	2027655	-29	-22
204	"13:57:33	1210	2823	2539	618116	2027825	-27	-21	617874	2027678	-24	-18
208	"13:57:45	1222	2884	2600	618163	2027862	-32	-25	617929	2027703	-26	-20
212	"13:57:57	1234	2947	2663	618213	2027901	-35	-29	617985	2027732	-24	-18
216	"13:58:09	1246	3001	2717	618262	2027924	-30	-23	618031	2027761	-26	-19
220	"13:58:21	1258	3054	2770	618312	2027944	-26	-20	618074	2027792	-26	-19
224	"13:58:33	1270	3112	2828	618362	2027972	-29	-23	618119	2027828	-28	-21
228	"13:58:45	1282	3177	2893	618416	2028006	-30	-23	618170	2027867	-32	-26
232	"13:58:57	1294	3238	2954	618467	2028042	-31	-24	618220	2027904	-34	-28
236	"13:59:09	1306	3296	3012	618517	2028072	-35	-28	618272	2027928	-29	-22
240	"13:59:21	1318	3361	3077	618575	2028099	-34	-28	618331	2027955	-27	-21

244	"13:59:33	1330	3424	3140	618634	2028121	-31	-24	618385	2027987	-29	-23
248	"13:59:45	1342	3488	3204	618694	2028143	-30	-24	618439	2028022	-30	-24
252	"13:59:57	1354	3553	3269	618754	2028169	-35	-28	618493	2028058	-33	-26
256	"14:00:09	1366	3616	3332	618810	2028198	-34	-28	618549	2028087	-34	-28
260	"14:00:21	1378	3682	3398	618868	2028228	-36	-30	618610	2028112	-32	-26
264	"14:00:33	1390	3745	3461	618924	2028258	-38	-31	618669	2028134	-30	-24
268	"14:00:45	1402	3821	3537	618994	2028288	-40	-34	618739	2028163	-34	-27
272	"14:00:57	1414	3885	3601	619051	2028318	-40	-34	618797	2028191	-35	-28
276	"14:01:09	1426	3946	3662	619108	2028339	-39	-33	618851	2028219	-36	-29
280	"14:01:21	1438	4003	3719	619159	2028364	-40	-34	618901	2028246	-37	-30
284	"14:01:33	1450	4065	3781	619217	2028386	-41	-34	618957	2028272	-39	-32
288	"14:01:45	1462	4127	3843	619279	2028395	-39	-33	619014	2028298	-40	-34
292	"14:01:57	1474	4188	3904	619335	2028417	-40	-33	619068	2028324	-40	-33
296	"14:02:09	1486	4251	3967	619391	2028445	-37	-31	619126	2028348	-40	-33
300	"14:02:20	1497	4299	4015	619436	2028465	-33	-26	619171	2028368	-40	-34
304	"14:02:33	1510	4355	4071	619486	2028489	-32	-26	619224	2028387	-40	-34
308	"14:02:45	1522	4419	4135	619543	2028518	-31	-25	619286	2028398	-39	-33
312	"14:02:56	1533	4484	4200	619599	2028551	-32	-26	619346	2028422	-39	-33
316	"14:03:09	1545	4553	4269	619659	2028584	-30	-24	619408	2028452	-36	-29
320	"14:03:21	1558	4613	4329	619713	2028611	-30	-24	619463	2028478	-32	-26
324	"14:03:32	1569	4669	4385	619762	2028638	-29	-23	619513	2028503	-32	-25
328	"14:03:45	1581	4726	4442	619812	2028666	-25	-18	619563	2028530	-32	-25
332	"14:03:57	1594	4783	4499	619861	2028695	-20	-13	619612	2028558	-32	-25
336	"14:04:09	1606	4836	4552	619904	2028726	-20	-14	619659	2028584	-30	-24
340	"14:04:20	1617	4892	4608	619950	2028757	-20	-13	619708	2028609	-30	-24
344	"14:04:32	1629	4949	4665	619999	2028787	-19	-12	619759	2028636	-29	-23
348	"14:04:44	1641	5001	4717	620040	2028818	-19	-12	619804	2028661	-25	-19
352	"14:04:56	1653	5057	4773	620087	2028850	-20	-13	619853	2028690	-21	-14
356	"14:05:08	1665	5115	4831	620135	2028881	-19	-12	619900	2028723	-20	-14
360	"14:05:20	1677	5177	4893	620187	2028917	-16	-10	619952	2028758	-20	-13
364	"14:05:32	1689	5245	4961	620239	2028959	-18	-11	620008	2028794	-19	-12
368	"14:05:44	1701	5307	5023	620285	2029002	-18	-11	620059	2028831	-19	-13
372	"14:05:56	1713	5373	5089	620330	2029049	-19	-12	620114	2028868	-19	-13
376	"14:06:08	1725	5433	5149	620371	2029093	-21	-15	620163	2028901	-17	-11
380	"14:06:20	1737	5474	5190	620402	2029121	-21	-15	620196	2028925	-17	-10
384	"14:06:32	1749	5513	5229	620430	2029147	-21	-15	620227	2028950	-17	-11
388	"14:06:44	1761	5554	5270	620461	2029175	-21	-14	620258	2028977	-18	-11
392	"14:06:56	1773	5595	5311	620490	2029202	-21	-14	620287	2029004	-18	-11
396	"14:07:08	1785	5636	5352	620521	2029230	-21	-14	620316	2029034	-18	-12
400	"14:07:20	1797	5676	5392	620551	2029258	-21	-14	620344	2029063	-20	-13
404	"14:07:32	1809	5715	5431	620579	2029284	-20	-14	620370	2029092	-21	-15
408	"14:07:44	1821	5761	5477	620619	2029308	-21	-15	620404	2029123	-21	-15
412	"14:07:56	1833	5817	5533	620672	2029324	-20	-14	620445	2029161	-21	-15
416	"14:08:08	1845	5876	5592	620727	2029347	-18	-12	620489	2029201	-21	-14
420	"14:08:20	1857	5938	5654	620779	2029380	-18	-11	620534	2029243	-21	-14
424	"14:08:32	1869	6015	5731	620853	2029403	-17	-11	620593	2029292	-21	-14
428	"14:08:44	1881	6084	5800	620914	2029434	-18	-12	620656	2029319	-21	-14
432	"14:08:56	1893	6155	5871	620972	2029474	-18	-12	620722	2029345	-19	-12
436	"14:09:08	1905	6216	5932	621012	2029521	-20	-13	620774	2029377	-18	-11
440	"14:09:20	1917	6274	5990	621047	2029568	-21	-15	620829	2029395	-18	-11
444	"14:09:32	1929	6326	6042	621057	2029619	-21	-14	620877	2029415	-18	-11
448	"14:09:44	1941	6390	6106	621099	2029666	-21	-15	620932	2029446	-18	-12
452	"14:09:56	1953	6455	6171	621149	2029708	-22	-16	620983	2029487	-19	-12
456	"14:10:08	1965	6510	6226	621191	2029745	-20	-14	621018	2029530	-20	-13
460	"14:10:20	1977	6573	6289	621241	2029781	-21	-15	621050	2029582	-21	-15
464	"14:10:31	1988	6638	6354	621297	2029816	-20	-14	621076	2029640	-21	-15
468	"14:10:44	2001	6701	6417	621350	2029850	-22	-16	621120	2029684	-22	-15
472	"14:10:56	2013	6762	6478	621401	2029883	-22	-16	621166	2029723	-22	-15
476	"14:11:08	2025	6825	6541	621451	2029921	-22	-16	621215	2029762	-21	-14
480	"14:11:19	2036	6884	6600	621502	2029952	-22	-15	621265	2029796	-21	-14

484	"14:11:31 2049	6949	6665	621557	2029986	-21	-15	621320	2029831	-21	-15
488	"14:11:44 2061	7012	6728	621612	2030017	-21	-14	621373	2029864	-22	-16
492	"14:11:55 2072	7069	6785	621660	2030047	-20	-14	621419	2029897	-22	-16
496	"14:12:07 2084	7135	6851	621719	2030077	-20	-14	621473	2029935	-22	-16
500	"14:12:19 2096	7207	6923	621784	2030108	-20	-14	621535	2029972	-21	-15
504	"14:12:32 2108	7275	6991	621842	2030144	-17	-11	621594	2030006	-21	-14
508	"14:12:43 2120	7338	7054	621895	2030177	-20	-13	621647	2030039	-20	-14
512	"14:12:55 2132	7398	7114	621944	2030212	-19	-13	621700	2030068	-20	-14
516	"14:13:07 2144	7458	7174	621991	2030249	-20	-13	621754	2030094	-20	-14
520	"14:13:19 2156	7517	7233	622034	2030289	-19	-12	621805	2030122	-19	-13
524	"14:13:31 2168	7581	7297	622081	2030333	-22	-15	621860	2030155	-18	-12
528	"14:13:43 2180	7646	7362	622129	2030377	-22	-15	621915	2030191	-20	-13
532	"14:13:55 2192	7713	7429	622178	2030422	-22	-15	621968	2030231	-20	-13
536	"14:14:07 2204	7778	7494	622227	2030465	-25	-18	622017	2030274	-19	-13
540	"14:14:19 2216	7841	7557	622276	2030505	-27	-21	622064	2030317	-21	-14
544	"14:14:31 2228	7905	7621	622328	2030543	-26	-19	622111	2030360	-22	-15
548	"14:14:43 2240	7972	7688	622376	2030589	-25	-19	622160	2030405	-22	-15
552	"14:14:55 2252	8038	7754	622421	2030637	-26	-20	622209	2030449	-24	-17
556	"14:15:07 2264	8106	7822	622465	2030689	-27	-21	622261	2030492	-27	-20
560	"14:15:19 2276	8174	7890	622509	2030742	-28	-21	622316	2030534	-26	-20
564	"14:15:31 2288	8241	7957	622552	2030792	-26	-19	622365	2030579	-25	-19
568	"14:15:43 2300	8305	8021	622594	2030840	-29	-22	622410	2030625	-26	-20
572	"14:15:55 2312	8369	8085	622638	2030888	-23	-16	622451	2030673	-27	-20
576	"14:16:07 2324	8435	8151	622683	2030936	-24	-18	622494	2030724	-28	-21
580	"14:16:19 2336	8500	8216	622727	2030983	-25	-19	622535	2030773	-26	-20
584	"14:16:31 2348	8565	8281	622776	2031026	-23	-17	622578	2030822	-27	-21
588	"14:16:43 2360	8633	8349	622831	2031067	-21	-14	622624	2030873	-25	-18
592	"14:16:55 2372	8698	8414	622885	2031102	-21	-15	622668	2030921	-24	-17
596	"14:17:07 2384	8767	8483	622942	2031142	-20	-14	622716	2030971	-25	-18
600	"14:17:19 2396	8831	8547	622992	2031180	-20	-14	622762	2031014	-24	-17
604	"14:17:31 2408	8896	8612	623043	2031221	-21	-14	622814	2031054	-22	-15
608	"14:17:43 2420	8961	8677	623092	2031264	-20	-14	622867	2031090	-21	-15
612	"14:17:54 2431	9032	8748	623145	2031311	-20	-14	622926	2031131	-20	-14
616	"14:18:07 2443	9095	8811	623192	2031353	-21	-14	622976	2031168	-20	-14
620	"14:18:19 2456	9157	8873	623242	2031390	-20	-13	623025	2031207	-21	-14
624	"14:18:31 2468	9224	8940	623297	2031428	-22	-15	623076	2031250	-21	-14
628	"14:18:43 2479	9293	9009	623351	2031470	-20	-14	623128	2031295	-20	-14
632	"14:18:55 2492	9365	9081	623413	2031509	-22	-15	623182	2031343	-21	-14
636	"14:19:06 2503	9433	9149	623468	2031547	-21	-14	623235	2031385	-20	-13
640	"14:19:18 2515	9501	9217	623521	2031590	-21	-14	623291	2031424	-22	-15
644	"14:19:30 2527	9562	9278	623570	2031627	-22	-16	623340	2031461	-21	-14
648	"14:19:43 2539	9627	9343	623622	2031666	-23	-16	623394	2031497	-21	-15
652	"14:19:54 2551	9697	9413	623678	2031708	-24	-17	623452	2031536	-21	-15
656	"14:20:06 2563	9773	9489	623738	2031755	-23	-17	623512	2031582	-21	-14

TABLE 5

SAMPLE INVES OUTPUT FILE (MB1-108.OUT)

```
  INVES:  1-D RESISTIVITY INVERSON PROGRAM

 ********************************************************************************
    Output File Name:  mb1-108.out
 ********************************************************************************

              For a SCHLUMBERGER ARRAY


 DA - Source of DAta:                EXISTING Data
 SP - Closest A/S SPacing:           2.01490302054227 METERS
 FI - No. of FIeld Readings:         6
 LA - No. of Model LAyers:           3
 PA - No. of Fixed PArameters:       0
 RC - RMS Percent Error Cutoff:      1
 DL - Min RMS Improvement Must Be >  .01  In Order To Continue Inversion
 IT - Max Number of Iterations:      15
 UN - UNits of Distance:             METERS

          ************ 1-D Layered Model ************
```

Layer	Initial Model Values				Final Model				Depth To Top
1	T1	10.00	R1	22.000	T1	13.12	R1	22.441	0
2	T2	0.02	R2	0.010	T2	0.02	R2	0.007	13
3			R3	40.000			R3	41.149	13

```
  Fixed Parameters:  0  of  5  Total Inversion Parameters

   Inverse Modeling RMS =       0.49

   Forward Modeling RMS =      12.85

 Final Model From ITERATION NO.   5
```

LAYER NO.	THICKNESS		RESISTIVITY	THICK*RES	THICK/RES
1	T1	13.12	R1 22.441	294.513	0.585
2	T2	0.02	R2 0.007	0.000	3.020
3			R3 41.149		

SPACING	OBSERVED	CALCULATED	% DIFF
7.500	21.680	21.814	-0.618
10.000	21.130	21.087	0.203
13.300	19.840	19.780	0.302
17.800	17.730	17.597	0.747
23.700	14.900	14.876	0.159
31.600	12.370	12.417	-0.381
42.200	11.500	11.644	-1.248
56.200	12.370	12.370	0.000

```
 RMS ERROR =      0.4923
```

TABLE 6

SAMPLE MAT AND RIVERBED ELEVATION FILE (MBR1TC.DAT)

		DIMCO AT TDC CENTER					TDC	
NTDC	TSEC (sec)	XMID (ft)	NORTH (ft)	EAST (ft)	-Riverbed- DEPTH (ft)	ELEV (ft NGVD)	MAT ELEV (ft NGVD)	R.BED ELEV
64	791	295	615692	2027182	-23	-16	-25.3	-25.8
68	803	352	615748	2027195	-26	-19	-19.1	-11.4
72	815	415	615810	2027209	-27	-21	-22.2	-19.6
76	827	483	615876	2027227	-33	-26	-32.7	-33.2
80	839	546	615936	2027242	-39	-32	-29.1	-24.9
84	851	602	615991	2027251	-41	-34	-20.6	-10.1
88	863	660	616049	2027257	-39	-32	-32.7	-32.9
92	875	721	616110	2027264	-33	-26	-32.1	-26.6
96	887	786	616173	2027274	-30	-23	-29.6	-24.3
100	899	851	616235	2027294	-38	-31	-36.0	-36.0
104	911	918	616300	2027313	-47	-40	-33.6	-26.6
108	923	986	616366	2027327	-47	-41	-36.3	-36.3
112	935	1052	616431	2027340	-43	-37	-29.0	-20.0
116	947	1115	616494	2027347	-42	-35	-32.5	-26.2
120	959	1178	616556	2027356	-40	-34	-33.3	-33.4
124	971	1240	616617	2027365	-37	-31	-29.3	-25.1
128	983	1304	616681	2027374	-34	-27	-28.9	-25.0
132	995	1373	616747	2027390	-34	-28	-28.9	-24.8
136	1007	1438	616809	2027410	-35	-28	-29.2	-24.6
140	1018	1502	616870	2027428	-36	-30	-33.3	-33.4
144	1031	1568	616934	2027444	-39	-32	-20.9	-10.2
148	1043	1636	617002	2027453	-36	-30	-30.1	-25.6
152	1054	1704	617069	2027463	-33	-26	-30.6	-25.3
156	1067	1774	617138	2027476	-32	-25	-20.3	-10.4
160	1079	1844	617206	2027491	-34	-27	-24.5	-24.5
164	1090	1906	617267	2027503	-29	-22	-30.7	-27.9
168	1102	1971	617331	2027515	-27	-21	-29.3	-29.3
172	1115	2039	617397	2027531	-24	-18	-25.8	-25.8
176	1126	2104	617458	2027552	-29	-23	-27.7	-25.6
180	1138	2169	617520	2027574	-35	-28	-28.1	-25.7
184	1150	2237	617584	2027594	-35	-28	-28.1	-28.1
188	1162	2301	617647	2027609	-33	-27	-25.3	-24.6
192	1174	2359	617703	2027621	-32	-25	-28.9	-26.3
196	1186	2420	617762	2027636	-31	-25	-28.1	-28.1
200	1198	2478	617817	2027655	-29	-22	-23.3	-11.6
204	1210	2539	617874	2027678	-24	-18	-33.4	-24.8
208	1222	2600	617929	2027703	-26	-20	-34.8	-24.9
212	1234	2663	617985	2027732	-24	-18	-28.2	-12.3
216	1246	2717	618031	2027761	-26	-19	-48.0	-17.7
220	1258	2770	618074	2027792	-26	-19	-42.2	-18.9
224	1270	2828	618119	2027828	-28	-21	-53.4	-17.6
228	1282	2893	618170	2027867	-32	-26	-46.9	-20.9
232	1294	2954	618220	2027904	-34	-28	-56.0	-18.9
236	1306	3012	618272	2027928	-29	-22	-49.2	-20.2
240	1318	3077	618331	2027955	-27	-21	-52.3	-19.6

244	1330	3140	618385	2027987	-29	-23	-55.1	-19.2
248	1342	3204	618439	2028022	-30	-24	-70.6	-18.4
252	1354	3269	618493	2028058	-33	-26	-66.6	-19.1
256	1366	3332	618549	2028087	-34	-28	-66.8	-21.6
260	1378	3398	618610	2028112	-32	-26	-49.6	-18.2
264	1390	3461	618669	2028134	-30	-24	-43.1	-18.1
268	1402	3537	618739	2028163	-34	-27	-36.0	-20.9
272	1414	3601	618797	2028191	-35	-28	-39.9	-40.4
276	1426	3662	618851	2028219	-36	-29	-27.0	-27.0
280	1438	3719	618901	2028246	-37	-30	-45.3	-44.4
284	1450	3781	618957	2028272	-39	-32	-38.3	-29.6
288	1462	3843	619014	2028298	-40	-34	-34.3	-20.1
292	1474	3904	619068	2028324	-40	-33	-42.9	-27.6
296	1486	3967	619126	2028348	-40	-33	-40.5	-25.6
300	1497	4015	619171	2028368	-40	-34	-36.8	-22.6
304	1510	4071	619224	2028387	-40	-34	-36.2	-23.7
308	1522	4135	619286	2028398	-39	-33	-30.1	-16.8
312	1533	4200	619346	2028422	-39	-33	-34.3	-25.6
316	1545	4269	619408	2028452	-36	-29	-35.7	-25.6
320	1558	4329	619463	2028478	-32	-26	-35.2	-22.8
324	1569	4385	619513	2028503	-32	-25	-35.3	-19.9
328	1581	4442	619563	2028530	-32	-25	-34.0	-17.9
332	1594	4499	619612	2028558	-32	-25	-41.8	-27.3
336	1606	4552	619659	2028584	-30	-24	-42.0	-27.3
340	1617	4608	619708	2028609	-30	-24	-37.6	-20.7
344	1629	4665	619759	2028636	-29	-23	-30.9	-14.5
348	1641	4717	619804	2028661	-25	-19	-19.5	-8.4
352	1653	4773	619853	2028690	-21	-14	-22.8	-14.0
356	1665	4831	619900	2028723	-20	-14	-23.7	-23.2
360	1677	4893	619952	2028758	-20	-13	-22.5	-22.5
364	1689	4961	620008	2028794	-19	-12	-16.6	-17.1
368	1701	5023	620059	2028831	-19	-13	-22.1	-21.8
372	1713	5089	620114	2028868	-19	-13	-14.8	-14.8
376	1725	5149	620163	2028901	-17	-11	-16.6	-17.1
380	1737	5190	620196	2028925	-17	-10	-14.2	-14.2
384	1749	5229	620227	2028950	-17	-11	-14.9	-14.4
388	1761	5270	620258	2028977	-18	-11	-14.3	-14.8
392	1773	5311	620287	2029004	-18	-11		
396	1785	5352	620316	2029034	-18	-12	-11.5	-5.0
400	1797	5392	620344	2029063	-20	-13		
404	1809	5431	620370	2029092	-21	-15	-15.4	-8.9
408	1821	5477	620404	2029123	-21	-15		
412	1833	5533	620445	2029161	-21	-15	-23.0	-22.2
416	1845	5592	620489	2029201	-21	-14		
420	1857	5654	620534	2029243	-21	-14	-11.5	-5.0
424	1869	5731	620593	2029292	-21	-14		
428	1881	5800	620656	2029319	-21	-14	-10.6	-0.2
432	1893	5871	620722	2029345	-19	-12	-17.6	-14.7
436	1905	5932	620774	2029377	-18	-11	-13.1	-6.4
440	1917	5990	620829	2029395	-18	-11		
444	1929	6042	620877	2029415	-18	-11	-12.5	-5.4
448	1941	6106	620932	2029446	-18	-12		
452	1953	6171	620983	2029487	-19	-12	-9.7	-0.1
456	1965	6226	621018	2029530	-20	-13	-11.5	-5.0
460	1977	6289	621050	2029582	-21	-15		
464	1988	6354	621076	2029640	-21	-15	-18.7	-15.2
468	2001	6417	621120	2029684	-22	-15	-11.5	-5.0
472	2013	6478	621166	2029723	-22	-15		
476	2025	6541	621215	2029762	-21	-14	-11.5	-5.0
480	2036	6600	621265	2029796	-21	-14		

484	2049	6665	621320	2029831	-21	-15	-13.2	-5.0
488	2061	6728	621373	2029864	-22	-16		
492	2072	6785	621419	2029897	-22	-16	-15.0	-8.0
496	2084	6851	621473	2029935	-22	-16		
500	2096	6923	621535	2029972	-21	-15	-17.2	-11.3
504	2108	6991	621594	2030006	-21	-14	-17.2	-11.3
508	2120	7054	621647	2030039	-20	-14	-18.1	-14.9
512	2132	7114	621700	2030068	-20	-14		
516	2144	7174	621754	2030094	-20	-14	-16.2	-12.8
520	2156	7233	621805	2030122	-19	-13		
524	2168	7297	621860	2030155	-18	-12	-13.6	-11.3
528	2180	7362	621915	2030191	-20	-13		
532	2192	7429	621968	2030231	-20	-13	-12.3	-6.6
536	2204	7494	622017	2030274	-19	-13		
540	2216	7557	622064	2030317	-21	-14	-14.0	-9.8
544	2228	7621	622111	2030360	-22	-15	-14.5	-9.7
548	2240	7688	622160	2030405	-22	-15	-15.4	-10.9
552	2252	7754	622209	2030449	-24	-17	-19.2	-13.1
556	2264	7822	622261	2030492	-27	-20	0	0
560	2276	7890	622316	2030534	-26	-20	0	0
564	2288	7957	622365	2030579	-25	-19	0	0
568	2300	8021	622410	2030625	-26	-20	0	0
572	2312	8085	622451	2030673	-27	-20		
576	2324	8151	622494	2030724	-28	-21		
580	2336	8216	622535	2030773	-26	-20		
584	2348	8281	622578	2030822	-27	-21		
588	2360	8349	622624	2030873	-25	-18		
592	2372	8414	622668	2030921	-24	-17		
596	2384	8483	622716	2030971	-25	-18		
600	2396	8547	622762	2031014	-24	-17		
604	2408	8612	622814	2031054	-22	-15		
608	2420	8677	622867	2031090	-21	-15	0	0
612	2431	8748	622926	2031131	-20	-14		
616	2443	8811	622976	2031168	-20	-14		
620	2456	8873	623025	2031207	-21	-14		
624	2468	8940	623076	2031250	-21	-14		
628	2479	9009	623128	2031295	-20	-14		
632	2492	9081	623182	2031343	-21	-14		
636	2503	9149	623235	2031385	-20	-13		
640	2515	9217	623291	2031424	-22	-15		
644	2527	9278	623340	2031461	-21	-14		
648	2539	9343	623394	2031497	-21	-15		
652	2551	9413	623452	2031536	-21	-15		
656	2563	9489	623512	2031582	-21	-14	0	0

FIGURES

A. EQUIPMENT CONFIGURATION

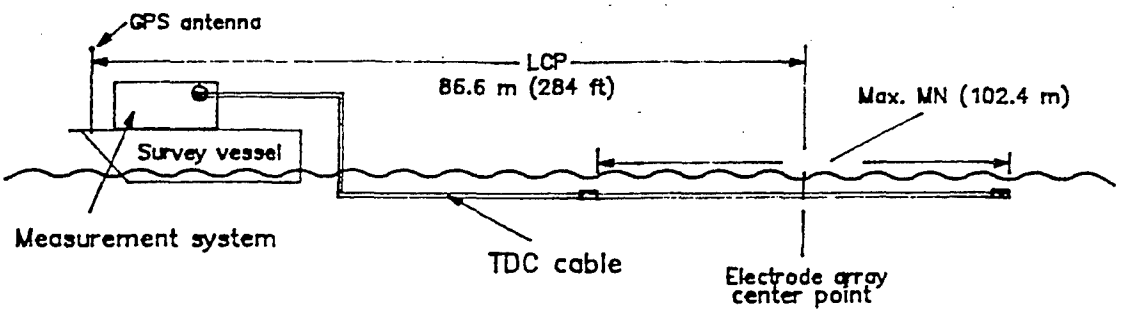

B. TDC MEASUREMENT SYSTEM SCHEMATIC

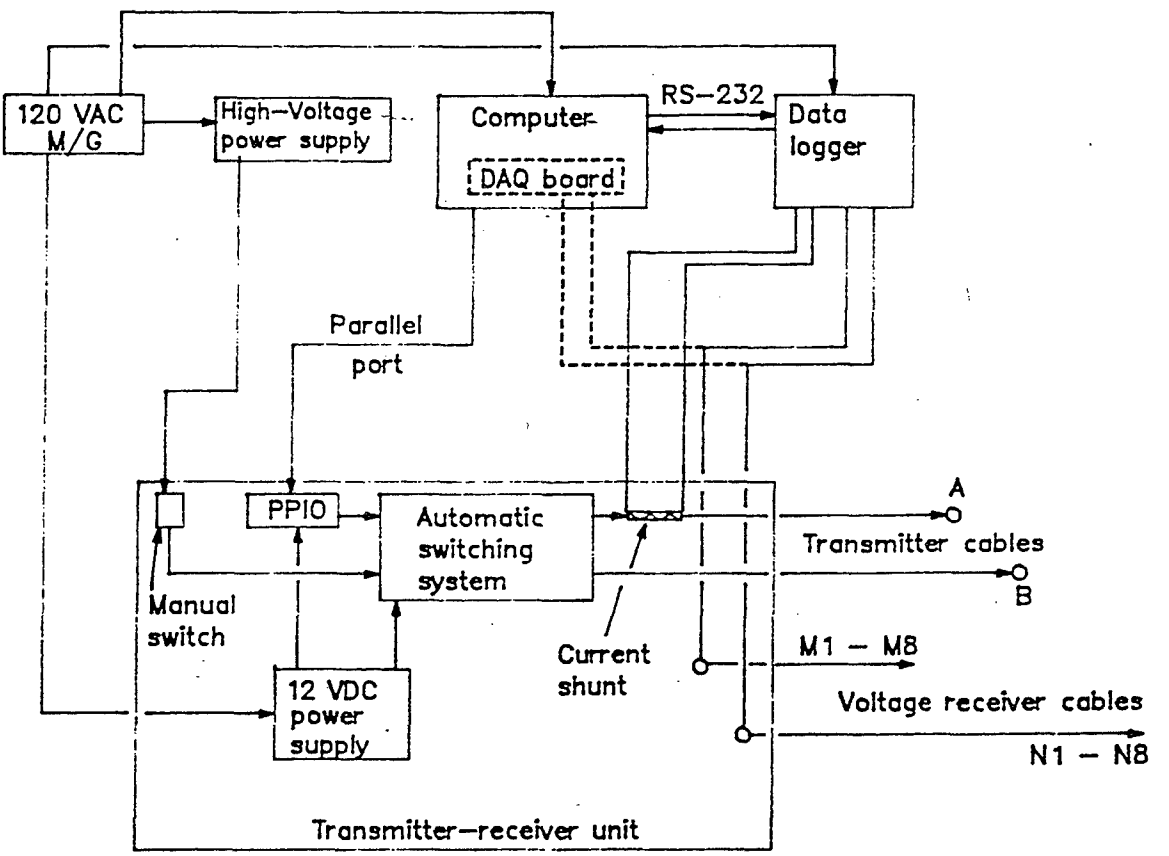

SP SURVEYS Geophysical Consultants	Towed Direct-Current Electrical Resistivity System (not to scale)	Figure 1

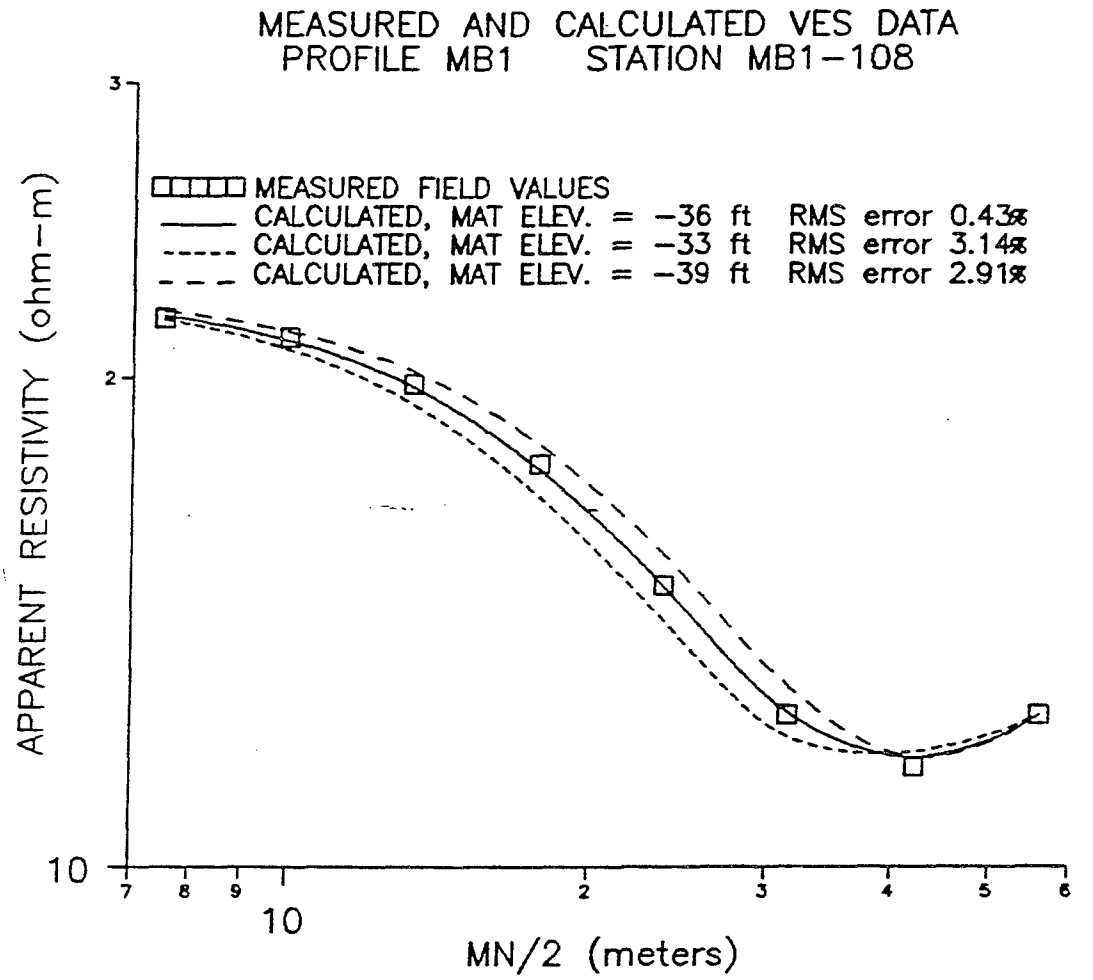

SP SURVEYS Geophysical Consultants	Mat Depth Resolution Study Missouri Bend Station MB1-108	Figure 2

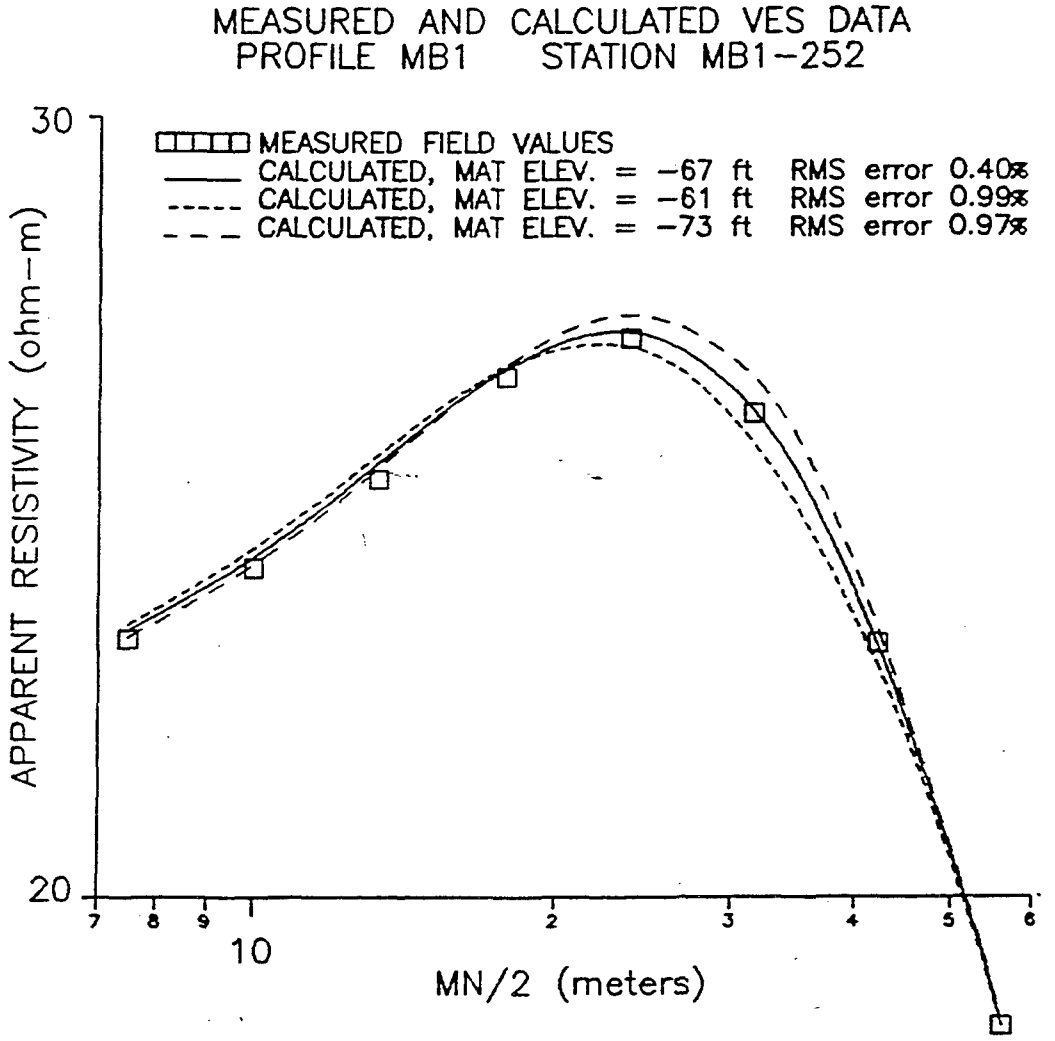

SP SURVEYS Geophysical Consultants	Mat Depth Resolution Study Missouri Bend Station MB1-252	Figure 3

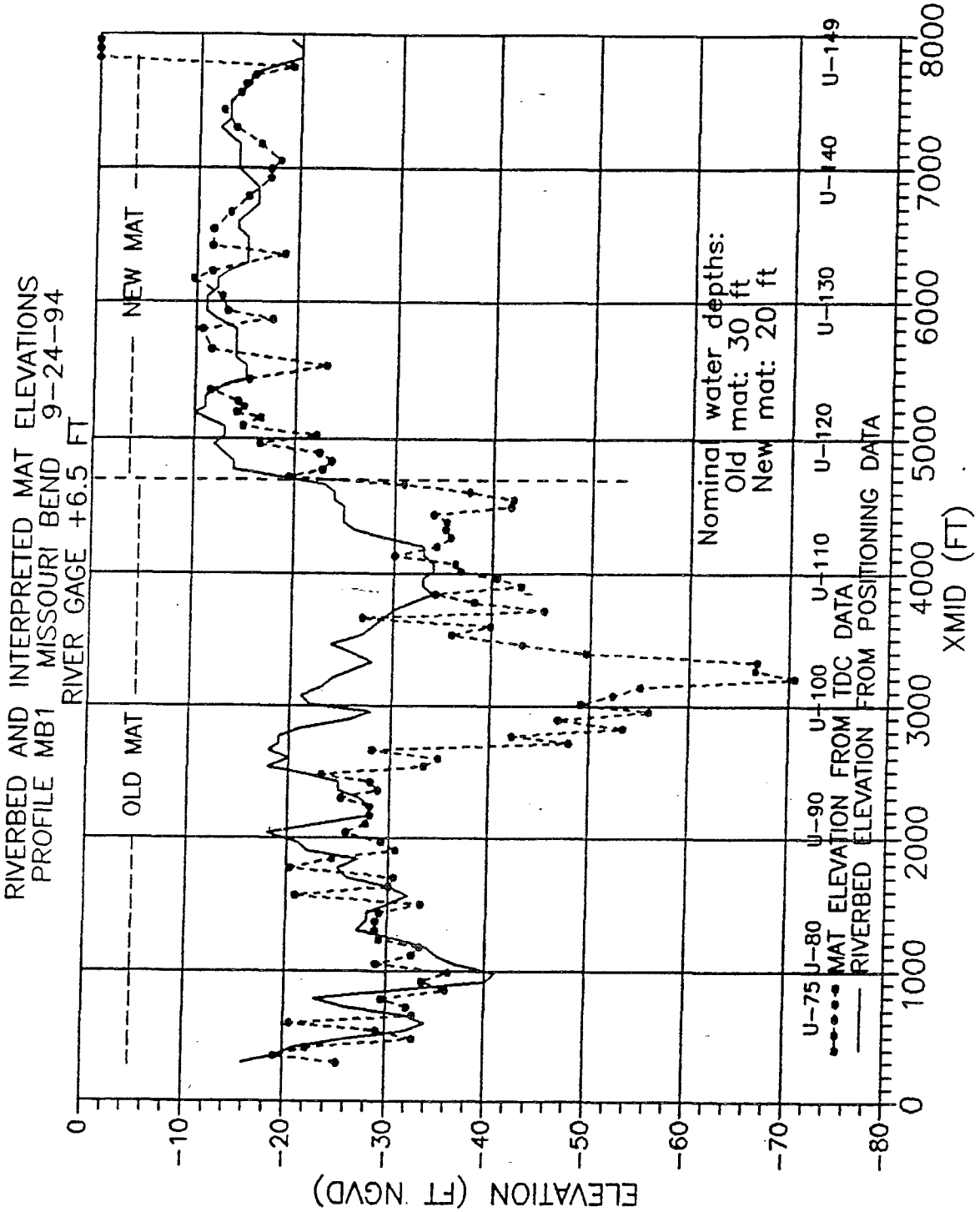

SP SURVEYS Geophysical Consultants	Mat and River Bed Elevation Plots Profile MB1 Missouri Bend	Figure 4

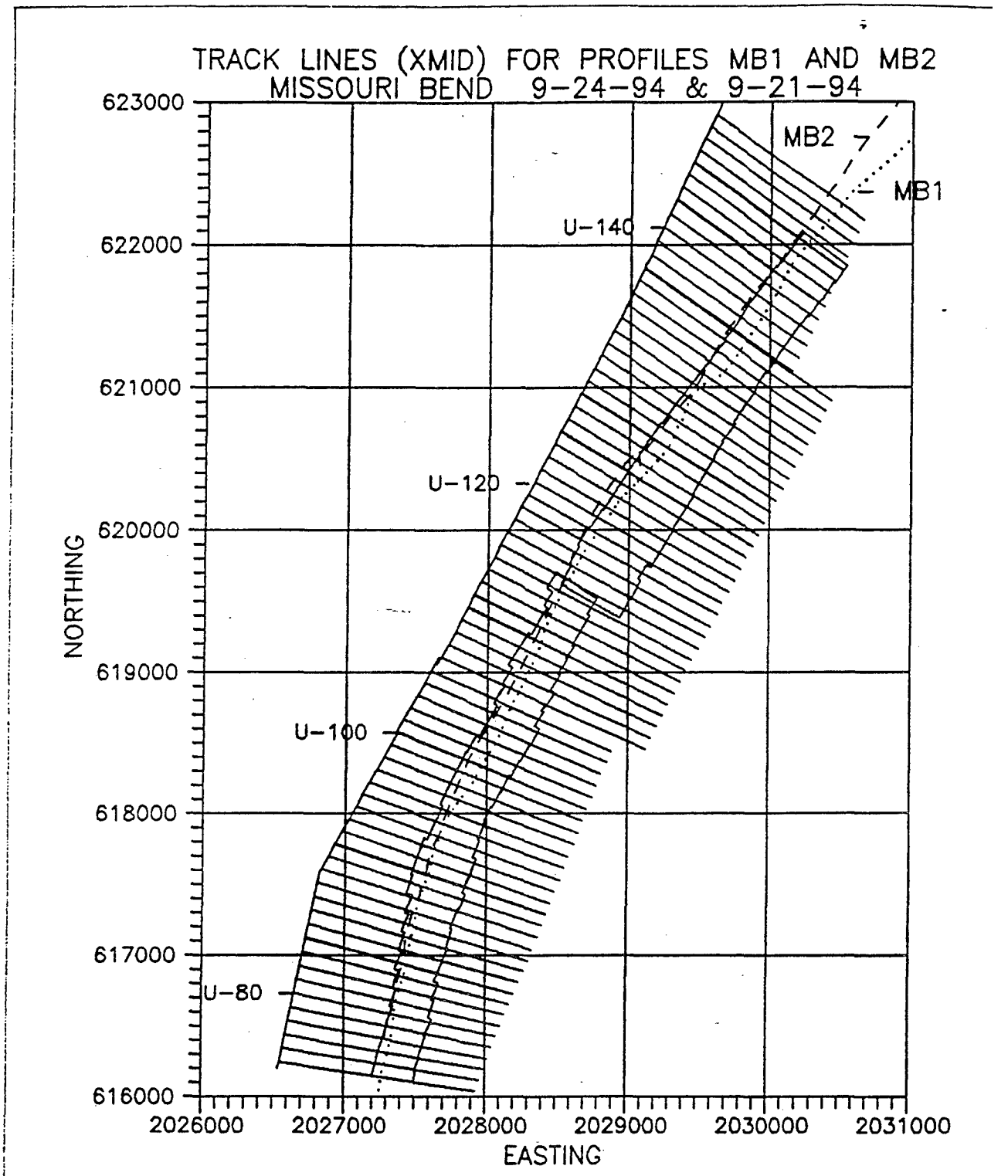

SP SURVEYS Geophysical Consultants	Survey Line Locations Profiles MB1 and MB2 Missouri Bend	Figure 5

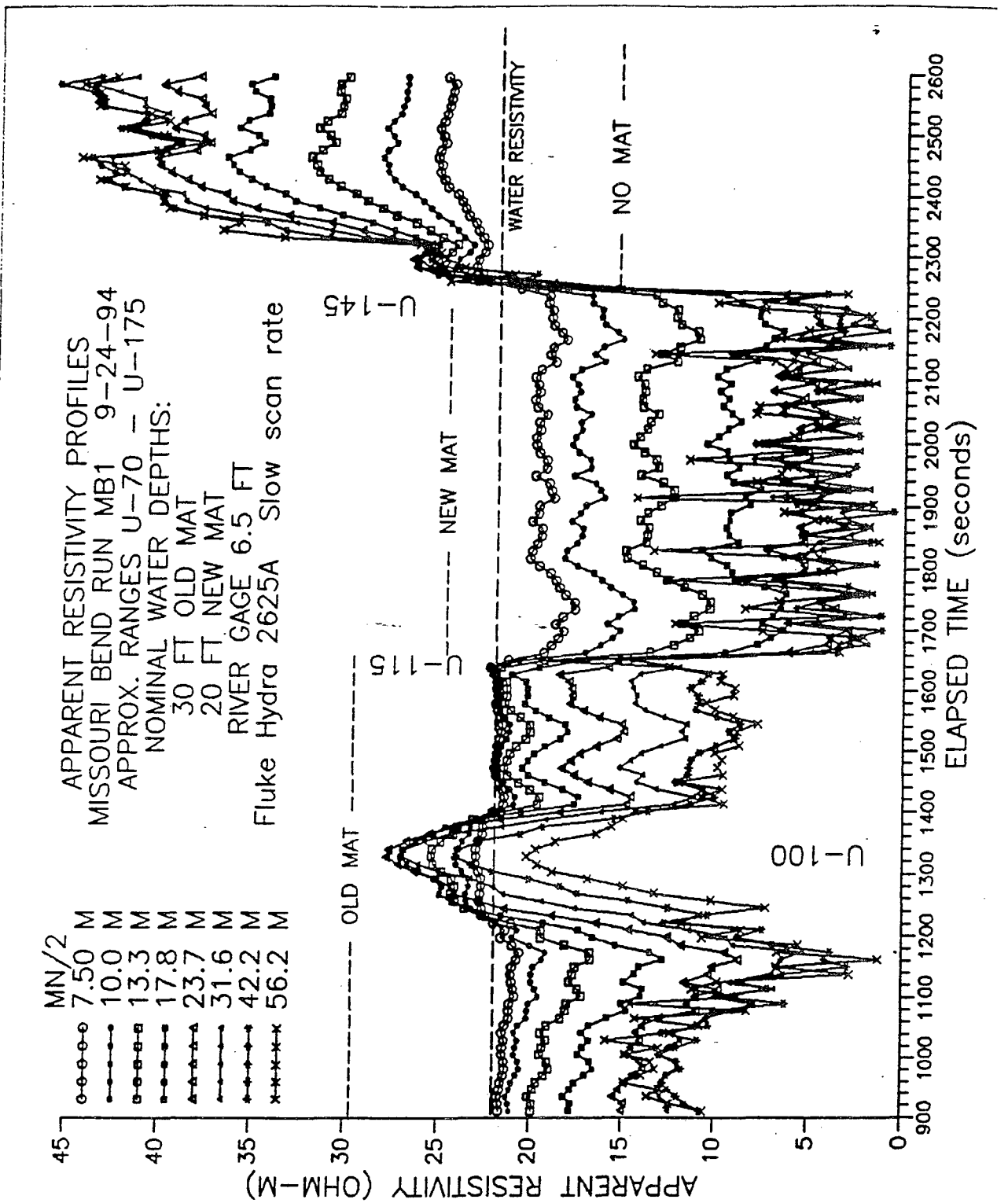

SP SURVEYS	Apparent Resistivity Plots	Figure
Geophysical Consultants	Profile MB1 Missouri Bend	6

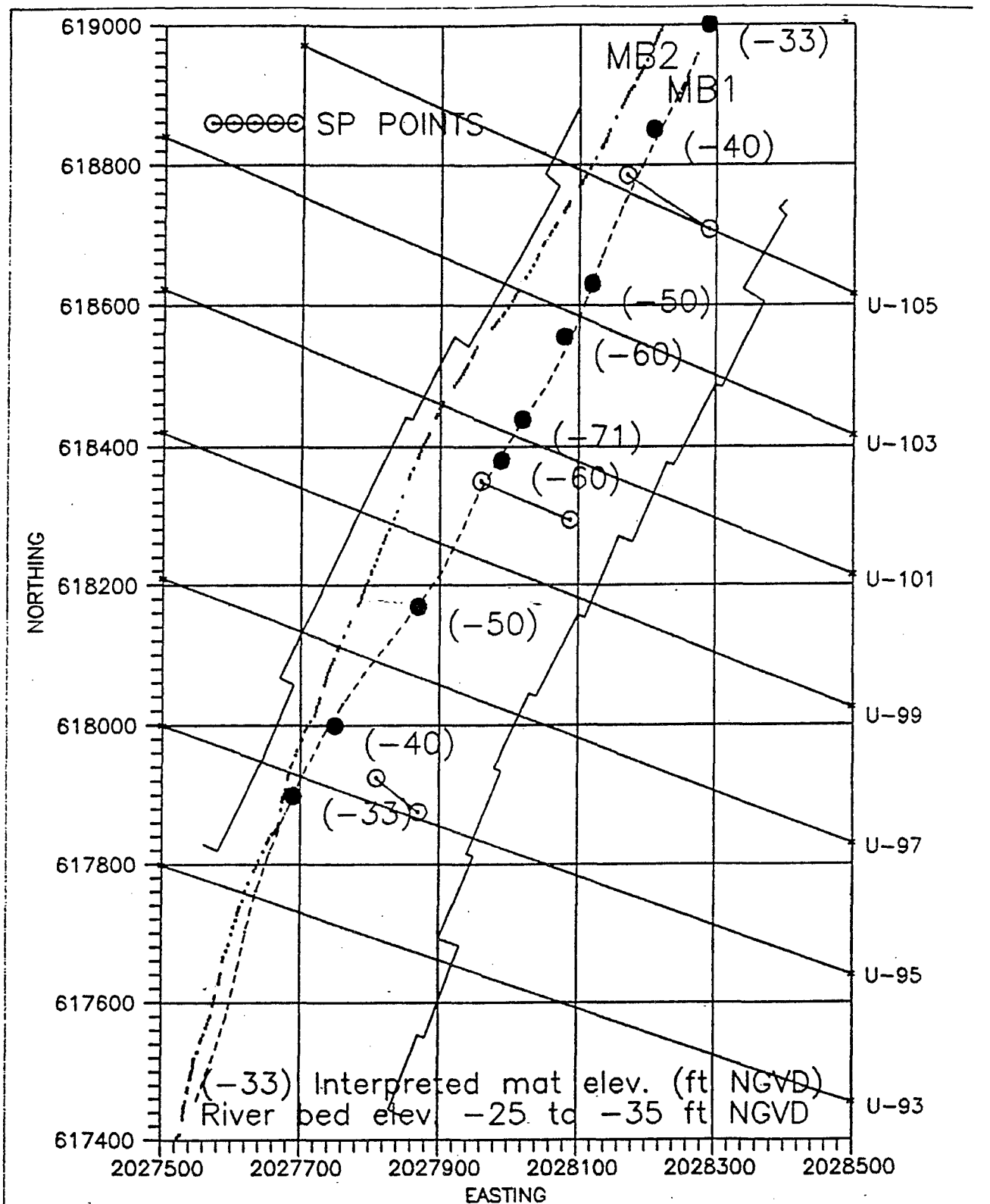

SP SURVEYS Geophysical Consultants	Plan Map Area of Buried Mat Profiles MB1 and MB2 Missouri Bend	Figure 7

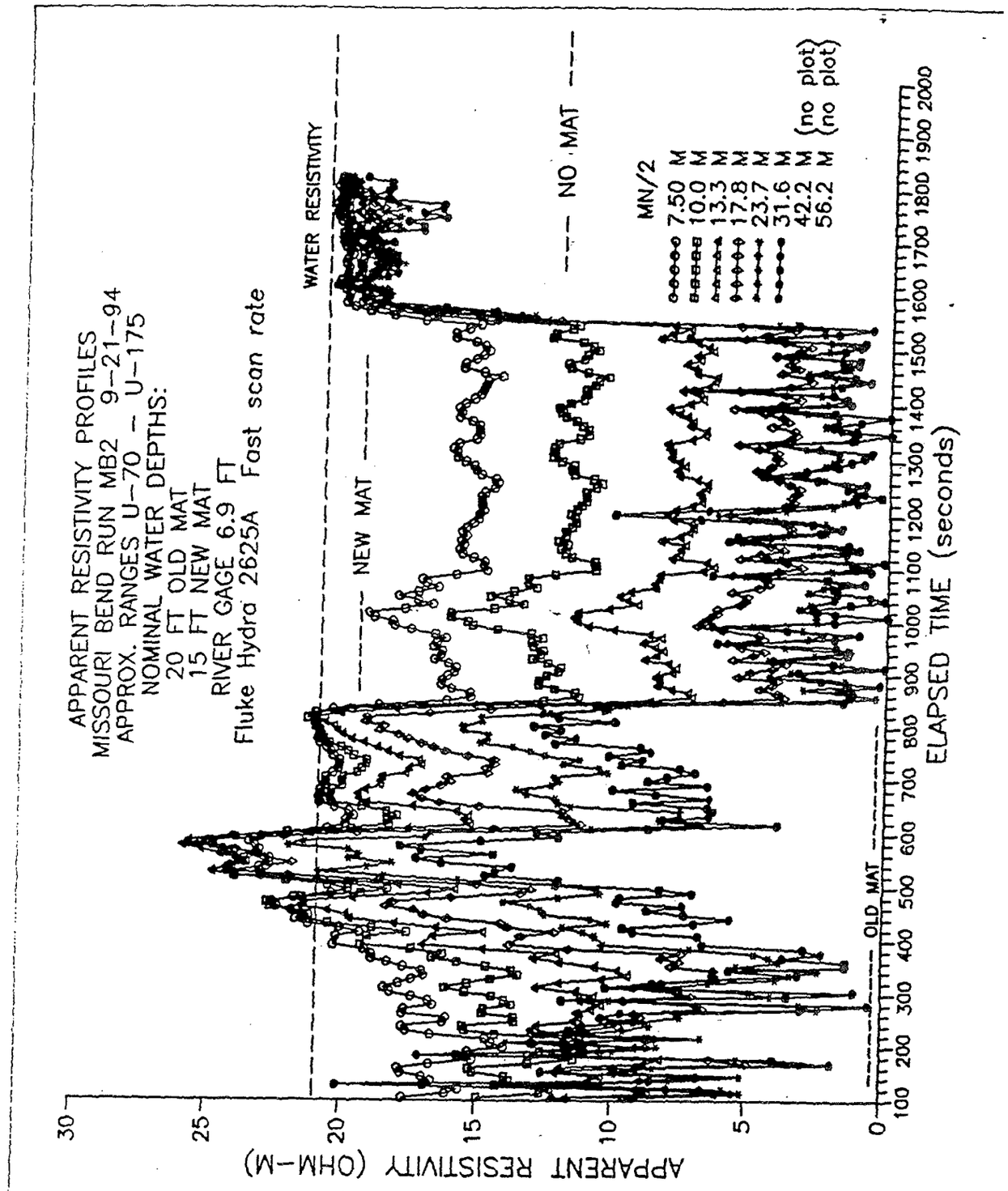

SP SURVEYS Geophysical Consultants	Apparent Resistivity Plots Profile MB2 Missouri Bend	Figure 8

Appendix D
Self-Potential Type Curves Generated by Articulated Concrete Mattresses

SELF-POTENTIAL TYPE CURVES

GENERATED BY ARTICULATED CONCRETE MATTRESSES

Prepared by:

Robert F. Corwin, Ph.D.
Consulting Geophysicist

SP SURVEYS
Geophysical Consultants
406 Sea View Drive
El Cerrito, CA 94530
(510) 527-2081

Prepared for:

U.S. Army Corps of Engineers
Waterways Experiment Station
3909 Halls Ferry Road
Vicksburg, MS 39180-6199

May 25, 1994

SELF-POTENTIAL TYPE CURVES

GENERATED BY ARTICULATED CONCRETE MATTRESSES

This report presents a series of self-potential (SP) profiles generated by program SPGENACM. The profiles show the effects of varying parameters of interest for design of SP surveys and interpretation of SP data obtained over articulated concrete mattresses (ACM's). The SP source models for the profiles were typical of those obtained from field measurements, using finite line sources and mat depths and geometries representative of ACM installations in the area of Baton Rouge, Louisiana.

SP anomaly amplitudes will vary as the source depth and configuration change. In order to better distinguish changes in the shapes of the profiles, peak-to-peak anomaly amplitudes for some of the plots were adjusted to similar scales within each plot by adjusting source current values. Field experience indicates that noise levels of measured SP profiles typically are less than 1 millivolt (mV). Therefore, profiles of similar amplitude that differ by more than about 1 mV over a significant length of the profile probably would be resolvable from typical field data.

Figure 1 shows a sketch of the mat and survey configuration used for this study. Table 1 lists the nominal values of each of the parameters. Similar parameter labels are used if the model includes more than two source lines. Unless otherwise noted, the profiles were calculated for a gradient array with an electrode separation SEP of 50 ft. This was the configuration used for most of the test surveys in the Baton Rouge area. A synthetic onshore gradient data file STD.POS with a line length f 1000 ft, station separation of 10 ft, and SP values of 1.0 mV was used as field data input to SPGENACM. This file is included on the enclosed disk.

Table 2 briefly summarizes the plots. Because the depth (H1) and location (X1) of the outer edge of the mat usually are the parameters best determined by the SP measurements, considerable attention has been given to investigating the effects of varying these parameters under a variety of conditions. Expanded descriptions of the plots are given on the following pages.

The model for this study is the horizontal line source shown on page 9 of the SPGEN documentation manual. It is assumed for this model that the sources are straight, horizontal lines and that the resistivity of the surrounding medium is perfectly uniform. Practically, this means that the effect of the contrast between water and river-bottom resistivity is not considered for these models. Also, it is assumed that the vessel survey line is perfectly straight and is oriented exactly perpendicular to the source lines.

TABLE 1

Mat and Survey Configuration Parameters

Parameter label	Definition	Standard value
SEP	Electrode dipole separation	50 ft
H1	Depth of outer line source	120 ft
H2	Depth of inner line source	40 ft
X1	Distance to outer line source	500 ft
X2	Distance to inner line source	750 ft
L1	Half-length of outer line source	1000 ft
L2	Half-length of inner line source	1000 ft
C1	Current of outer line source	+10 mA/ft
C2	Current of inner line source	-10 mA/ft
A	"Dip angle" of mat	19 degrees
LMAT	Distance between outer and inner line sources	250 ft

Note: Assumed water and river bed resistivity was 20 ohm-ft for all models.

TABLE 2

Summary of Type Curve Plots

Figure	Parameters varied; comments
2	Dipole separation SEP (= 25, 50, 100 ft; infinite)
3	Outer source depth H1 (= 40, 80, 120, 160, 200 ft) (no inner source line, X1 = 500 ft)
4	Outer source depth H1 (= 40, 80, 120, 160, 200, 240 ft) (with inner source line, X1 = 500 ft, X2 = 750 ft)
5	Outer source depth H1 (= 40, 80, 120, 160, 200, 240 ft) (with inner source line, X2 = 750 ft, X1 varies to maintain mat length LMAT = 250 ft)
6A	X-distance of outer source line X1 (= 500, 550, 600, 650, 700 ft). X2 constant at 750 ft.
6B	Same as 6A, with expanded Y-axis scale
7	Survey line Y-offset (L1 and L2 = 1000 ft, offset 0 - 1200 ft)
8	Effect of source line length (L1 = 0 to 1000 ft)
9	Comparison of point and line source profiles

DISCUSSION OF TYPE CURVE PROFILES

Figure 2: Effect of Dipole Separation

This plot shows the effect of varying the towed electrode dipole separation SEP (this value is labeled DI in program SPGEN). Source line current values were maintained constant at +/- 10 mV/ft. This allowed observation of the increase in measured anomaly amplitude associated with increasing dipole length.

The near-shore end of the survey line usually does not come close enough to shore to define the portion of the curve inshore of source 2. Therefore, the portion of the profile offshore of source 2 is of primary interest for interpretation. For the same mat parameters, the peak-to-peak amplitude of this segment of the profile increases from about 35 mV for a dipole separation of 25 ft to about 100 mV for SEP = 100 ft and about 170 mV for very large values of the separation. The location of the positive peak of the profile is better defined for the larger separations.

The tradeoff for this increased signal level is the somewhat greater noise level associated with the larger separation and an increase in operational difficulty. Large dipole separations probably would be desirable in cases where the mat is deeply buried and SP signal levels are relatively small.

Figure 3: Effect of Outer Source Depth (no inner source)

This plot shows the effect of varying the depth of the source line representing the outer edge of the mat, without the complicating effect of an inner line source. This represents the case where the inner source is well inshore of the outer source, or is deeply buried and produces a very small signal. The location X1 of the outer source was maintained constant at 500 ft. The amplitude of the source current C1 was adjusted to maintain the peak-to-peak amplitude of the profiles constant.

As expected from potential field theory, the anomaly wavelength decreases and the peaks become sharper with decreasing source depth. With no inner source present, the steepest negative gradient (inflection point) and zero crossing for each profile is located directly above the outer source.

Figure 4: Effect of Outer Source Depth (with inner source)

This plot is similar to that of Figure 3, but the model includes an inner source line located at X2 = 750 ft and H2 = 40 ft. Source currents C1 and C2 were maintained at +10 and -10 mV/ft, respectively.

For a shallow outer source depth H1 = 40 ft (equal to the inner source depth), the profile is symmetrical, with an outer anomaly

similar to those of Figure 3 combining with a "mirror image" above the inner source line. For a very deep outer source, the contribution of the outer source to the profile is essentially zero. Thus a "double-peaked" appearance and relatively large and well-defined outer positive peak indicate a relatively shallow depth to the outer source line.

The anomaly wavelength decreases, the peaks become sharper, and the amplitude of the positive peak increases with decreasing outer source depth. The steepest negative gradient (inflection point) of the profiles for the shallower sources is located directly above the outer source line. The zero crossing of the profile approaches closer to a location directly above the outer source line as the source depth decreases.

Figure 5: Effect of Outer Source Depth (mat length constant)

This model is similar to that for Figure 4, but instead of allowing the separation (LMAT) between the inner and outer sources to increase as the depth H1 of the outer source increases, LMAT was maintained constant at 250 ft and the "dip angle" A of the mat was varied from 0 degrees (H1 = 40 ft) to 53 degrees (H1 = 240 ft). As for Figure 4, current amplitudes were maintained constant at +/- 10 mV/ft. The plots and comments are similar to those for Figure 4.

Figures 6A and 6B: Effect of X-Location of Outer Source

These figures show the effect of varying the location X1 of the outer source line between X1 = 500 ft and X1 = 700 ft, while maintaining all other parameters constant (except inner source line current C2). C2 was varied to maintain the amplitude of the negative peaks of the profiles constant in order to better compare changes in profile shapes with changing outer source line location. The depth H1 of the inner source line was maintained at 200 ft. The location of the inner source line was maintained at X2 = 750 ft, and its depth H2 was maintained at 40 ft. The X and Y axis scales of Figure 6B are expanded from those of Figure E1 to show more detail in the area of interest for interpretation.

It is apparent that the locations of the inner negative and positive peaks of the profile are controlled by the position of the inner source line and so are not diagnostic of the X-position of the outer source line. The profile parameters that are indicative of X1 are the location of the outer positive maximum and the slope of the profile between this maximum and the negative minimum. As X1 approaches X2, the profiles begin to converge in the area between the sources, but remain well separated offshore of the outer source line. This indicates the importance of obtaining sufficient "background" data well offshore of the mat.

Figure 7: Effect of Survey Line Y-Offset

For all the previous models, it was assumed that the source line half-length L was 1000 ft and that the vessel survey line ran across the center of the source lines (i.e., that the source lines extended 1000 ft to either side of the survey line). Figure 7 shows the effect of offsetting the survey line from the center of the source lines. The source current strength was maintained constant at +/- 10 mA/ft.

For offsets of less than 500 ft, the SP profiles are virtually identical to that for zero offset. For an offset of 900 ft (survey line 100 ft from end of source lines), the profile begins to diverge noticeably from that for zero offset. For an offset of 1000 ft (survey line above end of source lines), the profile amplitude is reduced by about 1/2, although the profile shape and locations of the positive and negative peaks remain similar. For offsets of 1100 and 1200 ft (survey line 100 and 200 ft off the end of the source lines), the amplitude decays rapidly and the profile shape appears similar to that for a deeper mat.

These results indicate that data taken above the central portion of a mat field are not strongly affected by changes in source strength along the length of the mat. However, care must be taken not to mis-interpret data taken close to or past the end of a mat field as representing a more deeply-buried mat centered below the survey line. The use of as-installed mat location maps would be helpful in avoiding this type of error.

Figure 8: Effect of Source Line Length

This figure shows the effect of varying the half-length L1 of a single source line from zero (point source) to 1000 ft. The source depth was maintained at 80 ft and the source current was adjusted to maintain constant profile amplitude.

A source line length of 500 ft gives a profile very similar to that for 1000 ft. As the line length decreases further, the peaks of the profile become sharper, indicating an apparently shallower source depth for the shorter lines. As required by potential field theory, the amplitude-adjusted profile for a very short line (L1 = 1 ft) is almost identical to that for a point source.

Figure 9: Comparison of Point and Line Source Profiles

This figure examines the possibility of mis-interpreting a very short line source (approximated by a point source at 80 ft depth) as a longer line source at a shallower depth. As for Figure 8, source current values were adjusted to maintain constant profile amplitudes.

In the area close to the source, the profile for a line source with half-length L1 of 1000 ft at a depth of 50 ft matches the profile for the point source at a depth of 80 ft. However, these profiles diverge strongly at distances more than about 100 ft from the source. A line with L1 = 250 ft provides an approximate fit at distances greater than 300 ft from the source, but a poor fit closer to the source. Thus the maximum source depth error due to line length variation in this extreme case (L1 varying from 0 to 1000 ft) is about 30 ft. Examination of the entire profile helps to differentiate short source lines at greater depths from longer source lines at shallower depths.

FIGURE 1

Type Curve Study Parameters
(not to scale)

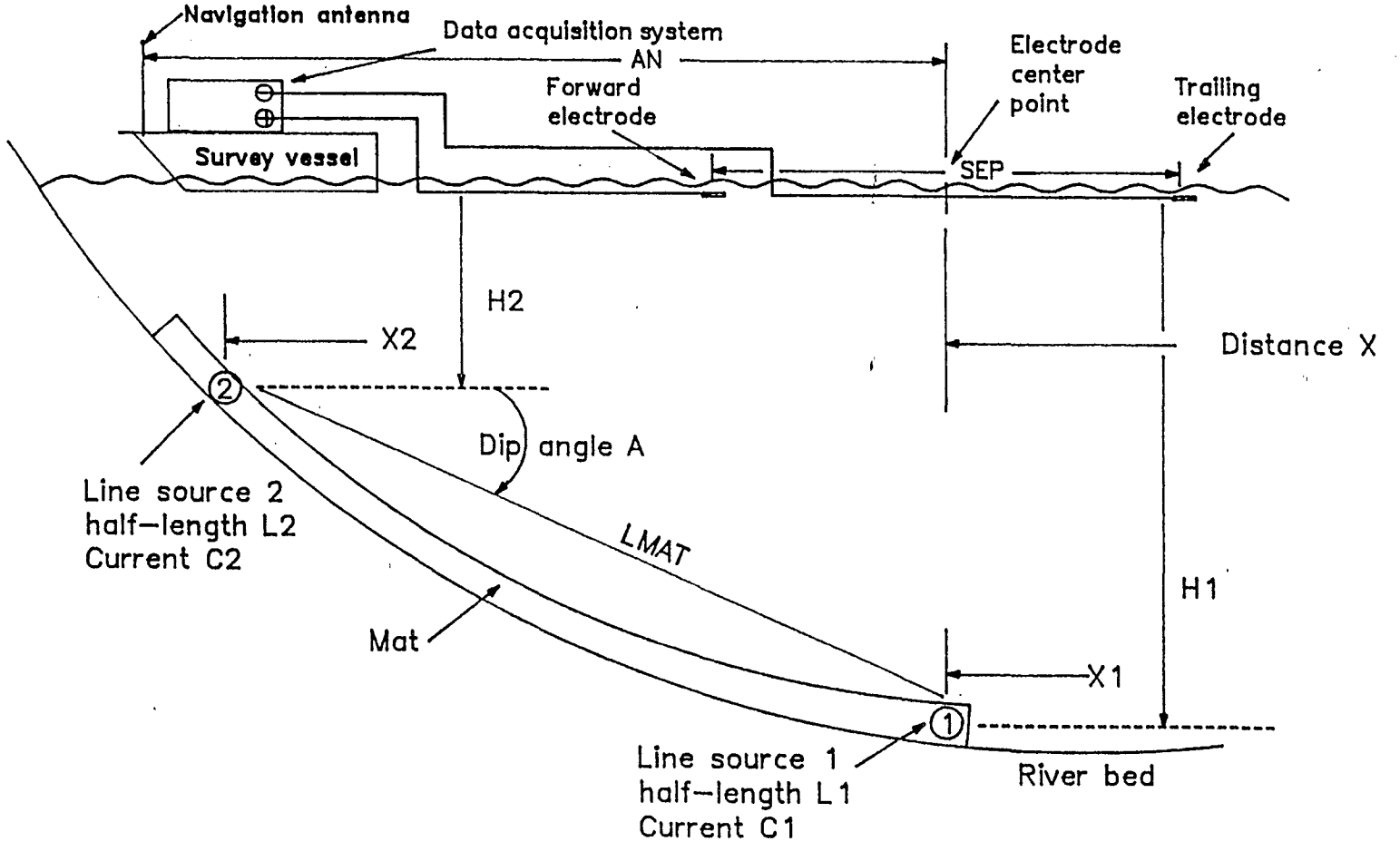

FIGURE 2

EFFECT OF DIPOLE SEPARATION

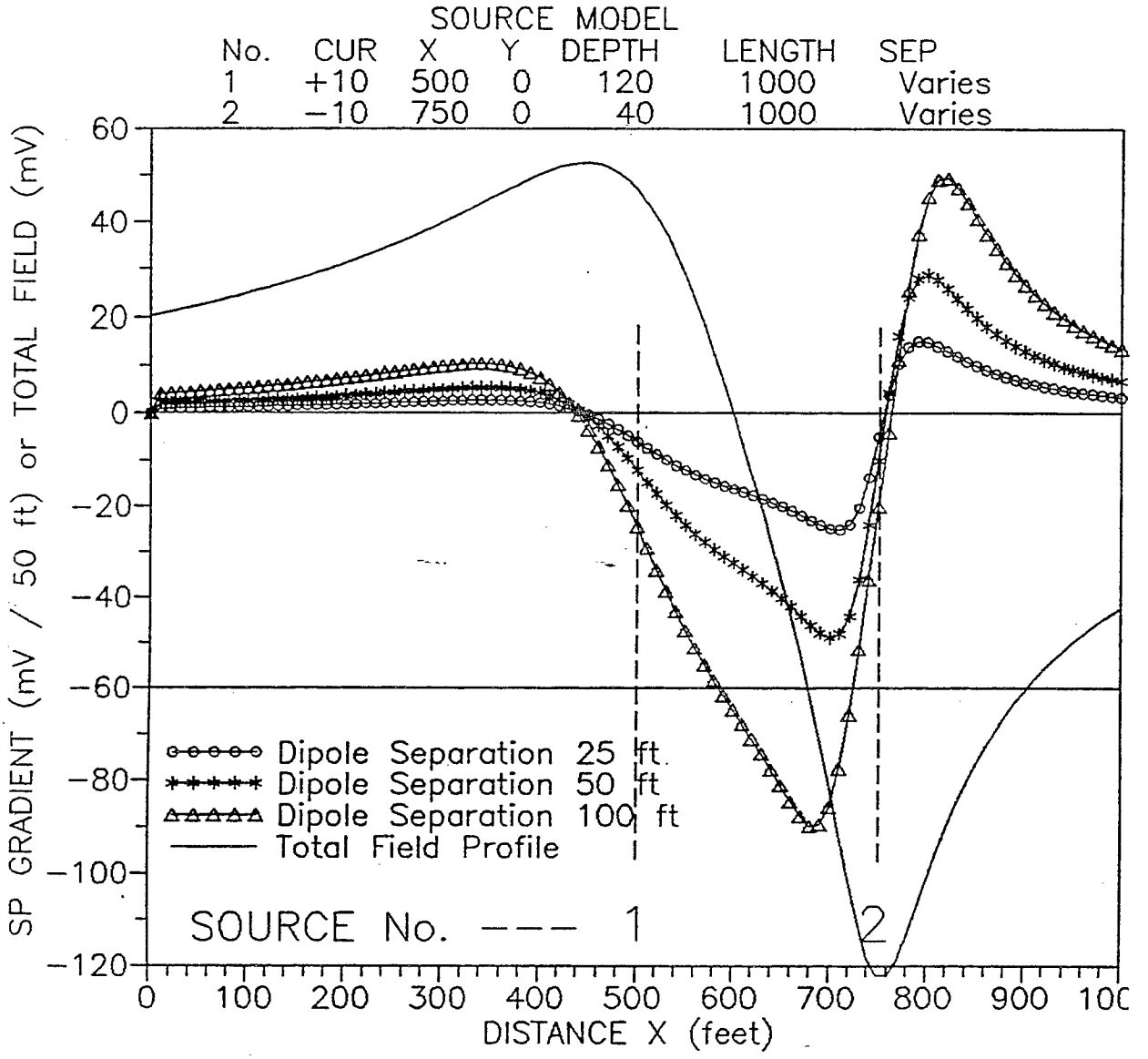

FIGURE 3

EFFECT OF DEPTH OF OUTER EDGE OF MAT
(source at outer edge only)

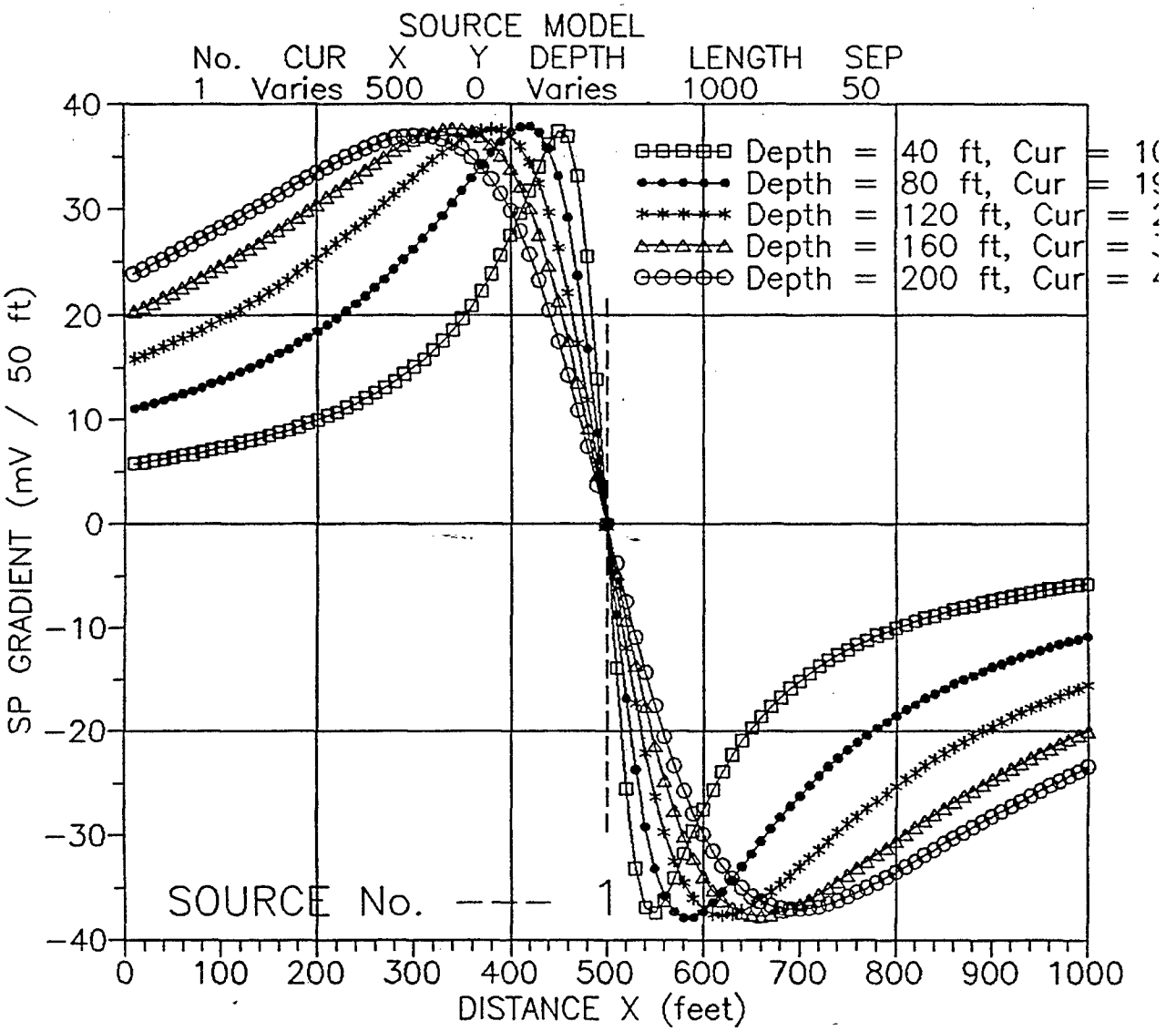

FIGURE 4

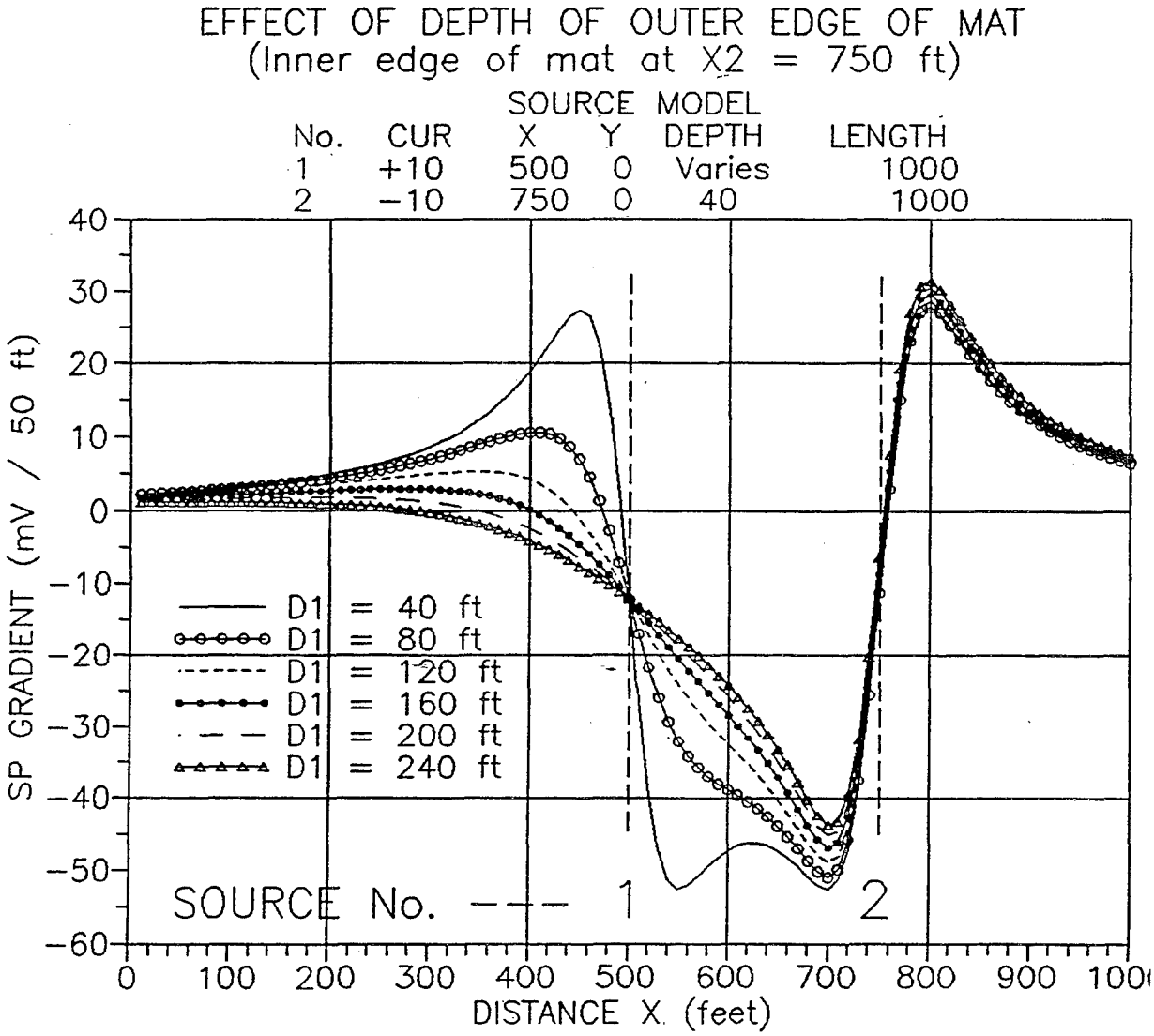
EFFECT OF DEPTH OF OUTER EDGE OF MAT
(Inner edge of mat at X2 = 750 ft)
SOURCE MODEL
No. CUR X Y DEPTH LENGTH
1 +10 500 0 Varies 1000
2 −10 750 0 40 1000
SP GRADIENT (mV / 50 ft)
DISTANCE X. (feet)
D1 = 40 ft
D1 = 80 ft
D1 = 120 ft
D1 = 160 ft
D1 = 200 ft
D1 = 240 ft
SOURCE No. --- 1 2

FIGURE 5

EFFECT OF DEPTH OF OUTER EDGE OF MAT
(X2 = 750 ft, X1 varies)

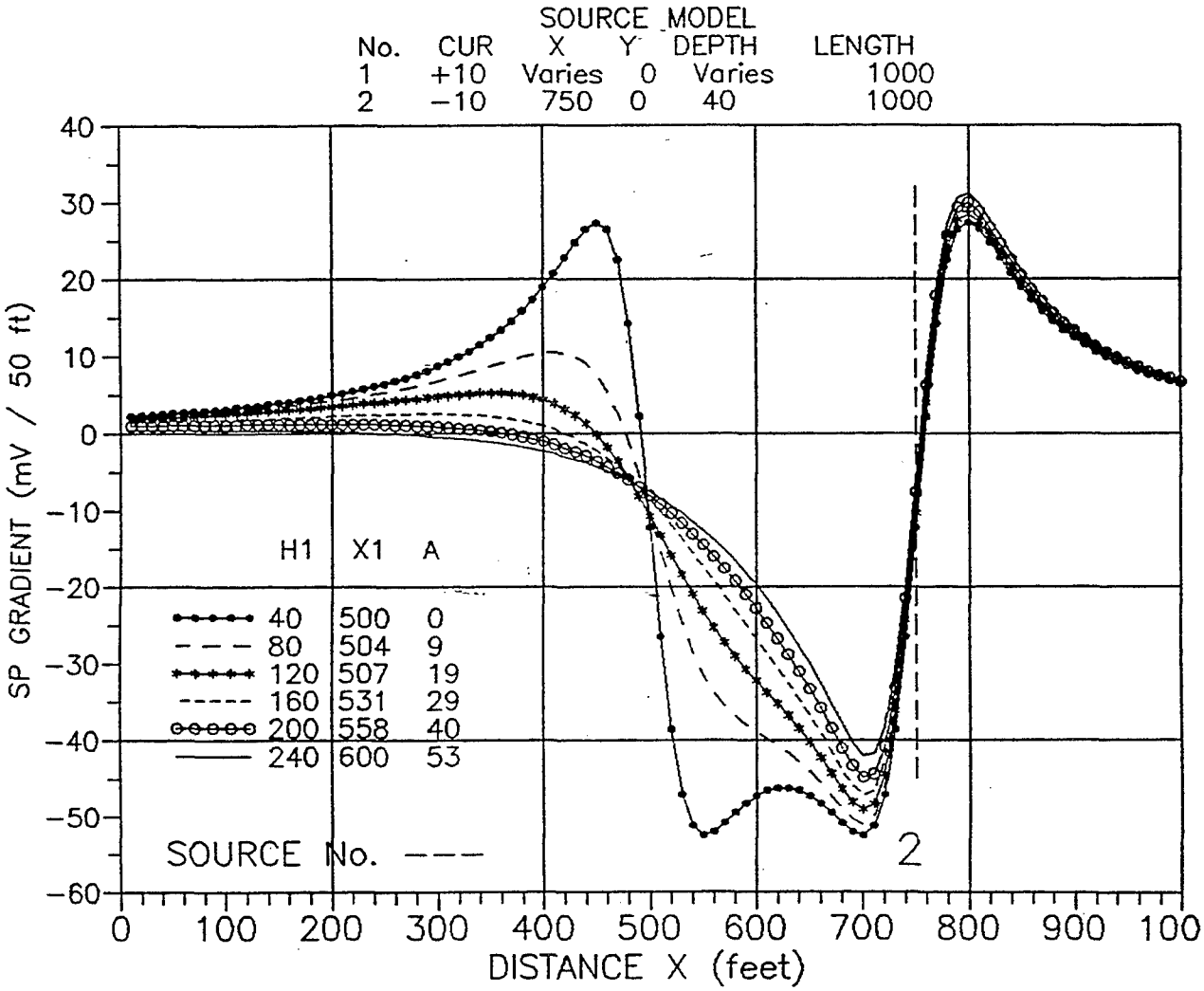

FIGURE 6A

EFFECT OF X–LOCATION OF OUTER EDGE OF MAT
(X2 = 750 ft, D1 = 200 ft, X1 and CUR2 vary)

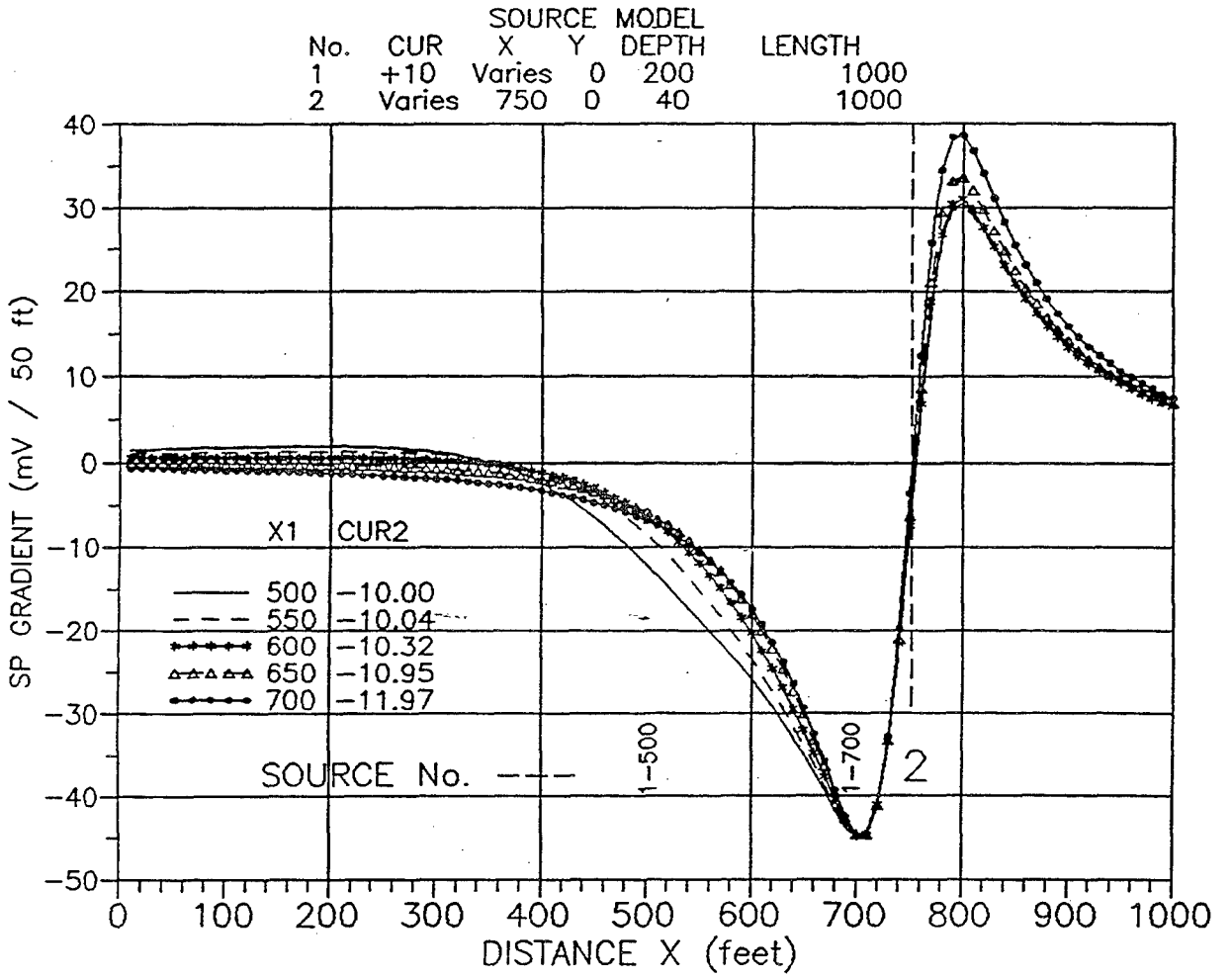

FIGURE 6B

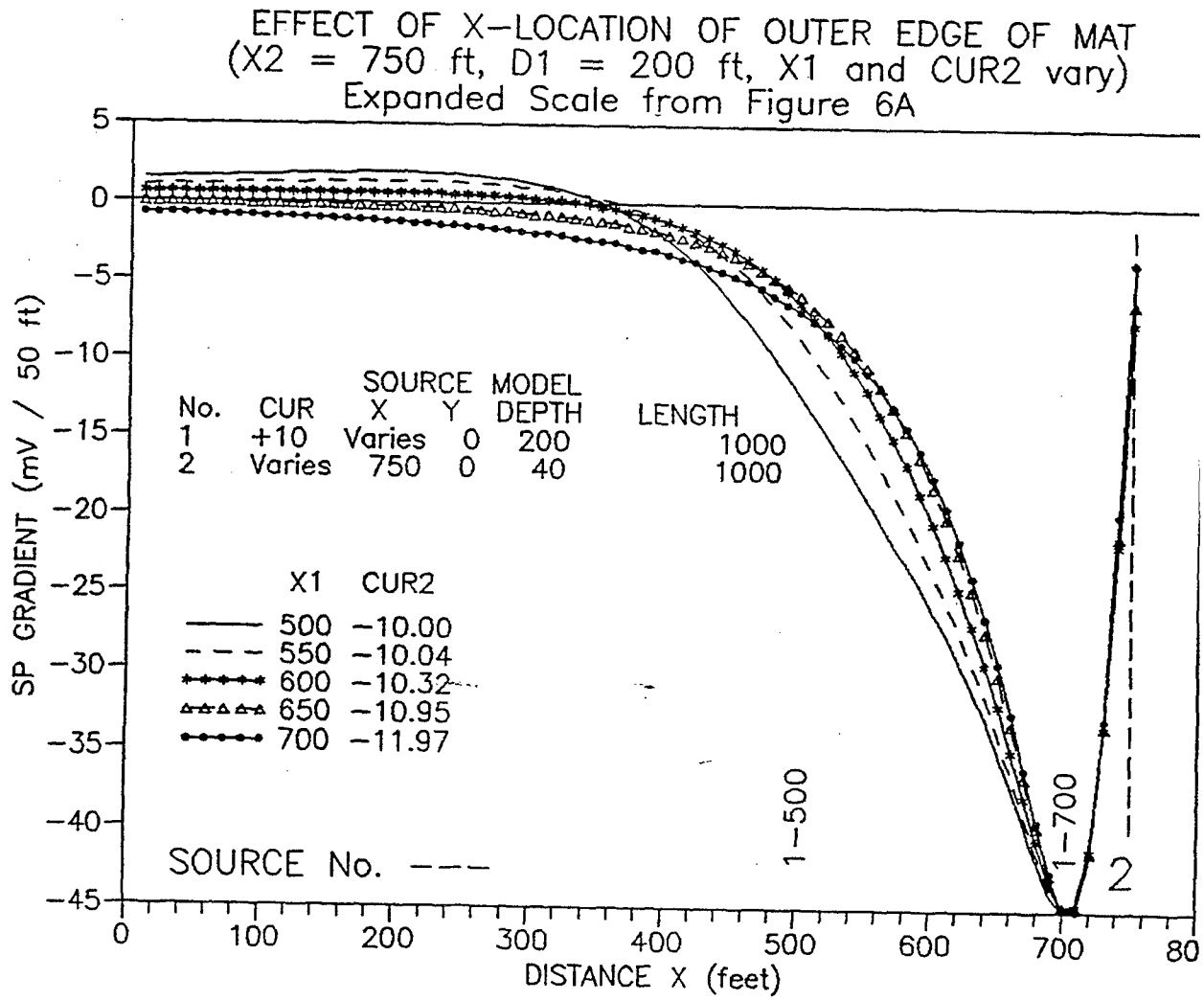
EFFECT OF X–LOCATION OF OUTER EDGE OF MAT
(X2 = 750 ft, D1 = 200 ft, X1 and CUR2 vary)
Expanded Scale from Figure 6A
SP GRADIENT (mV / 50 ft)
DISTANCE X (feet)
SOURCE MODEL
No. CUR X Y DEPTH LENGTH
1 +10 Varies 0 200 1000
2 Varies 750 0 40 1000
X1 CUR2
500 −10.00
550 −10.04
600 −10.32
650 −10.95
700 −11.97
SOURCE No. ---
1–500
1–700
2

FIGURE 7

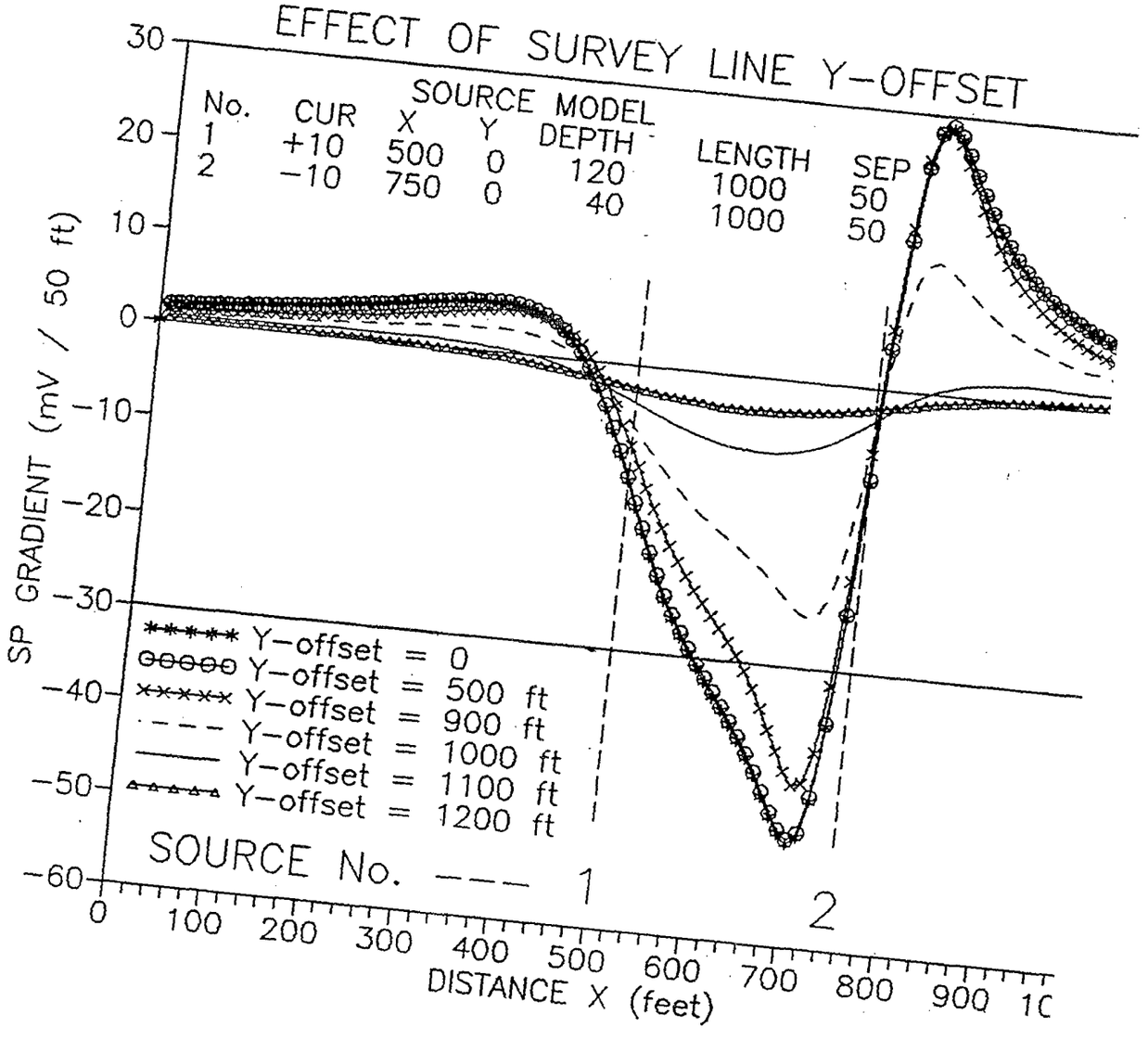
EFFECT OF SURVEY LINE Y-OFFSET
SOURCE MODEL
No. CUR X Y DEPTH LENGTH SEP
1 +10 500 0 120 1000 50
2 −10 750 0 40 1000 50
SP GRADIENT (mV / 50 ft)
30
20
10
0
−10
−20
−30
−40
−50
−60
Y-offset = 0
Y-offset = 500 ft
Y-offset = 900 ft
Y-offset = 1000 ft
Y-offset = 1100 ft
Y-offset = 1200 ft
SOURCE No. --- 1
2
0
100
200
300
400
500
600
700
800
900
DISTANCE X (feet)

FIGURE 8

EFFECT OF SOURCE LINE LENGTH

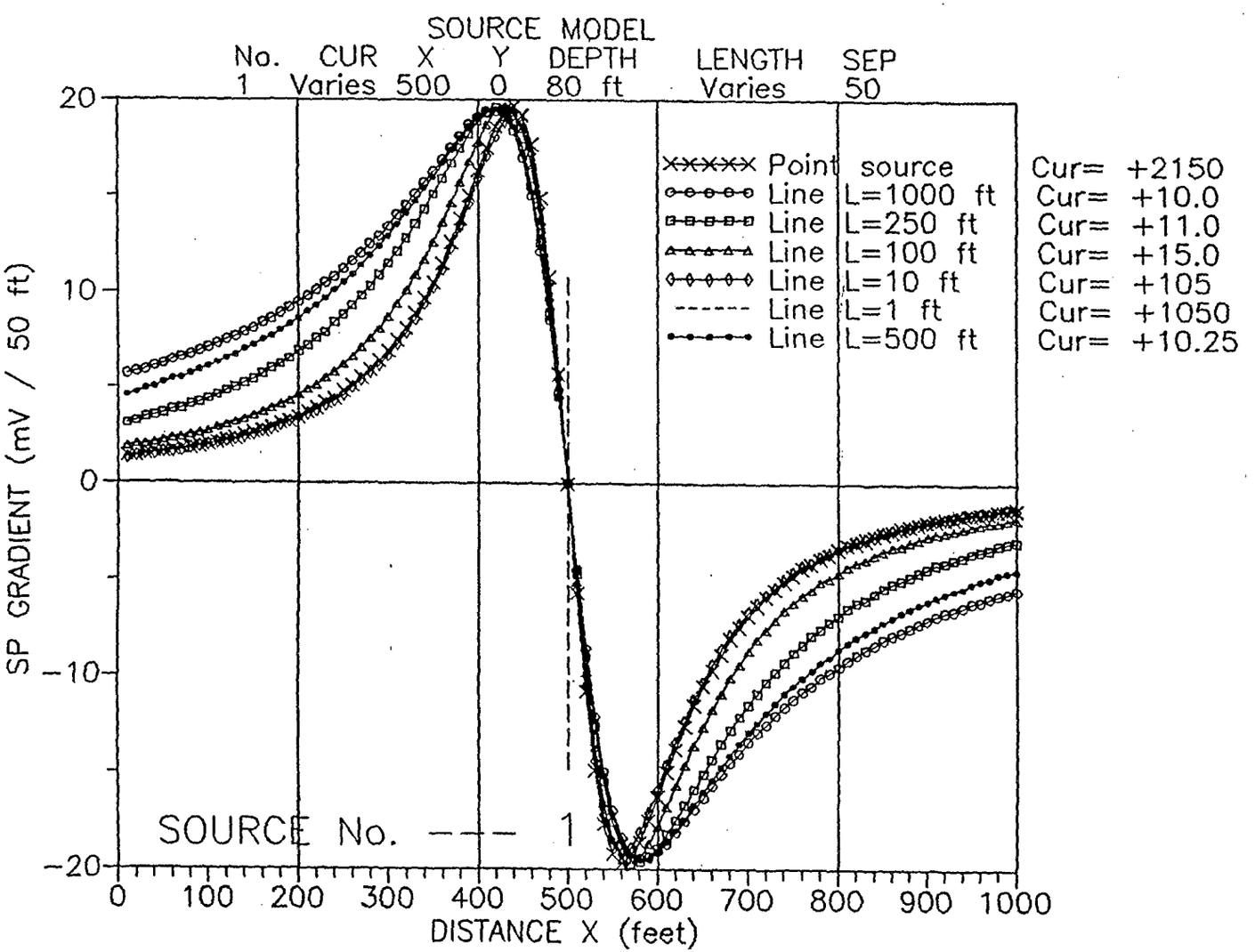

FIGURE 9

COMPARISON OF POINT AND LINE SOURCE PROFILES

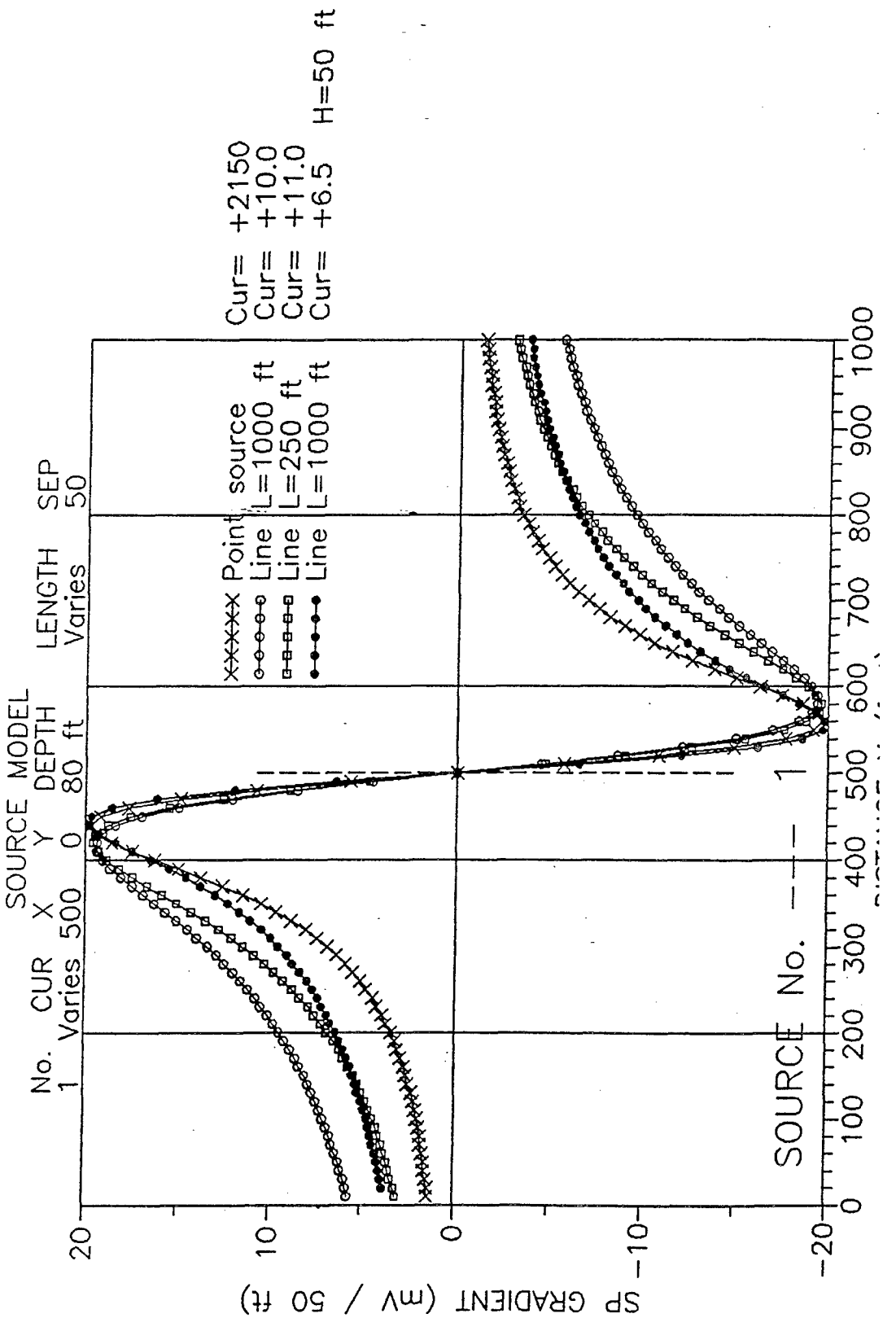

Appendix E
Phase I Report - Airborne Electromagnetic Techniques to Delineate Reinforced Concrete Slabs Buried Within River Bed Sediments

AIRBORNE ELECTROMAGNETIC TECHNIQUES TO DELINEATE REINFORCED CONCRETE SLABS BURIED WITHIN RIVER BED SEDIMENTS

PHASE I REPORT

TO

U.S. ARMY CORPS OF ENGINEERS
U.S. ARMY ENGINEERS WATER EXPERIMENT STATION
VICKSBURG, MS

BY

PRINCIPAL INVESTIGATOR: EDWARD C. MOZLEY

CO-INVESTIGATOR: TIMOTHY KOONEY

NAVAL OCEANOGRAPHIC AND ATMOSPHERIC RESEARCH LABORATORY
STENNIS SPACE CENTER, MS 39529-5004

INTRODUCTION:

The Naval Oceanographic and Atmospheric Research Laboratory (NOARL) has been developing airborne electromagnetic (AEM) techniques for the measurement of shallow water depths in sea water from the shoreline to depths in excess of 30 meters (m). This effort has fostered the development of a new generation of high power digital AEM systems capable of high resolution measurements of both water a sediment characteristics. During the development NOARL in conjunction with Right By Design, Geophex and Lawrence Berkeley Laboratory developed and tested both a measurement system and interpretation algorithms. The test efforts have indicated that sea water depths and conductivities can be reliably measured from an airborne platform (helicopter) at speeds of 85-90 knots. The system provides estimates of sediment conductivity that are reasonable for expected formation factors and water conductivities. The penetration is a strong function of the electrical conductivity of the media through which the induced electromagnetic energy diffuses. Therefore, the resolution of sediment characteristics would be limited in sea water (conductivity=5.6 siemens/meter (S/m)) to water depths of less than 60 ft. for a frequency of 150 Hz; however, in river water where the water conductivity would be an order of magnitude smaller, the system would penetrate through 180 ft. of water to map bottom conductivities.

The work described in this report was initiated to define the feasibility of using AEM methods to map the location of reinforced concrete slabs that are positioned along river banks to limit erosion. These slabs are covered with silt and in some cases washed away during high flow periods. In order to plan a corrective action, the accurate location and depth of the slabs are required. The U.S. Army Corps of Engineers (COE) have adapted acoustic systems, which were originally designed for hydrography and sediment classification applications, to mapping the location of the mats or slabs; however, acoustic methods provide limited depth of penetration in some areas of interest and it is proposed that AEM techniques would provide a means to compliment the acoustic information. The electromagnetic methods would detect the high conductivity of the embedded "fabric" of steel that connect the slabs together. The degree of success provided by electromagnetic techniques depends on the conductance of the slab. By using estimates for this quantity, the optimum system configurations may be designed with the aid of numerical simulations for both air and water based platforms. The proposed work was composed of three basic phases: experimental design, measurement of critical parameters, and implementation of a field validation test for proof of concept.

METHODOLOGY:

The first phase in this effort was composed of a modeling effort. A suite of simulations was completed that indicated the feasibility of using various electromagnetic (EM) system frequencies to map the depth and lateral extent of the concrete mat buried beneath the river channel. One and three dimensional models were generated to indicate the response and appropriate frequencies for estimated conductance values. This phase of the work assessed the coupling of the system and target over specified frequency ranges and quantified the affects of the water and surrounding sediments. The results of this phase indicated the necessary bandwidth and system configurations that were required to resolve the conductive slab. This phase of the program was completed in August 1991. Based

upon the successful results of this phase of the work, the next phase of the work should be implemented.

The second phase of the program would be to measure the EM response of the concrete mat, measure the effects caused by the conductivity of the overburden material, and test the system's ability to detect the mat using the system band width that was defined in the Phase I effort. This may be implemented by modifying an existing ground or airborne system such that it may be deployed on the water surface. This would provide a means of acquiring a suite of high density measurements for minimum deployment cost and maximum signal levels. For small slab targets, the floating system would be easier to position over a fixed set of well surveyed locations with known parameter values or characteristics. The measurement density could be precisely controlled and multiple measurements could be utilized to reject local noise sources. In summary, water surface measurements would provide a cost effective means to validate Phase I model results and provide a high resolution measure of the critical parameters. The measurements of the slab response over a band width appropriate for airborne systems will be used to infer the slab conductance and background conductivities. These important characteristics will determine the range in depth over which the targets may be detected from a remote platform.

The results that are provided under Phases I and II will define the feasibility of using specific AEM systems and dictate the bandwidth/signal-to-noise levels required. If Phases I and II are successful, the program should be completed with a phase III effort. This phase would be composed of an airborne test of NOARL's AEM system over a well defined suite of target cases. This is an important culmination of the effort that would validate the use of helicopter mounted EM systems for rapidly mapping depths of burial for concrete erosion mats from a platform not affected by water conditions.

PHASE I PREPARATION:

In order to obtain realistic values for background conductivities and establish a base model, COE scientist Steve Scott and COE contractor Robert Corwin were contacted. Their inputs plus our experience in coastal areas resulted in the assumption that the mean water conductivity would be approximately 0.04 S/m (or a resistivity of 5 Ohm-m) and an average sediment conductivity of 0.2 S/m (or a resistivity of 25 Ohm-m). A water depth of 15 m was selected as a reasonable value to test the concept of EM mapping over three dimensional mats.

The EM target in this study is the wire "fabric" or mesh that ties segments of the concrete mat together. In order get a estimate of its conductance, we visited the COE Vidalia Area Office and obtained the specifications for the articulated concrete mattress and visited the casting/storage facility to observe actual mats and construction materials. The concrete mat or mattress configuration is shown in the upper portion of figure 1. The electrically conducting components of the mat are confined to the steel wire that holds the individual concrete slabs together. The geometry and dimensions of this wire are shown in the lower portion of figure 1. The overall lateral dimensions of each mat section is 7.6 x 1.2 m (299 x 48 inches) that consists of 44.4 m of wire with a diameter of 3.8×10^{-3} m. Since the conductivity of the steel wire is

approximately $1.0x10^{7}$ S/m, the skin depth at frequencies from 100 to 1000 Hz ranges from $15.0x10^{-3}$ to $5.0x10^{-3}$ m. Since this is greater than the wire diameter, the currents inducted into the wire will flow throughout the volume of the wire and not be confined to its surface. In addition, all wire segments within the mat are electrically connected and each section of mat is electrically connected to the next with copper straps. Finally, the skin depth within the 0.2 S/m sediment ranges from 112 to 36 m for the 100 to 1000 Hz frequency band. These skin depths are well above the dimensions of the mesh or loop size that makes up the wire fabric as shown in the lower portion of figure 1. As a result, any currents that are induced into the sediments would be channeled (quasi-statically distorted) into the wire "fabric" in response to its relatively high conductivity and relatively small mesh size.

The above heuristic arguments support the hypothesis that the wire mesh imbedded in the concrete slabs, which is in turn buried in the sediment, will respond to an EM source as an equivalent thin sheet conductor. The equivalent thin conductor would have an equal volume of conductive material provided by the steel wire redistributed into a continuous sheet with the same lateral dimensions as the wire mesh. Using the diameter of the wire, total wire length and lateral dimensions of each section of mat as provided above, one obtains an equivalent thickness of $5.45x10^{-5}$ m for the steel sheet that may be "easily" simulated as a target (one or three dimensional) buried within a layered environment.

A second important point, which is associated with EM induction phenomena, is the similarity or "effective equivalence" between responses from thin layers (or thin finite conductors) with a common conductivity-thickness product. This product is defined as the conductance, which in the case of the mat defined above is 545 siemens. The estimation of this conductance value and the approximation of the real situation of an imbedded wire mesh within the sediments with a tractable thin sheet model are the major assumptions used in this study. This summarizes the rational that was used to establish background parameters and to define the type of numerical simulations, which are appropriate for the study.

In order to use the model results to design a measurement program, the total noise level of the proposed measurement system should be accurately estimated. Since the measurement system that was proposed for the Phase II portion of the program is the wide band NOARL AEM system adapted to a float measurement platform or vehicle, then an upper bound for the noise level of the system would be provided by high altitude airborne noise measurements made with this system during earlier surveys. The noise measures would provide an upper level noise estimate because they were made at an air-speed of 85 knots as compared to Phase II measurements that would be confined to a stable water surface or float platform deployed at one to four knots. The dominate cause of noise in this system is the vibration of the sensor coils in the earth's magnetic field. The slow water borne system would be very stable and acoustic vibrations should be greatly reduced. The AEM system was deployed in the Kings Bay, Georgia area in the summer of 1990 and these data indicated that the noise at 150, 390, and 4110 Hz was 2.5, 1.5, and 3.0 parts per million (ppm) of the primary fields respectively. These noise estimates were based on 1/6 second averages or a five sample stack, since the system acquired 30 samples per second. The noise magnitudes decrease as more data area averaged approximately as the inverse of the square root of the number of samples stacked. Therefore, an

average noise value of 1.0 ppm is reasonable for data that are smoothed to one second averages, which are appropriate for measurements acquired at speeds of less than 5 knots (sample intervals of less than 2.6 m). This will be used as a reference value to evaluate the feasibility of observing various model responses in the Phase II measurement scenario.

ONE-DIMENSIONAL SIMULATIONS:

The basic one-dimensional (1-D) or background model (water and sediment without an anomalous thin conductor or mesh) and two "equivalent" 1-D layered models with a conductance value of 545 siemens are shown in figure 2. The EM source is a vertical magnetic dipole or horizontal loop (T_z) and the response is the total vertical magnetic field (H_z). The EM source operates in the frequency domain over the band ranging from 90 to 5000 Hz and the receiver-source separation is 5.18 m. The deployment height of 1.0 meter was selected as a reasonable value for the Phase II measurements. The 1-D simulations were implemented with an in-house developed program BSAUT that calculates the response from a multi-layered earth model. The similarity between the normalized vertical field responses for the thick (0.3 m) and thin (5.45×10^{-5} m) layered anomalous zones is shown in figure 3. The abscissa in this figure defines the frequencies in Hz over which the transmitter operates on a logarithmic base ten scale and the ordinate defines the magnitude of the real (in-phase) and quadrature (imaginary) components of the anomalous vertical magnetic field normalized by the primary field in units of ppm. The anomalous response is defined as the total response from a thick layered, (3-D) thin layered, or three dimensional model minus the basic 1-D model response.

The family of normalized real and quadrature frequency responses for the basic 1-D model (water depth t_1=15 m) and four other water depths (t_1=5,10,20, and 30 m) are provided in figures 4 and 5 respectively. The vertical and horizontal coordinates are the same as in the previous figure. Note that the ordinate in figures 2, 3, and 4 all are in units of thousands of ppm, which is three orders of magnitude greater than the projected noise level of the measurement system that was given in the last section. These signatures could very easily be measured and the frequency characteristics of the anomalous fields given in figure 3 are very different from those shown in figures 4 and 5 for t_1=15 m. The family anomalous frequency responses that is provided with the introduction of a thin conductor with a conductance of 545 siemens (total field response minus the basic models shown in figures 4 and 5) is presented in figures 6 and 7 for water depths of 10, 15, 20 and 30 m. The anomalous response for a water depth of 5 m was not plotted on these figures because the response was so large that logarithmic scaling would have been required. Therefore, the presence of the thin layer conductor or mesh would be easily detected in the 1-D situation or when the lateral dimensions of the thin layer are large compared to the footprint, which has a circular geometry with a diameter that varies as a function of water depth and has a value approximately equal to the water depth at t_1=15 m. To stress the difference in the frequency response caused by adding the thin and thick conducting sheets, the normalized total field responses of the 1-D basic model for t_1=15 m with no conductive layer (empty model), the 1-D thin layer (for the same t_1, t_a=5.45×10^{-5} and sigma=1.0×10^{7} S/m), and the 1-D thick layer (for the same t_1, t_a=0.3, and sigma=1817 S/m) are presented in figure

8 for comparison. In this figure, it is clear that total or measured responses for "empty" model versus either of the models containing the thin anomalous layer with a conductance of 545 siemens may be easily identified. The great difference in the spectral signature between the case where the thin sheet is present and the one where it is absent indicates that an unambiguous interpretation is possible.

THREE-DIMENSIONAL MODEL VALIDATION:

In order to validate the 3-D integral equation algorithm that was used on the 3-D model study, a comparison with other numerical schemes was initiated. The software that NOARL used in the study was developed at the University of Utah by Doctors G. Newman and G. Hohmann to simulate the response from 3-D high contrast anomalous bodies buried in a layered media. The first test of the algorithm was compare the frequency response that was provided by the 3-D software without an anomalous body to a 1-D modeling algorithm with same layered model (the basic model shown in figure 2). The normalized frequency response for both algorithms are given in figure 9; the results are very similar for both real and quadrature responses. In this figure, the squares and the tilted triangles indicate the quadrature and real responses respectively for the 1-D model and the thin lines indicate the 3-D algorithm response without an anomalous body.

A second check on the algorithm was much more rigorous, and was composed of a check against the frequency response provided by a totally different forward simulation scheme that was developed by Dr. P. Wiedelt. This softwware now resides at the University of California at Berkeley (UC Berkeley). The algorithm simulates the response from a thin sheet that is defined only by its conductance and its lateral dimensions and is buried in a layered media. Dr. Kiha Lee at UC Berkeley constructed a model that was composed of a horizontal thin conductor in the same layered background as the 1-D case shown in figure 2 with a conductance of 545 siemens and lateral dimensions of 4.8 x 6.0 m. The University of Utah algorithm was used to simulate a similar model with a 3-D horizontal prism with a thickness of 0.3 m and the same lateral dimensions as Lee's model. The conductivity of the 3-D model was reduced to 1817 S/m so that the conductance of the prism would remain the same as in Lee's model.

The simulation results from both algorithms are shown in figure 10 as the normalized frequency response of the vertical magnetic field that is measured 1.0 meter above the water with an EM transmitter/receiver system centered over the finite conductor and oriented along the shortest lateral dimension. The results of Lee's thin sheet model are denoted as two-dimensional (2-D) Real and 2-D Quad (2-D is used since the thickness of anomalous is not specified directly) and are provided at 90, 390 and 1000 Hz in this figure. In contrast, the results of the University of Utah algorithm are indicated as 3-D Real and 3-D Quad for the "equivalent" finite thick sheet model and are given at 90, 100, 150, 200, 390, 500, 800, 1000, 2000, 4110, and 5000 Hz to more clearly define the frequency characteristics. The close agreement between the algorithms is clearly evident in this figure and we can proceed with the model study with a high degree of confidence that the results are accurate to approximately 10 percent or better.

THREE DIMENSIONAL SIMULATIONS:

The simulations of the 1.2x7.5 meter section of mat with a conductance of 545 siemens indicated that the responses were under the numerical noise of the algorithm. However, if five of these sections are connected side by side then the response becomes significant. The model geometry of this small finite prism simulation is shown in figure 11. The lateral dimensions are given as 6.0x7.5 m and the thickness of the conductor is 0.3 m. The prisms conductivity is 1817 S/m, which provides a conductance of 545 siemens. The model simulates a sequence of measurements along a profile in the x direction across the center of the flat rectangular prism at a height of 1.0 meter above the water. Two cases will be considered on this model.

The first case will be for a flat prism embedded in the sediment 0.3 m with its upper surface in contact with the 0.04 S/m (25 Ohm-m resistivity) water. The normalized anomalous (3-D minus 1-D layered background) frequency and spatial response for the real and quadrature components are presented as pseudo-sections in figures 12 and 13 respectively. The abscissa defines the position in feet along the profile of the center of the transmitter/receiver system with 0 indicating the center of the prism. The ordinate defines the frequency scale in Hz and the contours represent lines of constant magnitude of the normalized field component in units of ppm. The real component in figure 12 gives a broad large response greater than 40 ppm for all frequencies above 200 Hz and over a profile segment three times the width of the prism. The imaginary response in contrast has a relatively narrow range in frequencies from 100 to 1000 Hz that have a response, which is greater than 40 ppm, and the spatial range of this 40 ppm anomaly is confined to an area twice the width of the prism as shown in figure 13. The large magnitude and the distinctive frequency signature of these responses in contrast to the basic background responses given in figure 4 and 5 indicate that these five parallel segments of mat should be easily identified.

If one buries the prism 5 m below the sediment water interface, the response is significantly reduced but remains well above the 1 ppm noise level of the measurement system. The normalized anomalous responses for both the prism located at the water sediment interface and the prism buried within the sediment are provided in figure 14 for the case where the transmitter/receiver are centered over the prism and oriented across the short axis of the 6.0x7.5 meter prism. In this figure, the characteristic increase in the real response at higher frequencies for the unburied prism is clearly evident as is the band pass nature of the quadrature response that was observed in the pseudo-sections. The response from the buried prism has not only decreased in magnitude but has undergone a significant change in its frequency characteristics. The frequency signature for both the real and quadrature anomalous responses are very similar in shape to the 1-D anomalous response observed in figure 3 with a greatly reduced amplitude. In summary, these 3-D simulations indicate that a frequency range from 100 to 4000 Hz are sufficient to identify characteristic responses for both prisms deposited on the sediment and buried within the sediments. The degree of attenuation caused by burying the prism 5 m within the sediment indicates that this depth of burial may be at or approaching the maximum detectable depth for this geometry. The problem of identifying buried prisms or mats will be much more difficult than finding those located on top of the sediments.

As stated above, the magnitude of the response functions for even the buried prism is well above the background noise level of the measurement system. However, when the magnitude of the prism responses decreases to within a few percent of the background (1-D) responses then rapid changes in water depth or bottom conductivity can compound the complexity of the interpretation problem and an unambiguous identification may not be possible. The range of possible background deviations are uncertain and the ability to simulate their effects are beyond the scope of this preliminary study.

Since large contiguous sections of these small mats are routinely deployed over large areas, some large prism or sheet models were implemented. The normalized frequency response for a large prism with the same conductance as used in earlier models and the background parameters shown in figure 11 but with the lateral dimensions of 60x75 m is presented in figure 15. The anomalous 1-D response is also plotted for the sake of comparison. In addition, the response for a slightly smaller prism is plotted at 390 Hz. Both prisms give a similar response at 390 Hz and the 60x75 meter sheet has a frequency signature that closely tracks the 1-D solution. The only significant difference is that the finite sheet has a smaller real response, which is characterized by a nearly constant offset of approximately 20 percent. The same anomalous responses for the 1-D and 60x75 meter sheet as described in the last figure are plotted in figure 16. However, in figure 16 we have also added the response from a much larger prism with lateral dimensions of 120x120 m at 390 Hz. Now in this case, we see that the larger finite sheet has finally approached the 1-D solution to within the numerical error of the 3-D software. The same models that were presented as normalized anomalous field responses in the last figure are plotted in figure 17 as normalized total fields to show the frequency characteristic that would be observed by a measurement system. When compared to figures 4 and 5, it is again clear that these large sheet segments would be easy to identify.

Finally, the finite large sheet with lateral dimensions of 48x60 m, which was first mentioned in the discussion of figure 15, is again considered. The responses for this model are presented in figure 18 for 90 an 390 Hz for the 3-D thick (0.3 meter) prismatic model along with the full frequency response for corresponding 1-D model. In addition, the Wiedelt finite thin sheet model with the same conductance as the thick prism is shown as the 2-D Real and 2-D Quad at 90 Hz in this figure. The quadrature responses as has been seen on all large sheet models are nearly the same for the 3-D prism and 1-D algorithms. In this case, the quadrature response for the finite thin sheet (indicated as 2-D in the figure) is also in close agreement at 90 Hz. In the case of the real response, the picture is not as clear. The real response is approximately 20 percent below the 1-D response at both 90 and 390 Hz for the 3-D prismatic model as was observed earlier on this and the 60x75 meter model. However, for the 48x60 meter model we also have Lee's 90 Hz response which is clearly between the 1-D and 3-D responses. The difference between the finite thin sheet and the prismatic model is approximately 15 percent deviation which may indicate that for these large 3-D models a larger numerical error may exist than for the smaller prisms described in the first part of this section. However, it is stressed that these errors are small compared to magnitude of the responses and should not affect any of the conclusions reached in this report.

THREE MAJOR RESOLUTION ISSUES:

During a meeting with the COE personnel in late August 1991, three major issues were raised, that were not addressed in the earlier modeling work. The first of these was associated with the feasibility of finding small missing segiments of the mat located within much larger continuous sections. To address this question, the complimentary case to the one described in figures 11-13 above was implemented. For this case, the background 1-D model was composed of a 15 m deep, 25 Ohm-m water layer that was covering a thin conductor with a conductance of 545 siemens, which was in turn located on top of a 5 Ohm-m sedimentary half-space. The anomalous zone was composed of a 7.0 X 6.0 meter resistive (5 Ohm-m) "hole" centered at the origin X=0.0 m. The real anomalous response as a function of position and frequency are provided in figure 19. The 25 ppm contours in this figure approximately outline the edges (X=+/- 3.0 m) of the "hole" over most of the frequency band covered. The anomalous quadrature response is given in figure 20 and the edges of the "hole" are approximately defined by the 10 ppm contours from 300 to 3000 Hz. The much larger real response, which is approximately two orders of magnitude above the measurement noise, at the low frequency end of the band clearly provides the best indication of the void. This simulation shows that the missing set of five mat elements is easily detected in areas where the background parameters remain fairly uniform over the dimensions of the footprint.

The second issue that was raised during the review meeting was associated with the ability to locate the edge of the mat field. To address this question, a profile was generated across a large finite (60x75 m) slab with a conductance of 545 siemens laying under 15 meters of 25 Ohm-m water and over a 5 Ohm-m sedimentary half-space. The anomalous frequency response over the center of the slab was provided in figures 15 and 16. In order to define the field structure over the edge of the slab, a pseudo-section was generated for the anomalous real and quadrature components and displayed in figures 21 and 22 respectively. The fields indicated by the contours are logarithmically compressed due to the wide range in magnitude of responses. The compression was confined to those field values whose absolute value exceeded 1.0. For these values, the base 10 logarithm was applied to the absolute values. Then the original sign was restored and the resulting magnitudes were contoured. It is clear that the edge of the slab located at x= +/- 30 m is well defined by the sharp lateral gradient occurring at all frequencies below 500 Hz in both the real and quadrature components. For the real component, a value of 1.5 that corresponds to an anomalous field value of 31.6 ppm would define the edge. A range of +/- 1.0 meter would correspond to a range in compressed values from 1.2 to 1.8, which transforms to anomalous field values ranging from 15.8 to 63.1 ppm. This means that a variation of 1.0 meter away from the edge results in a factor of four change in the normalized fields, whose values are an order of magnitude above the instrumentation noise. This indicates that if the background parameters are uniform over the footprint that the edge of the mat can be located with approximately 1.0 meter accuracy in 15 m of water.

The third and final issue that was raised at this meeting, was associated with the ability to detect large thin sheet targets in up to 60 m of water and under 6-8 m of sediment. To address this issue an additional suite of 1-D models were generated and evaluated. The model results in terms of both total and

anomalous responses are provided in appendix A and cover a wide range of water depths (20-100 m) and depths of burial (0-8 m) for the targets. It should be remembered that the measurement noise is expected to be on the order of 1.0 ppm and that a dynamic range of 1 part in 4000 is achievable. The results provided by this family of simulations can easily be summarized as follows: 1) the variation in water depth will decrease signal levels and diminish the resolution of the target responses but even at the extreme depth of 60 m the responses are well above the projected noise levels in a layered situation and the targets should be detected; 2) the effect of burying the target greatly diminishes the magnitude of the response but detectable signals are observed at up to 8 m depth within uniform sediments even at extreme water depths; 3) even in those cases for water depths between 60-100 m where the specific depth of burial in the sediments will be dificult to resolve, the presence of the mat is well defined by frequency response below 1000 Hz. Therefore, it is feasible to use EM techniques in these tough situations; however, the background parameters such as sediment conductivity, water depths, and water conductivity must be relatively uniform over the EM system's footprint. If these parameters vary spatially in a significant manner then the target or thin sheet signature may be masked by the resulting perturbations in the fields.

CONCLUSIONS:

The preliminary model study has validated that the simulation accuracies are better than 15 percent and probably much better than 10 percent for small mat sections. The spectral and spatial characteristics indicate that both sections of mat and missing sections with lateral dimensions of 6.0x7.5 m are detectable and smaller sections could be found under stable background conditions. The 3-D simulations indicate that the edge of the mats may be located with an accuracy of approximately 1.0 meter over 15 m of water in a uniform environment. Also, the 3-D simulations indicated that sections of mat, which were buried within the sediments, may be located but that the low amplitude of the response could cause ambiguous interpretation results when the background conditions such as water depth or bottom conductivity changed rapidly. The 1-D and large 3-D models indicated that the large sections of mat should be easily identified, if all sub-sections are well connected electrically. Water depths of up to 60 m and burial depths of up to 10 m within the sediment are viable targets when background parameters are uniform and sheet dimensions are large compared to the footprint.

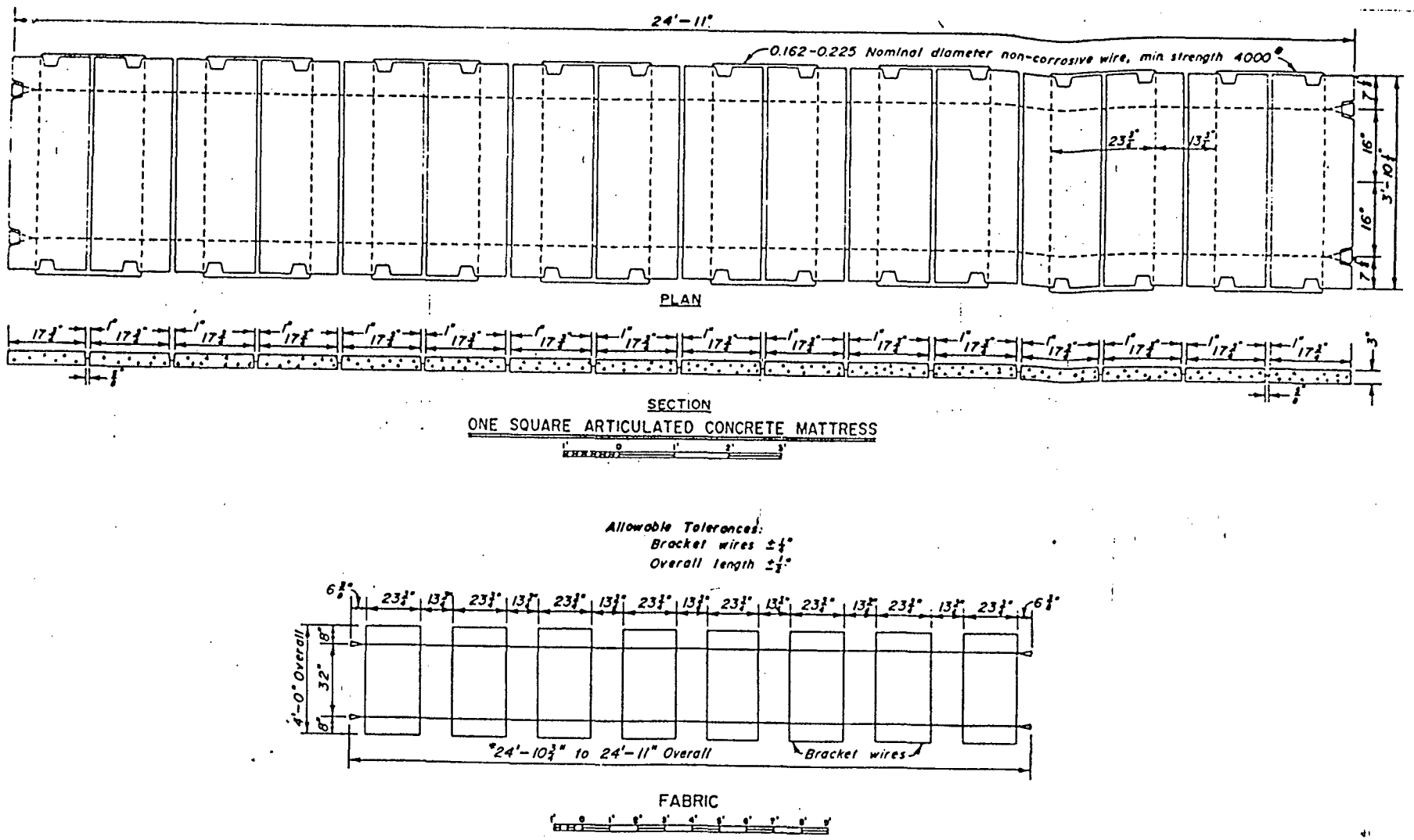

Figure 1 - Construction diagram for a single 25x4 ft (7.5x1.2m) section of concrete mattress.

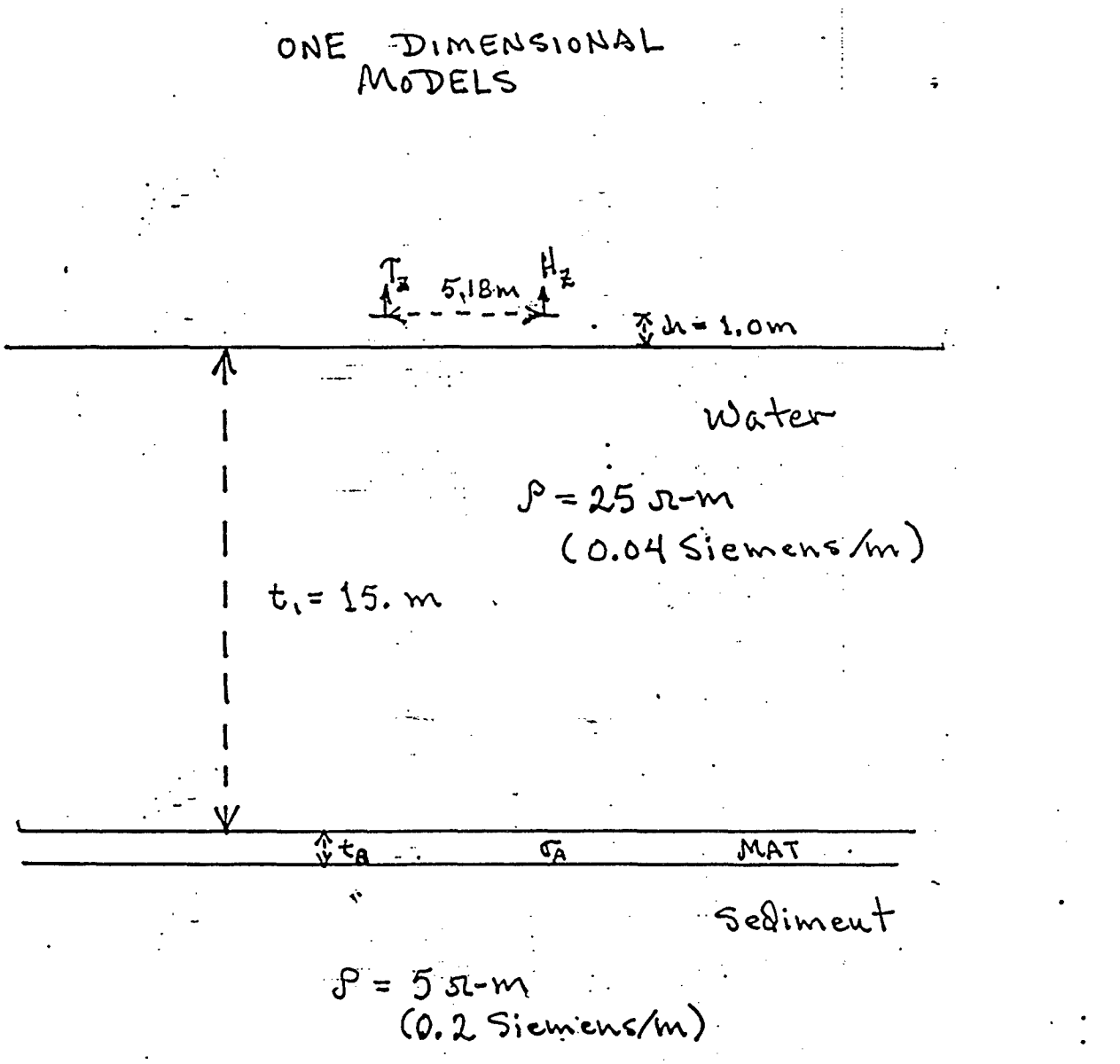

Figure 2 - Sketch and parameters used for one dimensional models for both BSAUT and Newman algorithms.

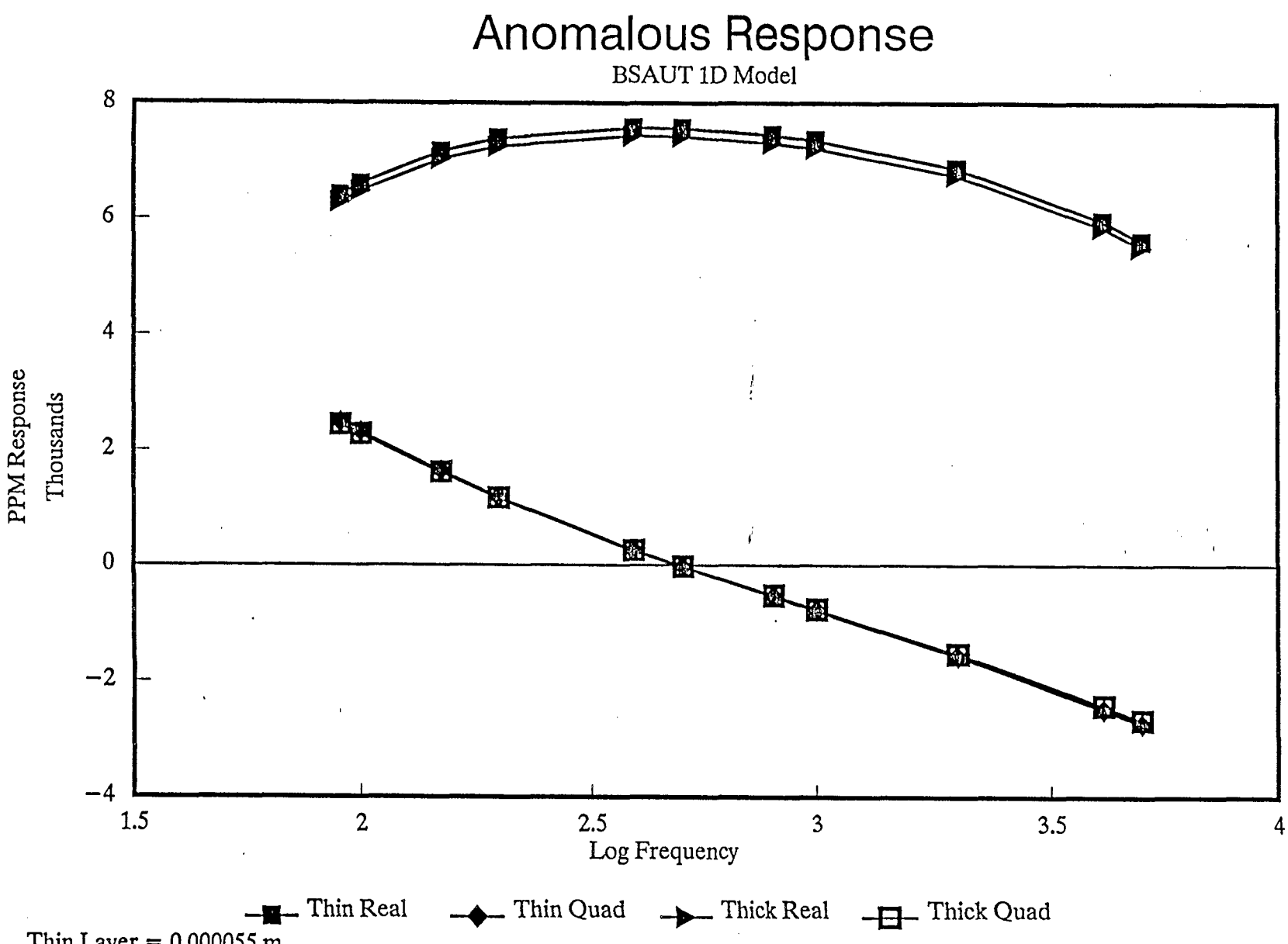

Figure 3 - Comparison of the anomalous responses of two 1D models utilizing the BSAUT algorithm. The

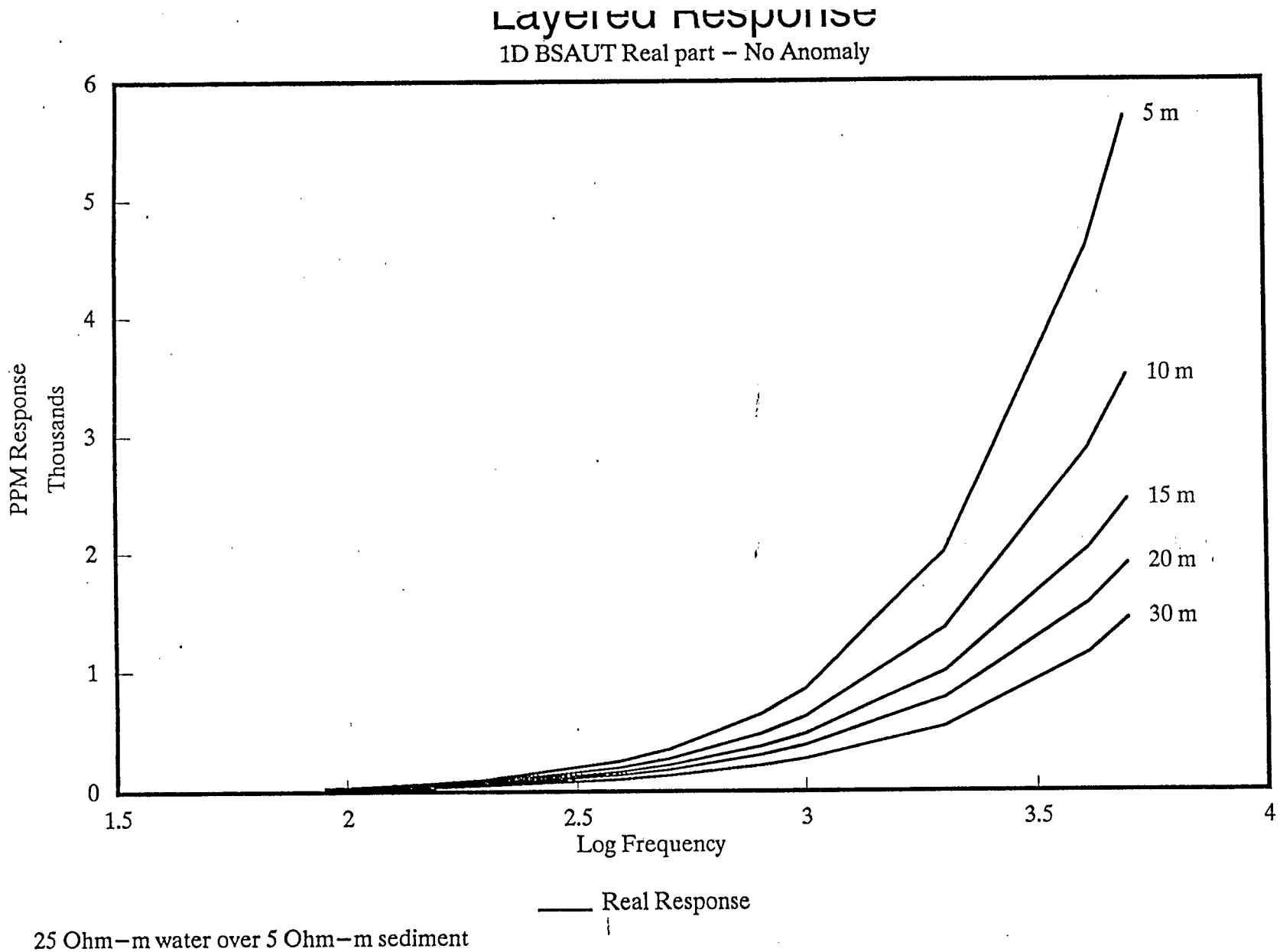

Figure 4 - Variations in the real component of the empty BSAUT layered response with depth of the 25 ohm-m

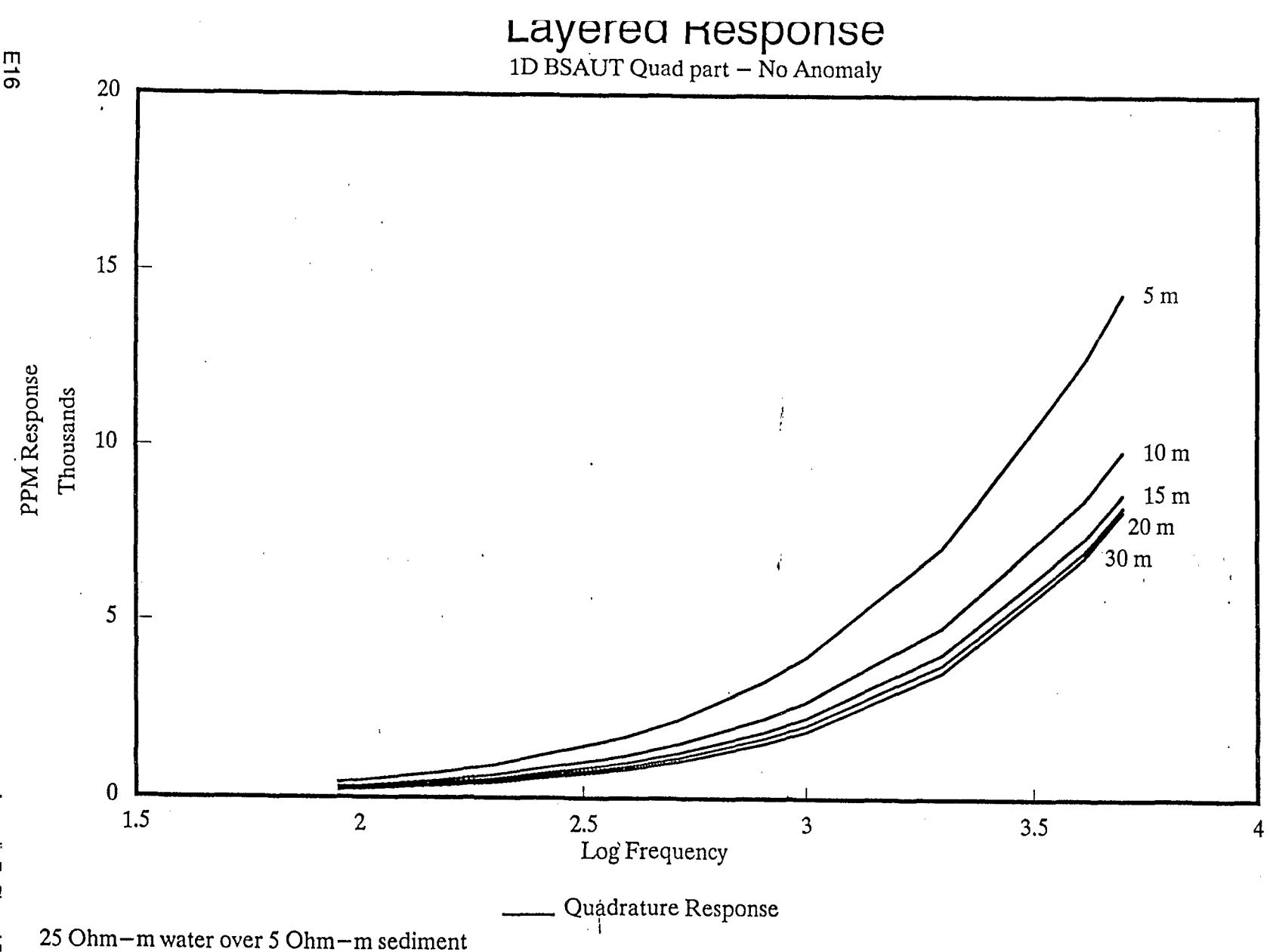

Figure 5 - Variations in the quadrature component of the empty BSAUT layered response with depth of the 25

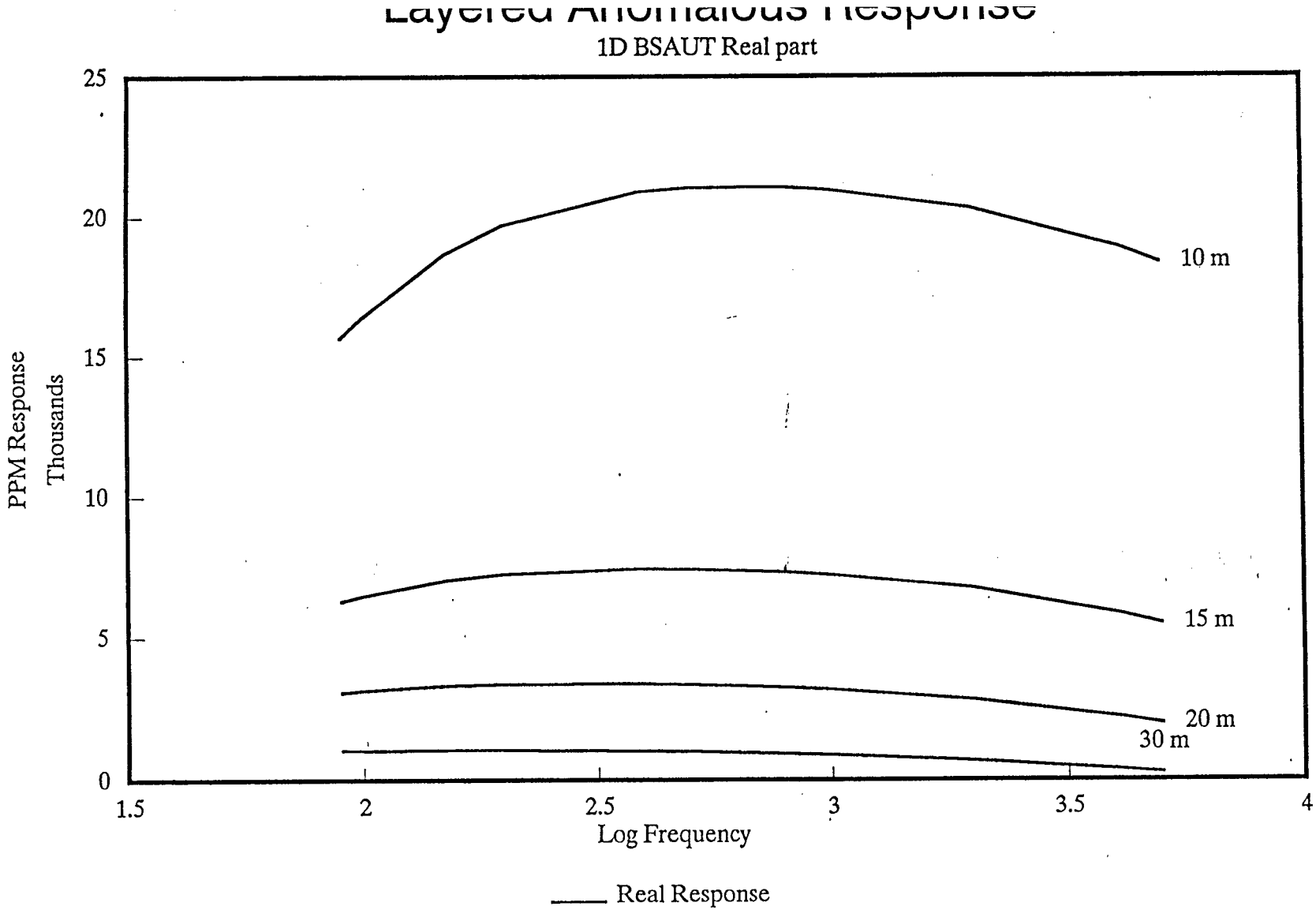

Figure 6 - Variation of the real component of the anomalous response due to a 545.4 conductance layer as the

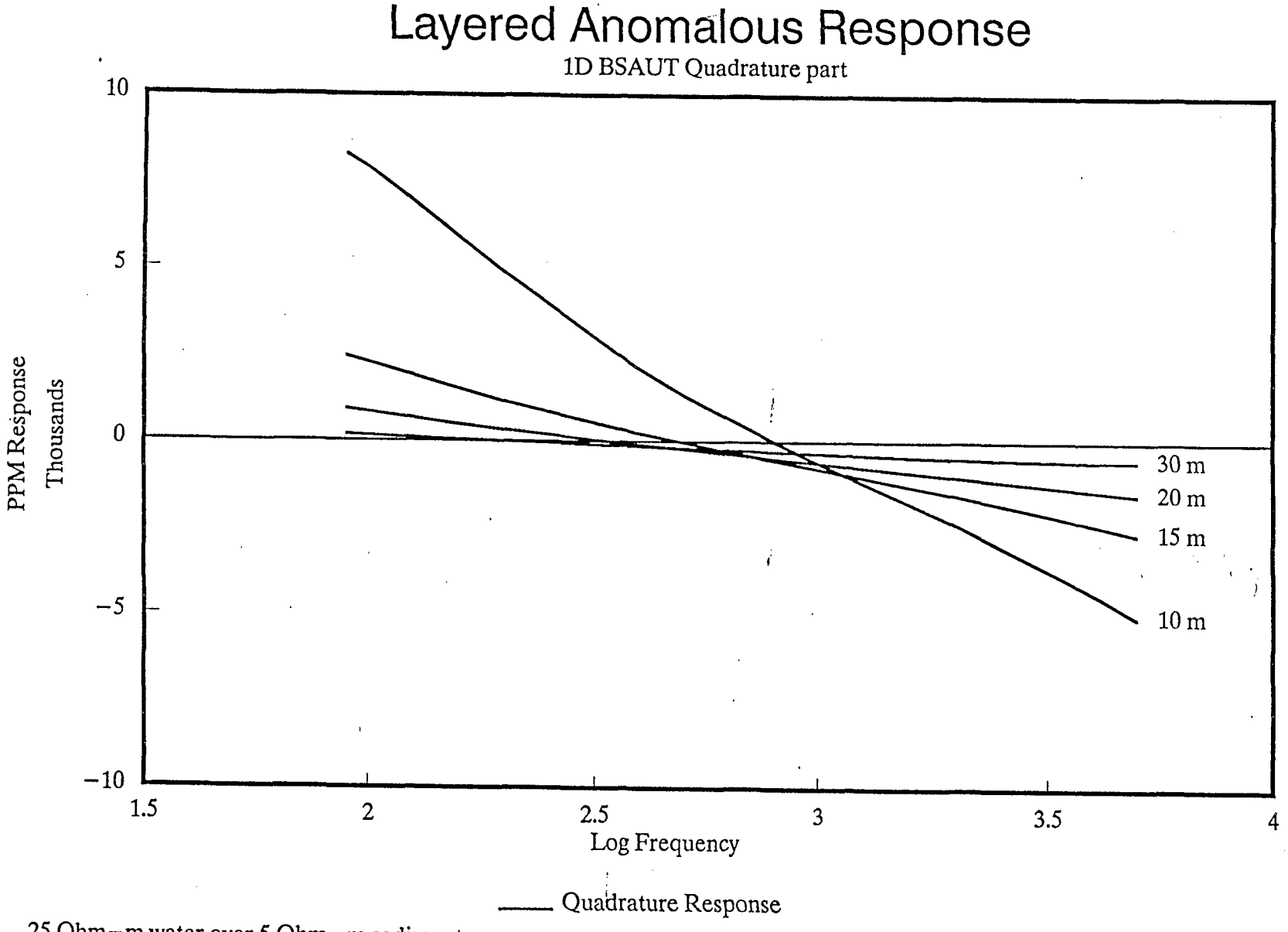

25 Ohm−m water over 5 Ohm−m sediment
Anomaly Sigma−t = 545.5 Siemens

Figure 7 - Variation of the quad component of the anomalous response due to a 545.4 conductance layer as the

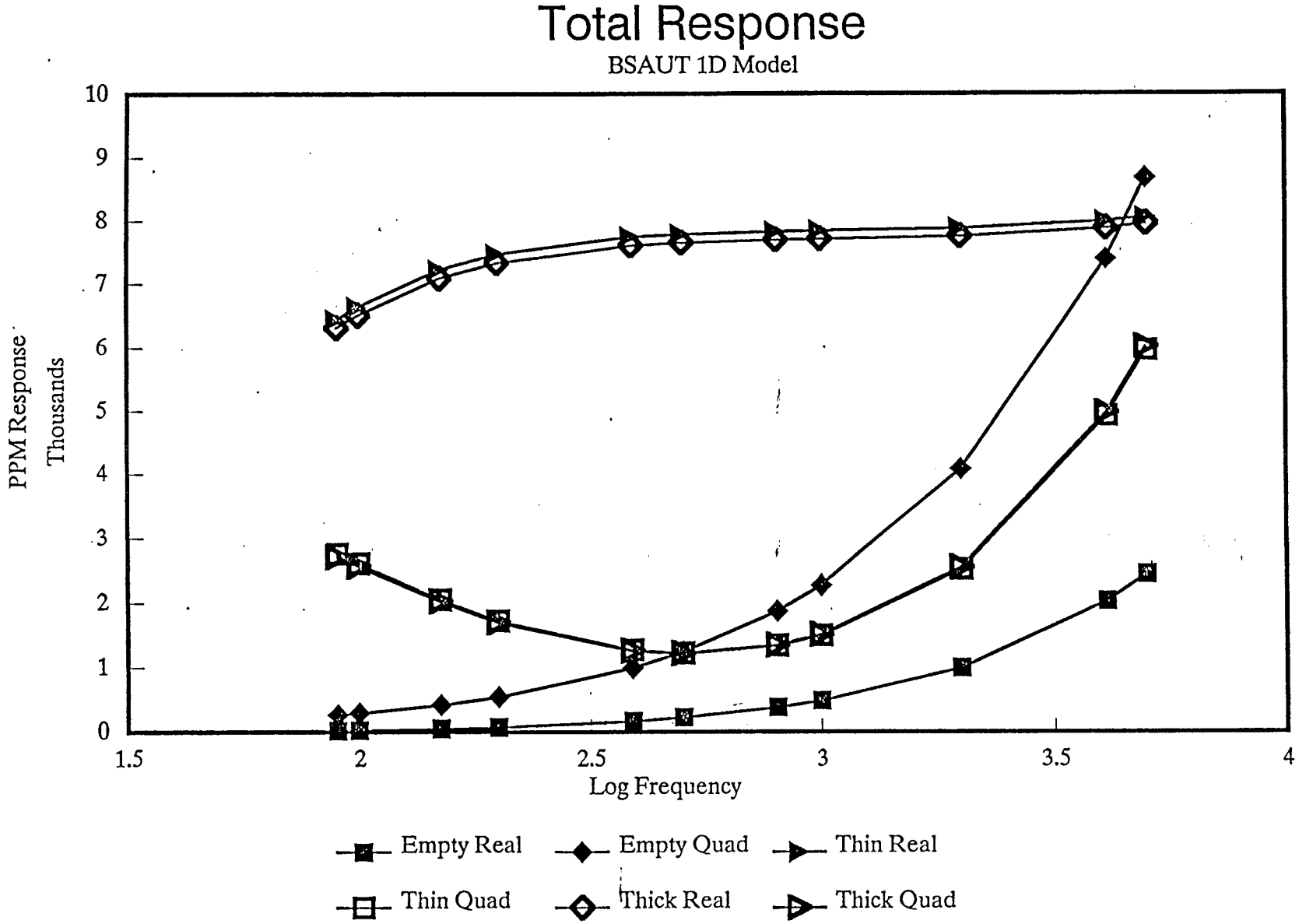

Figure 8 - The total response for thick and thin 1D models compared to the layered (empty) background

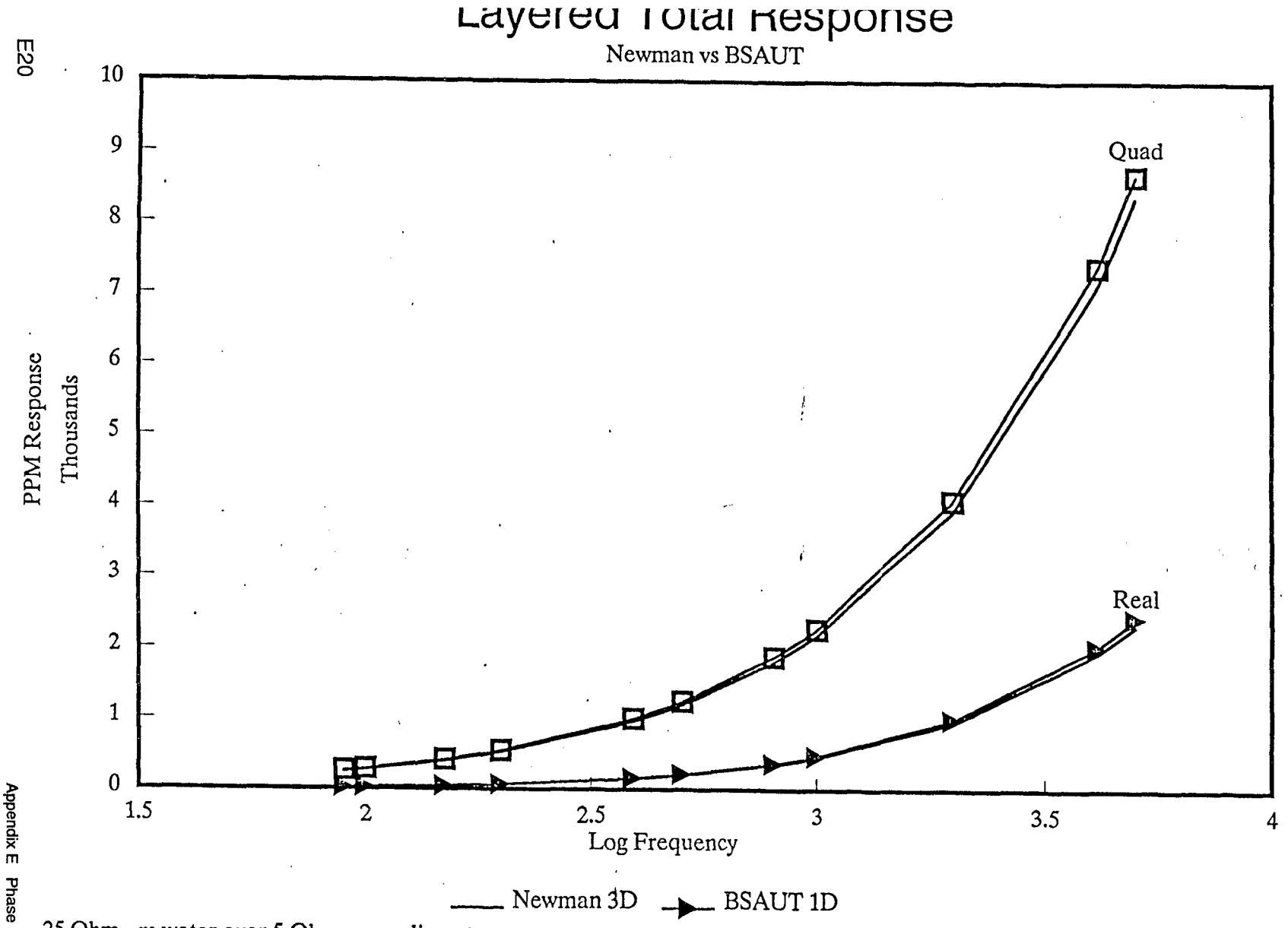

25 Ohm−m water over 5 Ohm−m sediment

Figure 9 - Comparison of the responses of a 15m thick 25 ohm-m layer over a 5 ohm-m water layer. A .3m thick 1818 Siemens/m layer lies between the water and a 5 ohm-m half space from the Newman 3D algorithm and

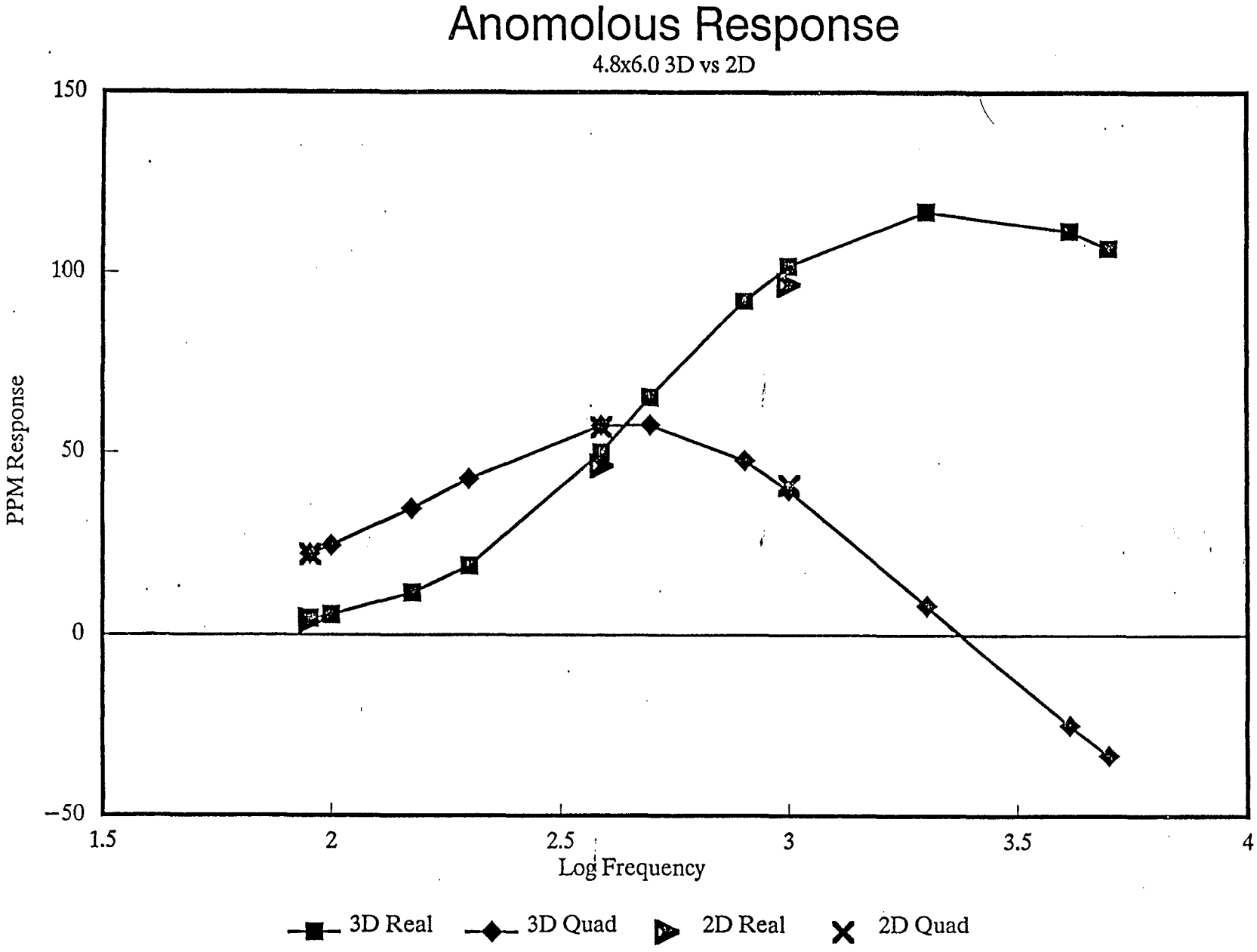

Figure 10 - Comparison of the anomalous responses of the 3D and 2D models of a 4.8 x 6.0m object with sigma

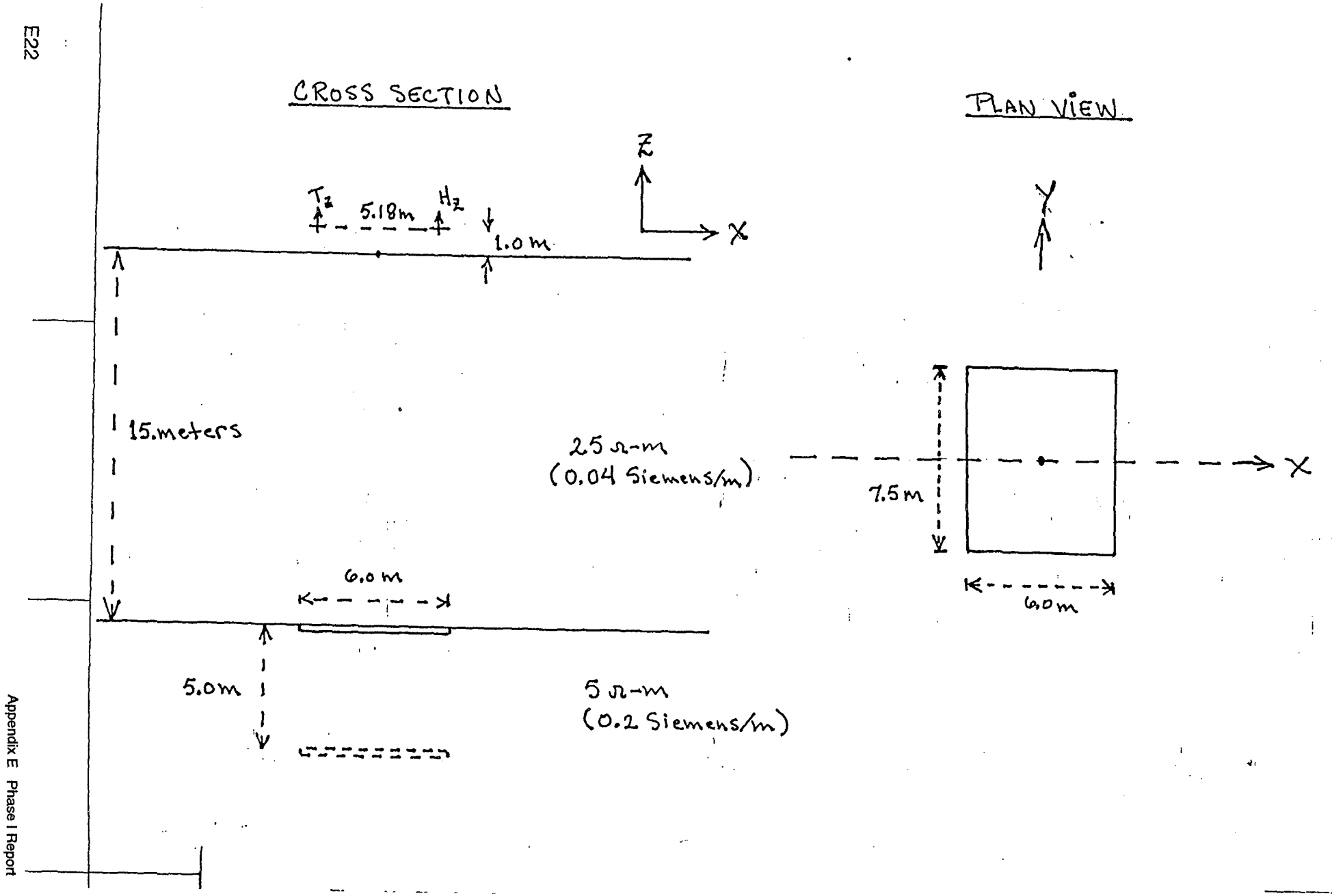
CROSS SECTION
PLAN VIEW
Z
X
T_z
5.18m
H_z
1.0 m
15.meters
25 Ω-m
(0.04 Siemens/m)
6.0 m
5.0m
5 Ω-m
(0.2 Siemens/m)
Y
X
7.5 m
6.0 m

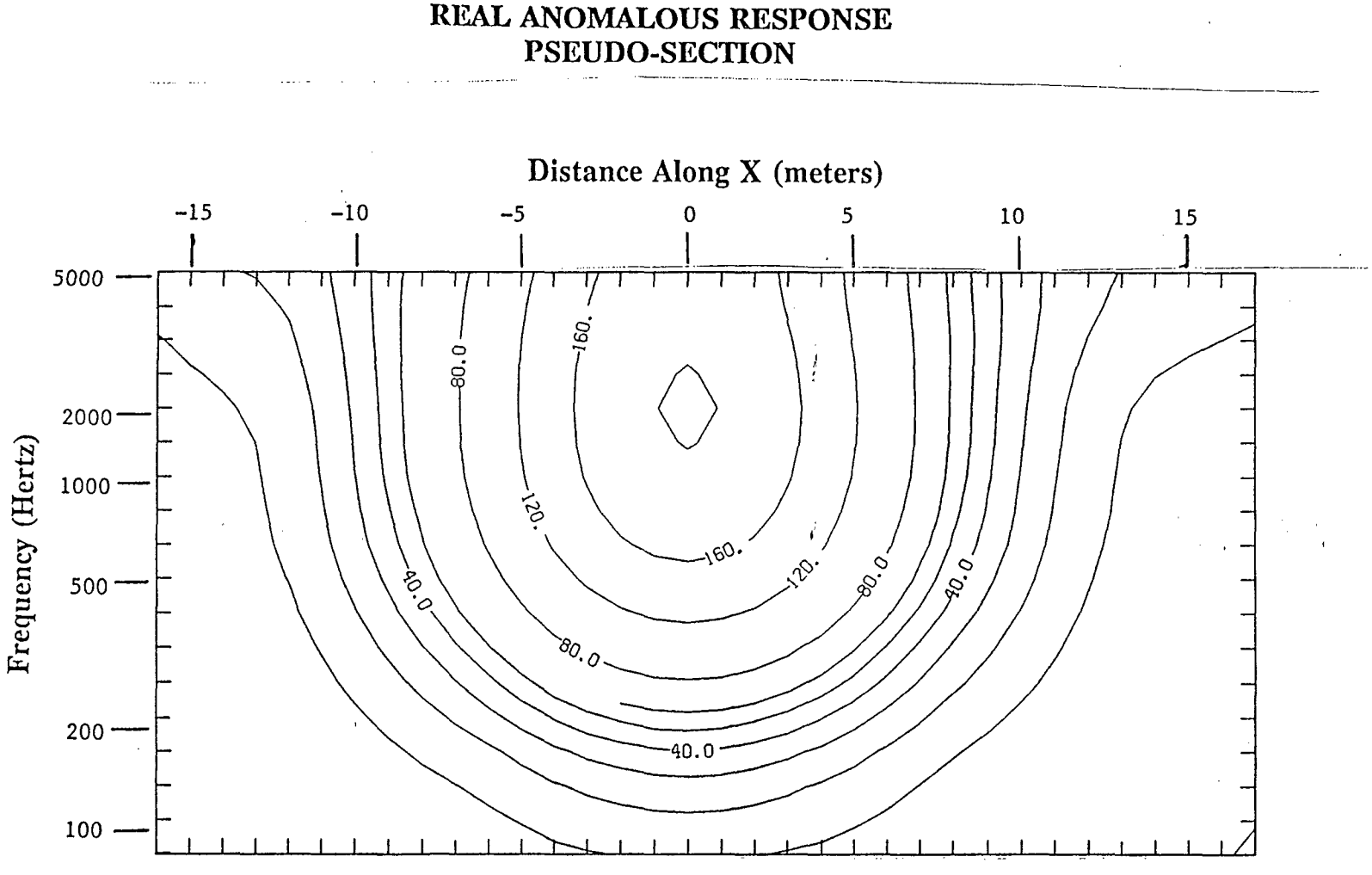

Figure 12 - Pseudosection of the real anomalous response of a 6.0 x 7.5 x 0.3 m thick slab with a conductivity of 1818 Siemens/m centered at (0,0). The transmitter is located at (X-2.59,0) and the receiver is located at (X+2.59,0). Response is indicated in ppm of source field.

QUADRATURE ANOMALOUS RESPONSE
PSEUDO-SECTION

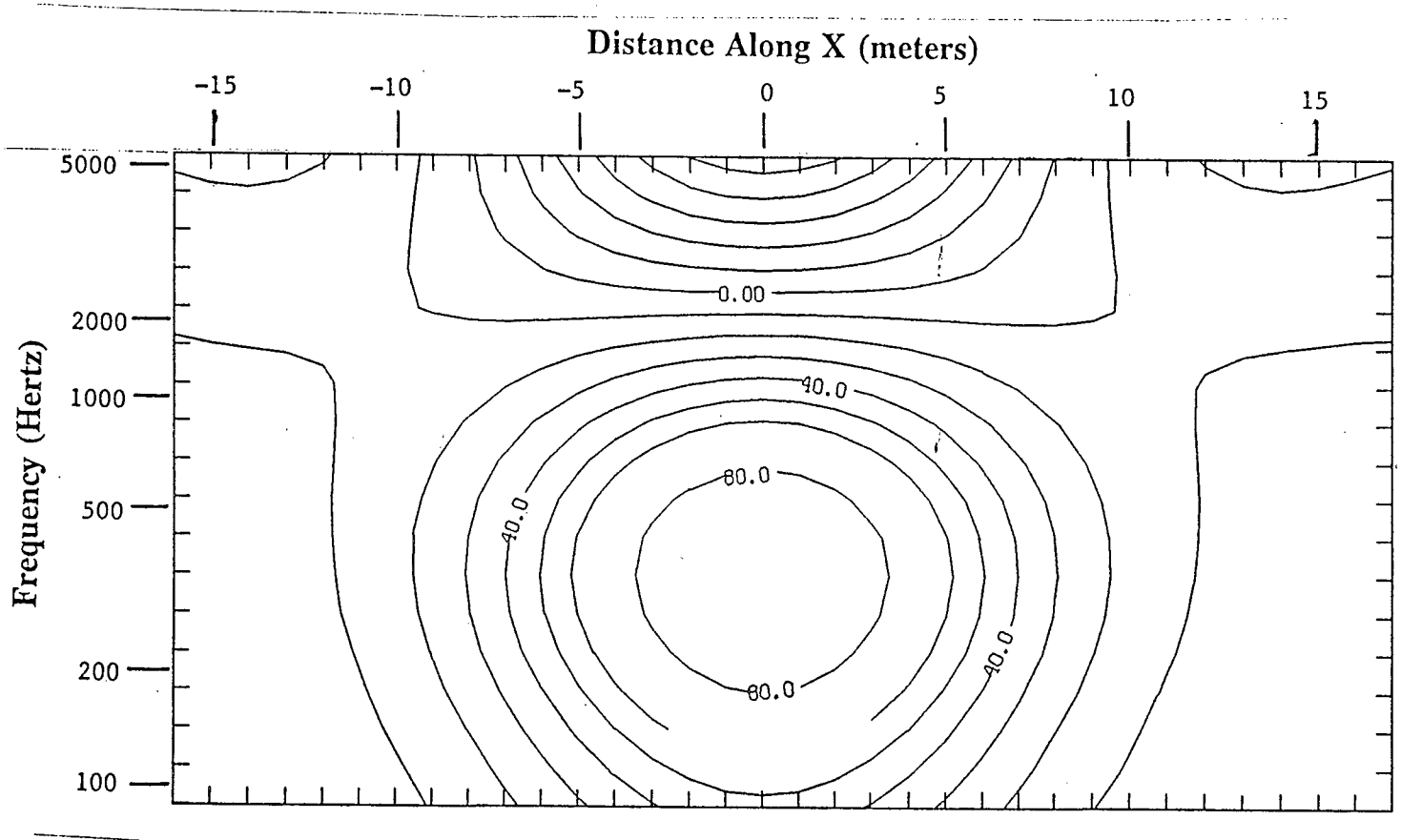

Figure 13 - Pseudosection of the quadrature anomalous response of a 6.0 x 7.5 x 0.3 m thick slab with a conductivity of 1818 Siemens/m centered at (0,0). The transmitter is located at (X-2.59,0) and the receiver is located at (X+2.59,0). Response is indicated in ppm of source field.

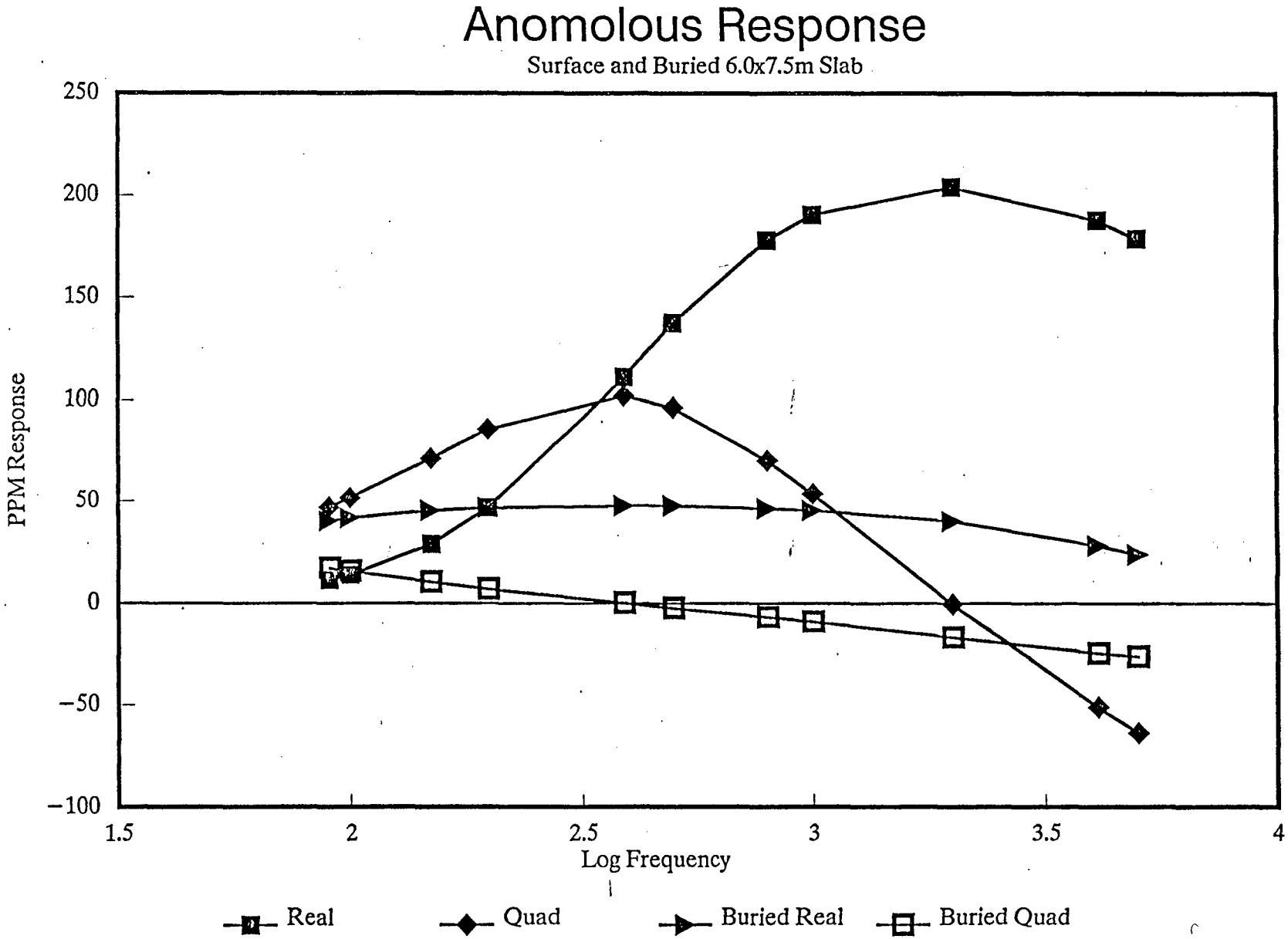

Figure 14 - Anomalous responses of identical 6.0 x 7.5 x .3m slabs, one with a top surface at the water sediment

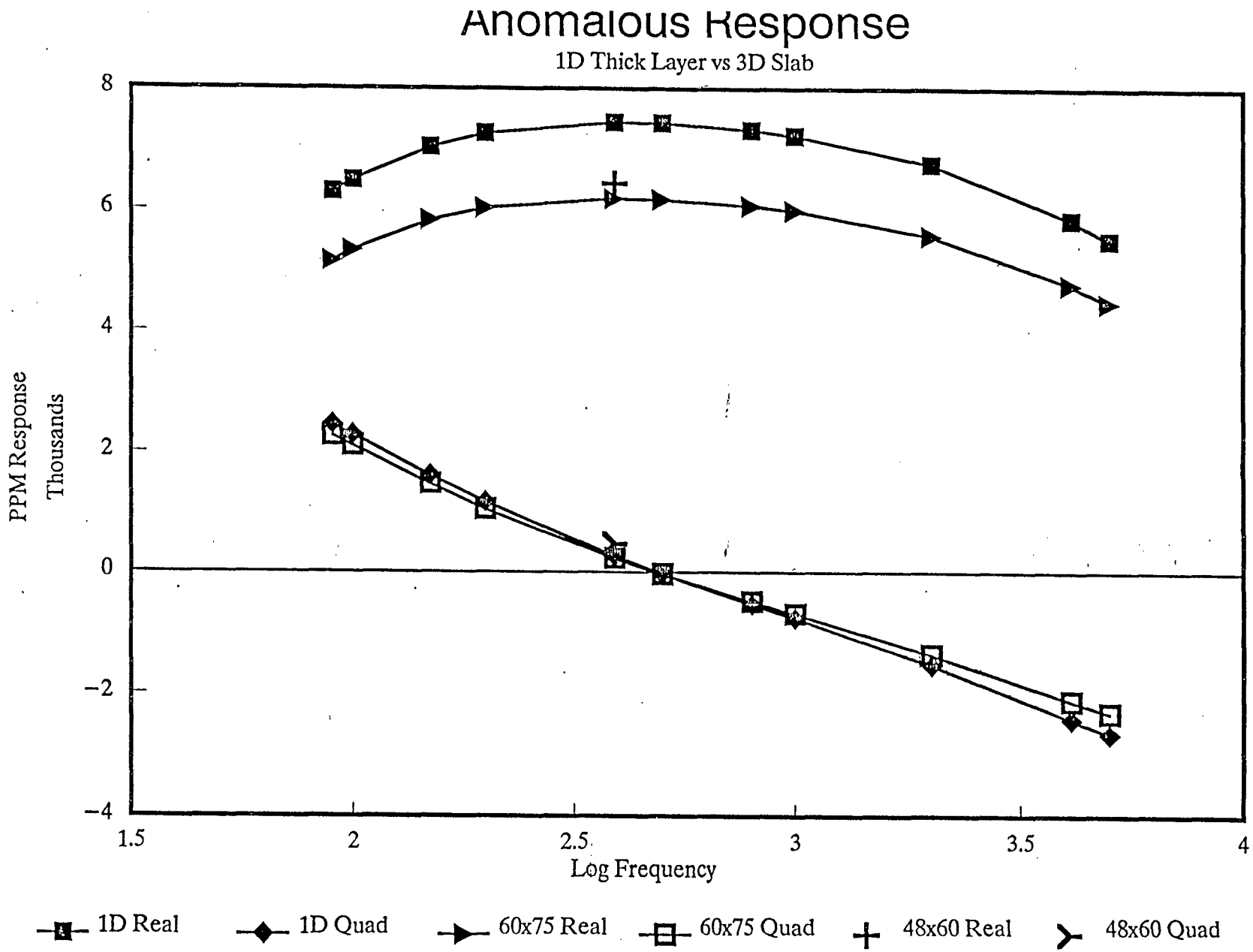

Figure 15 - Comparison of the anomalous responses of a 1D 3m thick sheet (sigma = 1818 Siemens/m) and

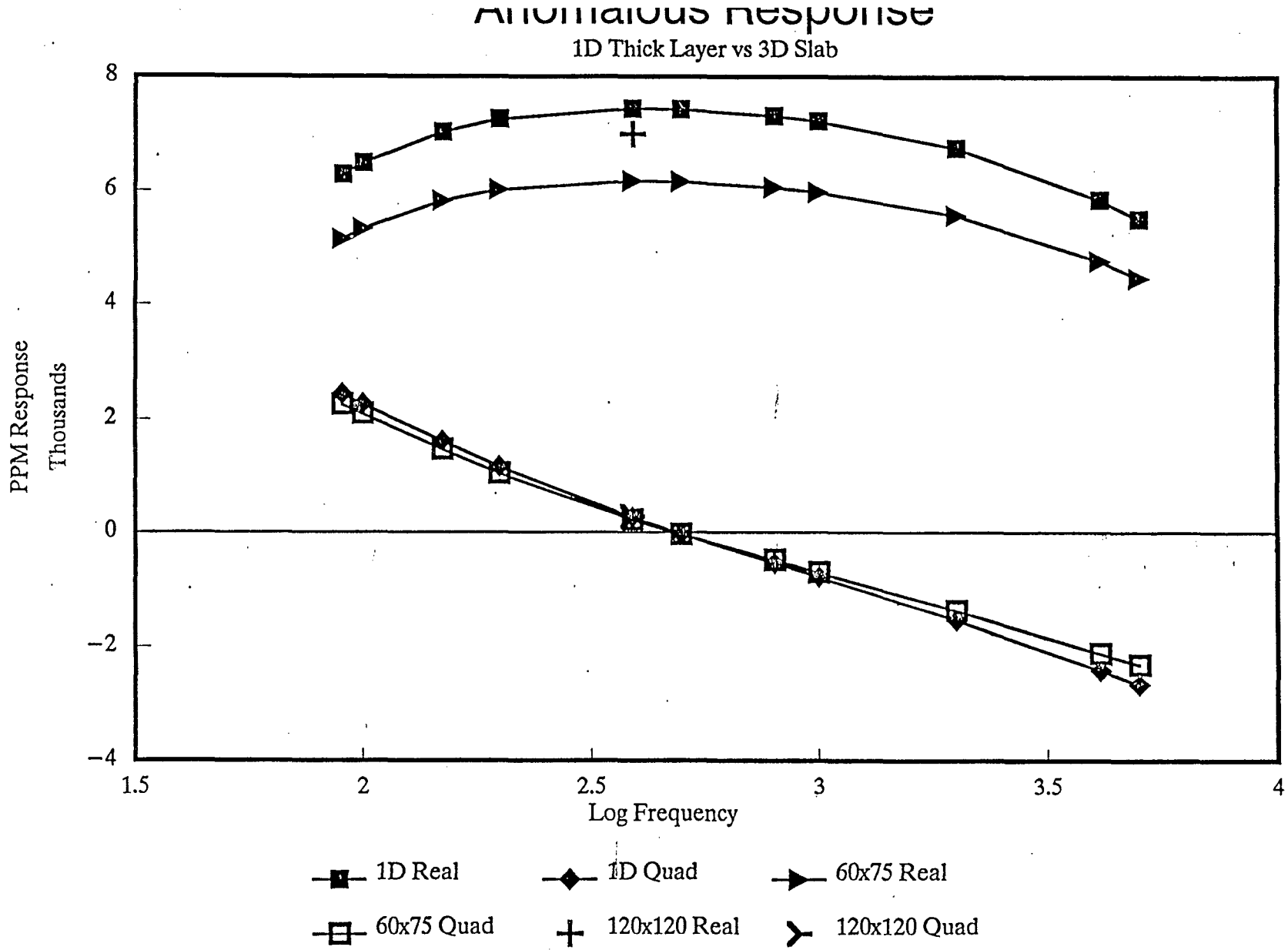

Figure 16 - Anomalous response of 1D and 3D models in ppm of the source field. The X axis represents logarithmic frequency. The 1D model is an infinite sheet .3m thick while the 3D models are 60 x 75 x .3m and

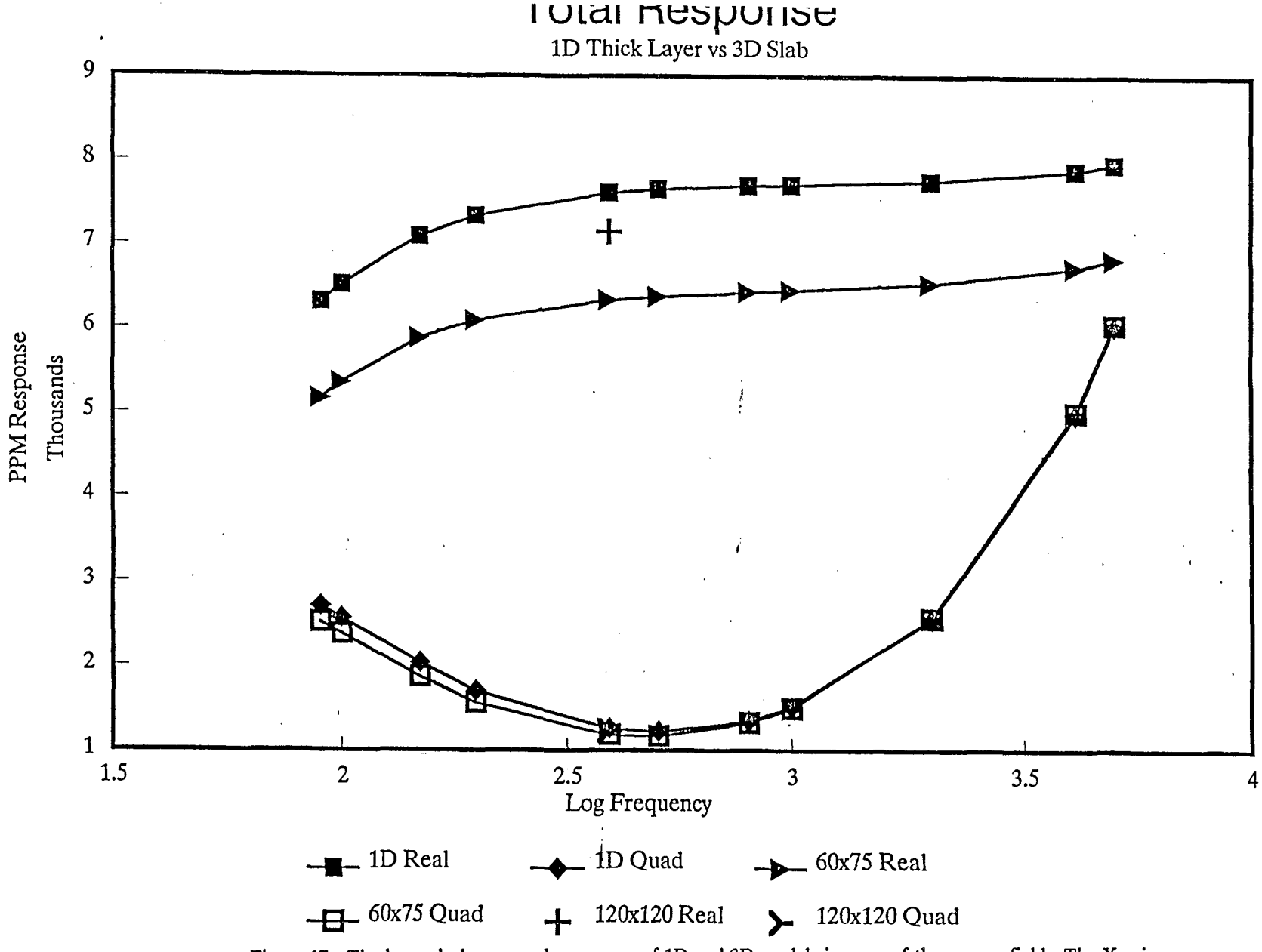

Figure 17 - The layered plus anomaly response of 1D and 3D models in ppm of the source field. The X axis represents logarithmic frequency. The 1D model is an infinite sheet .3m thick while the 3D models are 60 x 75

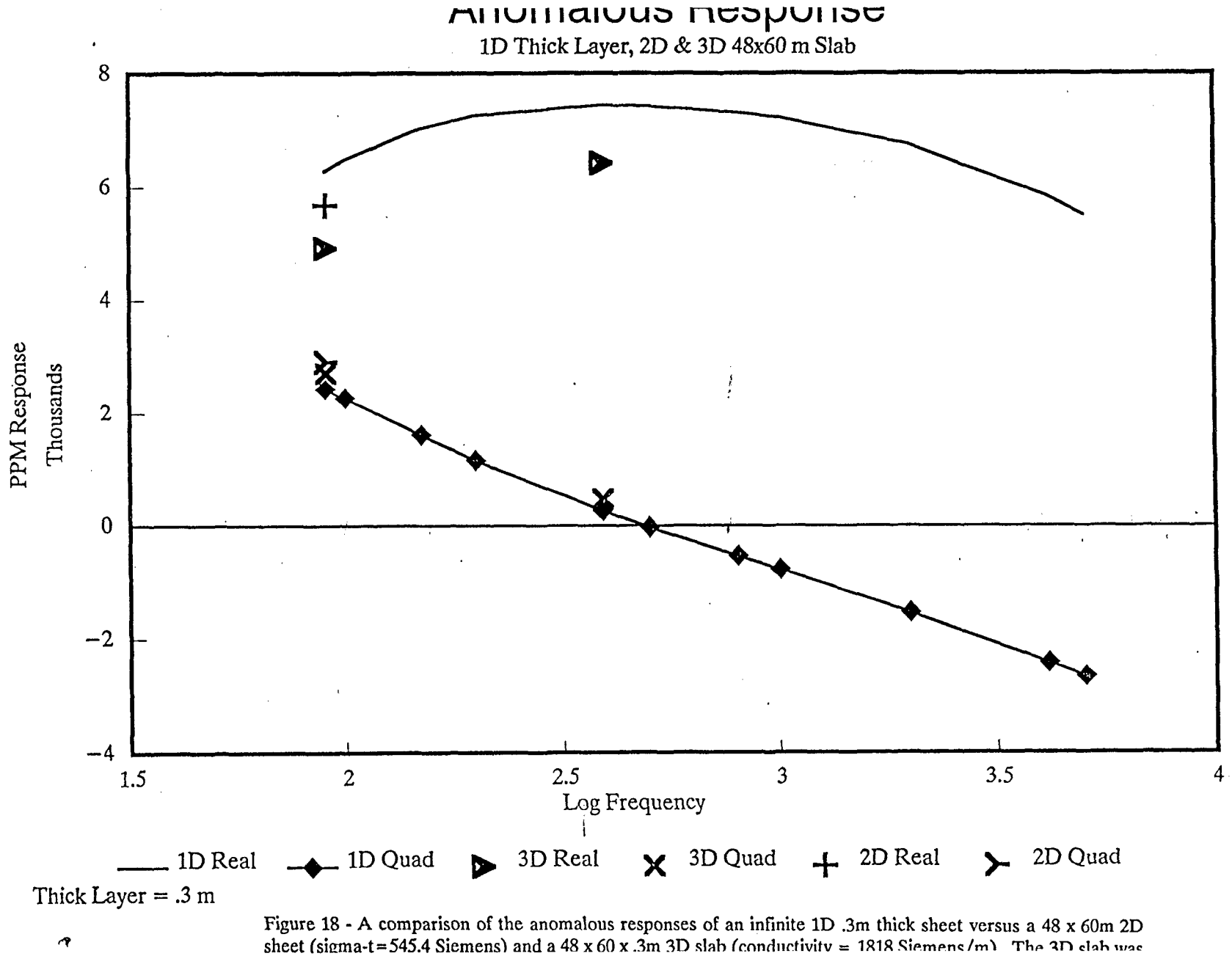

Figure 18 - A comparison of the anomalous responses of an infinite 1D .3m thick sheet versus a 48 x 60m 2D sheet (sigma-t=545.4 Siemens) and a 48 x 60 x .3m 3D slab (conductivity = 1818 Siemens/m). The 3D slab was

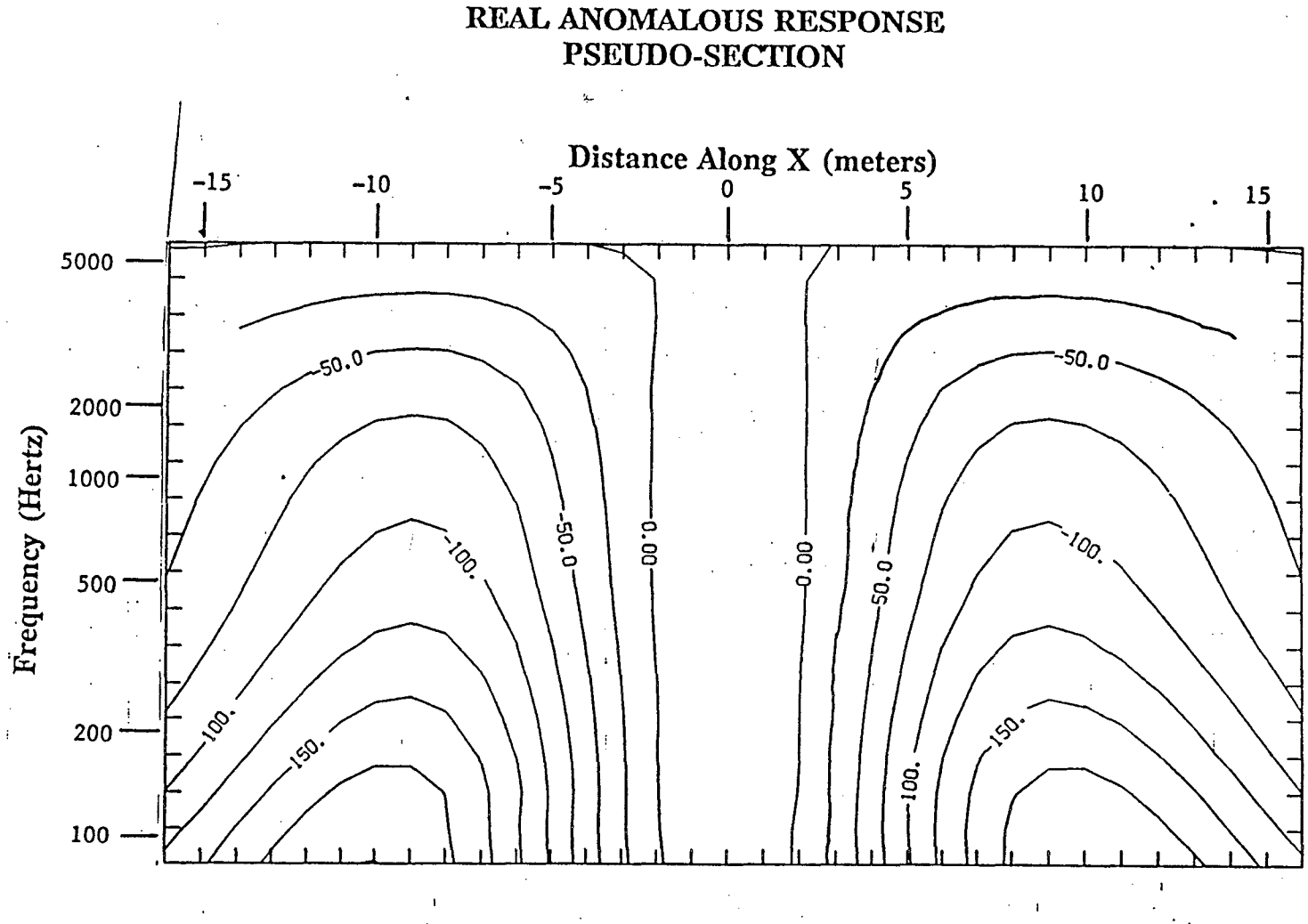

Figure 19 - Real anomalous response for a 6.0 x 7.5 m 0.5 Siemen "hole" in an infinite 0.3 m thick 1818 Siemens/m conductivity sheet. The hole is centered at (0,0). Contours are spaced at 25 ppm intervals. The transmitter is located at (X-2.59,0) and the receiver at (X+2.59,0).

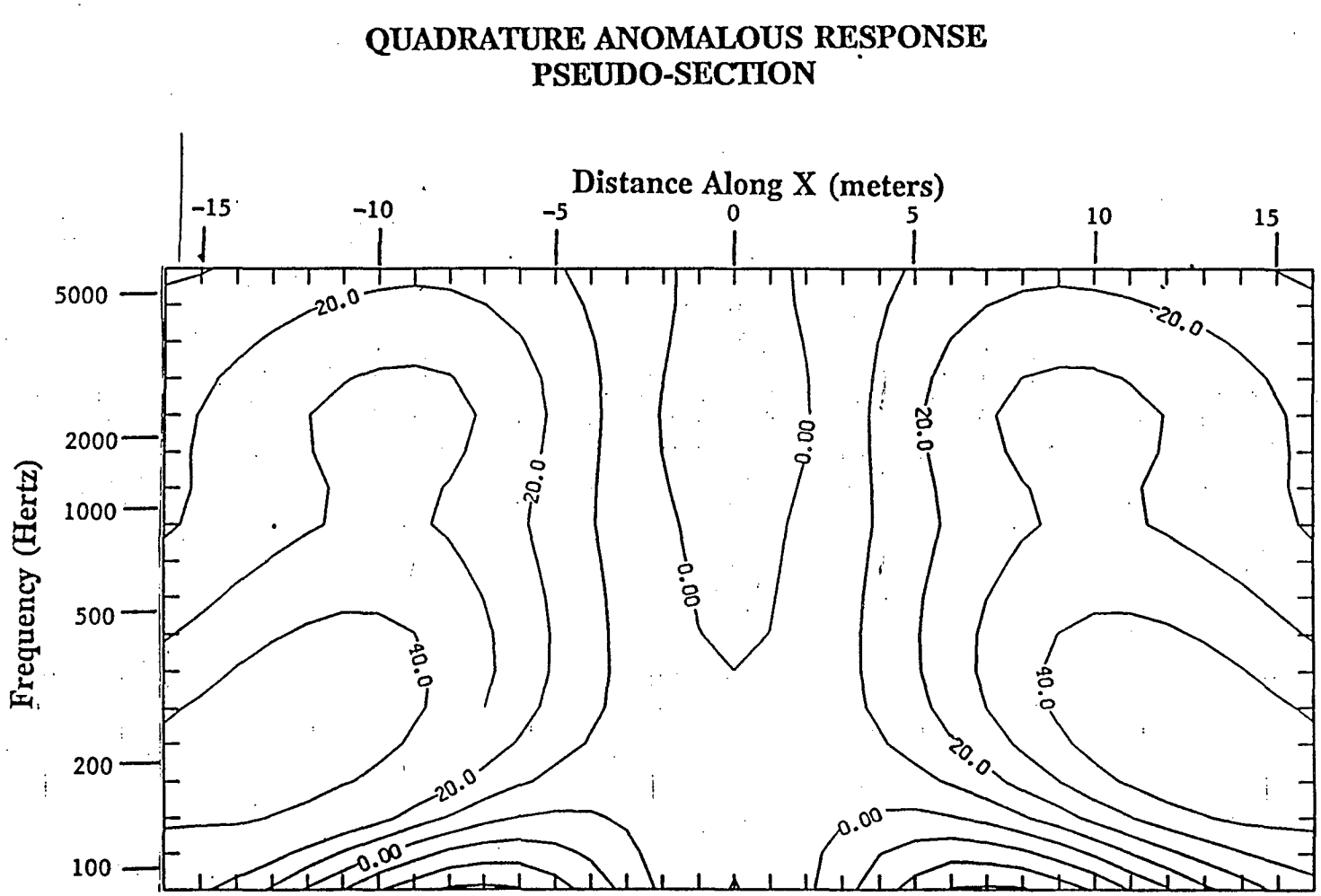

Figure 20 - Quadrature anomalous response for a 6.0 x 7.5 m 0.5 Siemen "hole" in an infinite 0.3 m thick 1818 Siemens/m conductivity sheet. The hole is centered at (0,0). Contours are spaced at 10ppm intervals. The transmitter is located at (X-2.59,0) and the receiver at (X+2.59, 0).

REAL ANOMALOUS RESPONSE PSEUDO-SECTION

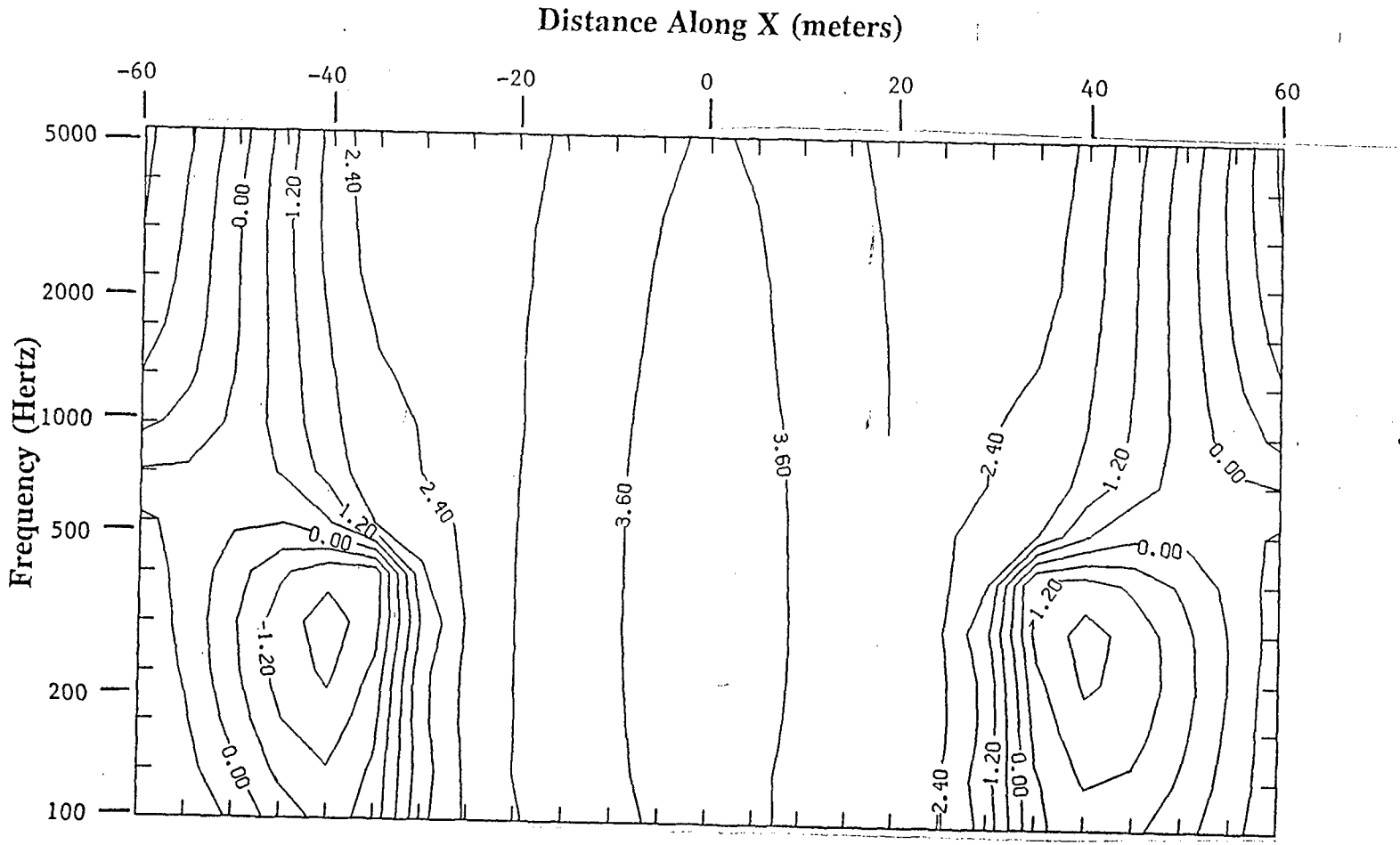

Figure 21 - Real anomalous response for a 60 x 75 x 0.3 m slab centered at (0,0) with a 1818 Siemens/m conductivity. Contours represent the logarithmically compressed response spaced at 0.6 unit intervals. The transmitter is located at (X-2.59.0) and the receiver at (X+2.59.0).

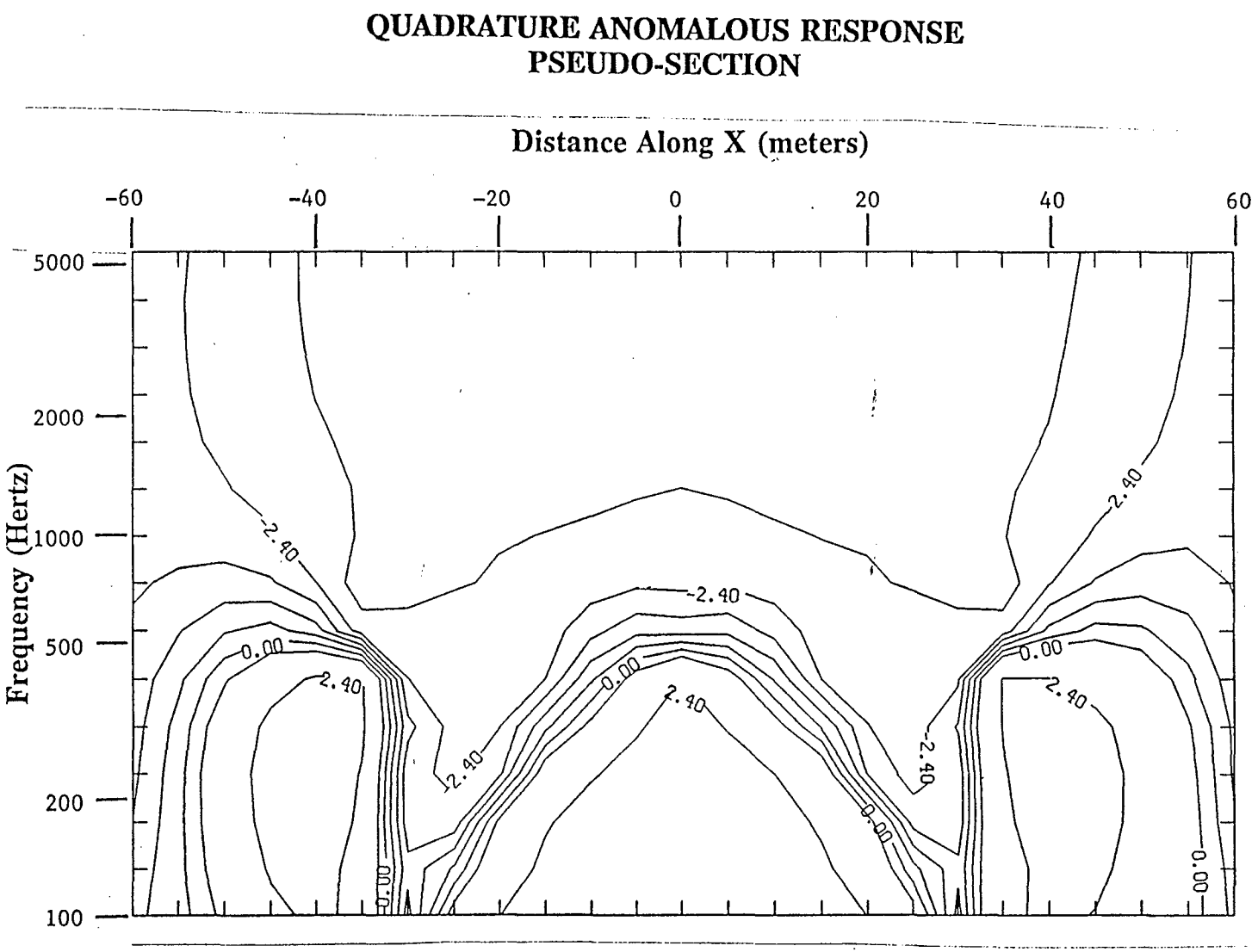

Figure 22 - Quadrature anomalous response for a 60 x 75 x 0.3 m slab centered at (0,0) with a 1818 Siemens/m conductivity. Contours represent the logarithmically compressed response spaced at 0.6 unit intervals. The transmitter is located at (X-2.59,0) and the receiver at (X+2.59,0).

APPENDIX A

The appendix provides the results for a suite of 1-D simulations composed of a thin conductive sheet with a 545 Siemen conductance buried at various depths ranging from 0 to 8 m within a uniform 5 Ohm-m half-space that is overlain by a 25 Ohm-m water layer that varies in depth from 20 to 100 m. The first two figures provide the real and quadrature total field responses for the thin sheet buried at 0, 2, 4, 6, and 8 m within the sediment under 20 m of water. The third and forth figures provide the same information except the water depth is 40 m. The fifth and sixth figures have same responses as the previous sets except the water depth is 60 m. The background model that is defined as only the water layer over the sedimentary half-space is provided in each of these six figures for reference. At a water depth of 60 m, the quadrature response approaches the background model at the resolution dictated by the large background signals. Therefore the responses at water depths greater than 60 m were not plotted as total normalized fields. The remaining figures A7-A16 provide the anomalous responses that are defined as the total response minus the background response. These responses are provided for the real and quadrature components at water depths of 20, 40, 60, 80 and 100 m. It should be noted that measurable responses are observed below 1000 Hz at all water depths calculated.

Total Response – Real

1D – 20 Meter Water Depth

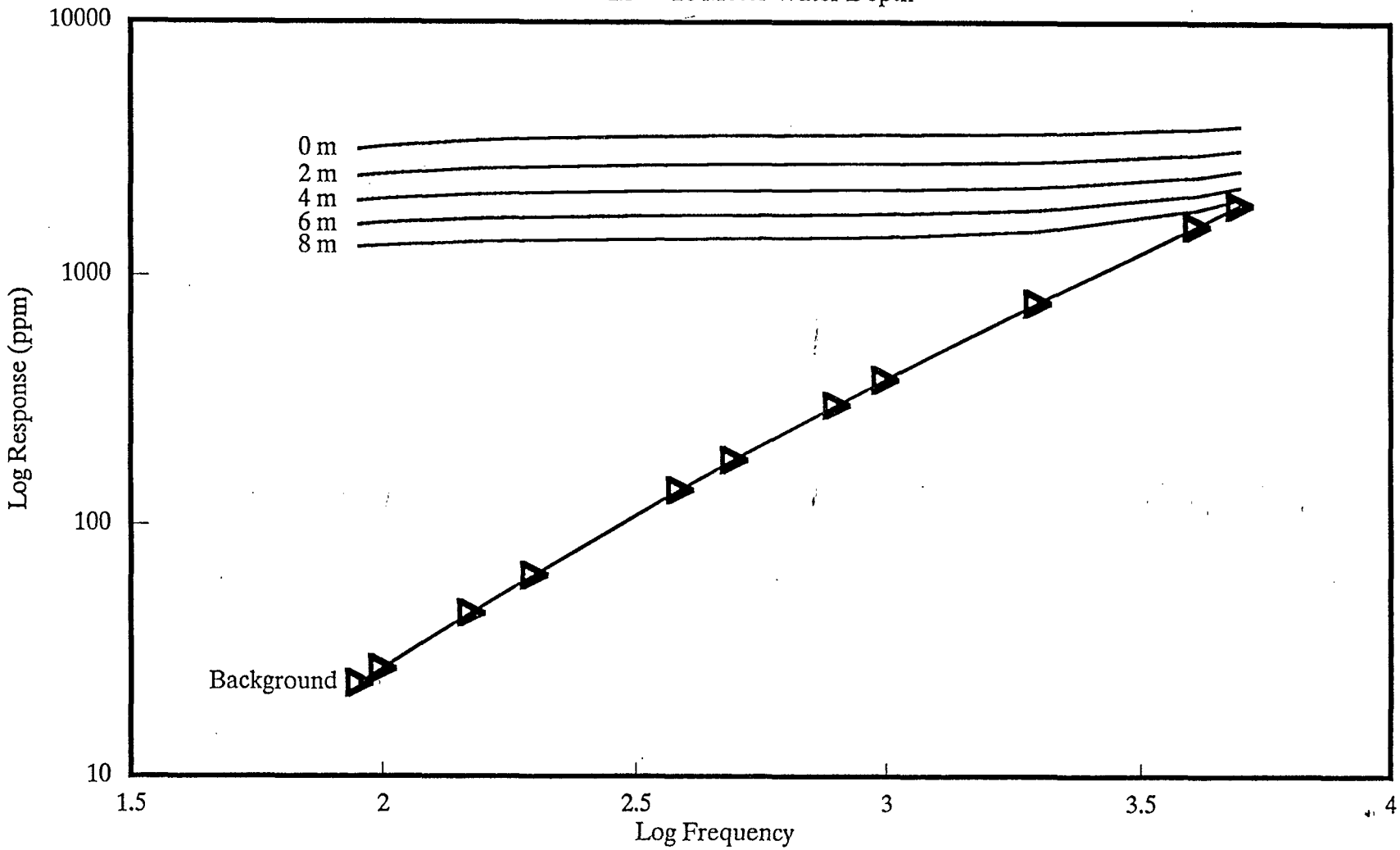

Conducting Layer Response Background – No Conductor

Water 25 Ohm–M Bottom 5 Ohm–M
Buried Layer at 5 Depths, 546 Siemens Conductance

Total Response – Quadrature

1D – 20 Meter Water Depth

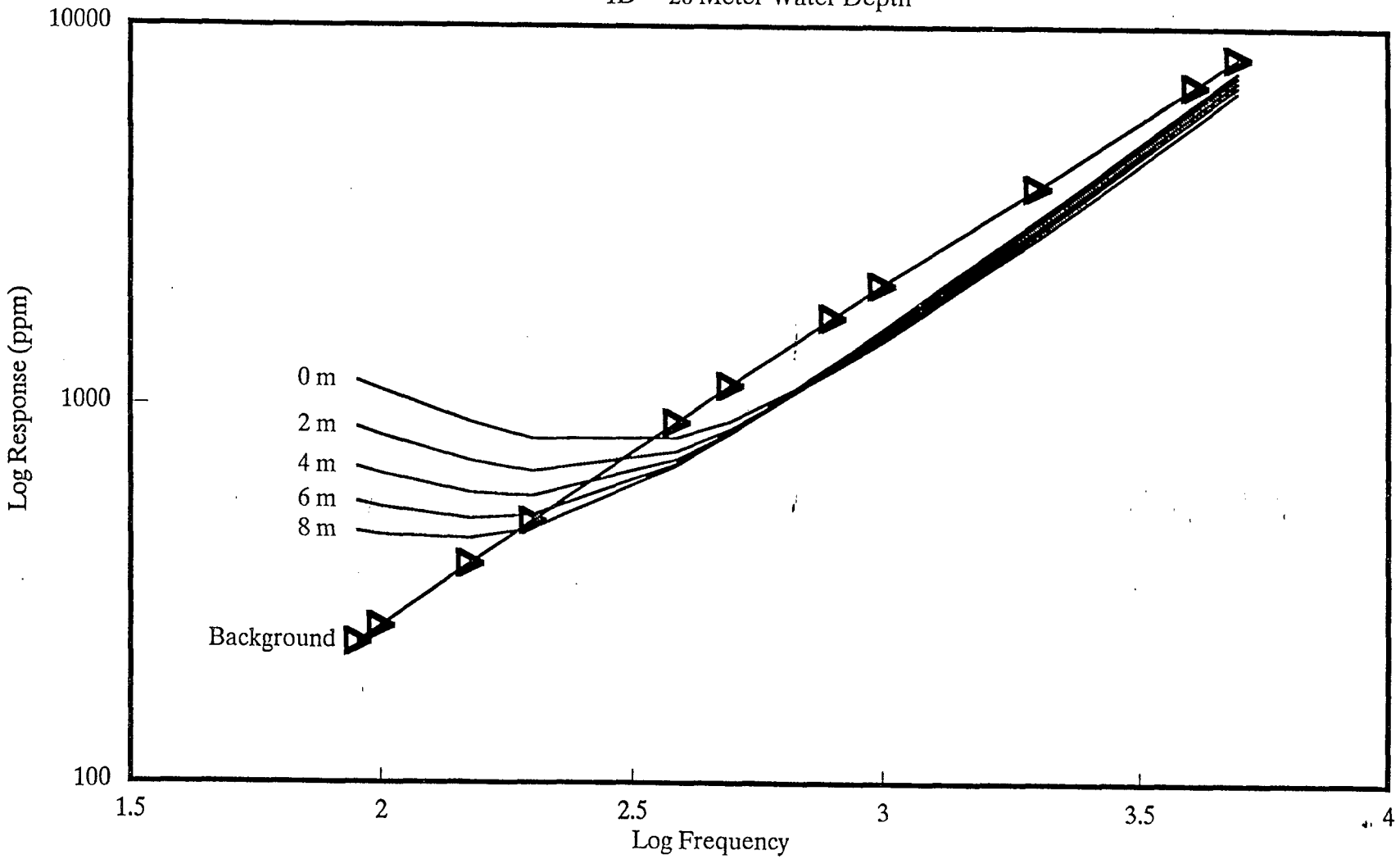

Conducting Layer Response Background – No Conductor

Water 25 Ohm–M Bottom 5 Ohm–M
Buried Layer at 5 Depths, 546 Siemens Conductance

Total Response – Real

1D – 40 Meter Water Depth

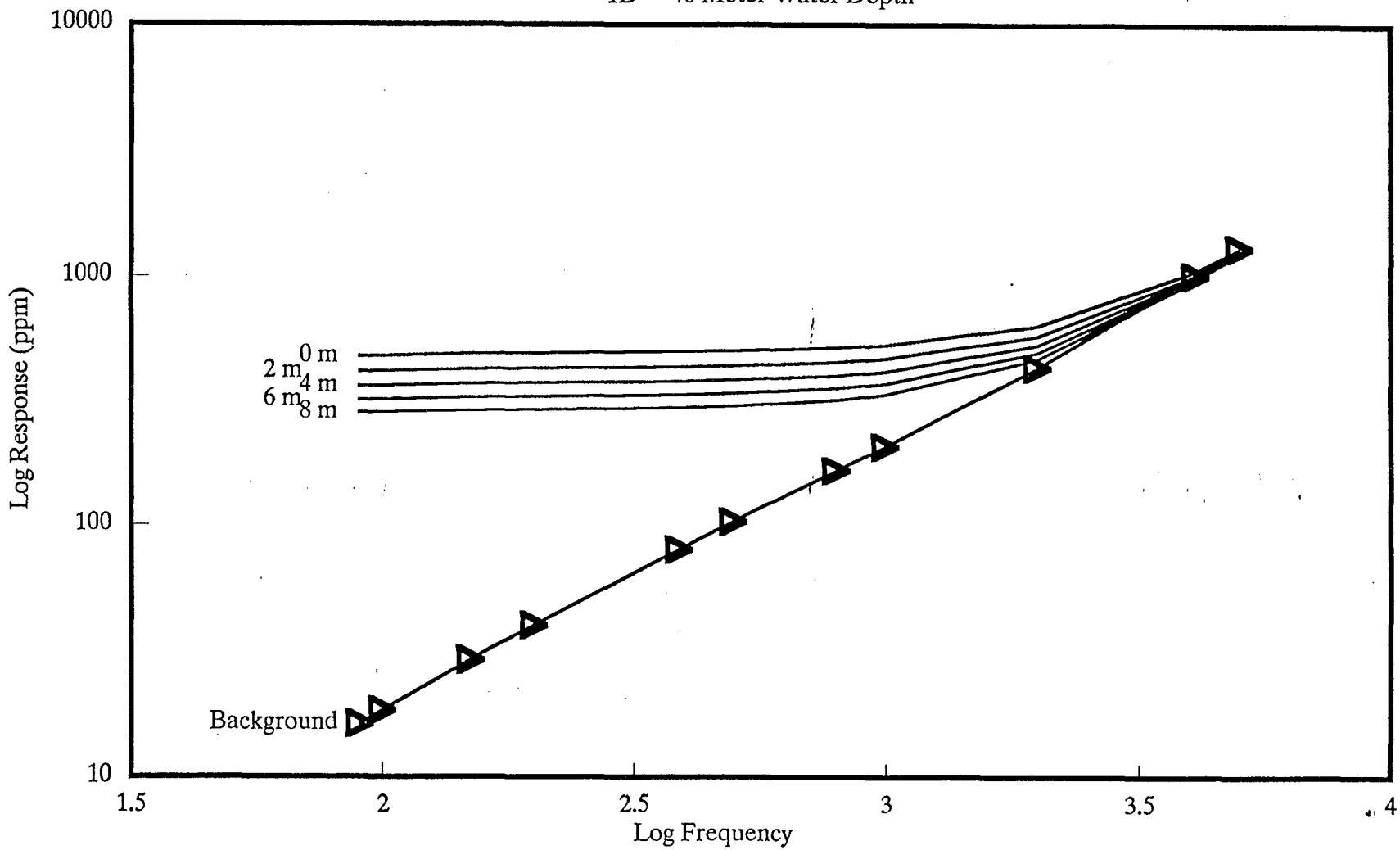

Conducting Layer Response Background – No Conductor

Water 25 Ohm–M Bottom 5 Ohm–M

Buried Layer at 5 Depths 546 Siemens Conductance

Total Response – Quadrature

1D – 40 Meter Water Depth

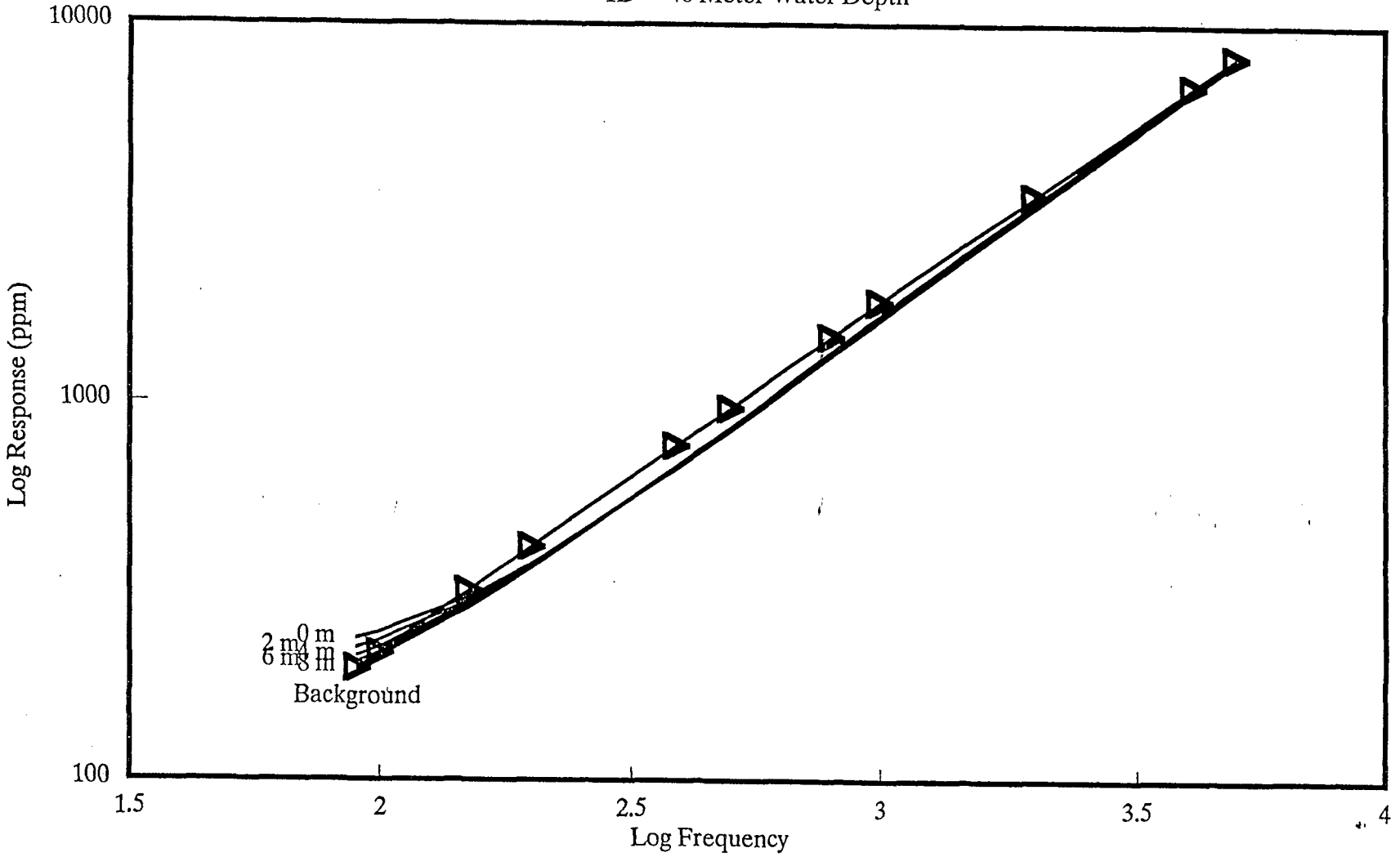

Conducting Layer Response — Background – No Conductor

Water 25 Ohm–M Bottom 5 Ohm–M
Buried Layer at 5 Depths, 546 Siemens Conductance

Total Response – Real

1D – 60 Meter Water Depth

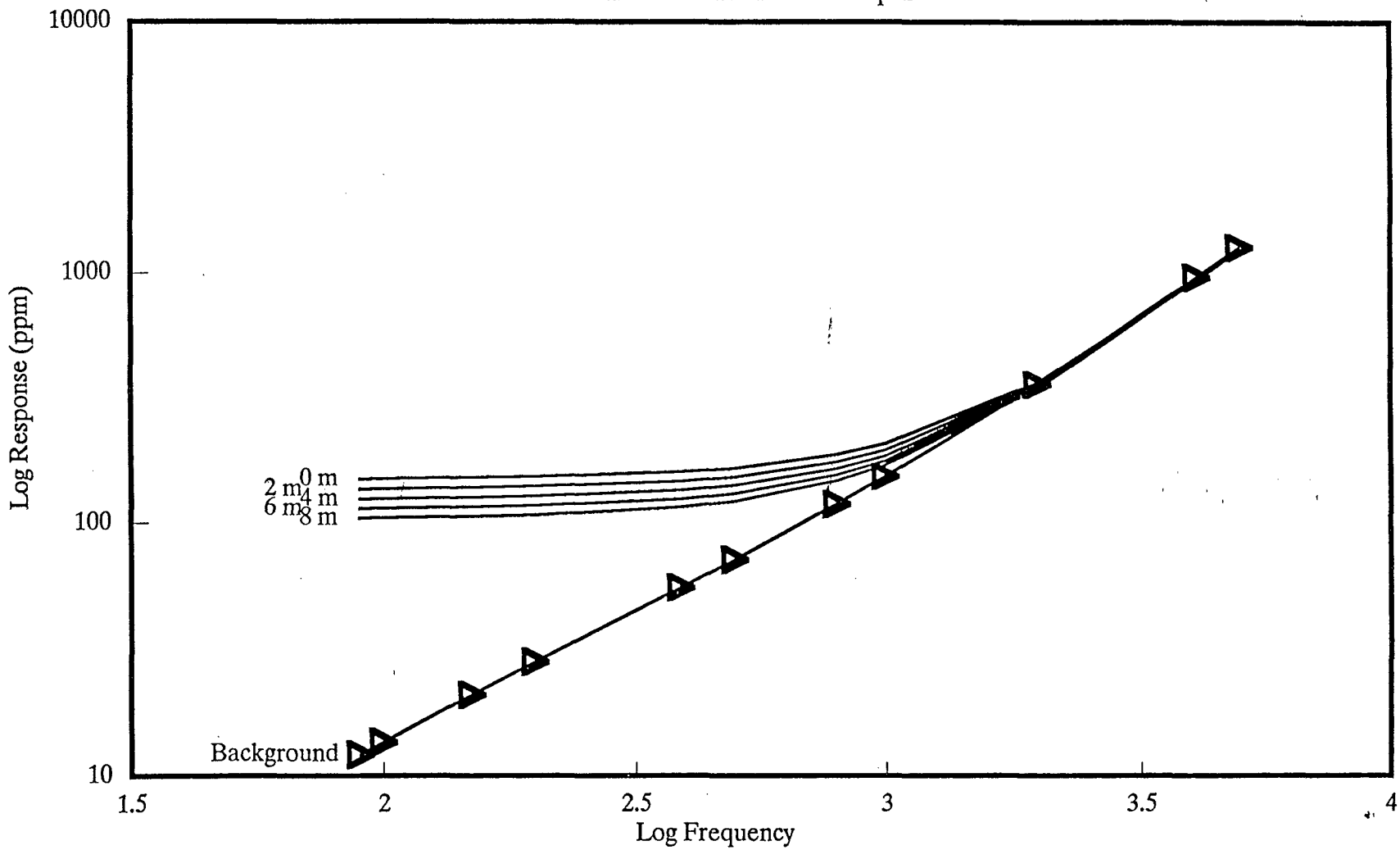

Conducting Layer Response Background – No Conductor

Water 25 Ohm–M Bottom 5 Ohm–M

Buried Layer at 5 Depths 546 Siemens Conductance

Total Response – Quadrature

1D – 60 Meter Water Depth

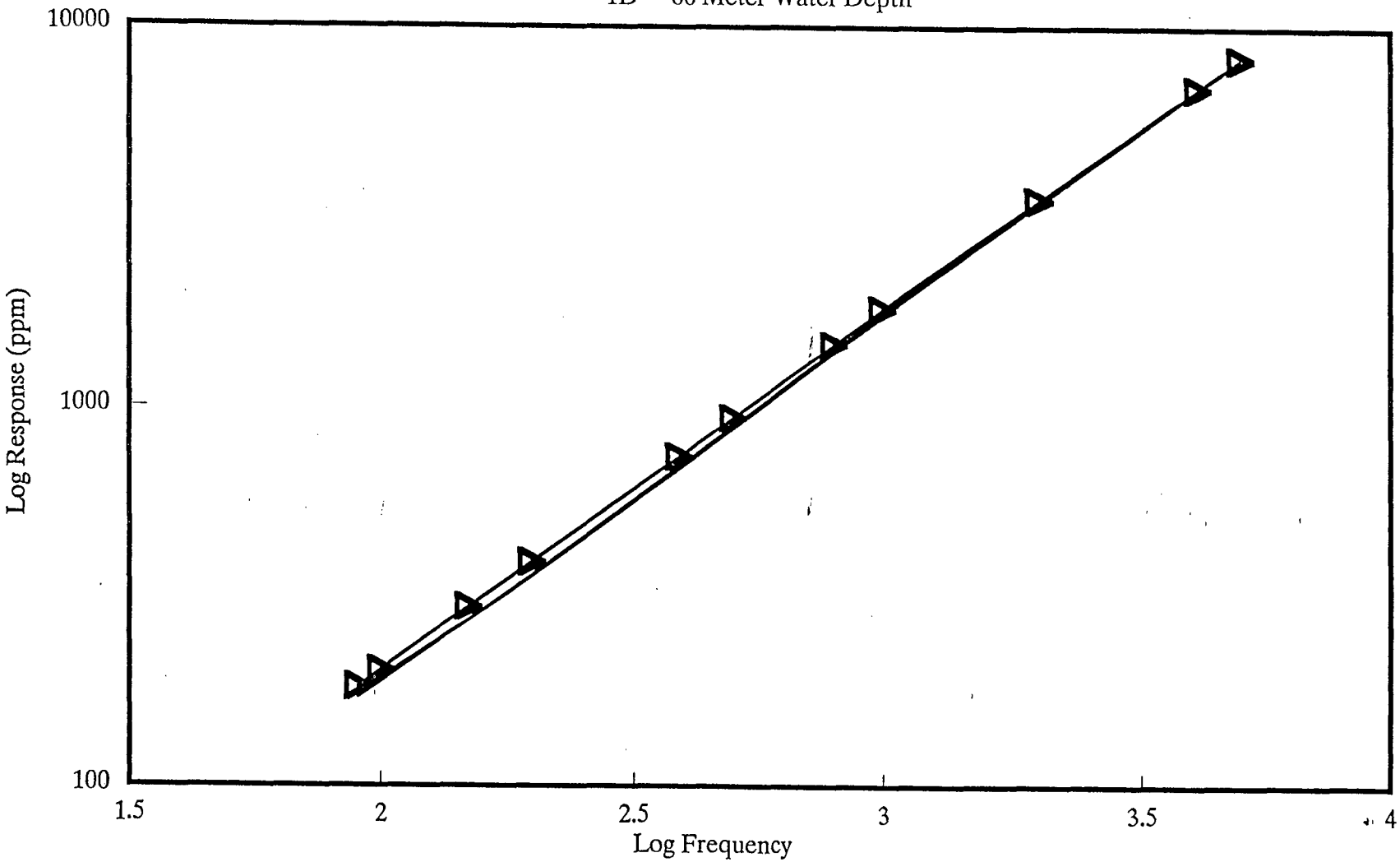

Conducting Layer Response Background – No Conductor

Water 25 Ohm–M Bottom 5 Ohm–M
Buried Layer at 5 Depths, 546 Siemens Conductance

Anomalous Response – Real

1D – 20 Meter Water Depth

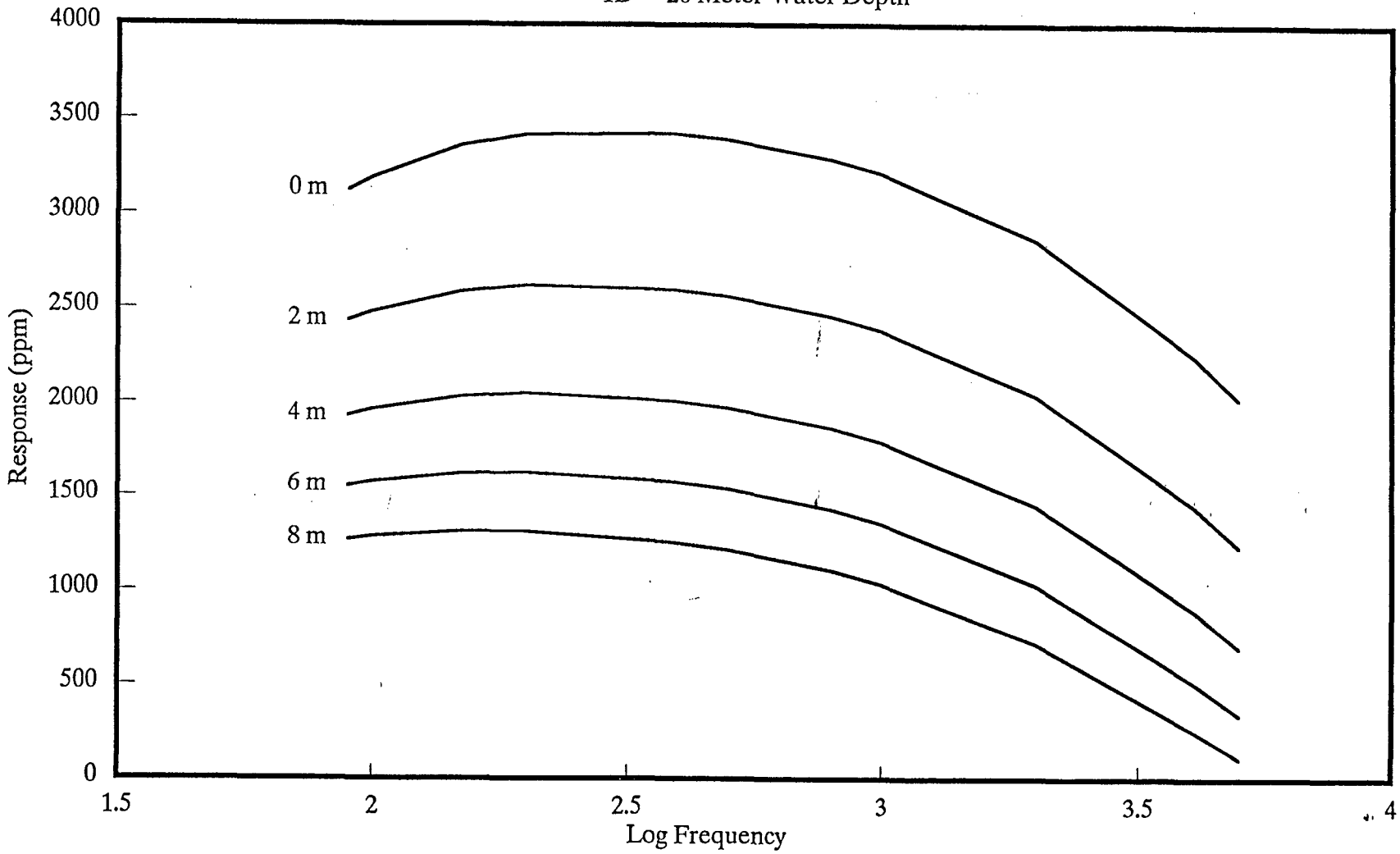

_____ Conducting Layer Response

Water 25 Ohm–M Bottom 5 Ohm–M
Buried Layer at 5 Depths, 546 Siemens Conductance

Anomalous Response – Quadrature

1D – 20 Meter Water Depth

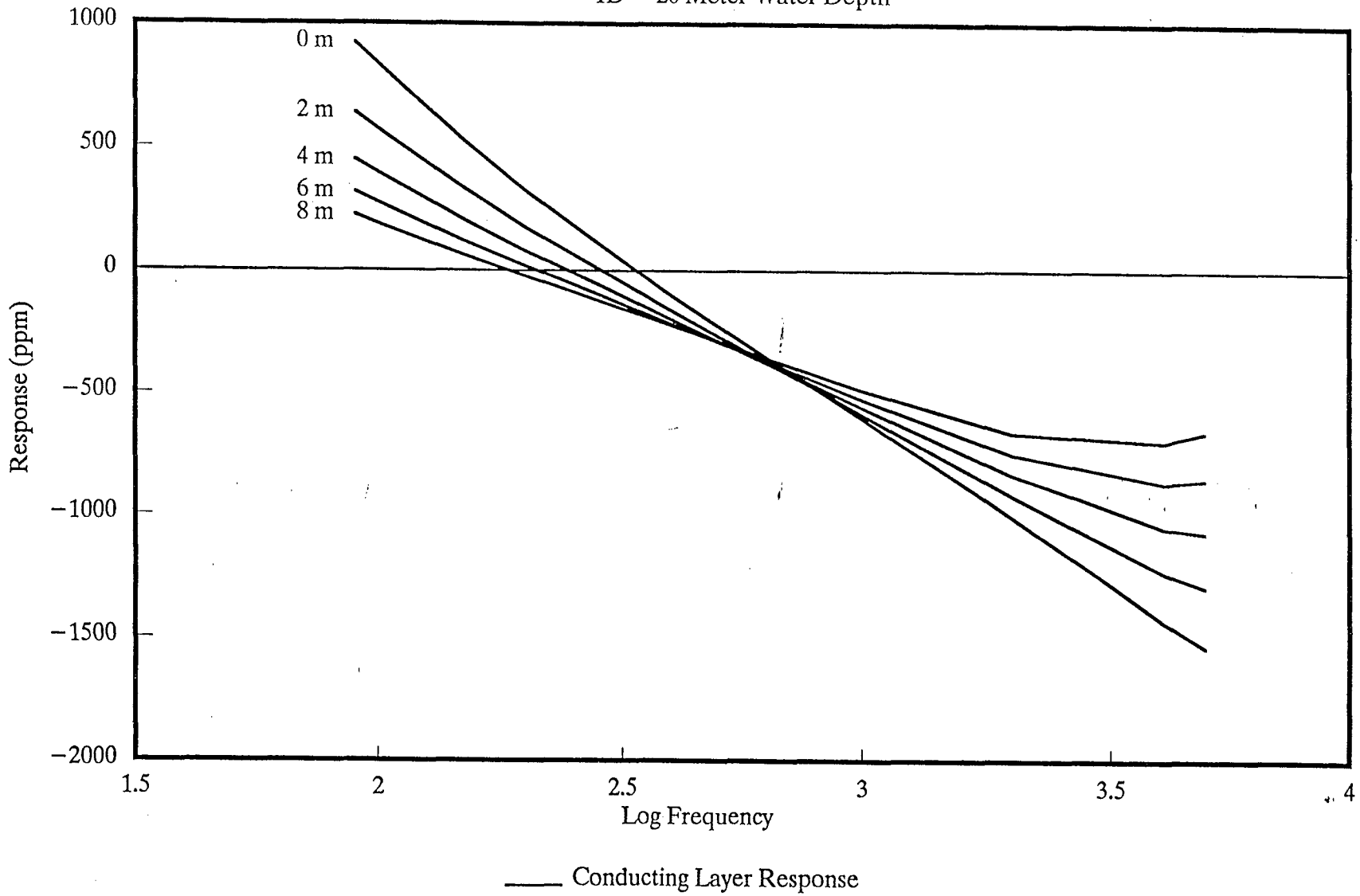

—— Conducting Layer Response

Water 25 Ohm–M Bottom 5 Ohm–M
Buried Layer at 5 Depths, 546 Siemens Conductance

Anomalous Response – Real

1D – 40 Meter Water Depth

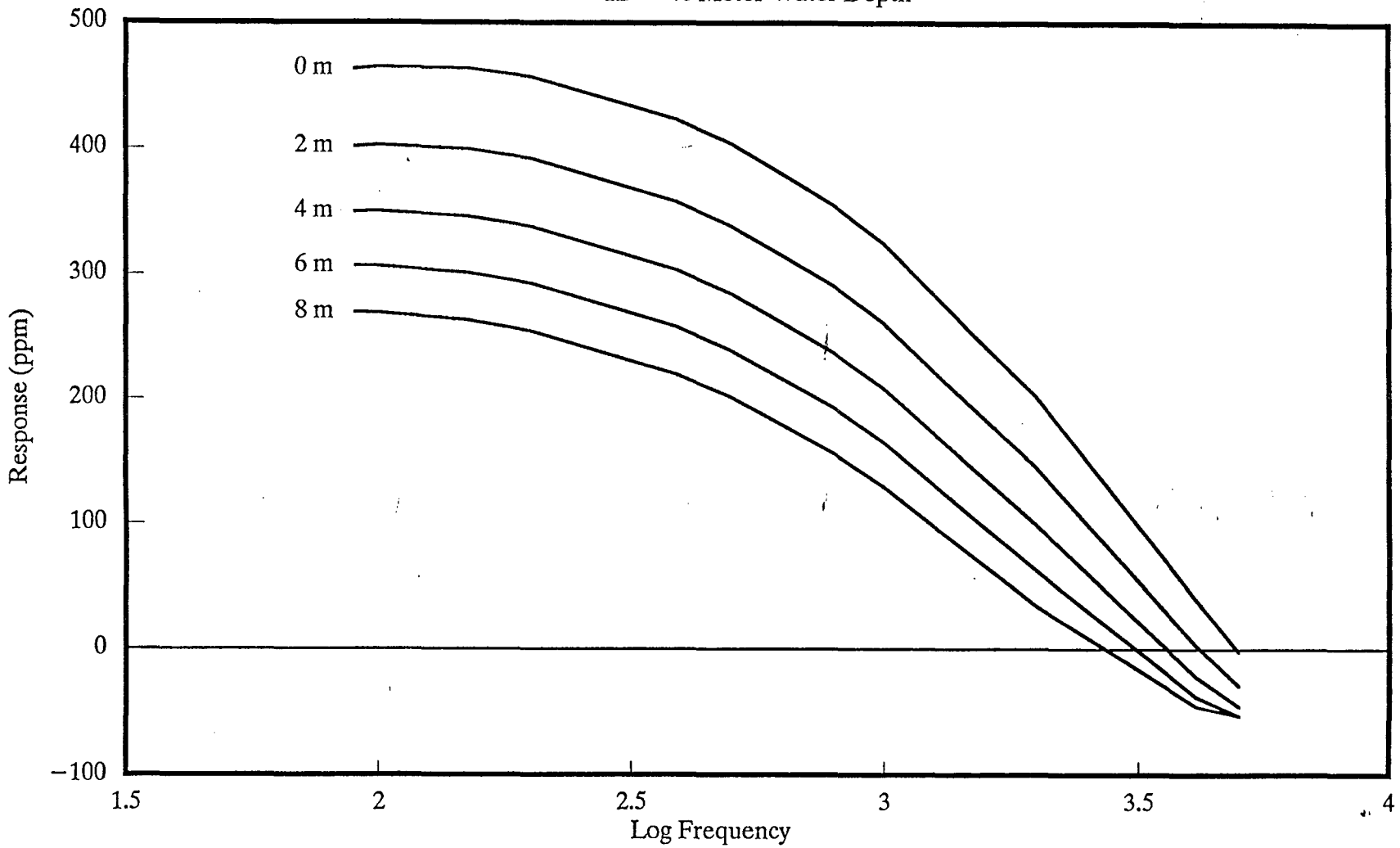

—— Conducting Layer Response

Water 25 Ohm–M Bottom 5 Ohm–M
Buried Layer at 5 Depths, 546 Siemens Conductance

Anomalous Response – Quadrature

1D – 40 Meter Water Depth

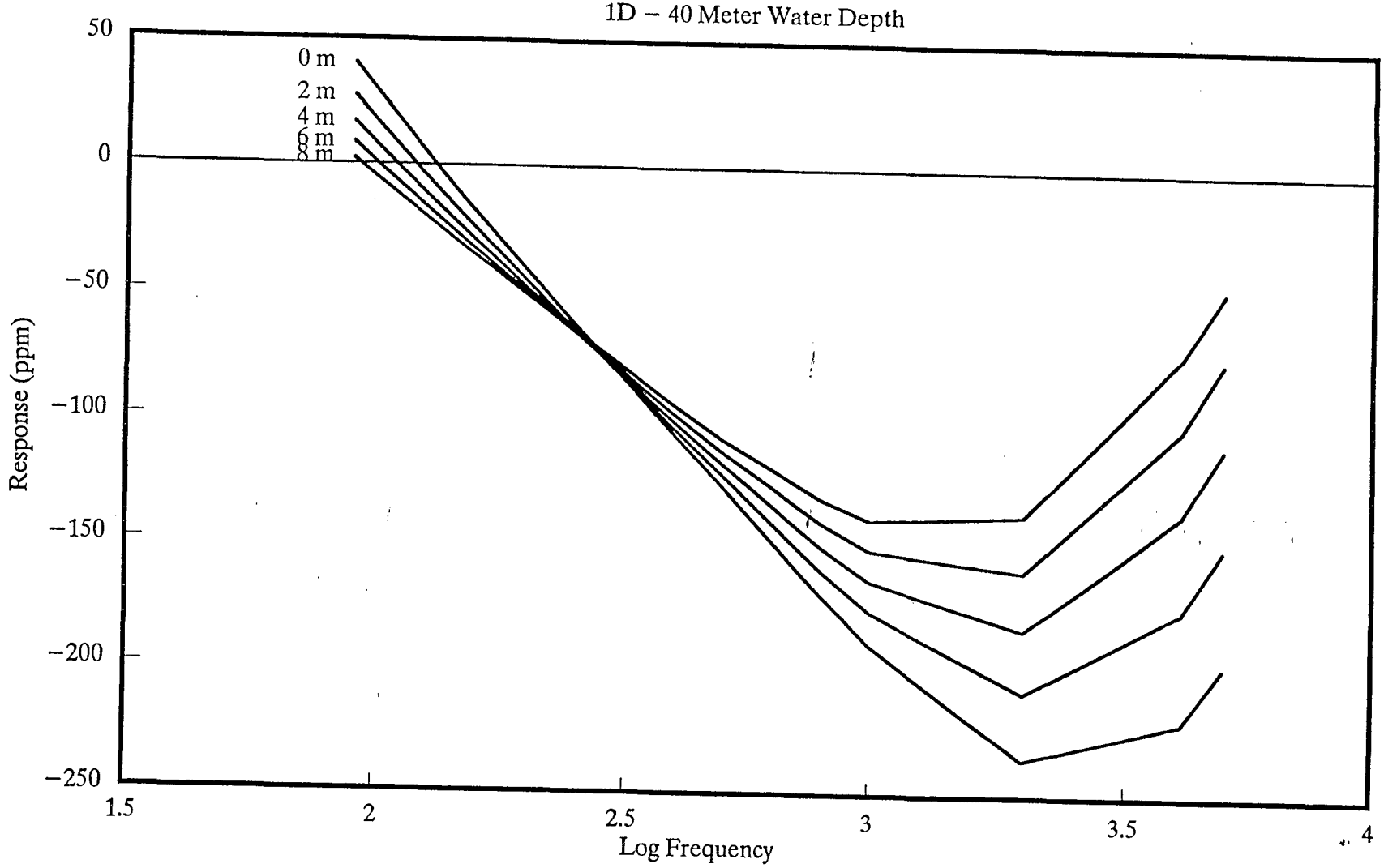

—— Conducting Layer Response

Water 25 Ohm–M Bottom 5 Ohm–M
Buried Layer at 5 Depths, 546 Siemens Conductance

Anomalous Response – Real

1D – 60 Meter Water Depth

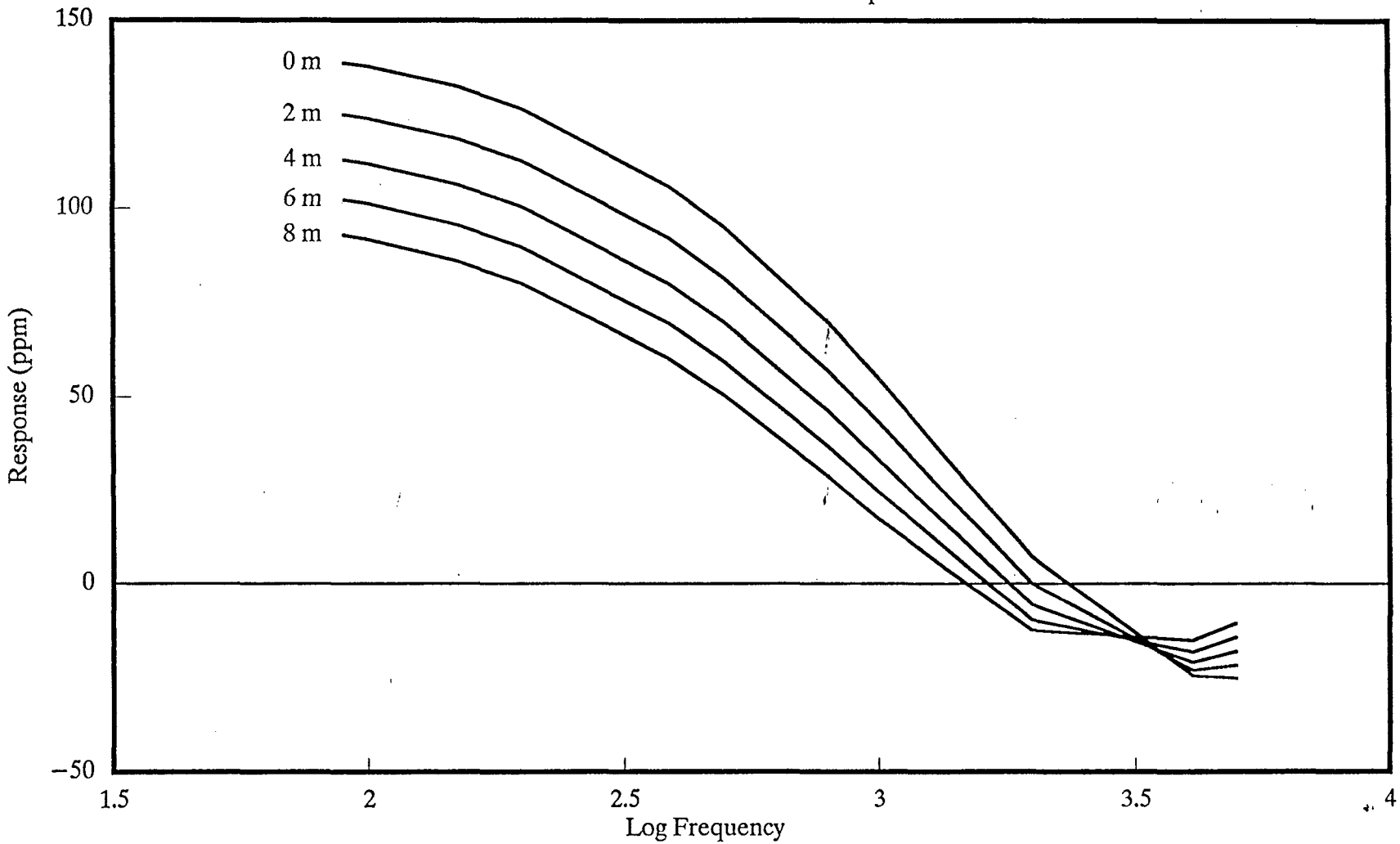

—— Conducting Layer Response

Water 25 Ohm–M Bottom 5 Ohm–M
Buried Layer at 5 Depths, 546 Siemens Conductance

Anomalous Response – Quadrature

1D – 60 Meter Water Depth

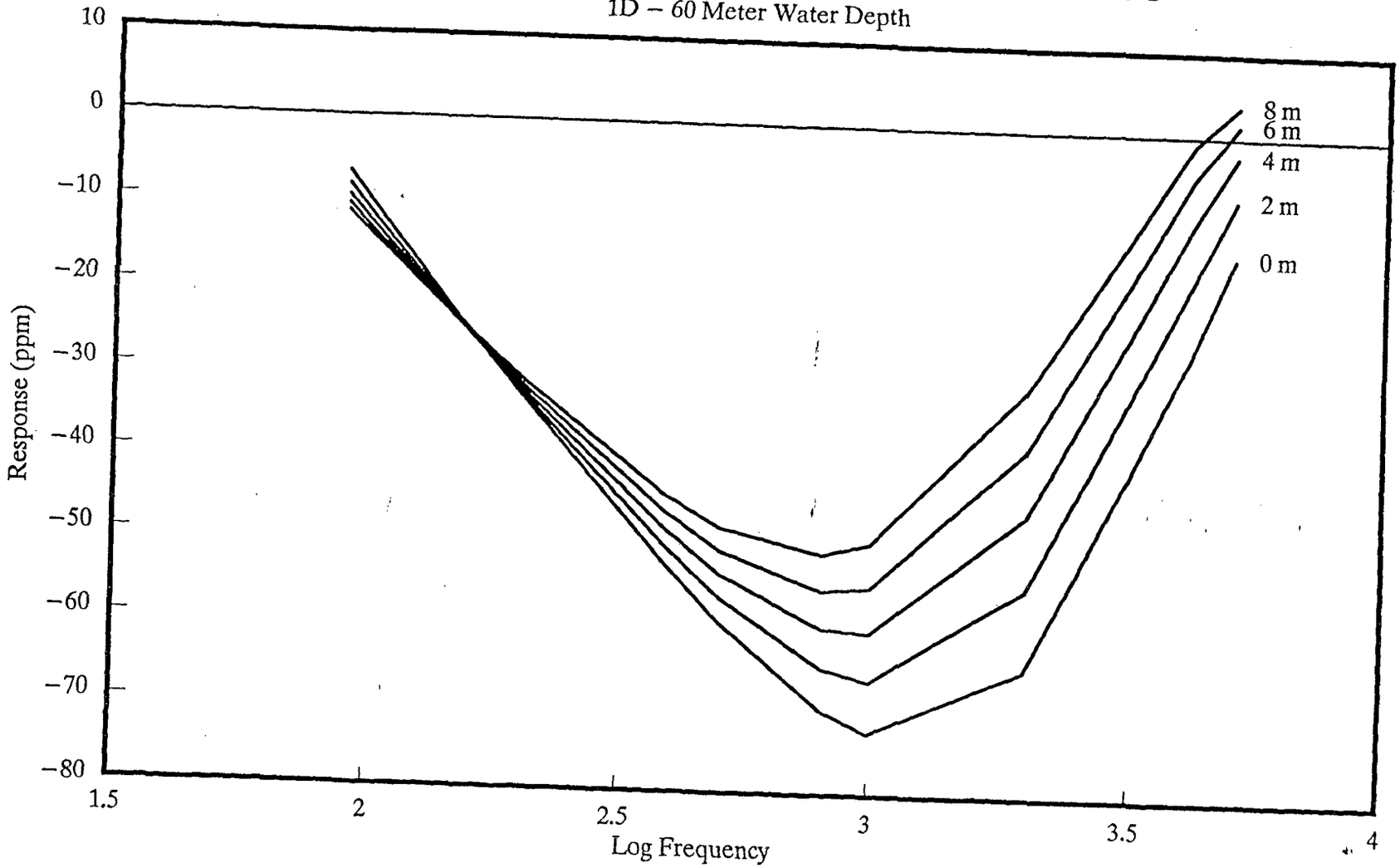

—— Conducting Layer Response

Water 25 Ohm–M Bottom 5 Ohm–M
Buried Layer at 5 Depths. 546 Siemens Conductance

Anomalous Response – Real

1D – 80 Meter Water Depth

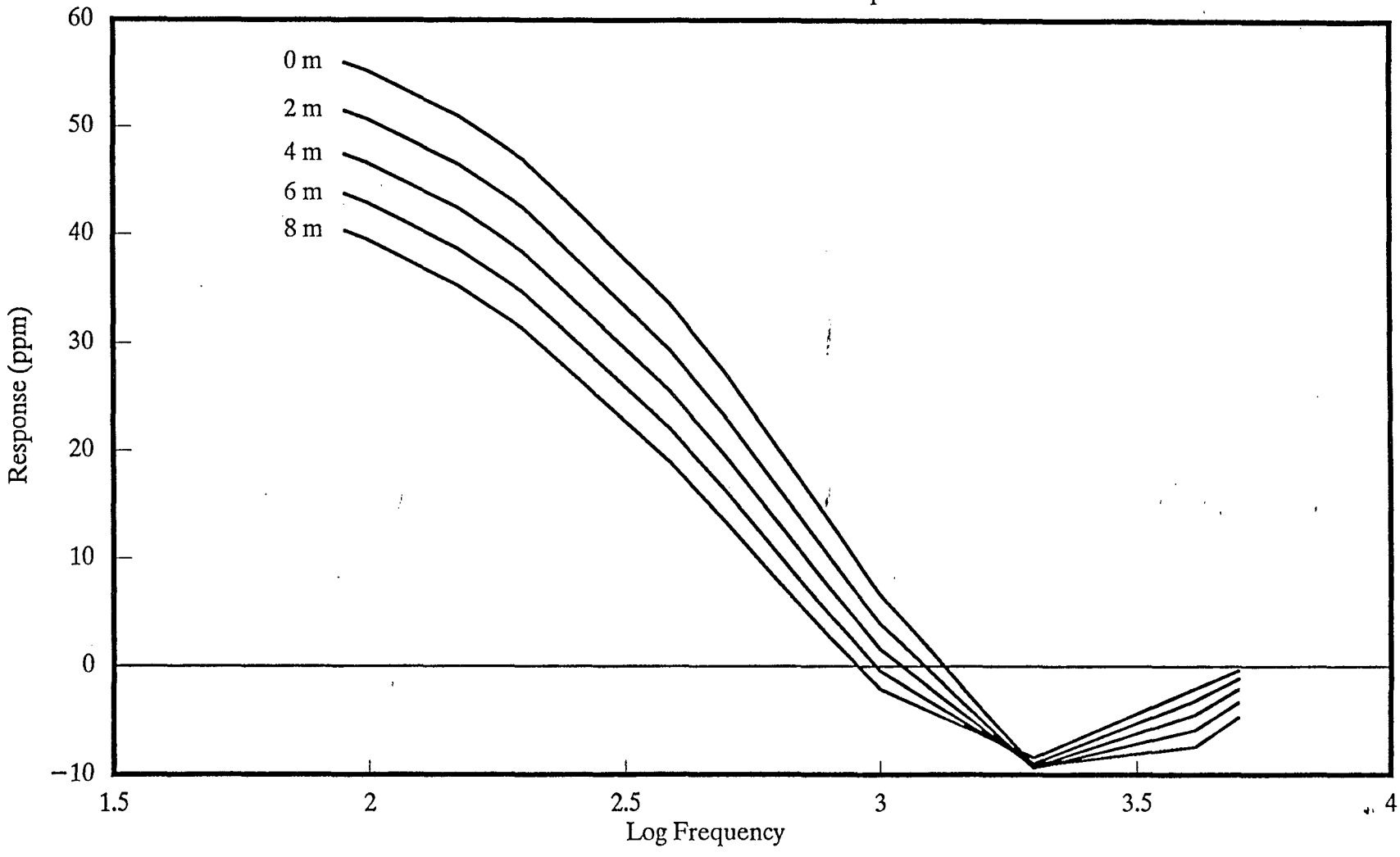

____ Conducting Layer Response

Water 25 Ohm–M Bottom 5 Ohm–M
Buried Layer at 5 Depths, 546 Siemens Conductance

Anomalous Response – Quadrature

1D – 80 Meter Water Depth

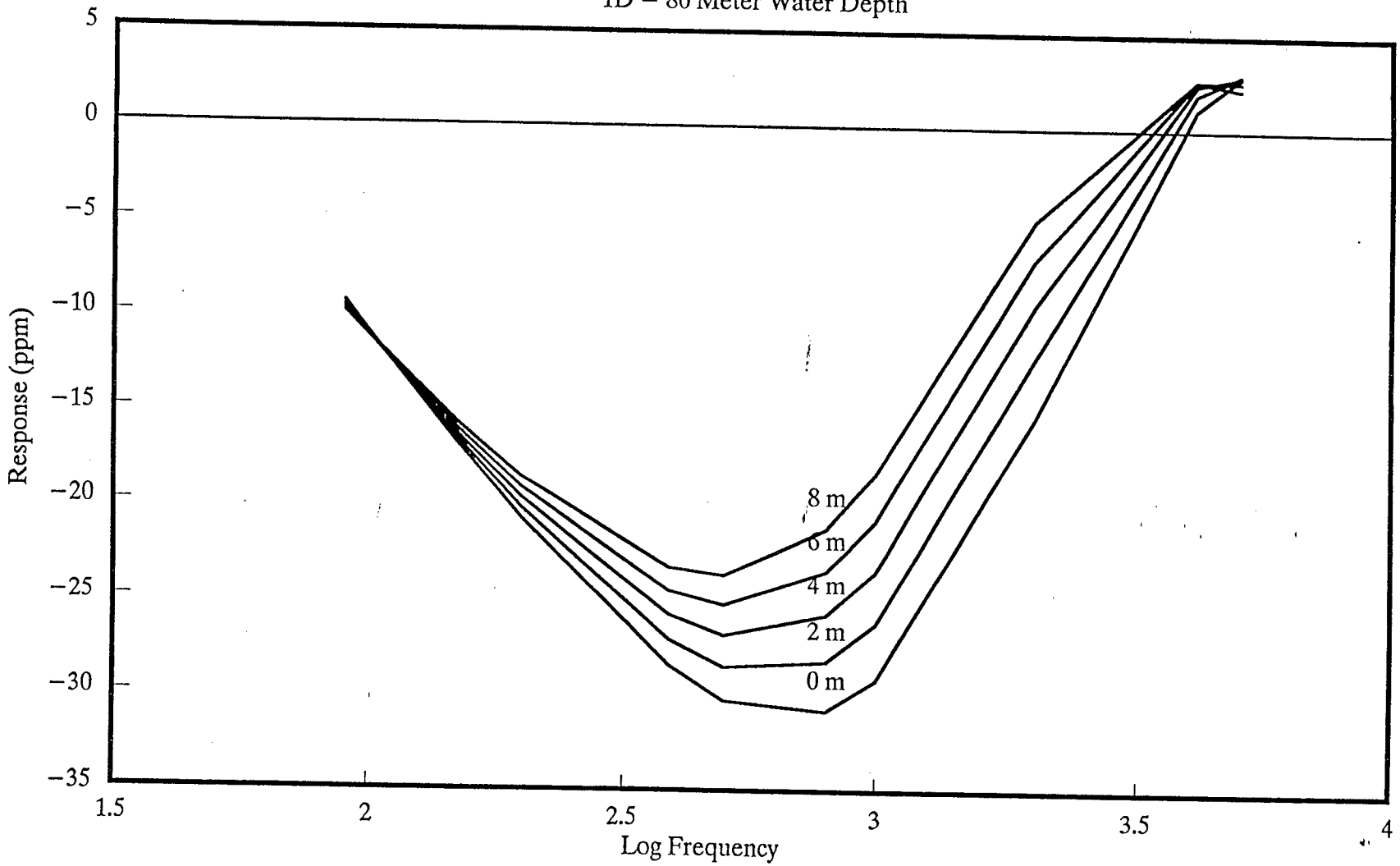

—— Conducting Layer Response

Water 25 Ohm–M Bottom 5 Ohm–M
Buried Layer at 5 Depths, 546 Siemens Conductance

Anomalous Response – Real

1D – 100 Meter Water Depth

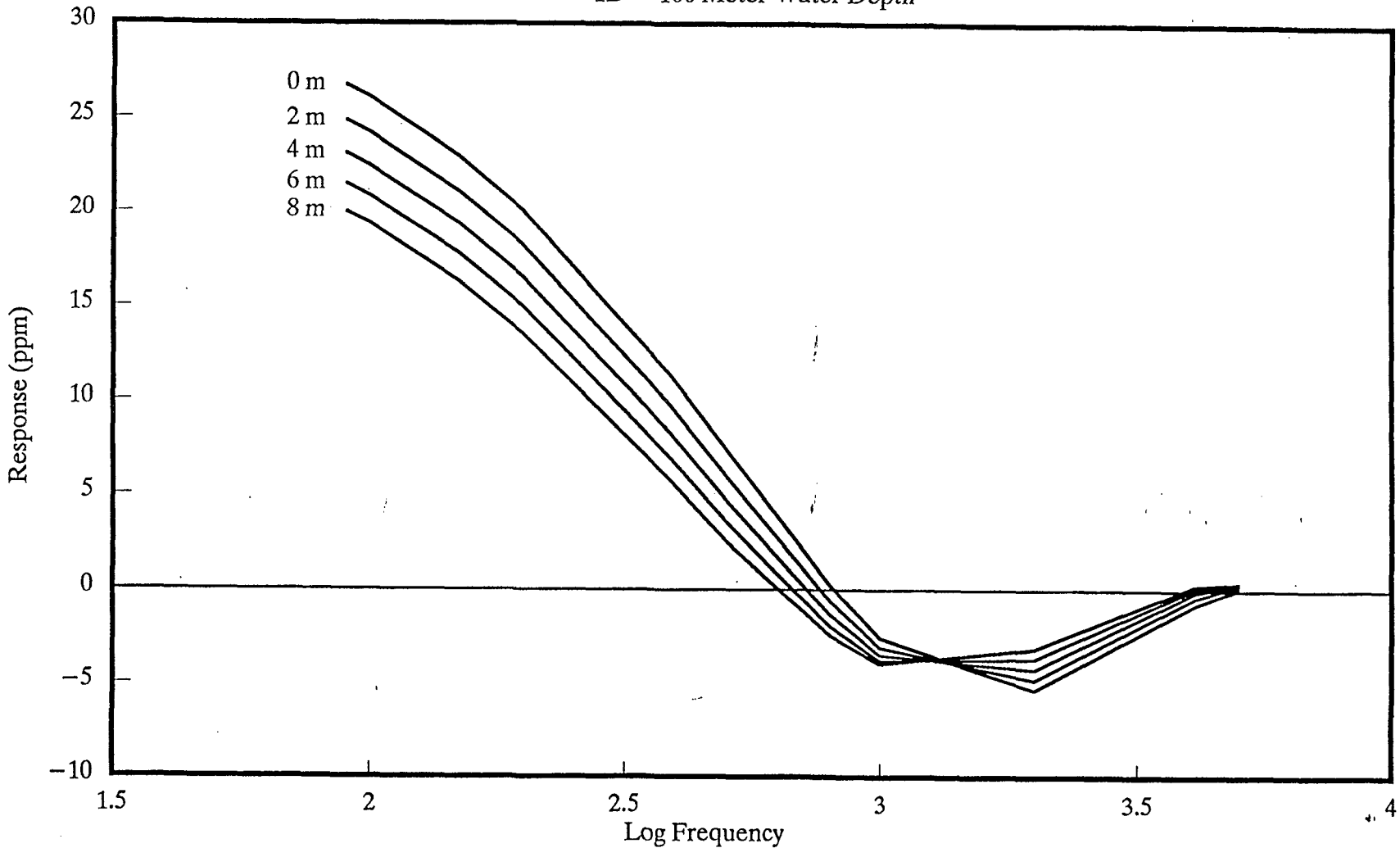

____ Conducting Layer Response

Water 25 Ohm–M Bottom 5 Ohm–M
Buried Layer at 5 Depths, 546 Siemens Conductance

Anomalous Response – Quadrature

1D – 100 Meter Water Depth

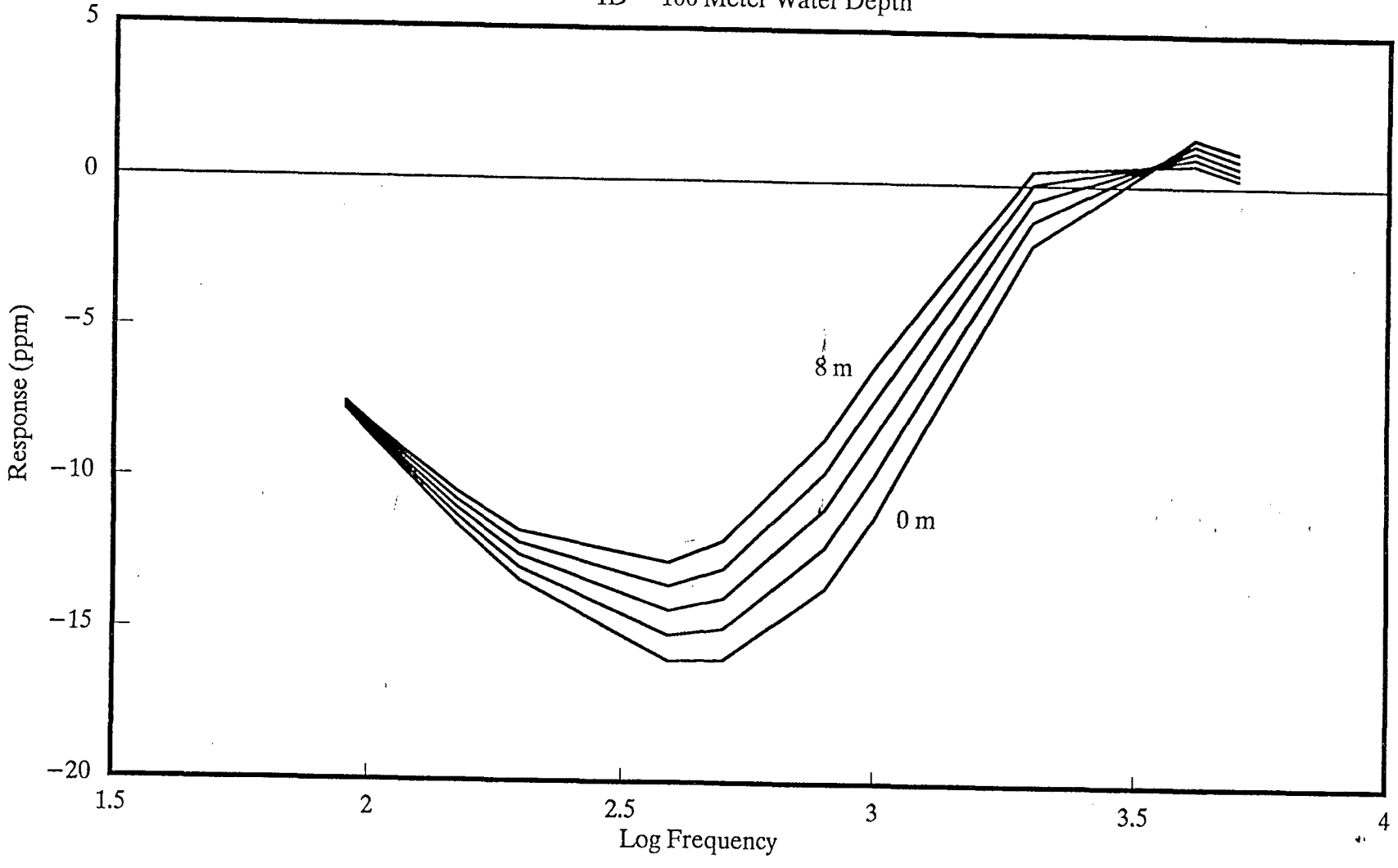

—— Conducting Layer Response

Water 25 Ohm–M Bottom 5 Ohm–M
Buried Layer at 5 Depths, 2m intervals, 546 Siemens Conductance

REPORT DOCUMENTATION PAGE

Form Approved
OMB No. 0704-0188

ic reporting burden for this collection of information is estimated to average 1 hour per response, including the time for reviewing instructions, searching existing data sources, gathering and ma
data needed, and completing and reviewing the collection of information. Send comments regarding this burden estimate or any other aspect of this collection of information, including sug
educing this burden, to Washington Headquarters Services, Directorate for Information Operations and Reports, 1215 Jefferson Davis Highway, Suite 1204, Arlington, VA 22202-4302, a
e of Management and Budget, Paperwork Reduction Project (0704-0188), Washington, DC 20503.

AGENCY USE ONLY *(Leave blank)*	2. REPORT DATE	3. REPORT TYPE AND DATES COVERED
	August 1998	Final report

TITLE AND SUBTITLE
Mapping Emplaced Articulated Concrete Mattress Using Geoelectrical and Electromagnetic Techniques

5. FUNDING NUMBERS
MIPR
W42-HEM-91-ED-51
MIPR
CELMK-PR-B94-5877

AUTHOR(S)
Keith J. Sjostrom, Dwain K. Butler, Robert F. Ballard

PERFORMING ORGANIZATION NAME(S) AND ADDRESS(ES)
U.S. Army Engineer Waterways Experiment Station
3909 Halls Ferry Road
Vicksburg, MS 39180-6199

8. PERFORMING ORGANIZATION REPORT NUMBER
Technical Report GL-98-17

SPONSORING/MONITORING AGENCY NAME(S) AND ADDRESS(ES)
U.S. Army Engineer Division, Lower Mississippi Valley
Vicksburg, MS 39180

10. SPONSORING/MONITORING AGENCY REPORT NUMBER

SUPPLEMENTARY NOTES
Available from National Technical Information Service, 5285 Port Royal Road, Springfield, VA 22161.

. DISTRIBUTION/AVAILABILITY STATEMENT
Approved for public release; distribution is unlimited.

12b. DISTRIBUTION CODE

ABSTRACT ***(Maximum 200 words)***

Articulated concrete mattresses (ACM) are structures placed parallel to the river current for the purpose of stabilizing tl concave banks in river bends, reduce the effects of erosion, and maintain the river channel. Over time, ACM's suffer structural fatigue or become damaged and must be remediated or replaced. The results of this research program reported herein describe the development of rapid, safe, and cost-effective geophysical procedures for detecting, delineating, and assessing the condition of emplaced ACM along the Lower Mississippi River. From 10 geophysical methods evaluated, tl self-potential (SP), towed electrical (TDC) resistivity, and electromagnetic (EM) methods were selected for further development. This report documents the geophysical concepts, field testing procedures, data analysis methods, results of investigation, and summary of the effectiveness in meeting the research objectives. The ACM is an excellent electrical tar for each geophysical method. Each method implemented can be used in both a high-resolution or reconnaissance mode ar able to rapidly detect the presence of ACM and delineate the mattress edges. Depth information to in-service ACM, even when the mat is buried under sediment, is best provided by the TDC resistivity, transient EM, and SP methods. The EM techniques are better in providing condition assessment information and detecting the individual mat segments.

SUBJECT TERMS
Articulated concrete mattress
Electrical resistivity method
Electromagnetic methods
Geophysical methods
Mississippi River
Self-potential method

15. NUMBER OF PAGES
356

16. PRICE CODE

SECURITY CLASSIFICATION OF REPORT	18. SECURITY CLASSIFICATION OF THIS PAGE	19. SECURITY CLASSIFICATION OF ABSTRACT	20. LIMITATION OF ABSTI
UNCLASSIFIED	UNCLASSIFIED		